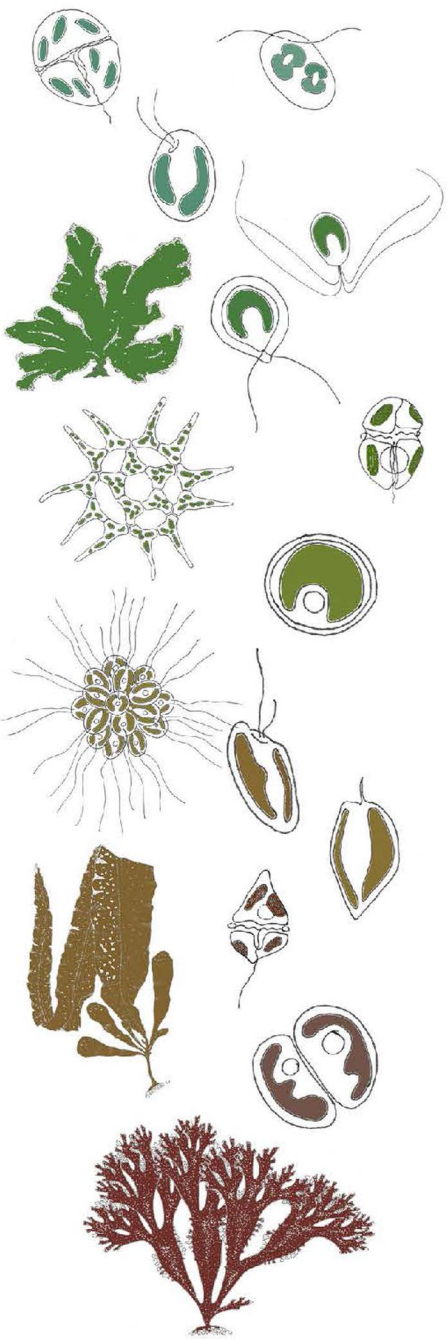
THIRD EDITION

Algae

Anatomy, Biochemistry, and Biotechnology

Laura Barsanti and Paolo Gualtieri





CRC Press
Taylor & Francis Group

Algae

A single-source reference on the biology of algae, the third edition of *Algae: Anatomy, Biochemistry, and Biotechnology* examines the most important taxa and structures for freshwater, marine, and terrestrial forms of algae. Its comprehensive coverage goes from algae's historical role through its taxonomy and ecology to its natural product possibilities.

In this update, the authors have gathered a significant amount of new material, including:

- more information on macroalgae
- detailed description of biotic associations
- updated description of biomass cultivation systems
- coverage of different "omic" approaches and tools used in algal investigation
- an expanded and updated algae utilization chapter

The book's unifying theme is the important role of algae in the earth's self-regulating life support system and its function within restorative models of planetary health. It also discusses algae's biotechnological applications, including potential nutritional and pharmaceutical products.

Written for students as well as researchers, teachers, and professionals in the field of phycology and applied phycology, this new full-color edition is both illuminating and inspiring.


Taylor & Francis
Taylor & Francis Group
http://taylorandfrancis.com

Algae

Anatomy, Biochemistry, and Biotechnology

Third Edition

Laura Barsanti
Istituto di Biofisica, Pisa, Italy

and

Paolo Gualtieri
Istituto di Biofisica, Pisa, Italy

CRC Press
Taylor & Francis Group
Boca Raton London New York

CRC Press is an imprint of the
Taylor & Francis Group, an **informa** business

Third edition published 2023
by CRC Press
6000 Broken Sound Parkway NW, Suite 300, Boca Raton, FL 33487-2742

and by CRC Press
4 Park Square, Milton Park, Abingdon, Oxon, OX14 4RN

CRC Press is an imprint of Taylor & Francis Group, LLC

© 2023 Laura Barsanti and Paolo Gualtieri

First edition published by CRC Press 2006

Second edition published by CRC Press 2014

Reasonable efforts have been made to publish reliable data and information, but the author and publisher cannot assume responsibility for the validity of all materials or the consequences of their use. The authors and publishers have attempted to trace the copyright holders of all material reproduced in this publication and apologize to copyright holders if permission to publish in this form has not been obtained. If any copyright material has not been acknowledged please write and let us know so we may rectify in any future reprint.

Except as permitted under U.S. Copyright Law, no part of this book may be reprinted, reproduced, transmitted, or utilized in any form by any electronic, mechanical, or other means, now known or hereafter invented, including photocopying, microfilming, and recording, or in any information storage or retrieval system, without written permission from the publishers.

For permission to photocopy or use material electronically from this work, access www.copyright.com or contact the Copyright Clearance Center, Inc. (CCC), 222 Rosewood Drive, Danvers, MA 01923, 978-750-8400. For works that are not available on CCC please contact mpkbookspermissions@tandf.co.uk

Trademark notice: Product or corporate names may be trademarks or registered trademarks and are used only for identification and explanation without intent to infringe.

Library of Congress Cataloging-in-Publication Data
Names: Barsanti, L., author. | Gualtieri, Paolo, author.
Title: Algae : Anatomy, biochemistry, and biotechnology / Laura Barsanti, Istituto di Biofisica, Pisa, Italy and Paolo Gualtieri, Istituto di Biofisica, Pisa, Italy.
Description: Third edition. | Boca Raton : CRC Press, 2023. | Includes bibliographical references and index.
Identifiers: LCCN 2022032392 (print) | LCCN 2022032393 (ebook) | ISBN 9781032035123 (hardback) | ISBN 9781032035147 (paperback) | ISBN 9781003187707 (ebook)
Subjects: LCSH: Algae.
Classification: LCC QK566 .G83 2023 (print) | LCC QK566 (ebook) | DDC 561/.93—dc23/eng/20220713
LC record available at https://lccn.loc.gov/2022032392
LC ebook record available at https://lccn.loc.gov/2022032393

ISBN: 978-1-032-03512-3 (hbk)
ISBN: 978-1-032-03514-7 (pbk)
ISBN: 978-1-003-18770-7 (ebk)

DOI: 10.1201/9781003187707

Typeset in Times
by Apex CoVantage, LLC

To Antonietta, my sister; to Silvana and Renzo, mam and dad, whom I cannot longer hug; and to Antonio and Luca, my two brothers, whom I hope to hug for many more years.

To Mario R. Tredici (1951-2022): es un soplo la vida…

Laura

To my Mom Lilli, to my two fathers Giuseppe and Bruno, and to my younger brother Mimmo, who loved me, but are no longer beside me.

I have survived them thanks to all the others (many) who loved me and still do, despite me.

Paolo


Taylor & Francis
Taylor & Francis Group
http://taylorandfrancis.com

Contents

Preface xiii
Authors' Biographies xv
Introduction xvii

Chapter 1 General Overview 1

Definition 1
Classification 2
Summaries of the 12 Algal Phyla 2
Cyanobacteria 2
Glaucophyta 8
Rhodophyta 9
Prasinodermatophyta and Chlorophyta 11
Charophyta 15
Haptophyta 17
Cryptophyta 18
Ochrophyta 19
Miozoa—Dinophyceae 23
Cercozoa—Chlorarachniophyceae 26
Euglenozoa—Euglenophyceae 26
Structure of Thallus—Cytomorphological Types 28
Unicells and Unicell Colonial Type 28
Filamentous Type 28
Siphonocladous Type 28
Siphonous Type 32
Parenchymatous and Pseudo-Parenchymatous Type 35
Palmelloid Type 36
Nutrition 37
Reproduction 38
Vegetative and Asexual Reproduction 38
Binary Fission or Cellular Bisection 38
Zoospores, Aplanospores, and Autospores 38
Autocolony Formation 38
Fragmentation 40
Resting Stages 40
Sexual Reproduction 41
Haplontic or Zygotic Life Cycle 41
Diplontic or Gametic Life Cycle 42
Diplohaplontic or Sporic Life Cycle 42
Occurrence and Distribution 42
Biotic Interactions 44
Viruses 44
Bacteria 48
Arthropods 50
Amphibians 51
Reptiles 53
Other Animals and Humans 53

Extreme Habitats 56
Cold Environments 56
Hot Environments 58
Dry Environments 60
Space 62
Endosymbiosis and the Origin of Eukaryotic Photosynthesis 63

Chapter 2 Biogeochemical Role of Algae 71

The Roles of Algae in Biogeochemistry 71
The Oxygen and Carbon Cycles 72
The Nitrogen Cycle 76
The Phosphorus Cycle 81
The Iron Cycle 83
The Silicon Cycle 88
The Sulfur Cycle 92
Limiting Nutrients 94

Chapter 3 Anatomy 101

Cytomorphology and Ultrastructure 101
Outside the Cell 101
Type 1—Simple Cell Membrane 101
Type 2—Cell Surface With Additional Extracellular Material 102
Mucilages and Sheaths 102
Scales 103
Frustules 107
Cell Walls 110
Loricas 111
Skeletons 112
Type 3—Cell Surface With Additional Intracellular Material in Vesicles 114
Type 4—Cell Surface With Additional Extracellular and Intracellular Material 116
First Level 119
Second Level 119
Third Level 121
Flagella and Associated Structures 122
Flagellar Shape and Surface Features 123
Flagellar Scales 123
Flagellar Hairs 126
Flagellar Spines 128
Internal Features 128
Axoneme 128
Paraxial Rod 129
Other Intra-Flagellar Accessory Structures 130
Transition Zone 132
Basal Bodies 136
Root System 138
Glaucophyta 139

Prasinodermatophyta, Chlorophyta, Charophyta 139
Haptophyta 145
Cryptophyta 145
Ochrophyta 147
Cercozoa—Chlorarachniophyceae 150
Miozoa—Dinophyceae 151
Euglenozoa—Euglenophyceae 152
How Algae Move 154
Swimming 154
Movements Other Than Swimming 165
Buoyancy Control 168
How a Flagellum Is Built: Intra-Flagellar Transport 170
How a Flagellar Motor Works 170
How a Paraxial Rod Works 171
The Photoreceptor Apparatus 171
Types of Photoreceptive Systems 173
Type I 173
Type II 175
Type III 177
Photoreceptive Proteins 177
Behavioral and Physiological Features 180
Sampling Strategies 181
Trajectory Control 182
Signal Transmission 183
An Example: Photoreceptor and Photoreception in *Euglena* 183
Chloroplasts 188
Cyanobacteria 189
Glaucophyta 189
Rhodophyta 191
Prasinodermatophyta, Chlorophyta, Charophyta 191
Haptophyta 192
Cryptophyta 192
Ochrophyta 193
Cercozoa—Chlorarachniophyceae 194
Miozoa—Dinophyceae 195
Euglenozoa—Euglenophyceae 197
The Nucleus, Nuclear Division, and Cytokinesis 198
Rhodophyta 199
Prasinodermatophyta, Chlorophyta, Charophyta 199
Cryptophyta 200
Miozoa—Dinophyceae 200
Euglenozoa—Euglenophyceae 201
Ejectile Organelles and Feeding Apparatus 203
Prasinodermatophyta, Chlorophyta, Charophyta 203
Haptophyta 203
Cryptophyta 204
Ochrophyta 205
Cercozoa—Chlorarachiophyceae 205
Miozoa—Dinophyceae 205
Euglenozoa—Euglenophyceae 207

Chapter 4 Photosynthesis 215

Light 215
Photosynthesis 218
Light-Dependent Reactions 219
PSII and PSI: Structure, Function, and Organization 227
ATP—Synthase 229
ETC Components 230
Electron Transport: The Z-Scheme 231
Proton Transport: Mechanism of Photosynthetic Phosphorylation 232
Pigment Distribution in PSII and PSI Super-Complexes of Algal Division 234
Light-Independent Reactions 235
RuBisCO 235
Calvin Benson Bassham Cycle 241
Carboxylation 242
Reduction 242
Regeneration 242
Photorespiration 242
The Photosynthesis-Irradiance Response Curve (P-vs-E Curve) 243
Photoacclimation 246
Photosynthesis in Light-Limited Environments 247
The Energy Relationships in Photosynthesis: The Balance Sheet 251

Chapter 5 Culturing 257

Collection, Storage, and Preservation 257
Culture Types 260
Culture Parameters 262
Temperature 263
Light 263
pH 263
Salinity 263
Mixing 263
Culture Vessels 264
Media Choice and Preparation 264
Freshwater Media 265
Marine Media 273
Seawater Base 273
Nutrients, Trace Metals, and Chelators 274
Vitamins 276
Soil Extract 277
Buffers 277
Sterilization of Culture Materials 284
Culture Methods 286
Microalgae 286
Batch Cultures 286
Continuous Cultures 289
Semi-Continuous Cultures 290
Commercial-Scale Cultures 290
Outdoor Ponds 291

Photobioreactors 293
Culture of Sessile Micro-Algae 296
Macroalgae 296
Onshore Cultivation 296
Offshore Cultivation 297
Nearshore Cultivation 297
Integrated Multitrophic Aquaculture 298
Quantitative Determinations of Algal Density and Growth 298
Growth Rate and Generation Time Determinations 303

Chapter 6 Utilization 307

Human Food 308
Cyanobacteria 308
Rhodophyta 310
Ochrophyta—Phaeophyceae 315
Chlorophyta 321
Animal Feed 324
Hydrocolloids 327
Agar 329
Alginates 330
Carrageenan 331
Fertilizers 332
Cosmetics 335
Functional Foods and Nutraceuticals 336
Harmful Algal Blooms and Toxins 346
Cyanophyceae 350
Prymnesiophyceae 351
Bacillariophyceae 351
Raphidophyceae 352
Dinophyceae 353
Algae as Tools for Environmental Monitoring 356
Flow Cytometry 356
Metagenomic Analysis 357
Remote Sensing 358
Digital Microscopy 358
Algae as Tools for Bioremediation 361
Heavy Metals 361
Food Industry Wastewater 364
Algae in a Bio-Based Economy 365
Algae-Based Products: Use and Market Scenarios 368
Exploitation of the Algae Potential for Different Target Markets 373
Sustainability 376

Chapter 7 Working With Light 385

How Light Behaves 385
Scattering 385
Absorption 386
Fluorescence 387
Interference 389

Reflection 389
Refraction 391
Dispersion 392
Diffraction 392
Lab Instruments 394
The Microscope 394
Bright Field Microscopy 396
Steps in Establishing Köhler Illumination 397
Numerical Aperture, Airy Disk, and Microscope Resolution 398
CCD Cameras for Optical Microscopy 399
Fluorescence Microscopes 401
Light Sources for Microscopy 402
Digital Microscopy 403
Hardware 403
Software 404
An Alternative "Simple" Method for Obtaining Algae Absorption Spectra 404
Field Instruments 406
Radiometry 408
Measurement Geometries: Solid Angles 408
Radiant Energy 408
Spectral Radiant Energy 408
Radiant Flux (Radiant Power) 409
Spectral Radiant Flux (Spectral Radiant Power) 409
Radiant Flux Density (Irradiance and Radiant Exitance) 409
Spectral Radiant Flux Density 410
Radiance 410
Spectral Radiance 410
Radiant Intensity 411
Spectral Radiant Intensity 411
Photometry 411
Luminous Flux (Luminous Power) 412
Luminous Intensity 412
Luminous Energy 414
Luminous Flux Density (Illuminance and Luminous Exitance) 414
Luminance 414
Lambertian Surfaces 414
Unit Conversion 416
Radiant and Luminous Flux (Radiant and Luminous Power) 416
Irradiance (Flux Density) 416
Radiance 417
Radiant Intensity 417
Luminous Intensity 417
Luminance 417
Geometries 417
PAR Detectors 418

Subject Index 421
Index 433

Preface

In the eight years since the second edition of this book was published, we have compiled a large amount of new material and data, based on our own experiences in reading, writing, and reviewing. With the aid of all this information, we have updated and revised the book, introducing changes and additions, hoping for a good result but aware of the fact that completeness is a far-away mirage.

As with the previous editions, this book has been thoughtfully considered and written for undergraduate and post-graduate students with a general scientific background who are having their first academic experience with topics such as algology and aquatic biology, as well as for researchers, teachers, and professionals in the fields of phycology and applied phycology. Our major commitment is still the same: to arouse the curiosity of both students and teachers (and of course of all the possible readers, no matter the level of education), challenging and stimulating them to move beyond the limit of the written page to further explore not only the topics highlighted in the book but also all the new ideas that can spring to mind (we hope!) after reading each chapter.

Though updated, the bibliography is still by no means exhaustive; we have not attempted to be comprehensive, and many excellent papers will still be missing. Our intention was to include only enough to lead the reader into the right part of the primary literature in a fairly directed manner and to provide a sort of orienteering compass in the "mare magnum" of scientific papers.

We are deeply grateful to the staff at CRC Press, Boca Raton (FL), particularly our patient and discerning editor, Alice Oven, for trusting us enough to ask for a third edition, and to the senior editorial assistant, Shikha Garg, who had to cope with all our mess.

Our sincere gratitude to Valter Evangelista for his skillful assistance and ability in helping us with the drawings and illustrations. For the artwork present in the book, we will be always grateful and indebted to Antonietta and Luca Barsanti, sister and brother of Laura. Their drawing work is wonderful and their artistic abilities unattainable. We are also indebted to Lorenzo Birindelli, a young new member of our research group, for his skillful ability in preparing all the new drawings and schemes and for his patience in keeping up with our ever-changing demands and moods without going mad. He dedicated six months of his life to us, and we are happy for him that he is still very young and will be able to do many more interesting things in his future. Grazie!


Taylor & Francis
Taylor & Francis Group
http://taylorandfrancis.com

Authors' Biographies



Dr. Laura Barsanti graduated in Natural Sciences from the University of Pisa (Italy), and though she dreamed of sailing the seas to study whales and dolphins, she ended up chasing microalgae on a microscope slide. She realized she liked it, and she kept doing it for more than 40 years at the Centro Studi Microrgansmi Autotrofi in Florence, then at the Biophysics Institute of the National Council of Research (CNR) in Pisa, where she still does it today. She has authored three books and edited three more and has published about 200 papers and patents.



Dr. Paolo Gualtieri graduated in Biology and Computer Science from the University of Pisa (Italy) and then took his PhD in Biophysics at the same university. He has been a visiting professor in many different research institutes around the world (Max Plank Institute for Biophysical Chemistry of Gottingen, Max Plank Institute for Biochemistry of Martinsried, CNRS Marine Station of Villefranche sur Mer, NIH Bethesda, University of Marburg, University of Regensburg, Computer Science Center of the University of Maryland, University of Tennessee, and Purdue University). At present, he is senior scientist at the Biophysics Institute of the National Council of Research (CNR) in Pisa (Italy) and adjunct professor at the University of Maryland, University College (College Park, MD, USA). He has given over 30 keynote international lectures, authored three books, and edited three more; he has published about 200 papers and patents and has served on many international boards. Paolo used to be a tennis teacher, and now he just plays; he has two Conservatory of Music diplomas in trumpet.


Taylor & Francis
Taylor & Francis Group
http://taylorandfrancis.com

Introduction

In our intention, the major commitment of this book is to arouse the curiosity of both students and teachers (and of course of all the possible readers, no matter the level of education), though it should serve as a means to encourage outstanding work in the field of phycology, especially the aspect of teaching. This book has been conceived and written for undergraduate and post-graduate students with a general scientific background, following courses on algology and aquatic biology, as well as researchers, teachers, and professionals in the fields of phycology and applied phycology. It does not pretend to be exhaustive, because information and data on the algal world are constantly expanding, growing, and changing and reaching an end point is impossible. Still, it is possible to give an idea of what is within and behind this vast topic, and this is what we have tried to do. For this reason, each of the chapters can be read on its own as a self-contained essay, used in a course, or assigned as supplemental reading for a course.

We have presented an overview of the classification of algae, keeping in mind that taxonomy is under constant and rapid revision at all levels, especially thanks to the continuous new genetic progress that challenges rigid concepts of the tree of life. Life cycles, means of reproduction, and a phylogenetic interpretation of the algae evolutionary process provide a conceptual framework for the following chapters. Freshwater, marine, and terrestrial forms have been described, and their levels of organization have been treated from the subcellular, cellular, and morphological standpoints, together with physiology, biochemistry, culture methods, and finally the current issues that involve algae and human society. Extensive original drawings and photographic illustrations provide detailed descriptions of many algal apparatus.

Compiling an exhaustive bibliography would have been a Sisyphean task, that is, useless and vain; hence, the lists of suggested reading at the end of each chapter are by no means complete but intended to convey an idea of the complexity and importance of these organisms by highlighting the most recent literature and reporting to a wider public the progress made in this field of research.


Taylor & Francis
Taylor & Francis Group
http://taylorandfrancis.com

1 General Overview

DEFINITION

The term *algae* has no formal taxonomic standing; nevertheless, it is routinely used to indicate a polyphyletic (i.e. including organisms that do not share a common origin but follow multiple and independent evolutionary lines), non-cohesive, and artificial assemblage of O_2-evolving, photosynthetic organisms (with several exceptions of colorless members undoubtedly related to pigmented forms). According to this definition, plants could be considered an algal division. Algae and plants produce the same storage compounds and use similar defense strategies against predators and parasites, and a strong morphological similarity exists between some algae and plants. Then, how can we distinguish algae from plants? The answer is quite easy since the similarities we have listed between algae and plants are much fewer than their differences. Plants show a very high degree of differentiation, with roots, leaves, stems, and a xylem/phloem vascular network; their reproductive organs are surrounded by a jacket of sterile cells; and they have a multicellular diploid embryo stage which remains developmentally and nutritionally dependent on the parental gametophyte for a significant period (and this feature is the source of the name embryophytes given to plants) and tissue-generating parenchymatous meristems at the shoot and root apices producing tissues that differentiate into a wide variety of shapes. Moreover, all plants have a digenetic life cycle with an alternation between a haploid gametophyte and a diploid sporophyte. Algae do not have any of these features: they do not have roots, stems, or leaves, nor well-defined vascular tissues; even though many seaweed are plant-like in appearance, and some of them show specialization and differentiation of their vegetative cells, they do not form embryos, their reproductive structures consist of cells that are all potentially fertile and lack sterile cells covering or protecting them, parenchymatous development is present only in some groups, and they have both monogenetic and digenetic life cycles. Moreover, algae occur in such dissimilar forms as microscopic single cell, macroscopic multicellular loose or filmy conglomerations, matted or branched colonies, or more complex leafy or blade forms, which contrast strongly with the uniformity in vascular plants. Evolution may have worked in two ways, one for shaping similarities and one for shaping differences. The same environmental pressure led to the parallel, independent evolution of similar traits in both plants and algae, while the transition from relatively stable aquatic environment to a gaseous medium exposed plants to new physical conditions that resulted in key physiological and structural changes necessary to invade upland habitats and fully exploit them. The bottom line is that plants are a separate group with no overlap with the algal assemblage.

The profound diversity of size, ranging from picoplankton only 0.2–2.0 μm in diameter to giant kelps with fronds up to 60 m in length; ecology and colonized habitats; cellular structure; levels of organization and morphology; pigments for photosynthesis; reserve and structural polysaccharides; and type of life history reflect the varied evolutionary origins of this heterogeneous assemblage of organisms, including both prokaryote and eukaryote species. The term "algae" refers to macroalgae and a highly diversified group of microorganisms known as microalgae. Estimates of the number of algae vary from 30,000 to over 1 million species, but most of the reliable estimates refer to the numbers given in the AlgaeBase site (htpps://www.algaebase.org), which currently documents 52,000 species described, including fossil algae (about 5,000 species of Cyanophyta and about 47,000 species of eukaryotic algae). This number includes about 16,500 species of diatoms, about 7300 species of red algae, about 2000 species of brown algae, about 6,700 species of green algae (Chlorophyta, mostly marine), about 5,000 species of charophytes (Charophyta,

DOI: 10.1201/9781003187707-1

mostly freshwater), about 3,500 species of dinoflagellates, about 1,500 species of euglenophytes, and a lot of smaller groups.

CLASSIFICATION

Over the past 30 years, molecular phylogenetic studies have led to extensive modification of traditional classification schemes for algae, and nowadays no easily definable classification system acceptable to all exists for this group of organisms, since taxonomy is under constant and rapid revision at all levels following the continuous new genetic and ultrastructural evidence. Keeping in mind that the polyphyletic nature of the algal group is somewhat inconsistent with traditional taxonomic groupings, though they are still useful to define the general character and level of organization, and remaining aware of the fact that taxonomic opinion may change as information accumulates, we will adopt a tentative scheme of classification mainly based on algaebase.org taxonomy (last access 3/24/2022).

As more and more analysis is done, more and more species are discovered and old assignments reassessed. Moreover, the recognition of the importance of horizontal (lateral) gene transfer (HGT a.k.a. LGT) and endosymbiotic gene transfer (EGT) in the transmission of genetic material between two organisms without sexual or asexual reproduction challenges a rigid concept of the tree of life and makes it very difficult for taxonomists to keep pace with the continuous progress in algae systematics. Therefore, the main purpose of the classification here reported is to categorize the diversity of the algae in a very practical manner, providing names that are useful for teaching students and searching the literature, without any claim of completeness.

Prokaryotic members of this assemblage are grouped into the kingdom Eubacteria, phylum Cyanobacteria, with the single class of Cyanophyceae. Members of the proposed division Prochlorophyta, considered artificial, are currently included in this class. Eukaryotic members are grouped into the three kingdoms of Plantae, with five phyla; Chromista, with four phyla; and Protozoa, with two phyla. Table 1.1 shows the different classes in the 12 phyla. Figure 1.1 shows examples of representatives of each class.

SUMMARIES OF THE 12 ALGAL PHYLA

Historically, the major groups of algae were classified on the basis of pigmentation; chemical nature of photosynthetic storage product; photosynthetic membranes (thylakoids) organization and other features of the chloroplasts; chemistry and structure of cell walls; number, arrangement, and ultrastructure of flagella (if any); occurrence of any other special features; and sexual cycles. Recently revised classifications incorporate advances resulting from the widespread use of phylogenomic-scale phylogenetic analyses and massively increased taxon sampling in rRNA-phylogenies. All these studies tend to assess the internal genetic coherence of the major phyla such as Cyanobacteria, Glaucophyta, Rhodophyta, Prasinodermatophyta, Chlorophyta, Charophyta, Haptophyta, Cryptophyta, Ochrophyta, Miozoa, Cercozoa, and Euglenozoa, confirming that these divisions are non-artificial. Table 1.2 attempts to summarize the main characteristics of the different algal groups.

Cyanobacteria

All blue-green algae (Figures 1.1a and 1.2) and prochlorophytes (Figure 1.3) are non-motile Gram-negative eubacteria. In structural diversity, blue-green algae range from unicells to branched and unbranched filaments to unspecialized colonial aggregations and are possibly the most widely distributed of any group of algae. They are planktonic, occasionally forming blooms in eutrophic lakes and an important component of the picoplankton in both marine and freshwater systems: benthic, as dense mats on soil or in mud flats and hot springs, as the “black zone” high on the seashore, and as

TABLE 1.1
Classification Scheme of the Different Algal Groups

	Kingdom	Subkingdom	Infrakingdom	Phylum	Class	Representative	Image
Prokaryota	Eubacteria	Negibacteria		Cyanobacteria	Cyanophyceae	*Arthrospira*	*1a*
Eukaryota	Plantae	Glaucoplantae		Glaucophyta	Glaucophyceae	*Cyanophora*	*1b*
		Biliphyta	Rhodaria	Rhodophyta	Cyanidiophyceae	*Cyanodioschyzon*	*1c*
					Bangiophyceae	*Porphyra*	*1d*
					Florideophyceae	*Phyllophora*	*1e*
					Compsopogonophyceae	*Erythrocladia*	*1f*
					Porphyridiophyceae	*Porphyridium*	*1g*
					Rhodellophyceae	*Glaucosphaera*	*1h*
					Stylonematophyceae	*Stylonema/Rhodosorus*	*1i/1l*
		Viridiplantae		Prasinodermatophyta	Palmophyllophyceae	*Palmophyllum*	*1m*
					Prasinodermatophyceae	*Prasinoderma*	
			Chlorophyta	Chlorophyta	Chlorodendrophyceae	*Tetraselmis*	*1n*
					Chlorophyceae	*Kirchneriella*	*1o*
					Mamiellophyceae	*Crustomastix*	*1p*
					Nephroselmidophyceae	*Nephroselmis*	*1q*
					Pedinophyceae	*Pedinomonas*	*1r*
					Pyramimonadophyceae	*Pyramimonas*	*1s*
					Trebouxiophyceae	*Chlorella*	*1t*
					Ulvophyceae	*Codium/Halimeda*	*1u/1v*
			Streptophyta	Charophyta	Mesostigmatophyceae	*Mesostigma*	*1z*
					Chlorokybophyceae	*Chlorokybus*	*1aa*
					Klebsormidiophyceae	*Klebsormidium*	*1ab*
					Charophyceae	*Nitella*	*1ac*
					Coleochaetophyceae	*Coleochaete*	*1ad*
					Zygnematophyceae	*Closterium*	*1ae*
	Chromista	Hacrobia		Haptophyta	Coccolithophyceae	*Coronocyclus*	*1af*
					Haptophyta incertae sedis	*Umbellosphaera*	*1ag*
					Pavlovophyceae	*Pavlova*	*1ah*
				Cryptophyta	Cryptophyceae	*Rhodomonas*	*1ai*

(*Continued*)

TABLE 1.1 ***(Continued)***
Classification Scheme of the Different Algal Groups

	Kingdom	Subkingdom	Infrakingdom	Phylum	Class	Representative	Image
		Harosa	Heterokonta	Ochrophyta	Bacillariophyceae	*Melosira*	*1al*
					Bolidophyceae	*Tetraparma*	*1am*
					Chrysophyceae	*Ochromonas/Gyraudiopsis*	*1an/1ao*
						Synura	*1ap*
					Dictyochophyceae	*Distephanus*	*1aq*
					Eustigmatophyceae	*Nannochloropsis*	*1ar*
					Pelagophyceae	*Chrysophaeum*	*1as*
					Phaeophyceae	*Undaria*	*1at*
					Phaeothamniophyceae	*Phaeothamnion/Aurearena*	*1au/1av*
					Picophagophyceae	*Picophagus*	*1az*
					Pinguiophyceae	*Pinguiococcus*	*1ba*
					Raphidophyceae	*Heterosigma*	*1bb*
					Schizocladiophyceae	*Schizocladia*	*1bc*
					Synchromophyceae	*Synchroma*	*1bd*
					Xanthophyceae	*Vaucheria*	*1be*
			Halvaria	Miozoa	Dinophyceae	*Prorocentrum/Pyrocystis*	*1bf/1bg*
	Protozoa			Cercozoa	Chlorarachniophyceae	*Gymnochlora*	*1bh*
		Eozoa	Euglenozoa	Euglenozoa	Euglenophyceae	*Euglena*	*1bi*
						Phacus	*1bl*
						Trachelomonas	*1bm*
						Peranema	*1bn*

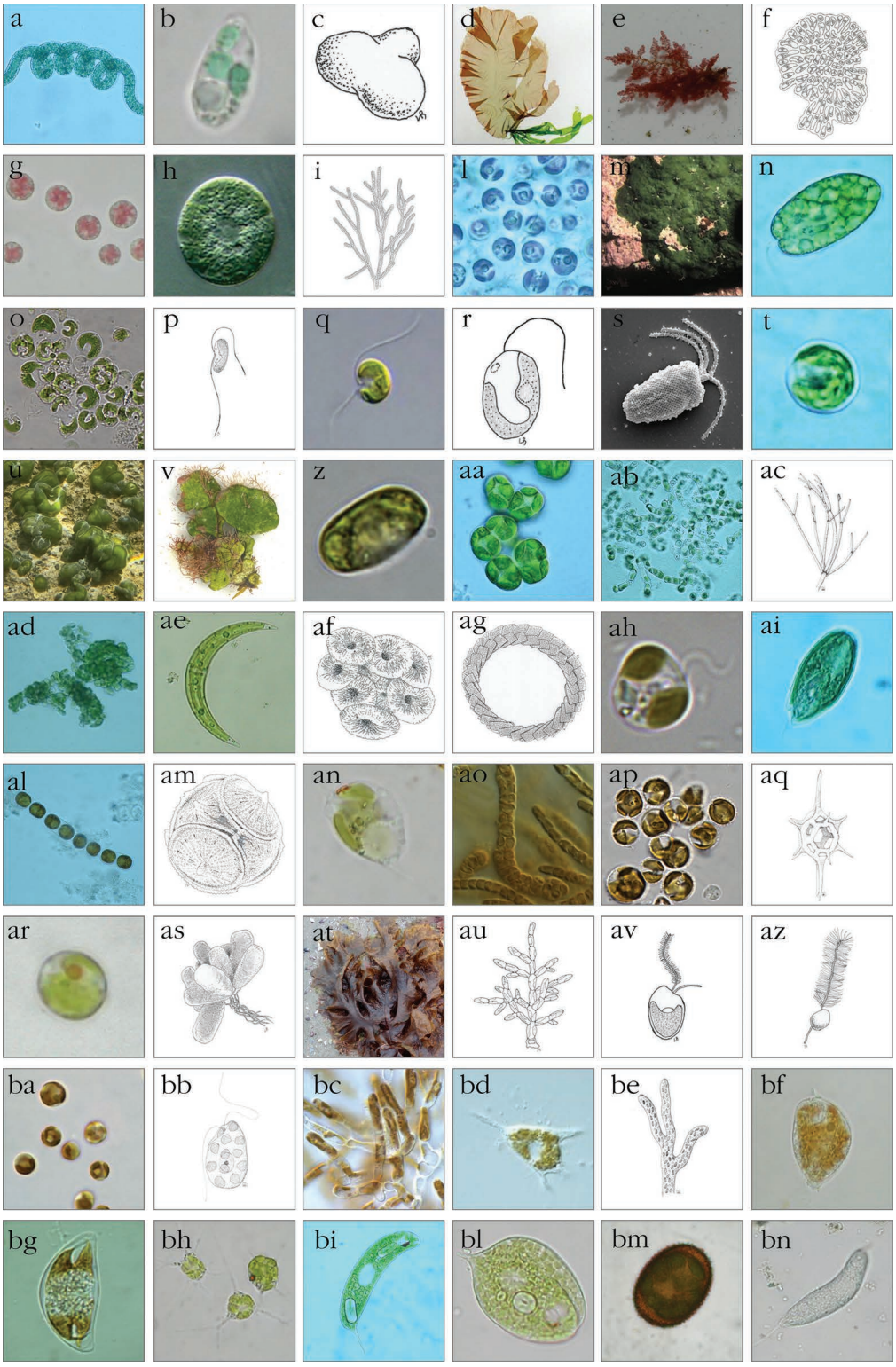


FIGURE 1.1 Examples of representatives of the different algal classes.

TABLE 1.2
The Main Pigments, Storage Products and Cell Coverings of the Algal Divisions

Phylum	Pigments (cf. Chapter 4)				Storage products
	Chlorophylls	**Phycobilins**	**Main carotenoids**	**Main xanthophylls**	
Cyanobacteria	*a, b*	C-phycoerythrin C-phycocyanin allophycocyanin	β-carotene	myxoxanthin zeaxanthin	cyanophycin (arginine and asparagine polymer) cyanophycean starch (α -1,4-glucan)
Glaucophyta	*a*	phycoerythrocyanin C-phycocyanin allophycocyanin	β-carotene	zeaxanthin	starch (α -1,4-glucan)
Rhodophyta	*a*	B-phycoerythrin R-phycoerythrin R-phycocyanin allophycocyanin	α-, and β-carotene	lutein	floridean starch (α -1,4-glucan)
Prasinodermatophyta	*a, b*	absent	α-, β- and γ-carotene	lutein prasinoxanthin	starch (α -1,4-glucan)
Chlorophyta	*a, b*	absent	α-, β- and γ-carotene	lutein prasinoxanthin	starch (α -1,4-glucan)
Charophyta	*a, b*	absent	α-, β- and γ-carotene	lutein prasinoxanthin	starch (α -1,4-glucan)
Haptophyta	*a*, c_1, c_2	absent	α- and β-carotene	fucoxanthin	chrysolaminaran (β -1,3-glucan)
Cryptophyta	*a*, c_2	B-phycoerythrin (545) R-phycocyanin allophycocyanin	α-, β-, and ε-carotene	alloxanthin	starch (α -1,4-glucan)
Ochrophyta	*a*, c_1, c_2, c_3	absent	α-, β- and ε-carotene	fucoxanthin violaxanthin neoxanthin diadinoxanthin	chrysolaminaran (β -1,3-glucan)
Miozoa (Dinophyceae)	*a*, c_1, c_2	absent	β-carotene	peridinin fucoxanthin diadinoxanthin dinoxanthin gyroxanthin	starch (α -1,4-glucan)
Cercozoa (Chlorarachniophyceae)	*a, b*	absent	absent	lutein neoxanthin violaxanthin	paramylon (β -1,3-glucan)
Euglenozoa (Euglenophyceae)	*a, b*	absent	β- and γ-carotene echinenone	diadinoxanthin	paramylon (β-1,3-glucan)

relatively inconspicuous components in most soils, and symbiotic in diatoms, ferns, lichens, cycads, sponges, and other systems. Numerically these organisms dominate the ocean ecosystems. There are approximately 10^{24} cyanobacterial cells in the oceans. To put that in perspective, the number of cyanobacterial cells in the oceans is two orders of magnitude more than all the stars in the sky. Pigmentation of cyanobacteria includes both chlorophyll *a*, blue and red phycobilins (phycoerythrin, phycocyanin, allophycocyanin), and carotenoids. These accessory pigments lie in the phycobilisomes, located in rows on the outer surface of the thylakoids. Their thylakoids, which lie free in the cytoplasm, are not arranged in stacks but singled and equidistant, in contrast to prochlorophytes and most other algae but similarly to Rhodophyta and Glaucophyta.

The reserve polysaccharide is cyanophycean starch, stored in tiny granules lying between the thylakoids. In addition, these cells often contain cyanophycin granules, that is, a polymer of arginine and asparagines. Some marine species also contain gas vesicles used for buoyancy regulation. In some filamentous cyanobacteria, heterocysts and akinetes are formed. Heterocysts are vegetative cells that have been drastically altered (loss of photosystem II; development of a thick, glycolipid cell wall) to provide the necessary anoxygenic environment for the process of nitrogen fixation (Figure 1.4). Some cyanobacteria produce potent hepato- and neurotoxins.

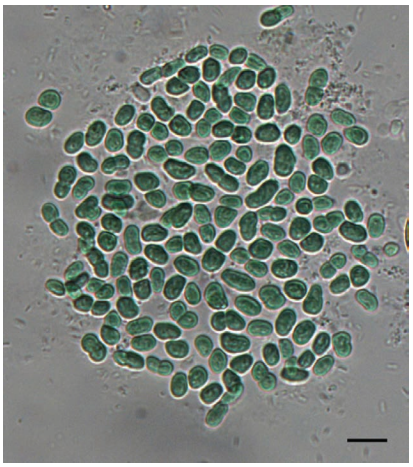


FIGURE 1.2 Cells of *Cyanothece* sp. Bar: 10 μm.



FIGURE 1.3 Cells of *Prochloron* sp. Bar: 10 μm.

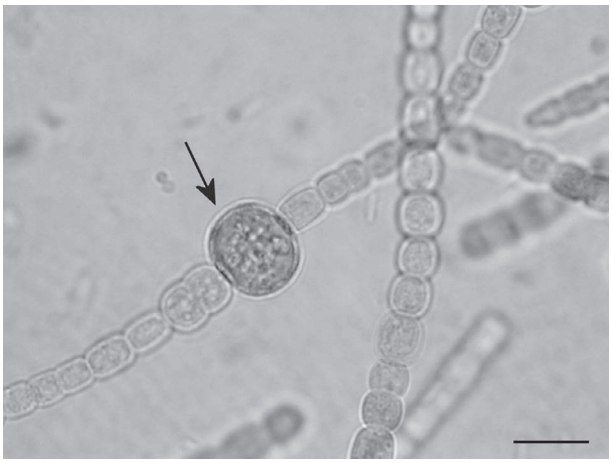


FIGURE 1.4 Heterocyst (arrow) of *Trichormus azollae*. Bar: 10 μm.

Prochlorophytes can be unicellular or filamentous, and, depending on the filamentous species, they can be either branched or unbranched. They exist as free-living components of pelagic nanoplankton and obligate symbionts within marine didemnid ascidians and holothurians and are mainly limited to living in tropical and subtropical marine environments, with optimal growth temperature at about 24°C. Prochlorophytes possess chlorophyll *a* and *b*, as euglenoids and land plants, but lack phycobilins, and this is the most significant difference between them and cyanobacteria, which extends the light-harvesting capacity of these algae into the blue and orange/red regions of the visible light spectrum. Other pigments are β-carotene and several xanthophylls (zeaxanthin is the principal one). Their thylakoids, which lie free in the cytoplasm, are arranged in stacks. Prochlorophytes have a starch-like reserve polysaccharide. These prokaryotes contribute a large percentage of the total organic carbon in the global tropical oceans, making up to anywhere from 25% to 60% of the total chlorophyll *a* biomass in the tropical and subtropical oceans. They are also able to fix nitrogen, though not in heterocysts. Both blue-green algae and prochlorophytes contain polyhedral bodies (carboxysomes) containing RuBisCO (ribulose-1,5-bisphosphate carboxylase/oxygenase, the enzyme that converts inorganic carbon to reduced organic carbon in all oxygen-evolving photosynthetic organisms) and have similar cell walls characterized by a peptidoglycan layer. Blue-green algae and Prochlorophytes can be classified as obligate photoautotrophic organisms. Reproduction in both divisions is strictly asexual, by simple cell division, or fragmentation of either the colony or the filaments.

Glaucophyta

This phylum contains only a single class, the Glaucophyceae (Figures 1.1b and 1.5). These algae are basically unicellular flagellates with a dorsiventral construction; they bear two unequal flagella, which are inserted in a shallow depression just below the apex of the cell. Glaucophyceae are rare freshwater inhabitants, sometimes also collected from soil samples. They possess only chlorophyll *a*; accessory pigments such as phycoerythrocyanin, phycocyanin, and allophycocyanin are organized in phycobilisomes. Carotenoids such as β-carotenes and xanthophylls zeaxanthin are also present in their chloroplast, which lies in a special vacuole and presents a thin peptidoglycan wall located between the two plastid outer membranes. Thylakoids are not

stacked. The chloroplast DNA is concentrated in the center of the chloroplast, where typically carboxysomes are present, which contain the RuBisCO enzyme. Starch is the reserve polysaccharide, which is accumulated in granular form inside the cytoplasm but outside the chloroplast. Glaucophyceae live photoautotrophically with the aid of blue-green plastids often referred to as cyanelles. Cyanelles are presumed to be a relic of the plastid's endosymbiotic origin, as glaucophytes are thought to have diverged before red algae and green plants split from each other. Sexual reproduction is unknown in this division.

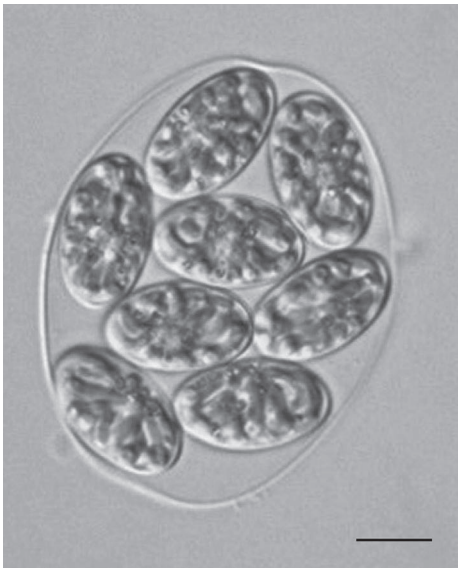


FIGURE 1.5 A group of eight autospores of *Glaucocystis nostochinearum* still retained within the parent cell wall. Bar: 10 μm.

Rhodophyta

This phylum contains seven classes, consisting mostly of seaweed but also including genera of free-living unicellular microalgae. They inhabit marine ecosystems but are also present in freshwater and terrestrial environments. The lack of any flagellate stages and centrioles and the presence of accessory phycobiliproteins (allophycocyanin, phycocyanin, and phycoerythrin) organized in phycobilisomes (shared with Cyanobacteria, Cryptophyta, and Glaucophyta) are unique features of these algae; chlorophyll *a* is the only chlorophyll. Stellate or discoid chloroplasts are enclosed by a double unit membrane; thylakoids do not stack at all but lie equidistant and singly within the chloroplast. One thylakoid is present around the periphery of the chloroplast, running parallel to the chloroplast internal membrane. The chloroplastic DNA is organized in blebs scattered throughout the whole chloroplast. The most important storage product is floridean starch, an α-1,4-glucan polysaccharide, which is deposited in the cytoplasm. Grains of this starch are located only in the cytoplasm, unlike the starch grains produced in the Chlorophyta, which lie inside the chloroplasts. Most rhodophytes live photoautotrophically. In the great majority of red algae, cytokinesis is incomplete. In most red algae, particularly species belonging to the Florideophyceae, daughter cells are separated by the pit connection, a proteinaceous structure that fills the junction between cells and successively becomes a plug. At least seven types of plug can be recognized on the basis of their ultrastructural

features, which give valuable taxonomic information about the different red algae groups. Early-diverging rhodophytes have no specialized meristematic region, and the growth is diffuse, since cell division may occur anywhere in the body. On the other hand, filamentous rhodophytes undergo apical growth via division of an apical cell located at the end of a filament. Species in which sexual reproduction is known generally have an isomorphic or heteromorphic diplohaplontic life cycle; a haplontic life cycle is considered an exception. The widespread occurrence of life cycles with two or three multicellular phases may be due to the absence of centrioles and flagella in the vegetative cells, spores, and gametes.

The earliest-diverging class, Cyanidiophyceae, includes extremophile unicellular algae, spherical or elliptical in shape, growing in volcanic and thermal areas under extremely low pH (0.05–5) and relatively high temperature (35°C–56°C). Unlike most eukaryotes, they are also capable of tolerating a large array of toxic chemical compounds such as sulfuric acid, arsenic, and other heavy metals. They reproduce by binary fission (*Cyanidioschyzon*, Figure 1.1c) or by formation of endospores (*Cyanidium*, *Galdieria*) and can be facultative heterotrophs or obligate photoautotrophs. These algae lack pyrenoids.

The class Bangiophyceae includes all multicellular genera in which the gametophyte has chloroplasts lacking a peripheral encircling thylakoid, and the Golgi is associated with both the endoplasmic reticulum (ER) and mitochondrion. They are found in marine and freshwater environments. The thallus construction is relatively simple: filamentous, as in *Bangia*, or foliose (blade-like), as in *Porphyra*. Many economically important genera found in intertidal and subtidal habitats, such as *Porphyra purpurea* and *P. umbilicalis*, belong to this class; they are harvested for human food across the North Atlantic and are under development as aquaculture crops for human and animal foods. *Porphyra* species (Figure 1.1d) are important reference red algae because of their multicellularity, high stress tolerance (e.g. to heat, freezing, high light, osmotic stress, and desiccation), ancient fossil record of the Bangiales, and capacity to synthesize an array of storage carbohydrates and light protection compounds. The life history of Bangiales such as *Porphyra* spp. involves an alternation between the economically important foliose blade (haploid gametophyte) and the microscopic, filamentous, diploid conchocelis phase (Chapter 6). The systematics of this class has been revised on the basis of the nuclear SSU rRNA gene and the plastid rbcL gene, assigning to the genus *Pyropia* species previously identified as *Porphyra* species.

The Florideophyceae (Figures 1.1e and 1.6) include all multicellular genera, both marine and freshwater, in which the gametophytes have chloroplasts with a peripheral encircling thylakoid, and the Golgi is associated with both ER and mitochondrion. The class contains species as seemingly different as the coralline algae, characterized for the deposition of $CaCO_3$ as calcite in the cell wall; *Botryocladia*, known as sea-grapes; and parasitic taxa. Coralline algae are divided in two morphological groups: geniculate, which possess uncalcified body regions conferring high flexibility and branching to the algae, such as *Corallina*, and non-geniculate, which lack uncalcified regions and are often crust-formers adhering to a substrate, such as *Lithothamnion*. Species belonging to the *Botryocladia* genus resemble a cluster of deep red grapes; the single thallus is divergently branched and bears numerous elongate, pyriform, sacchate branches. These hollow and inflated branches are filled with a colorless, acidic, polysaccharide, and protein mucilage, which makes them buoyant and better able to compete for light. As to parasite members, they are highly host specific such as *Gracilariophila oryzoides*, which is found only on the lower thallus portion of *Gracilariopsis andersonii*. Markers of red algal parasitism include the presence of diminished or absent pigmentation, reduced morphologies, and host-parasite cell connections. Parasitism has independently evolved over 100 times in eight different orders, and it develops only on other Florideophyceaen species. Parasites form cellular connections with their host by creating secondary pit connections between adjacent cells, finding a way to get into the host cell. Florideophyceae show a triphasic reproduction cycle: an isomorphic gametophyte and sporophyte generations are separated by the carposporophyte, a very different sporophyte that emerges from the development of the zygote. In general, the carposporophyte is a set of small filaments that terminate in diploid spores, carpospores. These spores disperse and germinate to form the sporophyte. This is generally pseudoparenchymatous and identical to the gametophyte.



FIGURE 1.6 Frond of *Halymenia floresii*. Bar: 10 cm.

The class Compsopogonophyceae includes microscopic filamentous algae (e.g. *Erythrocladia,* Figure 1.1f) and macroscopic multicellular species (e.g. *Compsopogon*). They live in coastal seawater or freshwater. They possess two distinctive ultrastructural characters in combination: the association of Golgi bodies with ER instead of mitochondria as in almost all red algae and the presence of a peripheral encircling thylakoid in the chloroplast. The color of chloroplasts is variable from greenish blue to red. Asexual reproduction occurs by monospores generated by the oblique division of vegetative cells. Sexual reproduction and alternation of generations are reported in the Erythropeltidales.

The three classes of Porphyridiophyceae (Figure 1.1g), Rhodellophyceae (Figure 1.1h), and Stylonematophyceae (Figures 1.1i and 1.1l), which together with the Compsopogonophyceae diverged relatively early, include ten recognized genera of unicellular red algae. In the Porphyridiophyceae, the Golgi bodies are invariably associated with ER and a mitochondrion (*Porphyridium*), while in the Rhodellophyceae (*Glaucosphaera*), the Golgi association can be either with ER or the functionally equivalent outer membrane of the nuclear envelope. The class Stylonematophyceae also includes pseudofilamentous or filamentous red algae, in which the width of the thallus is often only one cell across (*Stylonema*). In the first two classes, reproduction occurs by cell division, while in the Stylonematophyceae, reproduction occurs by both cell division and monospores.

Prasinodermatophyta and Chlorophyta

Members of the Prasinodermatophyta are restricted to dimly lit habitats and deep water (Figure 1.1m). They possess a unique type of multicellularity, forming well-defined macroscopic bodies composed of small, spherical, non-flagellate cells embedded in a firm gelatinous matrix (*Palmophyllum*).

Members of the Chlorophyta are common inhabitants of marine, freshwater, and terrestrial environments; within the phylum, a great range of somatic differentiation occurs, ranging from flagellates to complex multicellular thalli differentiated into macroscopic organs. The different level of

thallus organization (unicellular, colonial, filamentous, siphonous, and parenchimatous) has traditionally served as the basis of classification of this division. Chlorophytes show a wide diversity in the number and arrangement of flagella associated with individual cells (one or up to eight, in the apical or sub-apical region). All members of the chlorophytes have motile stages with two or four anterior isokont flagella (i.e. flagella are of equal length and equivalent function), although algae with two flagella of slightly unequal lengths have been described. Flagella are characterized by a "stellate structure"–type flagellar transition region. Within the cell, the flagellar basal bodies are associated with four microtubular rootlets, cruciately arranged, which alternate between two and higher numbers of microtubules, according to the formula X-2-X-2. When viewed from above the cell, the basal bodies and rootlets can have a perfect cruciate pattern, with the basal bodies directly opposed (DO), or they can be offset in a clockwise (CW) or counterclockwise (CCW) position.

According to the most recent classifications, Chlorophyta comprises the early-diverging Pyramimonadophyceae, which gave rise to the core chlorophytes (Chlorodendrophyceae, with the three major classes of Ulvophyceae, Trebouxiophyceae, and Chlorophyceae); the Pedinophyceae, sister class to the core chlorophytes; the Mamiellophyceae; and the Nephroselmidophyceae.

Chlorodendrophyceae possess a pair of flagella inserted in a pit; basal body orientation is CCW (Figure 1.1n). These algae are covered by organic scales, the outer layer of which is fused to form a theca. The class Chlorophyceae comprises mainly swimming cells with one or two pairs of flagella without mastigonemes (Figure 1.1o). Cells can be naked or covered by a more or less calcified cell wall (Figure 1.7). Either DO or CW arrangements are present in the members of this class. Mamiellophyceae are typically solitary cells with one or two chloroplasts, mono- or biflagellate, with isokont or anisokont flagella (Figure 1.1p). They may be scales covered or naked. Nephroselmidophyceae (Figure 1.1q) are laterally compressed, scales-covered cells, with laterally inserted anisokont flagella, and possess a single cup-shaped chloroplast. Pedinophyceae are unicellular, monoflagellate asymmetrical algae with CCW basal body orientation (Figure 1.1r). Rigid or thin hair-like appendages are present on the flagellum. Pyramimonadophyceae are a heterogeneous assemblage of unicellular motile algae either naked or covered on their cell body and flagella by non-mineralized organic scales (Figures 1.1s and 1.8). They are predominantly marine planktonic but also include several freshwater representatives. The class Trebouxiophyceae (Figures 1.1t and 1.9) encompasses motile and non-motile unicells, colonies, and multicellular filaments or small microscopic blades from freshwater or terrestrial habitats, with some species also present in brackish or marine water. Several species are symbiotic of fungi to form lichens or endosymbiotic of freshwater and marine protists, invertebrates, and plants. Swimming cells can have one or two pairs of flagella without mastigonemes. All the algae of the class possess a CCW basal body orientation.

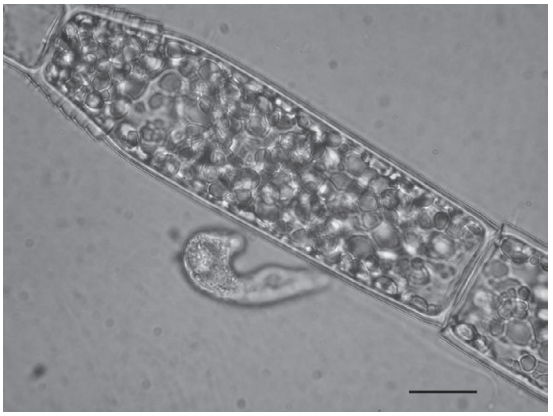


FIGURE 1.7 Filament of *Oedogonium* sp., with a *Peranema* sp. cell. Bar: 20 μm.

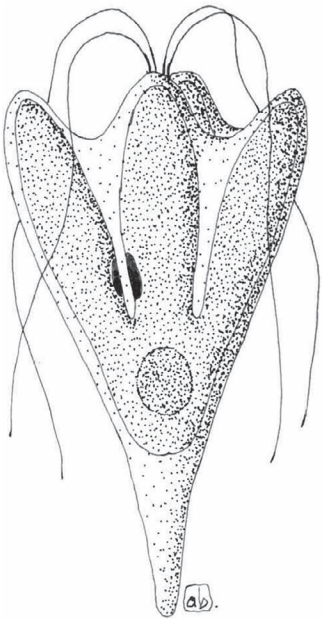


FIGURE 1.8 Unicell of *Pyramimonas longicauda*.

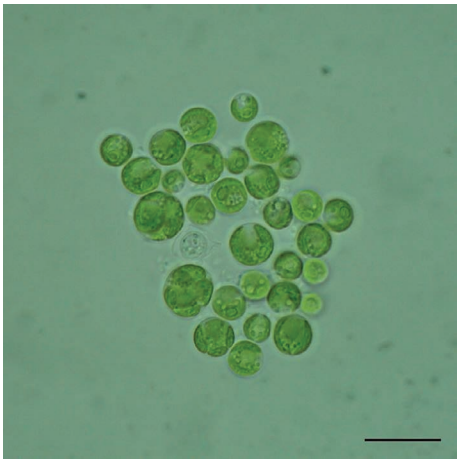


FIGURE 1.9 Group of *Chlorella* sp. cells. Bar 15 μm.

Ulvophyceae morphologies range from microscopic unicell to macroscopic multicellular plants and giant-celled organisms (Figures 1.1u, 1.10, and 1.11). Four main cytomorphological types can be distinguished: non-motile uninucleate unicells; multicellular filaments or blades composed of multinucleate cells; multicellular bodies composed of multinucleate cells with nuclei organized in regularly spaced cytoplasmic domains; and siphonous thalli consisting of a single giant tubular cell containing thousands to millions of nuclei, such as *Acetabularia* (Figures 1.1v and 1.12). In some species, siphonous thalli are encrusted with calcium carbonate. The majority of Ulvophyceae are marine algae, but several members also occur in freshwater or damp subaerial habitats. All the algae of the class possess a CCW basal body orientation.

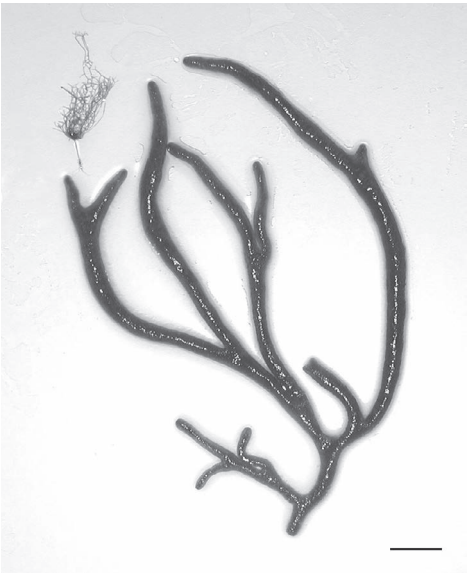


FIGURE 1.10 Thallus of *Codium* sp. Bar: 2 cm.

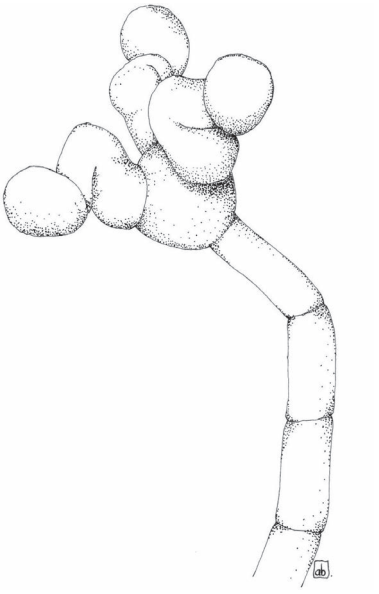


FIGURE 1.11 Thallus of *Trentepohlia arborum*.

Chlorophyta possess chlorophylls *a* and *b*, β- and γ-carotene, and several xanthophylls as accessory pigments. Chloroplasts are surrounded by a two-membrane envelope without any ER membrane. Within the chloroplasts, thylakoids are stacked to form grana. Pyrenoids, where present, are embedded within the chloroplast and often penetrated by thylakoids. The circular molecules of chloroplast DNA are concentrated in numerous small blobs (1–2 μm in diameter). The most important reserve polysaccharide is starch, which occurs as grain inside the chloroplasts; glucan or β-1,4-mannan can

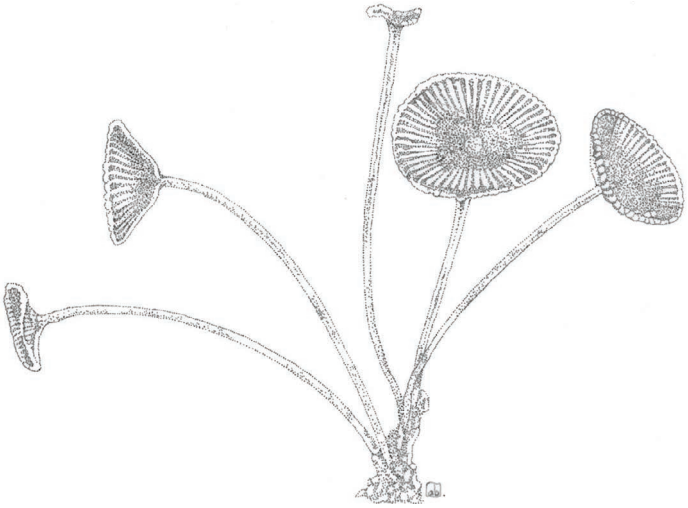


FIGURE 1.12 Portion of the thallus of *Acetabularia* sp.

be present in the cell wall of some Ulvophyceae. Eyespot, if present, is located inside the chloroplast and consists of a layer of carotenoid-containing lipid droplets between the chloroplast envelope and the outermost thylakoids.

Charophyta

Charophytes are the organisms most closely related to land plants. The six groups of the phylum have been recognized as distinct on the basis of ultrastructural, biochemical, and molecular data. Mesostigmatophyceae and Chlorokybophyceae form the earliest branching streptophytes; the only genus of Mesostigmatophyceae is *Mesostigma*, with two species, *M. viride* and *M. grande* (Figure 1.1z). These isogamous algae are freshwater, scaly, asymmetrical, and unicellular biflagellate and, unlike other charophytes, possess two multi-layered structures and an eyespot. Chlorokybophyceae (Figure 1.1aa) consist of a sole representative, *Chlorokybus atmophyticus*, occurring in moist terrestrial habitats where it forms colony-like sarcinoid packets of a few cells enveloped in a common mucilaginous matrix, which reproduce asexually by asymmetrical motile spores possessing a single multi-layered structure. Klebsormidiophyceae represent the common ancestor of the remaining streptophytes, in which multicellularity evolved in the form of unbranched filaments (Figures 1.1ab and 1.13). These freshwater or terrestrial algae, which can also form sarcinoid packets, reproduce by filament fragmentation and release of motile spores. Charophyceae are the most plant-like in appearance among the charophytes because of the independent evolution of macrophytic forms such as *Chara* (Figures 1.1ac and 1.14). Thalli consist of a central stalk of large, elongate, multinucleate cells and whorls of branches at nodes. All species are oogamous, with motile sperm produced in complex antheridia. Coleochaetophyceae (Figure 1.1ad) range in morphology from branched, filamentous algae to relatively complex discoid pseudo-parenchymatous thalli. They may be epiphytic, endophytic, or loosely attached to submerged vascular plants or other substrates. They are oogamous, with biflagellate zoospore and sperm. The Zygnematophyceae are the most species-rich clade of the Charophyta and the most morphologically diverse (Figure 1.1ae). Thalli include non-motile unicells, filaments, and small colonial forms (Figure 1.15). They possess an unusual mode of sexual reproduction by fusion of non-flagellate gametes. A very recent comprehensive genome-scale analysis of 160 nuclear genes

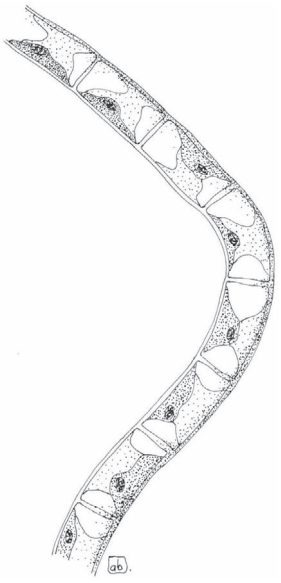


FIGURE 1.13 Filament of *Klebsormidium* sp.

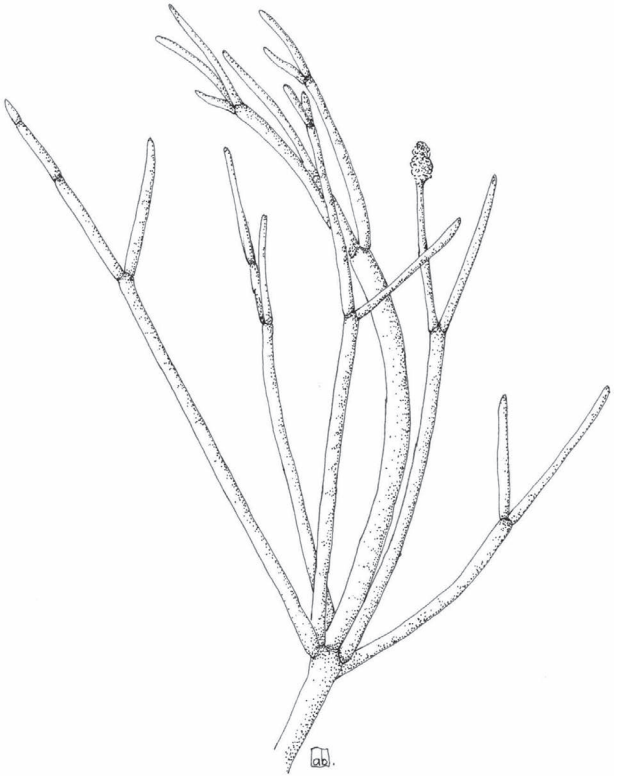


FIGURE 1.14 Thallus of *Nitella* sp.

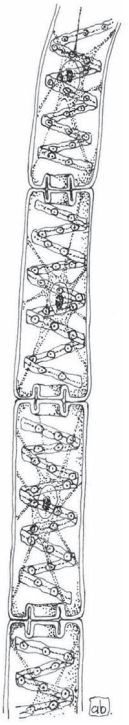


FIGURE 1.15 Simple filament of *Spirogyra* sp.

drawn from species distributed across all the charophyte groups supported the Zygnematophyceae as the closest living relative to land plants.

Haptophyta

This phylum contains only three classes, Coccolithophyceae, Haptophyta incertae sedis (Figures 1.1af, 1.1ag, and 1.16), and Pavlovophyceae (Figure 1.1ah). The great majority of these algae are unicellular, motile, palmelloid, or coccoid, but a few form colonies or short filaments. These algae are generally found in marine habitats, although there are a number of records from freshwater and terrestrial environments. Flagellate cells bear two naked flagella, inserted either laterally or apically, which may have different lengths. A structure apparently found only in algae of this division is the haptonema, typically a long, thin organelle reminiscent of a flagellum but with a different ultrastructure. The chloroplast contains only chlorophyll *a,* c_1, and c_2. The golden yellow-brown appearance of chloroplast is due to the accessory pigments such as fucoxanthin, β-carotene, and other xanthins. Each chloroplast is enclosed within a fold of ER, which is continuous with the nuclear envelope. Thylakoids are stacked in threes, and there are no girdle lamellae. Nucleic DNA is scattered throughout the chloroplast as numerous nucleoids. When present as in *Pavlova* (Figure 1.1ah), the eyespot consists of a row of spherical globules inside the chloroplast; no associated flagellar swelling is present. The most important storage product is the polysaccharide chrysolaminarin. The cell surface is typically covered with tiny cellulosic scales or calcified scales bearing spoke-like fibrils, radially arranged. Most haptophytes are photosynthetic, but heterotrophic nutrition is also possible. Phagotrophy is present in the forms that lack a cell covering. A heteromorphic diplohaplontic life cycle has been reported, in which a diploid planktonic flagellate stage alternates with a haploid benthic filamentous stage.



FIGURE 1.16 Unicell of *Helicosphaera carteri*.



FIGURE 1.17 Unicell of *Cryptomonas* sp. Bar: 6 µm.

Cryptophyta

The unicellular flagellates belonging to the division Cryptophyta are asymmetric cells dorsiventrally constructed (Figures 1.1ai and 1.17). They are mostly biflagellated, with two unequal, hairy flagella, sub-apically inserted, emerging from above a deep gullet located on the ventral side of the cell. The wall of this gullet is lined by numerous ejectosomes similar to trichocysts. Cryptophytes are typically free swimming in freshwater and marine habitats; palmelloid phases can also be formed, and some members are known to be zooxanthellae in host invertebrates or within certain marine ciliate.

These algae possess only chlorophyll *a* and c_2. Phycobilins are present in the thylakoid lumen rather than in phycobilisomes. The chloroplasts, one or two per cell, are bounded by four membranes. The outermost membrane is continuous with the nuclear envelope, and its surface is studded with ribosomes. Between the inner and outer membrane pairs is the periplastidial compartment, which contains the nucleomorph, the relict nucleus of the eukaryotic endosymbiont. Thylakoids are arranged in pairs, with no girdle lamellae. The pyrenoid projects out from the inner side of the chloroplast. The chloroplast DNA is condensed in small nucleoids scattered inside the chloroplast. The reserve polysaccharide accumulates in the periplastidial space as starch granules. Sometimes an eyespot formed by spherical globules is present inside the plastid, but it is not associated with the flagella. The cell is enclosed in a stiff, proteinaceous periplast made by polygonal plates. Most forms are photosynthetic, but there are some that are colorless and heterotrophic. The primary method of reproduction is simply by longitudinal cell division, but sexual reproduction has recently been documented.

Ochrophyta

One of the defining features of the members of this division is that when two flagella are present, they are different. Flagellate stages, when present, are therefore termed heterokont; that is, they possess a long mastigonemate flagellum, which is directed forward during swimming, and a short smooth one that points backwards along the cell. These algae are mostly marine, but they can be found also in freshwater and terrestrial habitats. They show a preponderance of carotenoids over chlorophylls that results in all groups having a golden rather than grass-green hue typical of other major algal divisions. The members of this division possess chlorophylls *a,* c_1, c_2, and c_3, with the exception of the Eustigmatophyceae, Aurearenales, and *Ochromonas* (Chrysophyceae), which have only chlorophyll *a*. The principal accessory pigments are β-carotene, fucoxanthin, and vaucheriaxanthin. The chloroplast is surrounded by four membranes: the normal plastidial double-membrane envelope, surrounded by a periplastidial membrane and by rough ER, which may be continuous with the outer membrane of the nuclear envelope. The periplastidial membrane is considered the remnants of the eukaryotic endosymbiont's (a red alga) plasmalemma. The chloroplast interior is occupied by thylakoids, which are grouped into stacks of three, called lamellae. One lamella usually runs along the whole periphery of the chloroplast, and it is termed the girdle lamella, absent only in the Eustigmatophyceae. The chloroplastic DNA is usually arranged in a ring-shaped nucleoid. The Ochrophyta species that reproduce sexually have haplontic (e.g. Chrysophyceae), diplontic (e.g. Bacillariophyceae), or diplohaplontic (e.g. Phaeophyceae) life cycles.

Bacillariophyceae or diatoms are a group of unicellular brown pigmented cells that are encased by a unique type of silica wall, composed of two overlapping frustules that fit together like a box and lid (Figures 1.1al, 1.18, and 1.19). Bolidophyceae are flagellated picoplanktonic algae, considered the closest, although separated, lineage to diatoms (Figure 1.1am). Chrysophyceae are predominantly single-celled flagellate individuals but also coccoid, filamentous, and parenchymatous (Figures 1.1an, 1.1ao, and 1.20). Most of these algae lack cell walls and have flagella inserted apically or slightly subapically. Cell coverings, when present, include organic scales, organic lorica, and cellulose cell walls. In this class there are also the Synurales, unicellular and colonial algae, important components of the species composition and biomass in freshwater environments worldwide (Figures 1.1ap and 1.21). A well-organized cell covering of siliceous, overlapping scales is characteristic of the class. These scales are morphologically unique for each species, and observations made with electron microscopy are usually required for species-level identification. They differ from closely related Chrysophyceae in the presence of only chlorophyll c_1, parallel basal body orientation, and the lack of eyespot. Dictyochophyceae are naked unicells that bear a single flagellum, anteriorly directed, with mastigonemes (Figures 1.1aq and 1.22). These algae possess several nucleoids scattered inside the chloroplast. The main reserve polysaccharide is chrysolaminarin, a



FIGURE 1.18 Marine diatom in chains. Bar: 10 µm.

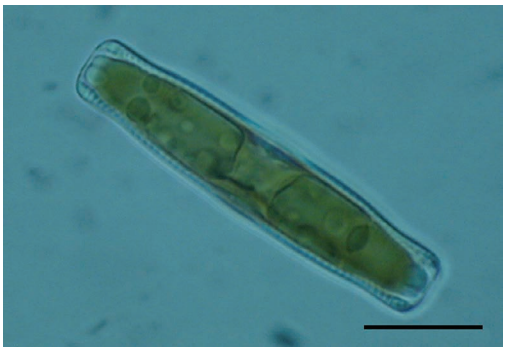


FIGURE 1.19 Freshwater diatom. Bar: 10 µm.



FIGURE 1.20 *Ochromonas* sp. motile unicell. Bar: 4 µm.

β-1,3-glucan, located inside the cytoplasm in special vacuoles. The eyespot consists of a layer of globules, enclosed within the chloroplast, and together with the photoreceptor, located in the smooth flagellum, forms the photoreceptive apparatus. The member of this phylum can grow photoautrophically but can also combine different nutritional strategies such as heterotrophy (phagotrophy). The class includes the silicoflagellates, a group characterized by formation of a silicified skeleton,

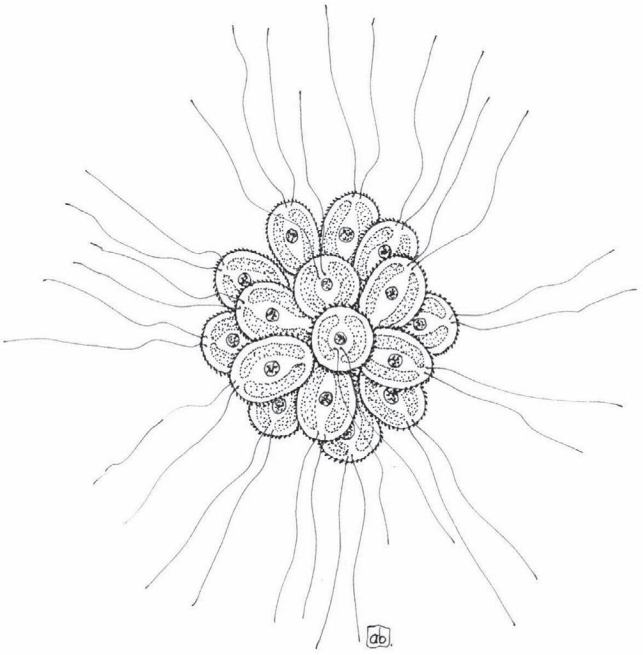


FIGURE 1.21 Free-swimming colony of *Synura uvella*.

and organically scaled members. All known species of Eustigmatophyceae are green coccoid unicells either single, in pairs, or in colonies, which exhibit little morphological diversity (Figures 1.1ar and 1.23). They are found in fresh and brackish water and seawater, as well as soil environments. Pelagophyceae include ciliated and coccoid members; cells can bear a single flagellum, anteriorly directed, or two flagella, the second posteriorly directed (Figure 1.1as). Phaeophyceae are multicellular, from branched filaments to massive and complex parenchymatous kelp (Figures 1.1at and 1.24). Flagellated stages possess two flagella, usually laterally inserted, one anteriorly and one posteriorly directed. Cells show an alginate and cellulose wall. Phaeothamniophyceae can be filamentous (Figure 1.1au), palmelloid, or coccoid; the vegetative cells are surrounded by a distinct cell wall of varying thickness. During cell division, an entirely new cell wall is formed inside the parent cell wall; that is, the new walls are formed by eleutheroschisis. Swimming stages have flagella inserted laterally. This class includes also non-motile algae such as *Aurearena* sp.; the cells are surrounded by a cell wall, with two unequal flagella lying inside the cell wall, or naked, motile, and biflagellate cells (Figure 1.1av). Picophagophyceae contain both photosynthetic and non-photosynthetic phagotrophs with filopodia or reticulopodia; the status of these algae as a distinct class has been questioned (Figure 1.1az). Pinguiophyceae are all single-celled microalgae from picoplankton size to over 40 μm (Figure 1.1ba). They deserve mention because of the unusually high percentage of polyunsaturated fatty acids, especially eicosapentaenoic acid (EPA, 20:5, n-3); this peculiarity is the basis for the choice of the Latin noun *pingue* (adj., fat) as the root for the class name. Raphidophyceae are all unicellular autotrophic cells (Figures 1.1bb and 1.25), relatively big in size (30–80 μm), with a globoid to ovoidal elongated shape. Sometimes they show a more sharpened point with a curved dorsal side and a flat ventral side. All the species lack a cell wall, and they have no covering outside the cell membrane; consequently the shape of the cell can vary with external conditions. They possess both trichocysts and mucocysts. Schizocladophyceae contain a single species, a marine filamentous alga isolated from the Tyrrhenian Sea; the cells possess a wall containing alginates but lacking cellulose (Figure 1.1bc). Synchromophyceae cell

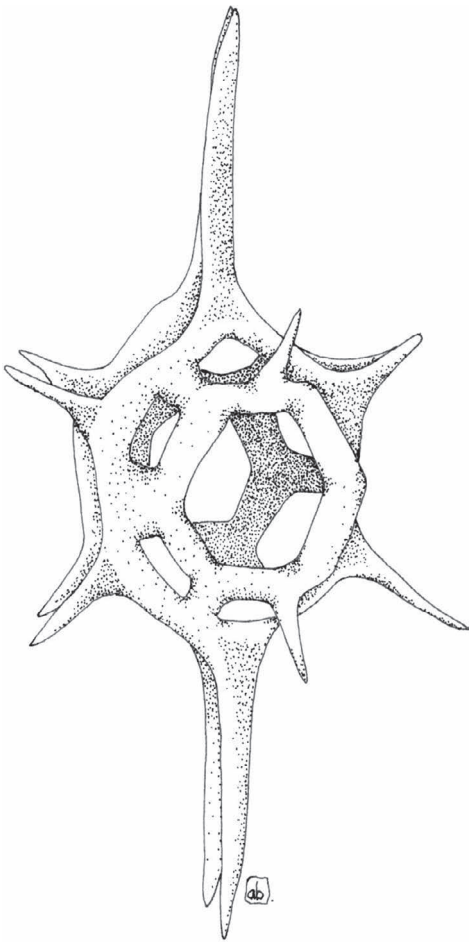


FIGURE 1.22 The silicoflagellate *Disthepanus speculum*.

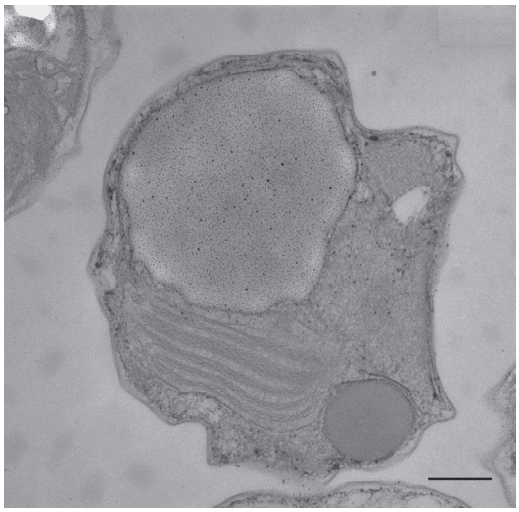


FIGURE 1.23 Transmission electron micrograph of *Nannochloropsis* sp. non-motile unicell. Bar: 0.5 µm.



FIGURE 1.24 Frond of *Bellotia eriophorum*. Bar: 5 cm.

types can be sessile, migrating, and floating amoebae, surrounded by a lorica, usually with one ostiole, through which reticulopodia protrude and fuse with neighboring cells to build up a meroplasmodium (Figure 1.1bd). The most striking and unique morphological feature of these algae is the aggregation of chloroplasts, each with two membranes, into groups of up to eight enclosed in a common periplastidial membrane and epiplastid rough ER. Xanthophyceae can be unicellular coccoids or flagellate, ameboid, or filamentous, but the most distinctive species are siphonous (Figures 1.1be and 1.26). Most Xanthophyceae are freshwater or soil algae, but a few are marine. They are both marine and freshwater.

Miozoa—Dinophyceae

Dinophyceae are typical unicellular flagellates but can also be non-flagellate, ameboid, coccoid, palmelloid, or filamentous (Figures 1.1bf, 1.1bg, 1.27, and 1.28). Dinoflagellates have two flagella with an independent beating pattern, one training, one girdling, which confer the characteristic rotatory swimming whirling motion. Flagella can be apically inserted (desmokont type) or emerging from a region close to the midpoint of the ventral side of the cell (dinokont type). Most dinoflagellates are characterized by cell-covering components that lie beneath the cell membrane. Around the cell there is a superficial layer of flat, polygonal vesicles, which can be empty or filled with cellulose plates. In dinokont-type dinoflagellates, these thecal plates generally form a bi-partite armor consisting of an upper, anterior half and a lower, posterior half, separated by a groove known as a cingulum where the transversal flagellum is located (Figure 1.28). A smaller groove, the sulcus, extends posteriorly from the cingulum and hosts the longitudinal flagellum. The two flagella emerge from a pore located at the intersection of the two grooves. Very often they are important components of the microplankton of freshwater and marine habitats. Though most are too large (2–2,000 μm) to be consumed by filter feeders, they are readily eaten by larger protozoa, rotifer, and planktivorous fishes. Some dinoflagellates are invertebrate parasites; others are endosymbionts (zooxanthellae) of tropical corals. Dinoflagellates possess chlorophylls *a,*

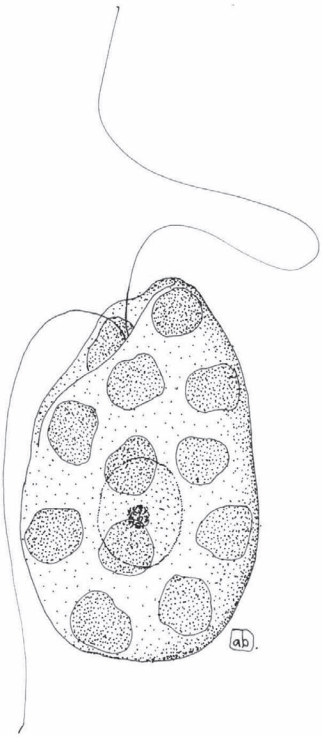


FIGURE 1.25 Unicell of *Heterosigma akashiwo*.

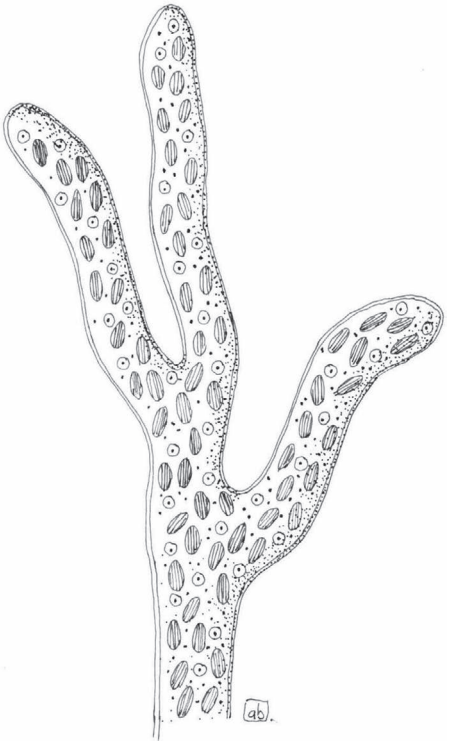


FIGURE 1.26 Siphonous thallus of *Vaucheria sessilis*.

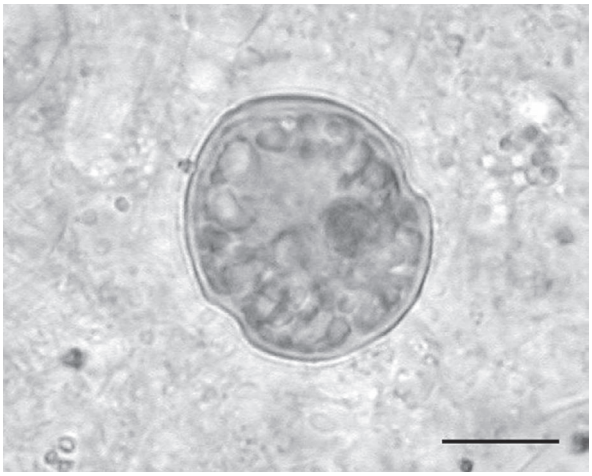


FIGURE 1.27 A marine dinoflagellate. Bar: 30 µm.

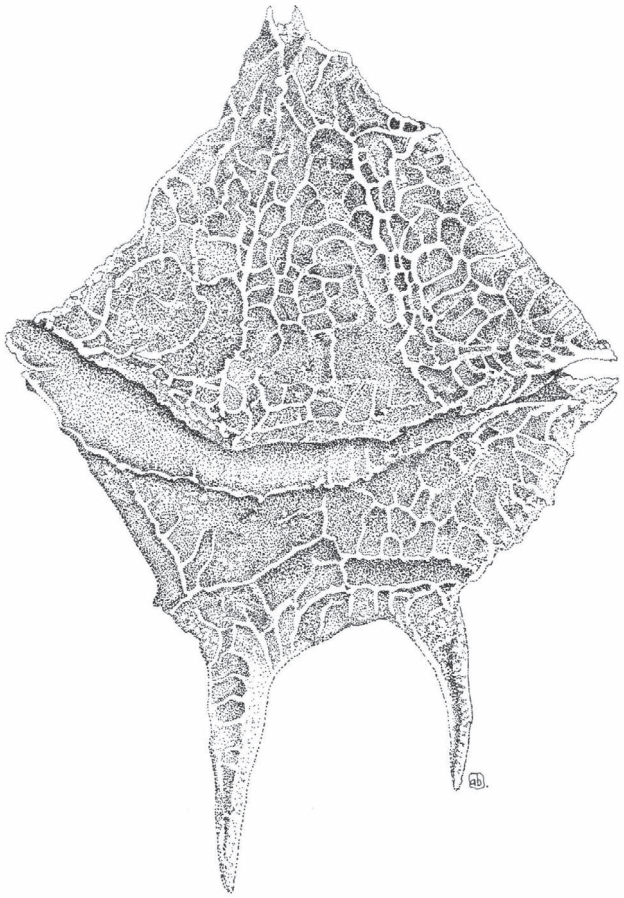


FIGURE 1.28 Dorsal view of *Gonyaulax* sp., a brackish water dinoflagellate.

c_1, and c_2; fucoxanthin; other carotenoids; and xanthophylls such as peridinin, gyroxanthin diester, dinoxanthin, diadinoxanthin, and fucoxanthin. The chloroplasts, where present, are surrounded by three membranes. Within the chloroplasts, the thylakoids are for the most part united in stacks of three. The chloroplast DNA is localized in small nodules scattered in the whole chloroplast, with typical pyrenoids. A really complex photoreceptive system is present in dinophytes such as *Warnowia polyphemus, W. pulchra*, or *Erythropsidinium agile* consisting of a "compound eye" composed of a lens and a retinoid. Most dinoflagellates are distinguished by a dinokaryon, a special eukaryotic nucleus involving fibrillar chromosomes that remain condensed during the mitotic cycles. The principal reserve polysaccharide is starch, located as grains in the cytoplasm, but oil droplets are present in some genera. At the surface of the cell there are trichocysts that discharge explosively when stimulated. Besides photoautotrophy, dinoflagellates exhibit an amazing diversity of nutritional types, since about half of the known species lack plastids and are therefore obligate heterotrophic. Some are notorious for nuisance blooms and toxin production, and many exhibit bioluminescence. Dinophyceae generally have a haplontic life history.

Cercozoa—Chlorarachniophyceae

Chlorarachniophyceae are naked, uninucleate cells that form a net-like plasmodium via filopodia (Figures 1.1bh, 1.29a and 1.29b). The basic life cycle of these algae comprises ameboid, coccoid, and flagellate cell stages. The ovoid zoospores bear a single flagellum that wraps around the cell during swimming. Chlorarachniophytes are marine algae. They possess chlorophyll *a* and *b*. Each chloroplast has a prominent projecting pyrenoid and is surrounded by four envelope membranes. Thylakoids are grouped in stacks of one to three. A nucleomorph is present between the second and third membranes of the chloroplast envelope. The origin of this organelle is different from the origin of the cryptophytes nucleomorph, since the chlorarachniophytes once came from a green algal endosymbiont. Paramylon (β-1, 3-glucan) is the storage carbohydrate. They can have phototrophic and phagotrophic engulfing bacteria, flagellates, and eukaryotic algae. Asexual reproduction is carried out by either normal mitotic cell division or zoospore formation. Sexual reproduction characterized by heterogamy has been reported for only two species.

Euglenozoa—Euglenophyceae

Euglenophyceae include mostly unicellular flagellates, although colonial species are common (Figures 1.1bi, 1.1bl, 1.1bm, 1.1bn, and 1.30). They are widely distributed, occurring in freshwater but also brackish and marine waters, most soils, and mud. They are especially abundant in highly heterotrophic environments. The flagella arise from the bottom of a cavity called a reservoir located in the anterior end of the cell. Cells can also ooze their way through mud or sand by a process known as metaboly, a series of flowing movements made possible by the presence of the pellicle, a proteinaceous wall that lies inside the cytoplasm. The pellicle can have a spiral construction and can be ornamented. The members of this division share their pigmentation with prochlorophytes, green algae and land plants, since they have chlorophyll *a* and *b*, β- and γ-carotenes, echinenone, and diadinoxanthins. However, plastids could be colorless or absent in some species. As in the Dinophyceae, the chloroplast envelope consists of three membranes. Within the chloroplasts, the thylakoids are usually in groups of three, without a girdle lamella; pyrenoids may be present. The chloroplast DNA occurs as a fine skein of tiny granules. The photoreceptive system consisting of an orange eyespot located free in the cytoplasm and the true photoreceptor located at the base of the flagellum can be considered unique among unicellular algae. The reserve polysaccharide is paramylon, β-1, 3-glucan stored in granules scattered inside the cytoplasm and not in the chloroplasts like the starch of the Chlorophyta. Though possessing chlorophylls, these algae are not photoautotrophic but rather

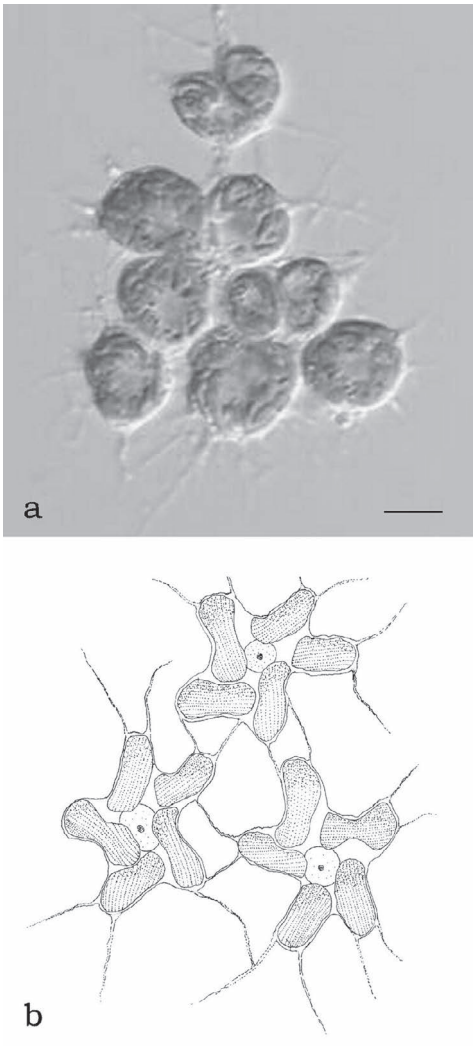


FIGURE 1.29 Plasmodial reticulum of *Chlorarachnion*: bright field microscope image (a), schematic drawing (b). Bar: 4 µm.



FIGURE 1.30 Unicell of *Euglena gracilis*. Bar: 10 µm.

obligate mixotrophic, because they require one or more vitamins of the B group. Some colorless genera are phagotrophic, with specialized cellular organelles for capture and ingestion of prey; some others are osmotrophic. Some of the pigmented genera are facultative heterotrophic. Only asexual reproduction is known in this division. Euglenophyceae possess unique cellular and biochemical features that place these microorganisms closer to trypanosomes than to any other algal group.

STRUCTURE OF THALLUS–CYTOMORPHOLOGICAL TYPES

An unrivalled diversity of morphological and cytological designs has evolved within algae, from microscopic unicells to macroscopic multicellular organisms, from simple filaments to giant-celled algae. Examples of the distinctive morphological characteristics within different groups are set forth in Table 1.3.

Unicells and Unicell Colonial Type

Many algae are solitary cells, unicell, with or without flagella, and hence motile or non-motile. *Nannochloropsis* (Ochrophyta) (Figures 1.1ar and 1.23) is an example of a non-motile unicell, while *Ochromonas* (Ochrophyta) (Figures 1.1an and 1.20) is an example of motile unicell. Other algae exist as aggregates of a few or many single cells held together loosely or in a highly organized fashion, the colony. In this type of aggregate, the cell number is indefinite, growth occurs by cell division of its components, there is no division of labor, and each cell can survive on its own. *Hydrurus* (Ochrophyta) (Figure 1.31) forms long and bushy non-motile colonies with cells evenly distributed throughout a gelatinous matrix, while *Synura* (Ochrophyta) (Figures 1.1ap and 1.21) forms free-swimming colonies composed of cells held together by their elongated posterior ends. Another quite unusual example of colony is *Tetraflagellochloris mauritanica* (Chlorophyta) (Figures 1.32a and 1.32b): up to 12 cells can be arranged in groups, which are connected by intercellular diaphragms and cytoplasmic bridges, without sharing any common colonial boundary. When the number and arrangement of cells are determined at the time of origin of the colony and remain constant during the life span period of the individual colony, the colony is termed coenobium. *Volvox* (Chlorophyta) (Figure 1.33), with its spherical colonies composed of up to 50,000 flagellated cells interconnected by cytoplasmic bridges, is an example of motile coenobium, as well as *Eudorina* (Chlorophyta) (Figure 1.34). *Hydrodictyon* (Chlorophyta), with its flat plat-like networks of several thousand cells, and *Pediastrum* (Chlorophyta) (Figure 1.35), with its flat colonies of cells characterized by spiny protuberances, are examples of non-motile coenobia.

Filamentous Type

Filaments result from cell division in the plane perpendicular to the axis of the filament and have cell chains consisting of daughter cells connected to each other by their end wall. Growth is diffuse, either apical or intercalary. Filaments can be simple as in *Oscillatoria* (Cyanobacteria) (Figure 1.36), *Spirogyra* (Chlorophyta) (Figure 1.15), or *Ulothrix* (Chlorophyta) (Figure 1.37) and can have false branching, as in *Tolypothrix* (Cyanobacteria) (Figure 1.38) or *Scytonema* (Cyanobacteria) (Figure 1.39), or true branching, as in *Cladophora* (Chlorophyta) (Figure 1.40). Filaments of *Stigonema ocellatum* (Cyanobacteria) (Figure 1.41) consist of a single layer of cells and are called uniseriate; those of *Stigonema mamillosum* (Cyanobacteria) (Figure 1.42), made up of multiple layers, are called multiseriate.

Siphonocladous Type

Algae with this cytomorphological design have multicellular thalli, with a basically uniseriate filamentous, branched, or unbranched organization composed of multinucleate cells as a consequence of uncoupled cell division and mitosis. The synchronously dividing nuclei are organized in non-motile, regularly spaced, nucleocytoplasmic domains that are maintained by

TABLE 1.3
The main thallus morphology in the different algal divisions

Phylum	Unicellular and non-motile	Unicellular and motile	Colonial and non-motile	Colonial and motile	Filamentous	Syphonous	Parenchymatous
Cyanobacteria	*Synechococcus* *Prochloron*	n.d.	*Anacystis*	n.d.	*Calothrix* *Prochlorothrix*	n.d.	*Pleurocapsa*
Glaucophyta	*Glaucocystis*	*Cyanophora*	n.d.	n.d.	n.d.	n.d.	n.d.
Rhodophyta	*Porphyridium*	n.d.	*Cyanoderma*	n.d.	*Goniotricum*	n.d.	*Palmaria*
Prasinodermatophyta	*Prasinoderma*	n.d.	*Palmophyllum*	n.d.	n.d.	n.d.	n.d.
Chlorophyta	*Chlorella*	*Dunaliella*	*Pseudo-sphaerocystis*	*Volvox*	*Ulothrix*	*Bryopsis*	*Ulva*
Charophyta	*Cosmarium*	*Mesostigma*	*Chlorokybus*	n.d.	*Klebsormidium*	n.d.	*Coleochaete*
Haptophyta	n.d.	*Chrysochromulina*	n.d.	*Corymbellus*	n.d.	n.d.	n.d.
Cryptophyta	n.d.	*Cryptomonas*	n.d.	n.d.	*Bjornbergiella*	n.d.	n.d.
Ochrophyta	*Triceratium*	*Ochromonas*	*Chlorobotrys*	*Synura*	*Ectocarpus*	*Vaucheria*	*Fucus*
Miozoa (Dynophyceae)	*Dinococcus*	*Gonyaulax*	*Gloeodinium*	n.d.	*Dinoclonium*	n.d.	n.d.
Cercozoa (Chlorarachniophyceae)	n.d.	*Chlorarachnion*	n.d.	n.d.	n.d.	n.d.	n.d.
Euglenozoa (Euglenophyceae)	*Ascoglena*	*Phacus*	*Colacium*	n.d.	n.d.	n.d.	n.d.

(n.a.: not available; n.d.: not detected).

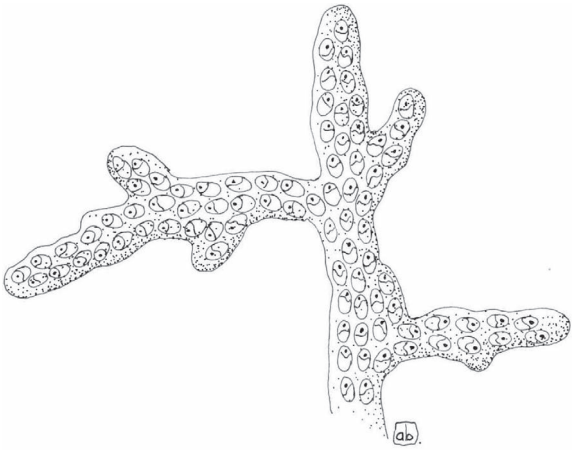


FIGURE 1.31 Non-motile colony of *Hydrurus foetidus*.

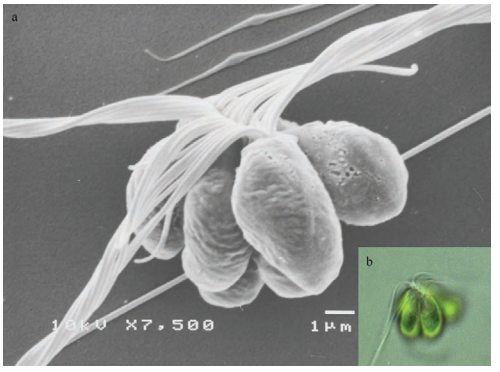


FIGURE 1.32 Free-swimming colony of *Tetraflagellochloris mauritanica*: SEM image (a), wide field optical microscope image (b).

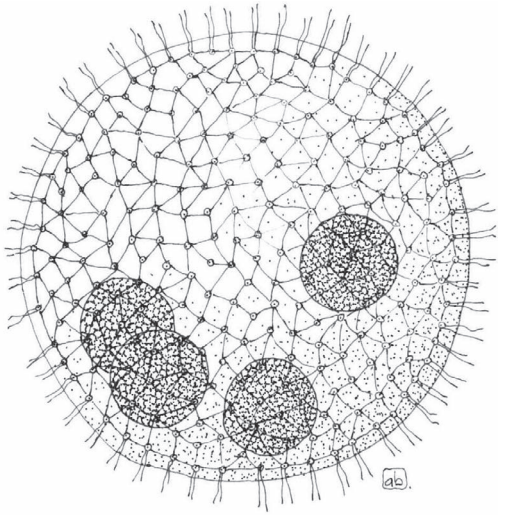


FIGURE 1.33 Motile coenobium of *Volvox aureus*.



FIGURE 1.34 Motile coenobium of *Eudorina* sp. Bar 20 µm.

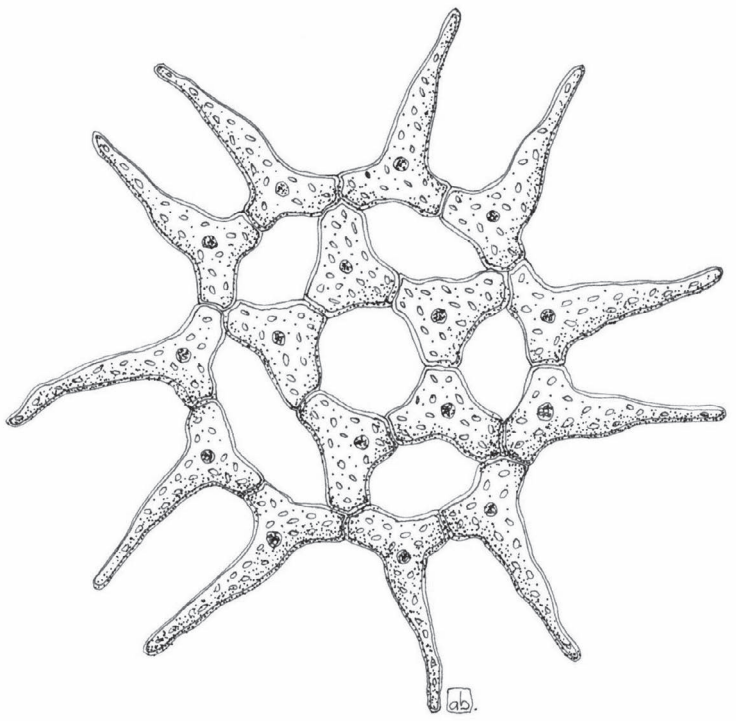


FIGURE 1.35 Non-motile coenobium of *Pediastrum simplex*.

perinuclear microtubule arrays. Despite lacking clear physical borders, such as a plasma membrane, these cytoplasmic domains behave like independent structural entities or pseudocells. This morphotype is present in members of the class Ulvophyceae (Chlorophyta) such as *Cladophora* sp. and *Anadyomene* sp.



FIGURE 1.36 Simple filament of *Oscillatoria* sp.

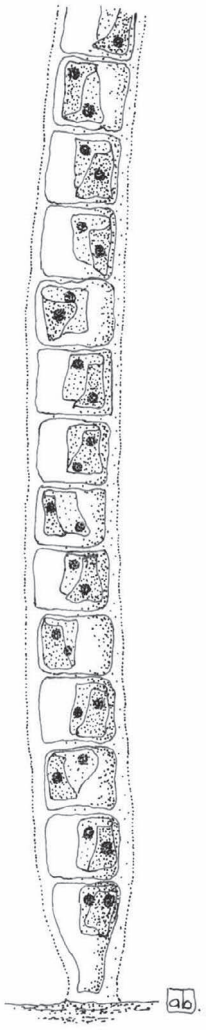


FIGURE 1.37 Simple filament of *Ulothrix tenerrima*.

Siphonous Type

Siphonous algae consist of a single giant tubular cell containing thousands to millions of nuclei dividing by asynchronous mitosis; hence, they are unicellular but multinucleate (or coenocytic). No cross-walls are present, and the algae often take the form of branching tubes. The sparsely branched tube of *Vaucheria* (Ochrophyta) (Figure 1.26) is an example of a coenocyte or apocyte, a single cell containing many nuclei. *Bryopsis* (Chlorophyta) and *Acetabularia* sp. (Chlorophyta) (Figures 1.1v and 1.12) are other quite diverse examples; the first is a fern-like, asymmetrically branched, marine alga composed of a single, tubular-shaped cell containing multiple nuclei and chloroplasts in a thin cytoplasmic layer surrounding a large central vacuole. The second is an umbrella-shaped alga, with a rhizoid, a stalk, and a cap-like whorl, growing in clusters attached on rocks. The single-compartment architecture of siphonous algae would suggest that they are particularly vulnerable to injury, but even if damage does occur, a complex, multistep wound response is triggered, and a wound can be plugged in seconds, regenerating the lost tissue. Many species can even use a small

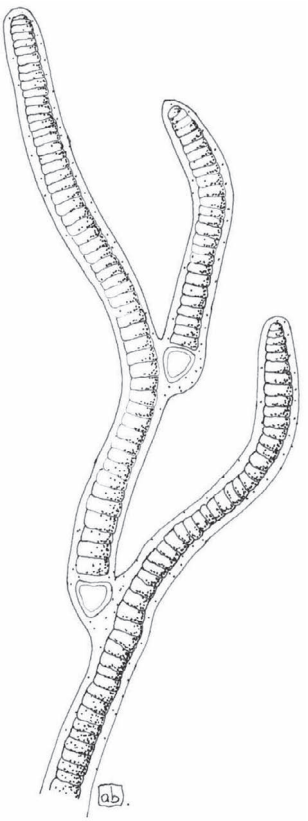


FIGURE 1.38 False branched filament of *Hassallia byssoidea*.

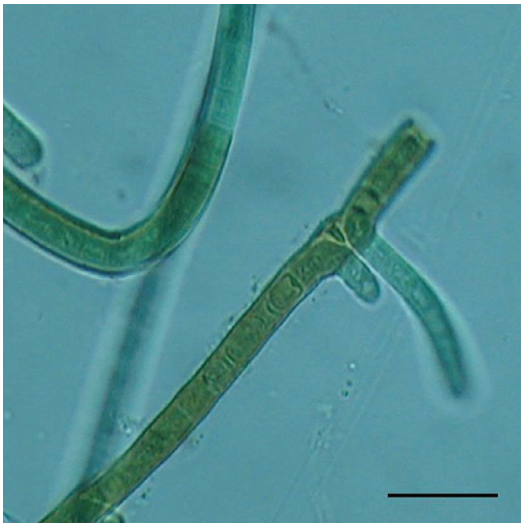


FIGURE 1.39 False branched filament of *Scytonema* sp. Bar 30 µm.



FIGURE 1.40 True branched filament of *Cladophora glomerata*.

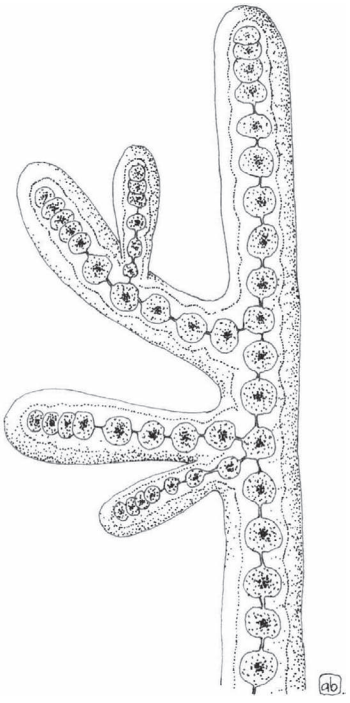


FIGURE 1.41 Uniseriate filament of *Stigonema ocellatum*.

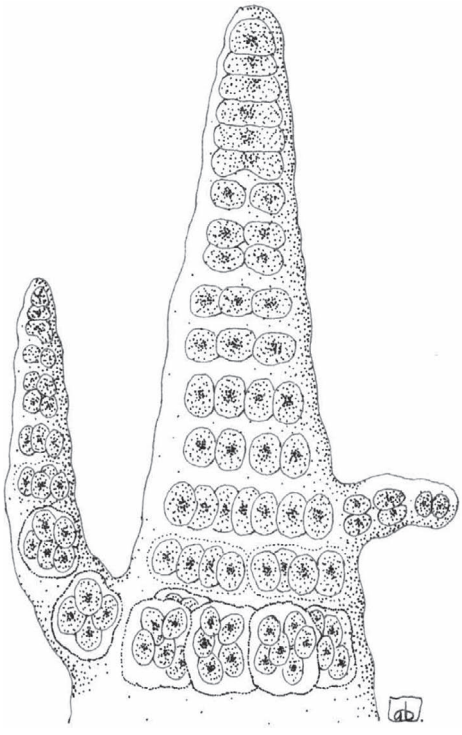


FIGURE 1.42 Pluriseriate filament of *Stigonema mamillosum*.

bit of excised tissue to regenerate the rest of the plant. This ability offers these algae considerable competitive advantage over other marine organisms. In some settings where they have been accidentally introduced, notably the Mediterranean Sea, certain species of siphonous green algae, with their multinucleate coenocytic body composed essentially of one very large, complex cell, such as the allocton *Caulerpa racemosa* var. *cylindracea* (Figure 1.43), have proved very successful, displacing native marine flora over large areas.



FIGURE 1.43 Frond of *Caulerpa racemosa* var. *cylindracea*. Bar 3 μm.

Parenchymatous and Pseudo-Parenchymatous Type

These algae are mostly macroscopic, with tissue of undifferentiated cells and growth originating from a meristem with cell division in three dimensions.

In the case of parenchymatous algae, cells of the primary filament divide in all directions, and any essential filamentous structure is lost; cells are often interconnected by intercellular plasmodesmata. This three-tissue dimensional organization is present in *Ulva* (Chlorophyta) (Figure 1.1u), where the thallus is simply organized in a two-cell layered sheet, and in many of the brown algae, such as *Laminaria, Fucus*, or *Macrocystis*. Parenchymatous construction is the basis of the ability of these brown macroalgae to grow to large sizes (more than 50 m) and form underwater forests. *Palmaria* (Florideophyceae, Rhodophyta) is a red alga with a complex parenchymatous structure (Figure 1.44). Pseudoparenchymatous algae are made up of a loose or close aggregation of numerous, intertwined, branched filaments held together by mucilage, especially in red algae, which collectively form the thallus, apparently composed of tissue but fundamentally and entirely based on a filamentous construction with little or no internal cell differentiation. Early in their evolutionary diversification, red algae underwent a key morpho-structural event, which confined the production of male and female gametangia to the apical cells. This event would have limited growth possibilities of the algae and prevented the evolution of parenchymatous thalli, which in turn limited the size and complexity of red algae. Other examples of this kind of thallus organization are *Hildenbrandia* (Florideophyceae, Rhodophyta), whose pseudoparenchymatous organization consists of an array of filaments closely packed into a thin, flat, deep, rose-colored crust growing on stone or other substrates; *Desmaretia* (Ochrophyta, Phaeophyceae), whose tissue construction is based on pluriseriate

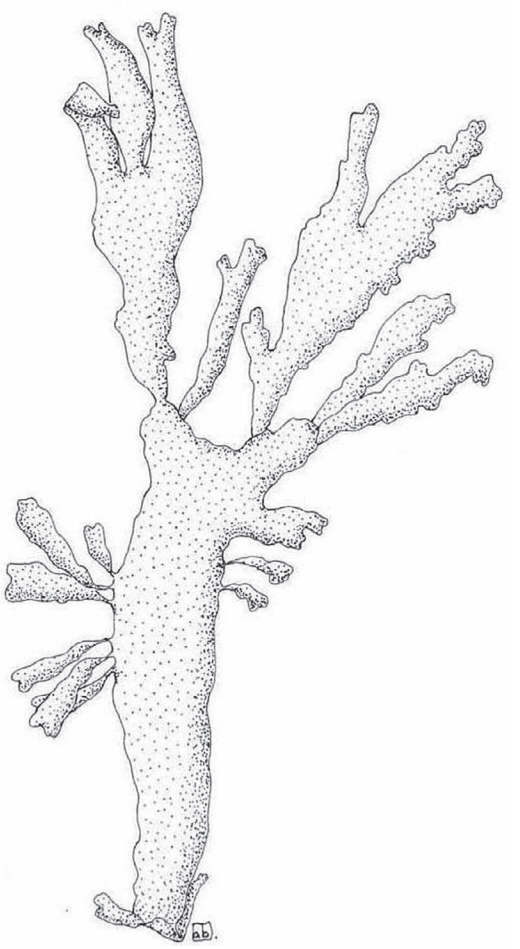


FIGURE 1.44 Parenchymatous thallus of *Palmaria palmata*.

filaments formed by vertical cell division; and *Cephaleuros* (Chlorophyta, Ulvophyceae), the most widespread parasitic alga infecting vascular plants such as magnolia, banana, and tea, whose pseudoparenchymatous thalli are more or less circular, composed of short cylindrical filamentous cells, and grow forming more or less circular cushions on the surface, beneath the cuticle, and/or within the intercellular space of the host plant.

Palmelloid Type

This type of thallus organization consists of non-motile, quite independent cells embedded within a common mucilaginous matrix. The name comes from the similarity with the algae belonging to the genus *Palmella* (Chlorophyta), which form gelatinous colonies, with non-flagellate, spherical, or ellipsoid cells uniformly arranged at the peripheral matrix. The palmelloid type can be present as a temporary phase of the life cycle in some species and as a permanent feature in others. Under unfavorable conditions, algae such as *Chlamydomonas* (Chlorophyta)*, Haematococcus* (Chlorophyta), or *Euglena* (Euglenozoa) (Figure 1.45) lose their flagella, round off, and undergo successive divisions, while the cells secrete mucus. Once favorable conditions are restored, the mucilage dissolves and cells revert to the flagellate conditions.

In members of the genus *Tetraspora* (Chlorophyta), this organization is a permanent feature: colonies are vesicular and sac-like, containing many hundreds of cells at the periphery, with long pseudocilia extending beyond the mucilaginous matrix. The palmelloid organization is also present in members of the Palmophyllales, an early-diverging chlorophytic lineage restricted to dimly lit habitats and deep water. These algae possess a unique type of multicellularity: they form well-defined macroscopic bodies composed of small spherical cells embedded in a firm gelatinous matrix.

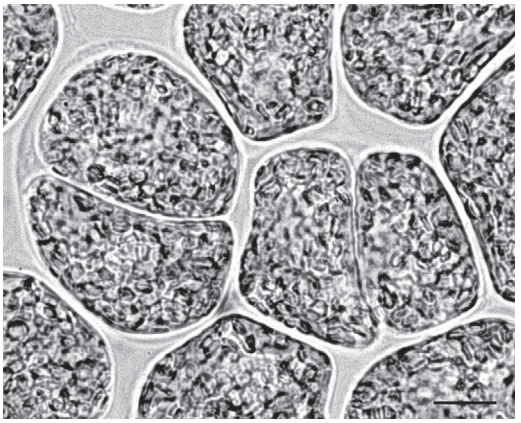


FIGURE 1.45 Palmelloid phase of *Euglena gracilis*. Bar 10 μm.

NUTRITION

Following our definition of the term *algae*, most algal groups should be considered photoautotrophs, that is, depending entirely upon their photosynthetic apparatus for their metabolic necessities, using sunlight as source of energy and CO_2 as a carbon source to produce carbohydrates and adenosine triphosphate. Most algal divisions contain colorless heterotrophic species that can obtain organic carbon from the external environment, either by taking up dissolved substances (osmotrophy) or by engulfing bacteria and other cells as particulate prey (phagotrophy). Algae also exist that cannot synthesize essential components such as the vitamins of the B_{12} complex, or fatty acids, and have to import them; these algae are defined as auxotrophic.

However, it is widely accepted that algae use a complex spectrum of nutritional strategies, combining photoautotrophy and heterotrophy. This ability is referred to as mixotrophy. The relative contribution of autotrophy and heterotrophy to growth within mixotrophic species varies along a gradient from algae whose dominant mode of nutrition is phototrophy, through those for which phototrophy or heterotrophy provide essential nutritional supplements, to those for which heterotrophy is the dominant strategy. Some mixotrophs are mainly photosynthetic and only occasionally use an organic energy source. Others meet most of their nutritional demand by phagotrophy but may use some of the products of photosynthesis from sequestered prey chloroplasts. Photosynthetic fixation of carbon and use of particulate food as a source of major nutrients (nitrogen, phosphorus, and iron) and growth factors (e.g. vitamins, essential amino acids, and essential fatty acids) can enhance growth, especially in extreme environments where resources are limited. Heterotrophy can be important for the acquisition of carbon when light is limited, and, conversely, autotrophy can maintain a cell during periods when particulate food is scarce.

On the basis of their nutritional strategies, we can classify algae into four groups:

- *obligate heterotrophic algae*: they are primarily heterotrophic but are capable of sustaining themselves by phototrophy when prey concentrations limit heterotrophic growth (example: *Gymnodinium gracilentum,* Miozoa);
- *obligate phototrophic algae*: their primarily mode of nutrition is phototrophy, but they can supplement growth by phagotrophy and/or osmotrophy when light is limited (example: *Dinobryon divergens,* Ochrophyta);
- *facultative mixotrophic algae*: they can grow equally well as photoautotrophs and as heterotrophs (example: *Fragilidium subglobosum,* Miozoa); and
- *obligate mixotrophic algae*: their primary mode of nutrition is phototrophy, but phagotrophy and/or osmotrophy provide substances essential for growth (in this group we can include photoautoxotrophic algae) (example: *Euglena gracilis,* Euglenozoa).

REPRODUCTION

Methods of reproduction in algae may be vegetative by division of a single cell or fragmentation of a colony, asexual by production of motile spore, or sexual by union of gametes. Vegetative and asexual modes allow stability of an adapted genotype within a species from one generation to the next. Both modes provide a fast and economical means of increasing the number of individuals while restricting genetic variability. Sexual mode involves plasmogamy (union of cells), karyogamy (union of nuclei), chromosome/gene association, and meiosis, resulting in genetic recombination. Sexual reproduction allows variation but is more costly because of the waste of gametes that fail to mate.

Vegetative and Asexual Reproduction

Binary Fission or Cellular Bisection

It is the simplest form of reproduction; the parent organism divides into two equal parts, each having the same hereditary information as the parents. In unicellular algae, cell division may be longitudinal, as in *Euglena* (Euglenozoa) (Figure 1.46), or transverse. The growth of the population follows a typical curve consisting of a lag phase, an exponential or log phase, and a stationary or plateau phase, where increase in density has leveled off (cf. Figure 5.3 in Chapter 5). In multicellular algae or in algal colonies, this process eventually leads to growth of the individual.

Zoospores, Aplanospores, and Autospores

Zoospores are flagellate motile spores that may be produced within a parental vegetative cell, as in *Tetraselmis* (Chlorophyta) (Figure 1.47). Aplanospores are aflagellate spores that begin their development within the parent cell wall before being released; these cells can develop into zoospores. Autospores are aflagellate daughter cells that will be released from the ruptured wall of the original parent cell. They are almost perfect replicas of the vegetative cells that produce them and lack the capacity to develop in zoospospores. Examples of autospore-forming genera are *Nannochloropsis* (Ochrophyta) and *Chlorella* (Chlorophyta). Spores may be produced within and by ordinary vegetative cells or within specialized cells or structures called sporangia.

Autocolony Formation

In this reproductive mode, when the coenobium/colony enters the reproductive phase, each cell within the colony can produce a new colony similar to the one to which it belongs. Cell division no longer produces unicellular individuals but multicellular groups, a sort of embryonic colony that differs from the parent in cell size but not in cell number. This mode characterizes green algae such as *Volvox* (Chlorophyta) (Figure 1.33) and *Pediastrum* (Chlorophyta) (Figure 1.48). In *Volvox*,

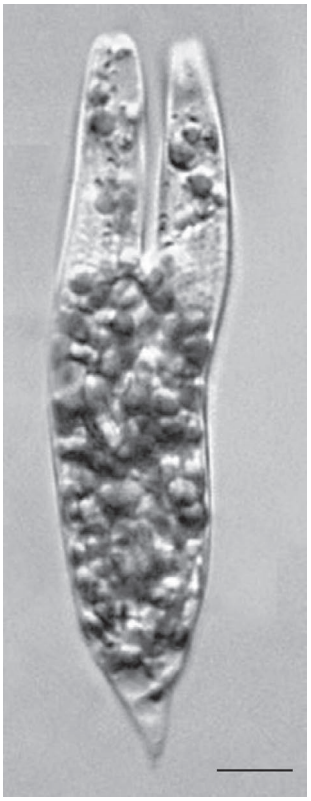


FIGURE 1.46 Cell division in *Euglena* sp. Bar: 5 µm.



FIGURE 1.47 Zoospores of *Tetraselmis* sp. within the parental cell wall. Bar 5 µm.

division is restricted to a series of cell which produce a hollow sphere within the parent colony, and with each mitosis, each cell becomes smaller. The new colony everts, its cell form flagella at their apical poles, and it is released by rupture of the parent sphere. In *Pediastrum*, the protoplast of some cells of the colony undergoes divisions to form biflagellate zoospores. These are not liberated but aggregate to form a new colony within the parent cell wall.

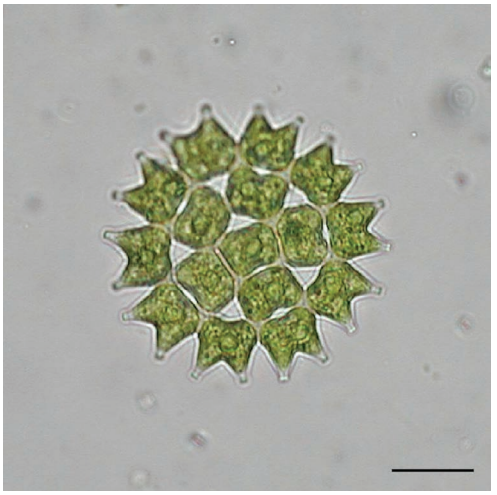


FIGURE 1.48 Non-motile coenobium of *Pediastrum* sp. Bar 10 µm.

Fragmentation

A more or less random process whereby non-coenobic colonies or filaments break into two to several fragments with the capacity of developing into new individuals.

Resting Stages

Under unfavorable conditions, particularly of desiccation, many algal groups produce thick-walled resting cells, such as hypnospores, hypnozygotes, statospores, and akinetes.

Hypnospores and hypnozygotes, which have thickened walls, are produced *ex novo* by protoplasts that previously separated from the walls of the parental cells. Hypnospores are present in *Ulothrix* spp. (Chlorophyta) and *Chlorococcum* spp. (Chlorophyta), whereas hypnozygotes are present in *Spyrogyra* spp. (Chlorophyta) and Dinophyceae (Miozoa) (Figure 1.49). Hypnospores and

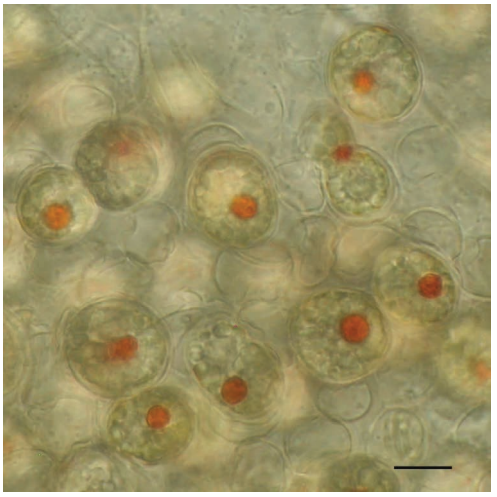


FIGURE 1.49 Dinoflagellate hypnozygote. Bar 10 µm.

hypnozygotes enable these green algae to survive temporary drying out of small water bodies and also allow aerial transport from one water body to another, for instance, via birds. It is likely that dinoflagellate cysts have a similar function.

Statospores are endogenous cysts formed within the vegetative cell by members of Chrysophyceae such as *Ochromonas* spp. The cyst walls consist predominantly of silica and so are often preserved as fossils. These statospores are spherical or ellipsoidal, often ornamented with spines or other projections. The wall is pierced by a pore and sealed by an unsilicified bung, and a nucleus, chloroplasts, and abundant reserve material lie within the cyst. After a period of dormancy, the cyst germinates and liberates its content in the form of one to several flagellated cells.

Akinetes are of widespread occurrence in the blue-green and green algae. They are essentially enlarged vegetative cells that develop a thickened wall in response to limited environmental nutrients or light. Figure 1.50 shows the akinetes of *Anabaena cylindrica* (Cyanophyta). They are extremely resistant to drying and freezing and function as a long-term anaerobic storage of the genetic material of the species. Akinetes can remain in sediments for many years, enduring very harsh conditions, and remain viable to ensure the continuance of the species. When suitable conditions for vegetative growth are restored, the akinete germinates into new vegetative cells.

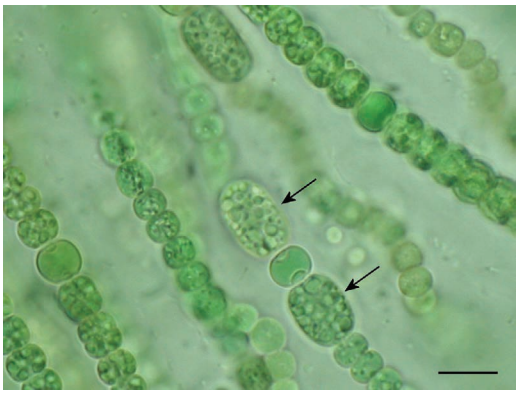


FIGURE 1.50 Akinetes (arrows) of *Anabaena* sp. Bar: 10 µm.

Sexual Reproduction

Gametes may be morphologically identical to vegetative cells or markedly differ from them, depending upon the algal group. The main difference is obviously the DNA content, which is haploid instead of diploid. Different combinations of gamete types are possible. In the case of isogamy, gametes are both motile and indistinguishable. When the two gametes differ in size, we have heterogamy. This combination occurs in two types: anisogamy, where both gametes are motile, but one is small (sperm) and one is large (egg), and oogamy, when only one gamete is motile (sperm), which fuses with one that is non-motile and very large (egg).

Algae exhibit three different life cycles with variation inside the different groups. The main difference is the point where meiosis occurs, the type of cells it produces, and whether there is more than one free-living stage present in the life cycle.

Haplontic or Zygotic Life Cycle

This cycle is characterized by a single predominant haploid vegetative phase, with meiosis taking place upon germination of the zygote. *Chlamydomonas* (Chlorophyta) (Figure 1.51) exhibits this type of life cycle.

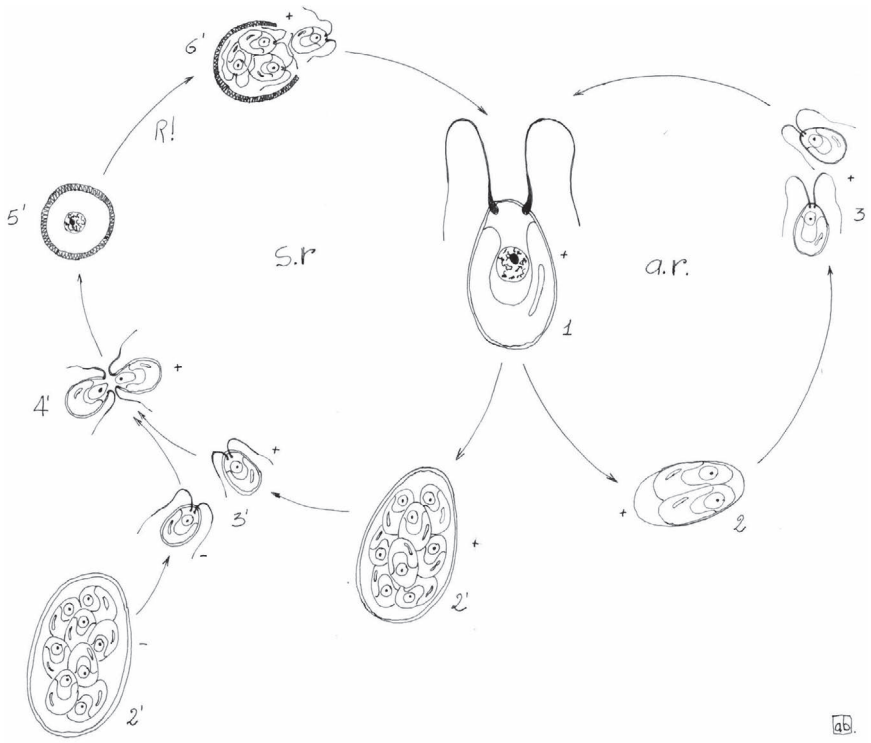


FIGURE 1.51 Life cycle of *Chlamydomonas* sp.: 1, mature cell; 2, cell producing zoospores; 2', cell producing gametes (strain+ and strain–); 3, zoospores; 3', gametes; 4', fertilization; 5', zygote; 6', release of daughter cells. R!: meiosis; a.r: asexual reproduction; s.r: sexual reproduction.

Diplontic or Gametic Life Cycle

This cycle has a single predominant vegetative diploid phase, and meiosis gives rise to haploid gametes. Diatoms (Figure 1.52) and *Fucus* (Ochrophyta) (Figure 1.53) have a diplontic cycle.

Diplohaplontic or Sporic Life Cycle

These cycles present an alternation of generation between two different phases consisting of a haploid gametophyte and a diploid sporophyte. The gametophyte produces gametes by mitosis; the sporophyte produces spores through meiosis. Alternation of generation in the algae can be isomorphic, in which the two phases are morphologically identical, as in *Ulva* (Chlorophyta) (Figure 1.54), or heteromorphic, with predominance of the sporophyte, as in *Laminaria* (Ochrophyta) (Figure 1.55), or with predominance of the gametophyte, as in *Porphyra* (Rhodophyta) (Figure 1.56).

OCCURRENCE AND DISTRIBUTION

The heterogeneous assemblage of prokaryotic and eukaryotic algal species possesses extreme physiological variability and plasticity and multifaceted growth strategies that allow them to colonize and thrive in a profound diversity of environmental settings, from aquatic to dry, from very cold to very hot, from fully lighted to deeply dark, and establish surviving, mutually beneficial interactions with many other organisms.

This incredible adaptability is the result of the pressure of both abiotic (physiochemical) and biotic factors. Abiotic factors are light, temperature, salinity, nutrient availability, pH, turbidity, and O_2 and CO_2 concentration; algae are not limited to temperate waters but can survive at very great depth and

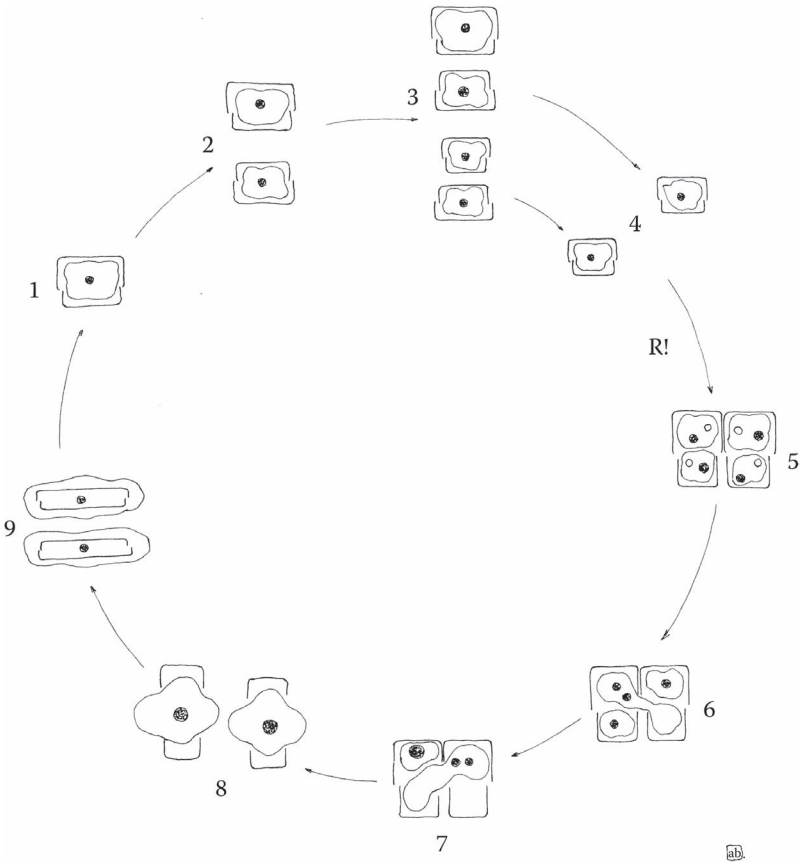


FIGURE 1.52 Life cycle of a diatom: 1, vegetative cell; 2–3, vegetative cell division; 4, minimum cell size; 5, gametogenesis; 6–7, fertilization; 8, auxospores; 9, initial cells. R!: meiosis.

very low irradiance and thrive beneath polar ice sheets. Upon adaptation to life on land, a considerable number of subaerial algae have colonized such surprising places as catacombs, tree trunks, hot springs, and snow banks and can also resist desiccation in the desert regions of the world, embedded within rocks. The activities of land algae facilitate the conversion of rock into soil, minimize soil erosion, and increase water retention and nutrient availability for plants growing nearby.

Biotic factors are, for example, competition within and between species for space, light, and nutrients or any limited source and associations-relations with other organisms. A variety of relations exist, which include epiphytism, parasitism, and symbiosis, each posing different problems for the algae to deal with. Some partnerships can be mutually beneficial, as in the case of algae living with fungi to form lichens or inside the cells of reef-building corals; in both these cases, algae provide oxygen and complex nutrients to their partner and in return receive protection and simple nutrients. These arrangements enable both partners to survive in conditions that they could not endure alone.

Algae can share their life with animals, growing on sloth hair, inside the jelly capsule of amphibian eggs, upon the carapaces of turtles or shells of mollusks, or camouflaging the dorsal scute of harvestmen. They can also establish pathogenic associations and cause infections in animals and humans.

We will describe examples of algae involved in biotic interactions with other organisms and thriving in extreme habitats (very cold, very hot, very dry, absence of gravity). Algal life in light-limited environments will be described in Chapter 4.

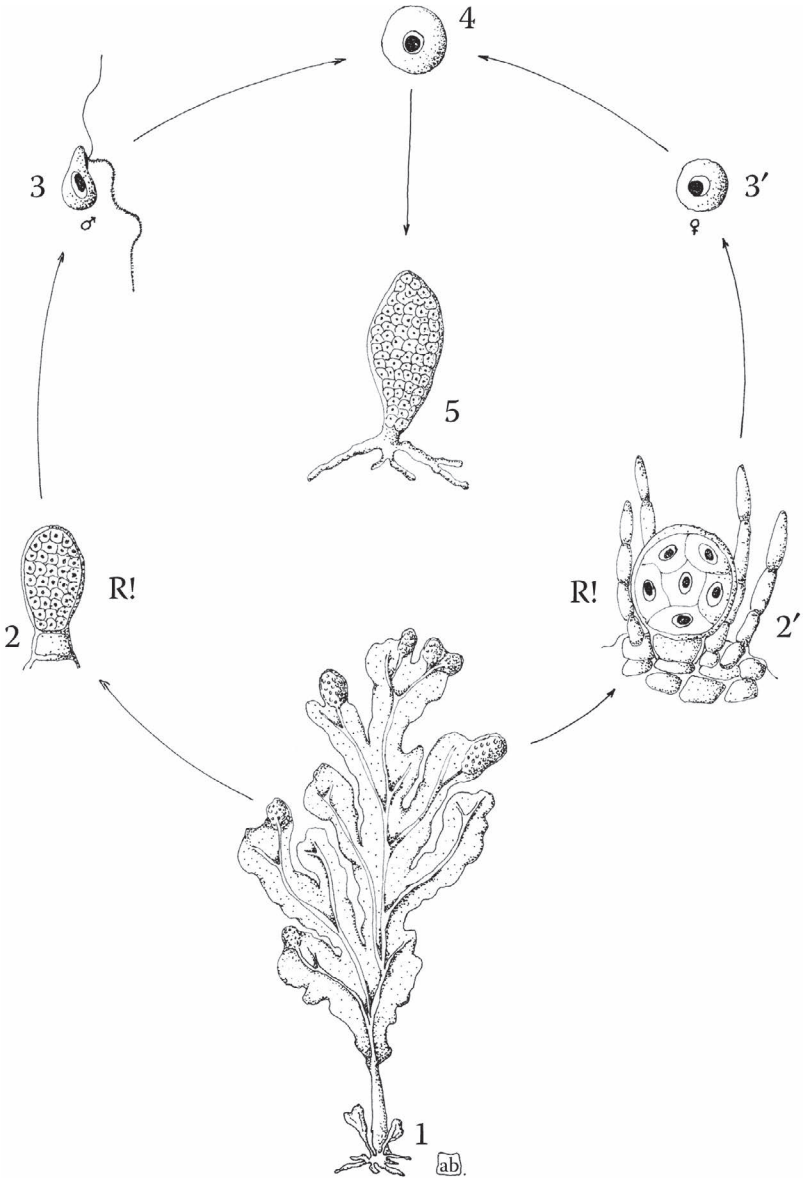


FIGURE 1.53 Life cycle of *Fucus* sp.: 1, gametophyte; 2, anteridium; 2', oogonium; 3, sperm; 3', egg; 4, zygote; 5, young sporophyte. R!: meiosis.

Biotic Interactions

Viruses

Viruses infecting eukaryotic algae, both micro- and macroalgae, are extremely diverse. They have been reported with DNA or RNA genomes in various architectures (linear, circular, double-stranded, single-stranded, segmented) and sizes (4.4 to 638 kb).

Virus abundance in aquatic systems is currently recognized to be about 10^6 to 10^9 of virus particles per mL of marine waters or even higher in freshwater systems and sediments. Viral particles are generally more abundant than any other microorganism, and their abundance is known to be tightly linked to that of the host they infect. The recent use of metagenomics has determined that

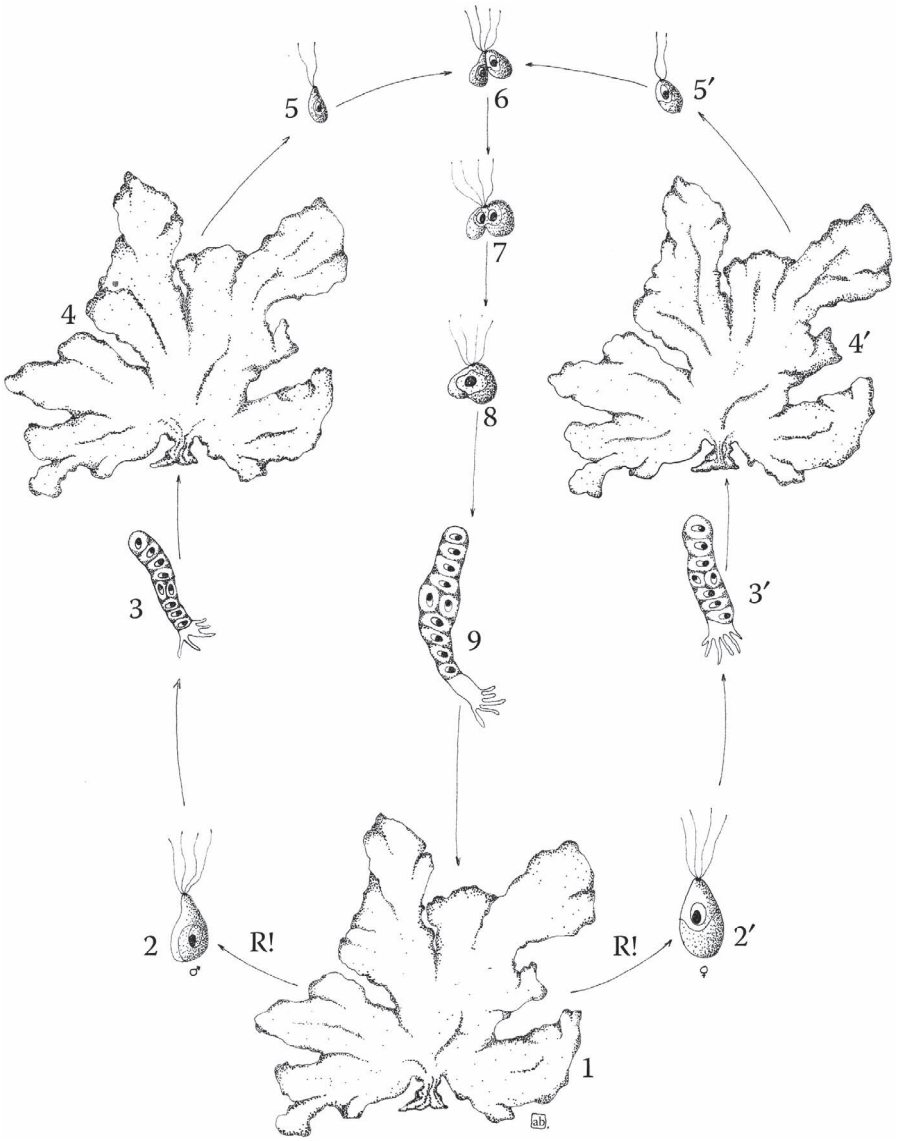


FIGURE 1.54 Life cycle of *Ulva* sp.: 1, sporophyte; 2, male zoospore; 2', female zoospore; 3, young male gametophyte; 3', young female gametophyte; 4, male gametophyte; 4', female gametophyte; 5, male gamete; 5', female gamete; 6–8, syngamy; 9, young sporophyte. R!: meiosis.

aquatic viruses are not only present in large quantities but that they are also characterized by a very wide genetic diversity worldwide. Since the discovery of high viral numbers and diversity, their role in aquatic ecosystems has been acknowledged as indispensable in structuring the microbial community and biogeochemical cycles. Briefly, 90% of aqueous systems are made up of microbes that can be roughly divided into two groups: phytoplankton and heterotrophic plankton, both of which are known to be infected by viruses. The structure and diversity of microbial communities can therefore be modified by viruses through selective removal, which can in turn release predation pressure and/or stimulate other trophic levels. Specifically in phytoplankton, viruses are known to be able to remove 25% of the photosynthetically fixed carbon and to restrict phytoplankton blooms. Viruses can also be responsible for the transfer of genetic material between species, through

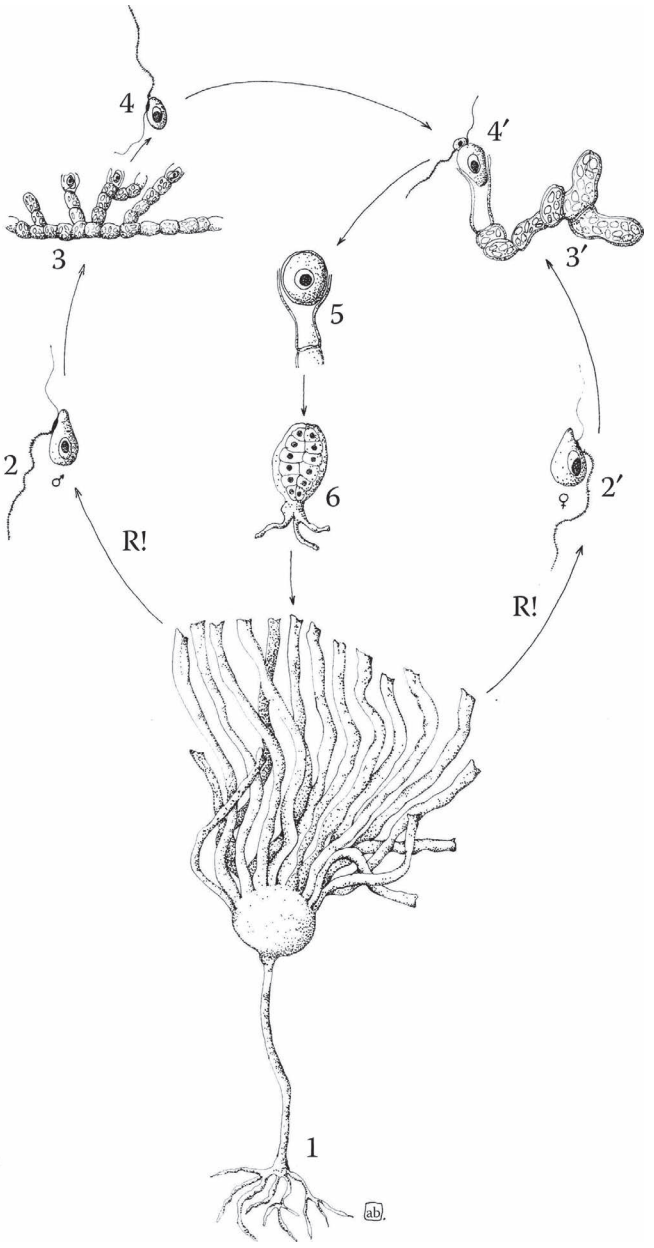


FIGURE 1.55 Life cycle of *Saccharina* sp.: 1, sporophyte; 2, male zoospore; 2', female zoospore; 3, male gametophyte; 3', female gametophyte; 4, sperm; 4', egg and fertilization; 5, zygote; 6, young sporophyte. R!: meiosis.

transformation or transduction (to date only reported in bacteriophages), and ultimately for the release of genetic material into the environment after the lysis of the host, making it available to other species. The role of aquatic viruses in biogeochemical cycles, mainly nutrient and energy cycling, involves the movement of material from living organisms into the particulate and dissolved pools of organic matter, referred to as the viral shunt. This is very important, as it increases respiration in the oceans and freshwater systems, reduces the direct transfer of microbes to higher trophic levels, increases primary productivity by making more nutrients available for autotrophs, recycles

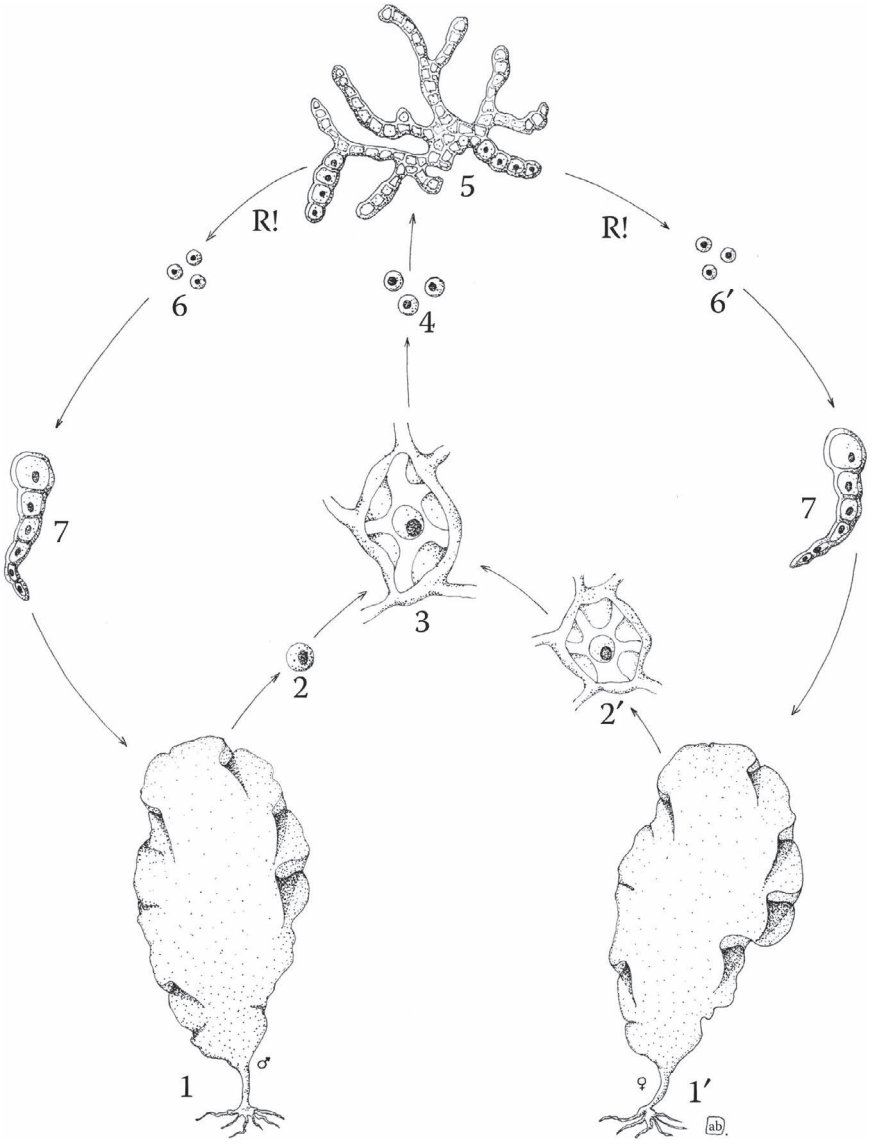


FIGURE 1.56 Life cycle of *Porphyra* sp.: 1, male gametophyte; 1', female gametophyte; 2, sperm; 2', egg; 3, fertilization and zygote; 4, spores; 5, sporophyte; 6, male spore; 6', female spores; 7, young male gametophyte; young female gametophyte. R!: meiosis.

carbon more intensively within the microbial loop, removes carbon from the classical grazing food web by diverting it to the microbial loop, and increases carbon that is exported to the deep ocean by the biological pump. The effects that algal viruses exert on their environments are of global importance, as phytoplankton activity is indispensable in all aquatic systems on Earth.

While algal viruses are important members in many aquatic environments, their contribution to these processes at the global scale primarily arises when they infect and lyse abundant bloom-forming algae. This includes harmful bloom formers and ecosystem-scale specialists like coccolithophores that form blooms large enough to be observed from outer space.

The first characterization of an algal-virus system dates back to 1983, when four double-stranded DNA (ds-DNA) viruses were identified from symbiotic *Chlorella* few hours after the isolation of the

algae from their hosts (*Paramecium bursaria, Hydra viridis*). Since then, this system has been fully investigated with genomes, transcriptomes, and proteomes documented in the literature, leading to the recognition of two main families of algal-infecting viruses: Phycodnaviridae and Mimiviridae.

Eukaryotic algal viruses in culture collections have been isolated from about 60 species, most of them belonging to the ds-DNA group; to date, the only single-stranded DNA (ss-DNA) algal-infecting viruses have been isolated by diatoms (Bacillariophyceae), and those currently in culture are those infecting the cosmopolitan genus *Chaetoceros*.

Also, ds-RNA and ss-RNA genomes of algal-infecting viruses have been isolated and characterized; a ds-RNA virus has been described for *Micromonas pusilla* and another one from *Chondrus crispus*.

ss-RNA viruses have received more attention, since their hosts are common marine phytoplankton, with some species capable of forming harmful blooms. Most of the alga-infecting ss-RNA viruses are members of the order Picornavirales, while the viruses infecting *Heterocapsa* (Dinophyceae) and *Heterosigma* (Raphidophyceae) are the sole members of the families Alvernaviridae and Marnaviridae (order Picornavirales), respectively. Other picornaviruses infect diatoms of the genus *Chaetoceros* and are generally thought to be highly species specific.

Viruses infect also cyanobacteria, the dominant autotrophs in most aquatic environments, such as freshwater and marine environments. Viruses infecting cyanobacteria are referred to as cyanophages and can play major roles in the dynamics, genetic diversity, and structure of cyanobacterial communities. Based on their morphological differences, cyanophages are generally categorized within three families, the Myoviridae, Podoviridae, and Siphoviridae, which belong to the order Caudovirales. They have linear double-stranded DNA genomes. Cyanophages are among the key factors determining the rate and direction of evolution in cyanobacterial populations; they play the role of genetic information stores and carriers and also regulate the sizes and genetic diversity of cyanobacterial populations. Viruses need hosts to reproduce their genomes. This mutually profitable partnership determines population histories in communities and provides grounds for the coevolution of cyanophages and cyanobacteria. Lytic cyanophages destroy cyanobacterial cells. The degree of lysis depends on the ratio between the amounts of virulent cyanophage particles and cyanobacterial cells sensitive to viral infection, and this ratio in turn depends on the population structure; availability of nutrient and energy sources; competition with other ecosystem members; and various environmental factors, particularly seasonal factors. The degree of lysis is negligible in oligotrophic marine communities due to the low population density and rare contacts between cyanophages and their hosts. In tropical regions of the ocean, cyanobacteria are more abundant; correspondingly, lysis is more intense, though it depends on the amount of viral particles, which rapidly die at high insolation and temperature.

Bacteria

Phytoplankton and bacterioplankton numerically dominate the ocean and freshwater planktonic community and are the primary producers and decomposers, respectively, which makes them the structural pillars of the ecosystem and its foremost functional entities. These plankton communities together influence the global carbon cycle and ultimately the climate, and though the primary function of heterotrophic bacteria is decomposition, it is now accepted that some bacteria also play a part in algal growth promotion. Therefore, the interactions between these two groups of plankton, which cover the whole range of possible symbiotic relationships and are likely to be universal in the environment, and the influence of their interaction on each other and on a global scale are areas of recent research interest.

A prerequisite for such association/exchange networks is the spatial assembly of interacting organisms. Each unicellular alga is surrounded by its phycosphere, an ecologically and physiologically integrated and microscopic chemically enriched zone, in which gradients of released compounds are maintained. In this key interface, cross-kingdom communications are mediated by the release and uptake of organic compounds, and intricate networks have evolved, which have revolutionized life on earth in many aspects.

Many notable examples are species specific, such as the green seaweed *Ulva mutabilis* (Ulvophyceae), which relies on different bacterial strains for successful morphogenesis. When grown under laboratory conditions, axenic gametes of *U. mutabilis*, rather than forming the typical blade- or tube-like morphology, develop into callus-like aggregates of undifferentiated cells with abnormal cell walls. These findings suggest the existence of chemical signaling between bacteria and the alga and, potentially, the complementarity of metabolic pathways. Similar interactions have also been found between the bacterium *Sulfitobacter pseudonitzschiae* and the diatom *Pseudonitzschia multiseries* (Bacillariophyceae); bacteria also have been shown to facilitate the acclimation of the brown seaweed *Ectocarpus siliculosus* (Phaeophyceae) to a freshwater environment.

Marine pelagic bacteria have evolved strategies to utilize resources released from living and decaying primary producing microalgae, controlling entire algal blooms by inducing algal lysis and facilitating uptake of metabolites released during the process. The interaction between *Kordia algicida* and *Skeletonema costatum* (Bacillariophyceae) is an example of this strategy: a protease produced by the bacterium causes the alga to lyse, and the concomitant release of organic compounds sustains bacterial growth. Other bacteria have evolved real hunting strategies, such as *Pseudomonas protegens*, which accumulates around the initially motile freshwater algal cells of *Chlamydomonas reinhardtii* (Chlorophyceae) and immobilizes prey by deflagellation. This process, triggered by the lipopeptide orfamide A, also leads to the disruption of algal Ca^{2+} homeostasis. The bacteria therefore shape their immediate environment and benefit from the resources released upon the following cell lysis.

More general interactions are seen with bacteria that play a key role in providing micronutrients to algae, but studies have also shown that macronutrients such as nitrogen, carbon, and phytohormones usually exchange between algae and bacteria. Examples of micronutrients are essential organic compounds, such as thiamine (vitamin B_1) and cobalamin (vitamin B_{12}). These compounds are required as enzyme cofactors, but many phytoplankton species are unable to synthesize them. Only prokaryotes (only a subset of both Eubacteria and Archaea) can synthesize cobalamin *de novo*, and levels free in the aquatic environment are generally too low to support algal growth. Direct provision of the vitamin from bacteria to algae occurs in the natural environment. There is specificity in this interaction, demonstrated by the fact that, although cyanobacteria are B_{12} producers, they make a variant known as pseudocobalamin that is considerably less bioavailable to eukaryotic algae than cobalamin, the variant produced by many heterotrophics. Thus, provision of photosynthates from algae may provide the signal to attract and retain cobalamin producers within the phycosphere. Similar to B_{12}, recent studies have demonstrated that bacteria can also provide either thiamine (vitamin B_1) or its precursors to phytoplankton, and, because thiamine is also often limited, phytoplankton blooms may similarly be limited by thiamine-producing bacteria or other microbes.

One of the most ubiquitous interactions in the marine ecosystem is the *Roseobacter*–algae interaction. Members of the *Roseobacter* lineage play a major role in biogeochemical cycling, especially carbon and sulfur, by oxidizing the greenhouse gas carbon monoxide and producing dimethylsulfide utilizing algal osmolytes.

The most widely studied interaction between a marine alga and its associated bacterium is that between the cosmopolitan coccolithophore *Emiliania huxleyi* (Coccolithophyceae) and *Phaeobacter inhibens*, a member of the *Roseobacter* lineage. This interaction is the closest example of classic continuum theory between algae and bacteria, not proven to be driven by environmental factors but rather surprisingly determined by algal molecules and a growth phase. These algae can quickly bloom and form dense populations ($>10^6$ cells·L^{-1}) over vast expanses of the upper ocean (>250,000 km^2), which then decline after every bloom. *Phaeobacter inhibens* attaches to the cells of *E. huxleyi* and exploits released dimethylsulfonium propionate as a source of carbon and sulfur. After association, bacteria initially increase algal growth by releasing the growth promoting indole-3-acetic acid (IAA). IAA production is further increased by supply of the biosynthetic precursor tryptophan by *E. huxleyi*.

When *E. huxleyi* reaches senescence, population declines, and cells start releasing p-coumaric acid as by-products of the degradation of cell wall lignin. Upon p-coumaric acid release, the bacterium responds with the production of 11 types of troponoids, which eventually kill algae. Its

relationship with the alga switches from mutualistic to pathogenic, and the bacterium switches from a sessile lifestyle on the algal cell wall to a motile phase.

During the brief period of high algal growth, the bacteria not only supply vitamins and phytohormones to algae but also provide antibacterial safeguards towards non-roseobacters in cohesion with algae.

Arthropods

Arthropods are a good host for algae. Cyanobacteria were reported to grow epizoically on the dorsal scute of the harvestman *Neosadocus* sp. (Arachnida, Opiliones) in Cardoso Island, southeast Brazil. The epizoic algae almost fully covered the harvestman's back, giving the animals a greenish coloration contrasting markedly with the brownish body and appendages. The growth of the algae did not affect behavior and locomotion of the animals, which would benefit from the presence of the photosynthetic organism by being camouflaged and thus protected from visual diurnal predators.

Arachnids are exploited also by green algae. Very recently a species of the well-known genus of green unicellular alga *Dunaliella* (Chlorophyceae) was found on the walls of a cave located in the in the Coastal Range hills of the Atacama Desert (Chile). The cave, situated about 75 m above sea level, is about 170 m deep, an average height of 50 m, and its entrance directly confronts the Pacific Ocean, less than 200 m away from it. The alga grows upon spider webs attached to the walls of the entrance-twilight transition zone of the cave. All previously reported members of this genus are found in extremely saline aquatic environments; hence, this is the first *Dunaliella* species able to thrive in a subaerial habitat. The identity of this alga as a new species, *Dunaliella atacamensis*, was assessed by molecular and morphological methods.

The Coastal Range, which separates the hyperarid Atacama Desert plateau from the Pacific Ocean, acts as a topographic barrier to clouds and moisture-rich marine air moving from the ocean. Thus, fog-originated water allows the presence of "fog oases" in this region, with a daily cycle with a maximum expansion over the coastal hills during the night and early morning hours. The cave interior acts like a funnel that continuously captures the incoming water-rich air of oceanic origin, in particular the south-facing walls exposed to the moisture-rich prevailing winds, the only area of the cave where the alga grows. This area is about 20 m away from the entrance, where the light is about 1.4% of the outside incident light. Most of the alga grows as colonies of green cells covering spider webs attached to the cave walls and not on the underlying rocks. The colonized spider webs are constantly subjected to the flow of the humid, rich air moving through them, condensing water droplets, especially during the night and early morning hours. Condensation of water onto the hygroscopic threads of spider webs is a well-known phenomenon. An alternative source of water could be dew, whose formation is induced by substrates with temperatures below the dew point of the ambient air. As the exposed surfaces of the cave cool by radiating heat during the late afternoon and night, atmospheric moisture could condense at a rate greater than that at which it can evaporate, resulting in the formation of water droplets on the spiderweb threads at the early hours of the morning, as observed.

D. atacamensis cells are non motile, mostly round or ovoid, with a diameter of 6 μm; they possess one cup-shaped chloroplast with a single pyrenoid surrounded by several starch bodies. Though no flagellum appears to be present, the cells possess small stub-like structures reminiscent of flagella. These stub-like structures are comparable to the short flagella of a *D. salina* mutant (Figure 1.57) and could have the function of primary "clinging" devices attaching the cell to the spiderweb thread. The cells form tetrads that join into colony-like structures in irregular clumps reminiscent of palmelloid stages of other *Dunaliella* species under reduced salinity conditions (≤10% NaCl). In the palmella stage, the cells usually lose their flagella and eyespot, become more rounded, and excrete a layer of exopolysaccharides (EPSs) in which they repeatedly divide, thus forming colonies of green cells. All these morphological characteristics are present in *D. atacamensis* cells.

Another interesting feature is the well-developed layer of EPS, which in *D. salina* strains is produced in response to the environmental stress caused by increasing salt concentrations. EPSs have been shown to be involved in the efficient capture and retention of ambient water by cyanobacteria

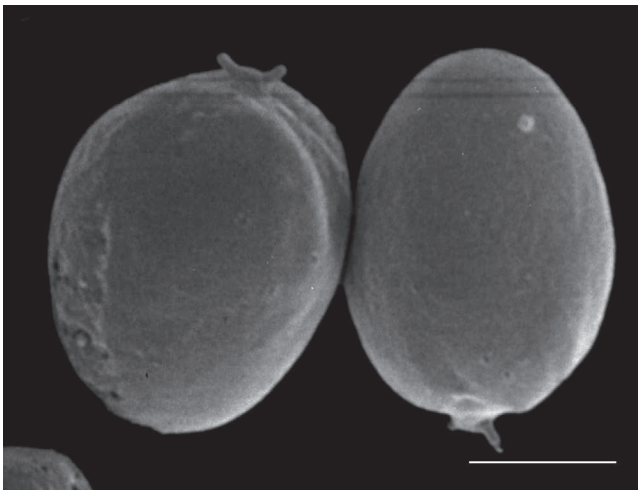


FIGURE 1.57 Scanning electron micrograph of the stumpy mutant of *Dunaliella salina*. Bar 3 μm.

in extreme environments, suggesting a similar role for the cave-inhabiting *D. atacamensis*. Since the thick layer of EPS could lower CO_2 diffusion in the cells, a pyrenoid might be advantageous in a subaerial habitat for carbon fixation in this extreme environment.

Different features previously evolved by *Dunaliella* species for living in hypersaline environments (i.e. colonial growth, pigments for avoiding photodamage, salt tolerance, glycerol production, EPS production) are highly advantageous for adapting to a subaerial environment with reduced water availability and perhaps different light regimes than those experienced by its aquatic ancestors. This process recapitulates the adaptations evolved by green algae for the sea-to-land transition, that is, from aquatic algae to land plants. As algae moved to land, they could make an efficient use of resources by exploiting a range of previously evolved traits that are likely to have played a key role in this successful process of extending the habitability range. These include cell wall biochemistry, desiccation resistance and tolerance, and structural complexity, as well as various reproductive strategies. Many of these traits characterize the enormous physiological variability of *Dunaliella* species, and *D. atacamensis* represents a beautiful example of this assertion.

Amphibians

Another mutualistic association with algae occurs in some amphibians. All amphibians lay eggs with a capsule, although the form and thickness of the capsule vary widely. Some amphibians, including the spotted salamander *Ambystoma maculatum* (Amphibia, Urodela) and the pickerel frog *Rana palustris* (Amphibia, Anura), embed their eggs in large masses of relatively firm jelly, which are attached to vegetation in ponds. Other amphibians, including the wood frog *Rana sylvatica* (Amphibia, Anura) and the spotted marsh frog *Lymnodynastes tasmaniensis* (Amphibia, Anura), lay their eggs in masses that float at the surface of the pond or are loosely attached to vegetation. The capsule, at least in aquatically developing amphibians, protects the eggs from predators, and it also resists exchange of respiratory gases. Amphibian egg masses in the wild are often inhabited by algae, for example, egg masses of *Ambystoma maculatum*. The algae were first noted by Orr in 1888, who speculated that they must have considerable influence on the respiration of the embryos. It is now well established that this relationship is symbiotic. The alga *Oophila ambystomatis* (Chlorophyceae) is found exclusively in amphibian egg masses, mostly in those of *Ambystoma maculatum* (it derives its name from this association) but also in those of *R. sylvatica* and some other species. Individual egg capsules appear green due to dense accumulations of algae surrounding the embryo. In *A. maculatum*, algae primarily enter salamander embryos through the blastopore before the formation of a patent stomodeum

and therefore before active feeding is possible. The embryonic association of the *Ambystoma*–alga symbiosis may indicate an inefficient immune system or an adaptive immune response that would otherwise remove invading intracellular algae. Some algal cells are also embedded within epithelial or mesenchymal tissues that are far from the alimentary canal, consistent with algae having entered salamander embryos directly by penetrating their embryonic integument. Molecular data are consistent with a process of oviductal transmission of algae from one salamander generation to the other, but horizontal transmission could be present as well, with the algae deriving from the environment. Algal cells leave direct sunlight by entering opaque salamander tissues. Behavioral stimuli, such as gradients of nitrogenous waste, which may instigate algal proliferation, could serve as the behavioral cue for tissue and cellular invasion against this light gradient.

The mutual benefit of this facultative association has been clearly established through exclusion experiments. Clutches raised in the dark do not accrue detectable algae. The presence of algae in these experiments correlates with earlier hatching, decreased embryonic mortality, more synchronous hatching, and reaching a larger size and later developmental stage at hatching. Additionally, algal growth is minimal in egg capsules after embryos are removed, indicating that the embryos and not the egg capsules aid algal growth. Intracapsular algae are thought to benefit from nitrogenous wastes released by the embryos, whereas salamander embryos benefit from the net increase of oxygen produced by the algae. Most intracellular algae and algae of the alimentary canal disappear by early larval stages. Their possible absorption may confer a further metabolic benefit to their host. Presence of the algae also correlates with decreased cilium-mediated rotation of early-stage embryos and increased muscular contractions during later embryonic stages, both of which may be secondary effects of modulated oxygen levels. The reciprocal benefits of hatchling survival and growth to the embryo, and population growth to the algae, reveal that this symbiosis is a true mutualism.

Algae are also important for tadpoles of other amphibians, establishing an ecologically important mutualism that is conditional and provides partner species with novel options for adjusting to changing environments. It is well know that organisms reaching their critical thermal maximum (CTM, the minimal high deep-body temperature that is lethal to an animal) are incapable of escaping the lethal conditions. This holds especially true for aquatic organisms in thermally uniform systems, which have no refuge from heat stress; further, temperature increases within such systems decrease the concentration of the necessary gases oxygen and carbon dioxide. Aquatic organisms that are stressed for these gases for respiration and photosynthesis would benefit from fortuitous mutualistic interactions in which the "by-product" gases evolved by metabolism can be absorbed reciprocally. Observations were conducted on numerous tadpoles of the dwarf American toad *Bufo americanus charlesmithi* (Amphibia, Anura) in a shallow temporary pool subjected to extended exposure to solar radiation, located in Ashley County (Arkansas, USA). The water became very warm by mid-afternoon, and some of the tadpoles possessed an atypical greenish coloration. The tadpoles were late stage, and some of them exhibited well-developed legs. Microscopic examination of live tadpoles from the pool revealed clusters of biflagellated green algae identified as *Chlorogonium* (Chlorophyceae) scattered as greenish blotches over the skin. Individuals of this alga were observed actively flagellating to maintain a position oriented to the skin of the tadpole. The distribution of the alga generally followed the pattern of cutaneous blood vessels on the dorsal surfaces of the legs, tail, and lateral body wall. The high CTM of toads helps them survive in warmer conditions and shortens the time required for development, thereby promoting metamorphosis prior to desiccation of the habitat. Rates of oxygen consumption in tadpoles increase with higher temperatures, but water at higher temperature holds a lower concentration of gases. Although tadpoles are tolerant to warmer temperatures, the O_2 deficits can lead to respiratory distress and death. Under conditions of low O_2, tadpoles of some species can supplement oxygen intake by gulping air, but the late development of the lungs precludes this in *Bufo*. Consumption of O_2 increases sharply prior to metamorphosis. Thus, the warmer water contains less O_2 at a time when more may be needed. Even after acclimatization to warmer temperatures, the CTM of tadpoles of most anuran species is 38°C–40°C, with a few exceptions above 41°C in species that develop in xeric (with very little moisture) or tropical habitats. On the other hand, the rate of photosynthesis tends to increase

with increases in temperature up to an optimum, after which it decreases rapidly, partly limited by the availability of inorganic carbon. The growth rate of algae slows in stagnant cultures because the rate of diffusion of CO_2 from the air become limiting, partly because CO_2 diffuses 10^4 times faster in air than in water. Green algae (Chlorophyta, including *Chlorogonium*) tend to dominate in temperatures of 15°C–30°C but are replaced by cyanobacteria above 30°C. Thermophilic algae thrive best in waters rich in CO_2, where conditions necessary to maintain high rates of photosynthesis are met. The pattern of association and distribution of *Chlorogonium* over the skin of tadpoles allows maximum potential for uptake of otherwise limited CO_2 released via cutaneous respiration by tadpoles. The relatively small size of *Chlorogonium* specimens also could indicate stress. The mean length of the cells taken from the tadpoles was 13.4 μm (range 7–22 μm), and the width ranged only between 1.5 and 3 μm. The normal measurements from species known to occur in the United States range from 19–59 μm in length and 5–18 μm in width. Smaller cells result in a higher surface/volume ratio, which could help maximize absorption in CO_2-limited environments.

The CTM at which tadpoles of *Bufo americanus* could survive independently is 39.5°C. In a heat-stress–inducing environment, however, the CTM could be expanded by over 4°C (to about 43°C) in the presence of a photosynthetic, mutualistic alga such as *Chlorogonium*. Considering these phenomena, it is hypothesized that the *Chlorogonium* and tadpoles are exhibiting a facultative symbiosis in which tadpoles gain O_2 produced via photosynthesis adjacent to the skin, and concomitantly *Chlorogonium* receive the metabolic CO_2 evolved from the tadpoles. Similar algal accumulations have been found on tadpoles of gray tree frogs (*Hyla versicolor*) and cricket frogs (*Acris crepitans*) at other locations within Arkansas (USA).

Reptiles

Algal occurrence on reptiles is limited to turtles. The green algal genus *Basicladia* Hoffman and Tilden (Ulvophyceae) contains species that are specifically epizoic on carapaces of turtles or shells of mollusks. Closely related to the genus *Cladophora* (Ulvophyceae), the genus *Basicladia* is mainly distinguished by its epizoic nature. Five species are recognized, and all are known only from freshwater turtles or snails. *Basicladia crassa* and *B. chelonum* have been reported from freshwater turtles in several states of the Rocky Mountains and the Caribbean. Outside of the United States, *B. sinensis* was described from the back of a turtle brought from China to an aquarium in California, and *B. ramulosa*, an exceptionally large species, is known from Australian turtles. The fifth taxon, *B. vivipara*, is known only from the freshwater snail, *Viviparus malleatus* Reeve (Gastropoda). In 1975, *B. crassa* was reported for the first time from Virginia on the carapace of a red-bellied turtle, *Chrysemis rubriventris*. The algae are characterized by a thallus with siphonocladous organization, with single, unbranched, sometimes twisted filaments. Rhizoids at the basal part are usually round, and they attach to the turtle shell. These algae are usually restricted to the turtle carapace, where they form a wide band thickly covering the marginals and ventral half of the pleural scutes but thinning as it extends dorsally. The rugose carapacial surface of this turtle is well suited for the attachment of algal rhizoids, but the basking habit of the turtle may account for the absence of most carapacial algae since they are subject to increased desiccation and solar radiation above the water level. Also, *C. rubiventris* sheds the epidermal scutes of its carapace periodically, thus freeing itself of any algae attached. However, it is not uncommon to find "moss-back" red-bellies in the spring, especially just after emergence from hibernation when air temperatures are still too cool for much basking. *B. crassa* and *B. chelonum* are able to survive periods of basking desiccation and even more heat than the turtles themselves. It is possible that repeated exposure to the sun's ultraviolet rays and the drying effect through frequent basking associated with the grazing action of herbivorous fish or amphipods would at least limit the growth of these algae.

Other Animals and Humans

A very particular and unusual symbiosis is that between sloths and green algae. Sloths are slow-moving arboreal mammals inhabiting tropical rainforests in Central and South America, represented

by six extant species in two genera, *Bradypus* (four species: *B. variegatus, B. torquatus, B. tridactylus, B. pygmaeus*), the three-fingered sloths, and *Choloepus* (two species: *C. hoffmanni, C. didactylus*), the two-fingered sloths. A versatile small-scale ecosystem of epibiotic symbionts that includes algae, ciliates, moths, insects, and fungi thrives in the fur of these animals, which has been described as "a moving island of biodiversity."

Among the many odd features of these sluggish tree-dwellers, perhaps the oddest of all is their hair, which, with its peculiar morphology and structure, seems to facilitate symbiotic algal growth unlike any other mammals. Sloth hair is long and coarse, and that of the three-fingered sloth (*Bradipus* spp.) has transverse cracks that increase in quantity and depth as sloths age. The hairs swell considerably when wet, and the moisture retained within cracks may sustain algal growth on the hair surface. Algae do not grow directly within the cracks but on the smooth outer surface of the hair, where access to photosynthetic radiation is not limited. Hairs of the two-fingered sloth (*Choloepus* spp.) have longitudinal grooves and do not absorb much water; algae are found within these grooves and do not coat the entire surface of the hairs. During the dry season, the hair of sloths usually has a dirty brown coloration, but during long periods of rain, it may show very appreciable greenish tinges brought about by the increased presence of symbiotic algae. The greenish color of the hair give the sloth excellent camouflage among the leaves; this camouflage is crucial to the sloth's survival, because its inability to move quickly makes it an easy target for predators that hunt by sight such as the harpy eagle (*Harpia harpyja*).

Recently, the genetic diversity of the eukaryotic community present in the fur of sloths belonging to all six extant species was investigated. Amplicon metagenomic studies of sloth fur to date reveal a variable array of algae across and within different sloth species. The majority of the green algal sequences obtained from the hair samples formed a clade of their own within the green algal class Ulvophyceae (Chlorophyta). This group received high support (100%) for its monophyly in all phylogenetic analyses that were employed. This clade, consisting of small (3–13 μm) thick-walled cells without pyrenoids, is likely to correspond to the green algal genus *Trichophilus* (Ulvophyceae), whose first description dates back to 1887. The clade was subdivided into three subclades that received moderate to high internal node support. Two subclades, A and C, were formed by rRNA gene clones originating from *Choloepus hoffmannii* hair samples. Clones in clade B originated from the hair of *Bradypus* species. Within clade B, the sequences from *B. tridactylus* were different from those of *B. variegatus* and *B. pygmaeus.*

Trichophilus spp. was the only green alga in the hair of the brown-throated sloth *B. variegatus* and the pygmy three-toed sloth *B. pygmaeus.* These species were also found on Hoffmann's two-toed sloth *Choloepus hoffmanni* and the pale-throated sloth *B. tridactylus*, together with terrestrial green algae from their surroundings, such as *Trentepohlia* (Ulvophyceae) (Figure 1.11) and *Myrmecia* (Trebouxiophyceae), while the maned three-toed sloth *B. torquatus* hosted a variety of purely terrestrial algae. The algae have a distinct distribution patterns in *Choloepus* and *Bradypus*, lying longitudinally along the grooves in the former and in short lateral tongues or lines in the latter. The algae found on the coat of *Bradypus tridactylus* lie between the cuticle scales, and the hair changes with age in apparently all species of *Bradypus.* Young hairs are white, gray, brownish, or black and do not possess the deep cracks seen in older hairs. The first traces of algae appear on these young hairs as tiny dots or extremely narrow transverse lines. Older hairs have larger, wider algal colonies and obvious deep transverse cracks. When wet, these cracks close considerably, but when dry, they give the effects of beads on a string. The oldest hairs are badly deteriorated, with the spongy cuticle worn off on one side, exposing the full length of the cortex. In the older hairs, living algae are absent. It was suggested that either the algae colonize the very narrow cracks in young hairs or the algae themselves initiate the cracks. The hair of all three *Bradypus* species readily absorbs water, but those of *Choloepus* do not. No evidence of algae was found in babies still at the age of clinging to their mothers, suggesting that at least *Trichophilus* is gained in childhood, most likely from the mother. This observation is supported by an earlier study noting that sloths gain the algae and other parasites by the time they are a few weeks old, which could provide them with

protective camouflage. Lack of healthy algal colonies has been observed in *Bradypus* kept in captivity; since they do not survive long under these conditions, algae have been suggested to provide nutrition or a particular trace element essential for the health of the animals.

Algae have also been reported to grow on the fur of polar bears (*Thalarctos maritimus*). These animals normally have creamy-white fur, presumably an adaptation for camouflage in a snowy environment. However, cases have been reported of polar bears kept in captivity in different American and Japanese zoos that turned green as result of algae growing on their fur. The coloration was particularly evident on the flanks, on the outer fur of the legs, and in a band across the rump. This coloration was clearly attributable to the presence of algae inside the hairs, specifically in the hollow medullae of many of the wider (50–200 μm), stiffer guard hairs of the outer coat. The thinner (less than 20 μm) hairs of the undercoat, which were not hollow, were colorless. The fact that some of these lumina were in connection with the external air or water could explain how the algal cells could have entered the hairs in the first place and how exchange of O_2 and CO_2 and uptake of water and mineral salts would be facilitated and could permit growth of the algae if suitably illuminated. Such a habitat has certain advantages, such as being warm and protected from most kind of potential predators. The algae isolated from the polar bear hairs and cultured under controlled conditions were identified as cyanobacteria.

Algae can also establish pathogenic association with both animals and humans. Among the genera most intensely investigated are *Prototheca*, which infect only vertebrates, and *Helicosporidium* (Trebouxiophyceae), which are known so far to invade only invertebrates.

Algae of the genus *Prototheca* (Trebouxiophyceae) are achlorophyllic unicells, spherical to oval in shape, ranging from 3 to 30 μm in diameter. Phylogenetic studies indicate that *Prototheca* spp. cluster with the photosynthetic alga *Auxenochlorella protothecoide* (Trebouxiophyceae) and *Helicosporidium*. Therefore, protothecal species are closely related to the green algae *Chlorella* (Trebouxiophyceae) but lack chloroplasts and possess a two-layered, instead of three-layered, cell wall; they are heterotrophic and require external sources of organic carbon and nitrogen. The life cycle is similar to that of algae of the genus *Chlorella*; reproduction is asexual by internal septation and irregular cleavage, with subsequent rupture and release of 2 to 16 autospores through a characteristic split in the cell wall of the parent cell. Released autospores then go on to develop into mature cells. The taxonomic status of the genus *Prototheca* has changed during the last decades, and currently the following five species are assigned to this genus: *P. zopfii, P. wickerhamii, P. stagnorum, P. ulmea*, and *P. blashkeae*. A sixth species, *P. moriformis*, is not generally accepted. Only two of these species have been documented to cause infections in humans and animals: *P. zopfii* and *P. wickerhamii*. These algae are globally ubiquitous and can be isolated from various reservoirs, such as environment, animals, and food. Typical sources of *Prototheca* species are the slime flux of trees; fresh and marine waters; soil and sewage; stables and animal buildings; excrement; various animals (cattle, deer, dogs); and food items such as butter, potato peels, bananas, and cow's milk.

In 1952, *P. zopfii* was first identified as a pathogen of bovine mastitis associated with reduced milk production characterized by thin watery secretion with white flakes. This form of mastitis is now endemic in the most countries of the world and represents a serious problem, since the affected animals must be culled from their herds to halt transmission of the disease. *Prototheca* also produce disease in humans, and the clinical conditions caused by this alga are generally referred to as protothecosis. The first case of human infection was diagnosed in 1961 in Sierra Leone on a rice farmer; it took the form of a verrucose foot lesion from which *P. zopfii* was isolated as etiological agent. Over the following years, the number of documented cases of protothecosis rose continuously, with about four new cases being diagnosed every year over the past decade. Only a few cases of systemic disease have been reported. Most infections are likely due to traumatic implantation of organisms, but a few cases of opportunistic infection have also been reported. Protothecosis has also been diagnosed among other very different species such as dogs, cats, sheep, deer, Atlantic salmon, carp, and flying foxes.

Despite its non-photosynthetic, obligate heterotrophic nature, *Prototheca* is known to have retained a plastid with starch granules; recent data indicate that several metabolic pathways (e.g.

carbohydrate, amino acid, lipid, and isoprenoid) are located in this non-photosynthetic plastid. The reconstruction of this complex metabolic network could represent a new approach in the treatment of protothecosis.

Algae of the genus *Helicosporidium* (Trebouxiophyceae) are obligate parasites of invertebrates, especially arthropods (insects, mites, crustaceans, and trematodes), which support the growth and development of the parasite in their hemolymph. This alga features three different life stages: cysts, filamentous cells, and vegetative cells. The life cycle begins with an orally transmitted cyst stage that is composed of three ovoid cells and a coiled, elongate filamentous cell enclosed within an outer pellicle. Within the gut of the host, cysts burst open and release a filamentous cell with surface barbs, along with three egg-shaped accessory cells. The barbed filaments proceed to invade the gut cells, penetrating them and emerging into the hemolymph. Vegetative cells have been observed to replicate within the phagocytic hemocytes and to develop extracellularly in the hemolymph. After multiple two- to four-cell autosporogenic cell divisions, a portion of the hemolymph-borne vegetative cells differentiate into cysts. Generally, the infection leads to the death of the host, but the exact mode of transmission remains poorly known.

Helicosporidia contain plastids, and although they have not yet been visually identified, molecular evidence has confirmed their existence. The *Helicosporidium* plastid genome is one of the smallest known (37.5 kb). Its reduced size results from loss of many genes commonly found in plastids of other plants and algae (including all proteins that function in photosynthesis), elimination of duplicated genes and redundant tRNA isoacceptors, and minimization of intergenic spaces. The *Helicosporidium* plastid genome is also highly structured, with each half of the circular genome containing nearly all genes on one strand. Both the structure and content of the plastid genome and the deduced function of the organelle show parallels with the relict plastid found in the apicomplexan malaria parasite *Plasmodium falciparum*. The apicomplexa and *Helicosporidium* are not closely related; indeed, among plastid types, they could hardly be more different: the apicoplast is a secondary plastid derived from a red alga, whereas the *Helicosporidium* plastid is a primary green algal plastid. The cryptic *Helicosporidium* plastid is probably also metabolically more diverse and retains several pathways that have been lost by *Plasmodium*, such as amino acid metabolic pathways. A possible explanation is that *Helicosporidium* can survive in a cyst form outside its host and thus might need more metabolic autonomy than *Plasmodium*, which is entirely host associated throughout its life cycle. These unrelated organisms each evolved from photosynthetic ancestors, and the convergence in form and function of their relict plastids suggests that common forces shape plastid evolution, following the switch from autotrophy to parasitism. If plastid reduction is a continuous process, then *Plasmodium* may simply be further along in the process of reducing a fully functioning plastid to the highly specialized relict we see today.

Extreme Habitats

Cold Environments

Unusual and extreme habitats for algae are represented by very cold environments, such as platelet ice layers, the snowfield, and glaciers. Algal cells adapting to cold temperatures have to take care of the following three processes:

- changing the ratio of saturated and unsaturated fatty acids in the lipids of the cell membranes to maintain membrane fluidity;
- adjusting the permeability of the cell membrane for water to react to osmotic changes of the outer medium; and
- when exposed to freezing temperatures, reducing the water content of the cell interior to prevent ice crystal formation.

Adaptive features include pigments, polyols (sugar alcohols, e.g. glycerin), sugars and lipids (oils), mucilage sheaths, motile stages, and spore formation. Moreover, since the algae living in regions that receive full solar exposure are adapted to a high–UV light environment, they can augment their UV protection capacity, especially during summer months, by producing secondary metabolites, including phenylpropanoids, carotenoids, xanthophylls, and mycosporine amino acids.

In some Antarctic coastal areas, a semi-consolidated layer of platelet ice (flat, disk-shaped ice crystals mixed with sea water, approximately 20% ice and 80% seawater by volume, approximately 0.1 m in diameter and 10 mm thick), ranging from a few cm to several meters in thickness, occur under sea ice located adjacent to floating ice shelves. The platelet ice is intermediate between the relatively impermeable congelation ice above and the water column below, and it is characterized by quite rapid nutrient exchanges. Because it is submerged beneath 1–2 m of consolidated ice, irradiance reaching the platelet ice is first attenuated by the overlying snow cover, sea ice crystals and brine inclusions, particles, and soluble material, resulting in a light field that is reduced in magnitude and restricted in spectral distribution. Nevertheless, reports of high algal production and biomass accumulation in the platelet ice of the Weddell and Ross Seas (Antarctica) attest to the success of the platelet ice microalgal community at growth in these low light conditions. The algae inhabiting the platelet ice layer are extremely shade adapted, typically attaining maximum photosynthetic rates at an irradiance of ≤20 μmol m^{-2} s^{-1}.

Platelet ice provides a much larger surface area for algal attachment and growth than the skeletal layer where most of the biomass within the congelation ice is concentrated. For example, a 0.02-m-thick skeletal layer with ice crystals spaced 0.6 mm apart provides approximately 67 m^2 of surface area per m^2 of horizontal surface, with relatively little interstitial space for seawater exchange. In contrast, a platelet layer 0.6 to 0.7 m thick would have a surface area of approximately 400 m^2 per m^2 of horizontal surface, with a large amount of interstitial space. In addition, the fixed position of the platelets provides a stable substrate that isolates the algae from vertical mixing and holds them in a higher and less variable light field than that available within the underlying water column. Vertical compression of the biomass also reduces the fraction of photosynthetic active radiation absorbed by the ice/water milieu of the platelet layer and increases the fraction absorbed by the algae for use in photosynthesis. Ice microbial communities are dominated by microalgae, primarily diatom species, such as *Nitzschia stellata*, *Pinnularia quadratarea*, *Fragilariopsis sublineata*, and *Melosira arctica* (Bacillariophyceae). The latter diatom has been extensively studied for the effect that its abundant secretion of mucus-like EPS might have on sea ice formation and durability. *Melosira arctica,* together with other unicellular algae, small crustaceans, and bacteria, inhabits the brine channels present in the platelet ice, in which the brine expelled from the ice crystals remains trapped. The particularly potent exopolymers of *M. arctica* lead to more disordered ice crystals, greater pore density, more complex pore geometries, and greater salt retention by the newly formed ice. Exopolymer-enhanced retention of salt in growing sea ice translates to greater retention of other source water impurities, including EPS-producing microalgae. The benefits of ice entrainment to algae include stable positioning to capture more light energy for photosynthesis and refuge from predation. By altering ice physical properties, EPSs precondition the bottom ice layer for optimal habitability, as well as for later survival as the growing ice front becomes colder interior ice with smaller pores of more concentrated brine and biologically protective EPS. The survival benefits extend to Bacteria and Archaea ubiquitous in cold winter ice. For filamentous ice algae that cross the ice–water interface, accessing nutrients in underlying waters, the EPS-mediated geometric complexities of the ice pore space may help anchor filaments.

Sea ice that retains more salt will also retain more of the dissolved constituents of the source water, from carbon dioxide and other greenhouse gases to iron and other nutrients essential to primary production. Their retention, alteration, and eventual release determine the biogeochemical imprint of sea ice on the surface ocean (and atmosphere). The reduction of ice permeability by EPS must also influence the role of sea ice as an inorganic carbon pump from atmosphere to underlying ocean, as well as its seeding and fertilization of surface waters during the melt season.

True snow algae are defined as those that grow and reproduce wholly within the water retained by snow during snowmelt. During summer months, large blooms occur, which can reach cell concentrations of 10^6 cells ml^{-1} and color whole snow banks red, orange, green, or gray depending on the species and habitat conditions. Most snow algae belong to Chlorophyta, such as *Chloromonas rubroleosa* (Chlorophyceae) and *Chlamydomonas nivalis* (Chlorophyceae). These algae color the snow red due to the excess of carotenoids and xanthophylls. Species from other algal groups are also important, and the dominant alga in many of the glaciers around the world is the saccoderm desmid *Mesotaenium berggrenii* (Zygnematophyceae), an alga that colors the snow grey due to its iron tannin compounds. Snow algae go through a complex life history, involving motile vegetative stages that undergo syngamy and thick-walled resting spores and zygotes. The latter allow them to survive the time when the snow has completely melted and probably to be spread by wind. Many of these algae possess vegetative and or motile cells that are usually green in color and immotile spores or cysts that may be red, orange, or yellow-green in color. The green vegetative cells color the snow green, whereas red and orange snow is generally caused by the spore stages, though some snow algae may be red pigmented in their vegetative state. The spores usually have thick walls and large amounts of lipid reserves, polyols, and sugars. They are able to withstand sub-zero temperatures in winter and also high soil temperatures and desiccation in summer, which would kill normal vegetative cells. The motile stages enable them to re-colonize the snow from germinating spores left behind on the soil as well as to position themselves at the optimum depth for photosynthesis in the snow/ice column. The cells of some species also secrete copious amounts of mucilage that enable them to adhere to one another and to snow crystals and prevent the cells from being washed away by melt water. The mucilage also forms a protective coat and delays desiccation, and it may have an additional function as an UV shield. A few species are common worldwide, but others are restricted to either the Northern or Southern hemispheres.

Snow algae sustain a highly diverse microbial community on snow fields and glaciers, which is composed of bacteria, heterotrophic flagellates, and ciliates. These organisms in turn sustain a community of cold-adapted animal species, such as midges, copepods, and snow fleas on Himalayan glaciers and ice worms and collembolas on North American glaciers. Blooms of snow algae can reduce the surface albedo (i.e. the ratio of reflected to incident light; see later) of snow and ice and largely affect their melting.

The ecology of snow algae is important for understanding the glacial ecosystem, since they can be used as indicators to date ice cores drilled from glaciers. Their biomass and community structure inside ice cores may also provide information on the paleo-environment.

Hot Environments

Another example of ecological diversification of algae is the colonization of thermal environments. In these complex high-temperature systems, the microbial and geochemical interactions are highly interwoven, providing many of the basic constituents for the primordial synthesis of organic molecules and for the evolution of fundamental metabolic processes. Present-day hydrothermal venting occurs in both terrestrial and marine environments, primarily as a direct result of geothermal activity associated with plate tectonic movement. Spreading centers, subduction zones, and hot spots release heat from the crust and generate high-temperature water. Wherever fissures develop around hydrothermal vents, water can percolate into the crust and react with the surrounding rock, heating the fluid and altering its chemistry. The altered water will eventually be forced back convectively to the surface as super-heated, highly reduced, hydrothermal fluid rich in gases and minerals. The hydrothermal fluid chemistry is a record of its path within the earth's crust and differs as a function of the underlying rock composition and the residence time of the fluid in the subsurface.

Thermal waters are widely distributed over the face of the earth, although springs are often concentrated in restricted areas. The antiquity of many individual springs is noteworthy. Historical records of springs in the Mediterranean go back to the ancient Greeks and Romans. The largest concentrations of hot springs and fumaroles are found in Yellowstone National Park (USA), Iceland,

New Zealand, Japan, and the USSR. Temperatures of hot springs range from 30°C up to boiling (90°C–100°C depending on altitude). Despite the geochemical constraints (physical and chemical parameters) defining the environmental conditions of hydrothermal systems, these systems do support a plethora of unicellular microalgae. The pH of the habitat defines the composition of phototrophic communities, which greatly differ between alkaline and acidic reaches.

Alkaline hot spring habitats across western North America, Asia, Africa, and possibly Europe have been studied for several decades to understand the composition, structure, and function of microbial communities of thermal environments. Hot spring outflows typically exhibit marked temperature gradients, and microbial communities containing *Synechococcus* (Cyanophyceae, Cyanobacteria) generally develop in these systems at temperatures between about 45°C and 73°C, which is the thermal maximum for photosynthetic life. Studies on the behavior of *C*-phycocyanin from *Synechoccocus lividus* showed that purified *C*-phycocyanin is stable up to least 70°C, and it is highly aggregated, with identical spectroscopic behaviors at 20°C and 70°C. For these characteristics, it is termed a temperature-resistant protein.

Thermoacidic environments are scattered disparately throughout the earth but cluster mainly in volcanic areas that have constant geothermal activity and low pH levels, due primarily to the presence of sulfuric acid as a result of the biological and abiological oxidation of elemental sulfur or hydrogen sulfide. The biology of acid hot springs is quite different from that of neutral/alkaline springs. Though most thermo-acidophiles are prokaryotes (Archea and Bacteria), photosynthetic prokaryotes, such as cyanobacteria, are completely absent from acid water even when the temperature has dropped to quite low values. The photosynthetic microorganisms of such acid water are rare kinds of eukaryotes found nowhere else on earth, the Cyanidiales (Cyanidiophyceae), a group of asexual unicellular red algae. Members of this order are able to live in extreme environments that combine low pH levels (–0.2 to 4.0) and moderately high temperatures of 40°C to 56°C throughout the globe. These algae often form well-developed mats in acidic geothermal locations. How this important physiological resistance is achieved is still not understood, though a strong proton pump or low proton membrane permeability are possibilities.

Three genera, *Cyanidium*, *Galdieria*, and *Cyanidioschyzon,* are recognized. The genera *Cyanidium* and *Cyanidioschyzon* are thought to include a single species each, *Cyanidium caldarium* and *Cyanidioschyzon merolae*, respectively, whereas the genus *Galdieria* has been classified into four species, *Galdieria sulphuraria*, *Galdieria maxima*, *Galdieria partita*, and *Galdieria daedala*, based on cell morphology. The three genera have been distinguished morphologically based on reproductive patterns, chloroplast and mitochondrion shapes, the presence or absence of a vacuole, cell size, and the presence or absence of a cell wall. Strains of the genus *Cyanidioschyzon* are smaller (usually 1 or 2 μm in breadth), with an oval, club-like shape. They reproduce by binary cytokinesis and lack rigid cell walls. *Galdieria* and *Cyanidium* have more spherical shapes, possess rigid cell walls, and reproduce through the formation of 4 to 32 small daughter cells within a mother cell. Chloroplasts vary from a multilobed shape in *G. sulphuraria* to a spherical shape in *Cyanidium*. These algae are not red but blue-green, due to their predominant pigments, C-phycocyanin and chlorophyll *a*. As in the case of *Synechococcus,* C-phycocyanin from *Cyanidium* fits the characteristics of a temperature-resistant protein. Its hallmark for stability is to remain inflexible toward structural change over a wide range of temperatures from 10°C to 50°C. The protein denatures irreversibly at the temperature at which the alga is no longer viable between 60°C to 65°C.

Geothermal environments are well known not only for their high temperature and their extremely acidic or basic pH but also for their elevated content of toxicants like arsenic and copper. Among the Cyanidiales, *Cyanidioschyzon* has been shown to influence arsenic cycling at elevated temperatures by oxidizing arsenite As(III) to arsenate As(V) and to methylate arsenic. The ability of this alga to transform arsenic represents a major mechanism for tolerance to high concentration of arsenic in acidic geothermal settings and contributes to the ecological fitness and ability of this red alga to flourish in such surroundings. Diatoms also have been proved to be thermophilous, acidophilous, and able to survive in toxic environments. An epipelic community of diatoms inhabits the arsenic-rich

hydrous ferric oxide mats that coat the sandy substratum of Beowulf Spring, Yellowstone National Park (YNP), USA, a strongly acidic (pH < 3) and thermophilous (temperature > 50°C) environment with potentially toxic concentrations of dissolved metals. Diatoms are present mainly in the regions of the spring characterized by temperature of 67°C, brown arsenic-rich mats, and pH 2.26. The diatom flora in this area are dominated by a deme within the *Nitzschia thermalis* complex, in association with *N. ovalis, Pinnularia acoricola*, and *Eunotia exigua*. The success of this community may be due to low diatom diversity, hence reduced inter-specific competition and absence of predators, coupled with the potential metabolism of toxic metals.

Dry Environments

Crusts can be defined as microbiotic assemblages formed by living organisms and their by-products, creating a complex surface structure of soil particles bound together by organic material. Some crusts are characterized by their marked increase in surface topography, often referred to as pinnacles or pedicles. Other crusts are merely rough or smooth and flat. The process of creating surface topography, or pinnacling, is due largely to the presence of filamentous cyanobacteria and green algae. These organisms swell when wet, migrating out of their sheaths. After each migration, new sheath material is exuded, thus extending sheath length. Repeated swelling leaves a complex network of empty sheath material that maintains soil structure after the organisms have dehydrated and decreased in size.

Biological sand crusts (BSCs) play an important role in stabilizing sandy desert areas by reducing soil erosion, which generally includes rain and wind erosion, and by their impact on biotic compositions. These crusts represent one of the harshest environments in nature. Organisms inhabiting this ecosystem face frequent hydration/dehydration cycles, extreme light intensities, temperature amplitude from subfreezing during winter nights but up to 60°C on mid-summer days, and vast osmotic potential changes from close to pure rainwater to salt crystals on the crust's upper layer.

To cope with the combination of declining water availability and rising light intensity to levels much higher than those required to saturate photosynthetic demand, photosynthetic organisms inhabiting BSCs must possess efficient survival mechanisms. Crucial for survival is the ability to sense diurnal changes in environmental conditions and rapidly activate metabolism and growth in the short periods when water and sufficient light intensity are available but to turn metabolism off during desiccation. Desert crusts are liable to experience rapid pH rise from around 8 and up to 10.5 consequent on the photosynthetic activity, thereby reducing the dissolved CO_2 level within the crusts. To cope with the limited CO_2 level, a CO_2 concentrating mechanism (CCM) (documented in many photosynthetic microorganisms) is likely activated to enable efficient CO_2 fixation. Indeed, a CCM was described in several crust cyanobacteria. The large fluxes of inorganic carbon and protons associated with CCM activity affect the pH homeostasis of the cells and may help dissipate excess light energy.

Although the erodibility of soil with and without crusts has been quantified, only a few studies have been focused on the specific effects of different algae in stabilization of sand dunes. The recovery rate of cryptogamic crusts (i.e. a thin crust made up of mosses, lichens, algae, and bacteria) in natural and artificial conditions has been examined, as well as the effect of the wind regime (including wind force and types), moisture, crust development, soil texture, vegetation coverage, season, and human activity on algal crust integrity. Most algal crust formation in arid areas is initiated by the growth of cyanobacteria during episodic events of available moisture, with subsequent entrapment of mineral particles by the mechanical net of cyanobacterial filaments and glue of extracellular slime. Algal crusts are critical to the ecosystem in which they occur. Evidence has shown that they may play important roles in the stabilization of soil surfaces and the improvement of soil structure, contributing significantly to soil fertility of these regions through such processes as nitrogen fixation; excretion of extracellular substances; and retention of soil particles, organic matter, and moisture. Nitrogen fixation by cyanobacteria and lichens (due to their

symbiotic cyanobacteria) making up the crusts is the primary source of nitrogen input in many of the arid ecosystems on a worldwide basis. The fascinating points herein are why and how the algal crusts, only a few millimeters thick, play such important roles and how the relevant organisms survive and even flourish in such a harsh environment with extreme desiccation, strong radiation, and large fluctuations of temperature.

Systematic investigations of algal crusts conducted in the Tengger Desert (China) have provided data on the vertical microdistribution of cyanobacterial and algal species within samples aged 42, 34, 17, 8, and 4 years. This vertical distribution was distinctly laminated into an inorganic layer with few algae (0.00–0.02 mm), an algae-dense layer that was relatively compact and densely inhabited with algae (0.02–1.0 mm), and an algae-sparse layer (1.0–5.0 mm). Due to extremely high irradiation, the surface of the inorganic layer was the harshest microenvironment of the desert crusts and therefore was colonized only with the cyanobacteria *Scytonema javanicum* (Cyanophyceae) and *Nostoc flagelliforme* (Cyanophyceae), desiccation-tolerant species possessing high UV-screening pigments. These two heterocystous, diazotrophic species were the only algae found at the depth of approximately 0.02–0.05 mm, while around 0.05–0.10 mm, the coccoid green alga *Desmococcus olivaceus* (Trebouxiophyceae), characterized by strong resistance to stressful environments, was the dominant species. The biggest algal biovolume was present at 0.10–0.15 mm, with the dominance of *Microcoleus vaginatus* (Cyanophyceae), a sheath-forming and polysaccharide-excreting cyanobacterium capable of stabilizing sand grains. The diversity of algal species was the largest in all crust samples at the depth of approximately 0.15–0.50 mm. Filamentous (*Anabaena azotica, Phormidium tenue, Lyngbya cryptovaginatus*) and unicellular (*Gloeocapsa* sp., *Synechocystis pevalekii*) cyanobacteria, unicellular coccoid green algae (*Chlamydomonas* sp., *Chlorococcum humicola*, Chlorophyceae), *Chlorella vulgaris* and *Palmellococcus miniatus* (Trebouxiophyceae), diatoms (*Navicula cryptocephala*, *Diatoma vulgare* var. *ovalis*, and *Hantzschia amphioxys* Bacillariophyceae), and euglenoids (*Euglena* spp. Euglenophyceae) were present. Within the range of approximately 0.50–1.00 mm, there were many more green algae and euglenoids than in the other strata. Because the upper 1 mm of the crust was the euphotic zone (i.e. the zone where enough light penetrates for photosynthesis to occur), more than 96% of the algal bio-volume was distributed in this algae-dense layer (0.02–1.0 mm). By the algae-sparse layer, dramatically reduced irradiance was inadequate for efficient photosynthesis, and therefore this layer had only about 4% of the total algal bio-volume. At 1.0–2.0 mm, species usually found were *L. cryptovaginatus*, *M. vaginatus*, *P. tenue, S. pevalekii*, *N. cryptocephala*, and *H. amphioxys*. At the depth of approximately 2.0–3.0 mm, *P. tenue* was the dominant species, together with diatoms, mainly *N. cryptocephala* and *H. amphioxys*. At the depth of approximately 3.0–4.0 mm, only diatoms were present. The existence of a diatom layer at the crust base might be the result of downward seepage of water and the high motility of these algae. The older the crusts, the nearer to the surface were *Nostoc* sp., *Chlorella vulgaris, Microcoleus vaginatus, Navicula cryptocephala*, and fungi, which might be less resistant to the surface stresses. This might reflect the slow but effective process of algal crust development at early stages, and this process might be beneficial to the transformation from algal crusts to lichen crusts at later stages in consideration of the integration of cyanobacteria and green algae, such as *Nostoc*, with fungi to form lichen.

Another inhabitant of BSC is *Chlorella ohadii* (Trebouxiophyceae), a green microalga isolated from soil crusts in the Negev desert of Israel. Characterized by subfreezing temperatures in winter and extremely high temperatures in summer, this desert is a very harsh habitat. The dry and arid environment is accompanied by intense sunlight during the long desert summer, forcing photosynthetic organisms to develop exceptional mechanisms to avoid photoinhibition. To thrive under these extreme conditions, *C. ohadii* possesses peculiar adaptations, which include a short generation time (2–4 hr), massive reduction of photosystem II (PSII) antenna size, accumulation of protective carotenoids, very rapid repair of photodamaged reaction center proteins, maintained maximum PSII efficiency in high light intensities of 3500 μE m^{-2} sec^{-1}, and metabolic flexibility.

Space

In 1973, the visionary astronomer and planetary scientists Carl Sagan, known worldwide for his crucial research on extraterrestrial life, hypothesized the possibility of re-engineering the planet Venus into a quite Earth-like place by simply seeding the clouds around the second planet from the sun "with a hardy variety of algae, a genus called Nostocaceae was suggested, which would perform photosynthesis in the vicinity of the clouds." His hypothetical scenario was based on the evidence that algae are capable of thriving in really extreme habitats (in the deserts under burning sun, under the ice in the poles); hence, they could have coped as well with the inhospitable atmospheres of other planets. Sagan was deeply convinced that algae would have in time changed the hostile environment of Venus by transforming the CO_2 present in the planet atmosphere into carbon and oxygen and making Venus a much more pleasant place for humans. Carl Sagan's terraforming vision of the planets around us by means of microorganisms was preceded by other visions that, well before the first space launch of a human, focused on the possibility of growing algae in space for the needs of cosmonauts' diets.

Since the beginning of space flight in the early 60s through today's planned experiments, microalgae have been investigated as possible and promising key components of on-board sustainable life-support systems, because they can absorb the exhaled CO_2 from the cabin air, produce O_2 as a side product, recycle waste as a nutrient source (e.g. urine and flash water) and produce edible biomass in situ in closed environmental systems at any place and at any time. With increasing mission durations up to years, space travelers will need oxygen, fresh water, and nutritional food to survive, and the supply will have to become independent from Earth; hence, the particular characteristics of microalgae will be of crucial importance to minimize resupply needs and the carried mass.

Regarding utilization in Earth orbit or deep space, microalgae require regeneration capacity towards cosmic radiation and the capability to withstand microgravity effects. To date, more than 50 experiments with algae flown in low earth orbit have been identified. The species that have been investigated are mainly Trebouxiophyceae from the genus *Chlorella* (*Chlorella vulgaris, Chlorella pyrenoidosa, Chlorella sorokiniana, Chlorella ellipsoidea*), which have been proven to survive continuous exposure to ionizing irradiation under preservation of more than 90% of their initial photosynthetic capacity, maintaining the highest oxygen-evolving capacity, and to withstand microgravity conditions for up to 180 days continuous culture. Other Chlorophyceae, such as *Chlamydomonas reinhardtii*, *Scenedesmus obliquus*, and *Sphaerocystis sphaerocystiformis*, and the trebouxiophycean *Rosenvingiella radicans* have also been flown. Among cyanobacteria, *Nostoc sphaeroides, Gloeocapsa* sp., and *Anabaena siamensis* have been employed in spaceflight experiments.

The cyanobacterium *Nostoc* sp. PCC7524 and a plastid mutant of the eukaryotic alga *Euglena gracilis* flew on board a Long March II Chinese rocket to space in 1987. In this experiment, the plastid mutant alga was the O_2 consumer and CO_2 producer, and the cyanobacterium produced O_2 and consumed CO_2. Both organisms survived the 4.5 days in space, and some of the cyanobacteria grew under illumination. This experiment is often referred to as the origin of MELiSSA, the Micro-Ecological Life Support System developed by the European Space Agency (ESA) in 1988, which combined physicochemical technologies with microbial and plant conversion of organic and inorganic waste into nutrients and biological air revitalization.

In later years, there were also some approaches with cyanobacteria like *Nostoc commune* var. *sphaeroides, Anabaena siamensis,* and *Arthrospira indica*. The latter was used in the *Arthrospira*-B experiment, which was launched to the International Space Station (ISS) in 2017 and which was the first approach to allow online measurements of the O_2 production rate and growth rate in space. Additionally, the cultures were kept axenic over the entire duration of over one month. To date, this experiment is the most sophisticated successful approach to run an instrumented photobioreactor on board a space station.

Algae in both photosynthetically active and inactive states have been shown to survive exposure to a variety of spaceflight cabin conditions, including radiation and weightlessness. Most importantly, it has been demonstrated that even direct exposure to the vacuum environment of space can

be withstood by inactive algae, which is important for stored inoculation cultures during emergencies such as a depressurization or during uncrewed time periods of a mission. This ability can greatly enhance the reliability of bioregenerative life support systems in general.

ENDOSYMBIOSIS AND THE ORIGIN OF EUKARYOTIC PHOTOSYNTHESIS

The origin of cyanobacteria can be equated with the origin of aerobic photosynthesis around 2.8 billion years ago, in the Archaean Era of Earth history. From that time to the present, cyanobacteria have played fundamental roles in driving much of the ocean carbon, oxygen, and nitrogen fluxes, establishing a major turning point in the biogeochemistry of our planet. Prior to the appearance of these organisms, all photosynthetic organisms were anaerobic bacteria that used light to couple the reduction of carbon dioxide to the oxidation of low free-energy molecules, such as H_2S or preformed organics. Cyanobacteria developed a key characteristic that distinguished them from their photosynthetic evolutionary precursors, the ability to extract electrons from water, releasing oxygen as a byproduct, with the help of two photosystems linked in series. Oxygenic photosynthesis exploits the energy of visible light to oxidize water and simultaneously reduces CO_2 to organic carbon, represented by $(CH_2O)_n$. Light energy is used as a substrate and chlorophyll *a* as a requisite catalytic agent.

Formally oxygenic photosynthesis can be summarized as:

$$CO_2 + H_2O + \text{light} \xrightarrow{\text{Chlorophyll } a} (CH_2O)_n + O_2$$

Thanks to endosymbiosis, the photosynthetic trait was acquired in the founding group of photosynthetic eukaryotes, the Plantae or Archaeplastida, and spread to give rise to the wide variety of photosynthetic eukaryotes on earth today. The origins of plastids in eukaryotic cells about 1.8 billion years ago are one the most profound effects of the endosymbiotic process. These organelles have been well established to have evolved from a single so-called "primary endosymbiotic event" involving the uptake of a β-cyanobacterium by a heterotrophic/phagotrophic eukaryote, whose ancestors had already acquired a mitochondrion via endosymbiosis of a proteobacterium. Plastid genomes rarely encode more than 200 proteins, which represent a small fraction of the proteins required for full functionality and an even smaller fraction of the few thousands proteins found in modern-day cyanobacteria. It is widely assumed that in the process of endosymbiosis, most endosymbiont genes were either lost, together with the corresponding function, or transferred to the host nucleus and merged into the chromosomes during the course of plastid integration. This migration of genes between two genomes is known as endosymbiotic gene transfer, a special case of horizontal gene transfer. Over time, some acquired targeting sequences that enabled their products synthesized on cytoplasmic ribosomes to be targeted back to the organelle. In addition, some host genes acquired targeting sequences that enabled their products to be imported into the organelle. All these processes played a fundamental role in the integration of endosymbiont and host. "Primary plastids" are surrounded by two bounding membranes and are only found in three major eukaryotic photosynthetic groups of Plantae, that is, Glaucophyta, Chlorophyta, and Rhodopyta.

Glaucophyta occupy a key position in the evolution of plastids; in fact, the plastids of glaucophytes contain chlorophyll *a*, present in cyanobacteria, and retain the remnant of a Gram-negative bacterial peptidoglycan wall that would have been between the two membranes of the cyanobacterial ancestor symbiont. The retention of this ancestral character is absent in both green and red plastids.

Chlorophyta (green algae and plants) constitute the second lineage of primary plastids. The simple two-membrane system surrounding the plastid, the congruence of phylogenies based on nuclear and organellar genes, and the antiquity of the green algae in the fossil record all indicate that the green algal plastid is of primary origin. In these chloroplasts, chlorophyll *b* was synthesized as a secondary pigment, phycobiliproteins were lost, and starch was stored. Another hypothesis suggested that the photosynthetic ancestor of green lineage was a prochlorophyte that possessed chlorophylls *a* and *b* and lacked phycobiliproteins.

The green lineage played a major role in oceanic food webs and the carbon cycle from about 2.2 billion years ago until the end-Permian extinction, approximately 250 million years ago. It was this similarity to the pigments of plants that led to the inference that the ancestors of land plants (i.e. embryophytes) would be among the green algae, and it is clear that phylogenetically, plants are a group of green algae adapted to life on land.

The plastids of Rhodophyta (red algae) constitute the third primary plastid lineage. Like the green algae, the red algae are an ancient group in the fossil record, and some of the oldest fossils interpreted as being of eukaryotic origin are often referred to the red algae, although clearly these organisms were very different from any extant alga. Like those of green algae, the plastids of red algae are surrounded by two membranes. However, they are pigmented with chlorophyll *a,* phycobiliproteins, organized into phycobilisomes, and are distinguished by the presence of phycoerithrin. Phycobilisomes are relatively large extrinsic antennas, water-soluble, and attached to the surface of the thylakoid membrane. Thylakoids with phycobilisomes do not form stacks like those in other plastids, and consequently the plastids of red algae (and glaucophytes) bear an obvious ultrastructural resemblance to cyanobacteria.

Though the plastids of these three lineages are all primary plastids, that is, having only two membranes around them, they differ more noticeably in their light-harvesting machinery. Green algae and plants have membrane-intrinsic antenna proteins (members of the light-harvesting complex, LHC, superfamily) that bind both chlorophylls *a* and *b* and are associated with both photosystems. Red algae have proteins of the same family that bind only chlorophyll *a* and are associated with photosystem I. Glaucophytes do not have this type of antenna, but, along with the red algae, they have phycobilisomes, extrinsic antennas which bind linear tetrapyrroles.

Molecular phylogeny supports two possible evolutionary scenarios for the branching order within Plantae, the red-first and glaucophyte-first hypotheses. The inability to unambiguously decide between these two using genome-wide analyses may be explained by the more than 1 billion years that have passed since primary endosymbiosis. The early period of Plantae evolution was likely characterized by a rapid radiation; reticulate evolution (by horizontal gene transfer) among taxa; and high rates of gene divergence, loss, and replacement that have diffused the evolutionary signal. This idea is supported by the findings regarding mitochondrial gene order and gene content that do not favor a particular order of branching.

As ancient as the primary endosymbiotic origin of plastid was (1.8 billion years ago), it is worth noting that cases of "recent" cyanobacterium-eukaryote endosymbiosis are known, for example, in the testate amoeba *Paulinella cromatophora* and the diatom *Rhopalodia gibba*. The photosynthetic consortium between *Paulinella* and an α-cyanobacterium was established 60 million years ago. This amoeba is surrounded by the cell wall called theca, which is composed of silica scales. Apart from typical eukaryotic organelles such as nucleus and mitochondria, it harbors two cyanobacterium-derived endosymbionts. The endosymbionts are photosynthetically active and deeply integrated with the host cell, and their genome has been reduced to one third in comparison to their cyanobacterial ancestors. The pennate diatom *Rhopalodia gibba* harbors endosymbionts closely related to extant cyanobacteria. Some of the closest free-living relatives of these so-called spheroid bodies are diazotrophic cyanobacteria of the *Cyanothece* sp. group. The spheroid bodies encode genes for nitrogen fixation and have the capacity to fix molecular nitrogen under light conditions only, unlike all other unicellular nitrogen-fixing cyanobacteria. Although the spheroid bodies are of cyanobacterial origin, they lack the typical photosynthetic pigmentation.

Plantae, that is, Glaucophyta, Chlorophyta, and Rhodopyta, represent just the beginning of the endosymbiosis story. In fact, whereas mitochondria originated once and have apparently never been lost, plastids have spread between eukaryotic lineages several times in events referred to as secondary and tertiary endosymbiosis, that is, the uptake and retention of a primary or secondary algal cell by another eukaryotic lineage. Euglenozoa and Cercozoa derived from this primary plastid lineage by two separate secondary endosymbiosis acquiring the plastid by engulfing a green alga. Two

independent lineages of green algae were captured by two distinct lineages of phagotrophic protists via secondary endosymbiosis; chloroplast genome analyses suggest that the chlorarachniophyte plastid is derived from a green alga belonging to the "core chlorophyte" group (Trebouxiophyceae, Ulvophyceae, Chlorophyceae), while the ancestor of the euglenophyte plastid is related to prasinophyte green algae. There is no strong similarity between the plastid of euglenids and chlorarachniophytes: euglenids have plastids bounded by three membranes and store paramylon in the cytosol, whereas chlorarachniophytes have plastids bounded by four membranes with a nucleomorph and store β-1-3-glucan in the cytosol.

Euglenozoa contains photoautotrophic species and species with different types of feeding strategies, osmotrophic (e.g. *Rhabdomonas*) or phagotrophic (e.g. *Peranema*). The plastid has been subsequently and independently lost in several branches within the phototrophic clade. Current knowledge on the phylogeny of euglenozoa implies that the secondary endosymbiotic event happened after the split of *Peranema* but before the split of *Eutreptia* and *Eutreptiella*, which form the basal lineages of the phototrophic clade. Recently, a number of red algal origin genes have been identified in the photosynthetic *Euglena gracilis* as well as in the heterotrophic *Peranema*. It is likely that these genes have been acquired via eukaryote-to-eukaryote lateral gene transfer, giving rise to a complex pattern of genome mosaicism in euglenids. These genes may come from prey organisms, and the lineage of euglenids might have experienced a cryptic red algal plastid endosymbiosis before the current green algal plastid was established. Derived genes may have contributed to the successful integration and functioning of the green algal secondary plastid in modern-day euglenids.

Multiple red algal–derived Calvin cycle genes have been detected also in Cercozoa (Chlorarachniophyceae) nuclear genomes. One possible explanation is that these genes were transferred from red alga prey organisms via horizontal gene transfer. The prey organism might have been captured by and retained in an ancestral and probably non-photosynthetic chlorarachniophyte as an endosymbiont, which was then replaced by a green algal endosymbiont, giving rise to the extant secondary plastid in Chlorarachniophyceae. The plastids of cryptophytes, ochrophytes, dinoflagellates, and haptophytes likely arose from a single initial event of secondary endosymbiosis of a red alga with a non-photosynthetic eukaryotic host. The red alga eventually evolved chlorophyll *c* plastids and engaged in several subsequent higher-order endosymbiosis with phylogenetically diverse hosts (in an order still to be resolved), hence giving rise to all the extant photosynthetic lineages. The derivation of chlorophyll *c*–containing plastids from the red algal lineage is still somewhat conjectural, but recent analyses of both gene sequences and gene content are consistent with this conclusion.

The cryptophytes were the first group in which secondary plastids were recognized, on the basis of their complex four-membrane structure. Like red algae, they have chlorophyll *a* and phycobiliproteins, but these are distributed in the intrathylakoidal space rather than in the phycobilisomes found in red algae, Glaucophyta, and Cyanophyta. In addition, cryptomonads possess a second type of chlorophyll, chlorophyll *c*, which is found in the plastids of the remaining red lineage clades; retain the nucleomorph, vestigial nucleus of their symbiont; and have starch in the periplastid space, the reserve polysaccharide of red algae.

Ochrophyta (including kelps, diatoms, chrysophytes, and related groups), Haptophyta (the coccolithophorids), and probably those dinoflagellates (Miozoa) pigmented with peridinin have chlorophylls *a* and *c*, along with a variety of carotenoids for pigmentation. Stacked thylakoids are found in those lineages (including the cryptomonads) that lack phycobilisomes.

The plastid situation in dinoflagellates is exceptionally complex; most of the phototrophic species harbor a plastid of red algal origin bound by three membranes and characterized by the carotenoid peridinin and chlorophylls *a* and c_2. It has been speculated that the ancestral peridinin-containing chloroplast was replaced by one from a cryptophyte, a haptophyte, a diatom, or a green alga, that is, by additional endosymbiotic events, namely tertiary endosymbiosis in the first three cases and serial secondary endosymbiosis for the green alga. These symbiotic

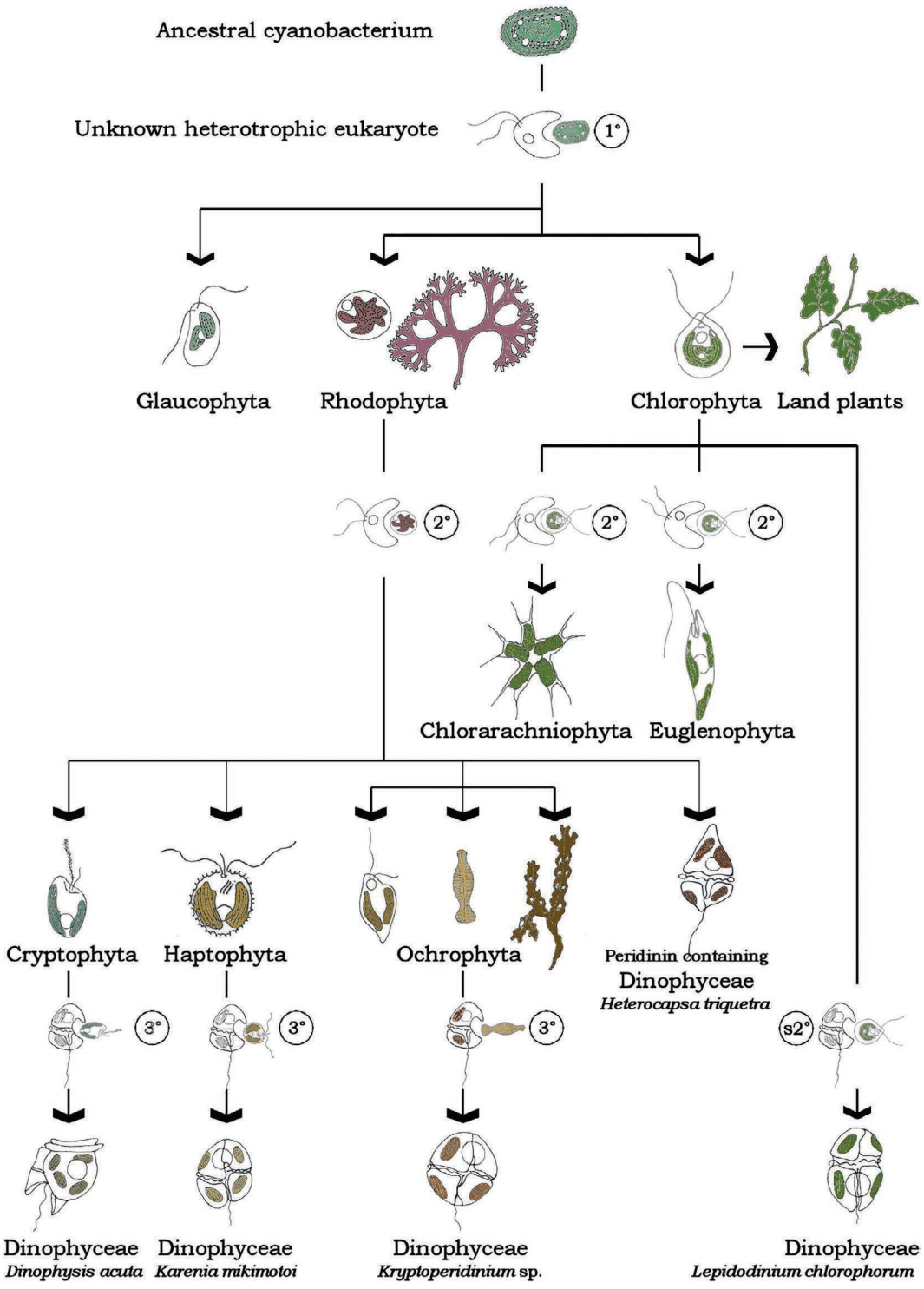


FIGURE 1.58 Hypothesis for algal evolution and endosymbiotic events. 1°, primary endosymbiosis; 2°, secondary endosymbiosis; s2°, serial secondary endosymbiosis; 3°, tertiary endosymbiosis.

relationships have not all reached the same level of permanence, and sometimes it is disputed whether the plastids are the traces of a stable symbiosis or kleptoplastids, that is, plastids obtained from ingested algal prey and retained, which may remain temporarily functional and be used for photosynthesis by the predator. In some cases, the endosymbiont is present in an almost unchanged form and was therefore established more recently (e.g. *Kryptoperidinium foliaceum*). In other cases, the symbiont has lost almost all organelles, and only the chloroplast remains (e.g. peridinin-containing species, *Heterocapsa*, *Peridinium*), indicating an older, more well-established symbiosis. Members of the Kareniaceae (*Karenia mikimotoi*, *Karlodinium micrum*) possess fucoxanthins as accessory pigments instead of peridinin; molecular data confirmed that the peridinin-containing chloroplast in this group has been superseded by a haptophyte-type containing fucoxanthin. Other dinoflagellates like *Dinophysis acuminata* have established a stable symbiosis with a cryptophyte symbiont, of which only the chloroplast remains, surrounded by three membranes. A diatom symbiont is present in a small group of closely related dinoflagellates named "dinotoms" consisting of only ten species such as *Durinskia baltica, Kryptoperidinium foliaceum, Peridinium quinquecorne,* and other species belonging to the genera *Galeidinium* and *Gymnodinium.* The endosymbionts have been shown to originate from three different diatom lineages, one pennate and two centric. Despite the loss of a distinctive cell wall, motility, and ability to divide mitotically, these endosymbionts have retained a large nucleus with vast amount of DNA and a large volume of cytoplasm, separated from the host by a single membrane, and their own mitochondria in addition to the chloroplasts. Another unique symbiosis is present in the dinoflagellate genus *Lepidodinium*; members of this genus such as *L. viride* (Figure 1.1bh, courtesy of Francisco Rodriguez Hernandez) and *L. chlorophorum* (formerly *Gymnodinium chlorophorum*) possess green-colored plastids containing chlorophylls *a* and *b*. The pigment composition, phylogenetic analyses of plastid-encoded genes, and a survey of nuclear genes encoding plastid-targeted proteins in *Lepidodinium chlorophorum* clearly indicated that the ancestral *Lepidodinium* cells replaced the original plastids containing Chl–*a* + *c* with the Chl–*a* + *b*–containing plastid of an endosymbiotic green alga belonging to the core chlorophytes. Only the symbiont chloroplast remains in these dinoflagellates. A schematic drawing of the hypothesis of the different symbiotic events is shown in Figure 1.58.

SUGGESTED READING

Abu-Ghosh, S., Dubinsky, Z. and Iluz, D. Acclimation of thermotolerant algae to light and temperature interaction. Journal of Phycology, 56, 662–670, 2020.

Adl, S.M., Simpson, A.G.B., Lane, C.E., Lukeš, J., Bass, D., Bowser, S.S., Brown, M.W., Burki, F., Dunthorn, M., Hampl, V., Heiss, A., Hoppenrath, M., Lara, E., le Gall, L., Lynn, D.H., McManus, H., Mitchell, E.A.D., Mozley-Stanridge, S.E., Parfrey, L.W., Pawlowski, J., Rueckert, S., Shadwick, L., Schoch, C.L., Smirnov, A. and Spiegel, F.W. The revised classification of eukaryotes. Journal of Eukaryotic Microbiology, 59, 429–514, 2012.

Algaebase. www.algaebase.org/

Anand, N., Thajuddin, N. and Dadheech, P.K. Chapter 3 – Cyanobacterial taxonomy: Morphometry to molecular studies. In: Cyanobacteria, Mishra, A.K., Tiwari, D.N. and Rai, A.N. (Eds.).

Academic Press, Cambridge, MA, 2019.

Andersen, R.A. Biology and systematics of heterokont and haptophyte algae. American Journal of Botany, 91, 1508–1522, 2004.

Bartlau, N., Wichels, A., Krohne, G., Adriaenssens, E.M., Heins, A., Fuchs, B.M., Amann, R. and Moraru, C. Highly diverse flavobacterial phages as mortality factor during North Sea spring blooms. bioRxiv, 10.11 01/2021.05.20.4449362021.2005.2020.444936, 2021.

Bendif, E.M., Probert, I., Hervé, A., Billard, C., Goux, D., Lelong, C., Cadoret, J.P., Véron, B. Integrative taxonomy of the pavlovophyceae (haptophyta): A reassessment. Protist, 162, 738–761, 2011.

Bhattacharya, D., Price, D.C., Yoon, H.S., Yang, E.C., Poulton, N.J., Andersen, R.A., et al. Single cell genome analysis supports a link between phagotrophy and primary plastid endosymbiosis. Scientific Reports, 2, 356, 2012.

Bourrelly, P. Les Algue d'eau douce. Initiation à la Systèmatique. Les algues verdes. Editions N.Boubèe, Paris, 1966.
Bourrelly, P. Les Algue d'eau douce. Initiation à la Systèmatique. Les algues jaunes et brunes. Editions N.Boubèe, Paris, 1968.
Bourrelly, P. Les Algue d'eau douce. Initiation à la Systèmatique. Eugleniens, Peridinies, Algues rouges et Algues bleues. Editions N.Boubèe, Paris, 1970.
Brodie, J., Ball, S.G., Bouget, F.Y., Chan, C.X., De Clerck, O., Cock, J.M., Gachon, C., Grossman, A.R., Mock, T. and Raven, J.A. Biotic interactions as drivers of algal origin and evolution. New Phytologist, 216, 670–681, 2017.
Burki, F., Okamoto, N., Pombert, J.-F. and Keeling, P.J. The evolutionary history of haptophytes and cryptophytes: phylogenomic evidence for separate origins. Proceedings of the Royal Society B: Biological Sciences, 279:1736, 2246–2254, 2012.
Carr, N.G. and Whitton, B.A. The biology of cyanobacteria. Blackwell Scientific, Oxford, 1982.
Charon, J., Murray, S. and Holmes, E.C. Revealing RNA virus diversity and evolution in unicellular algae transcriptomes. Virus Evolution, 7, veab070, 2021.
Chen, Y. and Zeng, Q. Temporal transcriptional patterns of cyanophage genes suggest synchronized infection of cyanobacteria in the oceans, Microbiome, 8, 1–9, 2020.
Cirri, E. and Pohnert, G. Algae–bacteria interactions that balance the planktonic microbiome. New Phytologist, 223, 100–106, 2019.
Coy, S.R., Gann, E.R., Pound, H.L., Short, S.M. and Wilhelm, S.W. Viruses of eukaryotic algae: Diversity, methods for detection, and future directions. Viruses, 10, 487, 2018.
Dial, R. and Ditto, J. The biogeography of the glacier biome. In: Encyclopedia of the world's biomes, Goldstein, M.I. and Della Sala, D.A. (Eds.). Elsevier, Oxford, 2020.
Dorrell, R.G. and Smith, A.G. Do red and green make brown? Perspective on plastid acquisition within chromoalveolates. Eukaryotic Cell, 10:7 856–868, 2011.
Garcia-Cuetos, L., Moestrup, Ø., Hansen, P.J. and Daugbjerg, N. The toxic dinoflagellate *Dinophysis acuminata* harbors permanent chloroplasts of cryptomonad origin, not kleptochloroplasts. Harmful Algae, 9:1, 25–38, 2010.
Graham, L.E. and Wilcox, L.W. Algae. Prentice Hall, Upper Saddle River, New Jersey, 2000.
Green, B. After the primary endosymbiosis: an update on the chromalveolate hypothesis and the origins of algae with Chl *c*. Photosynthesis Research, 107:1, 103–115, 2011.
Green, B.R. Chloroplast genomes of photosynthetic eukaryotes. The Plant Journal, 66, 33–44, 2011.
Häder, D.P. On the way to Mars—Flagellated algae in bioregenerative life support systems under microgravity conditions. Frontiers in Plant Science, 1621, 2020.
Heesch, S., Serrano–Serrano, M., Barrera–Redondo, J., Luthringer, R., Peters, A.F., Destombe, C., Cock, J.M., Valero, M., Roze, D. and Salamin, N. Evolution of life cycles and reproductive traits: insights from the brown algae. Journal of Evolutionary Biology, 34, 992–1009, 2021.
Helliwell, K.E., Lawrence, A.D., Holzer, A., Kudahl, U.J., Sasso, S., Kräutler, B., Scanlan, D.J., Warren, M.J. and Smith, A.G. Cyanobacteria and eukaryotic algae use different chemical variants of vitamin B12. Current Biology, 26, 999–1008, 2016.
Imanian, B., Pombert, J.F., Dorrell, Ri G., Burki, F. and Keeling, P.J. Tertiary endosymbiosis in two dinotoms has generated little change in the mitochondrial genomes of their dinoflagellate hosts and diatom endosymbionts. PLoS One, 7, 1–13, 2012.
Janouškovec, J., Horák, A., Oborník, M., Lukeš, J. and Keeling, P.J. A common red algal origin of the apicomplexan, dinoflagellate, and heterokont plastids. PNAS 15, 10949–10954, 2010.
Kaup, M., Trull, S. and Hom, E.F. On the move: Sloths and their epibionts as model mobile ecosystems. Biological Reviews, 96, 2638–2660, 2021.
Kawachi, M., Inouye, I., Honda, D., O'Kelly, C.J., Bailey, J.C., Bidigare, R.R., et al. The Pinguiophyceae classis nova, a new class of photosynthetic stramenopiles whose members produce large amounts of omega-3 fatty acids. Phycological Research, 50:1, 31–47, 2002.
Keeling, P.J. The number, speed, and impact of plastid endosymbiosis I eukaryotic evolution. Annual Review of Plant Biology, 64:27, 1–27.25, 2013.
Khan, A.L., Dierssen, H.M., Scambos, T.A., Höfer, J. and Cordero, R.R. Spectral characterization, radiative forcing and pigment content of coastal Antarctic snow algae: Approaches to spectrally discriminate red and green communities and their impact on snowmelt. The Cryosphere, 15, 133–148, 2021.
Kim, E. and Archibald, J.M. Plastid evolution: Gene transfer and the maintenance of "stolen" organelle. BMC Biology, 8, 73–76, 2010.

Knowles, B., Bonachela, J.A., Behrenfeld, M.J., Bondoc, K.G., Cael, B., Carlson, C.A., Cieslik, N., Diaz, B., Fuchs, H.L. and Graff, J.R. Temperate infection in a virus–host system previously known for virulent dynamics. Nature Communications, 11, 1–13, 2020.

Küpper, F.C., Tsiamis, K., Johansson, N.R., Peters, A.F., Salomidi, M., Manousakis, L., Kallergis, M., Graham, M.H., Kinlan, B. and Mystikou, A. New records of the rare deep-water alga *Sebdenia monnardiana* (Rhodophyta) and the alien *Dictyota cyanoloma* (Phaeophyceae) and the unresolved case of deep-water kelp in the Ionian and Aegean Seas (Greece). Botanica Marina, 62, 577–586, 2019.

Lane, C.E. and Archibald, J.M. The eukaryotic tree of life: endosymbiosis takes its TOL. Trends in Ecology & Evolution, 23:5, 268–275, 2008.

Leliaert, F., Smith, D.R., Moreau, H., Herron, M.D., Verbruggen, H., Delwiche, C.F. and De Clerck, O. Phylogeny and molecular evolution of the green algae. Critical Reviews in Plant Sciences, 31, 1–46, 2012.

Levin, G., Kulikovsky, S., Liveanu, V., Eichenbaum, B., Meir, A., Isaacson, T., Tadmor, Y., Adir, N. and Schuster, G. The desert green algae *Chlorella ohadii* thrives at excessively high light intensities by exceptionally enhancing the mechanisms that protect photosynthesis from photoinhibition. The Plant Journal, 106, 1260–1277, 2021.

Liu, X., Bogaert, K., Engelen, A.H., Leliaert, F., Roleda, M.Y. and De Clerck, O. Seaweed reproductive biology: Environmental and genetic controls. Botanica Marina, 60, 89–108, 2017.

Lukeš, J., Leander, B.S. and Keeling, P.J. Cascades of convergent evolution: The corresponding evolutionary histories of euglenozoans and dinoflagellates. PNAS 106, 9963–9970, 2009.

Mackiewicz, P., Bodył, A. and Gagat, P. Protein import into the photosynthetic organelles of *Paulinella chromatophora* and its implications for primary plastid endosymbiosis. Symbiosis, 58, 1–3, 99–107, 2012.

Malavasi, V., Soru, S. and Cao, G. Extremophile Microalgae: The potential for biotechnological application. Journal of Phycology, 56, 559–573, 2020.

Matsumoto, T., Ishikawa, S.A., Hashimoto, T. and Inagaki. Y. A deviant genetic code in the green alga-derived plastid in the dinoflagellate *Lepidodinium chlorophorum*. Molecular Phylogenetics and Evolution, 60:1, 68–72, 2011.

Miyagishima, S.Y. Mechanism of plastid division: From a bacterium to an organelle. Plant Physiology, 155:4, 1533–1544, 2011.

Moniruzzaman, M., Weinheimer, A.R., Martinez-Gutierrez, C.A. and Aylward, F.O. Widespread endogenization of giant viruses shapes genomes of green algae. Nature, 588, 141–145, 2020.

Nelson, D.R., Hazzouri, K.M., Lauersen, K.J., Jaiswal, A., Chaiboonchoe, A., Mystikou, A., Fu, W., Daakour, S., Dohai, B. and Alzahmi, A. Large-scale genome sequencing reveals the driving forces of viruses in microalgal evolution. Cell Host & Microbe, 29, 250–266, e258, 2021.

Niederwieser, T., Kociolek, P. and Klaus, D. A review of algal research in space. Acta Astronautica, 146, 359–367, 2018.

Nissimov, J.I., Campbell, C.N., Probert, I. and Wilson, W.H. Aquatic virus culture collection: An absent (but necessary) safety net for environmental microbiologists. Applied Phycology, 1–15, 2020.

Qiu, D., Huang, L., Liu, S. and Lin, S. Nuclear, mitochondrial and plastid gene phylogenies of *Dinophysis miles* (dinophyceae): Evidence of variable types of chloroplasts. PLoS One, 6:12, e29398, 2011.

Ramanan, R., Kim, B.-H., Cho, D.-H., Oh, H.-M. and Kim, H.-S. Algae–bacteria interactions: Evolution, ecology and emerging applications. Biotechnology Advances, 34, 14–29, 2016.

Revellame, E.D., Aguda, R., Chistoserdov, A., Fortela, D.L., Hernandez, R.A. and Zappi, M.E. Microalgae cultivation for space exploration: Assessing the potential for a new generation of waste to human life-support system for long duration space travel and planetary human habitation. Algal Research, 55, 102258, 2021.

Roach, T.N., Little, M., Arts, M.G., Huckeba, J., Haas, A.F., George, E.E., Quinn, R.A., Cobián-Güemes, A.G., Naliboff, D.S. and Silveira, C.B. A multiomic analysis of in situ coral–turf algal interactions. Proceedings of the National Academy of Sciences, 117, 13588–13595, 2020.

Stephens, T.G., Gabr, A., Calatrava, V., Grossman, A.R. and Bhattacharya, D. Why is primary endosymbiosis so rare? New Phytologist, 231, 1693–1699, 2021.

Timme, R.E., Bachvaroff, T.R. and Delwiche, C.F. Broad phylogenomic sampling and the sister lineage of land plants. PLoS One 27, 1–8, 2012.

Tirichine, L. and Bowler, C. Decoding algal genomes: Tracing back the history of photosynthetic life on Earth. The Plant Journal, 66, 45–57, 2011.

Treves, H., Murik, O., Kedem, I., Eisenstadt, D., Meir, S., Rogachev, I., Szymanski, J., Keren, N., Orf, I. and Tiburcio, A.F. Metabolic flexibility underpins growth capabilities of the fastest growing alga. Current Biology, 27, 2559–2567, e2553, 2017.

Van den Hoek, C., Mann, D.G. and Jahns, H.M. Algae—An introduction to phycology. Cambridge University Press, Cambridge, United Kingdom, 1995.

Xia S., Zhang, Q., Zhu, H., Cheng, Y., Liu, G. and Hu, Z. Systematics of a kleptoplastidal dinoflagellate, *Gymnodinium eucyaneum* Hu (Dinophyceae), and its cryptomonad endosymbiont. PLoS One, 8, 1, e53820, 2013.

Yamaguchi, H., Nakayama, T., Kai, A. and Inouye, I. Taxonomy and phylogeny of a new kleptoplastidal dinoflagellate, *Gymnodinium myriopyrenoides* sp. nov. (Gymnodiniales, Dinophyceae), and its cryptophyte symbiont. Protist, 162, 4, 650–667, 2011.

Zapata, M., Fraga, S., Rodríguez, F. and Garrido, J.L. Pigment-based chloroplast types in dinoflagellates. Marine Ecology Progress Series, 465, 33–52, 2012.

Zechman, F.W., Verbruggen, H., Leliaert, F., Ashworth, M., Buchheim, M.A., Fawley, M.W., Spalding, H., Pueschel, C.M., Buchheim, J.A., Verghese, B. and Hanisak, M.D. An unrecognized ancient lineage of green plants persists in deep marine waters. Journal of Phycology, 46, 1288–1295, 2010.

2 Biogeochemical Role of Algae

THE ROLES OF ALGAE IN BIOGEOCHEMISTRY

Biogeochemical cycling can be defined as the movement and exchanging of both elements and energy between the four different components of the Earth, namely the atmosphere (the air envelope that surrounds the Earth), the hydrosphere (includes all the Earth's water that is found in streams, lakes, seas, soil, groundwater, and air), the lithosphere (the solid inorganic portion of the Earth, including the soil, sediments, and rock that form the crust and upper mantle and extend about 80 km deep), and the biosphere (all the living organisms). Cycling means that the four spheres are not mutually exclusive but overlap and intersect in a quite dynamic way. The lithosphere and atmosphere overlap because soils contain air and exchange gases with the atmosphere, but soils contain also water, so the lithosphere and hydrosphere overlap. In turn, the atmosphere contains dust from the lithosphere and water from the hydrosphere, forming a continuum. Last, organisms are present everywhere in water bodies, soils, aquifers, and the atmosphere, so the biosphere overlaps with the other three spheres. Chemical elements are cyclically transferred within and among the four spheres, with the total mass of the elements in all of the spheres being conserved, though chemical transformations can change their form, leading to a dynamic equilibrium between the various forms.

The biogeochemical cycle of any element describes pathways which are commensurate with the movement of the biologically available form of that element throughout the biosphere (where the term "biological availability" is used to imply the participation of a substance in a "biological" reaction as opposed to its simple presence in biota). The most efficient cycles are often equated with a high atmospheric abundance of the element, as in the case of nitrogen, which forms about 78% of the Earth's atmosphere. These cycles ensure a rapid turnover of the element and have the flexibility to process it in a number of different forms or phases (i.e. solid, liquid, gaseous). All biogeochemical cycles are driven directly or indirectly by the radiant energy of the sun, except in a few rare situations, as in the case of phosphorus, whose turnover is determined by tectonic events. Energy is absorbed, converted, temporarily stored, and eventually dissipated, essentially in a one-way process (which is fundamental to all ecosystem function). In contrast to energy flow, all elements that become incorporated into organic material undergo cyclic conversions; that is, they get recycled over and over again on different time scales. Through geologic time, these biogeochemical cycling processes have fundamentally altered the conditions on Earth in a unidirectional manner, most crucially by decomposition of abiotically formed organic matter on the primitive Earth by early heterotrophic forms of life or changing the originally reducing atmosphere to an oxidized one via the evolution of oxygenic phototrophs.

Like all organisms, algae function to link metabolic sequences and properties to form a continuous, self-perpetuating network of chemical element fluxes. They have played key roles in shaping Earth's biogeochemistry and contemporary human economy, and these roles are becoming ever more significant as human impacts on ecosystems result in massive alteration of biogeochemical cycling of chemical elements. The Earth's initial atmosphere consisted of 80% N_2, 10% CO/CO_2, and 10% H_2 (by volume): no free O_2 appeared until the Great Oxygenation Event, ~2.4 billion years ago, when the development of oxygenic photosynthesis by cyanobacteria transformed the atmosphere composition to 78% N_2, 21% O_2, and 0.036% CO_2 and other minor gases (by volume). The petroleum and natural gas we consume as fuels, plastics, dyes, and so on in our everyday life rely on fossilized hydrocarbons mostly formed by the deposition of organic matter consisting of the remains

DOI: 10.1201/9781003187707-2

of several freshwater marine microalgae from the classes Eustigmatophyceae, Dinophyceae, and Chlorophyceae. These remains contain bacterially and chemically resistant, high aliphatic biopolymers (algaenans) and long-chain hydrocarbons that are selectively preserved upon sedimentation and diagenesis and make significant contribution to kerogens, a source of petroleum under appropriate geochemical conditions. Moreover, we are still using the remains of calcareous microorganisms, deposited over millions of years in ancient ocean basins, for building material. Diatomaceous oozes are mined as additives for reflective paints, polishing materials, and abrasives and for insulation. Fossil organic carbon, skeletal remains, and oxygen are the cumulative remains of algae export production that has occurred uninterrupted for over 3 billion years in the upper ocean.

About 99.9% of the algae biomass is accounted for by six major elements, carbon (C), oxygen (O), hydrogen (H), nitrogen (N), sulfur (S), and phosphorus (P), plus calcium (Ca), potassium (K), sodium (Na), chlorine (Cl), magnesium (Mg), iron (Fe), and silicon (Si). The remaining elements occur chiefly as trace elements, because they are needed only in catalytic quantities. Algae are especially important for the biogeochemical cycling of the chemical elements they uptake, assimilate, and produce, such as carbon, oxygen, nitrogen, phosphorus, silicon, iron, and sulfur, which eventually affect the life of all other organisms.

In this chapter, we will describe the biogeochemical cycles of carbon, oxygen, nitrogen, phosphorus, silicon, iron, and sulfur and the role algae play in these processes. In addition, we will discuss the ecological importance of recycling of the so-called growth-limiting nutrients, that is, those nutrients that can be in short supply, such as nitrate (NO_3^-, iron (bioavailable Fe), phosphate (PO_4^{3-}), and dissolved silicon [$Si(OH)_4$], which are most often found in concentrations well below the half-saturation levels required for maximum phytoplankton growth.

THE OXYGEN AND CARBON CYCLES

The oxygen and carbon cycles are closely related, because they are directly associated with photosynthesis and respiration processes.

The natural oxygen cycle is determined by the aerobic respiration of glucose (taking place in all living organisms), which consumes oxygen in free form (O_2), using it as an electron sink, and produces carbon dioxide and water, and by photosynthesis, which consumes carbon dioxide and water to produce carbohydrates and molecular oxygen as a by-product, as we will see in Chapter 4.

Today oxygen constitutes about 21% of the atmosphere, 85.8% of the ocean, and 46.1% by volume of the earth's crust. It has not always been like that. The primordial atmosphere of the Earth is thought to have contained mainly CO_2, N_2, H_2O, and CO with traces of H_2, HCN, H_2S, and NH_3 but to have been devoid of O_2 (only small amounts were derived from the photolysis of water), thus being neutral to mildly reducing. Today, the atmosphere contains 78% N_2, 21% O_2, and 0.04% CO_2 by volume and is strongly oxidizing. All the molecular oxygen present in the Earth's atmosphere has been produced as the result of oxygenic photosynthesis, the source of the original O_2 being photosynthetic activity in the primordial oceans. The development of aquatic photosynthesis coincided with a long and reasonably steady drawdown of atmospheric CO_2, from concentrations approximately 100-fold higher than in the present-day atmosphere to approximately half of the present levels. This drawdown was accompanied by a simultaneous evolution of oxygen from nil to approximately 21%, comparable to that of the present day. The current atmospheric oxygen concentration is maintained in equilibrium between production by photosynthesis and consumption by respiration, with annual fluctuations of ±0.002%. Over geological time scales, the drawdown of CO_2 was not stoichiometrically proportional to the accumulation of O_2 because photosynthesis and respiration are but two of the many biological and chemical processes that affect the atmospheric concentrations of these two gases. The removal rate of CO_2 from the atmosphere by photosynthesis on land is about 12×10^4 Tg yr^{-1} worldwide. Recent analyses suggest that the terrestrial biosphere has responded to anthropogenic CO_2 emissions over the past century with a maximal increase in photosynthetic activity that proportionally matched the increase in atmospheric CO_2 concentration. In particular, from 1982 to 2020, plants have indeed

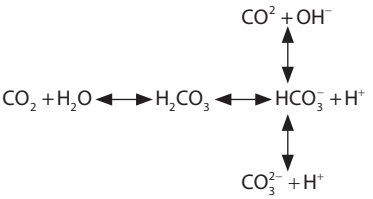
been photosynthesizing more, to the tune of 12% higher global photosynthesis. In that same time period, global carbon dioxide concentrations in the atmosphere grew about 17%, from 360 parts per million (ppm) to 420 ppm. The 12% increase in photosynthesis translates to 14×10^2 Tg yr^{-1} of additional carbon taken out of the atmosphere by plants each year, roughly the equivalent of the carbon emitted worldwide from burning fossil fuels in 2020 alone.

The concentration of oxygen in the oceans (85.8%) is influenced horizontally and vertically by physical features such as the thermocline (i.e. a layer in a large body of water, such as a lake, that sharply separates regions differing in temperature), which isolates deep water from exchange with the atmosphere and can be a zone of significant decomposition, causing an oxygen minimum. Oxygen is only sparingly soluble in water (oxygen solubility is inversely proportional to the temperature) and diffuses about 10^4 times more slowly in water than air. Deep water masses are brought to the sea surface in the polar zones where cooling gives rise to increased gas solubility and convection currents. These waters remain largely intact and move through the ocean basins with their oxygen concentration decreasing with time due to the decomposition of organic matter.

Carbon, the key element of all life on Earth, has a complex global cycle that involves both physical and biological processes, made up of carbon flows passing back and forth among four main natural reservoirs of stored carbon: the atmosphere, storing 75×10^4 Tg (0.001%) of the world's carbon as carbon dioxide (CO_2), carbon monoxide (CO), methane (CH_4), longer chain volatile hydrocarbons, and halogen compounds, chlorofluorocarbons and hydrochorofluorocarbons; the biosphere, that is, living organisms, storing 8×10^6 Tg (0.001%) of the world's carbon as compounds like fats, carbohydrates, and proteins; the hydrosphere, storing 39×10^6 Tg (0.06%) of the world's carbon as dissolved carbon dioxide; and the lithosphere, storing 10^6 Tg (0.002%) of the world's carbon in the form of fossils (e.g. oil, natural gas, lignite, and coal) and 62×10^{12} Tg (99.9%) in sedimentary rocks (e.g. limestone and dolomite). Carbon is also present in the mineral soil, in the bottom sediments of water bodies, in peat in bogs and mires, and in litter and humus, which contain 3×10^6 Tg (0.005%) of the world's carbon.

Carbon dioxide enters the ocean from the atmosphere because it is highly soluble in water; in the sea, free dissolved CO_2 combines with water and ionizes to form bicarbonate and carbonate ions, according to the following equilibrium:

1)



These ions are bound forms of carbon dioxide, and they (especially bicarbonate) represent by far the greatest proportion of dissolved carbon dioxide in seawater. On average, there are about 45 ml total CO_2 in one liter of seawater, but because of the equilibrium chemical reactions shown previously, nearly all of this occurs as bound bicarbonate and carbonate ions, which thus act as a reservoir of free CO_2. The amount of dissolved CO_2 occurring as gas in one liter of seawater is about 0.23 ml. When free CO_2 is removed by photosynthesis, the reaction shifts to the left, and the bound ionic forms release more free CO_2, so even when there is a lot of photosynthesis, carbon dioxide is never a limiting factor to plant production. Conversely, when CO_2 is released by the respiration of algae, plants, bacteria, and animals, more bicarbonate and carbonate ions are produced.

According to the general chemical reactions shown previously, the pH of seawater is largely regulated by the concentrations of bicarbonate and carbonate, and its value is usually 8 ± 0.5. Seawater acts as a buffered solution, since when CO_2 is added to seawater due to mineralization processes (i.e. the process of transforming organic materials back to inorganic forms of elements) and respiration, the number of hydrogen ions increases and the pH goes down (the solution becomes more acidic). If CO_2 is removed from water by photosynthesis, the reverse happens and the pH is elevated.

Some marine algae, both micro and macro, combine calcium with carbonate ions in the process of calcification to manufacture calcareous skeletal material. A well-known example of calcareous microalgae are the golden-brown scale-bearing coccolithophores, such as *Coccolithus* or *Emiliana* (Coccolithophyceae, Haptophyta). Examples of calcareous macroalgae, which are recognized as predominant contributors to the structures of the majority of reef limestone deposits, are the dark-purple crustose Corallinales (Rhodophyta), and the calcareous Chlorophyta such as *Halimeda* or *Udotea*.

Calcium carbonate ($CaCO_3$) may either be in the form of calcite or aragonite, the latter being a more soluble form. After death, this skeletal material sinks and is either dissolved, in which case CO_2 is again released into the water, or becomes buried in sediments, in which case the bound CO_2 is removed from the carbon cycle (sequestration). The amount of CO_2 taken up in the carbonate skeletons of marine organisms has been, over geological time, the largest mechanism for absorbing CO_2. At present, it is estimated that about 50×10^9 Tg of CO_2 occurs as limestone, 12×10^9 Tg in organic sediments, and 38×10^6 Tg as dissolved inorganic carbonate.

Calcification is not confined to a specific phylogenetically distinct group of organisms but evolved (apparently independently) several times in marine organisms. Carbonate sediments blanket much of the Atlantic Basin and are formed from the shells of both coccolithophores and foraminifera. As the crystal structure of the carbonates in both groups is calcite (as opposed to the more diagenically susceptible aragonite), the preservation of these minerals and their co-precipitating trace elements provides an invaluable record of ocean history. Although on geological time scales, huge amounts of carbon are stored in the lithosphere as carbonates, on ecological time scales, carbonate formation depletes the oceans of Ca^{2+} and, in so doing, potentiates the efflux of CO_2 from the oceans to the atmosphere. This calcification process can be summarized by the following reaction:

2) $$Ca^{2+} + 2HCO_3^- \leftrightarrow CaCO_3 + CO_2 + H_2O$$

As already noted, coccolitophores play a major role in calcification, especially *Emiliania huxleyi*. When the blooms of this haptophyte appear over large expanses of the ocean (white water phenomenon), myriad effects on the water and the atmosphere above can be observed. Although each cell is invisibly small, there can be as many as a thousand billion billion (10^{21}) of them in a large bloom, and the population as a whole has an enormous impact. *E. huxley* blooms are processed through the food web, with viruses, bacteria, and zooplankton all contributing to the demise and decomposition of blooms. Some debris from the bloom survives to sink to the ocean floor, taking chemicals out of the water column. While they live and when they die, the phytoplankton cells leak chemicals into the water. A bloom can be thought of as a massive chemical factory, extracting dissolved carbon dioxide, nitrate, phosphate, and so on from the water and at the same time injecting other chemicals such as oxygen, ammonia, dimethyl sulfide (DMS), and other dissolved organic compounds into the water. At the same time, the chemical factory pumps large volumes of organic matter and calcium carbonate into the deep ocean and to the ocean floor. Some of this calcium carbonate eventually ends up as chalk or limestone marine sedimentary rocks, perhaps to cycle through the Earth's crust and reappear millions of years later as mountains, hills, and cliffs. Coccolithophorids are primarily found at low abundance in tropical and subtropical seas and at higher concentrations at high latitudes in midsummer, following diatom blooms. Hence, export of inorganic carbon by diatoms in spring at high latitudes can be offset by an efflux of carbon to the atmosphere with the formation of coccolithophore blooms later in the year.

Coccolithophorid abundance increased through the Mesozoic and underwent a culling at the Cretaceous/Tertiary (K/T) boundary (i.e. the boundary between the Cretaceous and the first segment of the Cenozoic era, from 65 MYA until the present), followed by numerous alterations in the Cenozoic. The changes in coccolithophorid abundances appear to trace eustatic sea level variations, suggesting the transgressions lead to higher calcium carbonate fluxes. In contrast, diatom sedimentation increases with regressions, and since the K/T impact, diatoms have generally replaced coccolithophorids as ecologically important eukaryotic phytoplankton. On much finer time scales, during the Pleistocene, it would

appear that interglacial periods favored coccolithophorid abundance, while glacial periods favored diatoms. The factors that led to glacial–interglacial variations between these two functional groups are relevant to elucidating their distributions in the contemporary ecological setting of the ocean.

Coccolithophores influence regional and global temperature, since they can affect ocean albedo and ocean heat retention, and have a greenhouse effect. Coccoliths do not absorb photons, but they are still optically important since they act like tiny reflecting surfaces, diffusely reflecting the photons. A typical coccolith bloom (containing 100 mg m^{-3} of calcite carbon) can increase the ocean albedo from 7.5% to 9.7%. If each bloom is assumed to persist for about a month, then an annual coverage of 1.4×10^6 km^2 will increase the global annual average planetary albedo by

3) $$(9.7 - 7.5) \times (1/12) \times (1.4/510) = 0.001\%$$

where 510×10^6 km^2 is the surface area of the Earth.

This is a lower bound on the total impact, because light scattering by sub-bloom concentration coccoliths will have an impact over much larger areas (estimated maximum albedo impact = 0.21%). A 0.001% albedo change corresponds to a 0.002 Wm^{-2} reduction in incoming solar energy, whereas an albedo change of 0.21% causes a reduction of 0.35 Wm^{-2}. These two numbers can be compared to the forcing due to anthropogenic addition of CO_2 since the 1700s, estimated to be about 2.5 Wm^{-2}. Coccolith light scattering is therefore a factor of only secondary importance in the radiative budget of the Earth. However, the scattering caused by coccoliths causes more heat and light than usual to be pushed back into the atmosphere; it causes more of the remaining heat to be trapped near to the ocean surface, and only allows a much smaller fraction of the total heat to penetrate to deeper in the water. Because it is the near-surface water which exchanges heat with the atmosphere, all three effects just described conspire to mean that coccolithophore blooms may tend to make the overall water column dramatically cooler over an extended period, even though this may initially be masked by a warming of the surface skin of the ocean (the top few meters).

All phytoplankton growth removes CO_2 into organic matter and reduces atmospheric CO_2 by means of photosynthesis. However, coccolithophores are unique in that they also take up bicarbonate, with which they form the calcium carbonate of their coccoliths (calcification process). Coccolithophorid blooms are responsible for up to 80% of surface ocean calcification. In the equilibrium of the calcification process, an increase in CO_2 concentration leads to calcium carbonate dissolution, whereas a decrease in CO_2 levels achieves the reverse. While photosynthetic carbon fixation decreases the partial pressure of CO_2, as dissolved inorganic carbon is being utilized, conditions favoring surface calcification by coccolithophorid blooms contribute to the increase of dissolved CO_2.

The relative abundance of the components of the carbonate system (CO_2, H_2CO_3, HCO_3^-, and CO_3^{2-}) depends upon pH, dissolved inorganic carbon, and the total alkalinity, and the equilibrium between the components can shift very easily from being in one of these dissolved forms to being in another. How much of the total carbon is in each form is determined mainly by alkalinity and water temperature. When the seawater carbon system is perturbed by coccolithophore cells removing HCO_3^- to form coccoliths, this causes a re-arrangement of how much carbon is in each dissolved form, and this rearrangement takes place more or less instantaneously. The removal of two molecules of HCO_3^- and the addition of one molecule of CO_2 change the alkalinity, and this indirectly causes more of the dissolved carbon to be pushed into CO_2 form. Although the total dissolved carbon is obviously reduced by removal of dissolved carbon (bicarbonate ions) into solid calcium carbonate, the total effect, paradoxically, is to produce more dissolved CO_2 in the water. In this way, coccolithophore blooms tend to exacerbate global warming by causing increased atmospheric CO_2 (greenhouse effect) rather than ameliorating it, as is the case when dissolved CO_2 goes into new organic biomass. However, recent work is showing that additional properties of coccoliths may make the situation yet more complicated. Coccolith calcite is rather dense (2.7 kg l^{-1} compared to seawater density of 1.024 kg l^{-1}), and the presence of coccoliths in zooplankton fecal pellets and marine snow (the two main forms in which biogenic matter sinks to the deep ocean) causes them to

sink more rapidly. Slow-sinking organic matter may also adhere to the surfaces of coccoliths, hitching a fast ride out of the surface waters. If organic matter sinks faster, then there is less time for it to be attacked by bacteria and so more of the locked-in carbon will be able to escape from the surface waters, depleting the surface CO_2. Probably this co-transport of organic matter with coccoliths offsets the atmospheric CO_2 increase that would otherwise be caused and makes coccolithophore blooms act to oppose global warming rather than to intensify it.

THE NITROGEN CYCLE

The growth of all organisms depends on the availability of mineral nutrients, and none is more important than nitrogen, the fourth most abundant element in biomass, which is required in large amounts as an essential component of macromolecules, such as peptides, proteins, enzymes, chlorophylls, energy-transfer molecules (ATP, adenosine diphospate [ADP]), genetic materials (RNA, DNA), and other cellular constituents.

Nitrogen is present in all four different spheres of the Earth: the lithosphere contains about 98% of the global N (1.7×10^{11} Tg), distributed among its different compartments (crust, mantle, and core), with 2.1×10^9 Tg concentrated in the continental crust and oceanic sediments. The core and the mantle have been estimated to contain a total of over 1.6×10^{11} Tg of N. However, this N is not readily available to be cycled in the near-surface Earth environment. Some periodically enters the atmosphere and hydrosphere through volcanic eruptions, primarily as ammonia (NH_3) and nitrogen (N_2) gas. Most of the remainder (~2%, 4×10^9 Tg) is found in the atmosphere, where nitrogen gas (N_2) makes up more than 78% of the volume. The hydrosphere and the biosphere together contain relatively little N compared with the other spheres (~0.015%, 3 Tg). Nitrogen oceanic content averages 6.6×10^5 Tg, while lakes, rivers, and groundwater account for just 10^4 Tg. The N content of the terrestrial biosphere (1.4×10^4 Tg) is higher than that of the marine biosphere (1.8×10^3 Tg). Because of the presence of these many chemical forms in all the different spheres, with easily accessible reservoirs and numerous feedback controls, the N cycle is considered "perfect" and more complex with respect to the cycle of other nutrients.

Nitrogen has many chemical forms, both organic and inorganic, in the atmosphere, biosphere, hydrosphere, and lithosphere. It occurs in the gas, liquid (dissolved in water), and solid phases. N can be associated with carbon (organic species) and with elements other than carbon (inorganic species). Important inorganic species include nitrate (NO_3^-), nitrite (NO_2^-), nitric acid (HNO_3), ammonium (NH_4^+), ammonia (NH_3), the gas N_2, nitrous oxide (N_2O), nitric oxide (NO), and nitrogen dioxide (NO_2). Most organic N species in the four spheres are biomolecules, such as proteins, peptides, enzymes, and genetic material.

The key processes linking the major pathways of the nitrogen cycle are the following:

- N-fixation (biotic and abiotic): reduction of atmospheric N_2 into ammonia, NH_3.
- Assimilation: conversion of NO_3^- and NH_4^+ to organic nitrogen.
- Mineralization, or ammonification: conversion of organic nitrogen to NH_4^+.
- Nitrification: conversion of NH_4^+ to NO_2^- and successively NO_3^-.
- Denitrification: conversion of NO_3^- to gaseous forms of nitrogen (NO, N_2O, N_2).

Though complex microbial relationships regulate these processes, we can assume that fixation, mineralization, nitrification, and denitrification are carried out almost exclusively by bacteria, whereas algae play a main active role only in nitrogen fixation and assimilation. Greatly simplifying the overall nitrogen cycle, and from an algal point of view, atmospheric molecular nitrogen is converted by prokaryotic algae (cyanobacteria) to compounds such as ammonia (fixation), which are in part directly converted into amino acids, proteins, and other nitrogen-containing cell constituents of the fixators and in part excreted into the open environment. Eukaryotic algae, unable to perform fixation, incorporate fixed nitrogen, either ammonium or nitrate, into organic N compounds by

assimilation. When organic matter is degraded, organic compounds are broken down into inorganic compounds such as NH_3 or NH_4^+ and CO_2 through the mineralization process. The resultant ammonium can be nitrified by aerobic chemoautotrophic bacteria that use it as electron donor in the respiration process. The cycle is completed by denitrification carried out by usually facultative anaerobic bacteria that reduce nitrate used as electron acceptor in respiration to nitrogen gas.

All life forms require nitrogen compounds, still the most abundant portion of it (98%) is buried in the rocks and is therefore deep and unavailable, and the rest of the nitrogen, the N_2 gas (2%), can be utilized only by very few organisms. This gas cannot be used by most organisms because the extremely stable triple bond between the two nitrogen atoms makes the molecule almost inert. In order for N_2 to be used for growth, this gas must be "fixed" in the forms directly accessible to most organisms, that is, ammonia and nitrate ions.

A relatively small amount of fixed nitrogen is produced by atmospheric fixation (5–8%, 5 ± 3 Tg yr^{-1}); the high temperature and pressure associated with lightning result in the dissociation of O_2 molecules and the formation of O radicals, which can react with N_2 to form NO, subsequently stabilized by mixing with ambient air. These molecules then dissolve in rain, forming nitrates that are carried to the earth. Volcanic activity is also accompanied by the release of fixed N originating from the thermal fixation of atmospheric N_2. Abiotic processes associated with human activities are large additional sources of new fixed N. The largest source of anthropogenic fixed N is the Haber-Bosch process, in which atmospheric nitrogen and hydrogen (usually derived from natural gas or petroleum) can be combined to form ammonia (NH_3) using an iron-based catalyst, very high pressures, and a temperature of about 600°C. Ammonia can be used directly as fertilizer, but most of it is further processed to urea $(NH_2)_2CO$ and ammonium nitrate (NH_4NO_3). The modern rate of Haber-Bosch fixed N production (about 120 Tg N yr^{-1} in 2010) is similar to the rates of natural biological fixation on land and in the sea.

The major conversion of N_2 into ammonium, and thence into proteins, is a biotic process achieved by microorganisms, which represents one of the most metabolically expensive processes in biology, by which specialized groups of prokaryotes termed "diazotrophs" or "N_2-fixers" reduce N_2 gas to ammonia (NH_3) for the purpose of fulfilling their anabolic needs. Biological nitrogen fixation can be represented by the following equation, in which two moles of ammonia (but in solution, ammonia exists only as ammonium ions, that is, $NH_3 + H_2O \leftrightarrow NH_4^+ + OH^-$) are produced from one mole of nitrogen gas at the expense of 16 moles of ATP and a supply of electrons and protons (hydrogen ions):

4) $$N_2 + 8H^+ + 8e^- + 16\ ATP \rightarrow 2NH_3 + H_2 + 16ADP + 16\ P_i$$

All known diazotrophs are prokaryotes, and the ability to fix nitrogen is widely, though paraphyletically, distributed across both the bacterial and archaeal domains in at least 14 different phyla, though most of those experimentally investigated belong to the phylum Proteobacteria. Diazotrophs utilize all forms of energy metabolism (oxygenic and anoxygenic phototrophy, aerobic and anaerobic heterotrophy, chemolitotrophy) and are found in a variety of habitats within terrestrial and marine systems.

The capacity of nitrogen fixation in diazotrophs relies solely upon an ATP-hydrolyzing, redox active enzyme complex termed nitrogenase. In many of these organisms, nitrogenase makes up about 10% of total cellular proteins and consists of two highly conserved components, an iron protein (Fe-protein) and a molybdenum-iron protein (MoFe-protein). The Fe-protein is a γ_2 homodimer composed of a single Fe_4S_4 cluster bound between identical 32–40 KDa subunits. The Fe_4S_4 cluster is redox active and is similar to those found in small molecular weight electron carrier proteins such as ferredoxins. It is the only known active agent capable of obtaining more than two oxidative states and transfers electrons to the MoFe-protein. The MoFe-protein is a $\alpha_2\beta_2$ heterotetramer; the ensemble is approximately 250 Kda. The α subunit contains the active site for dinitrogen reduction, typically a $MoFe_7S_9$ metal cluster (termed FeMo-cofactor), although some organisms contain

nitrogenases wherein Mo is replaced by either Fe or V. These so-called alternative nitrogenases are found only in a limited subset of diazotrophs and, in all cases studied so far, are present secondarily to the MoFe-nitrogenase. MoFe-nitrogenase has been found to be more specific for and more efficient in binding N_2 and reducing it to ammonia than either of the alternative nitrogenases. The catalytic efficiency of these alternative nitrogenases is lower than that of MoFe-nitrogenase.

In addition to variations in metal cofactors, the nitrogenase complex is non-specific and reduces triple and double bond molecules other than N_2. These include hydrogen azide, nitrous oxide, acetylene, and hydrogen cyanide. The non-specificity of this enzyme and the alternative nitrogenases containing other metal co-factors implicate the role of varying environmental pressures on the evolutionary history of nitrogenase that could have selected for different functions of the ancestral enzyme. The nitrogenase enzyme system is extremely O_2 sensitive, since oxygen not only affect the protein structure but also inhibits the synthesis of nitrogenase in many diazothrops. The repression is both transient (lasting only a few hours) and permanent. The reactions occur while N_2 is bound to the nitrogenase enzyme complex. The Fe-protein is first reduced by electrons donated by ferredoxin. Then the reduced Fe-protein binds ATP and reduces the MoFe-protein, which donates electrons to N_2, producing di-imide (HN=NH). In two further cycles of this process (each requiring electrons donated by ferredoxin), HN=NH is reduced to imide (H_2N-NH_2), and this in turn is reduced to $2NH_3$. Depending on the type of microorganism, the reduced ferredoxin which supplies electrons for this process is generated by fermentation or photosynthesis and respiration.

As already stated, nitrogenase is highly sensitive to molecular oxygen (in vitro it is irreversibly inhibited by exposure to O_2). Therefore, during the course of planetary evolution, cyanobacteria have co-evolved with the changing oxidation state of the ocean and atmosphere to accommodate the machinery of oxygenic photosynthesis and oxygen-sensitive N_2 fixation within the same cell and/or colony of cells. Since nitrogen fixation occurs in a varied metabolic context in both anaerobic and aerobic environments, strategies have followed a very complex pattern of biochemical and physiological mechanisms for segregation that can be simplified in some spatial and/or temporal separation of the two pathways.

Nitrogenase is an ancient enzyme that almost certainly arose in the Archean ocean before the oxidation of the atmosphere by oxygenic photoautotrophs. An attractive hypothesis of the development of biological nitrogen fixation is that it arose in response to changes in atmospheric composition that resulted in the reduction in the production of abiotically fixed nitrogen. On the early Earth, concentrations of CO_2 in the atmosphere were high because of oxidation of CO produced by impacts of extraterrestrial bodies and only slow removal of CO_2 by weathering (the continents were smaller at this time, meaning that a smaller area of minerals was exposed for weathering). With these CO_2 conditions, the initial production rate of NO was estimated to be about 3×10^{11} g yr^{-1}. Atmospheric CO_2 levels declined with time, however, as the impact rate dropped and the continents grew. A rise in atmospheric CH_4 produced by methanogenic, methane-generating bacteria may have warmed the Archaean Earth and sped the removal of CO_2 by silicate weathering. As this happened, the production rate of NO by lightning dropped to below 3×10^9 g yr^{-1} because of the reduced availability of oxygen atoms from the splitting of CO_2 and H_2O. The resulting crisis in the availability of fixed nitrogen for organisms triggered the evolution of biological nitrogen fixation about 2.2 billion years ago. Under the prevailing anaerobic conditions of that period in Earth's history, anaerobic heterotrophs, such as *Clostridium,* developed. With the evolution of cyanobacteria and the subsequent generation of molecular oxygen, oxygen-protective mechanisms would be essential. A semi-temporal separation of nitrogen fixation and oxygenic photosynthesis combined with spatial heterogeneity was the first oxygen-protective mechanism developed by marine cyanobacteria such as *Trichodesmium* sp. and *Katagnymene* sp. A full temporal separation, in which nitrogen is only fixed at night, then developed in unicellular cyanobacteria diazotrophs and in some non-heterocystous filamentous diazotrophs (for example, *Oscillatoria limosa* and *Plectonema boryanum*). Finally, in yet other filamentous organisms, complete segregation of N_2 fixation and photosynthesis was

achieved with the cellular differentiation and evolution of heterocystous cyanobacteria (for example, *Nostoc* and *Anabaena*).

The non-heterocystous filamentous cyanobacteria *Trichodesmium* sp. and *Katagnymene* sp., unlike all other non-heterocystous species, fix nitrogen only during the day. Nitrogenase is compartmentalized in 15–20% of the cells in *Trichodesmium* sp., and 7% of the cells in *Katagnymene* sp. are often arranged consecutively along the trichome, but active photosynthetic components (photosystem I [PSI], PSII, RuBisCO, and carboxysomes) are found in all the cells, even those harboring nitrogenase (cf. Chapter 4). A combined spatial and temporal segregation of nitrogen fixation from photosynthesis and a sequential progression of photosynthesis, respiration, and nitrogen fixation over a diel cycle are the strategies used by these cyanobacteria. These pathways are entrained in a circadian pattern that is ultimately controlled by the requirement for an anaerobic environment around nitrogenase. Light initiates photosynthesis, providing energy and reductants for carbohydrate synthesis and storage, stimulating electron cycling through PSI, and poising the plastoquinone (PQ) pool at reduced levels. High respiration rates early in the photoperiod supply carbon skeletons for amino acid synthesis (the primary sink for fixed nitrogen) but simultaneously reduce the PQ pool further. Linear electron flow to PSI is never abolished. The reduced PQ pool leads to a down-regulation of PSII, which opens a window of opportunity for N_2 fixation during the photoperiod, when oxygen consumption exceeds oxygen production. As the carbohydrate pool is consumed, respiratory electron flow through the PQ pool diminishes, intracellular oxygen concentrations rise, the PQ pool becomes increasingly oxidized, and net oxygenic production exceeds consumption. Nitrogenase activity is lost until the following day.

A full temporal separation between oxygenic photosynthesis and nitrogen fixation occurs in *Plectonema boryanum* and *Oscillatoria limosa*. Transcription of nitrogenase and photosynthetic genes are temporally separated within the photoperiod; that is, nitrogenase is expressed primarily during the night. Nitrogenase is contained in all cells in equal amounts. The onset of nitrogen fixation is preceded by a depression in photosynthesis that establishes a sufficiently low level of dissolved oxygen in the environment. *Plectonema* sp. has a versatile physiology that allows it to reversibly modulate uncoupling of the activity of the two photosystems in response to intracellular nitrogen status. *Oscillatoria* sp. initiates nitrogen fixation in the dark and performs it primarily in the absence of light.

In non-heterocystous cyanobacteria, such as the filamentous *Symploca* sp. and *Lyngbya maiuscola* and the unicellular *Gloeothece* sp. and *Cyanothece* sp., temporal separation does not need a micro-aerobic environment. *Phormidium* sp. and *Pseudanabaena* sp. are other examples of cyanobacteria fixing only under micro-anaerobic conditions. Under contemporary oxygen levels, all of these organisms are relegated to narrow environmental niches.

In heterocystous cyanobacteria, such as *Anabaena* sp. and *Nostoc* sp., a highly refined specialization spatially separates oxygenic photosynthesis from N_2 fixation. Here, nitrogenase is confined to specialized heterotrophic cells, the heterocysts, which receive fixed C from nearby vegetative cells in exchange with fixed N. Heterocysts are characterized by a thick membrane that slows the diffusion of O_2, high PSI activity, loss of division capacity, inactivity of O_2-evolving PSII, aerobic respiration, and variation of phycobiliprotein content. This cell differentiates completely and irreversibly 12–20 hours after combined nitrogen sources are removed from the medium. The development of these cells, formed at intervals between vegetative cells, is a primitive form of cell differentiation. In this process, all PSII activity is gradually lost, and the proteins involved in oxygenic photosynthesis are degraded, while PSI activity is maintained. Simultaneously, the production of active nitrogenase is triggered. Nitrogen fixation is localized specifically in heterocysts, and light is used for cyclic electron flow around PSI to maintain a supply of ATP for the process. The primary organic nitrogen product (glutamate) is exported to adjacent vegetative and photooxygenic cells, while carbon skeletons, formed by the respiratory and photosynthetic processes in the latter cells, are translocated to the heterocysts. In some heterocystous cyanobacteria such as *Anabaena variabilis*, under anaerobic conditions, a different Mo-dependent nitrogenase can be

synthesized inside vegetative cells. This nitrogenase is expressed shortly after nitrogen depletion but prior to heterocyst formation, and can support the fixed N needs of the filaments independently of the nitrogenase in the heterocysts. Figure 2.1 shows the position of a heterocyst (H) and the akinetes (A) formed adjacent to it in a filament of *Anabaena* sp. The absorption spectra measured by microspectrophotometry (cf. Chapter 7) of these cells and a vegetative cell (V) are shown on the right side of the figure. The absorption spectrum of the heterocyst indicates that phycobiliproteins are lacking at this stage of development.

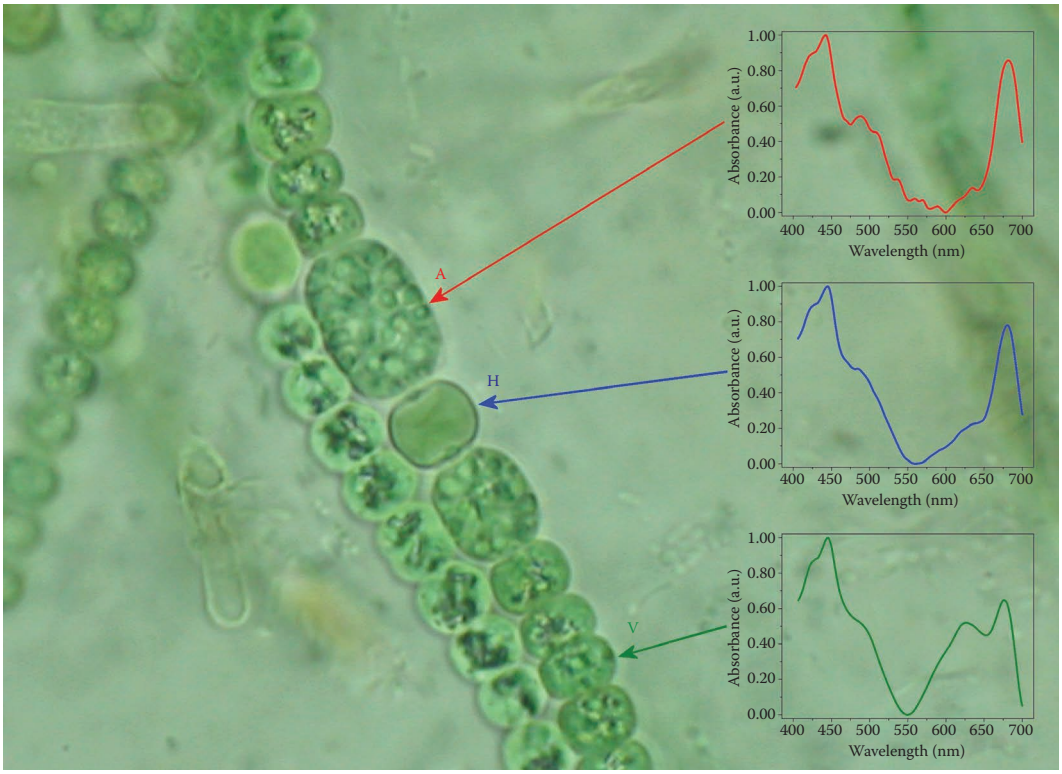


FIGURE 2.1 Position of a heterocyst (H) and the akinetes (A) formed adjacent to it in a filament of *Anabaena* sp. The absorption spectra measured by microspectrophotometry of these cells and a vegetative cell (V) are shown on the right side of the figure. The absorption spectra of the heterocyst and akinete indicate that phycobiliproteins are lacking at this stage of development. Scale bar = 5µm.

The metabolic cost of all the strategies use by diazotrophs to cope with the problem of nitrogenase damage by O_2 is extremely high and corresponds to about half of the energy used for N_2 fixation. For all eukaryotic algae, the only forms of inorganic nitrogen that are directly assimilable are nitrate (NO_3^-) nitrite (NO_2^-), and ammonium (NH_4^+). The more highly oxidized form, nitrate, is the most thermodynamically stable form in oxidized aquatic environments and hence is the predominant form of fixed nitrogen in aquatic ecosystems, though not necessarily the most readily available form. Following translocation across the plasmalemma (which is an energy-dependent process), the assimilation of NO_3^- requires chemical reduction to NH_4^+. This process is mediated by two enzymes, nitrate reductase and nitrite reductase. Nitrate reductase is located in the cytosol and uses nicotineamide adenine dinucleotide phosphate (NADPH) to catalyze the two-electron transfer:

5) $$NO_3^- + 2e^- + 2H^+ \rightarrow NO_2^- + H_2O$$

In cyanobacteria, nitrate reductase is coupled to the oxidation of ferredoxin rather than a pyridine nucleotide, as in eukaryotic algae. The nitrite formed by nitrate reductase is reduced in a six-electron transfer reaction:

6) $$NO_2^- + 6e^- + 8H^+ \rightarrow NH_4^+ + 2H_2O$$

Nitrite reductase utilizes ferredoxin in both cyanobacteria and eukaryotic algae; in the latter, the enzyme is localized in the chloroplasts. In both cyanobacteria and eukaryotic algae, photosynthetic electron flow is an important source of reduced ferredoxin for nitrite reduction. The overall stoichiometry for the reduction of nitrate to ammonium can be written as:

7) $$NO_3^- + 8e^- + 10H^+ \rightarrow NH_4^+ + 3H_2O$$

The incorporation of ammonium into amino acids is primarily brought about by the sequential action of glutamine synthetase (GS) and glutamine 2-oxoglutarate aminotransferase (GOGAT). Ammonium assimilation by GS requires glutamate as substrate and ATP and catalyzes the irreversible reaction:

8) $$\text{glutamate} + NH_4^+ + ATP \rightarrow \text{glutamine} + ADP + P_i$$

The amino nitrogen of glutamine is subsequently transferred to 2-oxoglutarate and reduced, forming 2 moles of glutamate:

9) $$\text{2-oxoglutarate} + \text{glutamine} + NADPH \rightarrow 2[\text{glutamate}] + NADP^+$$

Both GS and GOGAT are found in chloroplasts, although isoenzymes (multiple forms of an enzyme with the same substrate specificity but genetic differences in their primary structures) of both enzymes may also be localized in the cytosol. Whatever the location of the enzymes, however, glutamate must be exported from the chloroplast to the cytosol where transamination reaction (the reversible transfer of an amino group of a specific amino acid to a specific ketoacid, forming a new keto acid and a new amino acid) can proceed, thereby facilitating the syntheses of other amino acids.

THE PHOSPHORUS CYCLE

Phosphorus (P) is the 11th most abundant mineral in the earth's crust, and compared with carbon (C), sulfur (S), and nitrogen (N), it lacks a gaseous state. Hence, its cycle, which is the simplest of the biogeochemical cycles, has been described as "imperfect," as turnover of the buried sedimentary reservoir formed by the activity of ancient marine organisms is determined by tectonic events acting over tens and hundreds of million years.

Natural inorganic phosphorus deposits occur primarily as phosphate, that is, a phosphorous atom linked to four oxygen atoms (PO_4^{3-}), in the mineral apatite. The heavy molecule of phosphate never makes its way into the atmosphere; it is always part of an organism, dissolved in water, or in the form of rock. Cycling processes of phosphorus are the same in both terrestrial and aquatic systems. When rocks with phosphate are exposed to water (especially slightly acidic water) during the natural process of weathering, they gradually release the phosphorus as phosphate ions which are soluble in water, and the mineralized phosphate compounds break down.

Autotrophs (algae and plants) assimilate this dissolved phosphorus and alter it into organic phosphorus, using it in a variety of ways. It is an important constituent of the lipid portion of cell membranes, many coenzymes, DNA, RNA, and of course ATP. Heterotrophs obtain their phosphorous from the autotrophs they eat. When heterotrophs and autotrophs die (or when heterotrophs

defecate), the phosphate may be returned to the soil or water by the decomposers. There, it can be taken up by other autotrophs and used again. This cycle will occur over and over until at last the phosphorous is lost at the bottom of the deepest parts of the ocean, where it becomes part of the sedimentary rocks forming there. If the rock is brought to the surface and weathered, this phosphorous will be released.

Phosphates exist in three forms: orthophosphate ($H_2PO_4^-$, HPO_4^{2-}, PO_4^{3-}), metaphosphate (or polyphosphate) and organically bound phosphate, each compound containing phosphorous in a different chemical arrangement. These forms of phosphate occur in living and decaying plant and animal remains as free ions or weakly chemically bonded in aqueous systems; chemically bonded to sediments and soils; or as mineralized compounds in soil, rocks, and sediments. Orthophosphate forms are produced by natural processes, but major human-influenced sources include partially treated and untreated sewage, runoff from agricultural sites, and application of some lawn fertilizers. Orthophosphate is readily available to the biological community and typically found in very low concentrations in unpolluted waters. Poly-forms are used for treating boiler waters and in detergents. In water, they are transformed into orthophosphate and made available for autotroph uptake. Organic phosphate is phosphate that is bound or tied up in autotrophs, waste solids, or other organic material. After decomposition, this phosphate can be converted to orthophosphate.

Algae and plants are the key elements to passing on phosphates to other living organisms, but their importance in phosphorus cycling is connected mainly to the impact of this element on their growth. As already remarked, both phosphorus and nitrogen are among the nutrients that can become limiting; hence, an overloading of these two elements leads to dramatic changes in the structure and functioning of an ecosystem. Phosphorus, in the form of orthophosphate, is generally considered the main limiting nutrient in freshwater aquatic systems; that is, if all the phosphorus is used, autotroph growth will cease, no matter how much nitrogen is available. In phosphorus-limited systems, excess phosphorus will trigger eutrophic conditions. In these situations, the natural cycle of the nutrient becomes overwhelmed by excessive inputs, which appear to cause an imbalance in the "production versus consumption" of living material (biomass) in an ecosystem. The system then reacts by producing more phytoplankton/vegetation than can be consumed by the ecosystem. This overproduction triggers a series of events determining the aging process of the water body.

Under aerobic conditions, as water plants and algae begin to grow more rapidly than normal, there is also an excess die-off of the plants and algae as sunlight is blocked at lower levels. Bacteria try to decompose the organic waste, consuming oxygen and releasing more phosphate, which is known as "recycling" or "internal cycling." Some of the phosphate may be precipitated as iron phosphate and stored in the sediment where it can then be released if anoxic conditions develop. In deeper environments, the phosphate may be stored in the sediments and then recycled through the natural process of lithophication, uplift, and erosion of rock formations. In anaerobic conditions, as conditions worsen as more phosphates and nitrates may be added to the water, all of the oxygen may be used up by bacteria in trying to decompose all of the waste. Different bacteria continue to carry on decomposition reactions; however, the products are drastically different. The carbon is converted to methane gas instead of CO_2; sulfur is converted to hydrogen sulfide gas. Some of the sulfide may be precipitated as iron sulfide. Under anaerobic conditions, the iron phosphate precipitates in the sediments may be released from the sediments, making the phosphate bioavailable. This is a key component of the growth and decay cycle. The water body may gradually fill with decaying and partially decomposed plant materials to make a swamp, which is the natural aging process.

The problem is that this process can be significantly accelerated by man's activities. In fact, though P undergoes a biogeochemical cycle within the environment, anthropogenic redistribution through inefficient agricultural practice and inadequate nutrient recovery at wastewater treatment works have resulted in a sustained transfer of P from rock deposits to land and aquatic environments. Modern agriculture largely depends on inorganic phosphate-based fertilizers extracted from

geological non-renewable P reserves controlled by only a small number of countries. Their acquisition and application are critical political and resource issues for global food and environment security, and P may become increasingly inaccessible to low-income nations, vulnerable to volatile prices and supply insecurity. Estimates of mineable P depletion are uncertain (40–400 years), as mined products already show diminished P content and greater levels of heavy metal contamination. Moreover, about 80% of extracted P is being lost due to runoff, which in addition to P present in sewage discharges and agriculture losses causes unnecessary P accumulation in soils and rivers, highly detrimental for the environment. Currently, P together with other nutrients are not being effectively recycled back to agriculture from wastes because of ineffective wastewater treatment methods, economic costs, or regulatory concerns.

Microalgae have long been studied for sustainable wastewater treatment for the removal of P and for returning Pi back to soil in slow release form, thus helping to close the P-cycle. Microalgae have the added advantage of accumulating and storing it as polyphosphate granules (PolyP) in the form of acid-insoluble polyphosphate in vacuoles for future internal utilization under Pi deficiency. PolyPs are unbranched linear polymers of inorganic phosphate (Pi) linked by phospho-anhydride bonds of variable chain length, ranging from 10 to 100 s. After being degraded to Pi, acid-insoluble polyphosphate is used to sustain algal viability under Pi shortage. Moreover, microalgae can uptake more P than they need for survival when exposed to a P-abundant environment (known as P luxury uptake) as wastewater, up to four times that required by their normal metabolisms. Polyphosphate storage is stimulated within 1–2 h after P is fed in luxury uptake, and the resulting polyphosphate granules enable microalgae to divide several generations in the absence of any external P until polyphosphate runs out after longer-term P starvation. The excess P accumulation beyond their needs facilitates P use and decouples P transport from P assimilation to satisfy the P requirements of microalgae. Moreover, the accumulation of polyphosphate facilitates simultaneous heavy metal ion incorporation and thus promotes the remediation of heavy metal contamination.

THE IRON CYCLE

Iron (Fe) is the fourth most abundant element in the Earth's crust (5.63%) and one of the most important elements for the biosphere. It is abundant in respiratory and photosynthetic transport chains in the form of heme and as part of the iron-sulfur prosthetic group of ferredoxin; it is also present in the iron-rich nitrogenase protein complex of diazotrophs; hence, it is vital to metabolic processes such as photosynthesis, respiration, electron transport, nitrate reduction, and the detoxification of reactive oxygen species. It is estimated that about 80% of the iron present in phytoplankton cells is involved in the photosynthetic machinery; no doubt, then, that iron impacts phytoplankton growth, primary productivity, community structure, and biodiversity and, on a larger scale, ecosystem functioning and CO_2 fixation.

The chemical forms of iron in the oceans can be defined as particulate (≥0.45 μm) and dissolved (dFe) (≤0.45 μm), which in turn is categorized into colloidal (0.45–0.02 μm) and soluble iron (≤0.02 μm). Iron appears in two oxidation states: ferrous ions (Fe^{2+}), the reduced, more soluble, but thermodynamically unstable form, which is dominant in the earth's mantle, deep crust, and core, and ferric ions (Fe^{3+}), the less soluble oxidized form. The solubility of Fe^{2+} depends on temperature, oxygen level, and pH. The iron cycle can be defined as the cycling of this element between its 2+ and 3+ oxidation states, which can be entirely abiotic or facilitated by microorganisms. Abiotic processes include Fe^{2+} oxidation to Fe^{3+} in the presence of O_2 and the reduction of Fe^{3+} to Fe^{2+} by iron-sulfide minerals. The biological cycling of Fe^{2+} is mainly due to iron-oxidizing and iron-reducing microorganisms.

Despite its high abundance in the crust, iron bioavailability in aquatic systems is vanishingly scarce, its level decreasing over time with the increase in oxygen level since the Proterozoic era. At that time, when life first evolved about 3 billion years ago, the ocean was full of iron, as ancient banded iron formations show, and the metal was incorporated into a long list of essential cellular

functions (oxygen transport, sugar and other nutrient breakdown for energy, electron transfer during photosynthesis, nitrogen fixation). Iron started disappearing from the seas as soon as the first photosynthetic organisms evolved and started to breathe in carbon dioxide and exhale oxygen, during the Great Oxidation Event, ~2.4 billion years ago. When this happened, dissolved iron rapidly linked up with the newly plentiful oxygen atoms, forming iron oxides such as hematite, containing Fe(III) (Fe^{3+}, ferric iron), with an extremely low solubility: these oxides fell to the ocean floor, piling up in the banded iron formations worldwide present in sedimentary deposit, which account for more than 60% of global iron reserves and provide most of the iron ore presently mined. Most phytoplankton and other living organisms can't use iron in this state and require a different form, Fe(II) (Fe^{2+}, ferrous iron), which more readily dissolves and is absorbed by cells. Aquatic organisms therefore had to adapt to maintain sufficiently high levels of such a scarce resource, evolving efficient uptake systems, carefully controlling iron homeostasis within cells to avoid the formation of dangerous reactive oxygen species catalyzed by Fe(II). Under Fe deficiency conditions, phytoplankton modifies its photosynthetic machinery by reducing the concentration of Fe-rich cellular components and modifying the light-harvesting systems. These changes cause a decrease of both the photochemical efficiency of photosynthesis and growth rate. All these strategies have remained unchanged since the beginning of life on Earth, but the environment has completely changed, and in contemporary well-oxygenated waters, well mixed and with a mildly alkaline pH, free Fe^{2+} is instantly oxidized to Fe^{3+}, which then, unless bound to organic ligands, will precipitate as ferric-hydroxide, resulting in an extreme reduction of available Fe concentration.

In large areas of the oceans, dissolved Fe (dFe) concentrations in surface waters are extremely low, often ≤1 nM, while for large lakes such as Ontario or Geneva, iron is present in concentrations ranging from 0.5 to 312 nM. The vertical and spatial distributions of dFe have similar patterns in large lakes and the ocean. Vertical distributions are nutrient-like, with low concentrations at the surface as a result of biological uptake and increasing concentrations with depth due to remineralization, aggregation and settling, and sediment resuspension. In the global ocean, average dFe concentrations vary from 0.07 nmol at the surface to 0.76 nmol at depth. Fe seasonal variability exhibits a net decrease of dFe concentrations at the level of the deep layer chlorophyll *a* maximum during spring to summer months and an increase due to winter mixing. This indicates that biological activities and mixing processes are important for Fe distribution. A spatial gradient of dFe in the epilimnion of lakes has been observed, from nearshore (dFe mean: 31.7 nM) to isolated areas (dFe mean: 1.5 nM), showing a strong increase of dFe concentration along the coastline as a result of lake-edge sources. Elevated Fe concentrations are indeed generally found in nearshore waters, often in the range of 100–1,000 times higher than that found in the open ocean. Despite a relatively high concentration of Fe in rivers, very little riverine Fe reaches the open ocean, as most of it is removed by precipitation, coagulation, and sedimentary processes favored by the increase of salinity in estuaries.

Iron sources are numerous; Fe reaches marine waters via atmospheric aerosols, riverine input, melting of sea ice, icebergs, glacial ice particulates, volcanic ashes, continental margins, transport of hydrothermal Fe residuals, anoxic sediments, and recycling by organisms from viruses to mammals. Globally the largest input into the oceans comes from atmospheric dust deposition, although exceptions to this may be upwelling areas or coastal regions with large river inputs. It is estimated that ~3 times more dFe enters the oceans via atmospheric deposition than via rivers. In the case of lakes, the dominating Fe sources are river inputs (e.g. fluvial influx and wastewaters), atmospheric inputs (e.g. precipitation and dust), sediment resuspension, and reductive remobilization of Fe from the sediment. These sources are mainly balanced with outflow and sedimentation processes. The high contribution of fluvial inputs to dFe concentrations can be explained by lakes' large watershed area, where Fe from the products of weathered rocks and soil around watersheds accumulates. Fe limitation is widespread, limiting phytoplankton growth in about 30–50% of the world oceans; according to the "iron hypothesis" of the oceanographer John Martins, and to the results of in-situ iron addition experiments, the limitation of accessible Fe to sustain phytoplankton growth is the

primary factor leading to low phytoplankton biomass in high nutrient, low chlorophyll (HNLC) regions, which include high-latitude areas as well as important upwelling regions such as the subarctic north Pacific, the equatorial Pacific, and the Southern Ocean, characterized by excess concentrations of phosphate and nitrate. In these areas the concentration of bioavailable Fe affects the primary production and as a consequence the strength of the biological pump and associated carbon drawdown from the atmosphere. Terrestrial dust-borne new Fe transported over long distance then becomes a significant source of Fe to the remote regions where riverine and shelf sediment Fe is minimal.

Fe limitation is not restricted to HNLC regions; areas of the Atlantic Ocean and the Coral Sea exhibit reduced primary productivity due to low nutrient concentrations, specifically nitrate (NO_3), and are termed "low nutrient, low chlorophyll (LNLC)" regions. Here Fe becomes a co-limiting factor due to its crucial role in nitrogen assimilation and N_2 fixation. In these cases, an input of Fe is unlikely to have the same effect as that seen in HNLC regions, as the concentrations of other vital nutrients are too low to initiate growth. Fe deficiencies and limitations also exist in natural lake waters; bioassay approaches have demonstrated that Fe additions can stimulate phytoplankton growth and photosynthetic efficiency, suggesting that the phytoplankton communities of these waters are at least Fe stressed or even Fe limited.

Fe^{2+} uptake is carried out by proteins involved in high-affinity uptake systems and general divalent metal ion transporters. The two most widely distributed eukaryotic divalent metal-ion uptake protein families are natural resistance-associated protein (NRAMP) and zinc-regulated transporter (ZRT)–iron-regulated transporter (IRT)–like proteins (ZIPs). NRAMP and ZRT proteins function as general divalent metal ion transporters capable of Fe^{2+} uptake as well as intracellular Fe^{2+} transport and are present in almost all algal species. Fe^{3+} uptake is mediated by three main mechanisms: transferrin proteins capable of direct uptake of Fe^{3+}, present in mammals, plants, and algae; high-affinity uptake systems found in plants, algae, fungi, and humans; and the production of Fe^{3+}-binding organic ligands. Among the transferrin proteins, those belonging to the iron starvation–induced proteins (ISIPs) group are up-regulated under low iron conditions, and some of them are expressed solely under iron limitation. High-affinity uptake systems include an iron reductase (FRE), a multicopper oxidase (MCO), and an iron permease. The first step of a high-affinity uptake system is the reduction of Fe^{3+} by FRE, creating a pool of soluble Fe^{2+} in close vicinity to the cell. The accumulated pool of Fe2 + is re-oxidized to Fe^{3+} via an MCO. The iron permease then internalizes the oxidized Fe^{3+}. The reduction of iron is also necessary to release iron from siderophores or other organic compounds. Siderophores are organic ligands synthesized in bacteria from amino acids via non-ribosomal peptide synthases. In general, siderophores are weak acids forming octahedral structures that complex Fe^{3+} via electronegative oxygen atoms. The selectivity for Fe^{3+} prevents the binding of other dissolved divalent metal ions. Specific transporter proteins are responsible for uptake of the siderophore-iron complex, and iron is released from the complex via reduction to Fe^{2+}. Algae do not produce siderophores, but some algal species can use iron siderophores produced by other organisms.

Algae possess four different iron acquisition strategies for iron uptake: siderophore-mediated uptake, reductive high-affinity uptake, transferrin-mediated uptake of Fe^{3+}, and Fe^{2+} uptake via general divalent metal uptake proteins.

Different algal groups use different uptake strategies. Among prokaryotes, cyanobacteria have significantly higher iron demand than heterotrophic prokaryotes, as demonstrated by the non-diazotroph *Synechocystis*, which can store as much as 50% of cellular iron in bacterioferritin. Some other non-diazotrophs cyanobacteria, such as *Synechococcus*, can produce large numbers of siderophores, while the great majority of these microalgae can only import iron-loaded siderophores from the outer membrane into the periplasmic space by means of TonB-dependent transporters (TonB: outer membrane receptors), which are characterized by high affinity and high specificity for siderophores. Once in the periplasm, the siderophores are first bound to a periplasmic protein and then transported across the inner membrane. In the case of *Synechocystis*, the cells use the reductive

pathway for iron acquisition, which allows the reduction and dissociation of a great number of ferric chelates by means of an unique non-specific reductive system, energetically more favorable with respect to siderophore synthesis and transport.

In the case of diazotrophs, the mechanisms of iron uptake are more complex and less elucidated. Nitrogen fixation allows growth in nitrogen-starved waters; however, this process is iron intensive, as the nitrogenase protein complex is composed of the iron-rich proteins NifH (4 iron atoms per homodimer) and NifDK (15 iron atoms per homodimer). Biological nitrogen fixation in cyanobacteria is believed to have evolved in the anoxic ocean where Fe(II) was soluble and thus more bioavailable. Consequently, the scarcity of readily available iron in the modern ocean limits nitrogen fixation. At the same time, oxygenic photosynthesis and nitrogen fixation must be separated due to the extreme sensitivity of the nitrogenase Fe–S clusters to oxygen (cfr. nitrogen cycle). Thus, diazotrophs must balance nitrogen and iron metabolism both in terms of iron utilization and spatial and temporal arrangement of these incompatible reactions.

Trichodesmium is filamentous, non-heterocystous cyanobacteria, which is a successful bloom-forming nitrogen fixer from oligotrophic tropical and subtropical oceans, generating 60 to 80 Tg of new N annually, almost 40% of annual global nitrogen fixation. *Trichodesmium* contributes to sustaining marine life via the active release and release upon death and decay of key nutrients such as carbon and nitrogen, making it a vital player in the biogeochemical cycling of basic elements in contemporary and past oceans. Its thousands of kilometers, wide blooms comprise individual filaments as well as colonies in fusiform (tuft) and radial (puff) shapes, composed of tens to hundreds of individual filaments. The blooms are often associated with dust deposition, specifically in the tropical Atlantic, downwind from the Saharan desert dust plume. Atmospheric dust is a significant source of iron in iron-limited regions of the ocean, but this dust rapidly sinks below the surface, and the low solubility of iron from dust restricts its acquisition by phytoplankton. *Trichodesmium* possesses a higher intracellular iron quota (i.e. the minimum concentration of iron required by an individual cell to sustain its metabolic functions) than other phytoplankton, which results from the combination of iron-rich photosynthetic complexes and nitrogenase. A unique adaptation to this high iron quota is found in colonies of *Trichodesmium,* which can utilize airborne dust deposited on the ocean surface as a source of nutrients, with large colonies more likely to encounter dust particles compared with single cells or filaments, since their intricate morphology ensures the effective capture and retention of particles. Colonies further improve dust retention by active particle shuttling from the periphery to the colony core where dust and oxides are actively dissolved in a coordinated movement by trichomes. They have been shown to display a preference for iron-rich particles over iron-free particles. The preferred collection of iron-rich particles and rejection of iron-free particles suggest the ability to chemically sense iron and optimize the supply of this element by selectively utilizing iron-rich dust particles. The main mechanisms for dissolving mineral iron from dust include reductive dissolution and siderophore-mediated dissolution, both thought to be involved in *Trichodesmium* dust. The presence of H_2, which is produced during N_2 fixation, strongly stimulates mineral iron uptake by natural colonies of *Trichodesmium*, and it has been suggested that H_2 acts as a source of electrons for the reduction of mineral iron by the cells. *Trichodesmium* colonies also host many associated siderophore-producing bacteria. These siderophores have been shown to solubilize iron from its mineral state in dust and make it available to *Trichodesmium* cells. It is not known whether *Trichodesmium* takes up siderophores by a reductive or non-reductive mechanism, but the cells may contain proteins capable of siderophore transport. Interactions of this type are typically mutualistic, with the heterotrophic bacteria facilitating *the* cyanobacterium iron acquisition and *cyanobacterium* colonies providing the carbon and nitrogen substrate for bacterial colonization in the form of exudates.

Another diazotroph that deserves mention is the unicellular *Crocosphaera watsonii* found in the tropical and subtropical open ocean. Its intracellular iron levels change throughout the day, increasing at night with the expression of nitrogenase. Analysis of the *C. watsonii* transcriptomes revealed a temporal pattern to iron demand, correlating with increased expression of flavodoxin and the iron

homeostasis genes in the evening. This suggests coordination with nitrogenase activity. A similar increase in evening expression of these iron-related genes is also seen in *Cyanothece*, another unicellular diazotroph. In *Crocosphaera*, the synthesis of photosynthesis-related proteins peaks in the day, and the proteins are degraded as evening approaches. Conversely, the nitrogenase complex proteins are absent in the day and synthesized at night. At the same time, bacterioferritin protein levels cycle, with peaks matching both the maximum iron utilization points for photosynthesis and nitrogen fixation, suggesting a role in handling the iron being transferred between the two systems. *C. watsonii* minimizes its iron quota and creates temporal separation of the two incompatible systems by shifting iron from photosynthesis in the day to nitrogen fixation at night.

In the case of eukaryotic phytoplankton, most progress to date has been made in understanding the genetic underpinnings of iron homeostasis in green algae and diatoms, in particular *Ostreococcus* (Mamiellophyceae) and *Thalassiosira*, *Phaeodactylum*, and *Pseudo-nitzschia* (Bacillariophyceae). *Ostreococcus* spp. are marine green algae described as the smallest free-living eukaryotes, which possess very small, dense nuclear genomes of 12.5–13.0 Mbp. For comparison, the diatom *Phaeodactylum tricornutum* genome is 27.4 Mbp, and the *Chlamydomonas reinhardtii* genome is 120 Mbp. Two species of *Ostreococcus* have been sequenced from contrasting environments: *O. lucimarinus* from the open coastal waters of the Pacific Ocean and *O. tauri* from a more nutrient-replete oyster production lagoon on the Mediterranean coast of France. Results suggest the presence of genes for divalent metal transporters ZIP and NRAMP, genes with similarity to prokaryotic siderophore uptake, and genes that could represent a siderophore biosynthesis pathway (*O. lucimarinus*). Much like other marine phytoplankton, the iron quota is minimized: iron-free plastocyanin substitutes for cytochrome *c*6; flavodoxin is present; and Ni–SOD, Cu/Zn–SOD, and Mn–SODs appear to replace Fe–SOD. Transcript levels of ferritin and a ferredoxin family protein in *O. tauri* are clock regulated, both peaking at dusk.

Diatoms, which carry out nearly 20% of photosynthesis on earth, are often found in the most iron-limited regions of the ocean. Iron fertilization experiments often result in blooms dominated by diatoms, suggesting diatoms have adaptations that allow survival in iron limited waters and a subsequent rapid multiplication when iron becomes available. The recent metatranscriptomic data show that diatoms possess a unique transcriptional response to the sudden appearance of iron. While other phytoplankton in the community increase gene expression for a broad array of iron proteins like ferredoxin, cytochrome *c*6, and Fe–SOD, diatoms appear to prioritize expression of genes related to photosynthesis and nitrate uptake, reduction, and assimilation. This strategy allows rapid diatom growth and bloom domination.

Iron-regulated ferric reductase genes have been identified in *T. pseudonana* and *P. tricornutum*. These could reduce Fe(III) and Fe bound by siderophores (Fe–S), as could photoreduction (hv). Fe(II) could then enter the cytoplasm through iron-regulated transporters: ZIP in *P. tricornutum* and NRAMP in *T. pseudonana*. In this diatom, extracellular Fe(II) could also be reoxidized and transported through a yeast-like Fe(III) uptake system, utilizing the iron-regulated multi-copper ferroxidase (TpFET3) and Fe(III) permeases (TpFTR1 and TpFTR2). If ferritin is present, it can store iron, likely in the plastid.

Among *Pseudo-nitzschia* species, which frequently dominate diatom blooms, the oceanic *P. granii* is more tolerant of iron limitation than the coastal species *P. multiseries*, presumably because *P. granii* utilizes ferritin to store iron during times of iron availability. In addition to the utilization of ferritin, *Pseudo-nitzschia* is of interest because it is a eukaryotic marine phytoplankton which secretes the phytosiderophore-like compound domoic acid (DA), which is also a neurotoxin and causes wildlife death and amnesic shellfish poisoning in humans (cfr. Chapter 6). DA binds iron and copper and is structurally similar to the plant siderophore mugineic acid secreted into soil by graminaceous plants. Similarly to this acid, DA could facilitate the extraction of iron from terrestrial sediments found in coastal waters. DA production has been observed to be induced by both metal availability and limitation: elevated copper, copper limitation, iron limitation, and iron fertilization. This suggests DA plays a role in both metal uptake during rapidly growing blooms

and survival during limitation. DA binds iron with a low affinity, but the concentrations of DA in naturally occurring blooms are predicted to be sufficient to facilitate iron uptake. The ability to monopolize iron availability via a species-specific phytosiderophore could thus explain the dominance of *Pseudo-nitzschia* in blooms.

THE SILICON CYCLE

The biogeochemical cycle of silicon (Si) might be interpreted as those processes which link sources and sinks of silicic acid [$Si(OH)_4$] generated in aqueous environments by the weathering of Earth's crust by CO_2-rich rainwater. Silicic acid is the only precursor in the processing and deposition of silicon in biota. The biogeochemical cycle of silicon does not facilitate a high biospheric abundance of the element; in fact, the silicon cycle differs from the cycles of carbon, nitrogen, and sulfur, and it is similar to phosphorus in that there is no atmospheric reservoir. The silicon cycle, like those for phosphorus and the divalent metals Ca and Mg, has a significant abiotic drain. The cycle actually consists of two parts: the terrestrial or freshwater cycle and the marine cycle, the former feeding the latter. However, its replenishment can only occur via the marine sedimentary cycle. This is dependent upon geotectonic processes, such as mountain building and subduction and, as such, will incur delays of tens to hundreds of millions years before marine silicon is returned to the terrestrial environment.

The substantial losses of biospheric silicic acid to abiotic sinks may be compensated for in nature by its overall abundance in the Earth's crust. It is the second most abundant element in the lithosphere (28%), iron being the first (35%), and the seventh most abundant element in the universe. It is found in the Earth's crust in silicate minerals, the most prevalent of which are quartz, the alkali feldspars, and plagioclases. The latter two minerals are aluminosilicates and contribute significantly to the aluminum content of the crust. All of these minerals are broken down by the process of weathering.

The dominant form of weathering is the carbonation reaction (Urey reaction), which begins with the production of carbonic acid (H_2CO_3), from rainwater and gaseous CO_2. Carbonic acid is a weak acid but dissolves silicate rocks over geological timescales; the by-products of silicate weathering include calcium and magnesium ions (Ca^{2+} and Mg^{2+}), bicarbonate ions (HCO_3^-), and dissolved silica (SiO_2). These dissolved products are carried by streams and rivers down to the ocean, where their precipitation is either inorganic or organic by the various organisms that use them to make shells of silica or calcium carbonate ($CaCO_3$).

This reaction results in enhanced removal of CO_2 from the atmosphere, because the net effect of silicate mineral weathering is to convert soil carbon, derived ultimately from photosynthesis, into dissolved HCO_3^-.

On a geological timescale, this transfer is an important control on the CO_2 content of the atmosphere and hence global climate. Weathering is a complex function of rainfall, runoff, lithology, temperature, topography, vegetation, and magnitudes. Algae, plants, and their associate microbiota directly affect silicate mineral weathering in several ways: by generation of organic substances, known as chelates, with the ability to decompose minerals and rocks by the removal of metallic cations; by modifying pH through production of CO_2 or organic acids such as acetic, citric, phenolic, and so on; and finally by altering the physical properties of a soil, particularly the exposed surface areas of minerals and the residence time of water.

Silicifiers are among the most important aquatic organisms and include three classes: Bacillariophyceae, Bolidophyceae, and Dictyochophyceae, with diatoms being the world's largest contributors to biosilicification. All these organisms globally consume vast amounts of Si concomitantly with N, P, and organic C, connecting the biogeochemistry of these elements and contributing to the sequestration of atmospheric CO_2 in the oceans.

Since amorphous silica (SiO_2) is an essential component of the diatom cell wall, silicon availability is a key factor in the regulation of diatom growth in nature; in turn, the use of silicon by diatoms

dominates the biogeochemical cycling of silicon in the sea, with each atom of silicon weathered from land passing through a diatom an average of 39 times before burial in the sea bed.

Several thousand million years ago, little if any of the life on Earth was involved in the processing of silicic acid to amorphous silica ($SiO_2 \times nH_2O$). The concentration of silicic acid in the aqueous environment was high, on the millimolar order, and reflected equilibration according to the dominant mineral weathering reactions at that time. The prevalence of these environments rich in silicic acid is indicated in the fossil record by evidence of blue-green algae found encased in silica cherts. It is important to recognize that implicit in this observation is the acceptance that early biochemical evolution proceeded within environments which, relative to the conditions which prevail today, were extremely rich in silicic acid. Concomitant with the advent of dioxygen, and its subsequent gradual increase in the atmosphere, there occurred an increasing number of organisms within which silicic acid was processed to silica. The most important of these, in terms of their diversity, ubiquity (both freshwater and marine species), and biomass, were the diatoms. Diatoms are characterized by a silica frustule which surrounds their cell wall. Silicic acid is freely diffusible across the cell walls and membranes, and, in most cell types of most organisms, the intracellular concentration of silicic acid equilibrates with the extracellular environment according to a "Donnan equilibrium" (the equilibrium characterized by an unequal distribution of diffusible ions between two ionic solutions separated by a membrane which is impermeable to at least one of the ionic species present). However, while the intracellular concentration of the silicic acid in the diatom has not been measured, it is likely that it is under kinetic, as opposed to thermodynamic, control and that it is maintained at an extremely low level, probably less than 1 μmol. This kinetic control of the intracellular silicic acid concentration may be achieved through the condensation and polymerization of silicic acid in a number of chemical (e.g. pH-controlled) and physical (e.g. membrane-bound) compartments, eventually resulting in amorphous silica. This biogenic silica is then deposited in a controlled manner to form the intricate and elaborate silica frustules.

Evidence provided by biochemical and ultrastructural data showed that diatoms were derived from a secondary endosymbiotic event involving a red alga that occurred sometime between 1200 and 700 Ma and that was common to all ochrophytes, dinoflagellates, and coccolithophores. The diatom genome sequences analyzed to date confirm a red algal endosymbiont, but the abundance of genes apparently derived from a green algal source has led to the controversial hypothesis that a green algal endosymbiont preceded the red alga and that many of its genes were retained prior to the arrival of the red alga, whereas the red algal genes that were acquired later were not. In such a scenario, diatoms (and other photosynthetic algae) bear red algal–derived chloroplasts driven to a significant extent by green algal genes encoded in the nucleus, which may have provided a selective advantage in ocean environments and thus underlie why such organisms have come to dominate in the ocean whereas photosynthetic organisms harboring green algal-derived plastids dominate terrestrial habitats. An additional feature is the presence of several hundreds of bacterial genes scattered throughout diatom genomes, representing around 5% of total gene content. Many such genes appear to have ancient origins because they are shared among several diatoms and encode functions essential for diatom biology. Diatom-specific transposable elements additionally appear to have been instrumental in generating the rich diversity of species found today. The chimeric nature of diatom genomes has brought together unique combinations of genes that collectively encode non-canonical pathways of nutrient assimilation and metabolite management, including for a urea cycle that is integral to nitrogen metabolism and a novel configuration coupling photosynthesis and respiration between diatom chloroplasts and mitochondria. Diatom genomes have furthermore been found to encode large numbers of cyclins, key regulators of cell division, that may underlie their impressive proliferative capacity during oceanic blooms, as well as specialized stress-responsive light-harvesting chlorophyll-binding proteins that may be of particular importance for survival in polar-adapted diatoms. The peculiarities of the diatom toolbox used to manage silicon metabolism and to generate their silicified cell walls are also being revealed, and it is emerging that such

processes are deeply integrated within diatom primary metabolism, such as for the generation of frustule-localized long chain polyamines as offshoots of the urea cycle.

What is ascertained, and is becoming more and more clear, is the formative role played by diatoms and other silica-forming organisms, such as silicoflagellates, radiolarian, and sponges, in the biogeochemical cycle of silicon.

The reactions of condensation of silicic acid and subsequent polymerization to form biogenic silica eventually (i.e. upon the death of the organism) result in a net loss of silicic acid to the biosphere. The rate of the forward reaction (condensation and polymerization) is orders of magnitude higher than that of the reverse (regeneration of silicic acid pool), with the result that, concomitant with the rise of the diatoms and other silica-forming organisms, there was a significant reduction in the environmental silicic acid concentration. Silica frustules are formed in a matter of hours to days, whereas the rate at which silicic acid is returned to the biosphere through the dissolution of the frustules of dead diatoms as they sink in the water column is on the order of 10^{-9} μmol $m^{-2}s^{-1}$. In addition, the dissolution of these sinking frustules can be greatly influenced by the chemistry of the water column. For example, the frustule is a highly adsorptive surface and is implicated in the removal of metal ions, for example, aluminum, from the water column. These adsorptive processes tend to stabilize the frustule surface towards dissolution and thereby reduce the amount of silicic acid returned to the biosphere during sedimentation. Once the frustules have settled to the bottom, their silica enters the sedimentary cycle, whereupon it is unlikely to reappear in the biosphere for tens of millions of years.

The biologically induced dramatic decline in the environmental silicic acid concentration had the effect of accelerating the rate of mineral weathering. This, in turn, consumed more carbon dioxide and precipitated a gradual reduction in the atmospheric concentration of this "greenhouse" gas. The impact of the emergence of diatoms and other silica-forming organisms, and latterly the spread of rooted vascular plants, on the biogeochemical cycle of silicon contributed significantly to the global cooling which has resulted in the climate of today. The diatoms, in particular, are extremely successful organisms and will continue to deposit silica frustules of varying silica content at micromolar concentrations of environmental silicic acid. In this way they are a continuous accelerant of mineral weathering almost regardless of how low the environmental silicic acid concentration may fall.

From the advent of the silica-forming organisms, the process of biochemical evolution has continued in silicon-replete, though no longer of millimolar concentration, environments. Diatoms in sedimentary deposits of marine and continental, especially lacustrine, origin belong to different geologic ranges and physiographic environments. Marine diatoms range in age from Early Cretaceous to Holocene, and continental diatoms range in age from Eocene to Holocene; however, most commercial diatomites, both marine and lacustrine, were deposited during the Miocene. Marine deposits of commercial value generally accumulated along continental margins with submerged coastal basins and shelves where wind-driven boundary currents provided the nutrient-rich upwelling conditions capable of supporting a productive diatom habitat. Commercial freshwater diatomite deposits occur in volcanic terrains associated with events that formed sediment-starved drainage basins. Marine habitats generally are characterized by stable conditions of temperature, salinity, pH, nutrients, and water currents, in contrast to lacustrine habitats, which are characterized by wide variations in these conditions. Marine deposits generally are of higher quality and contain larger resources, owing to their greater areal extent and thickness, whereas most of the world's known diatomites are of lacustrine origin.

Unlike many other algae, whose division cycles are strongly coupled to the diel light cycle, diatoms are capable of dividing at any point of the diel cycle. This light independence extends to their nutrient requirements, with nitrate and silicic acid uptake and storage continuing during the night through the use of excess organic carbon synthesized during the day. Moreover, the silica frustule has recently been shown to play a role in CO_2 acquisition, which indicates that Si limitation can induce CO_2 limitation in diatoms. Specifically, the silica frustule facilitates the

enzymatic conversion of bicarbonate to CO_2 at the cell surface by serving as a pH buffer, thus enabling more efficient photosynthesis. This control by diatoms and the reduction in silicate input from rivers due to cooling and drying of the climate offers a feedback mechanism between climate variability, diatom productivity, and CO_2 exchange. These features of diatom physiology almost certainly contribute to the in situ observation that diatoms have greater maximum growth rates relative to comparable algae. Further, as long as silicic acid is abundant (and other nutrients non-limiting), diatoms are found to dominate algal communities. They typically dominate well-mixed coastal and upwelling regions and are often the main component of oceanic spring blooms, because they can divide more rapidly than other phytoplankton when conditions become favorable for growth. They also dominate at high latitudes and in polar environments, in particular along the sea-ice edge where other photosynthetic organisms are rare, making the Arctic and Southern Ocean ecosystems especially dependent on them. As stated, the importance of diatoms for the biogeochemistry of these regions over geological time periods is evidenced by the enormous deposits of siliceous mud and oozes more than 1 km thick in places. The rise of diatoms in the last few millions of years is accompanied by the establishment of the main petroleum source rocks, derived from carbon export. The often spatial coincidence of silica and fossil fuels, together with the worldwide survey of biomarkers (such as 24-norcholestane or C28-C29 steranes) in sediments and source rocks, indicate a crucial role of diatoms in the formation of today's reserves. Moreover, several petroleum basins overlap with regions where diatoms thrive, such as oceanic coastal environments and the Arctic Ocean. Although previous assessments suggest that petroleum source rocks are relatively low in abundance in the Southern Ocean, this region may hold significant resources as well.

Diatoms are estimated to contribute up to 45% of total oceanic primary production, around one fifth of all the photosynthesis on Earth, similar to all terrestrial rainforests combined, making them major players in the cycling of all biological elements. They globally uptake and process more than 240 Tmol Si yr^{-1}. Nowadays, risk to diatoms comes from both climate-forced impacts and anthropogenic sources. Reduced input of silicate due to damming of rivers and changes in water use patterns and increased input of inhibitory levels of ammonium to estuaries and adjacent coastal waters affect diatom success. The high ammonium concentrations prevalent in some estuaries, a result of anthropogenic inputs from sewage treatment plants and agricultural runoff, inhibit the uptake of nitrate by diatoms, which draw primarily on nitrate for high growth rates.

Aside from their role in the silicon cycle, diatoms have also attracted attention because of their importance to the export of primary production to the ocean's interior. Aggregation and sinking are important aspects in the life history of many diatom species, and high sinking velocities, whether as individuals, aggregates, or mats, allow diatoms to rapidly transport material out of the surface mixed layer. Additionally, mesozooplankton grazers that consume diatoms produce large, fast-sinking fecal pellets. These processes remove nutrients and carbon from the productive surface waters before they can be remineralized, making the diatoms crucial to "new" (or export) production. So long as silicic acid is available, diatoms act as a conduit for nutrients and carbon to deep waters, contrasting with the production of other algae, which "trap" nutrients in a regeneration loop at the surface.

Though diatoms are by far the most important organisms that take up silicic acid to form their encasing structures, silicoflagellates (Dictyochophyceae) also deserve mention. These unicellular heterokont algae belong to a small group of siliceous marine phytoplankton. Silicoflagellates live in the upper part of the water column and are adapted for life in tropical, temperate, and frigid waters. Silicoflagellates have a multi-stage life cycle, not all stages of which are known. The best-known stage consists of a naked cell body with a single anterior flagellum and numerous plastids contained within an external lateral skeleton. This skeleton is composed of hollow beams of amorphous silica, forming a network of bars and spikes arranged to form an internal basket. The siliceous skeleton of silicoflagellates is very susceptible to dissolution, and therefore their preservation is often hindered by diagenetic processes; moreover, their abundance is relatively low compared to that of other

siliceous microfossils, since they form a small component of marine sediments; both these reasons make their presence rare in the sedimentary record.

THE SULFUR CYCLE

Sulfur is an essential element for autotrophs and heterotrophs. In its reduced oxidation state, the nutrient sulfur plays an important part in the structure and function of proteins. Three amino acids found in almost all proteins (cysteine, cystine, and methionine) contain carbon-bound sulfur. Sulfur is also found in sulfolipids, some vitamins, sulfate esters, and a variety of other compounds.

In its fully oxidized state, sulfur exists as sulfate and is the major cause of acidity in both natural and polluted rainwater. This link to acidity makes sulfur important to geochemical, atmospheric, and biological processes such as the natural weathering of rocks, acid precipitation, and rates of denitrification. The sulfur cycle is also one of the main elemental cycles most heavily perturbed by human activity. Estimates suggest that emissions of sulfur to the atmosphere from human activity are at least equal to or probably larger in magnitude than those from natural processes. Like nitrogen, sulfur can exist in many forms: as gases or sulfuric acid particles. The lifetime of most sulfur compounds in the air is relatively short (e.g. days). Superimposed on these fast cycles of sulfur are the extremely slow sedimentary-cycle processes or erosion, sedimentation, and uplift of rocks containing sulfur. Sulfur compounds from volcanoes are intermittently injected into the atmosphere, and a continual stream of these compounds is produced from industrial activities. These compounds mix with water vapor and form sulfuric acid smog. In addition to contributing to acid rain, the sulfuric acid droplets of smog form a haze layer that reflects solar radiation and can cause a cooling of the earth's surface. While many questions remain concerning specifics, the sulfur cycle in general, and acid rain and smog issues in particular, are becoming major physical, biological, and social problems.

The sulfur cycle can be thought of as beginning with the gas sulfur dioxide (SO_2) or the particles of sulfate (SO_4^{2-}) compounds in the air. These compounds either fall out or are rained out of the atmosphere. Algae and plants take up some forms of these compounds and incorporate them into their tissues. Then, as with nitrogen, these organic sulfur compounds are returned to the land or water after the algae and plants die or are consumed by heterotrophs. Bacteria are important here as well since they can transform the organic sulfur to hydrogen sulfide gas (H_2S). In the oceans, certain phytoplankton can produce a chemical that transforms organic sulfur to SO_2 that resides in the atmosphere. These gases can re-enter the atmosphere, water, and soil and continue the cycle. An estimated 1320 Tg of sulfur is fixed by marine phytoplankton into organic material annually, of which ~600 Tg is subsequently released into seawater as dissolved organic sulfur (DOS) by various biological processes. The majority of these phytoplankton-derived metabolites are taken up from the DOS pool by marine bacteria on short time scales (minutes to days). The more reduced the sulfur atom is in DOS compared to sulfate, the more readily it can be incorporated into cellular material, and the more energy it yields for bacteria when oxidized back to sulfate. A fraction of the DOS pool (~25 Tg) is volatile and effluxes to the atmosphere (~4% of annual DOS inputs), whereas another ~1 Tg of DOS (0.2%) becomes part of the ocean's non-labile dissolved organic matter pool, with an estimated average lifetime of ~4,000 years.

All living organisms require S as a minor nutrient, in roughly the same atom proportion as phosphorus. Sulfur is present in freshwater algae at a ratio of about 1 S atom to 100 C atoms (0.15 to 1.96% by dry weight), and the S content varies with species, environmental conditions, and season. Vascular plants, algae, and bacteria (except some anaerobes that require S^{2-}) have the ability to take up, reduce, and assimilate SO_4^{2-} into amino acids and convert SO_4^{2-} into ester sulfate compounds.

Reduced volatile sulfur compounds, which are released to the oxygen-rich atmosphere, are chemically oxidized during their atmospheric lifetime and finally end up as SO_2 (oxidation state +4) and sulfuric acid (H_2SO_4) and particulate SO_4^{2-} (oxidation state +6) and methane sulfonate (oxidation

state +6). It is mainly these compounds that are removed from the atmosphere and brought back to the earth by dry and wet deposition.

Since the oxidation state of sulfur in H_2SO_4 (+6) is the most stable under oxic conditions, sulfate is the predominant form of sulfur in oxic waters and soils. Thus, the reduction of sulfate to a more reduced sulfur species is a necessary prerequisite for the formation of volatile sulfur compounds and their emission to the atmosphere. Biochemical processes which lead to this reduction can be considered the driving force of the atmospheric sulfur cycle.

Two types of biochemical pathways of sulfate reduction are important in the global cycles: dissimilatory and assimilatory sulfate reduction. Dissimilatory reduction of sulfate is a strictly anaerobic process which takes place only in anoxic environments. Sulfate-reducing bacteria reduce sulfate and other sulfur oxides to support respiratory metabolism, using sulfate as a terminal electron acceptor instead of molecular oxygen. Since the process is strictly anaerobic, dissimilatory sulfate reduction occurs largely in stratified, anoxic water basins and in sediments of wetlands, lakes, and coastal marine ecosystems. The process is particularly important in marine ecosystems, including salt marshes, because sulfate is easily available due to its high concentration in seawater (28 mM; 900 mg l^{-1}).

In contrast to animals, which are dependent on organo-sulfur compounds in their food to supply their sulfur requirement, other biota (bacteria, cyanobacteria, fungi, eukaryotic algae, and vascular plants) can obtain sulfur from assimilatory sulfate reduction for synthesis of organo-sulfur compounds. Sulfate is assimilated from the environment, reduced inside the cell, and fixed into sulfur-containing amino acids and other organic compounds. The process is ubiquitous in both oxic and anoxic environments. Most of the reduced sulfur is fixed by the intracellular assimilation process, and only a minor fraction of the reduced sulfur is released as volatile gaseous compounds, as long as the organisms are alive. Despite the small absolute amount, this is the largest natural source of sulfur that is released into the atmosphere. However, after death of the organisms, microbial degradation liberates reduced sulfur compounds (mainly in the form of hydrogen sulfide [H_2S] and DMS but also as organic sulfides) to the environment. During this stage, volatile sulfur compounds may escape to the atmosphere. However, as with sulfides formed from dissimilatory sulfate reduction, the sulfides released during decomposition are chemically unstable in an oxic environment and are re-oxidized to sulfate by a variety of microorganisms.

Sulfate is taken up into the cell by an active transport mechanism and inserted into an energetically activated molecule, APS (adenosine-5'-phosphosulfate), which can be further activated at the expense of one more ATP molecule to PAPS (3'-phosphoadenosine-5'-phosphosulfate). It is then transferred to a thiol carrier (a molecule with a -SH group) and reduced to the −2 oxidation state. In contrast to nitrate assimilation, where the various intermediates are present free in the cytoplasm, sulfur remains attached to a carrier during the reduction sequence. In a final step, the carrier-bound sulfide reacts with *O*-acetyl-serine to form cysteine. Cysteine serves as the starting compound for the biosynthesis of all other sulfur metabolites, especially the other sulfur-containing amino acids homocysteine and methionine. Cysteine and methionine are the major sulfur amino acids and represent a very large fraction of the sulfur content of biological materials.

One aspect of the sulfur metabolism of algae deserves special mention because of its atmospheric consequences: many types of marine algae, including planktonic algae, such as Coccolithophyceae, Dinophyceae, Bacillariophyceae, Chrysophyceae, and prasinophytes, and macroalgae belonging to the Chlorophyceae and Rhodophyceae produce large amounts of dimethylsulfonium propionate from sulfur-containing amino acids (methionine). Dinoflagellates accumulate DMSP to high millimolar concentrations and taurine to micromolar concentrations; the coccolithophore *Emiliania huxleyi* is also high in DMSP, along with di-hydroxy-propanesulphonate (DHPS) and cysteate, at millimolar and micromolar concentrations, respectively. Diatoms are the most versatile synthesizers of sulfur metabolites, producing DMSP, DHPS, cysteate, and sulfolactate and, in some species, isethionate and taurine. Cyanobacteria metabolomes contain millimolar concentrations of cysteate. These sulfur metabolites are released from phytoplankton into the marine DOS pool via a number

of mechanisms. Export from living cells (either passive or active) released into sea water by viral lysis or protist grazing and leakage from cells during bloom senescence are the main processes allowing heterotrophic bacteria access to a pool of labile organic sulfur.

DMSP is the precursor of DMS, its enzymatic cleavage product, which is a gas with a strong smell and in turn is a major source of atmospheric sulfur. Marine organisms generate about half the biogenic sulfur emitted to the atmosphere annually, and the majority of this sulfur is produced as DMS. Because reduced sulfur compounds such as DMS are rapidly oxidized to sulfur dioxides that function as cloud condensation nuclei, the production of DMS can potentially affect climate on a global scale. DMS has also an peculiar role: birds use DMS as a foraging cue, as algae being consumed by fish release DMS, as a consequence bringing the presence of the fish to the attention of the birds.

DMSP can function as osmoregulator, buoyancy controller, cryoprotectant, and antioxidant. Freshwater algae do not produce DMSP, since, being an osmolyte, it has no significance in freshwater systems. It has also been postulated that DMSP production is indirectly related to the nitrogen nutrition of algae, with DMSP being a store for excess sulfate taken up while assimilating the molybdenum necessary to synthesize nitrate reductase or nitrogenase. The cleavage of DMSP by means of the enzyme DMSP lyase produces gaseous DMS and acrylic acid. DMSP can also be released from phytoplankton cells during senescence, whereas zooplankton grazing on healthy cells is thought to facilitate the release of DMSP from ruptured algal cells during sloppy feeding. Once released from algal cells, DMSP undergoes microbially mediated conversion by cleavage into gaseous DMS and acrylate.

It had been known for many years that the global budget of sulfur could not be balanced without a substantial flux of this element from the oceans to the atmosphere and thence to land. Once emitted from the sea, DMS is transformed in the atmosphere by free radicals (particularly hydroxyl and nitrate) to form a variety of products, most importantly sulfur dioxide and sulfate in the form of small particles. As already stated, these products are acidic and are responsible for the natural acidity of atmospheric particles; human activities in burning fossil fuels add further sulfur acidity to this natural process. In addition, sulfate particles (natural and human-made) can alter the amount of radiation reaching Earth's surface both directly by scattering of solar energy and indirectly by acting as the nuclei on which cloud droplets form (cloud condensation nuclei, CCN), thereby affecting the energy reflected back to space by clouds (denser cloud albedo). The reduction of the amount of sunlight that reaches the earth surface leads to the consequent reduction of global temperature. This drop in temperature is suggested to cause a decrease in the primary production of DMSP (in other words, DMS). Thus, DMS is considered counteractive to the behavior of greenhouse gases like CO_2 and CH_4. Removal of the algae-DMS–derived sulfur from the air by rain and deposition of particles is an important source of this biologically important element for some terrestrial ecosystems.

LIMITING NUTRIENTS

Among the elements required for algal growth, there are some that can become limiting. The original notion of limitation was introduced by von Liebig more than a century ago to establish a correlation between the yield of a crop and the elemental composition of the substrate required for the synthesis of that crop. Von Liebig stated that if one crop nutrient is missing or deficient, plant growth will be poor, even if the other elements are abundant. That nutrient will be defined as the "limiting nutrient." This concept has come to be known as Liebig's "Law of the Minimum." Simply stated, Liebig's law means that growth is controlled not by the total of nutrients available but by the nutrient available in the smallest quantity with respect to the requirements of the plant. Liebig likens the potential of a crop to a barrel with staves of unequal length. The capacity of this barrel is limited by the length of the shortest stave and can only be increased by lengthening that stave. When that stave is lengthened, another one becomes the limiting factor.

The concentration of a nutrient will give some indication whether the nutrient is limiting, but the nutrient's supply rate or turnover time is more important in determining the magnitude or degree of limitation. For example, if the concentration of a nutrient is limiting, but the supply rate is slightly less than the uptake rate by the algae, then the algae will only be slightly nutrient limited. Not all algae are limited by the same nutrient, but it occurs at the species level; for example, all diatoms are limited by silicate. Moreover, there is a considerable variation in the degree, kind, and seasonality of nutrient limitation, which is related to variations in riverine input but also to conditions and weather in the outflow area.

In general, the growth rate of a population of organisms would be proportional to the uptake rate of that one limiting factor. Nutrient-limited growth is usually modeled with a Monod (or Michaelis-Menten) equation:

$$\mu = \mu_{max}[LN]/([LN]+ K_m) \quad (10)$$

where μ is the specific growth rate of population as a function of $[LN]$; $[LN]$ is concentration of limiting nutrient; μ_{max} is maximum population growth rate (at "optimal" conditions); and K_m is the Monod coefficient, also called the half-saturation coefficient because it corresponds to the concentration at which μ is one-half of its maximum. When the concentration of limiting nutrient $[LN]$ equals K_m, the population growth rate is $\mu_{max}/2$.

As $[LN]$ increases, μ increases, and so the algal population (number of cells) increases. Beyond a certain $[LN]$, μ tends asymptotically to its maximum (μ_{max}), and the population tends to its maximum yield. If this concentration is not maintained, primary productivity rapidly returns to a level comparable to that prior to the nutrient enrichment. This productivity variation is the seasonal blooming. Normal becomes abnormal when there is a continuous over-stimulation of the system by excess supply of one or more limiting nutrients, which leads to intense and prolonged algal blooms throughout the year. The continuous nutrient supply sustains a constant maximum algal growth rate (μ_{max}). Therefore, instead of peaks of normal blooms, followed by periods when phytoplankton is less noticeable, we have continuous primary production. When this occurs, we refer to it as eutrophication. In this process, the enhanced primary productivity triggers various physical, chemical, and biological changes in autotroph and heterotroph communities, as well as changes in processes in and on the bottom sediments and changes in the level of oxygen supply to surface water and oxygen consumption in deep waters. Eutrophication is considered a natural aging process for lakes and some estuaries, and it is one of the ways in which a water body (lake, rivers, and seas) transforms from a state where nutrients are scarce (oligotrophic) through a slightly richer phase (mesotrophic) to an enriched state (eutrophic).

Eutrophication can result in a series of undesirable effects. Excessive growth of planktonic algae increases the amount of organic matter settling to the bottom. This may be enhanced by changes in the species composition and functioning of the pelagic food web by stimulating the growth of small flagellates rather than larger diatoms, which leads to lower grazing by copepods and increased sedimentation. In areas with stratified water masses, the increase in oxygen consumption can lead to oxygen depletion and changes in community structure or death of the benthic fauna. Bottom-dwelling fish may either die or escape. Eutrophication can also promote the risk of harmful algal blooms that may cause discoloration of the water, foam formation, death of benthic fauna and wild or caged fish, or shellfish poisoning of humans. Increased growth and dominance of fast-growing filamentous macroalgae in shallow sheltered areas is yet another effect of nutrient overload which will change the coastal ecosystem, increase the risk of local oxygen depletion, and reduce biodiversity and nurseries for fish.

Human activities can greatly accelerate eutrophication by increasing the rate at which nutrients and organic substances enter aquatic ecosystems from their surrounding watersheds, for example, introducing detergents and fertilizers that are very rich in phosphorus into water bodies. The resultant aging, which occurs through anthropogenic activity, is termed cultural eutrophication.

Globally, nitrogen and phosphorus are the two elements that immediately limit, in a Liebig sense, the growth of photosynthetic organisms. Silicon could also become a more generally limiting nutrient, particularly for diatom growth. These nutrients are present in algal cells in a species-specific structural ratio, the so-called *Redfield ratio*, which determines the nutrient requirement of the species and whose value depends on the conditions under which species grow and compete. The Redfield ratio is 106 C:16 N:1 P (mean ratio by weight ≈ 40:7:1); over the past decades, high-resolution measurements have revealed notable deviations of N:P in the oceans from the Redfield ratio, and a clear meridional N:P pattern is observed. For instance, N:P in the cold, nutrient-rich, high-latitude oceans is ~13:1, whereas in the warm, nutrient-depleted (oligotrophic), mid-latitude oceans, it is ~28:1, values that are respectively lower and higher than the Redfield ratio. Similar patterns have also been observed across seasons. N:P is higher in the summer (warm and nutrient-depleted) and lower in the winter (colder and nutrient-replete) at many sites.

The Redfield ratio is accepted as a general indicator for balanced growth with potential for near-optimum growth rates. Consequently, the species composition of an environment will be determined not only by nutrient availability but also by their proper relation, since changes in nutrient ratio cause shifts in phytoplankton communities and subsequent trophic linkages. Diatoms require relatively nutrient-rich conditions and typically display lower-than-Redfield N:P. In contrast, cyanobacteria, which do well in nutrient-poor regions, display higher ratios under laboratory conditions. Thus, a diatom-dominated biomass, as generally observed at high latitudes, may explain low N:P in these locations, while cyanobacteria-dominated biomass may explain high N:P in oligotrophic systems.

Nitrogen generally limits overall productivity in the marine system, most often at higher salinities and during low-flow periods. However, since a marine system is in stoichiometric balance (i.e. microorganisms alter their external chemical environment, which is reflective of their own elemental biomass composition), any nutrient can become limiting. Phosphorus limitation occurs most often in freshwater system, in environments of intermediate salinities, and along the coasts during periods of high fresh water input. The occurrence of silicon limitation appears to be more spatially and temporally variable than phosphorus or nitrogen limitation and is more prevalent in spring than summer.

In the case of phosphorus, the limitation of algal growth can be at least twofold. First, there is limitation of nucleic acid synthesis. This limitation can be at the level of genome replication or at the level of RNA synthesis (a form of transcriptional control). The limitation can affect photosynthetic energy conversion by reducing the rate of synthesis of proteins in the photosynthetic apparatus, which is effectively negative feedback on photosynthesis. Second, a more immediate response to phosphorus limitation is on the rate of synthesis and regeneration of substrates in the Calvin-Benson cycle, thereby reducing the rate of light utilization for carbon fixation. Cells can also undergo a decrease in membrane phospholipids; moreover, the inability to produce nucleic acids under P limitation limits cell division, leading to an increased cell volume.

On a biochemical level, nitrogen limitation directly influences the supply of amino acids, which in turn limits the translation of mRNA and hence reduces the rate of protein synthesis. Under nitrogen-limited conditions, the efficiency of PSII also decreases, primarily as a consequence of thermal dissipation of absorbed excitation energy in the pigment bed. This appears to be due mainly to a decrease in the number of PSII reaction centers relative to the antennae. The functional absorption cross-section of PSII increases under nitrogen-limiting conditions, while the probability of energy transfer between PSII reaction centers decreases. From a structural point of view, the reaction centers behave as if they were energetically isolated, with a significant portion of the light-harvesting antenna disconnected from the photochemical processes. As nitrogen limitation leads to a reduction of growth and photosynthetic rates, it also leads to a reduction in respiratory rates. The relationship between the specific growth rate and specific respiration rate is linear, with a positive intercept at zero growth, which is termed "maintenance respiration." The

molecular basis of the alterations is unclear; however, the demands for carbon skeletons and ATP, two of the major products of the respiratory pathways, are markedly reduced if protein synthesis is depressed.

The requirement for silicon for construction of the diatom frustule makes this group uniquely subject to silicate limitation. Since silicic acid uptake, silica (SiO_2) frustule formation, and the cell division cycle are all tightly linked, under silica limitation, the diatom cell cycle predominantly stops at the G_2 phase, before the completion of cell division. Thus, an inhibition of cell division linked to an inability to synthesize new cell wall material under silicon limitation can lead to an increase in the volume per cell. This increase could also be partly explained by the formation of auxospores with a larger cell diameter.

SUGGESTED READING

Anbar, A.D. and Knoll, A.H. Protezoic ocean chemistry and evolution: A bioorganic bridge? Science, 297, 1137–1142, 2002.

Astier, J., Rossi, J., Chatelain, P., Klinguer, A., Besson-Bard, A., Rosnoblet, C., Jeandroz, S., Nicolas-Francès, V. and Wendehenne, D. Nitric oxide production and signalling in algae. Journal of Experimental Botany, 72, 781–792, 2021.

Behnke L. and LaRoche, J. Iron uptake proteins in algae and the role of iron starvation-induced proteins. European Journal of Phycology, 55:3, 339–360, 2020.

Benoiston, A.-S., Ibarbalz, F.M., Bittner, L., Guidi, L., Jahn, O., Dutkiewicz, S. and Bowler, C. The evolution of diatoms and their biogeochemical functions. Philosophical Transactions of the Royal Society B: Biological Sciences, 372, 20160397, 2017.

Berman-Frank, I., Lundgren, P. and Falkowski, P. Nitrogen fixation and photosynthetic oxygen evolution in cyanobacteria. Research in Microbiology, 154, 157–164, 2003.

Berman-Frank, I., Lundgren, P., Chen, Y., Kupper, H., Kolber, Z., Bergman, B. and Falkowski, P. Segregation of nitrogen fixation and oxygenic photosynthesis in the marine cyanobacterium *Trichodesmium*. Science, 294, 1534–1537, 2001.

Capone, D.G., Zehr, J.P., Paerl, H.W., Bergman, B. and Carpenter, E.J. *Trichodesmium*, a globally significant marine cyanobacterium. Science, 276, 1221–1229, 1997.

Conley, D.J. Biochemical nutrient cycles and nutrient management strategies. Hydrobiologia, 410, 87–96, 2000.

Conley, D.J. Terrestrial ecosystems and the global biogeochemical silica cycle. Global Biogeochemical Cycles, 16, 1121–1128, 2002.

Cottingham, P., Hart, B., Adams, H., Doolan, J., Feehan, P., Grace, N., Grayson, R., Hamilton, D., Harper, M., Hibbert, B., Lawrance, I., Oliver, R., Robinson, D., Vollenbergh, P. and Whittington, J. Quantifying nutrient-algae relationships in freshwater systems.: Outcomes of a workshop held at Monash University on the 8th August 2000. CRCFE Technical Report 8, CRCFE, Canberra, 2000.

Duhamel, S., Diaz, J.M., Adams, J.C., Djaoudi, K., Steck, V. and Waggoner, E.M. Phosphorus as an integral component of global marine biogeochemistry. Nature Geoscience, 14, 359–368, 2021.

Edwards, A.M., Platt, T. and Sathyendranath, S. The high-nutrient, low-chlorophyll regime of the ocean: Limits on biomass and nitrate before and after iron enrichment. Ecological Modeling, 171, 103–125, 2004.

Exley, C. Silicon in life: A bioinorganic solution to bioorganic essentiality. Journal of Inorganic Biochemistry, 69, 139–144, 1998.

Falkowski, P.G. Rationalizing elemental ratio in unicellular algae. Journal of Phycology, 36, 3–6, 2000.

Gabric, A., Gregg, W., Najjar, R., Erickson, D. and Matrai, P. Modeling the biogeochemical cycle of dimethylsulfide in the upper ocean: A review. Chemosphere—Global Change Science, 3, 377–392, 2001.

Gallon, J.R. N_2 fixation in phototrophs: Adaptation to a specialized way of life. Plant and Science, 230, 39–48, 2001.

Galloway, J.N., Dentener, F.J., Capone, D.G., Boyer, E.W., Howarth, R.W., Seitzinger, S.P, Cleveland, C.C., Green, P.A, Holland, E.A., Karl, D.M., Porter, J.H., Townsend, A.R. and Vorosmarty, C.J. Nitrogen cycles: Past, present and future. Biogeochemistry, 70, 153–226, 2004.

Gao, X., Bowler, C. and Kazamia, E. Iron metabolism strategies in diatoms. Journal of Experimental Botany, 72, 2165–2180, 2021.

Inokuchi, R., Kuma, K., Miyata, T. and Okada, M. Nitrogen-assimilating enzymes in land plants and algae: Phylogenic and physiological perspectives. Physiologia Plantarum, 116, 1–11, 2002.

Jackson, R.L., Gabric, A.J., Cropp, R. and Woodhouse, M.T. Dimethylsulfide (DMS), marine biogenic aerosols and the ecophysiology of coral reefs. Biogeosciences, 17, 2181–2204, 2020.

Kasamatsu, N., Hirano, T., Kudoh, S., Odate, T. and Fukuchi, M. Dimethylsulfopropionate production by psychrophilic diatom isolates. Journal of Phycology, 40, 874–878, 2004.

Kellogg, L.H., Turcotte, D.L. and Lokavarapu, H. On the role of the Urey reaction in extracting carbon from the earth's atmosphere and adding it to the continental crust. Frontiers in Astronomy and Space Sciences, 62, 2019.

Klausmeier, C.A., Litchman, E., Daufresne, T. and Levin, S.A. Optimal nitrogen-to-phosphorus stoichiometry of phytoplankton. Nature, 429, 171–174, 2004.

Leong, Yoong Kit, Chew, Kit Wayne, Chen, Wei-Hsin, Chang, Jo-Shu and Show, Pau Loke. Reuniting the biogeochemistry of algae for a low-carbon circular bioeconomy. Trends in Plant Science, 26:7, 2021.

Letscher, R.T., Hansell, D.A., Carlson, C.A., Lumpkin, R., Knapp, A.N. Dissolved organic nitrogen in the global surface ocean: Distribution and fate. Global Biogeochemical Cycles, 27, 141–153, 2013.

Lomans, B.P., van der Drift, C., Pol A. and Op den Camp, H.J.M. Microbial cycling of volatile organic sulfur compounds. Cellular and Molecular Life Sciences, 59, 575–588, 2002.

Lundgren, P., Soderback, E., Singer, A., Carpenter, E.J. and Bergman, B. *Katagnymene*: characterization of a novel marine diazotroph. Journal of Phycology, 37, 1052–1062, 2001.

Moran, M.A. and Durham, B.P. Sulfur metabolites in the pelagic ocean. Nature Reviews Microbiology, 17, 665–678, 2019.

Morrissey, J. and Bowler, C. Iron utilization in marine cyanobacteria and eukaryotic algae. Frontiers in Microbiology, 3, 43, 2012.

Norman, L., Cabanesa, D.J., Blanco-Ameijeiras, S., Moisset, S.A. and Hassler, C.S. Iron biogeochemistry in aquatic systems: From source to bioavailability. CHIMIA International Journal for Chemistry, 68, 764–771, 2014.

Olejarz, J., Iwasa, Y., Knoll, A.H. and Nowak, M.A. The great oxygenation event as a consequence of ecological dynamics modulated by planetary change. Nature Communications, 12, 1–9, 2021.

Otsuki, T. A study of the biological CO_2 fixation and utilization system. The Science of Total Environment, 27, 121–25, 2201.

Raven, J.A. and White, A.M. The evolution of silicification in diatoms: Inexplicable sinking and sinking as escape? New Phytologist, 162, 45–61, 2004.

Raymond, J., Siefert, J.L., Staples, C.R. and Blankenship, R.E. The natural history of nitrogen fixation. Molecular Biology and Evolution, 21, 541–554, 2004.

Seibach, J. (Ed.). Cellular origin and life in extreme habitats. Volume 3, Kluwe, Dordrecht, 2002.

Sethi, D., Butler, T.O., Shuhaili, F. and Vaidyanathan, S. Diatoms for carbon sequestration and bio-based manufacturing. Biology (Basel), 9:8, 217–248, 2020. doi:10.3390/biology9080217

Sharpley, A.N., Daniel, T., Sims, T., Lemunyon, J., Stevens, R. and Parry, R. Agricultural phosphorus and eutrophication. United states department of agriculture. Agricultural Research Service ARS, 149, 2003.

Slocombe, S.P., Zúñiga-Burgos, T., Chu, L., Wood, N.J., Camargo-Valero, M.A. and Baker, A. Fixing the broken phosphorus cycle: Wastewater remediation by microalgal polyphosphates. Frontiers in Plant Science, 11, 982, 2020.

Sunda, W., Kleber, D.J., Keine, R.P. and Huntsman, S. An antioxidant function for DMSP and DMS in marine algae. Nature, 418, 317–320, 2002.

Sutak, R., Camadro, J.M., Lesuisse, E. Iron uptake mechanisms in marine phytoplankton. Front. Microbiology, 11, 566691, 2020. doi:10.3389/fmicb.2020.566691

Tang, K. Chemical diversity and biochemical transformation of biogenic organic sulfur in the ocean. Frontiers in Marine Science, 7, 68, 2020.

The Open University. Ocean Chemistry and deep-sea sediments. Butterworth-Heinemann, Oxford, 2001.

Tuo, S.-H., Lee Chen, Y.-L., Chen, H.-Y. and Chen, T.-Y. Free-living heterocystous cyanobacteria in the tropical marginal seas of the western North Pacific. Journal of Plankton Research, 39, 404–422, 2017.

Van Alstyne, K.L. and Houser, L.T. Dimethylsulfide release during macroinvertebrate grazing and its role as an activated chemical defense. Marine Ecology Progress Series, 250, 175–181, 2003.

Voss, M. and Hietanen, S. The depth of nitrogen cycling. Nature, 493, 616–618, 2013.

Wang, S., Koedooder, C., Zhang, F., Kessler, N., Eichner M, Shi D. and Shaked, Y. Colonies of the marine cyanobacterium *Trichodesmium* optimize dust utilization by selective collection and retention of nutrient-rich particles. iScience. 9, 25:1, 103587, 2021. doi:10.1016/j.isci.2021.103587. PMID: 35005537; PMCID: PMC8718973

Weber, T. Southern ocean upwelling and the marine Iron cycle. Geophysical Research Letters, 47, 1–5, 2020. doi:10.1029/2020GL090737
Yool, A. and Tyrrel, T. Role of diatoms in regulating the ocean's silicon cycle. Global Biogeochemical Cycles, 17, 1103–1124, 2003.
Zehr, J.P. and Capone, D.G. Changing perspective in marine nitrogen fixation. Science, 368, eaay9514, 2020. doi:10.1126/science.aay9514
Zuo, Z. Why algae release volatile organic compounds, the emission and roles. Front: Microbiology. 10, 491, 2019. doi:10.3389/fmicb.2019.00491
http://eea.europa.eu/publications/soer-2020
http://history.nasa.gov/CP-2156/contents.htm
http://nca2014.globalchange.gov/report/sectors/biogeochemical-cycles
http://nca2018.globalchange.gov/
http://science.nasa.gov/earth-science/focus-areas/carbon-cycle-and-ecosystems
www.physicalgeography.net/
www.soes.soton.ac.uk/staff/tt/eh/biogeochemistry.html


Taylor & Francis
Taylor & Francis Group
http://taylorandfrancis.com

3 Anatomy

CYTOMORPHOLOGY AND ULTRASTRUCTURE

The description of the algal cell will proceed from the outside structures to the inside components. Details will be given only for those structures that are not comparable with analogous structures found in most animals and plants. The reader is referred to a general cell biology textbook for the structure not described in the following.

Outside the Cell

The cell surface forms the border between the external word and the inside of the cell. It serves a number of basic functions, including species identification; uptake and excretion/secretion of various compounds; protection against desiccation, pathogens, and predators; cell signaling; and cell–cell interaction. It serves as an osmotic barrier, preventing free flow of material, and as a selective barrier for the specific transport of molecules. Algae, besides naked membranes more typical of animal cells and cell walls similar to those of higher plant cells, possess a wide variety of cell surfaces. The terminology used to describe cell surface structures of algae is sometimes confusing; to avoid this confusion, or at least to reduce it, we will adopt terminology mainly based on that of Presig et al. (1994).

Cell surface structures can be grouped into four different basic types:

- simple cell membrane (Type 1)
- cell membrane with additional extracellular material (Type 2)
- cell membrane with additional intracellular material in vesicles (Type 3)
- cell membrane with additional intracellular and extracellular material (Type 4)

Type 1—Simple Cell Membrane

This cell surface consists of a simple or modified plasma membrane. The unit membrane is a lipid bi-layer, 7–8 nm thick, rich with integral and peripheral proteins. Several domains exist in the membrane, each distinguished by its own molecular structure. Some domains have a characteristic carbohydrate coat enveloping the unit membrane. The carbohydrate side chains of the membrane glycolipids and glycoproteins form the carbohydrate coat. Differences in thickness of plasma membrane may reflect differences in the distribution of phospholipids, glycolipids, and glycoproteins (Figure 3.1).

A simple plasma membrane is present in the zoospores and gametes of Chlorophyceae (Chlorophyta), Xanthophyceae (Ochrophyta), and Phaeophyceae (Ochrophyta); in the zoospores of the Eustigmatophyceae (Ochrophyta); and in the spermatozoids of Bacillariophyceae (Ochrophyta). This type of cell surface usually characterizes very short-lived stages, and in this transitory naked phase, the naked condition is usually rapidly lost once zoospores or gametes have ceased swimming and have become attached to the substrate, since wall formation rapidly ensues. A simple cell membrane covers the uninucleate cells that form the net-like plasmodium of the Chlorarachniophyceae (Cercozoa) during their whole life history. Most Chrysophyceae occur as naked cells, whose plasma membrane is in direct contact with water, but in *Ochromonas,* the membrane is covered with both a carbohydrate coat and surface blebs and vesicles, which may serve to trap bacteria and other particles that are subsequently engulfed as food. The properties of the membrane or its domains may change from one stage in the life cycle to the next.

DOI: 10.1201/9781003187707-3

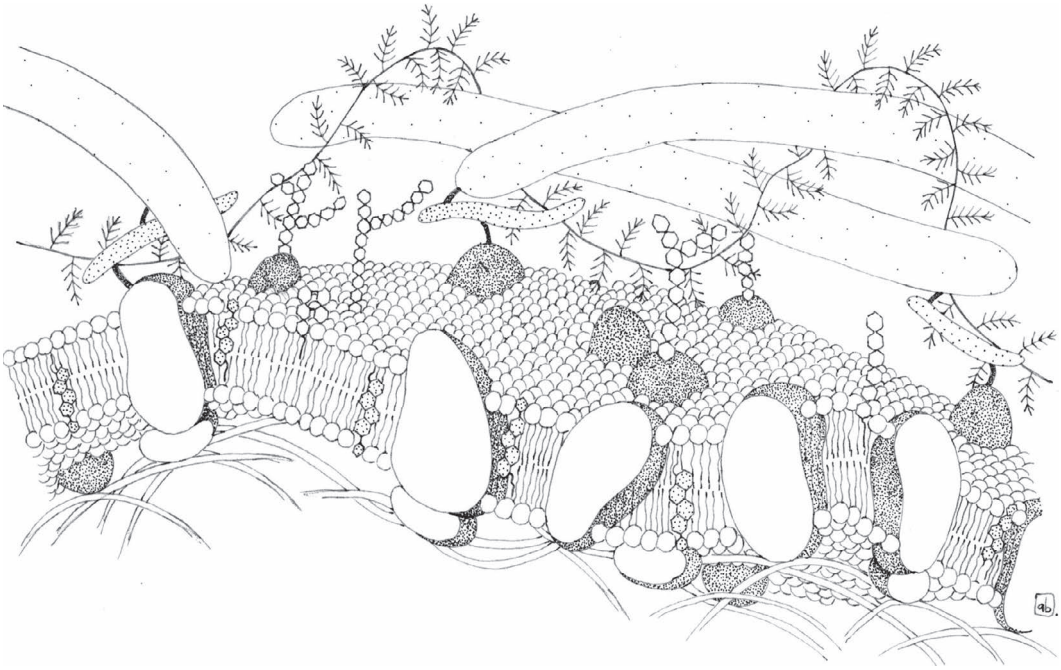


FIGURE 3.1 Schematic drawing of a simple cell membrane.

Type 2—Cell Surface With Additional Extracellular Material

Extracellular matrices occur in various forms and include mucilage and sheaths, scales, frustule, cell walls, loricas, and skeleta.

The terminology used to describe this membrane-associated material is quite confusing, and unrelated structures such as the frustule of diatoms, the fused scaled covering of some prasinophyceae, and the amphiesma of dinoflagellates have been given the same name: theca. Our attempt has been to organize the matter in a less confusing way (at least in our opinion).

Mucilages and Sheaths

These are general terms for some sort of outer gelatinous covering present in both prokaryotic and eukaryotic algae. Mucilages are always present, and we can observe a degree of development of a sheath that is associated with the type of the substrate the cells contact (Figure 3.2). All cyanobacteria secrete a gelatinous material, which, in most species, tends to accumulate around the cells or trichome in the form of an envelope or sheath. Coccoid species are thus held together to form colonies; in some filamentous species, the sheath may function in a similar manner, as in the formation of *Nostoc* balls or in development of the firm, gelatinous hemispherical domes of the marine *Phormidium crosbyanum*. Most commonly, the sheath material in filamentous species forms a thick coating or tube through which motile trichomes move readily. Sheath production is a continuous process in cyanobacteria, and variation in this investment may reflect different physiological stages or levels of adaptation to the environment. Under some environmental conditions, the sheath may become pigmented, although it is ordinarily colorless and transparent. Ferric hydroxide or other iron or metallic salts may accumulate in the sheath, as well as pigments originating within the cell. Only a few cyanobacterial exopolysaccharides have been defined structurally; the sheath of *Nostoc commune* contains cellulose-like glucan fibrils cross-linked with minor monosaccharides, and that of *Microcystis flos-aquae* consists mainly of galacturonic acid, with a composition similar to that of pectin. Cyanobacterial sheaths appear as a major component of soil crusts found throughout the world, from hot desert to polar regions, protecting soil from erosion,



FIGURE 3.2 Transmission electron microscopy image of the apical cell of *Leptolyngbya* spp. trichome in longitudinal section. The arrows point to the mucilaginous sheath of this cyanobacterium. Osmiophilic eyespot globules are present inside the cell. Scale bar 0.15 μm. Courtesy of Patrizia Albertano.

favoring water retention and nutrient bio-mobilization, and affecting chemical weathering of the environment they colonize.

In eukaryotic algae, mucilages and sheaths are present in diverse divisions. The most common occurrence of this extracellular material is in the algae palmelloid phases, in which non-motile cells are embedded in a thick, more or less stratified sheath of mucilage. This phase is so called because it occurs in the genus *Palmella* (Chlorophyceae), but it also occurs in other members of the same class, such as *Asterococcus* sp. (Chlorophyceae), *Hormotila* sp. (Chlorophyceae), *Gloeocystis* sp. (Chlorophyceae), and *Spirogyra* sp. (Zygnematophyceae). A palmelloid phase is present also in *Chroomonas* sp. (Cryptophyceae) and *Gloeodinium montanum* vegetative cells (Dinophyceae) and in *Euglena gracilis* (Euglenophyceae) (cf. Figure 1.45 of Chapter 1). Less common are cases in which filaments are covered by continuous tubular layers of mucilages and sheath. This occurs in the filaments of *Geminella* sp. (Trebouxiophyceae). A more specific covering exists in the filaments of *Phaeothamnion* sp. (Phaeothamniophyceae), since under certain growth conditions, cells of the filaments dissociate and produce a thick mucilage that surrounds them in a sort of colony resembling the palmelloid phase. Mucilages are present also in Rhodophyta; they are produced in the Golgi apparatus and are often abundant in reproductive cells, where mucilages expand upon hydration, playing an important role as a motility aid in the dispersal and attachment of these cells.

Scales

Scales can be defined as organic or inorganic surface structures of distinct size and shape. Scales can be distributed individually or arranged in a pattern, sometimes forming an envelope around

the cell. They occur only in eukaryotic algae, in the divisions of Ochrophyta, Haptophyta, and Chlorophyta. They can be as large as the scales of Haptophyta (1 μm) but also as small as the scales of Prasinodermatophyceae (50 nm). There are at least three distinct types of scales: non-mineralized scales, made up entirely of organic matter, primarily polysaccharides, which are present in the Prasinodermatophyceae; scales consisting of calcium carbonate crystallized onto an organic matrix, such as the coccoliths produced by many Haptophyta; and scales constructed of silica deposited on a glycoprotein matrix, formed by some members of the Ochrophyta.

Most taxa of Prasinodermatophyta possess several scale types per cell, arranged in one to five layers on the surface of the cell body and flagella, those of each layer having a unique morphology for that taxon. These scales consist mainly of acidic polysaccharides involving unusual 2-keto sugar acids, with glycoproteins as minor components. Members of the class Pyramimonadophyceae such as *Pyramimonas* sp. exhibit one of the most complex scaly coverings. It consists of three layers of scales. The innermost scales are small, square, or pentagonal; the intermediate scales are either naviculoid or spiderweb or box shaped (Figure 3.3); the outer layer consists of large basket- or crown-shaped scales. It is generally accepted that scales of the Prasinophytes are synthesized within the Golgi apparatus; developing scales are transported through the Golgi apparatus by cisternal progression to the cell surface and released by exocytosis. In some genera, such as *Tetraselmis* (Chlorodendrophyceae) and *Scherffelia* (Chlorodendrophyceae), the cell body is covered entirely by fused scales. The scale composition consists mainly of acidic polysaccharides. These scales are produced only during cell division. They are formed in the Golgi apparatus, and their development follow the route already described for the scales. After secretion, scales coalesce extracellularly inside the parental covering to form a new cell wall.

In the Haptophyta, cells are typically covered with external scales of varying degrees of complexity, which may be unmineralized or calcified. The unmineralized scales consist largely

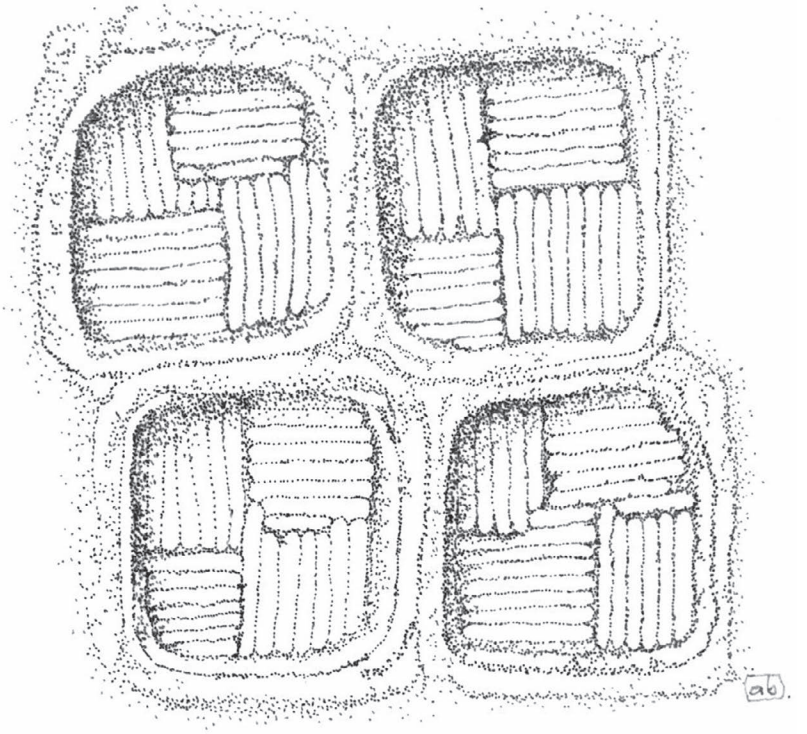


FIGURE 3.3 Box-shaped scales of the intermediate layer of *Pyramimonas* sp. cell body covering.

of complex carbohydrates, including pectin-like sulfated and carboxylated polysaccharides, and cellulose-like polymers. The structure of these scales varies from simple plates to elaborate, spectacular spines and protuberances, as in *Chrysochromulina* sp. (Coccolithophyceae) (Figure 3.4), or to the unusual spherical or clavate knobs present in some species of *Pavlova* (Pavlovophyceae).

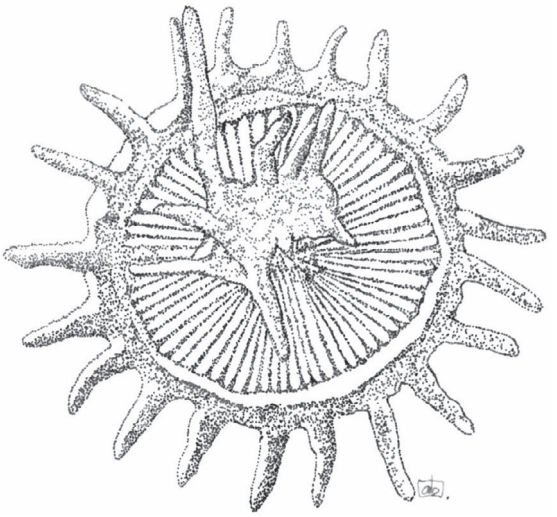


FIGURE 3.4 Elaborate body scale of *Chrysochromulina* sp.

Calcified scales termed coccoliths are produced by the coccolithophorids, a large group of species within the Haptophyta. In terms of ultrastructure and biomineralization processes, two very different types of coccoliths are formed by these algae: heterococcoliths (Figure 3.5) and holococcoliths (Figure 3.6). Some life cycles include both heterococcolith and holococcolith-producing forms. In addition, there are a few haptophytes that produce calcareous structures that do not appear to have either heterococcolith or holococcolith ultrastructure. These may be products of further biomineralization processes, and the general term nannolith is applied to them.

Heterococcoliths are the most common coccolith type and mainly consist of radial arrays of complex crystal units. The sequence of heterococcolith development has been described in detail in *Pleurochrysis carterae* (Coccolithophyceae), *Emiliana huxleyi* (Coccolithophyceae), and the nonmotile heterococcolith phase of *Coccolithus pelagicus* (Coccolithophyceae). Despite the significant diversity in these observations, a clear overall pattern is discernible in all cases. The process commences with formation of a precursor organic scale inside Golgi-derived vesicles; calcification occurs within theses vesicles with nucleation of a proto-coccolith ring of simple crystals around the rim of the precursor base-plate scale. This is followed by growth of these crystals in various directions to form complex crystal units. After completion of the coccolith, the vesicle dilates, its membrane fuse with the cell membrane, and exocytosis occurs. Outside the cell, the coccolith joins other coccoliths to form the coccosphere, that is, the layer of coccoliths surrounding the cell (cf. Figure 1.16 of Chapter 1).

Holococcoliths consist of large numbers of minute morphologically simple crystals. Studies have been performed on two holococcolith-forming species, the motile holococcolith phase of *Coccolithus pelagicus* and *Calyptrosphaera sphaeroidea*. Like the heterococcoliths, the holococcoliths are also underlaid by base-plate organic scales formed inside Golgi vesicles. However, holococcolith calcification is an extracellular process. Experimental evidence revealed that calcification occurs in a single highly regulated space outside the cell membrane but directly above the stack of Golgi vesicles. This extracellular compartment is covered by a delicate organic envelope or "skin." The

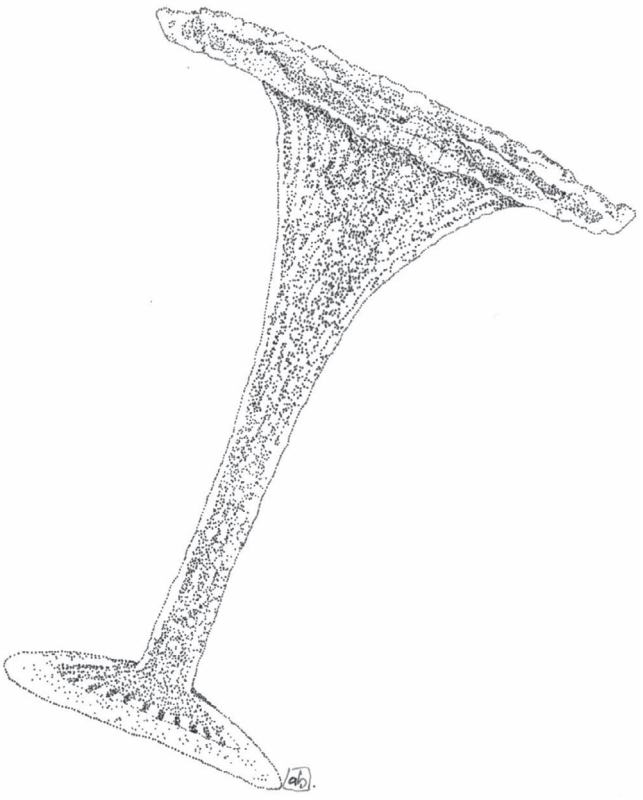


FIGURE 3.5 Heterococcolith of *Discosphaera tubifera*.

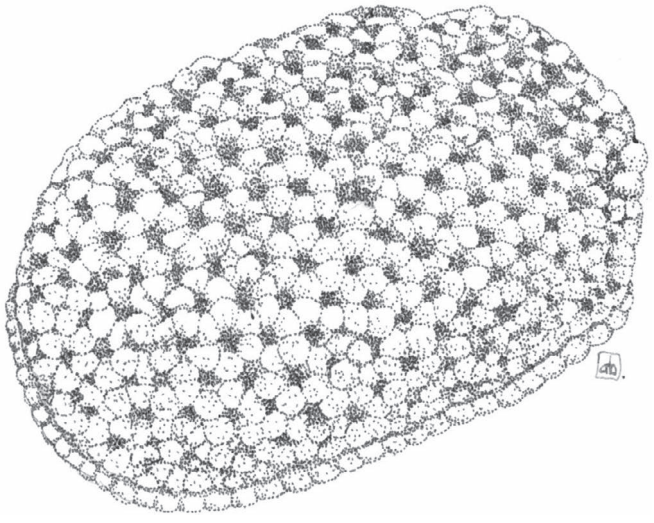


FIGURE 3.6 Holococcolith of *Syracosphaera oblonga*.

cell secretes calcite that fills the space between the skin and the base-plate scales. The coccosphere grows progressively outward from this position. As consequence of the different biomineralization strategies, heterococcoliths are more robust than the smaller and more delicate holococcoliths.

Coccolithophorids, together with corals and foraminifera, are responsible for the bulk of oceanic calcification. Their role in the formation of marine sediment and the impact their blooms may exert on climate change was discussed in Chapter 2.

Members of the Chrysophyceae (Ochrophyta), such as *Synura* sp. and *Mallomonas* sp., are covered by armor of silica scales, with a very complicated structure. *Synura* scales consist of a perforated basal plate provided with ribs, spines, and other ornamentation (Figure 3.7). In *Mallomonas*, scales may bear long, complicated bristles (Figure 3.8). Several scale types are produced in the same cell and deposited on the surface in a definite sequence, following an imbricate, often screw-like pattern. Silica scales are produced internally in deposition vesicles formed by the chrysoplast endoplasmic reticulum, which function as molds for the scales. Golgi body vesicles transporting material fuse with the scale-producing vesicles. Once formed, the scale is extruded from the cell and brought into the correct position on the cell surface.

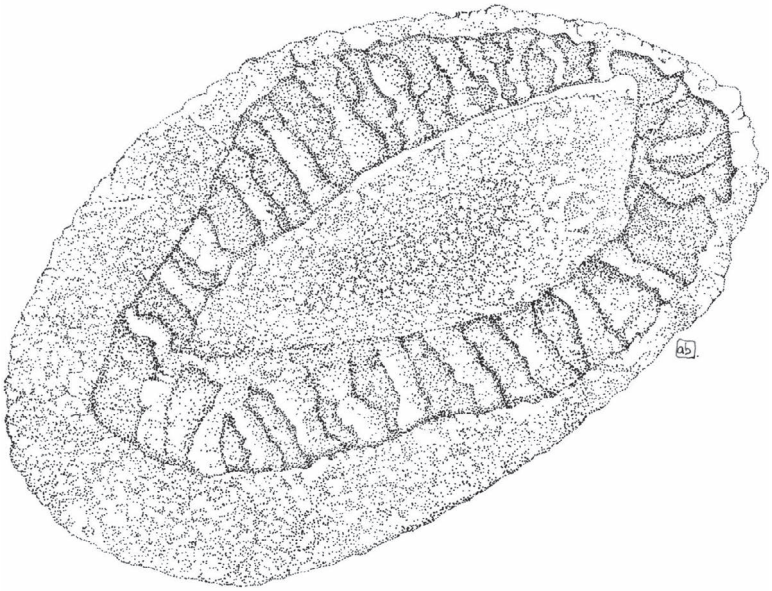


FIGURE 3.7 Ornamented body scale of *Synura petersenii*.

Frustules

This structure is present only in the Bacillariophyceae (Ochrophyta), commonly known as diatoms. The frustule is an ornate cell membrane made of amorphous hydrated silica, which displays intricate patterns and designs unique to each species. This silicified envelope consists of two overlapping valves, an epitheca and a slightly smaller hypotheca. Each theca is composed of a highly patterned valve and one or more girdle bands (cingula) that extend around the circumference of the cell, forming the region of theca overlay. Extracellular organic coats envelop the plasma membrane under the siliceous frustule. They exist in the form of both thick mucilaginous capsules and thin tightly bound organic sheaths. The formation of the frustule has a place in the silica deposition vesicles, derived from the Golgi apparatus, wherein the silica is deposited. The vesicles eventually secrete their finished product onto the cell surface in a precise position.

Diatoms can be divided artificially into centric and pennate according to the symmetry of their frustule. In centric diatoms, the symmetry is radial; that is, the structure of the valve is arranged in reference to a central point (Figure 3.9). However, within the centric series, there are oval, triradiate, quadrate, and pentagonal variations of this symmetry, with a valve arranged in reference to two, three, or more points. Pennate diatoms are bilaterally symmetrical about two axes,

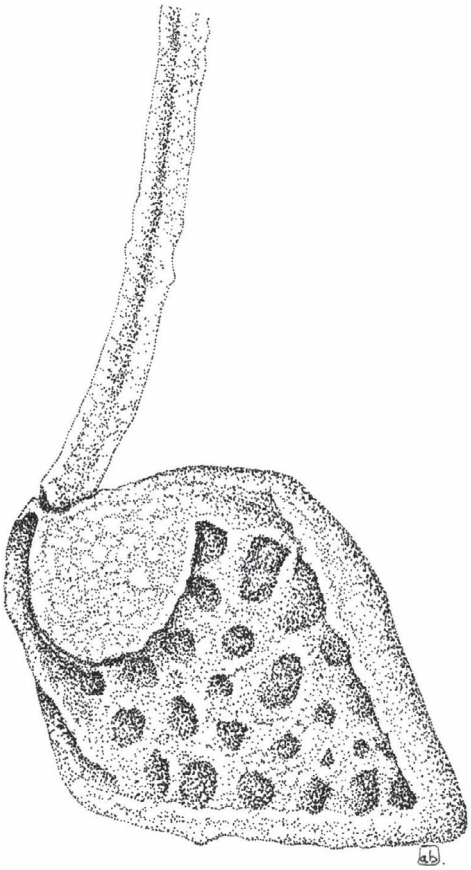


FIGURE 3.8 Body scale of *Mallomonas crassisquama*.

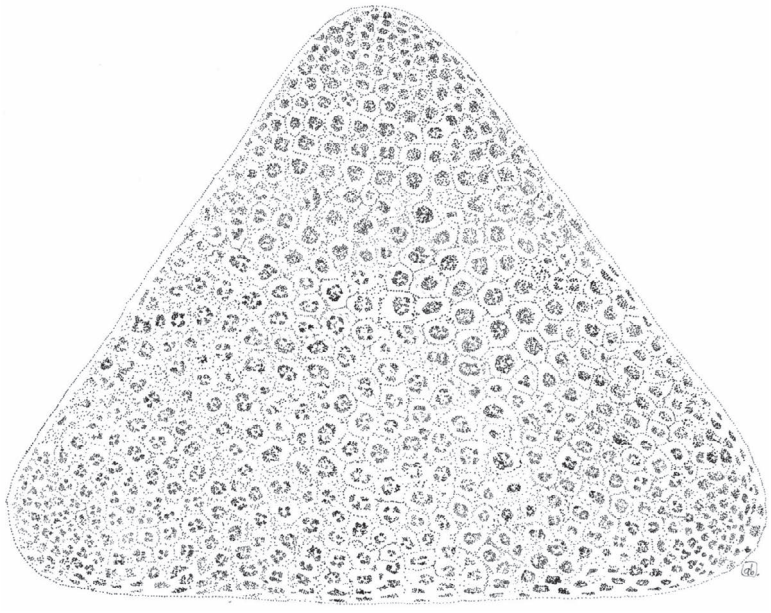


FIGURE 3.9 *Triceratium* sp., a centric diatom.

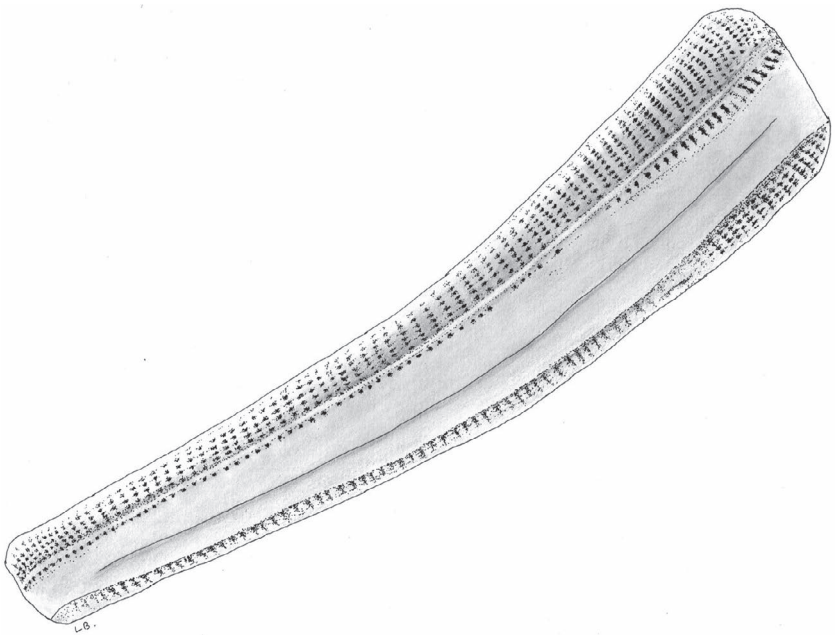


FIGURE 3.10 *Rhoicosphenia* sp., a pennate diatom.

apical and trans-apical, or only one axis (Figure 3.10); some genera possess rotational symmetry (cf. Figure 1.18 of Chapter 1). Valves of some pennate diatoms are characterized by an elongated fissure, the raphe, which can be placed centrally or run along one of the edges. At each end of the raphe and at its center, there are thickenings called polar and central nodules. Additional details in the morphology of the frustule are the stria, lines composed of areolae, pores through the valve that can go straight through the structure or can be constricted at one side. Striae can be separated by thickened areas called costae. Areolae are passageways for gases, nutrient exchanges, and mucilage secretion for movement and attachment to substrates or other cells of colony. Other pores, known as portules, are present on the surface of the valve. There are two types of portules: fultoportulae (Figure 3.11), found only in the order Thalassiosirales, and rimoportulae (Figure 3.12), which are universal. The structure of the fultoportulae is an external opening on the surface of the valve, extended or not into a protruding structure (Figure 3.11). The other end penetrates the silica matrix and is supported with two to five satellite pores. The portules themselves function in the excretion of several materials, among them β-chitin fibrils. These fibrils are manufactured in the conical invaginations in the matrix under the portule. This may be the anchoring site for the protoplast. The rimoportula is similar to the fultoportulae, except that it has a simpler inner structure. The rimoportula does not have satellite pores in the inner matrix. However, the rimoportula does have some elaborate outer structures that bend, have slits, or are capped. Sometimes the valve can grow out beyond its margin in structures called setae that help link adjacent cells into linear colonies as in *Chaetoceros* spp., or it can possess protuberances as in *Biddulphia* spp. that allow the cells to gather in zig-zag chains (Figure 3.13). In other genera such as *Skeletonema*, the valve presents a marginal ridge along its periphery consisting of long, straight spines, which make contact between adjacent cells and unite them into filaments. Some genera also possess a labiate process, a tube through the valve with internally thickened sides that may be flat or elevated.

Diatoms are by far the most significant producer of biogenic silica, dominating the marine silicon cycle. It is estimated that over 30 million km^2 of ocean floor are covered with sedimentary

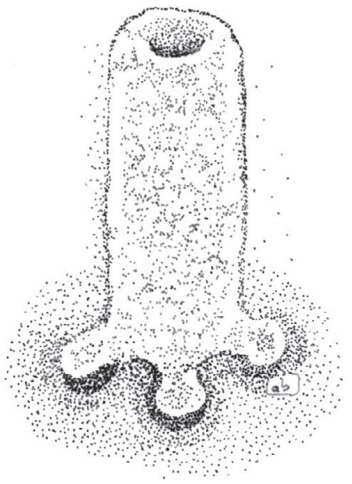


FIGURE 3.11 Fultoportula of *Thalassiosira* sp.



FIGURE 3.12 Rimoportula of *Stephanodiscus* sp.

deposits of diatom frustules. The geological and economical importance of these silica coverings, as well as the mechanism of silica deposition, were discussed in Chapter 2.

Cell Walls

A cell wall, defined as a rigid, homogeneous, and often multilayered structure, is present in both prokaryotic and eukaryotic algae.

In the Cyanobacteria, the cell wall lies between the plasma membrane and the mucilaginous sheath; its fine structure of the cell wall is of Gram-negative type. The innermost layer, the electron-opaque layer or peptidoglycan layer, overlays the plasma membrane, and in most cyanobacteria, its width varies between 1 and 10 nm but can reach 200 nm in some *Oscillatoria* species. Regularly arranged discontinuities are present in the peptidoglycan layer of many cyanobacteria; pores are located in single rows on either side of every cross wall and are also uniformly distributed over the cell surface. The outer membrane of the cell wall appears as a double-track structure tightly connected with the peptidoglycan layer; this membrane exhibits a number of evaginations representing sites of extrusion of material from the cytoplasm through the wall into the slime. The cell wall of genera such as *Prochloron* is comparable with that of the cyanobacteria in structure and contains muramic acid.

A eukaryotic algal cell wall is always formed outside the plasmalemma and is in many respects comparable to that of higher plants. It is present in the Rhodophyta, Eustigmatophyceae (Ochrophyta) (Figures 3.14a and 3.14b), Phaeophyceae (Ochrophyta), Xanthophyceae (Ochrophyta), Chlorophyceae (Chlorophyta), and Charophyceae (Charophyta). Generally, cell walls are made up of two components, a microfibrillar framework embedded in an amorphous mucilaginous material composed of polysaccharides, lipids, and proteins. Encrusting substances such as silica, calcium carbonate, or sporopollenin may be also present. In the formation of algal cell walls, the materials required are mainly collected into Golgi vesicles that then pass it through the plasma membrane, where enzyme complexes are responsible for synthesis of microfibrils in a predetermined direction.

In the Rhodophyta and in particular in the Florideophyceae, the cell wall consists of more than 70% of water-soluble highly hydrophilic sulfated polygalactans, which are polymers of β-(1–4) galactose and α-(1–3) linked 3,6 anhydro galactose. These are the major constituents of agars (less highly sulfated) and carrageenans (more highly sulfated), commercially very important in the food and pharmaceutical industries for their ability to form gels. In the

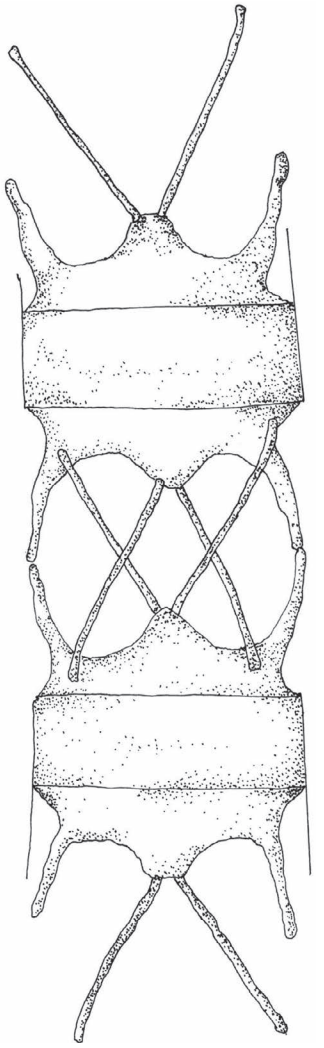


FIGURE 3.13 Cells of *Biddulphia* sp.

Phaeophyceae (Ochrophyta) cell wall, mucilagine are composed primarily of alginic acid; the salts of this acid have valuable emulsifying and stabilizing properties. In the Xanthophyceae (Ochrophyta), the composition of the wall is mainly cellulosic, while in the Chlorophyceae (Chlorophyta), xylose, mannose, and chitin may also be present in addition to cellulose. Some members of the Chlorophyceae (Chlorophyta) and Charophyceae (Charophyta) have calcified walls.

Loricas

These enveloping structures are present in some members of the class Chrysophyceae, (Ochrophyta) such as *Dinobryon* sp. or *Chrysococcus* sp., and in some genera of the Chlorophyceae, such as *Phacotus*, *Pteromonas*, and *Dysmorphococcus*. These loricas are vase-shaped structures with a more or less wide apical opening where the flagella emerge. These structures can be colorless or dark and opaque due to manganese and iron compound impregnation. As we can expect, different shapes correspond to different species. In *Dinobryon* sp., the lorica is an interwoven system of fine cellulose or chitin fibrils (Figure 3.15). In *Chrysococcus*

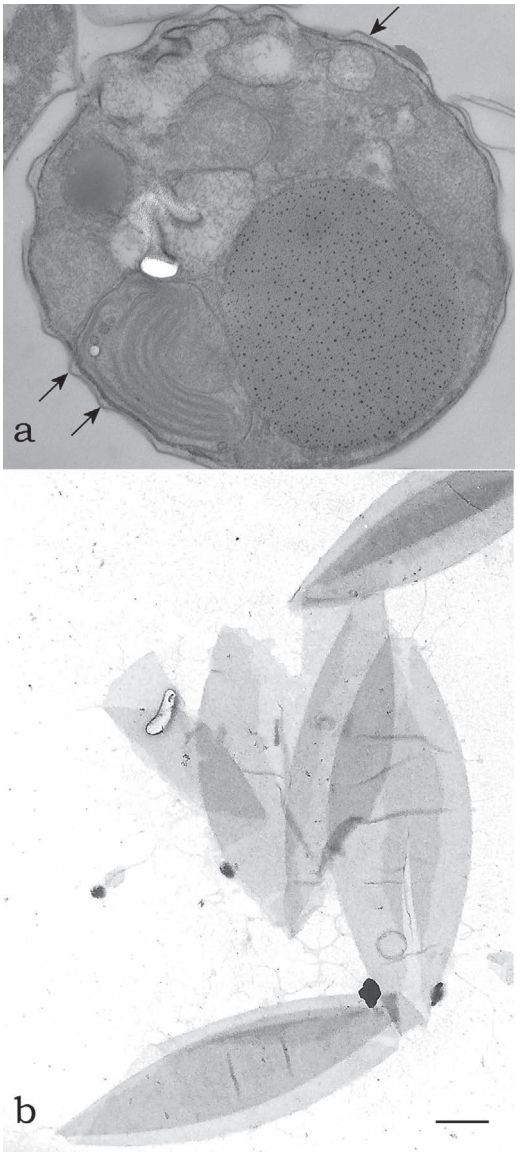


FIGURE 3.14 Transmission electron microscopy image of *Nannochloropsis* sp. in transversal section: arrows point to the cell wall (a), negative staining of the shed cell walls (b). Scale bar 0.5 μm.

sp., it can consist of imbricate scales. In *Phacotus,* the lorica is calcified, ornamented, and composed of two cup-shaped parts that separate at reproduction. In *Pteromonas*, the lorica extends into a projecting wing around the cell and is composed of two shell-like portions joined at the wings (Figure 3.16).

Skeletons

A siliceous skeleton is present in a small group of marine organisms called silicoflagellates belonging to the class Dictyochophyceae (Ochrophyta). This skeleton is placed outside the plasma membrane; it is a three-dimensional structure resembling a flat basket, which consists of a system of branched tubular elements bearing spinose endings (Figure 1.51 of Chapter 1).

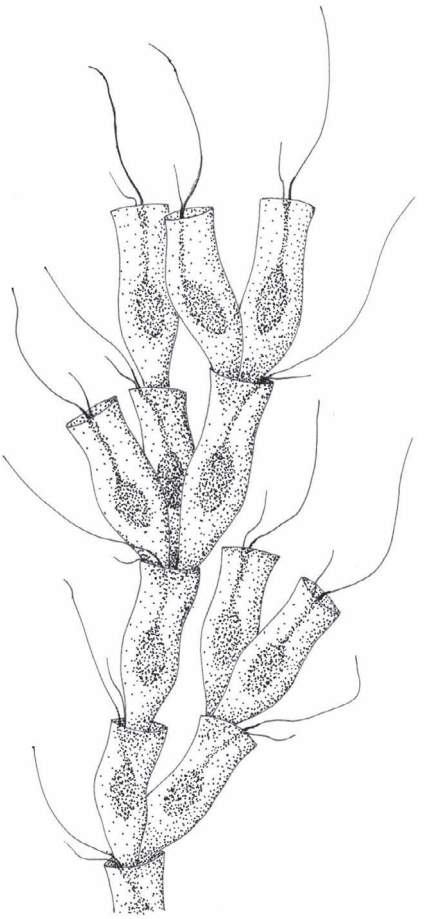


FIGURE 3.15 Tree-like arrangement of *Dinobryon* sp. cells showing their loricas.

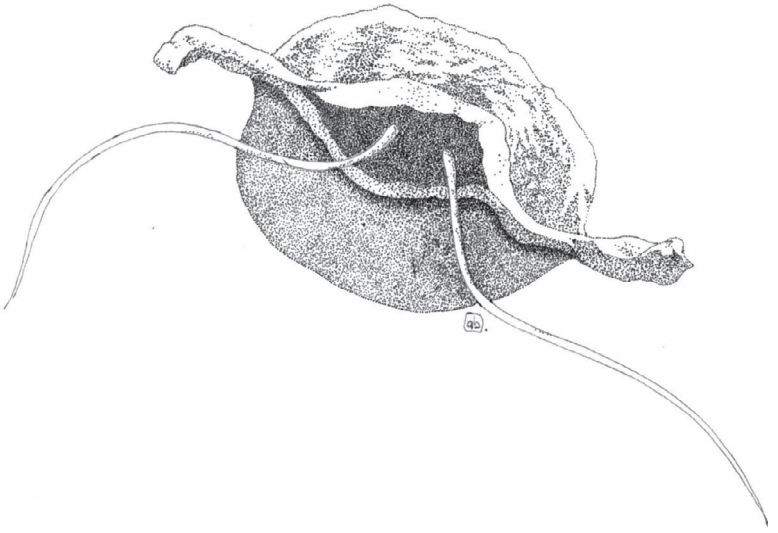


FIGURE 3.16 Lorica of *Pteromonas protracta*.

The protoplast is contained inside the basket and has a spongy or frothy appearance, with a central dense region containing the nucleus and the perinuclear dictyosomes and numerous cytoplasmic pseudopodia extending outward and containing the plastids. Sometimes a delicate cell covering of mucilage can be detected.

Type 3—Cell Surface With Additional Intracellular Material in Vesicles

In this type of cell surface, the plasma is underlined by a system of flattened vesicles. An example is the complex outer region of dinoflagellates (Dinophyceae) termed amphiesma. Beneath the cell membrane that bounds dinoflagellate motile cells, a single layer of vesicles (amphiesmal vesicles) is almost invariably present. The vesicles may contain cellulosic plates (thecal plates) in taxa that are thus termed thecate, or armored, or the vesicles may lack thecal plates, such taxa being termed athecate, unarmored, or naked. In athecate taxa, the amphiesmal vesicles play a structural role. In thecate taxa, thecal plates, one in each vesicle, adjoin one another tightly along linear plate sutures, usually with the margin of one plate overlapping the margin of the adjacent plate. Cellulosic plates vary from very thin to thick and can be heavily ornamented by reticula or striae; trichocyst pores, which may lie in pits termed areolae, penetrate most of them.

A separate layer internal to the amphiesmal vesicles may develop. It is termed the pellicle, though in the case of dinoflagellates, the term "pellicle" refers to a surface component completely different from the euglenoid pellicle and hence with a completely different accepted meaning, and in our opinion, its use should be avoided. The layer consists primarily of cellulose, sometimes with a dinosporine component, a complex organic polymer similar to sporopollenin that makes these algae fossilizable. In some athecate genera, such as *Noctiluca* sp., this layer forms reinforce the amphiesma, and the cells are termed pelliculate. This layer is also sometimes present beneath the amphiesma, as in *Alexandrium* sp. or *Scrippsiella* sp., and forms the wall of temporary cysts.

According to Dodge and Crawford (1970), the amphiesma construction falls into eight reasonably distinct categories (Figure 3.17):

1) simple membrane underlaid by a single layer of vesicles 600–800 nm in length, rather flattened, circular, or irregular in shape, with a gap of at least 40 nm between adjacent vesicles that may contain dense granular material; beneath the vesicles there are parallel rows of microtubules, which lie in groups of three; this simple arrangement is present in *Oxyrrhis marina*;
2) simple membrane underlaid by closely packed polygonal (generally hexagonal) vesicles 0.8–1.2 μm in length, frequently containing fuzzy material; these vesicles and the cell membrane are occasionally perforated by trichocyst pores; beneath the vesicles microtubules lie in rows of variable number; this type of amphiesma has been found in *Amphidinium carterae*;
3) as in category 2), but with plug-like structures associated with the inner side of the vesicles; these plugs are cylindrical structures 120 nm long and are arranged in single lines between single or paired microtubules; an example of this arrangement is present in *Gymnodinium veneficum*;
4) as in category 2), but with thin (about 20 nm) plate-like structure in the flattened vesicles; this amphiesma characterizes *Aureodinium pigmentosum*;
5) in this group, the vesicles contain plates of medium thickness (60 nm), which slightly overlap; in *Woloszynskia coronata*, the plates are perforated by trichocyst pores;
6) the plates are thicker (up to 150 nm) and reduced in number, with a marked diversity of form; each plate has two or more sides bearing ridges, and the remaining sides have tapered

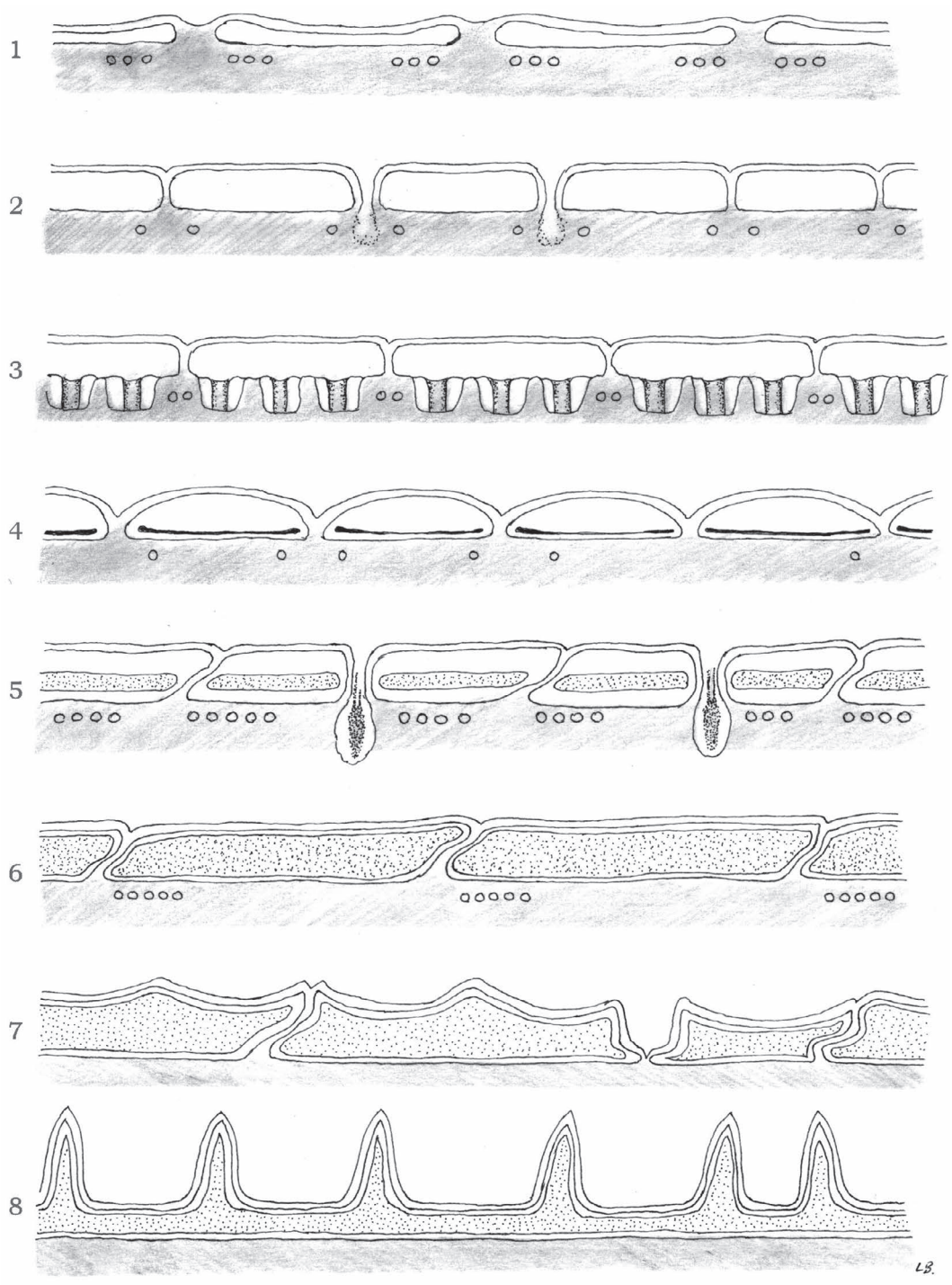


FIGURE 3.17 Diagram of the eight distinct categories of the dinoflagellate amphiesma. See text for details.

flanges; where the plates join, one plate bears a ridge and the opposite bears a flange; *Glenodinium foliaceum* belongs to this category;

7) the plates can be up to 25 μm across and up to 1.8 μm thick; they bear a corrugated flange on two or more sides and a thick rim with small projections on the opposing edges; these plates may overlap to a considerable extent, and their surface may be covered by a pattern of reticulations; a distinctive member of this category is *Ceratium* sp.;
8) amphiesma consisting of two large plates, with one or more small plates in the vicinity of the flagellar pores at the anterior end of the cell; plates can be very thin and perforated by two or three simple trichocyst pores, as in *Prorocentrum nanum*, or thick and with a very large number (up to 60) of trichocyst pores, as in *Prorocentrum micans*.

The arrangement of thecal plates is termed tabulation, and it is of critical importance in taxonomy of dinoflagellates. Tabulation can also be conceived of as the arrangement of amphiesmal vesicles with or without thecal plates. The American planktologist and parasitologist Charles Kofoid developed a tabulation system allowing reference to the shape, size, and location of a particular plate; plates were recognized as being in series relative to particular landmarks such as the apex, cingulum (girdle), and sulcus. His formulas (i.e. the listing of the total number of plates in each series) were especially useful for most gonyaulacoid and peridinioid dinoflagellates. Apart from some minor changes introduced afterwards, the Kofoid system is still the standard in the description of new taxa. Plates are numbered consecutively from that closest to the midventral position, continuing around to the cell left. A system of superscripts and other marks are used to designate the plate series. Two complete transverse series of plates are present in the epitheca: apical (’) and precingular (’’), counted from the ventral side in a clockwise sequence. Also, the hypotheca is divided into two transverse series: postcingular (’’’) and antapical (’’’’). Some genera also possess an incomplete series of plates on the dorsal surface of the epitheca, termed anterior intercalary plates (a), and on the hypotheca, termed posterior intercalary plates (p). Cingular (C) and sulcal (S) plates are also identified (Figure 3.18). Thus, for example, the dinoflagellate *Protoperidinium steinii* has the formula 4’, 3a, 7’’, 3C, 6S, 5’’’, 2’’’’, which indicates four apical plates, three anterior intercalary plates, seven precingular plates, three cingular plates, six sulcal plates, five postcingular plates, and two antapical plates.

Type 4—Cell Surface With Additional Extracellular and Intracellular Material

Both the surface structure of Cryptophyceae (Cryptophyta) and that of Euglenophyceae (Euglenozoa) can be grouped under this type.

The main diagnostic feature of the members of the Cryptophyceae is their distinctive kind of cell surface, colloquially termed periplast. Examples are *Chroomonas* (Figure 3.19) and *Cryptomonas*; in these algae, the covering consists of outer and inner components, present on both sides of the membrane, variable in their composition. The inner component is composed of protein and may consist of fibril material, a single sheet or multiple plates with various shapes, hexagonal, rectangular, oval, or round. The outer component may have plates, heptagonal scales, mucilage, or a combination of any of these. The pattern of these plates can be observed on the cell surface when viewed with scanning electron microscopy (SEM) and freeze-fracture transmission electron microscope (TEM), but it is not easily detectable under light microscopy view.

Euglenophyceae possess an unusual membrane complex called a pellicle, consisting of the plasma membrane overlying an electron-opaque semi-continuous proteic layer made up of overlapping strips. These strips or striae that can be described as long ribbons usually arise in the flagellar pocket and extend from the cell apex to the posterior. Each strip is curved at both edges, and in transverse section, it shows a notch, an arched or slightly concave ridge, a convex groove, and a heel region where adjacent strips interlock and articulate. The strips can be arranged helically

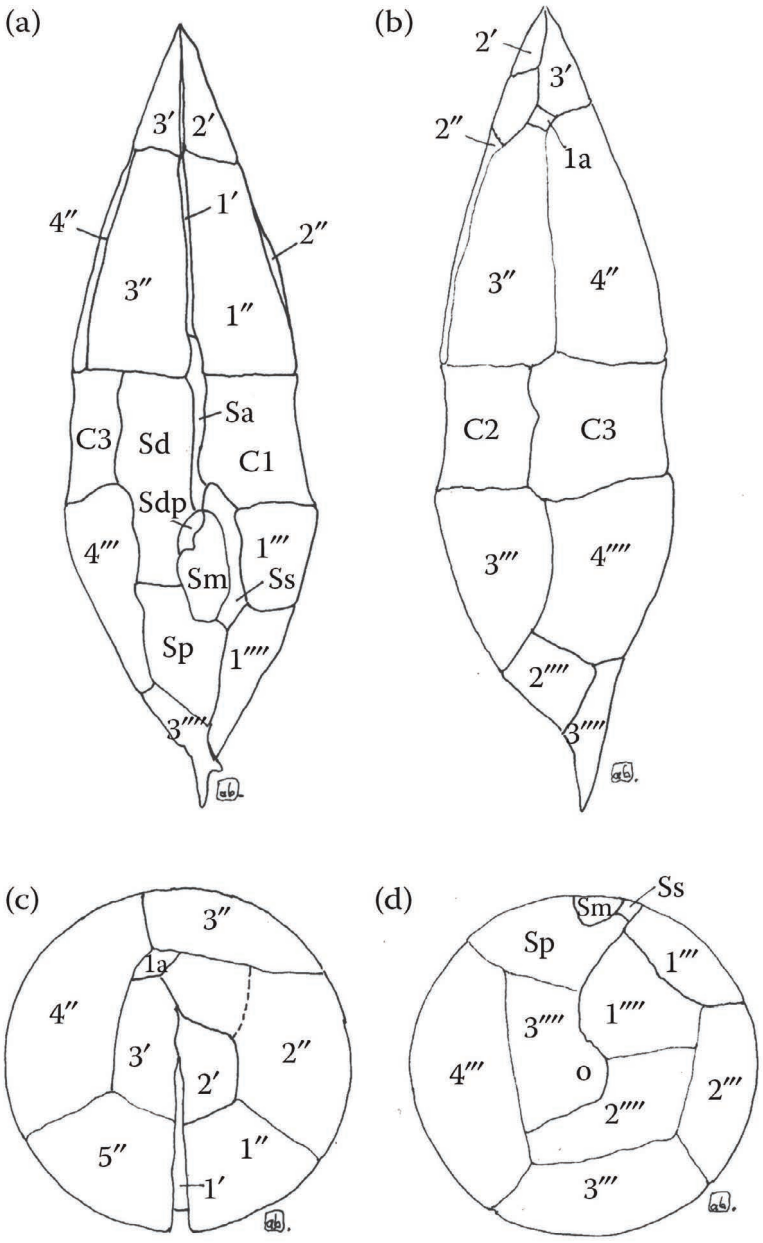


FIGURE 3.18 Line drawings of the thecal plate patterns of *Lessardia elongata* with the corresponding numeration. Ventral view (a), dorsal view (b), apical view (c), antiapical view (d). See text for details.

or longitudinally; the first arrangement, very elastic, is present in the "plastic euglenoids" (e.g. *Euglena, Peranema, Distigma*), either heterotrophic or phototrophic, where there are more than 16 strips. Their relational sliding over one another along the articulation edges permits the cells to undergo "euglenoid movement" or "metaboly." This movement is a sort of peristaltic movement consisting of a cytoplasmic dilation forming at the front of the cell and passing to the rear. The return movement of the cytoplasm is brought about without dilation. The more rigid longitudinal arrangement is present in the "aplastic euglenoids" (e.g. *Petalomonas, Ploeotia, Entosiphon*), all heterotrophic, where there are usually fewer than 12 strips. These euglenids are not capable of metaboly.

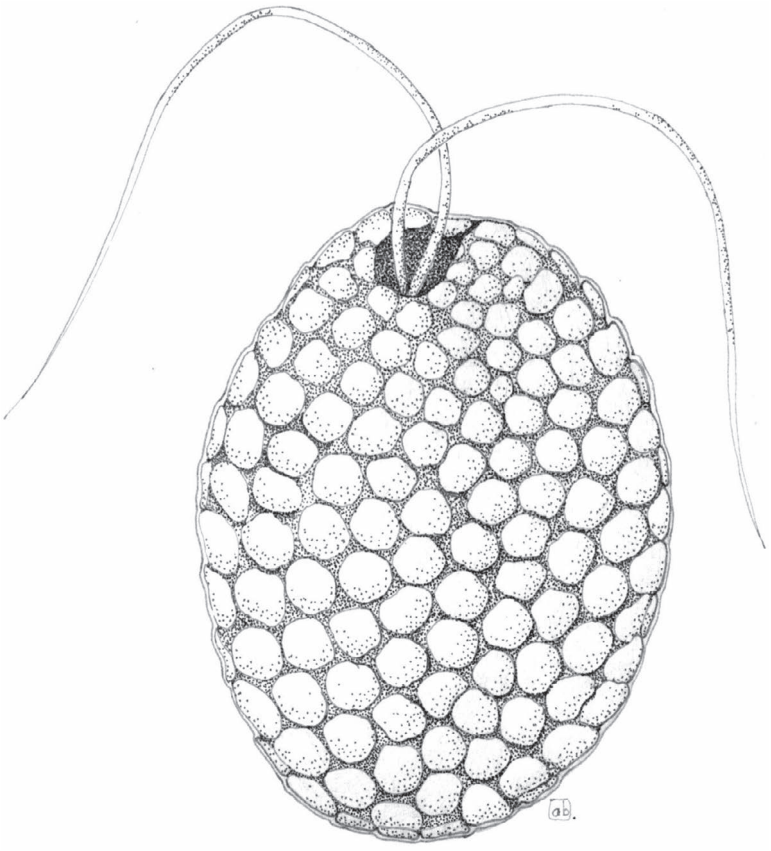


FIGURE 3.19 Periplast of *Chroomonas* sp.

The ultrastructure of the pellicular complex shows three different structural levels (Figure 3.20):

- the plasma membrane with its mucilage coating (first level)
- an electron-opaque layer organized in ridges and grooves (second level)
- the microtubular system (third level)

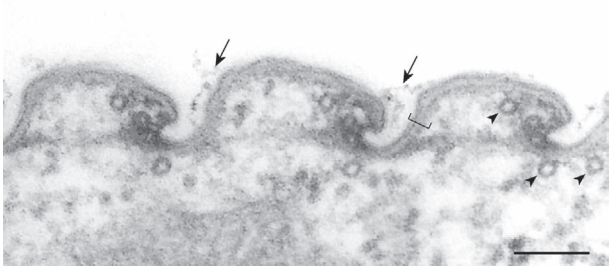


FIGURE 3.20 Transmission electron microscopy image of the surface of *Euglena gracilis* in transverse section, showing the three different structural levels of the pellicle. Arrows point to the first level (mucus coating); a square bracket indicates the second level (ridges and grooves); arrowheads point to the third level (microtubules). Scale bar 0.10 μm.

First Level

A dense irregular layer of mucilaginous glycoprotein covers the external surface of the cell. It has a fuzzy texture that, however, has a somewhat ordered structure of oriented threads. Mucilage bodies present beneath the cell surface secrete mucilaginous glycoproteins. The consolidation of the secretory products and their arrangement at one pole or around the periphery of the cell leads to the formation of peduncles (stalks of fixation) and other enveloping structures homologues to the loricas of Chrysophyceae and Chlorophyceae. Peduncles are present in *Colacium*, a euglenophyte that forms small arborescent colonies (Figure 3.21). Its cells, with reduced flagella, are attached by their anterior pole by a peduncle consisting of an axis of neutral polysaccharides and a cortex of acid polysaccharides. Loricas are present in *Trachelomonas* sp. (Figures 1.22 and 1.1bm of Chapter 1), *Strombomonas verrucosa* (Figure 3.23), and *Ascoglena*; they are very rigid, made up of mucilaginous filaments impregnated with ferric hydroxide or manganese compounds which confer an orange, brown, to black coloration to the structure. These loricas fit loosely over the body proper of the cell. They possess a sharply defined collar that tapers to a more or less wide apical opening where the flagella emerge or possess a wide opening on one pole and attached to a substrate at the other pole, as in *Ascoglena*.

Beneath the mucus coating, there is the plasma membrane (Figure 3.24). This cell membrane is continuous, covers the ridges and grooves on the whole cell, and can be considered the external surface of the cell. The protoplasmic face (PF) of the plasma membrane shows that the strips are covered with numerous peripheral membrane proteins of about 10 nm.

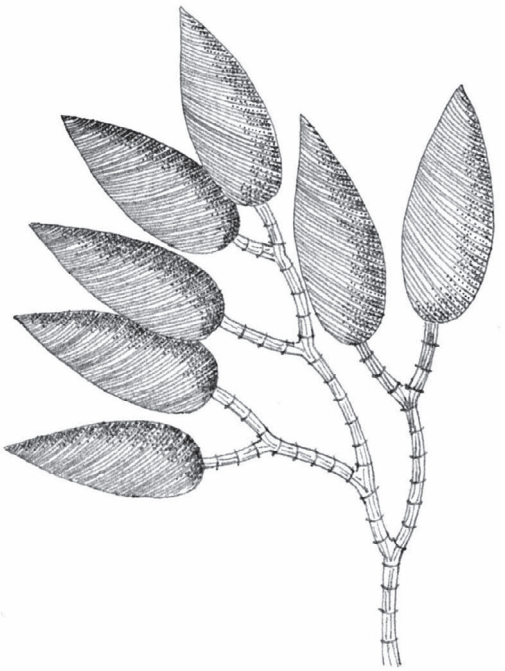


FIGURE 3.21 A small arborescent colony of *Colacium* sp. in which the cells are joined to one another by mucilaginous stalks.

Second Level

This peripheral cytoplasmic layer has a thickness that varies with the species. It consists of roughly twisted proteic fibers with a diameter from 10 to 15 nm arranged with an order texture or parallel striation (Figure 3.25a). The overall structure resembles the wired soul present in the tires, which gives the tire its resistance to tearing forces. Transversal fibers are detectable in some euglenoids, which connect the two longitudinal edges of the ridge of each strip (Figure 3.25b).

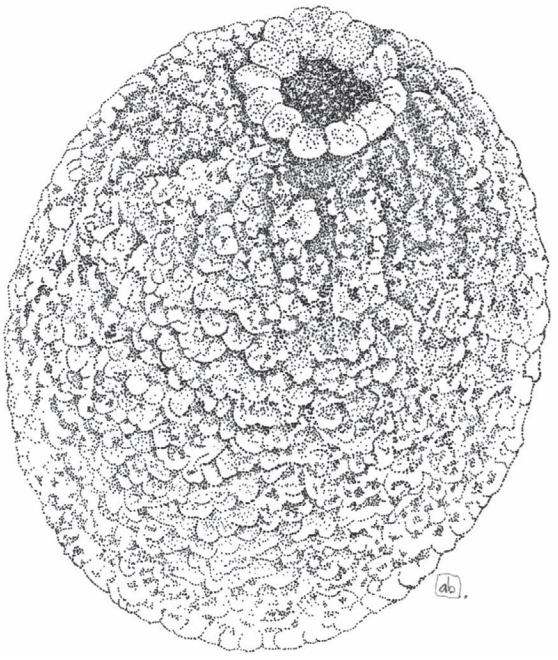


FIGURE 3.22 Lorica of *Trachelomonas* sp.

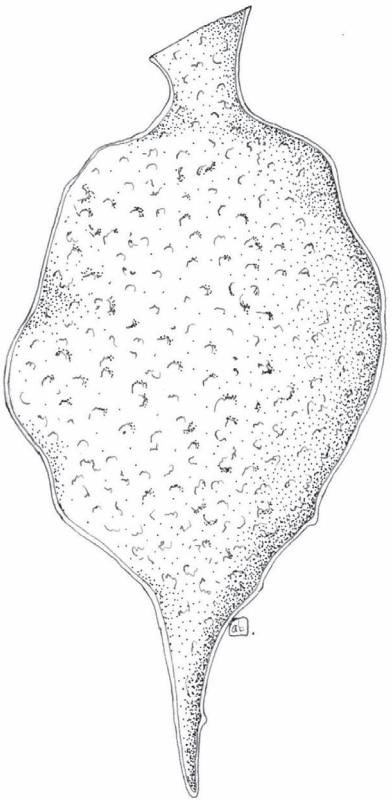


FIGURE 3.23 Lorica of *Strombomonas verrucosa*.

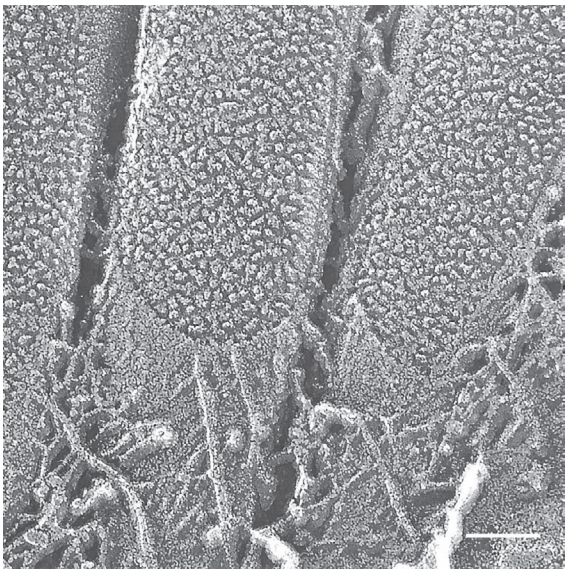


FIGURE 3.24 Deep-etching image of *Euglena gracilis* showing the mucus coating of the cell surface and the protoplasmic fracture of the cell membrane. Scale bar 0.10 µm. Courtesy of Pietro Lupetti.

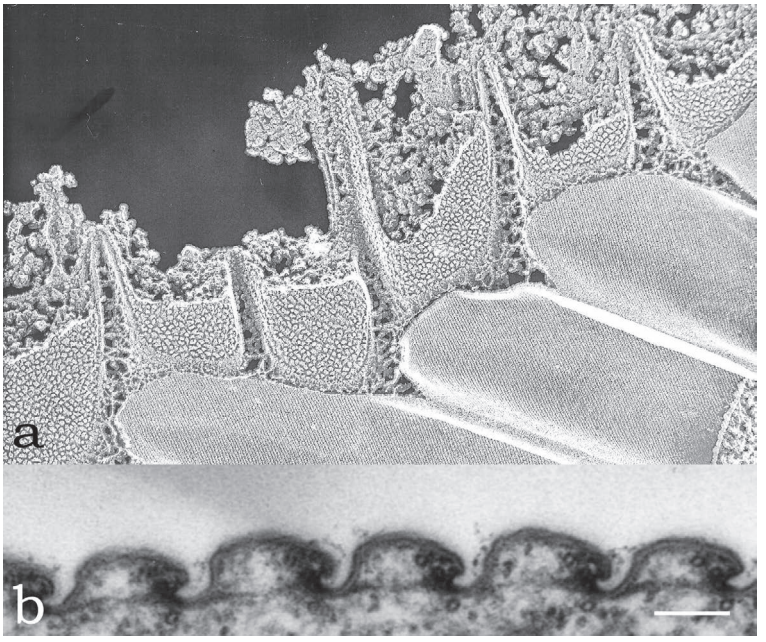


FIGURE 3.25 Deep-etching image of *Euglena gracilis* showing the second structural level of the pellicular complex and the regular texture of the internal face of the pellicle stripes (a). Transmission electron microscopy image of the pellicle of *Euglena gracilis* in transverse section showing the transversal fibers connecting the edges of successive ridges (b). Scale bars 0.10 µm.

Third Level

There is a consistent number and arrangement of microtubules associated with each pellicular strip, which are continuous with those that line the flagellar canal and extend into the region of

the reservoir. Within the ridge in the region of the notch, there are three to five, usually four, microtubules about 25 nm in diameter running parallel along each strip. Two of these are always close together and are located immediately adjacent to the notch adhering to the membrane (Figure 3.20).

The lack of protein organization in the groove regions gives higher plasticity to these zones and, together with presence of parallel microtubules in the ridge regions, gives the characteristic pellicular pattern to the surface of euglenoids.

The solid structure of the pellicle confers a very high degree of flexibility and resistance to the cells. Our experience with *Euglena gracilis* allow us to say this alga possesses one of the strongest coverings present in these microorganisms. A pressure of more than 2000 psi (about 150 bar) is necessary to break the pellicular structure of this alga.

Flagella and Associated Structures

Flagella can be defined as motile cylindrical appendages found in widely divergent cell types throughout the plant and animal kingdom, which either move the cell through its environment or move the environment relative to the cell.

Motile algal cell are typically biflagellate, although quadriflagellate types are commonly found in green algae; it is generally believed that the latter have been derived from the former, and a convincing example of this derivation is *Polytomella agilis* (Chlorophyceae) from *Chlamydomonas* sp. (Chlorophyceae). A triflagellate type of zoospore such as that of *Acrochaete wittrockii* (Ulvophyceae) may have originated from a quadriflagellate ancestor by reduction, whereas the few uniflagellate forms are most likely descendants of biflagellated cells. Intermediate cases exist which carry a short second flagellum, as in *Mantoniella squamata* (Mamiellophyceae) or *Euglena gracilis* (Euglenophyceae), where one flagellum is reduced to a stub (Figure 3.26); in some species, one flagellum of the pair is reduced to a non-functional basal body attached to the functional one, as in the uniflagellate swarmer of *Dictyota dichotoma* (Phaeophyceae). A special case of multiflagellate alga is the naked zoospore of *Oedogonium* (Chlorophyceae), where the numerous flagella form a ring or crown around the apical portion of the cell (stephanokont zoospore).

The characteristics of the flagella in a pair, that is, relative length and surface features, have led to a specific nomenclature. When the two flagella differ in length and surface features, one being hairy and the other smooth, they are termed "heterokont." This term applies to all

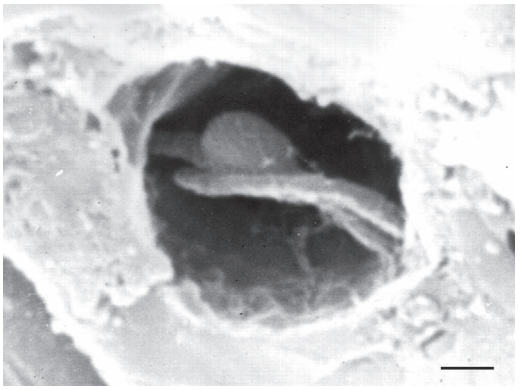


FIGURE 3.26 Scanning electron microscopy image of the reservoir of *Euglena gracilis* in longitudinal section showing the locomotory emerging flagellum bearing the photoreceptor and the non-emerging flagellum reduced to a stub. Scale bar 0.50 μm. Courtesy of Franco Verni.

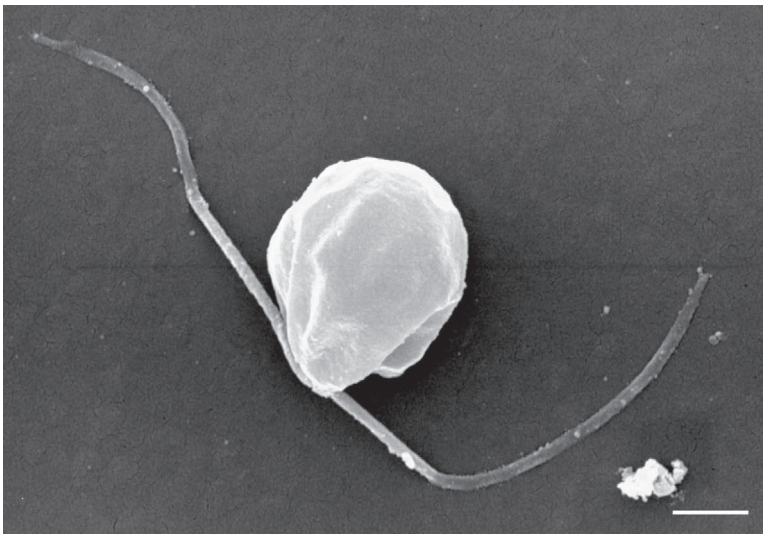


FIGURE 3.27 Scanning electron microscopy image of an isokont cell (*Dunaliella* sp.). Scale bar 3 μm.

members of the Ochrophyta. When the two flagella are equal in length and appearance, the term "isokont" is used (Figure 3.27), which applies to Haptophyta and to Chlorophyceae and Charophyceae. Within this group, there are a few genera whose flagella differ in length, which are termed "anisokont."

Description of flagella anatomy will proceed from the outside to the inside, from the surface features and components to the axoneme and additional inclusions to the structures anchoring the flagella to the cell.

Flagellar Shape and Surface Features

Deviations from the cylindrical shape are rare among the algae. Usually the flagellar membrane fits smoothly around the axoneme, and a total diameter of 0.25–0.35 μm, excluding scales, hairs, and so on, holds for most species. If extra material is present between the axoneme and the flagellar membrane, the flagellum diameter increases either locally, as in the case of flagellar swellings, or through almost the entire length, as in the case of paraxial rods. Minor deviations from the cylindrical shape are caused by small extensions of the membrane to form one or more longitudinal keels running the length of the flagellum. Greater extension of the membrane forms a ribbon or wing supported along the edge by a paraxial rod. More variations are present in the flagellar tip, since flagella can possess a hairpoint; that is, their distal part is thinner with respect to the rest of the flagellum, or be blunt-tipped, with an abundance of intermediates between these two types.

The flagellar surface is smooth in many algae, where only a simple plasma membrane envelopes the axoneme. Sometimes, however, a distinct, apparently homogeneous dense layer covers the flagellar membrane throughout (Figures 3.28, 3.51c, and 3.51d). One of the two flagella of Ochrophyta is smooth, and smooth flagella are present in members of the Haptophyta, such as *Chrysochromulina parva* (Coccolithophyceae), and in many Chlorophyta, such as *Chlamydomonas reinhardtii* (Chlorophyceae).

Flagellar Scales

Flagella may bear a high variety of coverings and ornamentation, which often represent a taxonomic feature. The occurrence of flagellar scales follows that of cell body scales, since they are



FIGURE 3.28 Transmission electron microscopy image of a *Dunaliella* sp. flagellum in transverse section, showing the homogeneous fuzzy coating of its membrane. Scale bar 0.10 μm.

present only in eukaryotic algae in the divisions of Ochrophyta, Haptophyta, and Chlorophyta. As for cell body scales, they have a silica-based composition in the Ochrophyta, a mixed structure of calcium carbonate and organic matter in the Haptophyta, and a completely organic nature in the Chlorophyta.

Members of the Ochrophyta fall into two groups: one possessing exactly the same type of scale on both the flagellar and body surface and the other showing flagellar scales different in structure and arrangement from body scales. An example of the first group is *Sphaleromantis* sp. (Chrysophyceae), whose flagella and cell body are closely packed with scales of very peculiar appearance, resembling the branched structure of a tree. Examples of the second group are *Mallomonas* sp. and *Synura* sp. (Chrysophyceae); in both genera, flagellar scales are not arranged in a regular pattern, are very small (under 300 nm), and possess different morphological types, the most characteristic being the annular type. Like body scales, flagellar scales are produced in deposition vesicles, extruded from the cell and brought into the correct position in relation to the other scales and the cell surface.

As noted, flagella of the Haptophyta are usually equal in length and appearance (isokont); however, members of the genus *Pavlova* (Pavlovophyceae) possess two markedly unequal flagella, the anterior much longer than the posterior, and carrying small, dense scales in the form of spherical or clavate knobs. These scales are often arranged in regular rows longitudinally or can be randomly disposed on the flagellum. Scales are formed inside the Golgi apparatus and then released to the cell surface by fusion of the plasmalemma and the cisternal membrane.

Flagellar scales are known from many Chlorophyta, such as Chlorodendrophyceae, Nephroselmidophyceae, and Mamiellophyceae, and Prasinodermatophyta such as Prasinodermatophyceae. These algae possess non-mineralized organic scales on their cell body and flagella, the same type of scale rarely being present on both surfaces. On the flagella, the scales are precisely arranged in parallel longitudinal rows, sometimes in one, two, or even three layers on top of each other. Each layer usually contains only one type of scale. The four flagella of *Tetraselmis* sp. (Chlorodendrophyceae) are covered by different types of scales: pentagonal scales attached to the flagellar membrane (Figure 3.29), rod-shaped scales covering the pentagonal scales, and hair scales organized in two rows on opposite side of the flagellum. A fourth type termed "knotted scales" is present only in some strains, but their precise arrangement is not known. In *Nephroselmis spinosa* (Nephroselmidophyceae), the flagellar surface is coated by two different types of scales arranged in two distinct layers. Scales of the inner layer, deposited directly on the membrane, are

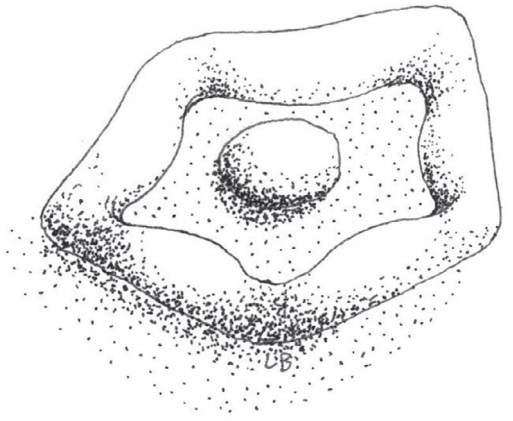


FIGURE 3.29 Pentagonal scale of the flagellar membrane of *Tetraselmis* sp.

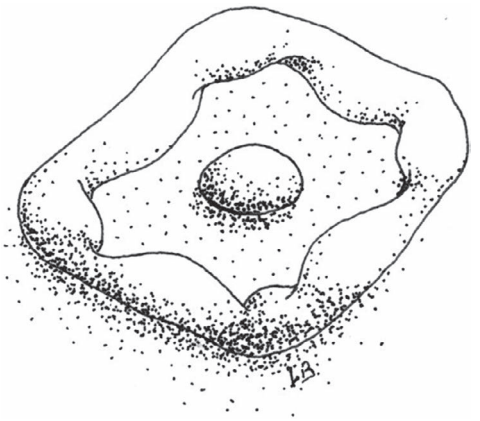


FIGURE 3.30 Square scale of the flagellar membrane of *Nephroselmis spinosa*.

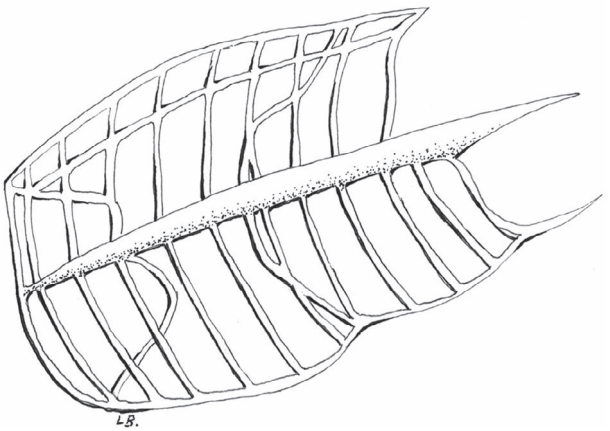


FIGURE 3.31 Limuloid scale of the flagellar membrane of *Pyramimonas* sp.

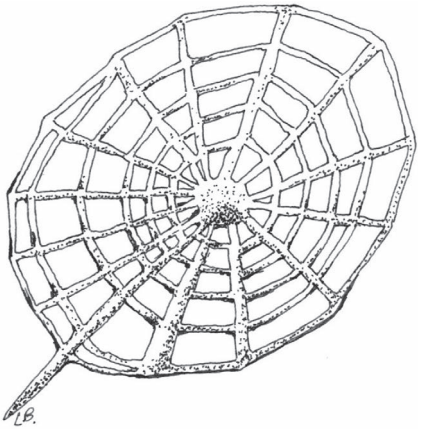


FIGURE 3.32 Spider-web scale of the flagellar membrane of *Mamiella gilva*.

small and square, 40 nm across (Figure 3.30); scales of the outer layer are rod shaped, are 30–40 nm long, and are deposited atop the inner scales. As in *Tetraselmis* (Chlorodendrophyceae), hair scales of at least two different types are also present covering the flagella. In *Pyramimonas* sp. (Pyramimonadophyceae), the scales are extremely complex in structure and ornamentation and belong to three different types. Minute pentagonal scales, 40 nm wide, form the layer covering the membrane, which in turn is covered by limuloid scales, 313 nm long and 190 nm wide, arranged in nine rows (Figure 3.31); each flagellum also bears two rows of almost opposite tubular hair scales, 1.3 μm long. Spider-web scales with an ellipsoid outline are present in *Mamiella gilva* (Mamiellophyceae), which are ornamented by a radial spoke elongated into a conspicuous spine (Figure 3.32).

The scales are synthesized within the Golgi vesicles. The vesicles then migrate to the base of the flagella and from there are extruded and arranged on the flagella.

Flagellar Hairs

Flagellar hairs can be grouped into two types: tubular and non-tubular (simple) hairs.

Tubular hairs consist of two or more distinct regions, at least one of which is thick and tubular, while the distal elements may be simpler. This type of hair is further divided into cryptophycean hairs, tripartite hairs, and prasinophycean hairs.

Cryptophycean hairs are unique for arrangement to the Cryptophyceae (Cryptophyta), being attached in two opposite rows on the longer flagellum and on a single row on the shorter one. On the long flagellum, the hairs consist of a tubular proximal part, 1.5–2.5 μm long, and a non-tubular distal filament, 1 μm long, while the hairs on the shorter flagellum are shorter, 1–1.5 μm long, with a distal filament, 1 μm long.

Tripartite hairs are the hair type of the Ochrophyta (Figures 3.33a and 3.33b). These hairs consist of three morphological regions: a short basal region, a tubular hollow shaft, and a distal region. The basal part is 0.2–0.3 μm long and tapers towards the site of attachment to the flagellar membrane, at which point dense structures are present that connect the hairs to the peripheral axoneme microtubules. The hollow shaft shows a range of length from 0.7–0.8 μm to 2 μm and a diameter of about 16 nm. The distal parts of each hair, called terminal filaments or fibers, are extremely fragile and hence difficult to detect because they are readily shed during electron microscopy preparation. In some cases, they are organized in a 2+1 structure, that is, two short filaments 0.3 μm long and one long filament 1 μm long; however, differences exist in their number, length, and diameter.

Cells of the Prasinodermatophyceae carry hairs on all their flagella, whether one, two, four, or eight, which are very diverse in morphology. They can vary in length from 0.5 to 3 μm, and a single flagellum may carry more than one hair type. In *Pyramimonas orientalis* (Pyramimonadophyceae), both lateral and apical hairs are bipartite and of the same length, with the lateral hairs divided into a short, thick base of 160 nm and a long, thin distal part of 650 nm, and the apical hairs possess a long, thick base and a very short, thin tip. Another example of flagellar hairs is *Mantoniella* sp. (Mamiellophyceae), bearing hairs on the flagellar tip that are longer than those on the side. In *Nephroselmis* (Nephroselmidophyceae) and *Tetraselmis* (Chlorodendrophyceae), there is a single hair type divided into two regions of roughly the same length (0.5 μm).

Unlike tubular hairs, simple, non-tubular hairs are not differentiated into regions; they are thin and very delicate, probably consisting of a single row of subunits. These hairs occur in a variety of

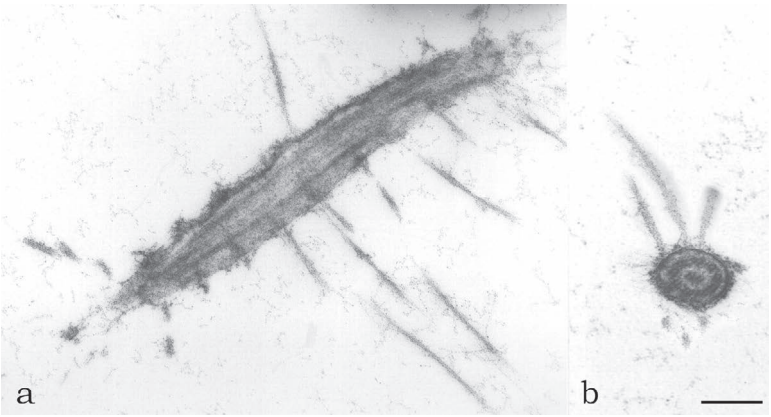


FIGURE 3.33 Transmission electron microscopy image of the long trailing flagellum of *Ochromonas danica* in both longitudinal (a) and transverse sections (b), showing the tripartite hairs. Scale bar 0.25 μm.

groups but are unique in the Euglenophyceae and Dinophyceae, whose hairy coverings share certain features not known to occur in any other algal group.

In Euglenophyceae, long, simple hairs are arranged in a single row on the emergent part of the flagella. In genera with two emergent flagella, the hair covering is similar on the two flagella. In *Euglena gracilis*, these long hairs consist of a single filament 3–4 μm long, with a diameter of 10 nm, while in *Eutreptiella gymnastica*, they are 4–5 μm long and assembled in unilateral bundles. In addition to these long hairs, euglenoid flagella carry a dense felt of shorter hairs, which in *Euglena* are approximately half as long and half as thick as the long hairs. These short hairs, precisely positioned with respect to each other and to axonemal components, consist of a sheath about 240–300 nm in length, which represents the basic unit. The units, each formed by loops, side arms, and filaments, lie parallel to each other in the longitudinal direction of the flagellum (Figure 3.34); two groups of short hairs are arranged helically on each narrow side of the flagellum, separated from each other by two membrane areas without hair attachments. In Dinophyceae, both the longitudinal and the transverse flagellum carry hairs, but unlike Euglenophyceae, the hairy coverings on the two flagella are different. The transverse flagellum carries unilateral hairs except in the proximal part; they are 2–4 μm long and arranged in bundles, each bundle consisting of different-sized hairs. In *Oxyrrhis marina*, hairs are of three different lengths, the longest in the middle. Hairs on the

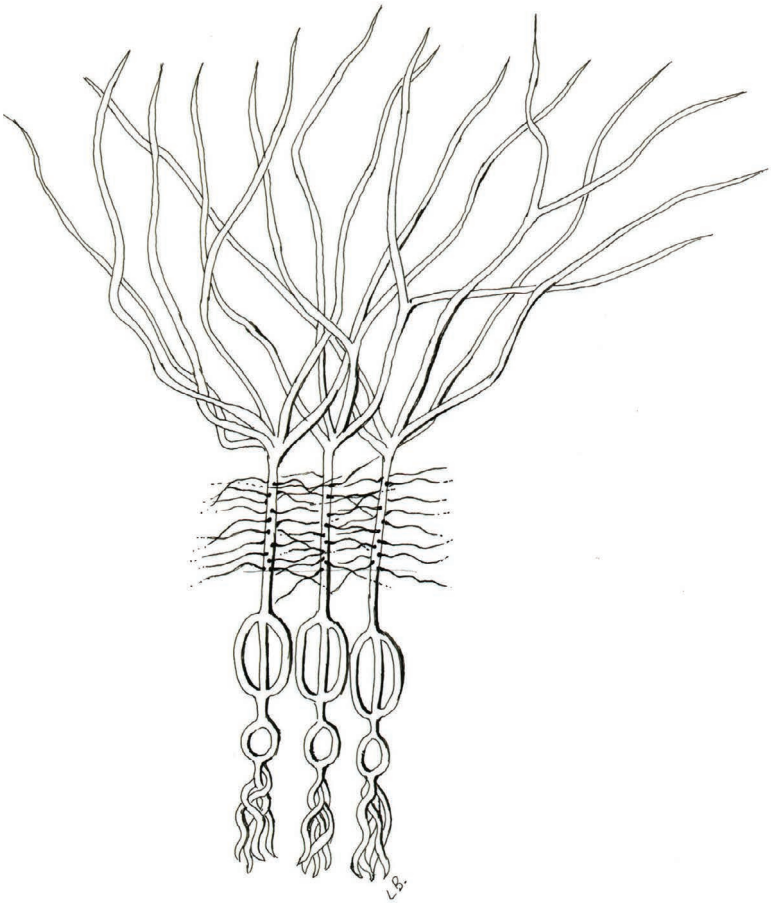


FIGURE 3.34 Short hairs of *Euglena* flagellum.

longitudinal flagellum are shorter than those on the transverse flagellum (0.4–0.75 μm) but similar in diameter (10 nm).

Simple, non-tubular hairs are also present in some Glaucophyta and Chlorophyta.

Flagellar Spines

Flagellar spines are a peculiarity of unknown function confined to male gametes of a few oogamous brown algae. The spermatozoids of *Dictyota* sp. (Phaeophyceae) are unique in possessing a longitudinal row of 12 very short spines on their single hairy flagella (these spermatozoids are basically biflagellate, but the second flagellum is reduced to its basal body only). Spines are absent on the distal 2.5–3 μm of the flagellum and on the proximal 10 μm. In other Phaeophyceae such as *Himanthalia*, *Xiphophora*, and *Hormosira*, spermatozoids possess only a single spine, up to 1.0 μm long. In all these algae, each spine is made up of electron-dense material located between the flagellar membrane and the peripheral axonemal doublets.

Internal Features

Axoneme

The movements of the flagella are generated by a single functional unit, the axoneme, which consists of a long cylinder, from 10 to 100 μm long, with a 0.2 μm diameter. Its structure, as seen in cross-sections by electron microscopy, is almost ubiquitous: it is made of nine equally spaced outer microtubule doublets (A and B) approximately 40 nm in diameter surrounding two central microtubules, the central pair (Figure 3.28). This arrangement is maintained by a delicate series of linkages to give the classical 9 + 2 pattern. The nine outer doublets are numbered starting from 1 located in the plane orthogonal to the plane, including the central pair, and counting clockwise when looking from the tip of the flagellum. The former plane allows the definition of the curvature directions during beating as left or right relative to it. Doublets are transiently linked by outer/inner dynein arms (ODAs and IDAs) that represent the flagellar motor and permanently interconnected by nexin links; the radial spokes connect the central pair to the peripheral microtubules of the outer doublets. Divergence from the basic 9 + 2 pattern is rare but includes the spermatozoid of some centric diatoms (9 + 0) and *Golenkinia minutissima* (Chlorophyceae) (9 + 1), as well as the haptonema of the Coccolithophyceae (Figure 3.35). This structure develops between the two flagella of these algae, and it is sometimes longer than the flagella themselves. It resembles a flagellum but contains a central shaft of six to eight microtubules arranged in a cylinder, with no doublets. In transverse section, the microtubules are disposed in an arc of a circle or in a ring and are surrounded by a limb of the smooth endoplasmic reticulum. The distal part of the haptonema is fairly straightforward. It is surrounded by plasma membrane, which is continuous over the tip of the haptonema and may be smooth, be drawn into a tip, or form a spathulate projection.

The bulk of axonemal proteins (70%) is made of tubulins, the building blocks (heterodimers) that polymerize linearly to form microtubules. Those tubulins, which constitute the wall of microtubules, belong to the *a* and *b* families, whose sequences have been conserved during evolution (other families, *g*, *d*, *e*, are responsible for microtubule nucleation at the level of the basal bodies/centrosomes). High molecular diversity among tubulins is generated by a series of post-translational modifications such as acetylation, detyrosylation, poly-glutamylation, or poly-glycylation. Tektin filaments are present at the junction between the A and B microtubules of each doublet. The internal and external arms that graft to the peripheral doublets represent 10–15% of the global protein mass of axonemes and are essentially formed by the "dynein-ATPases" motor (the Greek word "dyne" means force). Microtubular dyneins are large multimolecular complexes with a pseudo-bouquet shape and a molecular mass ranging from 1.4 MDa (bouquets with two heads) to 1.9 MDa (bouquets with three heads) for the whole molecule and approximately 500 kDa for the largest subunits containing the ATP hydrolysis site. The size of

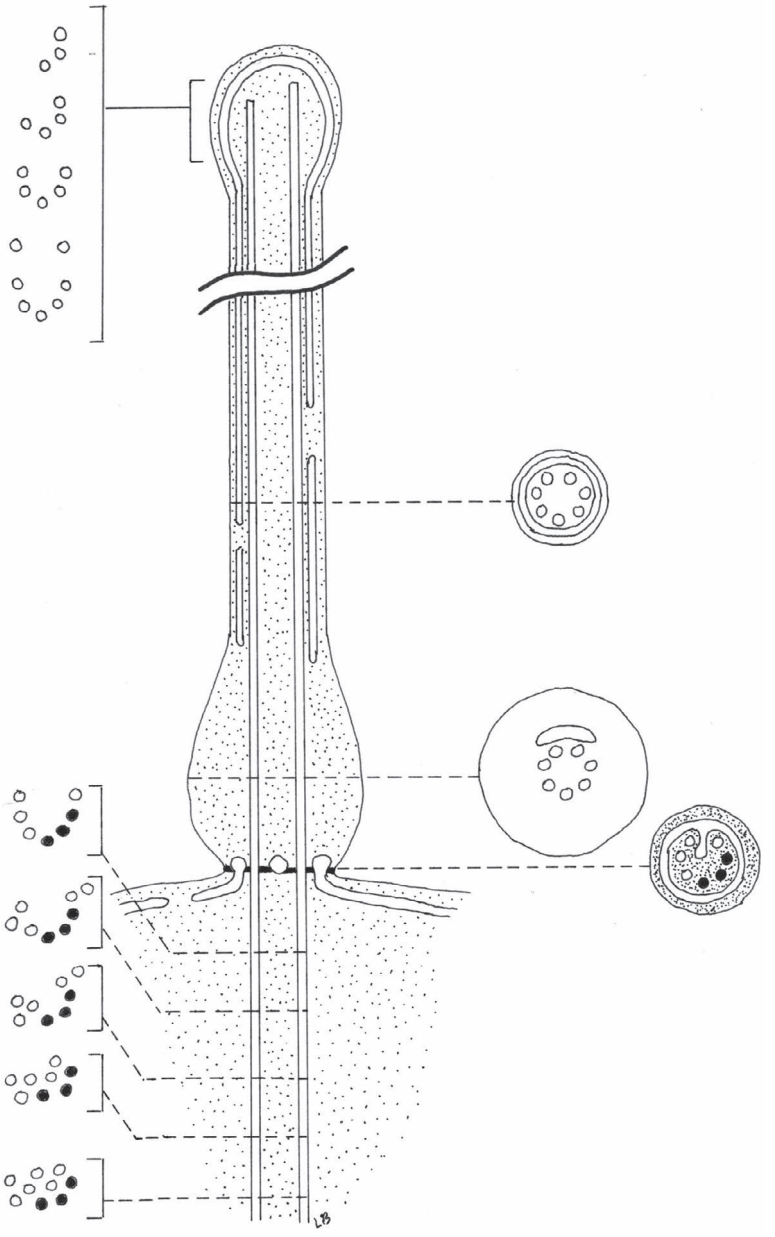


FIGURE 3.35 Schematic drawing of the generalized representation of the structure of the haptonema of *Chrysochromulina*.

both outer and inner dynein arms is approximately 50 nm. Among the 250 different polypeptides present in the axoneme, as estimated by bi-dimensional electrophoresis, only a few have been associated with a function.

Paraxial Rod

In addition to the 9 + 2 axoneme, algal flagella may contain a number of other structures within the flagellar membrane. Among those extending through the entire length of the flagella, there is the

paraxial rod, which is known only in the order of Pedinellales (Dictyochophyceae, Ochrophyta) and in members of the Euglenophyceae and Dinophyceae. The paraxial rod is also termed the paraflagellar rod (PFR). Paraflagellar rods are complex and highly organized lattice-like structures that run parallel to the axoneme. Among the different groups, PFRs are very similar structurally and biochemically.

In the Pedinellales, the membrane of the single emergent flagellum is expanded into a sheath or fin supported along the edge by the rod, which is cross-banded. Thanks to the presence of the fin, these algae are excellent swimmers. Their axoneme beats in a distinct planar wave.

Paraflagellar structures of characteristic appearance are present in some dinoflagellates. A hollow cylinder with the wall composed of helically arranged filaments is present in the single emergent (longitudinal) flagellum of *Noctiluca* gametes and in the longitudinal flagellum of both *Gyrodinium lebouriae* and *Oxyrrhis marina*. This rod is about as big as the axoneme in diameter and runs along the axoneme to which it is attached for almost its entire length. The thin filaments (nanofilaments with a 2–4 nm diameter) of its highly geometrically organized network are periodically attached to some of the outer doublet microtubules of the axoneme, which in *O. marina* is doublet number 4. A different type of paraxial rod is present in the complex-shaped transverse flagellum of dinoflagellates. This rod takes a nearly straight path along the inner wall of the sulcus and is regularly banded in the transverse direction. In contrast, the axoneme itself is distinctly helical.

A rod is present in most members of Euglenophyceae. In genera with two emergent flagella, such as *Eutreptia* and *Eutreptiella*, both flagella carry a paraxial rod. In *Eutreptiella*, where the two flagella differ in length, the rods also differ from each other in thickness and fine structure, the longer flagellum carrying a more complex rod than the shorter flagellum. In genera with a flagellar apparatus reduced to one long emergent flagellum and one short flagellum not extending beyond the reservoir region, only the emergent flagellum retains the rod, which extends its entire length. An example is *Euglena gracilis*; in this alga, the rod arises just above the flagellar transition zone and is located latero-ventrally with respect to the axoneme and the cell body. In thin cross-sections of isolated and demembranated flagella, the rod appears hollow, with an outer diameter of 90 nm. Images obtained from negative staining preparations show that the rod is made up of several coiled filaments, with a diameter of 22 nm, forming a 7-start left-handed helix with a pitch of 45° and a periodicity of 54 nm. Extending from the surface of the rod, a series of goblet-like projections can be observed, which form the point of attachment between the rod and one of the axonemal doublet microtubules (Figures 3.36a and 3.36b). The PFR does not assume any consistent orientation with respect to the central-pair microtubules of the emergent flagellum.

Two major protein components of the PFR have been identified in euglenoids and dinoflagellates with a number of possible minor protein constituents. These major proteins (referred to as PFR_1 and PFR_2) migrate in the sodium dodecyl sulphate polyacrylamide gel electrophoresis as a doublet of similar abundance. Depending on the organism, the mobility for PFR1 ranges from 70 to 80 kDa and for PFR2 from 62 to 70 kDa. Coils are a common structural motif in the filament formed using PFR1 and PFR2 proteins. Database searches reveal a 41-residue conserved region of the PFR_1/PFR_2 family that bears a significant relationship to a conserved motif within the central coiled rod of tropomyosin.

Other Intra-Flagellar Accessory Structures

Other intra-flagellar accessory structures are present in dinoflagellates besides the PFR: the so-called R fiber (Rf) and the so-called striated fiber (Sf). These structures do not show any kind of lattice or precisely organized structure. However, they deserve mention since they run for long distances along the axonemal structure and therefore are also candidates for modulating axonemal beating, possibly by Ca^{2+}-dependent contraction or through dipole-dipole forces.

The Rf is made of thin filaments 2–4 nm in diameter. It may be as large as the axoneme or the PFR in diameter (300–500 nm), runs along the major part of the axoneme, and is attached to it

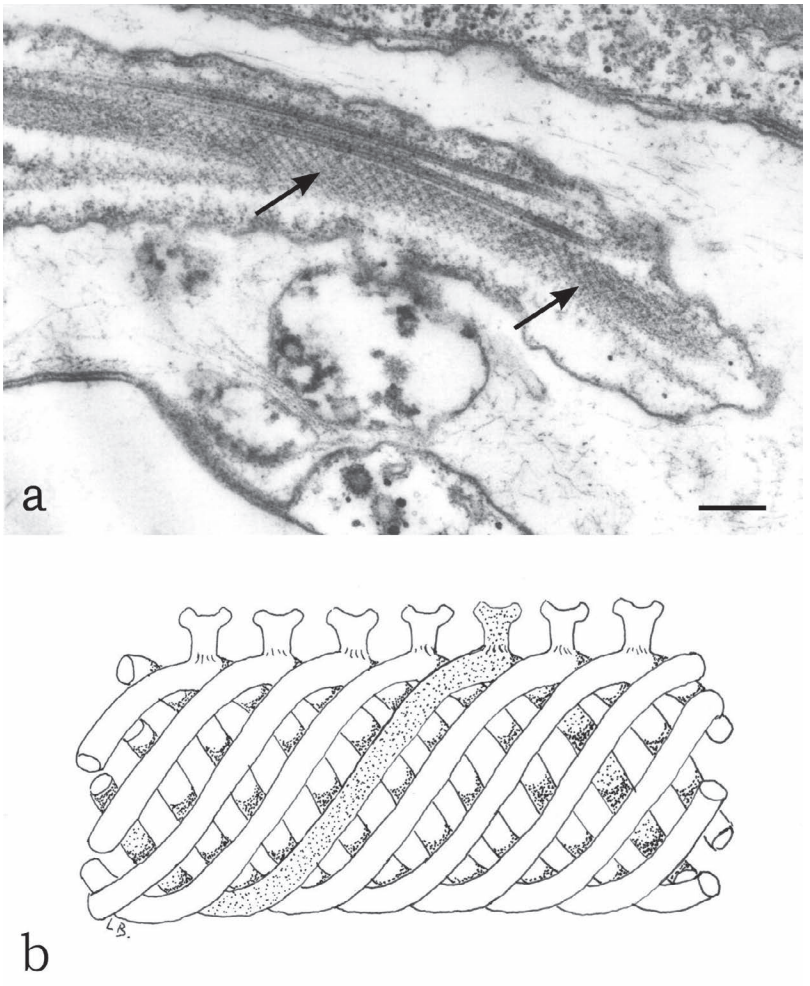


FIGURE 3.36 Transmission electron microscopy image of the locomotory flagellum of *Euglena gracilis* in longitudinal section. Arrows point to the PFR (a). Schematic drawing of the PFR showing the coiled filaments and goblet-like projections (b). Scale bar 0.40 μm.

via the PFR, the PFR linking the Rf to the axoneme. The Rf may contract and shows transversal striations of variable periodicities and thickness only during its contraction but not in its relaxed or fully contracted state (Figure 3.37). The precise structure of the Rf varies according to the fixation conditions for TEM, mostly depending upon the Ca^{2+} concentration, suggesting that its contractility is Ca^{2+} dependent. In some dinoflagellates, such as *Ceratium furca*, the Rf is a good candidate for the induction of the complete retraction of the longitudinal flagellum in the flagellar pocket, a movement that cannot be explained by the axoneme structure itself. In this retracted state, the Rf is contracted and the axoneme is highly folded (more tightly that during the usual flagellar beating). Therefore, the Rf could modulate the properties of the PFR and of axoneme motility through constraints imposed on the PFR.

The striated fiber is also made of thin filaments. It is much smaller than the PFR or the axoneme in diameter (about 35 nm) and runs along three-fourths of the axoneme. Its transversal striations suggest its implication in contractile processes that could modulate axonemal motility through gradual changes in the axonemal wavelength and/or amplitude.

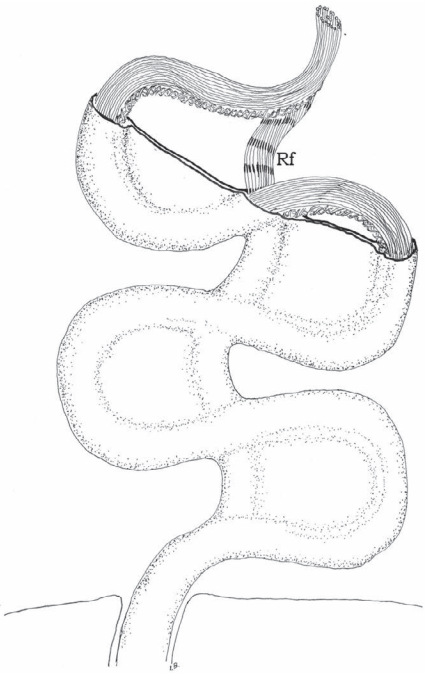


FIGURE 3.37 Schematical drawing of longitudinal flagellum of *Ceratium furca* during its contraction showing the striated Rf.

Transition Zone

While both the flagellar axoneme and the basal body that continues it are very constant in morphology among the different algae, the transition region where they meet varies considerably and is considered one of the most useful indicators of phylogenetic relationships. This region sometimes contains particular structures such as helices, star-shaped bodies, and transverse partitions referred to as basal plates. Five main types of transition zones may be distinguished, taking into account that secondary variations can appear within each.

The Type 1 transition zone is the simplest, with only one basal plate situated at the level of the point of inflexion of the flagellar membrane (Figure 3.38). Immediately above it, the flagellum shows a slight narrowing. Radial fibers connect the peripheral doublets to sub-membrane swellings. This type of transition zone is present in the Phaeophyceae (Ochrophyta).

In Type 2 zones, the basal plate is replaced by a sort of plug located beneath the point of inflexion of the flagellar membrane, far from the point of origin of the central pair of doublets (Figure 3.39). In this transition zone, the nine outer doublets show strong dilatation, which leaves room for a fibrillar spiral suspended on the doublets by short spokes. The spiral can reach the central doublet or be much shorter. Each outer doublet is associated via other spokes with a thickening of the membrane, whose folding forms a star with nine characteristic arms (Figures 3.40a and 3.40b). This transition region is typical of the Euglenophyceae. Among these algae, *Entosiphon sulcatum* is unique for its long transition region, the spiral of which surrounds the proximal 1 μm of the central doublet.

Type 3 transition regions possess a double system of complex plates. Variations exist due to the distance separating the plates or the presence of interposition material between them. In the Dinophyceae, the basal plate is duplicated and ring shaped; above it, there are two median discs, the uppermost supporting the central doublet of the axoneme (Figure 3.41a). In the Cryptophyta,

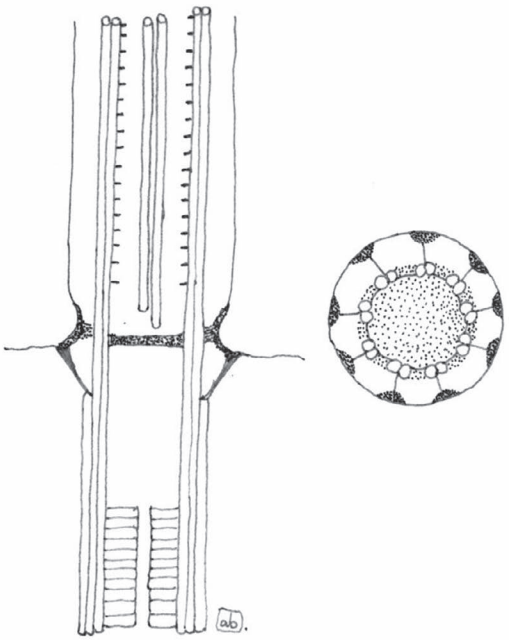


FIGURE 3.38 Type 1 transition zone (Phaeophyceae, Ochrophyta).

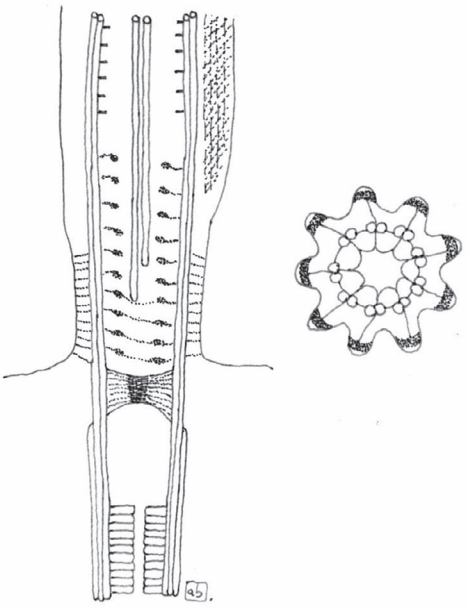


FIGURE 3.39 Type 2 transition zone (Euglenophyta).

an apical plate is located at the level of the narrowing of the flagellum above the point of inflexion of the flagellar membrane; the central doublet is right above this plate. A second plate bearing a ring-shaped thickening is located beneath it. In *Cyanophora* (Glaucophyceae, Glaucophyta), the apical plate has the same localization present in Cryptophyta, but it is ring

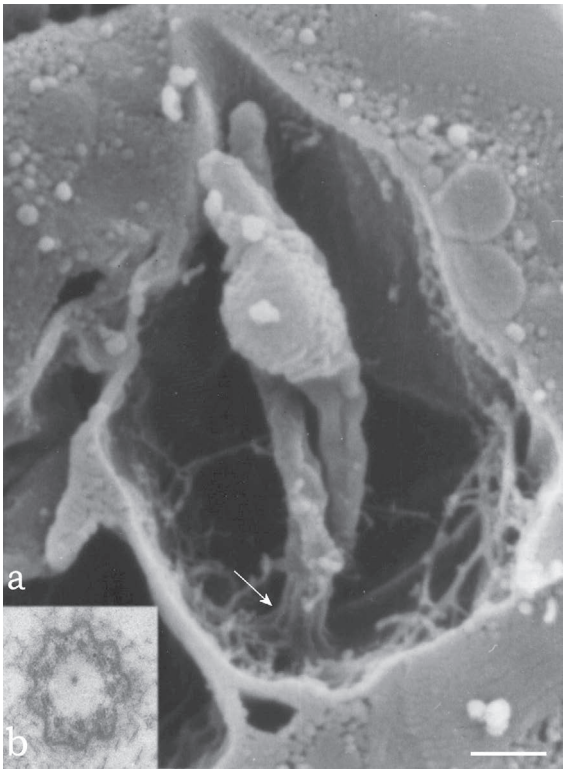


FIGURE 3.40 Scanning electron microscopy image of the reservoir region of *Euglena gracilis*, showing the two flagella arising from the bottom of the reservoir. The arrow points to the thickened folding of the flagellum membrane, typical of the transition zone (a). Transmission electron microscopy image of the transition zone in transverse section, showing the characteristic star configuration (b). Scale bar 0.50 μm.

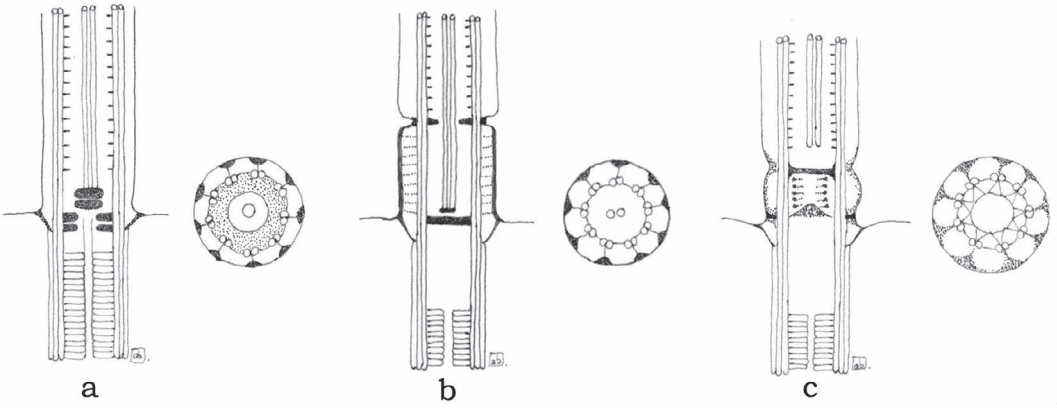


FIGURE 3.41 Type 3 transition zone of Dinophyta (a), Glaucophyta (b), and Haptophyta (c).

shaped and traversed by the central doublet that continues towards the basal plate situated at the level of the point of inflexion of the flagellar membrane (Figure 3.41b). Further variations of this type are present in Haptophyta, where two widely spaced plates are present, the apical below the central doublet. Each plate corresponds to a flagellar constriction, and the space

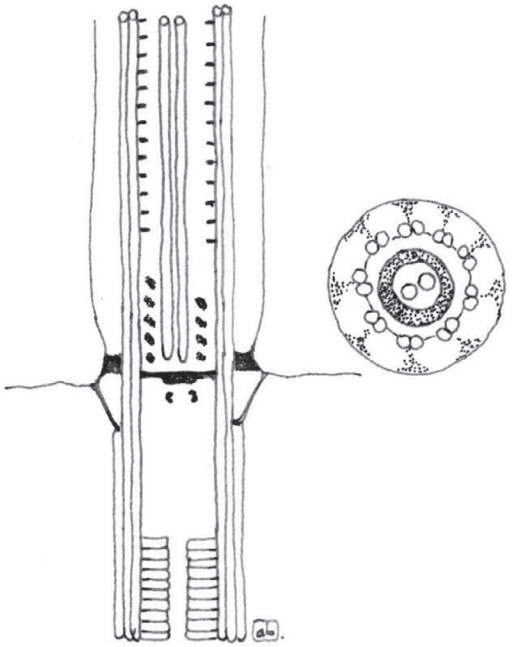


FIGURE 3.42 Type 4 transition zone of Chrysophyceae, Xanthophyceae, Eustigmatophyceae (Ochrophyta).

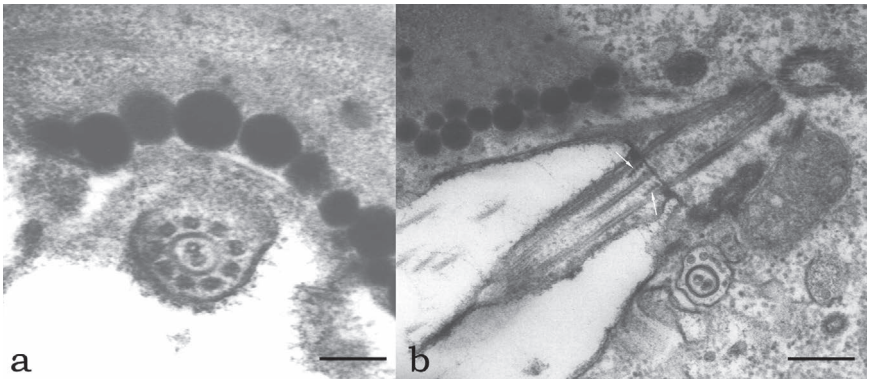


FIGURE 3.43 Transmission electron microscopy image of the transition zone of *Ochromonas danica* in transverse section (a), scale bar 0.20 μm; longitudinal section of the short flagellum of *Ochromonas* (b); arrows point to the double rows of punctae representing the turn of the helix. Scale bar 0.40 μm.

between them possibly contains fibrillar material; in cross-section, a stellate structure is visible, the arm of which connects with the a-tubules of the peripheral doublets (Figure 3.41c).

In Type 4 zones, there is only one basal plate situated at the point where the flagellum emerges, but this type of transition region is characterized by a very peculiar structure called "transitional helix" (Figure 3.42). In longitudinal sections, this appears as a double row of punctae equidistant from the doublets, representing four to six turns of a helix (Figures 3.43a and 3.43b). Some variations occur in the number of gyres, which in a short flagellum may be only one. This helix is present in Chrysophyceae, Xanthophyceae, and Eustigmatophyceae (Ochrophyta).

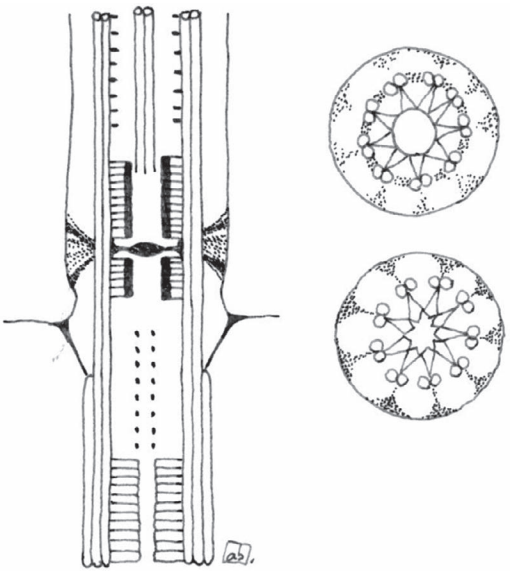


FIGURE 3.44 Type 5 transition zone (Chlorophyta).

Type 5 zones are characterized by the so-called "stellate pattern" (Figure 3.44); typically, it is divided into a longer distal and a shorter proximal part, separated by a basal plate. In the longitudinal section, the structure resembles an H, with the cross-bar located at a short distance above the cell surface (cf. Figure 3.46a). Transversely, the cross-bar may or may not extend to the peripheral doublets of the axoneme. Variations concern the length of the proximal part, the location of the plate, and the appearance of additional rings. This transition zone is typical of Chlorophyta.

Basal Bodies

A flagellum cannot be dissociated from its base, the basal body or kinetosome. This structure has a cylindrical form, with an average diameter of 0.2 μm, and a variable height (average 0.5 μm). The wall of the cylinder is discontinuous and consists of nine microtubular triplets tilted to the radii at an angle of 130° and interconnected by transverse desmosomes. The complete tubule A consists of 13 protofilaments, and the incomplete tubules B and C have 10 protofilaments. The proximal part of the basal body contains a fibro-granular structure termed the cartwheel, composed of a longitudinal central tubule and nine series of spokes joined to the triplets. This structure seems to be present in nearly all species of algae, with variations reported mainly for the length of the basal body. While most green algae usually possess very short basal bodies (250–450 nm), those of the Prasinodermatophyceae are often twice as long (560–690 nm). Some members of the Haptophyta, such as *Chrysochromulina* (Coccolithophyceae), also possess very long basal bodies (850–875 nm), but this length can reach a value of 1300 nm in some Euglenophyceae, such as *Entosiphon*.

In some Chlorophyta, two structures are present in association with the proximal ends of the basal bodies: the terminal cap and the proximal sheaths. The terminal cap is a more or less prominent electron-dense flap located on the anterior surface of the basal body, which folds over and covers in part its proximal end. The proximal sheath is located posterior to the proximal end of the basal body and can have a half-cylindrical shape or be wedge shaped, narrow proximally and broadening distally.

Variations in the number of basal bodies mainly reflect variations in the number of flagella. It is possible to distinguish:

1) cells with only one basal body, carrying one flagellum; this situation is very rare and is present in the euglenophyte of uncertain affinity *Scytomonas pusilla* and in the gametes of the diatoms *Lithodesmium* and *Biddulphia*;
2) cells with two neighboring basal bodies, forming the so-called primordial pair, indicated as 2A;
3) cells with numerous basal bodies.

In the case of two basal bodies, two possibilities exist: only one basal body, generally situated close to the nucleus or linked to it, possesses a flagellum, as in the spores of *Hydrurus* (Chrysophyceae), or both basal bodies possess a flagellum. The latter is the most frequently occurring situation in flagellate algae. Most often the basal bodies are inclined towards each other; sometimes they are perpendicular, or they may also be parallel facing the same direction or antiparallel facing opposite directions. In the Glaucophyta, the two basal bodies are inclined towards each other; in the Ochrophyta, they are parallel in *Mallomonas* and *Synura* (Chrysophyceae) and almost perpendicular in *Ochromonas* (Chrysophyceae); they lie at an obtuse angle to each other in the Xanthophyceae and Phaeophyceae, and are inclined to each other at an angle of about 90° in the Eustigmatophyceae and Raphidophyceae. In the Haptophyta the angle between the two basal bodies can be acute or obtuse; in both Cryptophyceae and Euglenophyceae the basal bodies are almost parallel, while in the Dinophyceae they lie at almost 180° to each other and slightly overlap. In the Chlorophyta, the angle between the two basal bodies can vary (about 90° in *Chlamydomonas*, 180° in *Acrosiphonia* zoid), and the couple can assume three different configurations:

1) 11 o'clock–5 o'clock configuration, in which the basal bodies are anticlockwise rotated relative to the first configuration (Figure 3.45a);
2) 12 o'clock–6 o'clock configuration, in which the basal bodies are in line with each other (Figure 3.45b);
3) 1 o'clock–7 o'clock configuration, in which the basal bodies are clockwise rotated relative to the first configuration (Figure 3.45c).

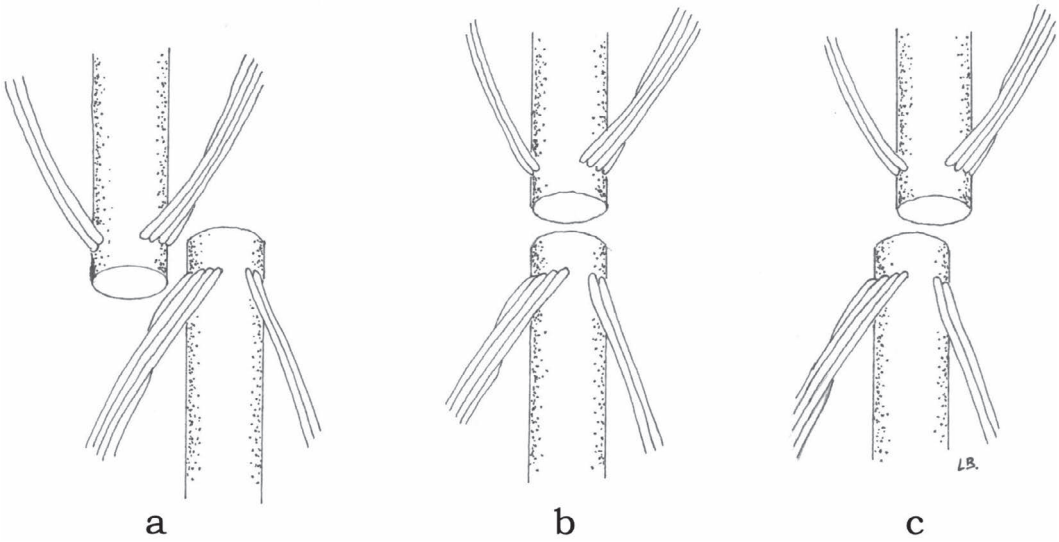


FIGURE 3.45 Schematical drawing of cruciate arrangements of basal bodies and roots of Chlorophyta. 11 o'clock–5 o'clock type (a), 12 o'clock–6 o'clock type (b), 1 o'clock–7 o'clock type (c).

The 11 o'clock–5 o'clock configuration is present in Ulvophyceae, while both the 12 o'clock–6 o'clock and 1 o'clock–7 o'clock configurations are present in the Chlorophyceae.

In the case of many basal bodies, the increase in their number and the corresponding increase in the number of flagella can result from:

1) a replica of each basal body of the pair, as in the stephanokont zoospore of *Oedogonium* (Chlorophyceae);
2) a replica of the primordial pair, indicated by the formula X·2A, as in the dinoflagellate *Phaeopolykrikos* sp. (Dinophyceae), where the primordial pair has undergone four replicas (4·2A);
3) the addition of new basal bodies in the surroundings of the primordial pair without a replication of it, indicated by the formula 2A + N; algae with four flagella, as in *Tetraselmis suecica* (Chlorodendrophyceae) or *Pyramimonas lunata* (Pyramimonadophyceae), with a formula 2A + 2N, while algae with eight flagella, such as *Pyramimonas octopus* (Pyramimonadophyceae), are indicated by the formula 2A + 6N.

Figure 3.46a shows an example of flagellum assemblage relative to the longitudinal section of a flagellum of *Tetraflagellochloris mauritanica* (Chlorophyceae) in the region between the basal bodies and the 9 + 2 axonemal structure. The basal bodies are composed of nine tilted microtubular triplets with connections between the A- and C-tubules of adjacent triplets. At the proximal end of each basal body, the hub-and-spoke complex of the cartwheel is present (Figure 3.46b). This structure consists of a central hub with a central dot and nine spokes that are connected to the A tubules by nine electron-dense knobs (Figure 3.46b). In the median longitudinal section, a series of projections seems to extend into the lumen of the basal body along the microtubular triplets, distally to the cartwheel. The lumen of the basal body is filled with filaments (asterisks; Figures 3.46a and 3.46c).

The transition zone (tz), characteristic of green algae (square brackets; Figure 3.46a), is distal to the end of the C-microtubules of the basal body.

This region contains two distinct stellate structures that are separated by the transitional plate. The stellate structure is formed by filaments that connect the A tubules of every third axonemal doublet with each other, constituting a nine-pointed star with a central ring-like hub (Figure 3.46d). In longitudinal sections, the two stellate structures form an H-piece with uneven arms composed of the distal (~800 nm long) and proximal (~320 nm long) stellate structures and separated by the transitional plate (Figure 3.46a). Differently from other chlorophycean algae such as *Chlamydomonas*, both the distal and the proximal stellate structures are attached to the same transitional plate, which in our preparation does not seem to extend to the microtubule doublets. Figure 3.46d shows a cross-section through the proximal stellate structure of the transitional region; projections attached to the A-B tubule junction extend to the flagellum membrane. Figure 3.46e shows the internal 9 + 2 structure of the axoneme.

Root System

All algal flagella appear to possess flagellar roots, that is, microtubular or fibrillar, often cross-banded structures, which extend from the basal bodies into the cytoplasm either underlying the plasma membrane or projecting into the cell and making contact with other organelles such as the nucleus, the mitochondria, the Golgi apparatus, or the chloroplasts. Diverse functions have been assigned to the flagellar roots: anchoring devices and/or stress absorbers, sensory transducers, and skeletal and organizational structures for morphogenetic processes.

The great diversity of morphology and arrangement of the flagellar root systems among the different algae make it necessary to describe them separately in each division. As mentioned,

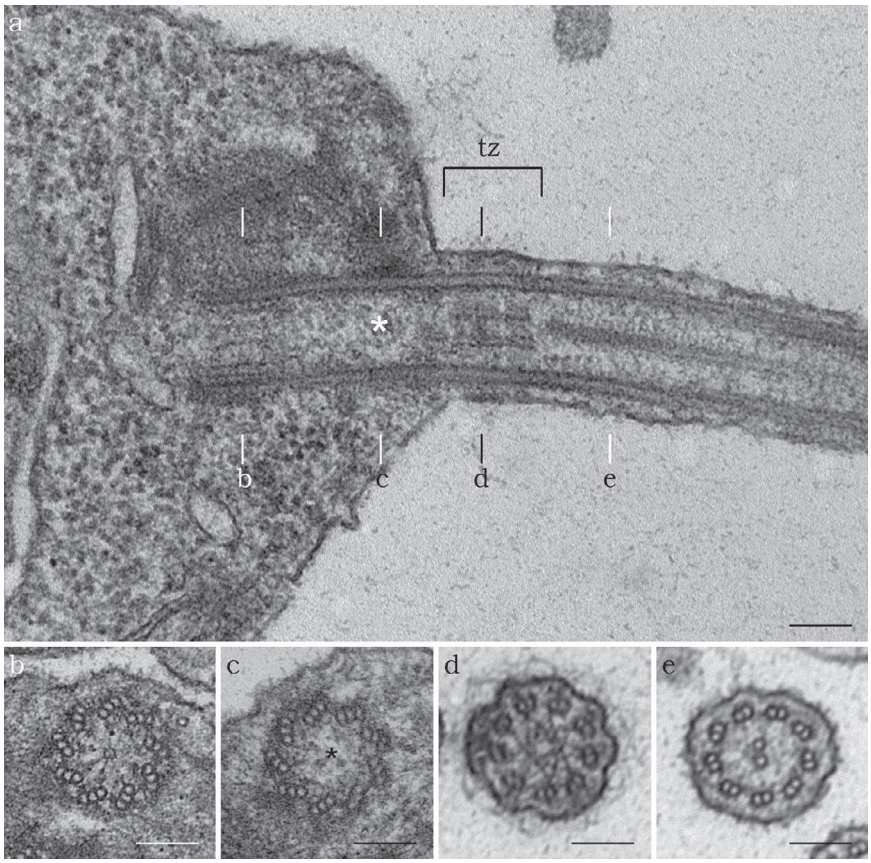


FIGURE 3.46 Longitudinal section of a flagellum of *Tetraflagellochloris mauritanica* between the basal body and the 9 + 2 axonemal structure.

The level of each section in the series of transverse sections (b–e) is indicated in the longitudinal section (a). See text for details; scale bar: 0.5 μm.

Cyanobacteria and Rhodophyta lack any flagellar apparatus; hence, they will not be considered in the following.

Glaucophyta

In the cyanelle-containing genera *Gloeochaete* and *Glaucocystis*, four roots are arranged in a cruciate manner, that is, spreading out more or less evenly from the basal bodies. All four roots appear identical, each containing about 20 microtubules in *Glaucocystis* and about 50 in *Gloeochaete*. In *Cyanophora*, there are two roots. In all these genera, each root contains a multilayered structure consisting of a band of microtubules, which overlies several layers of parallel plates (Figure 3.47).

Prasinodermatophyta, Chlorophyta, Charophyta

The flagellar apparatus of most of these algae are characterized by a cruciate root system. A cruciate root system consists of four roots spreading out more or less evenly from the basal bodies, with opposite roots usually possessing identical numbers of microtubules. Since in

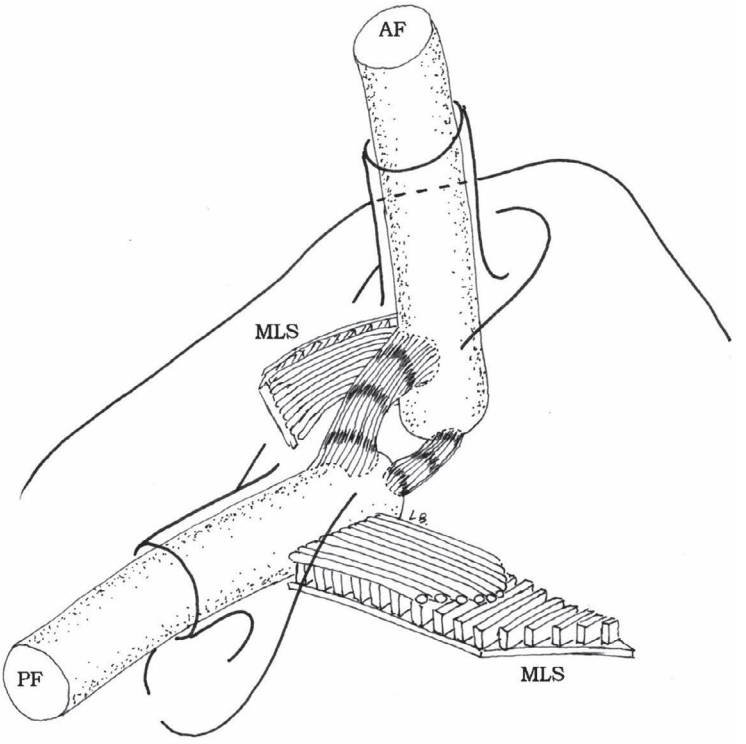


FIGURE 3.47 Root system of Glaucophyta. AF: anterior flagellum; PF: posterior flagellum; MLS: multilayered structure.

most members of these two phyla, two of the roots are two stranded, the general arrangement of microtubular root follows the X-2-X-2 system, with X varying from three to eight microtubules.

The root system is cruciate, with a 4-2-4-2 system in the tetraflagellate *Pyramimonas* (Pyramimonadophyceae) and *Tetraselmis* (Chlorodendrophyceae); a 4-2-0-0 system in *Mantoniella squamata* (Mamiellophyceae), due to the reduction of one of the two flagella and the lack of roots; a 4-3-0-(7–12) system in *Nephroselmis* (Nephroselmidophyceae); and a 4-6-4-6 system in *Mesostigma* (Mesostigmatophyceae). When four microtubular roots are present, as in *Pyramimonas*, they extend up the sides of the flagellar pit towards the anterior of the cell, where they join the microtubules of the cytoskeleton, which radiate from the flagellar region below the membrane. An elaborate system of non-striated fibers connects the basal bodies, which are associated with one or more rhizoplasts. These contractile structures extend from the proximal ends of the basal bodies down to the chloroplast, where they branch over the chloroplast surface and get in contact with it. Some tetraflagellate members of this class possess a synistosome, a longitudinally striated fibrous band connecting two of the basal bodies, and an asymmetrical structure termed lateral fibrous band, which forms an arc on one side of the four basal bodies. Proximal connective fibers may be present between the basal bodies. The microtubular root system of flagellate Chlorophyceae has the X-2-X-2 pattern. The roots diverge from the basal bodies and run beneath the cell membrane towards the posterior of the cell. Fibrous roots are generally present and associated with two-membered microtubular roots. Rhizoplasts extend from the basal bodies to the nucleus. The basal bodies are connected by a robust upper striated connective and two lower striated connectives (Figure 3.48).

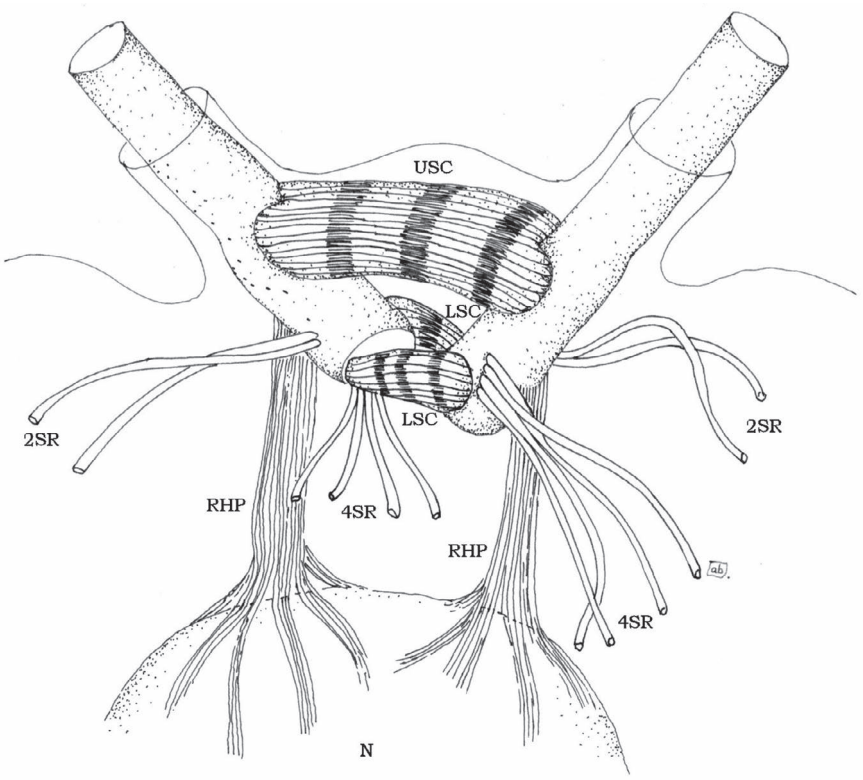


FIGURE 3.48 Root system of Chlorophyceae (Chlorophyta). 2SR: two-stranded roots; R4: four-stranded roots; RHP: rhizoplasts; N: nucleus; USC: upper striated connective; LSC: lower striated connectives.

In the stephanokont zoospore of *Oedogonium* sp., the flagellar bases are connected by a transversely striated fibrous band running around the top of the zoospore above the flagella. Three-membered microtubular roots perpendicular to the basal bodies depart from them and extend towards the posterior of the cell. Other striated components are present in close association with the microtubular roots.

The unusual root system of the recently identified chlorophycean *Tetraflagellochloris mauritanica* deserves a more detailed description. The four basal bodies are arranged in two pairs in a nearly diamond shape; the two opposite basal bodies, numbered 1 and 2, are closer to each other than the other two, which are located on the sides of the first pair and do not touch (Figure 3.49). A complex system of striated roots and radiating microtubules occurs around the four basal bodies, anchoring the four flagella in the cell by a cruciate root system. One pair of striated roots, with one root more prominent than the other, originates at each of the two closer basal bodies (white asterisk and white arrowhead, respectively, Figure 3.50a). Smaller striated roots originate at the second pair of basal bodies (arrowhead, Figure 3.50b). In transverse and longitudinal sections, these striated roots reveal a periodicity of 300–330 nm (asterisk, Figure 3.50c) and a clear distal tapering where they underlie the plasmalemma (Figure 3.50d). Microtubular roots are also present: two-stranded microtubular roots (arrows, Figure 3.50e) and four-over-one roots (arrow, Figure 3.50f). The striated roots are closely associated with the microtubular roots (arrow, Figures 3.50c and 3.50d). In TEM and SEM images (Figures 3.51a and 3.51b), the tapered ends of the striated roots form two symmetrical shoulders in the posterior part of the cell, just below the flagellar emergence; the microtubular

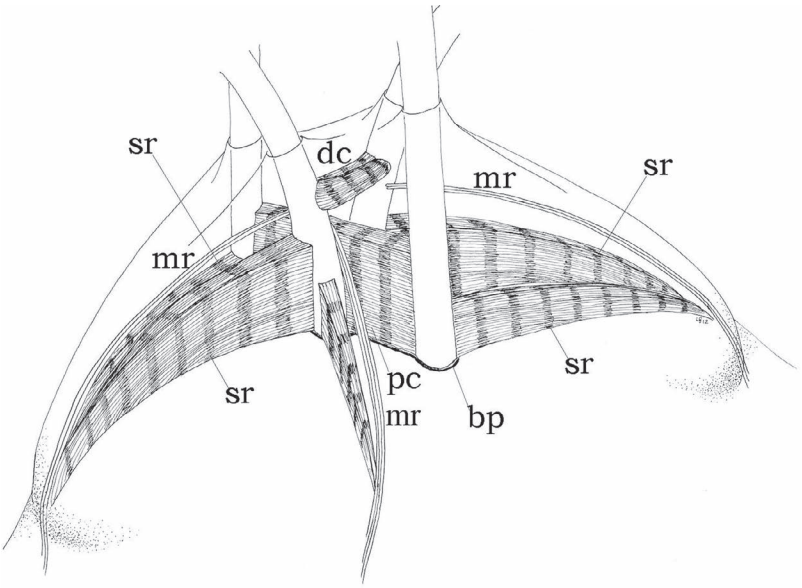


FIGURE 3.49 Schematic drawing of the posterior part of *Tetraflagellochloris mauritanica* illustrating the main components of the flagellar apparatus; sr, striated root; mr, microtubular root; dc, distal connection; pc, proximal connection; bp, basal plate. See text for details.

roots curve above the shoulders and down the sides of the cell for some distance. Basal bodies 1 and 2 lie in a V configuration (Figures 3.49 and 3.51c), while those of the other pair lie parallel to each other (Figures 3.49 and 3.51d). In the V configuration, the basal bodies are joined by a striated distal connection that is positioned immediately below the flagellar transition zone (arrow, Figure 3.51c). The two basal bodies are also joined at their bottom by a basal plate (double arrowheads, Figure 3.51c). The basal bodies of the other flagellar pair show a similar connection system: a prominent proximal connection showing alternating electron-dense zones resembling a striation (asterisk, Figure 3.51d) and a basal plate (arrowheads, Figure 51c). The arrow in Figure 3.51d indicates the cross-sectioned connecting fiber that joins flagellas1 and 2. Immediately below the connecting fiber, the microtubular roots are visible (double asterisks).

The microtubular rootlets of the flagellate reproductive cells of Ulvophyceae follow the X-2-X-2 arrangement of most green algae, with X = 4 in *Ulva* and X = 5 in *Ulothrix*. Striated bands connect the rootlets to the basal bodies, which are connected anteriorly by an upper connective; in some genera, additional striated bands between the basal bodies and striated components associated with the two-membered root can be detected. In *Chaetomorpha,* X is 3, while in *Cladophora*, X is 4. The microtubular rootlet systems of the biflagellate cells extend posteriorly nearly parallel to one another and to the basal body from which they arise. In the X-membered rootlets, an electron-dense strut or wing connects one of the uppermost microtubules to the subtending singlet, and the entire rootlet is usually subtended by a massive, more or less striated structure. Also the two-membered rootlets may be accompanied by such structures. An upper transversely striated connective links the basal bodies.

The flagellar apparatus of the reproductive cells of the Bryopsidales (Ulvophyceae) is anchored in the cell by four microtubular roots following the usual X-2-X-2 pattern. Each of the microtubules in the rootlet may be subtended by an electron-dense wing. The basal bodies

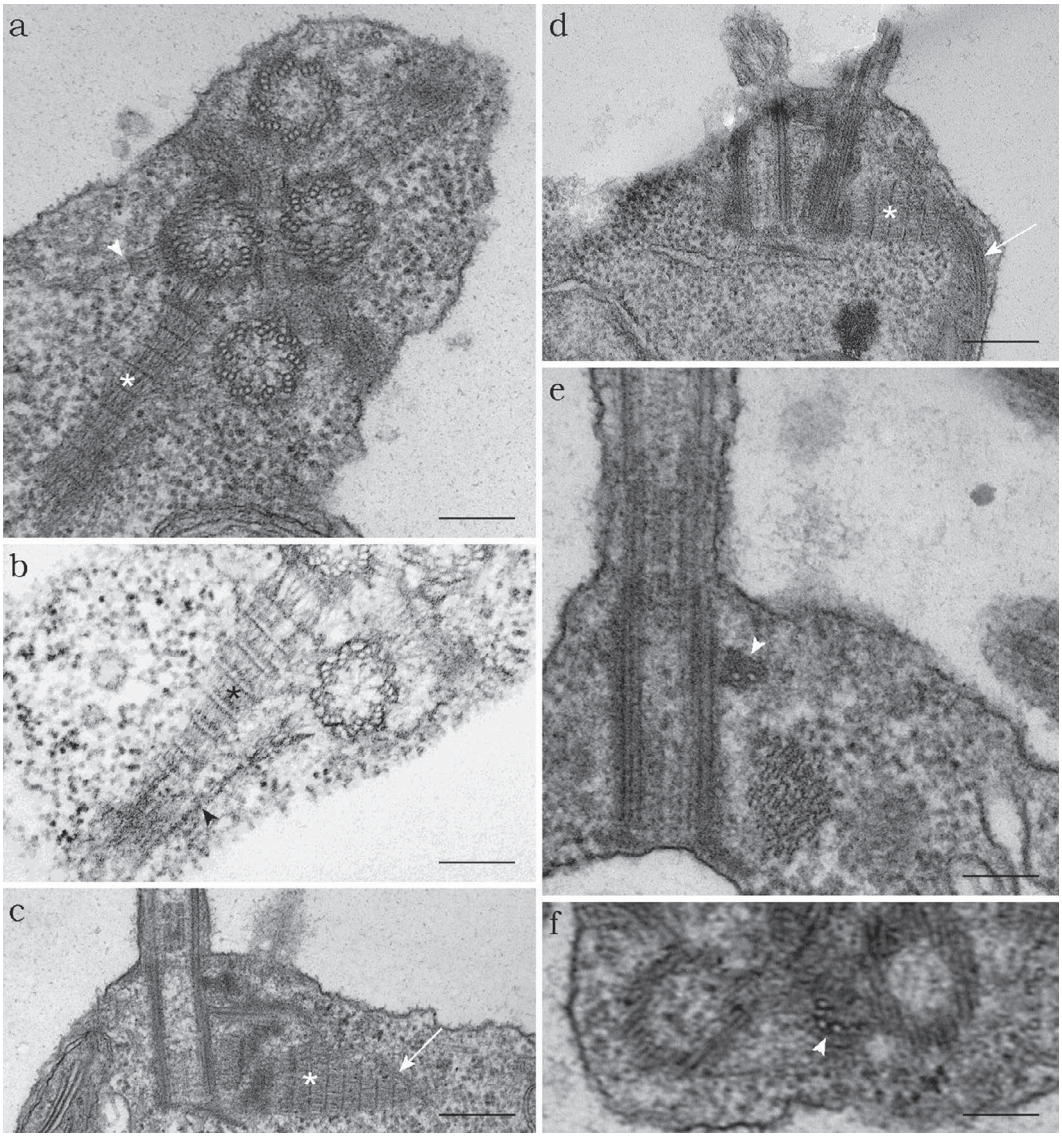


FIGURE 3.50 (a) TEM image of a transverse section of *Tetraflagellochloris mauritanica* showing the arrangement of the four basal bodies and the two striated roots originating at one basal body of the closer flagellar couple; arrowhead, minor root; asterisk, major root; scale bar: 1 µm; (b) similar section showing the smaller striated root (arrowhead) originating at one basal body of the more distant flagellar couple; scale bar: 1 lm; (c, d) TEM image of longitudinal sections of the posterior part of *T. mauritanica* cells showing the striated roots (asterisks) and the microtubular roots (arrows); scale bar: 1 µm. (e) two-stranded microtubular root (arrow). Scale bar: 1 µm. (f) four-over-one microtubular root (arrow); scale bar: 1 µm.

are connected anteriorly by a non-striated upper connective, with a typically pronounced arched appearance. Transversely striated bands connecting the rootlets to the basal bodies are also present. Species exist in this class that produce stephanokont zoospores with more than 30 flagella. In these cells, the basal bodies are connected by a non-striated fibrous upper ring, which can be

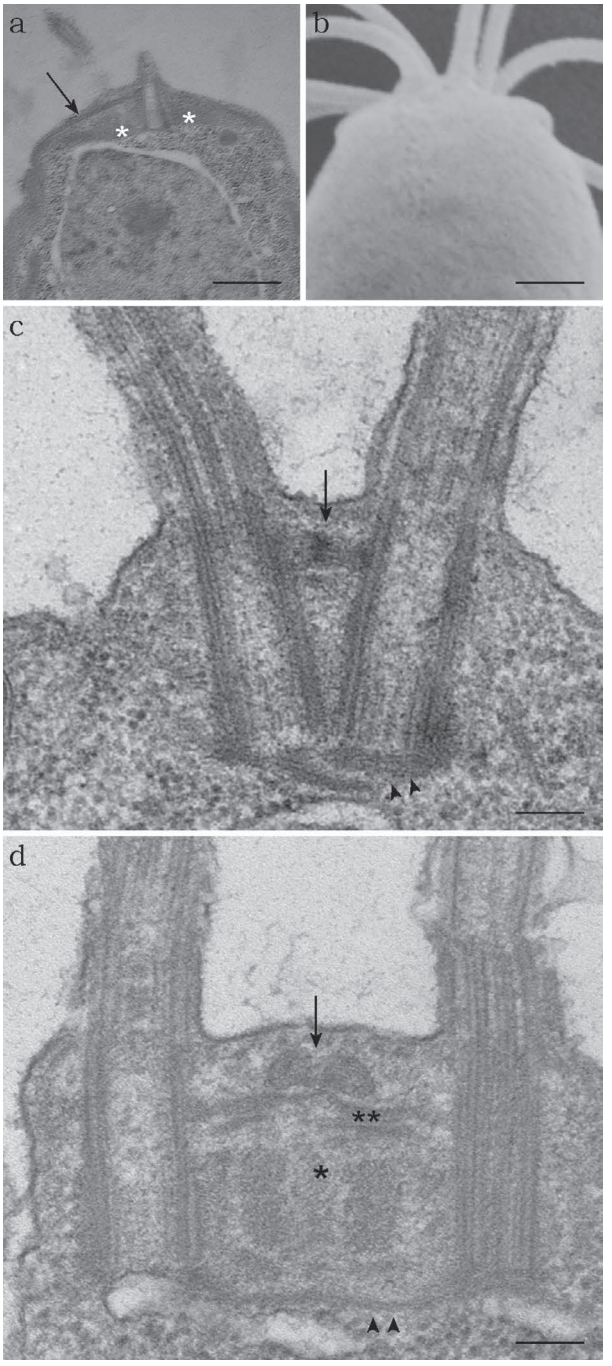


FIGURE 3.51 (a) TEM image of a longitudinal section of the posterior part of *T. mauritanica* showing the microtubular roots (arrow) in close association with the tapered ends of the striated roots, which form two symmetrical shoulders (asterisks); scale bar: 1 μm; (b) the posterior part of a cell visualized by SEM, showing the lateral wings formed by the association of microtubular roots and striated roots; scale bar: 1 μm; (c) V configuration of the basal bodies of the longer and closer flagellar pair; arrow: striated distal connecting fiber; double arrowheads: basal plate; scale bar: 1 μm; (d) as in (b), but showing the parallel configuration of the basal bodies of the shorter flagella; arrow: cross-sectioned striated distal connecting fiber; asterisk: proximal connection; double arrowheads: basal plate; double asterisks: microtubular roots, scale bar: 1 μm.

considered the result of the fusion of many non-striated upper connectives. The proximal ends of the basal bodies are partially enclosed in a second lower ring of amorphous material. Four- and six-membered microtubular roots depart from between the basal bodies. The microtubular root system of the Trentepohliales (Ulvophyceae) motile cells (tetraflagellate zoospores and biflagellate gametes) do not follow the X-2-X-2 pattern but show a 6-4-6-4 arrangement in *Trentepohlia* sp. The dorsiventrally compressed form of the flagellate cells forces the basal bodies and the root system components in a flattened arrangement. Basal bodies are aligned perpendicular to the long axis of the cell, with a parallel or antiparallel arrangement, and the microtubular rootlets, especially in the gametes, extend posteriorly nearly parallel to one another and to the basal body from which they arise. Two of the rootlets (the four-membered rootlets in *Trentepohlia* sp.) are associated with a complex columnar structure resembling the multilayered structure of the Charophyceae.

The root system and the associated structures of the biflagellate motile cells of Dasycladales have a X-2-X-2 pattern, with the basal bodies and microtubular rootlets showing a flattened arrangement. A striated distal fiber connects the proximal ends of the basal bodies, from which two prominent rhizoplasts depart.

No flagellate reproductive cells are present in the Zygnematophyceae. Biflagellate cells of Coleochaetophyceae such as *Chaetosphaeridium* sp. and *Coleochaete* sp. are characterized by a unilateral construction, in which the two equal flagella emerge on one side of the cell, below the apex. A transversely striated connective links the basal bodies. The system anchoring the flagella in the cell consists of a single lateral root of about 60 microtubules, which extends from the basal bodies along the cell side down to the posterior. At the level of the basal bodies, this broad root enters a multilayered structure in which the microtubules are located between two laminate plates.

In the biflagellate male gametes of the Charophyceae, the basal bodies are connected to each other by a conspicuous fibrous linkage; the root system consists of a main broad band of microtubules and a small secondary root.

Haptophyta

In the Haptophyta, there are different types of flagellar roots. Members of the order Pavlovales, such as *Pavlova* and *Diacronema*, possess a fibrous root, non-striated, which extends from the base of the anterior flagellum and passes into the cell along the inner face of the nucleus, becoming progressively wider. In some species, another fibrous root originates at the base of the haptonema. Two microtubular roots extend from the base of the posterior flagellum: a seven-stranded root which runs under the periplast and a two-stranded root arising almost at right angles to the seven-stranded root, running inside the cell opposite the haptonema. Fibrous connecting bands are present between the basal bodies (Figure 3.52). In the algae of the order Coccolithales, such as *Pleurochrysis*, the structure of the flagellar root system is more complex. Three main microtubular roots are associated with the two basal bodies, two broad roots, 1 and 2, arising near the left flagellum, and a smaller root, 3, arising near the right flagellum. Root 1 extends from the basal body up towards the cell apex and then curves backwards to run inside the cell. A fibrous root is associated with root 1. Closely packed microtubules organized in a bundle branch off perpendicularly from both roots 1 and 2. The basal bodies are connected to each other by distal, intermediate, and proximal connecting bands. Accessory connecting bands link the haptonema to the basal bodies and the left basal body to the broad microtubular root 1 (Figure 3.53).

Cryptophyta

The flagellar roots of these algae include two characteristic components, the rhizostyle and the compound rootlet. The rhizostyle is a posteriorly directed microtubular structure. It originates

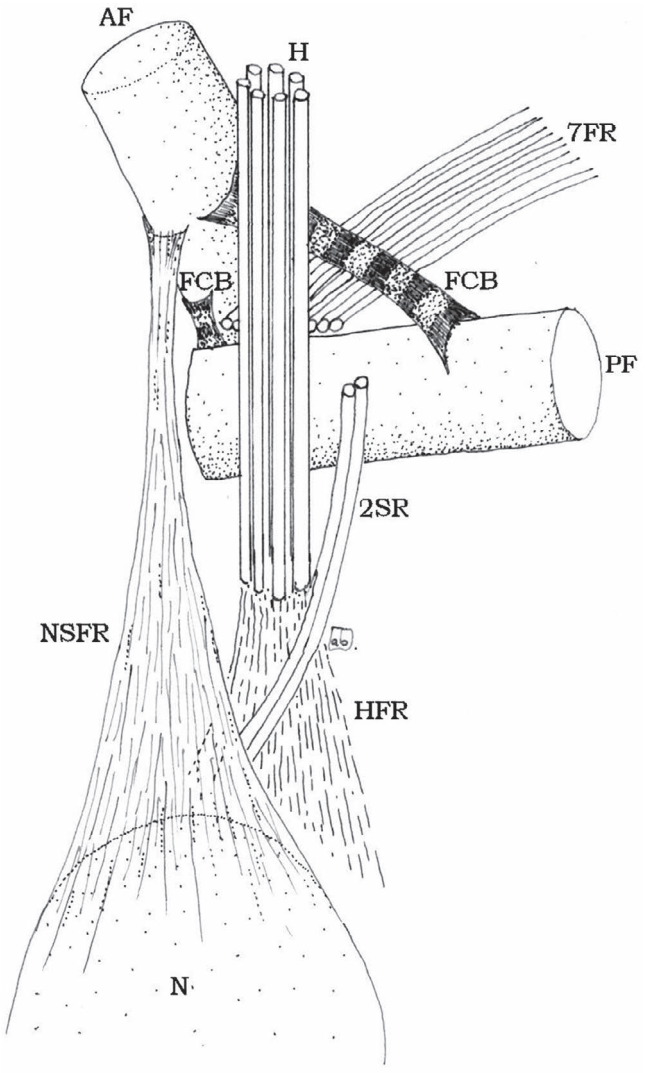


FIGURE 3.52 Root system of Pavlovales (Haptophyta). AF: anterior flagellum; PF: posterior flagellum; NSFR: non-striated fibrous root; H: haptonema; HFR: haptonema fibrous root; 2SR: two-stranded root; 7SR: seven-stranded root; FCB: fibrous connecting band; N: nucleus.

alongside the basal body of the dorsal flagellum and extends deep into the cell, parallel to the gullet, behind the layer of trichocysts, and ends in the posterior part of the cell. On the way, it runs through a groove in the nuclear surface. In many cryptomonads, such as *Chilomonas*, each rhizostyle microtubule bears a wing-like lamellar projection. The compound rootlet consists of a cross-banded fibrous band and microtubular roots. The fibrous band originates from the basal bodies of the dorsal flagellum but perpendicularly to the rhizostyle. A microtubular root arises near the rhizostyle and passes between the basal bodies in close association with the fibrous band; a second microtubular root extends dorso-laterally in a curved path, and a third root, which can be very short, originates near the rhizostyle and extends anteriorly. In addition to this rootlet, a conspicuous 12-stranded microtubular root is present in *Chilomonas*, together with a mitochondrion-associated lamella root, while a delicate cross-banded anchoring fiber

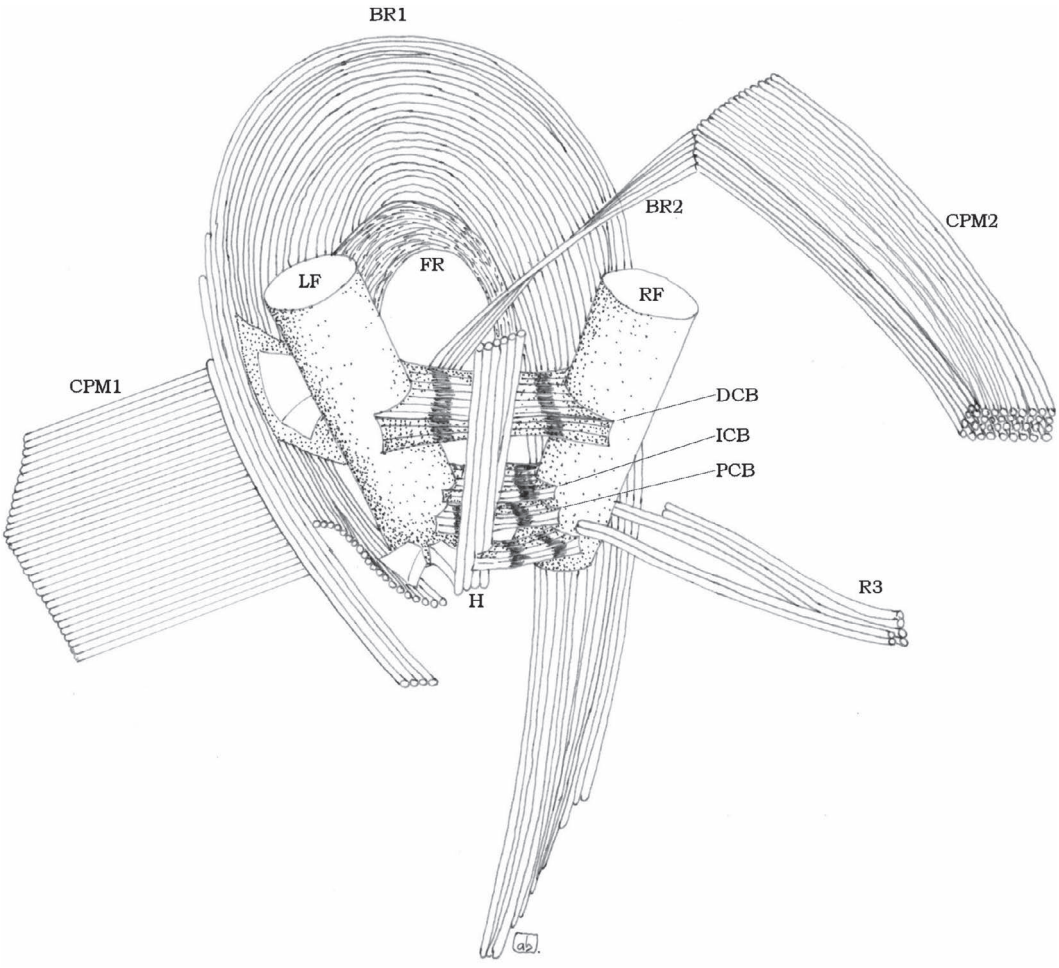


FIGURE 3.53 Root system of *Pleurochrysis* sp. (Haptophyta). LF: left flagellum; RF: right flagellum; H: haptonema; BR1, BR2: broad microtubular roots; FR: fibrous root; R3: small microtubule root; CPM1, CPM2: closely packed microtubules; DCB: distal connecting band; ICB: intermediate connecting band; PCB; proximal connecting band.

connecting one of the basal bodies to the ventral groove is present in *Cryptomonas*. The striated components of the root system have been shown to contain the contractile protein centrin (Figure 3.54).

Ochrophyta

The root system of *Ochromonas* can be considered the basic type of the Chrysophyceae. A single large cross-banded contractile root, termed the rhizoplast, is typically present, associated with the basal body of the longer pleuronematic flagellum. After leaving the basal body, this fibrous root passes closely against the edge of the chloroplast and reaches the tip of the pyriform nucleus. It then splits into several branches, ramifying over the nuclear surface, with some branches located in the narrow space between the nucleus and the associated Golgi body. Four microtubular roots, R1, R2, R3, and R4, anchor the two flagella in the cell, R1 and R2 associated with the basal body of the long pleuronematic flagellum and R3 and R4 associated with the basal body of the short smooth flagellum. The three-stranded R1 describes an arc in the anterior part of the cell just beneath the cell

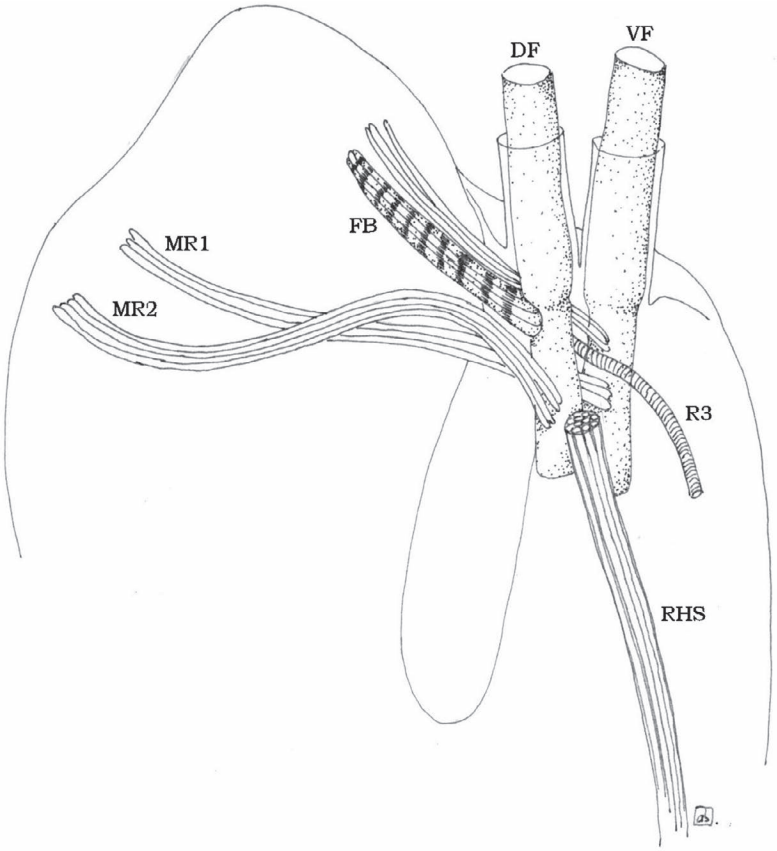


FIGURE 3.54 Root system of Cryptophyta. DF: dorsal flagellum; VF: ventral flagellum; RHS: rhizostyle; FB: fibrous band; MR1, MR2: microtubular roots; R3: root.

membrane. The two-stranded R2 originates at the opposite side of the basal body, running along the cell membrane. R3 and R4, consisting of a species-specific number of microtubules, arise from the opposite sides of the basal body of the short flagellum and form a loop around and under this flagellum. R1 forms the base of attachment of numerous microtubules running towards the posterior end of the cell, with cytoskeletal function (Figure 3.55).

No complete analysis of the flagellar root systems of Xanthophyceae exists. The typical root system as presently understood appears to consist of three different types of structures: a descending root originating near the basal bodies, resembling the rhizoplast in extending from the basal bodies along the nuclear surface, between the nucleus and the Golgi body, but differing in being unbranched and in consisting of a succession of rectangular blocks rather than fibers as in the Chrysophyceae; a cross-banded fibrillar root composed of slightly curved bands, originating together with, but at right angles to, the descending root and terminating at the cell membrane; microtubular roots in various numbers near the basal bodies, each of which contains three or four microtubules. In *Vaucheria* (Xanthophyceae), the system is completely different; neither a descending root nor a cross-banded fiber is present, but its anterior protrusion is supported by a single broad microtubular root of eight to nine microtubules arranged in a row. This root originates near the base of the anterior pleuronematic flagellum and from there passes forward along the cell membrane to the tip of the protrusion, turns around, and runs back on the opposite side of the cell, again along the membrane.

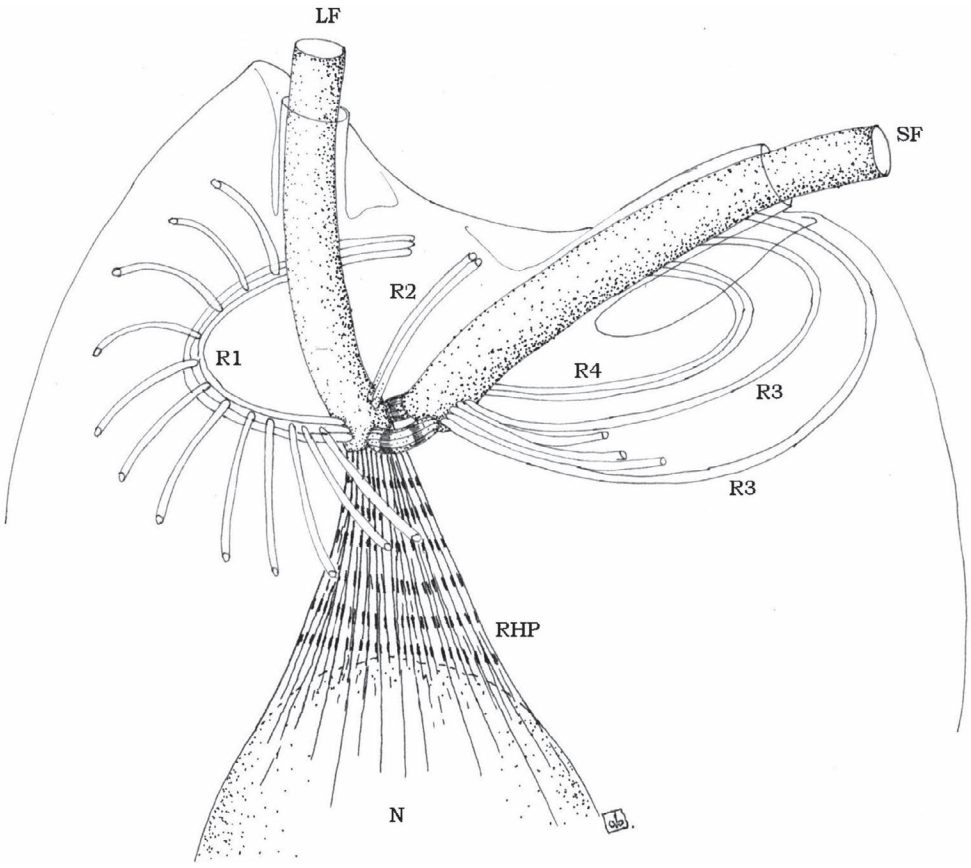


FIGURE 3.55 Root system of *Ochromonas* sp. (Ochrophyta). LF: long flagellum; SF: short flagellum; R1, R2, R3, R4: microtubular roots; RHP: rhizoplast; N: nucleus.

Only few data are available on the flagellar roots of Eustigmatophyceae. Both microtubular and cross-banded fibrillar types are present. The microtubular structures, consisting of two to five microtubules, arise close to the basal bodies and pass anteriorly and posteriorly in the cell. The cross-banded roots are narrow and pass from the region of the flagellar bases along the anterior flattened face of the nucleus.

The ultrastructure of the flagellar root system has been described only in one species of Bacillariophyceae, *Biddulphia laevis*. In the spindle-shaped spermatoids of this centric diatom, a system of microtubules radiates from the only basal body present into the cell to form a cone on the anterior part of the nucleus, and at least some of these microtubules extend throughout the length of the cell. They appear to maintain the elongated shape of the nucleus and thus probably of the cell itself.

An elaborate root system connects the basal bodies to the anterior surface of the nucleus in the Raphidophyceae. In *Chattonella*, two or three roots have been described, one multi-layered and associated with the pleuronematic flagellum and one with the smooth flagellum. The latter is a band of nine to ten microtubules, which extends from the anterior part of the cell, passing between the basal bodies and joining with other microtubules before extending along the nucleus in a depression of its surface. A large number of distinctly cross-banded fibrous roots are also present, extending from the flagellar bases to sheath the anterior cone of the nucleus.

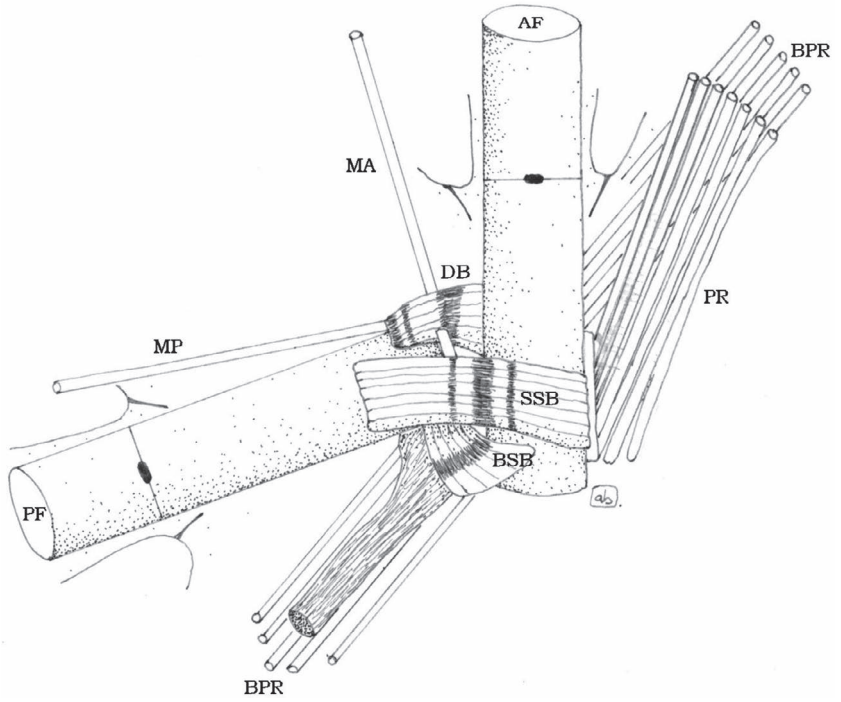


FIGURE 3.56 Root system of *Fucus* sp. (Ochrophyta). AF: anterior flagellum; PF: posterior flagellum; PR: proboscis root; BPR: bypassing microtubular root; MA: minor anterior root; MP: minor posterior root; DB: deltoid band; SSB: strap-shaped band; BSB: button-shaped band.

In the Phaeophyceae, the structure of the flagellar root system appears remarkably uniform. The main characteristic of the system is the root supporting the flat, elastic proboscis in spermatozoids of brown algae. In *Fucus*, this root is very broad and usually contains 7 microtubules (but there can be up to 15 microtubules), which travel from the base of the anterior flagellum along the plasmalemma to the anterior end of the cell, where the proboscis is located. Here, they bend back and run along the cell membrane on the opposite side. A by-passing microtubular root of about five microtubules originates in the anterior part of the cell, runs along the proboscis root, by-passes the basal bodies without contact, and continues towards the posterior part of the cell. Two other minor microtubular roots, consisting of only one microtubule, are present, one extending anteriorly, the other posteriorly. The basal bodies are interlinked by three cross-banded connectives, the deltoid and the strap-shaped and button-shaped bands (Figure 3.56).

Cercozoa—Chlorarachniophyceae

The single flagellum of the ovoid zoospores of *Chlorarachnion reptans* possesses a root system that consists of a microtubular component appearing as a 3 + 1 structure near the level of emergence of the flagellum, soon increasing to 8 + 1, and a second root with a homogeneous substructure that occupies a distinct concavity in the nuclear envelope.

In contrast to *Chlorarachnion reptans*, cells of *Bigelowiella natans* are basically biflagellate. The second flagellum, however, is exceptionally short and consists only of a barren basal body inserted

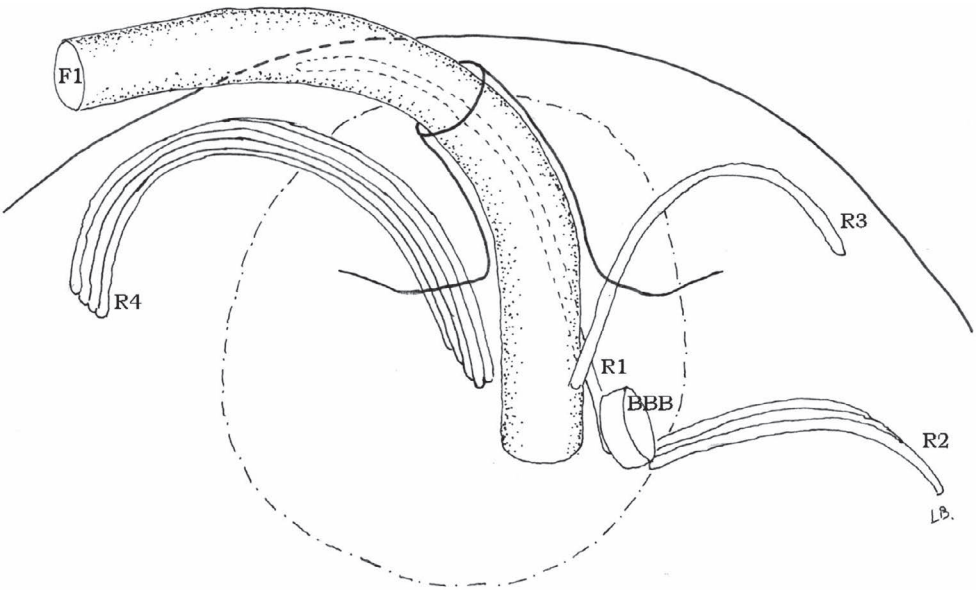


FIGURE 3.57 Root system of *Bigelowiella natans* (Chlorarachniophyta). F1: main flagellum; BBB: barren basal body; R1, R2, R3, R4: microtubular roots.

at an approximately right angle to the emergent flagellum. In this alga, the four flagellar roots consist of microtubular structures only with no cross-banded roots. A microtubular root is present on either sides of the long flagellum basal body; the largest and most conspicuous root, which attaches to the outside of the long flagellum basal body, is five stranded and forms an "L" in the area between the nucleus and the plasma membrane. Just before terminating, this root becomes two stranded. The second microtubular root associated with the long flagellum basal body emerges from the corner between the two basal bodies and is one stranded. The third flagellar root emerges on the outside of the short basal body, and it is three stranded. The four microtubular roots are the most unusual; they are one stranded and seem to emerge within the lumen to the short basal body next to the cartwheel structure (Figure 3.57).

Miozoa—Dinophyceae

The root apparatus of these algae is quite complex for number and appearance of ancillary structures associated to the microtubular roots and for the spatial relationship between roots and other cell organelles. Minor features can be considered species specific, while major components are common to almost all the dinoflagellates. The longitudinal basal body and the transverse basal body are interconnected by a small striated connective band. A multimembered microtubular root, the longitudinal root, originates on the left side of the longitudinal basal body and continues posteriorly along the sulcus. A cross-striated fibrous root, the transverse striated root, emanates from the left side of the transverse basal body and runs along the transverse flagellar canal and the cingulum. Striated connectives link the transverse striated root to both the longitudinal root and the longitudinal basal body and the proximal portion of the longitudinal basal body to the longitudinal root. The most distinct connective is a large electron-opaque fiber termed the nuclear fibrous connective, which links the proximal parts of the longitudinal root, the transverse striated root, and the transverse and longitudinal basal bodies with the nucleus. Fibrous rings with

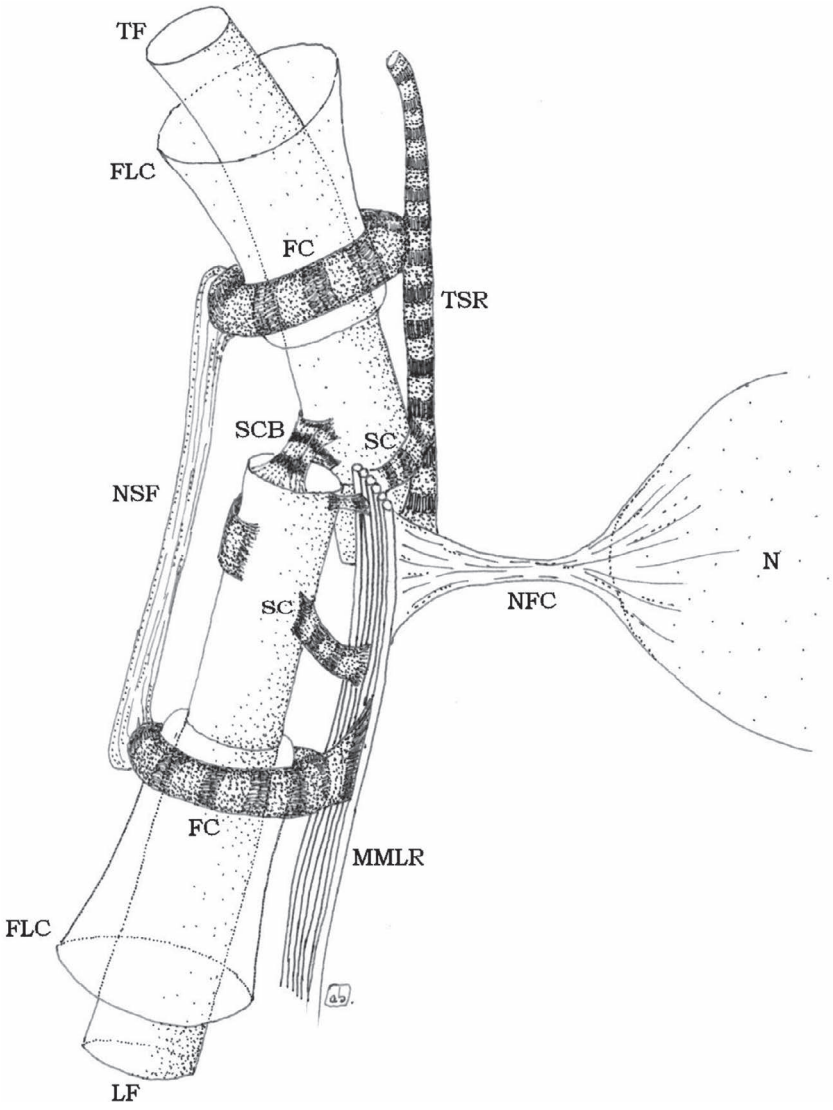


FIGURE 3.58 Root system of Dinophyceae. TF: transverse flagellum; LF: longitudinal flagellum; SCB: striated connective band; MMLR: multimembered longitudinal root; TSR: transverse striated root; SC: striated connectives; NFC: nuclear fibrous connective; N: nucleus; FC: fibrous collars; FC: flagellar canals; NSF: non-striated fiber.

cross-striations, called fibrous collars, encircle the flagellar canals, the longitudinal striated collar less conspicuous than the transverse striated collar. A non-striated fiber interconnects the two collars. The fibrous elements of this complex root apparatus are likely to contain centrin (Figure 3.58).

Euglenozoa—Euglenophyceae

Euglenoids show a rather uniform root structure, with one microtubular root opposite each basal body and a single microtubular root in between, termed dorsal, intermediate, and ventral roots (Figure 3.59). The dorsal root is anchored to the dorsal basal body at the side furthest

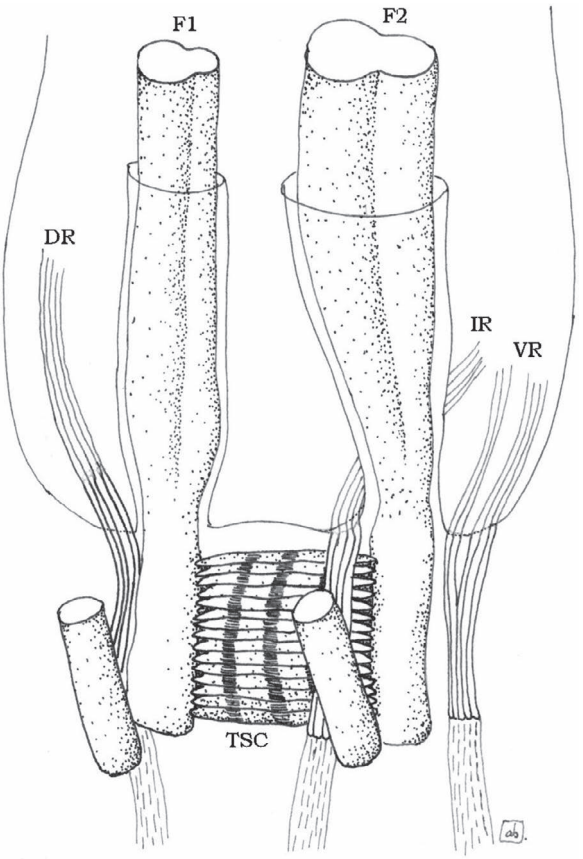


FIGURE 3.59 Root system of Euglenophyceae. F1, F2: flagella; DR: dorsal root; IR: intermediate root; VR: ventral root; TSC: transversely striated connective.

from the ventral basal body; the intermediate and ventral roots are both associated with the ventral basal body at its dorsal and ventral side, respectively. In *Euglena mutabilis*, the dorsal and the intermediate roots consist of three microtubules, while the ventral root consists of five microtubules; in *E. gracilis*, the ventral root is formed by five microtubules, as in *E. mutabilis*, while the microtubules of the dorsal root are more numerous. These roots extend from the basal bodies along the reservoir and into the cytoplasm, usually along the cell periphery, but in some species toward the nucleus. Flagellar roots are believed to play an important role in maintaining cell shape. In some species, the two flagellar basal bodies are connected by a conspicuous transversely striated connective.

Besides the intra-flagellar accessory structures described previously, euglenoids with two emergent flagella possess extra-flagellar accessory structures, the so-called rootlets. Two major classes of rootlets have been described: microtubular rootlets and filamentous rootlets. Microtubular rootlets are usually made of a complex and species-specific network (geometry, number of elements) anchoring the flagellar apparatus in the whole cell body. However, due to known functions of microtubules in other systems, these microtubules could not only play a role of anchor but also provide a stable oriented network along which cargos could be transported from inside the cell body to the flagellar apparatus.

The filamentous rootlets are made of filaments that can contain centrin. These appendages are attached to the pair of basal bodies located at the base of the flagella and extend

inside the cytoplasm, usually in the direction of the nucleus or along the plasma membrane. Classically, they have been considered anchoring structures providing the role of roots to the whole flagellar apparatus. However, they are contractile structures as well that may show transversal striations (centrin type, not assembling type) whose periodicity varies with their contraction state.

HOW ALGAE MOVE

Cytoplasm, cell walls, and skeletons of algae have a density greater than the medium these organisms dwell in. The density of fresh water is 1.0 $g \cdot cm^{-3}$, and that of sea water ranges from 1.021 to 1.028 $g \cdot cm^{-3}$, but most cytoplasmic components have a density between 1.03 and 1.10 $g \cdot cm^{-3}$; the silica forming the diatom frustule and the scales of Chrysophyceae have a density of 2.6 $g \cdot cm^{-3}$, and both calcite and aragonite of Haptophyta coccoliths reach an even higher value of 2.7 $g \cdot cm^{-3}$. With these density values, algae must inevitably sink. Therefore, one of the problems facing planktonic organisms (organisms that wander in the water and/or are carried about by the movements of the water rather than by their own ability to swim) is how to keep afloat between whatever levels are suitable for their life. The phytoplankton must obviously remain floating quite close to the surface because only here is there sufficient illumination for photosynthesis. There are broadly two solutions by which algae can keep afloat and regulate their orientation and depth: a dynamic solution, obtaining lift by swimming, and a static solution, by buoyancy control or through adaptations reducing sinking rates. In many cases, the two solutions function together.

Swimming

Life in water strongly conditions shape and size of phytoplankton, which in turn affect both metabolism and motility, since cells need to access nutrients, whose diffusion is limited by gradients, and have to harvest enough light to fulfill photosynthetic requirements, despite sinking. Uptake and propulsion must be simultaneously optimized to explore and exploit environmental resources. The algae are all good movers or, better, good swimmers.

What does swimming mean? It means that an organism immersed in a liquid environment is able to sustain movement by deforming its body shape (cell body plus flagella) in a periodic way. Algae swim more or less continuously and control their level chiefly by this means. For example, dinoflagellates, which can achieve speeds of 200–500 $\mu m\ sec^{-1}$, are said to maintain themselves near the surface by repeated bursts of upward swimming, alternating with short intervals of rest during which they slowly sink.

Motility is present in unicellular algae or colonies that are propelled by flagella; in some classes, it is confined only to gametes and asexual zoospores provided with flagella, which are used as a motor system for their displacement in the fluid medium. Algae, as biological microswimmers, self-propel by moving its/their flagellum/a. According to the type of far-field fluid flow that they induce, algae are classified as pushers and pullers. While pushers force fluid outward along their swimming direction and draw fluid into the sides of their bodies, pullers force the fluid inward along their swimming direction and repel fluid from their sides.

The physics governing swimming at the micrometer scale experienced by algae is different from the physics of swimming at the macroscopic scale. Forward movement of a swimming alga is resisted by two things: the inertial resistance of the fluid that must be displaced, which depends upon the density of the fluid, and the viscous drag experienced by the moving organism, that is, the rearward force exerted on the organism by the fluid molecules adhering to its surface when it passes through the viscous fluid.

The world of microorganisms is the world of low Reynolds numbers, a world where inertia plays little role and viscous forces dominate the flow. The Reynolds number (R) is defined as the ratio of inertial and viscous forces; it depends upon the size of the organism (related to the linear dimension, l), its velocity (u), and the density (ρ) and viscosity (η) of the fluid medium according to the equation:

1) $$R = (\text{inertial forces}) \times (\text{viscous forces})^{-1} = l \times u \times \rho \times \eta^{-1}$$

Since the ratio between the viscosity and the density is the kinematic viscosity ($v = \eta \times \rho^{-1}$ in $cm^2\ s^{-1}$), Equation 1 can be written as:

2) $$R = l \times u \times v^{-1}$$

In water, the kinematic viscosity is $10^{-2}\ cm^2\ s^{-1}$.

A 50-µm-long alga swimming at 10 µm × s^{-1} has the minuscule Reynold's number of 5×10^{-4}; hence, inertial effects are vanishingly small, and the major constraint is the viscous drag; this means that what an alga is doing at the moment is entirely determined by the forces that are exerted on it *at that moment* and by nothing in the past. Therefore, when the flagellum stops, forward movement of the cell will cease abruptly without gradual deceleration. The physics of low R numbers imposes also constraints on the possible shape changes that will result in progress. Considering some periodic motion of a low-R microalga swimmer, all the possible shapes of the swimmer can be constructed. In the absence of inertial effects, the motion of the swimmer's deformable body undergoing an ordered sequence of body-shape changes will be described by the rotation and displacement of the body.

Swimming strategies employed by larger organisms that operate at high Reynolds numbers, such as fish, birds, or insects, are ineffective at the small scale. The Reynolds number might get up to 10^5 for a fish 10 cm long swimming at 1 m s^{-1}. If the same fish were swimming at the Reynolds number of an alga, it would be as if it were swimming inside molasses. Any attempt to move by imparting momentum to the fluid, as is done in paddling, would be foiled by the large viscous damping. Therefore, microorganisms have evolved propulsion strategies that successfully overcome and exploit drag.

But why the do algae swim? All algae in an aquatic environment have a need to exchange molecules such as O_2, CO_2, and NH_3 with environment. Since all solid boundaries in a liquid medium have a boundary layer associated with them in which water movement is reduced (due to the no-slip boundary), this layer will impede the nutrient uptake of the organisms by creating a small depleted layer around them. Turbulence is very ineffective in transporting nutrients towards such small organisms, as the smallest length scale of turbulent eddies is on the order of several millimeters. Therefore, algae must rely on molecular diffusion to overcome the nutrient gradient across the boundary layer. Diffusion, that is, the slow mixing caused by the random motion of molecules, is important because of another very particular feature of a low Reynolds number: stirring is not any good. The alga's problem is not the energy supply; the problem is its environment. At a low Reynolds number, you cannot shake off your environment. If you move, you take it along with you; it only gradually falls behind.

Algae use their motility (be it sinking or swimming) to generate movement relative to the water and hence replenish the boundary layer with nutrients. However, depending on the size of the organism, the motive for swimming must differ, since its effects differ significantly. For small algae in the 1–10 µm range, diffusion is about 100 times more effective in supplying nutrients than movement. This is often expressed as the Sherwood number (S):

3) $$S = (\text{time for transport by diffusion}) \times (\text{time for transport by movement})^{-1}$$
$$= (L^2 \times D^{-1}) \times (L \times u^{-1})^{-1} = (L \times u)^{-1} \times D$$

where L is the distance over which the nutrient is to be transported, u is the water velocity, and D is the diffusion constant.

For scales on the order of 1 μm, the ratio is $\approx 10^{-2}$. Diffusion is about 100 times faster than movement. Hence, in this world of low Reynolds numbers, nothing is gained by trying to reduce the diffusion barrier by generating turbulent advection. In this contest, the only possible advantage of undertaking locomotion for the alga is that it might encounter nutrients in a higher concentration. For this purpose, a helical swimming path is more useful than a straight one in spite of the longer distance for the same displacement. This is because a helical swimming path enables detection of the three-dimensional component of a gradient, whereas the straight path allows detection of only one dimension. Purcell (1977) summarized it by saying that the organism does not move like a cow that is grazing in a pasture; it moves to find greener pastures. Only species that swim very fast, such as the dinoflagellates (about 500 μm × s^{-1}), can overcome the diffusion limitation. This high velocity should be related to the effective increase in the probability to catch more prey and therefore to the heterotrophic metabolism of the algal species.

Algae have evolved propulsion strategies that successfully overcome and exploit viscous drag. How, then, is propulsion achieved at low R? Since time doesn't matter, the deformation that produces the swimming must be asymmetrical. Therefore, the pattern of flagellar beating must be three-dimensional and asymmetric; that is, the forward stroke should be different from the reverse stroke. If the deformation were symmetrical, that is, identical when reversed (reciprocal motion), the net displacement of the cell would be zero.

For optimum propulsive efficiency, cell body size should be 15–40 times the flagellum radius (about 0.1 μm), and this ratio is present in many algae. When the cell body size is larger than predicted, as in *Euglena*, the effective radius of the flagellum is modified by simple, non-tubular hairs.

Beat patterns of most smooth flagella (i.e. without hairs) are three-dimensional, and the direction in which the microorganism moves is opposite to the direction in which the waves are propagated along the length of the flagellum so that, in almost all cases, when the cell body is to be pushed along, a wave must be initiated at the base of the smooth flagellum. Although basal initiation is more common than distal, both are known. The velocity of forward movement is always a small fraction of the velocity of the wave running along the flagellum, and its propulsive efficiency depends on the ratio of its amplitude and wavelength.

Unlike smooth flagella, the propulsive force generated by a flagellum bearing tubular hairs is in the same direction as the direction of wave propagation. These stiff hairs remain perpendicular to the axis of the flagellum as it bends (Figure 3.60). A wave moving away from the cell body will cause the hairs to act as oars, and the overall effect will be to propel the cell flagellum first.

Control characteristics, and thus behavioral peculiarities, are connected with the functioning of the propelling structure of the cell. If the cell is asymmetric, it advances spinning along its axis; it can correct its trajectory only by sudden steering obtained by changing the insertion angle of flagella or by the stiffening of internal structures. This behavior can be attributed to all heterokont or uniflagellate algae. In the case of a symmetric cell, it can accomplish a gradual smooth correction of its trajectory going forward without spinning (or rotating with a very long period) and displacing the barycenter of the motor couple. This behavior can be attributed to all isokont cells.

Examples of main swimming patterns among algae will be described in the following according to the number (one or more) and type of flagella (smooth or hairy).

In *Ochromonas* sp. (Ochrophyta), only the flagellum bearing hairs seems to be active during swimming (Figure 3.60). It is directed forward and executes simultaneous undulatory and helical waves that travel from its base to the tip. The resulting flagellum movements cause the whole body of the cell to rotate as it moves forward. The shorter flagellum trails backward

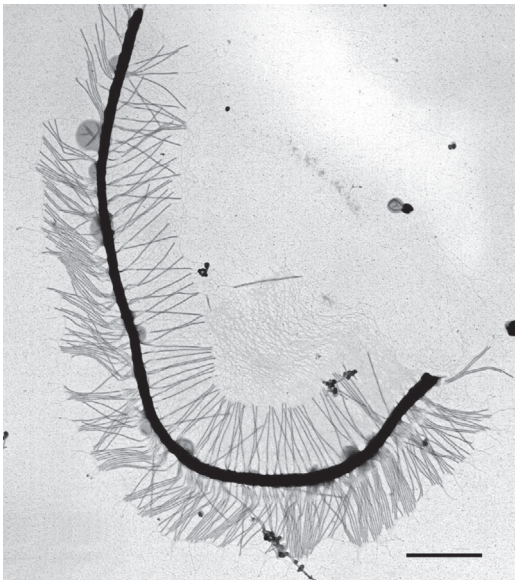


FIGURE 3.60 Negative staining of the trailing flagellum of *Ochromonas danica*. Scale bar 1 μm.

passively, lying against the cell; it is capable of acting as a rudder to steer the cells. The two rows of stiff hairs cause a reversal of the flagellum thrust. Water is propelled along the flagellum from the tip to the base so that the cell is towed forward in the direction of the flagellum (Figure 3.61).

As noted, the emergent flagellum of *Euglena* sp. (Euglenophyta) bears simple hairs 3–4 μm long. These long hairs are arranged in tufts of three to four and form a single row that runs along the flagellum spirally with a low pitch. The flagellar hairs increase the thrust of the flagellum against the surrounding water. During swimming, the long flagellum trails beside the cell body and performs helical waves, generated in a base-to-tip mode (Figure 3.62).

A peculiar swimming pattern is present in the ovoid zoospores of *Chlorarachnion reptans* and *Bigelowiella natans* (Chlorarachniophyceae), which bear a single flagellum inserted a little below the cell apex. This flagellum bears very delicate hairs markedly different from the tubular hairs of Ochrophyta. During swimming, the flagellum wraps back around the cell in a downward spiral, lying in a groove along the cell body. The cells rotate around the longitudinal axis during swimming, and the anterior or posterior end of the cell moves in either a narrow or wide helical path, which appears as a side-to-side rocking or wobbling (Figure 3.63).

In desmokont dinoflagellates such as *Prorocentrum* sp., the longitudinal flagellum, which extends apically, beats with an anterior-to-posterior whipping action, generating a wave in a tip-to-base mode. The second flagellum, perpendicular to the first, is coiled and attached to the cell body except for the tip, which beats in a whiplash motion, while the attached part undulates (Figure 3.64). In dinokont dinoflagellates, such as *Peridinium* sp. or *Gymnodinium* sp., the two flagella emerge at the intersection of the cingulum (transverse furrow) and sulcus (longitudinal sulcus). The longitudinal flagellum extends apically, running in the sulcus, and is the propelling and steering flagellum, while the ribbon-shaped transverse flagellum is coiled, lies perpendicular to the first, and runs around the cell in the cingulum. It is thought to be responsible for driving the cell forward, and it also brings about rotation. The longitudinal flagellum beats with a planar waveform, which contributes to forward movement. The longitudinal flagellum can also reverse

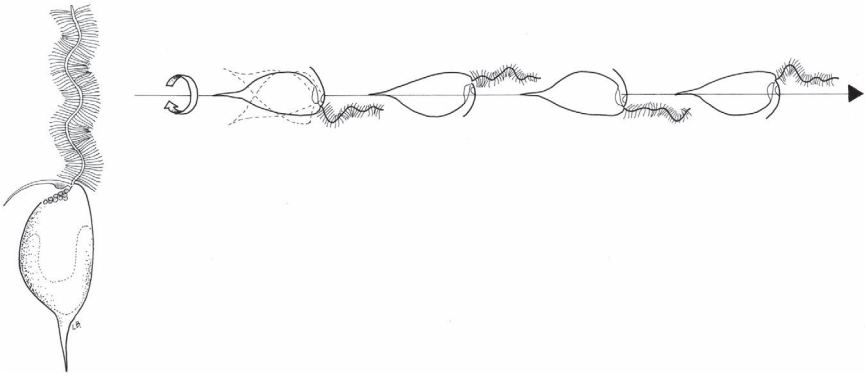


FIGURE 3.61 Swimming pattern of *Ochromonas danica*.

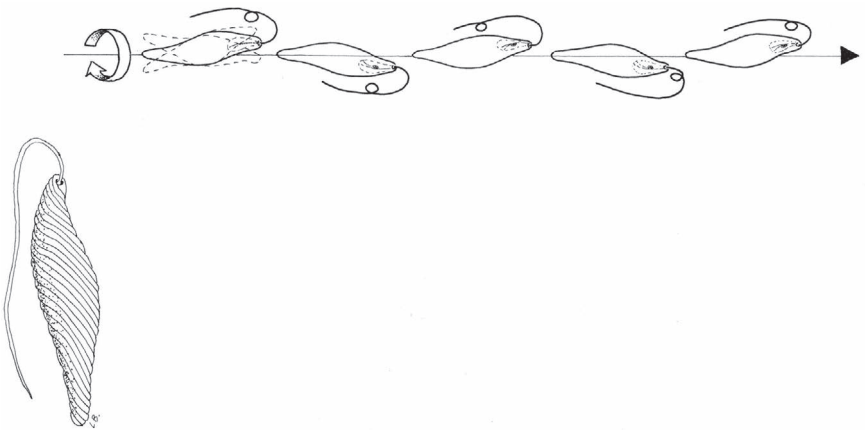


FIGURE 3.62 Swimming pattern of *Euglena gracilis*.

the swimming direction: it stops beating, points in a different direction by bending, and then resumes beating. This steering ability is related to a change in orientation of basal bodies and contraction of the structures associated with the axoneme. In the transverse flagellum, a spiral wave generated in a base-to-tip mode is propagated along the axoneme, bringing about backward thrust and rotation and the same time (Figure 3.65).

In the Chlamydomonadales, flagella are organized in pairs, and motile cells are typically biflagellate, such as *Chlamydomonas* or *Dunaliella*. In these algae, successful propulsion relying on repetitive periodical motion is assigned to the rhythmic beating of flagella. The beating of the flagella in a pair needs some sort of synchronization to generate a strategy of efficient swimming, which can be defined as the power consumption to swim a certain distance compared with the power the cell would need to drag the body through the fluid. Since at low R numbers, thrust is generated by the same mechanism that resists motion, that is, viscous drag, swimming efficiency is only a few percent. Its value mainly depends on the flagellar length, the payload to transport (i.e. the cell body), the ratio between flagellar and cell body length, and the amplitude and wavelength of the flagellar undulatory wave.

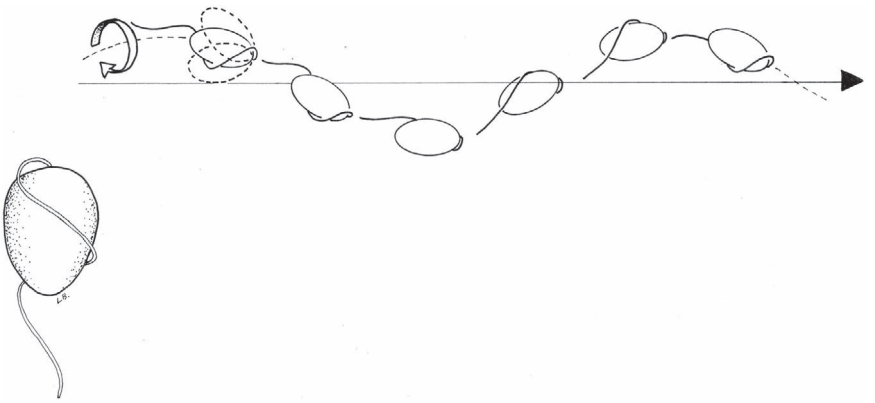


FIGURE 3.63 Swimming pattern of *Bigelowiella* sp.

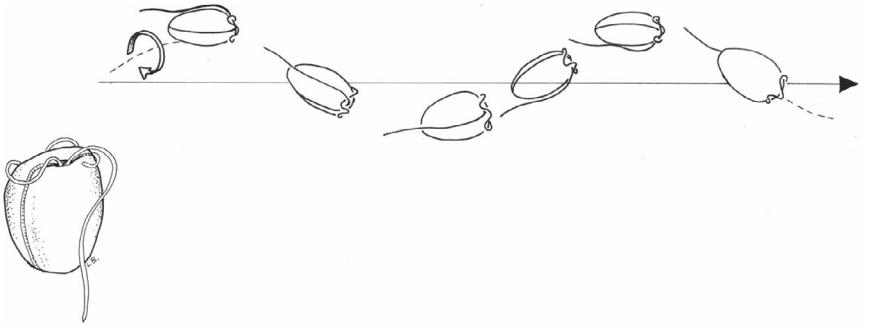


FIGURE 3.64 A desmokont dinoflagellate (*Prorocentrum* sp.) and its swimming pattern.

Swimming cells can switch between synchrony and asynchrony, and flagella within a single organism can be functionally distinct. Oscillations of the flagella are correlated with cell responses and sensitivity to the surrounding environment, are self-sustained, and yet are stable in the presence of small to moderate biochemical and background fluctuation.

Synchronization mainly occurs according to two stereotypical ways: the first is present in biflagellated algae such as *Chlamydomonas*. This alga is a typical "puller," in which propulsion acts from the front of the swimmer by the breaststroke-like beating of its pair of anterior flagella. The two flagella beat synchronously with identical frequencies and phases. The second way is present in multiflagellated algae, such as *Volvox* colonies. The flagella exhibit metachronal waves in which flagellar phases vary monotonically with position.

In isokont biflagellate algae such as *Chlamydomonas* or *Dunaliella* (Chlorophyta), during the effective stroke, the flagella bend only at the base and push more water backwards than what adheres to them during the forward recovery stroke, thus bringing about net forward movement. Cells also rotate while swimming. Speeds ranging from 100 to 200 μm s^{-1} can be reached by these cells during forward swimming. Backward swimming is also possible, during which the flagella perform undulatory movement (Figure 3.66).

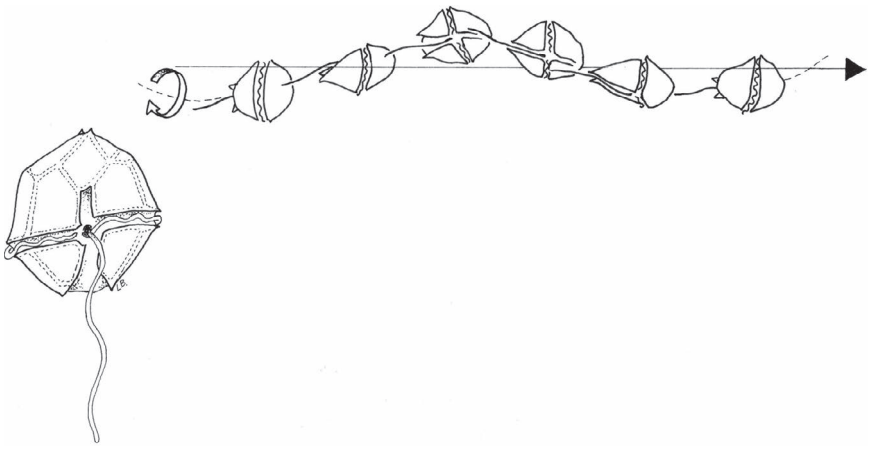


FIGURE 3.65 A dinokont dinoflagellate (*Peridinium* sp.) and its swimming pattern.

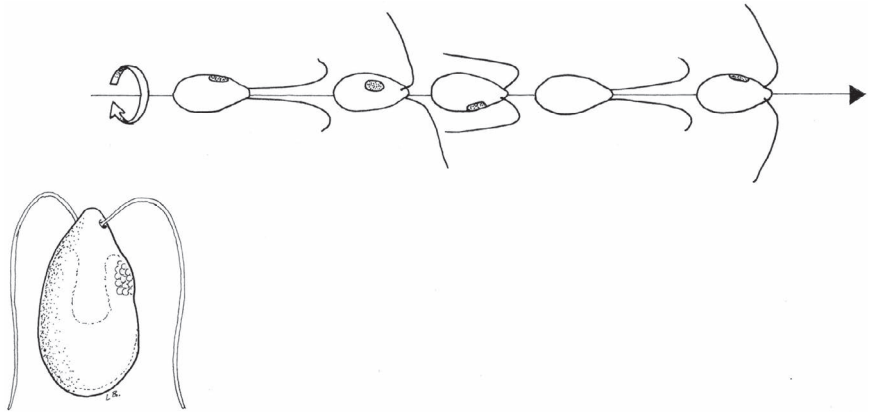


FIGURE 3.66 Swimming pattern of isokont biflagellate algae (*Dunaliella salina*).

When there are four flagellar and different in length (two shorter and two longer), as in *Tetraflagellochloris mauritanica* (Chlorophyceae), the swimming motion is more complex. This alga can either be single or form non-coenobial colonies consisting of up to 12 attached cells (Figure 3.6). Cells show a peculiar swimming motion, consisting of alternating short, rapid swimming phases and longer resting phases. They swim mainly with the anterior end forward by beating the four flagella, which beat synchronously and uni-directionally behind the cell. The planar, undulatory waves propagate from the base and along the lengths of the four flagella, a swimming behavior considered quite primitive. Cells suddenly stop by throwing the flagella forward, which recover the bent configuration of the resting phase by performing what appears to be a "braking" movement (Figure 3.67). The cells can also swim backward, although this motion seems to be used only during settling, with a ciliary beating that proceeds in fits and starts and appears to be rigid and limited to the part of the flagella distal to the bend.

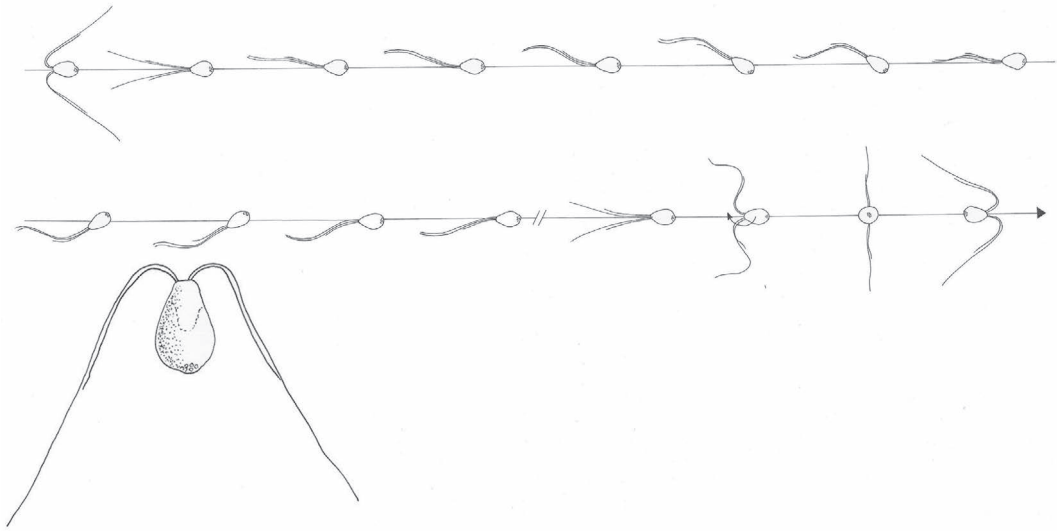


FIGURE 3.67 Swimming pattern of a quadriflagellate alga (*Tetraflagellochloris mauritanica*).

All the different swimming patterns described here can be thoroughly investigated in detail by digital microscopy (cf. Chapter 7). This methodology allows the exact determination of velocity, trajectories, swimming phases (forward, backward, rotation, etc.), and flagellar movements, which can be a very useful tool to investigate behavioral and physiological aspects of cells.

A typical lab-scale digital microscope setup can acquire and process images at a rate of 25 frames/s for track reconstruction or at a rate of 500 frames/s for the analysis of flagellar movements. The first step for track reconstruction is the determination of cell velocity to detect moving algal cells and get rid of other objects, such as debris and dead cells. Velocity determination is performed by continuously differencing each frame of the image from a previous frame, with a delay of 40 ms or multiples of 40 ms. For determination of the translational velocity value of a cell, the distance covered by the cell and the time lapse are measured. If no stimuli are applied to the environment, the swimming velocity of the cells can be considered constant. The frame difference operation between moving cells will produce objects with increasing area value up to the whole cell size during the delay progression: the greater the delay between the frames, the less two successive images of the cell are superimposed. There is a delay for which the difference operation gives two separate images of the same cell. This delay, together with the distance covered by the cell, allows the calculation of the velocity. The same delay is chosen for track reconstruction, so the overlapping of the images of the same cell in successive frame is avoided, the cell is properly segmented, and its features (e.g. barycenter) are extracted. The tracks of the cells are reconstructed, joining the cells whose barycenters lay within a prefixed distance range and whose calculated motion vector forms an angle with the forecast motion vector within a prefixed angle value. The track ends when no more barycenters satisfy these conditions. The distance range and the angle value are set on the basis of the swimming parameters of the algae. When the reconstruction procedure encounters more than one cell that satisfies the selection criteria, the algorithm chooses the cell which allows the construction of the motion vector with the smallest deviation angle from the forecast motion vector. To minimize the problem of intersecting tracks of cells swimming freely under the microscope, a low depth of focus can be used so that the cells swimming in the in-focus

layer are not hidden by the cells swimming in the out-of-focus layers. The result of the reconstruction procedure is a list containing the movement parameters of all the swimming algae, which are required to investigate their behavior.

The track reconstruction algorithm has already been tested on many unicellular algae, both mono- and pluri-flagellated, such as *Euglena gracilis, Dunaliella salina*, and *Tetraflagellochloris mauritanica*, to elucidate the different swimming patterns.

The shape of *Euglena gracilis* can be described by an ellipsoid about 50 μm long, with a maximum diameter of about 10 μm. Digital microscopy showed that *Euglena* navigates its environment exhibiting two different movements: helical swimming and local spinning. Light intensity determines swimming speed, rolling frequency, and sideways turning: at low light intensities (overcast daylight, or less than 1 Wm^{-2}), cells swim along helical paths, whereas at high light intensities (skylight, or greater than 10 Wm^{-2}), cells spin locally. *Euglena* senses light signals via the photoreceptor located inside the dorsal flagellum and periodically shaded by the eyespot. The light signal is converted into different three-dimensional (3D) flagellar beating patterns, which change the cell orientation and position in 3D space. This change in turn affects the detected light signal. During helical swimming, the velocity ranges from about 50 to 100 μm s^{-1}, and the cells rotate around their long axis anticlockwise at a frequency of about 1–2 Hz. Their dorsal flagellum beats at 20–40 Hz. During swimming, it trails beside the cell body and performs helical waves, generated in a base-to-tip mode, twisting into two loops that are distributed on both sides of the cell. The thrust of the flagellum against the surrounding water is increased by 3–4-μm-long hairs arranged in tufts of three to four, forming a single row that runs along the flagellum in a spiral pattern. The frequencies of body rolling and helical swimming are coupled, identical, and phase locked. For high light intensities, when the light sensor saturates, cells spin; that is, they do not rotate along their long axis but along their short axis in a plane perpendicular to the electrical vector of the light, in either a clockwise or anticlockwise direction. The flagellum twists into one loop extending towards the front of the cell and bends to the side opposite to the turning direction. The rotation is more or less continuous, and the cell position is unaffected. For intermediate light intensities, a polygonal swimming behavior emerges from periodic switching between the two beat patterns that resemble those of helical swimming and spinning, which coincide with the swimming and turning phases of the polygon. The number of spinning beats determines the turning angle and hence the order of the polygon.

These behaviors combine to cope with abrupt changes in the light environment. When cells coming from low light encounter a higher light intensity, then polygonal swimming or localized spinning occurs, making the cells turn around to avoid the light barrier. When cells previously at low light experience a suddenly strong spatially homogeneous light, they initially spin and then swim in polygons of increasing order (eventually intermittently skipping the turning phases) and thereby increase their "search radius" before ultimately escaping into darker regions and switching back to pure helical motion. When cells under low light are suddenly exposed to a spatial light gradient, they alternate between spinning, polygonal swimming, and helical swimming, thereby executing a biased random walk down the light gradient in a "run-and-tumble" way (Figure 3.68).

The stumpy mutant of *Dunaliella salina* has been investigated for the peculiar movement of its short flagella (Figure 1.57, Chapter 1). Digital microscopy has shown that these cells, despite their stump flagella, are not passively transported by the medium flow but actively move with an average velocity of 0.2 μm s^{-1}, which is significantly lower than the calculated average velocity of the wild type (100 μm s^{-1}) (Figure 3.69). To see details of the mutant movement, images were acquired using lateral illumination. The eyespot of Chlorophyta such as *Chlamydomonas* and *Dunaliella* is a quarter-wavelength multi-layered organization of osmophilic granules, which reflects very efficiently the light that strikes it. As the cell

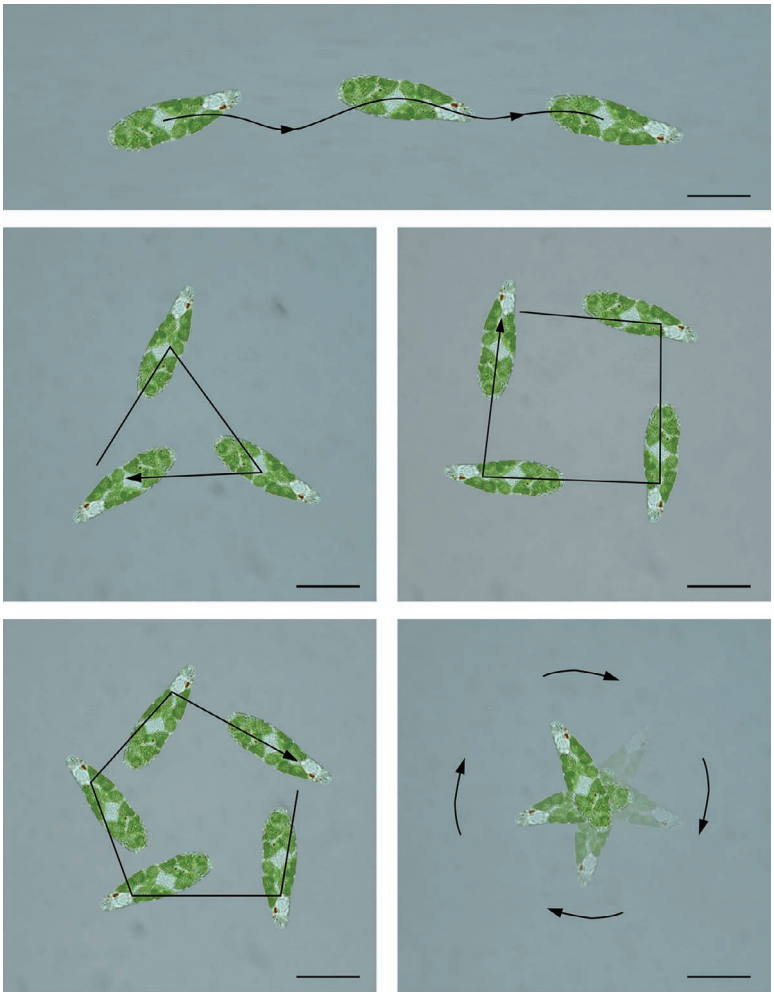


FIGURE 3.68 The different swimming movements of *Euglena* cell: helical swimming, polygonal swimming, localized spinning. Scale bar μm 20 μm.

moves, this brilliant spot becomes visible, and its positions indicate if the cell rotates or not. Digital microscopy has shown that mutant cells do not rotate around their longitudinal axis but oscillate irregularly around it, unlike wild-type cells, which rotate at 2 Hz while swimming (Figure 3.69). Mutant cells cannot swim because their flagella are not capable of producing and propagating a bending wave due to its extremely reduced length. Still, they can move. A possible explanation for this motion is that the mutant performs gliding, whereby the contact with a solid substrate (e.g. the glass of a microscope slide) draws the cell along the surface. The overall movement of the mutant can be described by alternately oscillating the body to the left and to the right like the clapper of a bell, and up-and-down pivotal along a small arch, hinging upon the left or the right stump. Moreover, the motion of the mutant lacks the coherent pattern of movement along a sinusoidal path of the wild type. It moves with a biased random walk; hence its nearing the stimulus direction is indirect and by chance.

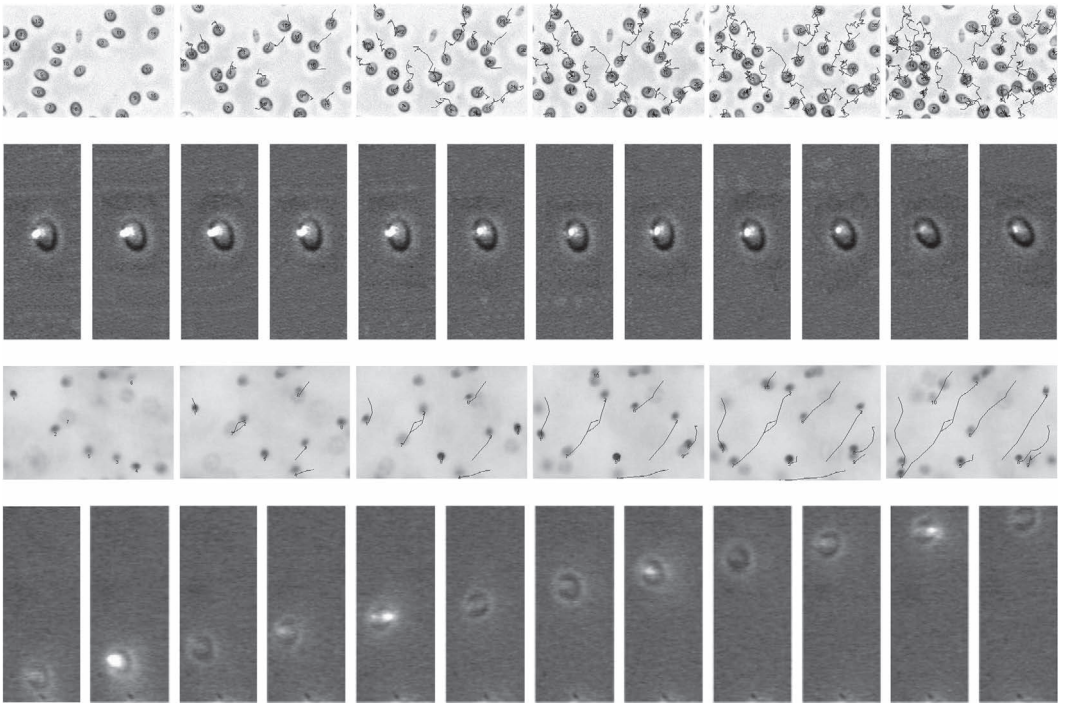


FIGURE 3.69 Swimming movements of *Dunaliella salina* stumpy mutant compared with the swimming movement of wild-type cell.

In the case of *Tetraflagellochloris mauritanica*, digital microscopy has enabled comprehension of the complex swimming motion of this quadriflagellated algae capable of both swimming and floating in resting position. This complex swimming motion consists of rapid phases of forward swimming of variable length along a straight path, which is followed by in-place random reorientations and/or phases of slow backward swimming, which can reverse the swimming direction (Figure 3.70a). Backward and forward swimming are both normal modes of swimming for this alga.

During forward swimming, cells move like "pushers"; the four rear-mounted flagella beat synchronously with a frequency of about 10 Hz, uni-directionally and perfectly phase-locked behind the cell; undulatory retrograde waves are produced at the base-proximal part of the flagella and run along them to the tip (Figure 3.70b).

During backward swimming, cells move like "pullers"; the right and left flagella couples beat asynchronously alternatively and sequentially every 400 ms, that is, one pair of flagella has finished one effective beat before the other enters the effective beat of its next cycle (Figure 3.70c). Each single beat of a flagella pair contains two components: the power stroke and the recovery stroke, the former faster (about 80 ms) than the latter (about 120 ms). Moreover, during the power stroke, the initiation of the wave is faster than its propagation to the tip, where the velocity slows down. The flagella then extend completely before curving closer to the cell body in the recovery movement. In backward swimming, the cells follow an almost straight path with a velocity that is positive during both the power stroke and the recovery stroke. The transition between the phases as well as the beginning and end of the motion are marked by the flagella in the bent configuration of the cell resting position (first frame in Figures 3.70b and 3.70c). All the sequences begin with the cells in their resting configuration, with the flagella extended laterally in the typical geniculate position.

In the case of a cell pair, forward swimming retraces the same steps of the single cell motion, from a resting position to a mirror resting position, gained by flipping the cell bodies onto the flagellar insertion (Figure 3.70d). However, the pair, while swimming, rotates around its axis of symmetry instead of rocking. In the case of colonies, forward swimming followed by resting phases is the only mode of swimming (Figure 3.70e). All sequences begin with the cells in their resting configuration, with the flagella extended laterally in the typical geniculate position. Colonies proceed rotating around their axis of symmetry, with a frequency of about 2 Hz. In this case, the resting position at the end of the motion is the same as the beginning; that is, the colonies cannot flip.

The velocity of single cells ranges from 260 to 350 μm s^{-1} during the forward motion and slows down to 85 to 120 μm s^{-1} when the cells move backward. Cells do not rotate, since the cell has a symmetrical ellipsoidal body marked by the eyespot in the anterior portion of the cell. The velocity of forward swimming pairs and colonies ranges from 83 to 115 μm s^{-1}.

Digital microscopy has also allowed the detection of the different shapes the flagella assume during their beating. To swim forward, the cell initiates the motion by pushing the body forward and simultaneously throwing the flagella behind in an arched concave position. As the cell proceeds, the four flagella gain an extended shape with a marked reduction of the curvature, which becomes almost convex, and join to get ready for flagellar beating. Undulatory waves then initiate at the base-proximal part of the flagella and run along them to the tip to propel the cell forward. During forward swimming, the cell body rocks around the swimming direction axis. At the end of the swimming phase, the cell slows down and undulatory waves stop because the flagella begin to separate in the proximal portion. The separation proceeds and also involves the distal portion of the flagella, which again takes an arched concave position, with the flagellar tips facing toward the axis of symmetry of the cell. A definite stop occurs when the cell body hinges onto the flagellar insertion to rotate backward; the result of this flipping is a resting configuration that mirrors that of the first frame. Backward swimming can begin either from the resting position or from forward swimming without flipping. During this motion, the right and left flagella pairs alternate their beating in sequence: the movement of a pair begins when the movement of the other ceases. Also in this case, the resting configuration marks the end of the motion. During forward swimming, the four flagella of *T. mauritanica* beat synchronously, uni-directionally, and perfectly phase locked behind the cell; undulatory retrograde waves are produced at the base-proximal part of the flagella and run along them to the tip in a flagella-like beating without any asynchronic episode (Figure 3.70f). When *T. mauritanica* swims backward, the flagella beat with time-shifted mirror symmetry and a phase variation from 0 to 2π (Figure 3.70g). This swimming mode is quite uncommon among unicellular algae, and it is not a transitory effect like a slip, but it is a true gait. The cell body rocking during backward swimming (the eyespot end of the cell body rocks toward the side opposite the side of the moving flagella pair, that is, counterclockwise) (Figure 3.70h), and the consequent differential changes in hydrodynamic friction are not enough to restore the synchronicity between the two flagella couples due to their length and mass and the small size of the cell body.

The mode of coordination of *T. mauritanica* can be described qualitatively as "serial coordination"; that is, the flagella pair beat alternatively and sequentially, unlike the mode of synchronization of wild-type *Chlamydomonas* described as "bilateral coordination"; that is, flagella movement is synchronized.

Movements Other Than Swimming

In some algae, movement cannot occur unless the cells are in contact with a solid substratum. This kind of movement, in some cases termed gliding, is present in cyanobacteria, in the red alga *Porphyridium* (Rhodophyta), in diatoms, and in some desmids (Chlorophyta).

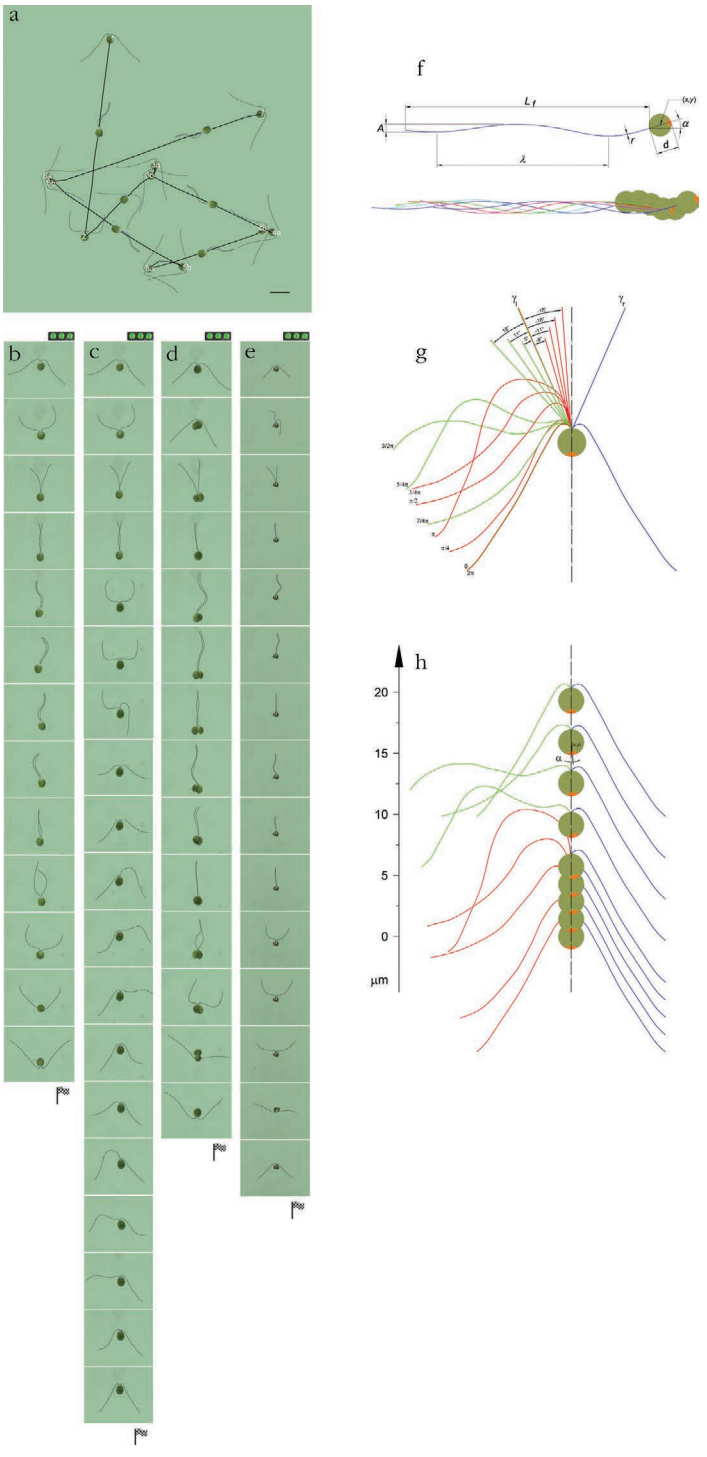


FIGURE 3.70 All the possible shapes of the different swimming movements of *Tetraflagellochloris mauritanica*: complex swimming motion (a), forward and backward movement of a single cell (sequences b, c), forward movement of a pair (sequence d), and forward movement of a colony (sequence e). The traffic light indicates the start of the swimming sequence, while the checkered flag indicates the end of the sequence. Model swimmer and time sequence of single cell optimal stroke (f). Asynchronous beat cycle of a single cell during backward swimming (g). Asynchronous beat cycle of the left flagella pair during backward swimming (h). Scale bar 10 µm.

The most efficient gliders among the cyanobacteria are found in the filamentous forms such as *Oscillatoria*, *Arthrospira*, *Phormidium*, and *Anabaena*, which can travel at up to 10 $\mu m \cdot s^{-1}$. Some species, such as *Phormidium uncinatum* and *Oscillatoria*, rotate about their long axis while gliding, while others, such as *Anabaena variabilis*, translate laterally. Other unicellular coccoid cyanobacteria, such as *Synechocystis*, move by "twitching," a flagella-independent form of translocation over moist surfaces. This type of motility is analogous to social gliding motility (S-motility) in myxobacteria, which involves coordinated movements of cells close to each other (cell–cell interactions) and requires both type IV pili operating in a manner similar to a grappling hook and fibrils (extracellular matrix material consisting of polysaccharides and protein). While moving, cyanobacterial gliders secrete mucilage, or slime, which plays an active role in gliding. Mucilage is extruded from rows of fine pores clustered circumferentially around the septa. These pores are part of a larger structure called the junctional pore complex (JPC), which spans the entire cell wall, peptoglycan layer, and outer membrane. The channels formed by the JPCs are inclined relative to the cell axis, this angle providing directionality to the extruded slime, and are oppositely directed on either side of the septum. Propulsion of the filament results from the adherence of the slime to both the filament surface and the substratum, combined with its extrusion from a row of JPCs on one side of each septum. Switching slime extrusion to the JPCs on the other side of the septum would result in a reversal of the direction of gliding. In *P. uncinatum*, the pores are aligned in a single row, whereas in *A. variabilis*, several rows of pores line both side of the septum. The outer surface of gliding cyanobacteria consists of parallel arranged fibrils of a glycoprotein known as oscillin, a Ca-binding protein required for motility. The surface striations formed by these fibrils would act as channels for the extruded slime to flow along. Therefore, if the fibrils are helically arranged, the cell will rotate as it glides; if the fibrils are aligned radially, the cell will not rotate. In all species studied to date, this correlation is consistent and provides a structural explanation for why some species rotate as they glide while others do not.

In diatoms, motility is restricted to pennate species possessing a raphe. These diatoms display a characteristic jerky movement forward or backward, with species-specific path patterns. The general velocity of their movement is 1–25 $\mu m \cdot s^{-1}$, but they can accelerate up to 100–200 $\mu m\ s^{-1}$. Raphid diatoms possess an actin-based cytoskeletal system located just beneath the plasma membrane at the raphe. Transmembrane components with an adhesive extracellular domain are connected to these actin bundles, and their interaction is somehow involved in both adhesion and motility mechanisms. Microtubules are also present in this region; in addition, secretory vesicles containing polysaccharides often appear near the actin filaments at the raphe, providing the mucilage strands that project from the raphe and adhere to the substratum during the gliding process.

At least two models exist which provide a reasonable explanation for diatom locomotion. In the first model, a force applied to the transmembrane protein–actin connectors, parallel to the actin bundles, would result in movement of the transmembrane proteins through the cell and subsequent movement of the cell in the opposite direction to the force. In the second model, the energy required for motility would be generated by a conformational change of the adhesive mucilage on hydration that occurs when it is secreted from the raphe. In this model, the actin bundles restrict the secretion of mucilage to one end of the raphe, which generates a net force moving the cell over the site of secretion. In both models, the secreted mucilage plays a central role either by providing traction to translate the force into cell movement or by generating the energy through conformational changes on hydration.

A slow gliding movement over solid substrata has been observed in *Porphyridium* sp. (Rhodophyta) and in some desmids (Chlorophyta). In *Porphyridium*, the mucilage produced in mucilage sacs located inside the cell is excreted through the membrane. In desmids, mucilage is excreted through the cell wall by flask-shaped pores. As they move, these gliding cells leave behind a fibrillar mucilaginous trail, whose swelling by water pushes the cells forward.

TABLE 3.1
Swimming and Gliding Speeds of Some Planktonic Algae

Name	Mean Speed
Gymnodinium gracilentum	500 μm × s^{-1}
Symbiodinium sp.	250 μm × s^{-1}
Tetraflagellochloris mauritanica	200 μm × s^{-1}
Tetraselmis suecica	180 μm × s^{-1}
Chattonella sp.	120 μm × s^{-1}
Cryptomonas	110 μm × s^{-1}
Chlorarachnion reptans	110 μm × s^{-1}
Euglena gracilis	100 μm × s^{-1}
Dunaliella salina	95 μm × s^{-1}
Ochromonas danica	80 μm × s^{-1}
Bigelowiella natans	70 μm × s^{-1}
Pavlova salina	50 μm × s^{-1}
Synechococcus	25 μm × s^{-1}
Oscillatoria spp.	10 μm × s^{-1}
Porphyridium spp.	0.66 μm × s^{-1}
Leptolyngbya spp.	0.004 μm × s^{-1}

Table 3.1 presents swimming and gliding speeds of some planktonic algae.

Buoyancy Control

The alternative to swimming is to float by means of some type of buoyancy device. In some of the brown algae attached to the seashore (*Fucus vesicolosus, Ascophyllum nodosum, Sargassum* sp., Ochrophyta), the fronds gain buoyancy from air bladders (pneumatocysts) within the thallus, which stands erect when submerged. Oxygen and nitrogen, in roughly the same proportion as in air, form the bulk of the gas, but there are also small, variable amounts of CO_2 and CO. Oxygen and CO_2 derive partly from the metabolic activities of the cells in the pneumatocyst wall, and diurnal changes in the composition and pressure of pneumatocyst gases have been shown. However, equilibration takes place between the gases in the pneumatocyst and in the surrounding water (or air). This is the source of nitrogen in the vesicles and the major source of O_2 and CO_2. In *Ulva* sp. (Chlorophyta), gas bubbles are entrapped in the central area of its tubular hollow thallus, which may aid in keeping the stipe upright by flotation. In other seaweed such as *Codium fragile* (Chlorophyta), gas trapped among the filaments achieves the same buoyancy effect of pneumatocysts.

Buoyancy regulation in cyanobacteria involves production of intracellular gas-filled structures (also termed vacuoles), not delimited by membranes and made up of assemblages of hollow cylinders, whose proteinaceous walls are permeable to gas but not to water. The density of this structure is about 0.12 g·cm^{-3}, about one eighth of that of water, and if sufficient gas-filled structures are present in a cell, it can become positively buoyant. In cyanobacteria, buoyancy is regulated by varying gas-filled structure formation and cytoplasmatic composition through synthesis and breakdown of photosynthetic products. The production of gas-filled structures is induced by low-light conditions (for example, in deep layers with insufficient light). Here, photosynthesis is reduced, osmotic pressure of newly synthesized sugars is small, and ballast materials such as carbohydrates are not produced at a high rate; therefore, they will not increase cell density, which in turn would increase sinking. Under these conditions, gas-filled structures can be produced at

a high rate, and cells increase their buoyancy. Conversely, if cell osmotic potential is high (high sugar production, increased amount of ballast in the form of secondary photosynthetic products), turgor pressure increases, it may collapse gas-filled structures, and cells become negatively buoyant and sink in the water column. A rise in turgor pressure with light irradiance has been found in many cyanobacteria; however, for this rise to result in gas-filled structure regulation, the pressure reached must exceed the lowest pressure of gas-filled structures. This occurs, for example, in *Anabaena flos-aquae* with a critical collapse pressure distributed about a mean of 6 bars. In *Trichodesmium* sp., gas-filled structures can withstand pressures of 12–37 bars depending on the species, and turgor pressure collapse is not possible as a buoyancy regulation mechanism in this genus; carbohydrate ballasting is considered the only plausible mechanism for rapid buoyancy shifts in this cyanobacterium.

Other algae obtain buoyancy from liquids of lower specific gravity than seawater or freshwater in a way similar to a bathyscaphe. Liquid-filled floats have the advantage of being virtually incompressible, but because of their higher density, they must constitute a much greater proportion of the organism's overall volume than is necessary with gas-filled floats if they are to give equivalent lift. The large central vacuole of diatoms contains cell sap of reduced density, obtained by the selective accumulation of K^+ and Na^+, which replaces the heavier divalent ions, conferring some buoyancy. In young, fast-growing cultures, diatom cells often remain suspended or sink only very slowly, although in older cultures, they usually sink more rapidly. Studies of the distribution of diatoms in the sea suggest that some species undergo diurnal changes of depth, usually rising nearer the surface during daylight and sinking lower in darkness, possibly due to slight alterations of their overall density effected by changes in specific gravity of the cell sap or in some cases by formation or disappearance of gas vacuoles in the cytoplasm. The dinoflagellate *Noctiluca* also gains buoyancy from a high concentration of NH_4^+ ions in its large vacuoles; the exclusion of relatively heavy divalent ions, especially sulfate; and a high intracellular content of Na^+ ions relative to K^+. As a result, the density of the cell sap in the vacuoles is less than that of seawater, and the cells can therefore be positively buoyant and float.

When buoyancy control is not possible by these mechanisms, algae can keep afloat and regulate their orientation and depth through adaptations reducing sinking rates. The rate at which a small object sinks in water varies with the amount by which its weight exceeds that of the water it displaces and inversely with the viscous forces between the surface of the object and the water. The viscous forces opposing the motion are approximately proportional to the surface area, and therefore, other things being equal, the greater the surface area, the slower the sinking rate.

There are a number of structural features of planktonic organisms which increase their surface area and must certainly assist in keeping them afloat. The majority of planktonts are of small size and therefore have a large surface-to-volume ratio. In many cases, modifications of the body surface increase its area with very little increase in weight. These modifications generally take two forms: a flattening of the body or an expansion of the body surface into spines, bristles, knobs, wings, or fins.

A great range of flattened or elaborately ornamented shapes occurs in diatoms such as *Chaetoceros* sp. In dinoflagellates, also, the cell wall is in some cases prolonged into spines (*Ceratium*) or wings (*Dinophysis*). Among the Chlorophyceae, the wall of the peripheral cells of *Pediastrum* colonies may bear clusters of very long and delicate chitinous bristles regarded as buoyancy devices. In *Scenedesmus*, the cells are also clothed by a large number of bristles with a complex structure, which seem to help keep the cells in suspension.

Reduction of the sinking rate is also obtained by an increase in lipid content, which has a density of about 0.86 g cm^{-3}. Oil droplets are common inclusions in the cytoplasm of algae; lipids stored in this form are present in the Chrysophyceae and Phaeophyceae (Ochrophyta) and in the Haptophyta, Cryptophyta, and Dinophyta. The thermal expansion of these compounds may be of some significance in effecting diurnal depth changes through reduction of cell density but without producing neutral buoyancy.

How a Flagellum Is Built: Intra-Flagellar Transport

The mechanisms that determine and preserve the size and function of cellular organelles represent a fundamental question in cell biology only partially understood up to now, and flagella have provided a handy model system to investigate organelle size-control analysis. It was discovered that flagella are dynamic structures and that flagellar length is regulated by a process called intra-flagellar transport (IFT). IFT is a motile process within flagella in which large protein complexes move from one end of the flagellum to the other, and flagellar length is regulated by a balance between continuous assembly of tubulin at the tip of the flagellum, counterbalanced by continuous disassembly. According to Iomini *et al*. (2001), the IFT cycle consists of four phases. In phase I, which takes place in the basal body region of the flagellum, anterograde particles are assembled from retrograde particles by remodeling and/or exchange of subunits with the cell body cytoplasm, with a concurrent decrease in number. In this phase, the precursors of the flagellar structures that make up the cargos are also loaded onto the particles. In phase II, the particles are transported from the base to the distal end of the flagellum by a heterometric kinesin II with a velocity of about 2 μm sec^{-1}. In phase III, which occurs at the distal end of the flagellum, anterograde particles are remodeled into retrograde particles with a concurrent increase in number, probably upon or after unloading their cargo. Finally, in phase IV, retrograde particles are transported by a cytoplasmic flagellar dynein from the distal end back to the basal body region of the flagellum with a velocity of about 3 μm sec^{-1}, higher than that of anterograde particles.

How a Flagellar Motor Works

Movement can arise by shape change of permanently linked elements, by reversible interactions causing movement of elements relative to each other, by reversible assembly and disassembly, and so on, all of which need energy input. We know that such changes can occur in proteins, the most likely molecules serving these locomotory functions in real movement system. But what drives and controls these changes? In principle, the problem is not difficult. Altering the ionic milieu, changing its environment chemically or electrically can alter the tertiary and/or quaternary structure of a protein. In most control systems, if not all, a change in the environment brings about a change in the properties of the motor, acting either directly or indirectly on the component of the motor. We need only two proteins to make a motor using the sliding filament mechanism: a globular protein (such as tubulin) and an anchor protein (such as the dynein-dynactin complex). If the globular protein can polymerize, we can assemble it into a linear polymer that can be attached via the anchor protein to another structure some distance away. The transformation of chemical energy into mechanical work depends upon a conformational change of the anchor protein, which uses the hydrolysis of ATP in ADP. Provided the anchor protein repeats the conformational change upon each monomer of the globular protein in turn, the "boat" can be hauled "hand over hand" toward the distant anchorage. Provided some kind of metachrony regulates adjacent motor molecules, we can link our small movements in a temporal series to amplify the amount of movement that can be achieved. Each step costs hydrolysis of one ATP molecule per anchor protein. The simplest and most obvious solution is either to have more than one anchor protein or to have a dimer working out of phase, being careful not to detach before the new attachment is formed. For instance, most (but not all) microtubular motors (dyneins, kinesins) work as dimers whose subunits walk along microtubule walls just like human legs walk on a surface. Once we have two hands to pull on the rope, we can indeed move hand over hand; the one-armed man cannot do more than pull once. Flagellum movements are due to the transient interaction between two anchored microtubules, coupled to a linkage control. The generation of sliding of adjacent doublets by flagellar dynein is combined to the resisting forces localized near the active sliding rows of dyneins. During the cycle of binding/release obtained by dynein conformational change coupled to ATP hydrolysis, chemical energy is converted into mechanical energy used for sliding. Due to their regular spacing every 24 nm along the axoneme, several

adjacent dyneins participate in this local sliding, and their functioning proceeds by local waves that propagate step by step all the way along the flagella. The postulated regulator has therefore to trigger the functioning of the different dyneins alternatively along the length as well as around the section of the axoneme, but its molecular nature remains unknown.

The model of Lindemann (1994) accounts for wave generation and propagation, regulated by geometrical constraints. This model, the so-called "geometric clutch," is based on the way a cylinder with nine generatrix (the nine outer doublets of the axoneme) changes form when submitted to bending. In the zone of curvature, the doublets located outside the curvature are brought apart, while the doublets located inside the curvature come closer to each other. This makes the corresponding dynein molecules efficient for sliding. In contrast, dynein molecules located outside the curvature are too far for binding to adjacent microtubules: no active sliding can occur in this zone. This model is consistent with ultrastructural data of electron microscopy. As previously, the functioning of the axonemal mechanics needs transient connections, which could possibly be disrupted by intrinsic proteolytic activities due to the combined activities of a protease/ligase system.

How a Paraxial Rod Works

Since the PFR and the axoneme are very tightly connected, both structures have to move together. It can be argued that the PFR contributes to regulate flagellar movements. This could be done by providing a more rigid structure that can vary its stiffness in time, that is, modifying the flagellum beating pattern.

We need only one protein to build a device for information transfer and control, that is, a protein with two conformational, alternate states such as intermediate filament proteins, which can form lattice-like structures. The propagation of conformational changes along these proteins can be used to transport and/or transduce sensory information. Each protein can be considered a dipole in one of the two possible states. We can imagine that the conformational change is transmitted by one dipole to the neighbor proteins as a wave. Therefore, a current flow through these lattice-like structures could be generated by the mobile electrons of the proteins that interact with their immediate neighbors via dipole–dipole forces.

The α-helical coiled-coils structural motif in the rod filament is well suited for electron propagation (Figure 3.36b). A current might be propagated distally, via PFR_1 and PFR_2 protein–protein charge transfers in the lattice-like rod filaments. The current flows through these lattice-like structures, and the sole constraint is that each lattice site should possess a dipole moment proportional to the magnitude of the mobile charge unit and the distance over which it hops, that is, about one or two nanometers. This wave produces a contraction in the PFR and a varying internal resistance that modulates the flagellar beats. The contraction occurs by displacement of the goblet appendages of the PFR along the axonemal microtubules, which reduces the distance between the coiled filaments, hence generating longitudinal waves of contraction along the paraxial rod. The stiffening should swing the flagellum sideways, damping out some undulatory waves of the axoneme.

THE PHOTORECEPTOR APPARATUS

In aquatic ecosystems, light is a physical factor of fundamental importance to both photosynthetic and non-photosynthetic heterotrophic organisms. They are able to sense and respond to light stimuli, an ability essential to optimizing physiological processes, and to time their lives to feeding, reproduction, defense, and virtually all their functions. One of the most striking responses is phototaxis, in which motile photosynthetic microorganisms adjust their swimming path with respect to incident light in a finely tuned manner. Phototaxis has many advantages: it allows photosynthetic organisms to position themselves for optimal light capture and efficient photosynthesis and facilitates avoidance responses in those situations where light is intense enough to damage pigments and chloroplasts. In the case of many sexually reproducing species, such as *Ulva* sp., both female and

male gametes show positive phototaxis, which may cause the co-localization of both gametes near the surface of seawater, improving the possibility of encounters. On the other hand, zygotes usually become negatively phototactic, enabling them to swim towards the bottom of the seashore, where they can find a suitable substratum. Also, non-photosynthetic organisms (heterotrophic) have been shown to benefit from the ecological advantages of phototaxis. For example, the marine dinoflagellate predator *Oxyrrhis marina* can orient to light and is able to use photosensory response to locate patches of phytoplankton prey by detecting chlorophyll *a* fluorescence.

The full exploitation of light information necessitates proper perceiving devices, able to change the small signal represented by the light falling upon them into a larger signal and response of an entirely different physical nature; that is, these devices, termed photoreceptors, must act as sensors to perceive wavelength and direction of light and as transducers to convert the light signal into chemical and/or electrical information but also as amplifiers and eventually as transmitters. Hence, photoreceptors can be considered algal "eyes," with many similarities with the complex vision systems of higher organisms, since they possess optics, photoreceptors, and signal transduction chain components.

The proper functioning of these basic visual systems relies on some necessary and universal structural, behavioral, and physiological features, such as the following:

- Shading device (structural)
- Photoreceptor and photoreceptive proteins (structural)
- Sampling strategies (behavioral)
- Trajectory control (behavioral)
- Signal transmission (physiological)

The shading device and photoreceptor are the structural elements used to screen the environment and provide information about the intensity and directionality of the incident light. These two elements are always in close association. The shading device, termed an eyespot, is usually an absorbing element that prevents light coming from certain directions from reaching the detector.

In flagellate algae, eyespot position is usually strictly defined with respect to the plane of beat of the flagella, though variation exists along the longitudinal cell axis, the eyespot being located either more anteriorly or more posteriorly or even apically (Figure 3.71). The position of the eyespot gives the algae distinctive left–right asymmetry. The typical organization of the eyespot consists of a single layer of closely packed globules containing mainly carotenoids that can play the shading role thanks to their strong absorbance in the 400–500 nm range.

The most common (and primitive) type of photoreceptor consists of extensive two-dimensional patches of photosensitive proteins, embedded in the plasma membrane in close association with the eyespot; the proteins have a ordered disposition in order to maximize light absorption. For detecting the direction of light of a specific spectral range, a photoreceptor demands a high

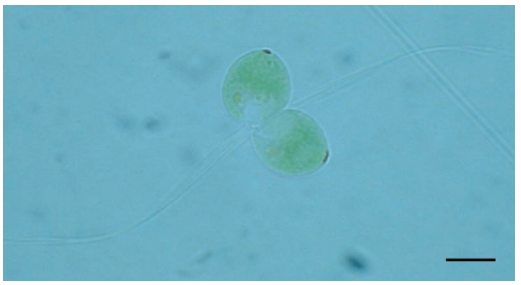


FIGURE 3.71 Apical eyespot of *Tetraflagellochloris mauritanica*. Scale bar 5 µm.

packing density of chromophore molecules organized in a lattice structure, with a high absorption cross-section of the chromophore, that is, a high probability of photon absorption by the chromophore and very low dark noise. Dark noise is the noise inherent in a receptor, constant and independent of light level, which arises from the random thermal motions of the molecules. For detecting patterns of light, the number and location of photoreceptors with fixed size and exposure time must be viewed according to the pattern of motion of algae; therefore, the design of the photoreceptive apparatus in conjunction with the helical movement of the cell produces a highly directional optical device, allowing effective tracking of the light direction. The function of photoreception is inseparable from the presence of photoreceptive proteins but not necessarily from the presence of an eyespot; hence, when the eyespot is absent, its function must be performed by the whole algal body.

Only a few photoreceptors can be identified by optical microscopy (cf. Figure 1.30 of Chapter 1), whereas the eyespot is always easily recognizable because of its size and color, usually orange-red (Figure 3.71).

Types of Photoreceptive Systems

Depending on their organization and structure, photoreceptive systems can be grouped into three main types.

Type I

A single layer of photoreceptor molecules is present inside the whole cell membrane or located in just the patch of membrane that covers the eyespot, when present (Figure 3.72). Lacking the eyespot, the whole algal body performs the shading function. This means that this type of photoreceptive system could be not detectable by optical microscopy and that investigating techniques such as microspectroscopy (cf. Chapter 7) and immunofluorescence are needed to localized photoreceptive proteins. This type of photoreceptive system is typical of Chlorophyta but is also present in Cyanobacteria, Ochrophyta, Haptophyta, Cryptophyta, and Dinophyceae.

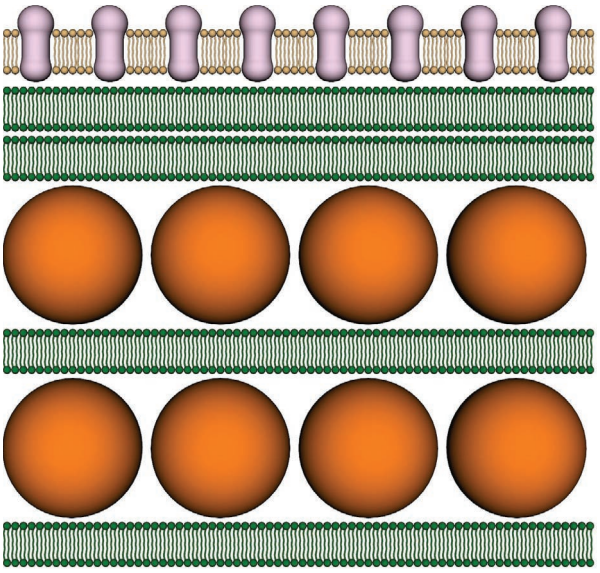


FIGURE 3.72 Schematic drawing of Type I photoreceptor system. Not to scale.

In Chlorophyta such as *Haematococcus* sp., *Spermatozopsis* sp., and *Dunaliella* sp., the eyespot is situated on one side of the cell, sometimes slightly protruding beyond the cell surface, as in the gametes of *Ulva*; its area can range from about 0.3 to 10 μm^2. The globules range from 80 to 190 nm in diameter, and their number varies from 30 to approximately 2000. The most common organization consists of a single layer of closely packed globules lying between the outermost thylakoid and the two-layered chloroplast membrane. Additional layers of globules can be present underneath the first layer, individual layers subtended or not by a single thylakoid. In most species, the globules show a hexagonal packing, which enables the highest possible packing density. In both *Pandorina* and *Volvox* colonies, the eyespots of cells in the anterior of the colony are larger than those of the posterior, consisting of up to nine layers, marking the occurrence of some degree of colony polarity.

The photoreceptor of *Chlamydomonas reinhardtii* can be considered the model of Type I photoreceptors. The eyespot is about 1 μm in length, located at the equator of the cell, usually composed of two organized rows of carotenoid-filled lipid globules separated by thylakoid membranes and packed under the chloroplast envelope. The layered structure of the shading organelle in this type of photoreceptor reflects orthogonal light toward the photoreceptor and blocks light originating from other directions. The photoreceptor of the green alga *Chlamydomonas* consists of an extensive two-dimensional patch of photosensitive proteins in the plasma membrane that lies directly over the closely apposed chloroplast envelope at the level of the eyespot (Figure 3.72). Immunofluorescence microscopy has revealed that this photoreceptor contains rhodopsin-like proteins.

In Cyanobacteria, phototactic orientation has been described in *Anabaena variabilis*, *Pseudoanabaena* sp., and *Phormidium*, although no defined structure for light sensing has been detected so far. The first identification of a complex photoreceptive system leading to evidence of a photoreceptive protein was performed in *Leptolyngbya* sp. This deep red cyanobacterium lives in Roman hypogea at extremely low light intensity (10^{13} photons $m^{-2}s^{-1}$). It possesses an orange eyespot at the tip of the apical cell of the trichome. Electron microscopy revealed that this eyespot is characterized by osmiophilic globules of about 100 nm in diameter arranged in a peripheral cap extending 2–3 mm from the apex and with a possible layered pattern (Figure 3.2) Microspectrophotometric analysis of the tip of the apical cell of *Leptolyngbya* trichomes revealed a complex absorption spectrum with two main bands. The band centered at 456 nm is due to the absorption of the carotenoid present in the eyespot, whereas the band centered at 504 nm can be assigned to rhodopsin-like proteins packed in the plasma membrane of the tip of the apical cell.

In Ochrophyta, data exist indicating that photoreceptor molecules are present inside the cell membrane of eggs of the fucoid brown alga *Silvetia compressa* (Figure 3.73a). Immunofluorescence microscopy highlighted the presence of a rhodopsin-like protein in the egg membrane (Figure 3.73c) Figure 3.73b shows a fluorescent image of a non-labeled egg. Since no eyespot can be detected in these algal stages, the shading function is assigned to the whole cell body.

In the Haptophyta, the eyespot is present only in some species of the order Pavlovales. It consists of a single layer of globules situated at the anterior end of one of the chloroplast, beneath the posteriorly directed flagellum, at the level of its emersion from the cell. In these algae, the photoreceptor has not been yet localized, but we can presume it is positioned inside the membrane in close association with the eyespot.

In the Cryptophyta, the presence of an eyespot is limited to a small number of species belonging to the genus *Chroomonas*. The eyespot is situated in the center of the cell, within a conical lobe of the chloroplast. It consists of a single layer of about 35 closely packed globules, attached to the chloroplast envelope and the endoplasmic reticulum. Also in these algae, the photoreceptive proteins should be located inside the plasma membrane overlaying the eyespot.

In the Dinophyceae, the eyespot is chloroplastic in *Peridinium* sp., consisting of a layer of globules under the chloroplast envelope, situated behind the longitudinal sulcus and truly extraplastidic in *Woloszynskia coronata*, where it consists of an irregular cluster of globules located beneath the

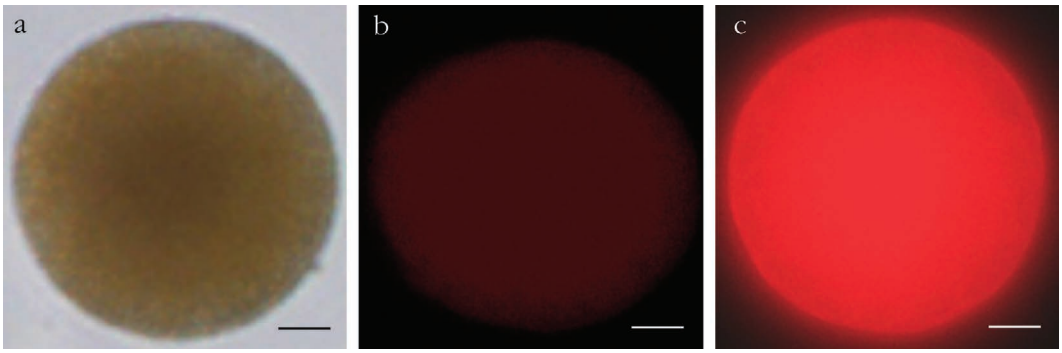


FIGURE 3.73 A *Silvetia compressa* egg in bright field microscopy (a), under fluorescence microscopy (b), and labeled with anti-rhodopsin antibody (c). The two arrows point to the cell membrane layer of the cell in which photoreceptive protein are located. Scale bar 2 μm.

sulcus, immediately adjacent to the subthecal microtubules. In the latter, neither connection with the chloroplast nor membranes surrounding the eyespot are present. *Glenodinium foliaceum* and *Peridinium balticum* possess another type of eyespot. It is a roughly triangular body situated behind the sulcus and is an independent structure bounded by a three-membrane envelope. Basically, there are two layers of pigmented globules, separated by a vesicle of granular material. The eyespot can fold back upon itself, making more layers. In *Amphidinium lacustre*, the eyespot is an elongated structure located along the right edge of the sulcus. Its color is a shade of greenish-yellow rather than the red-orange color commonly found in eyespots; it consists of up to six flat rows of bricklike units, each row contained in a vesicle bounded by a unit membrane. No data exist on the photoreceptor location in these dinoflagellates, but the assumption is the same as that made for the Haptophyta and Cryptophyta, that photoreceptive proteins must be located inside the plasma membrane close to the eyespot.

A separate case is that of *Alexandrium hiranoi* and *Gymnodinium mikimotoi*. Both dinoflagellates show phototactic responses but lack a detectable eyespot; hence, the shading function is performed by the cell body.

Type II

The photoreceptor consists of a multilayered membrane structure of photoreceptive protein. The eyespot is outwardly concave and is located close to this structure. This type of photoreceptive system is present in Ochrophyta and Euglenozoa.

In Ochrophyta, complex photoreceptors, consisting of layered electron-dense material organized in a rounded, wedge-shaped, or T-shaped organelle, are present inside the smooth flagellum of the motile stages of Xanthophyceae, Eustigmatophyceae, and Phaeophyceae. In the Xanthophyceae, the eyespot consists of a single layer of about 40 globules located at one side of the anterior end of the chloroplast. It is contained by the outermost thylakoid of the chloroplast, bounded by the chloroplast envelope and its associated endoplasmic reticulum. The cell membrane above the eyespot forms a depression through which the posterior smooth flagellum passes. The eyespot depression accommodates the photoreceptor. In the Eustigmatophyceae, the prominent eyespot occupies nearly the whole anterior part of the cell, adjacent to the flagellar insertion. It consists of an irregular collection of globules situated in a slight bulge of the zoospore but not enclosed by a membrane. The anterior hairy flagellum bears a photoreceptor swelling which fits alongside the eyespot. In the Phaeophyceae, the eyespot is situated in the posterior part of the cell inside a strongly reduced chloroplast and behind a depression of the cell surface through which the posterior flagellum runs. The

eyespot appears concave in shape and prominent, containing a single layer of about 60 globules. The photoreceptor swelling is localized at level of the eyespot.

An example of Chrysophyceae photoreceptor can be found in *Ochromonas danica*: the eyespot, located at the anterior end of the cell, consists of a single layer of carotenoid globules contained by the outermost thylakoid of the chloroplast. The cell membrane above the eyespot forms a slight invagination; this depression accommodates the photoreceptor consisting of a 3D assemblage of proteins located inside the base of the smooth flagellum (Figure 3.74).

In the members of the Euglenophyceae, the eyespot consists of a loose collection of globules situated on the dorsal side of the reservoir, the anterior invagination characteristic of these organisms. The globules vary in size (from 240 to 1200 nm) and number and can lie in a single layer or be bunched together. Individual globules may be membrane bound, but there is never a membrane surrounding the whole complex, and no association with any chloroplast component is present. The position of the eyespot within the reservoir region can vary among the species, but it is always in front of the photoreceptor situated on the long or emergent flagellum (Figure 3.75). The photoreceptor of *Euglena gracilis* can be considered the model of type II photoreceptor. This organelle is a 3D ordered assemblage of stacked membranes formed by 2D crystals of photoreceptive proteins. The organelle is located inside the membrane of the locomotory flagellum, connected to its axoneme by the paraxial rod. Figure 3.76a shows a portion of the photoreceptor at high magnification: the ordered disposition of the membrane layers is evident, made easily recognizable by osmium tetroxide staining of the phospholipid head groups. The periodicity is about 50 Å, comparable to the distance between the hydrophilic head layers of a typical membrane bilayer. About 50 membrane layers are present in the photoreceptor. Electron micrograph of negatively stained 2D lamellae, obtained by ionically induced uncoupling of the 3D compact structure of the photoreceptor, reveals stain excluding units protruding from the surface of the layer, arranged into a regular mesh (Figure 3.76b). After Fourier analysis, this mesh shows the ordered patches formed by the oligomers of the photoreceptive membrane spanning protein assembled in a hexagonal lattice visible in the grey scale contour plot (Figure 3.76c) that is a magnification of the central zone of Figure 3.76b. The membrane layers composing the photoreceptor are characterized by in-plane hydrophobic interactions, while their closely stacked disposition is due to the interlayer interactions between charged

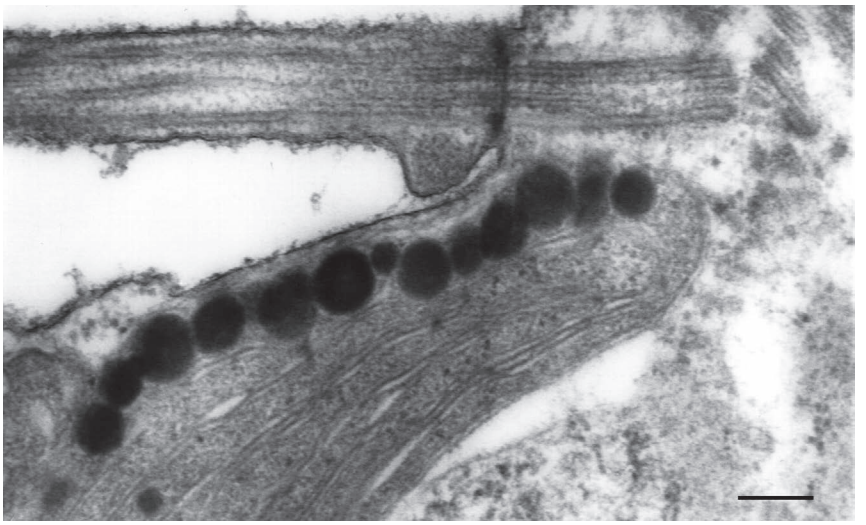


FIGURE 3.74 Transmission electron microscopy image of the photoreceptive system of *Ochromonas danica* in longitudinal section, showing the photoreceptor inside the trailing flagellum. Scale bar 0.30 μm.

protein extramembrane domains and the membrane in adjacent layers through charge density matching. About 10^6 photoreceptive proteins assembled in a hexagonal lattice span the membrane layers. Because of these characteristics, the photoreceptor of *Euglena* as a whole can be defined as a Type I crystal, that is, an ordered assemblage of stacked membranes formed by 2D crystals of membrane proteins. The *Euglena* photoreceptor structure is an example of a perfect device to absorb light with a maximal cross-section (insert in Figure 3.76a). Figure 3.77 shows the isolated *Euglena* photoreceptor–PFR complex.

Type III

This organization is present only in some dinoflagellates of the order Warnowiales, such as *Nematopsides* sp. and *Erythropsidinium* sp. The photoreceptor system is very specialized, and it is termed ocellus. It is situated towards the left side of the ventral surface of the cell. It consists of a refractile structure termed a hyalosome, thought to act as a lens, subtended by a domed pigmented part, divided into two sections, a retinoid and a pigmented cup. Between the lens and the retinoid is a chamber representing an invagination of the cell covering, which is lined by the cell membrane and allows the contact of the ocellus with the external medium. The pigmented cup wrapping the retinoid represents the eyespot and is made up of pigment-containing droplets enclosed in a vesicular layer. Small droplets contain carotenoid pigments; large droplets contain melanoid pigments. The retinoid is an extremely complex membranous construction made up of numerous regularly arranged layers, giving an almost paracrystalline appearance.

Photoreceptive Proteins

Over the past 15 years, genome sequencing and sequence comparison tools have revealed that genes encoding rhodopsin-like photoreceptive proteins are shared among distant taxa in all three domains of life: Archaea, Eubacteria, and Eukarya. As far as the algal word is concerned, reports from different research groups worldwide have provided examples of the broad distribution of type I rhodopsin-based photoreceptors among the different algal divisions and allowed the assumption that these proteins are present in all the algae of the supergroups of Plantae (Glaucophyta, Rhodophyta, Chlorophyta) and Chromista (Haptophyta, Cryptophyta, Ochrophyta, Miozoa), that is, those originating from a primary symbiotic event and those originating from a secondary or tertiary symbiotic event. In fact, genes encoding functional rhodopsins probably related to photoreception or ionic transport

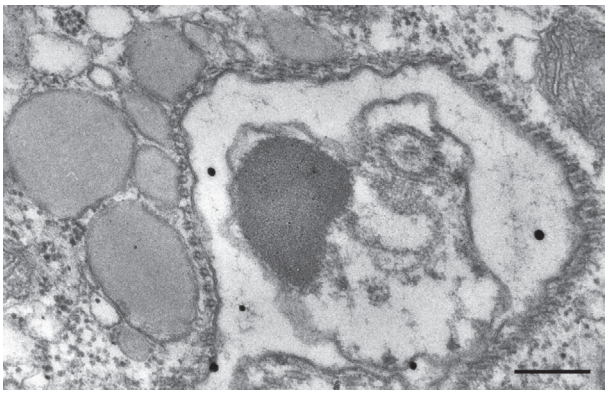


FIGURE 3.75 Transmission electron microscopy image of the photoreceptive system of *Euglena gracilis* in transverse section, showing the photoreceptor and the PFR inside the trailing flagellum and the eyespot in front of them inside the cell. Scale bar 0.50 μm.

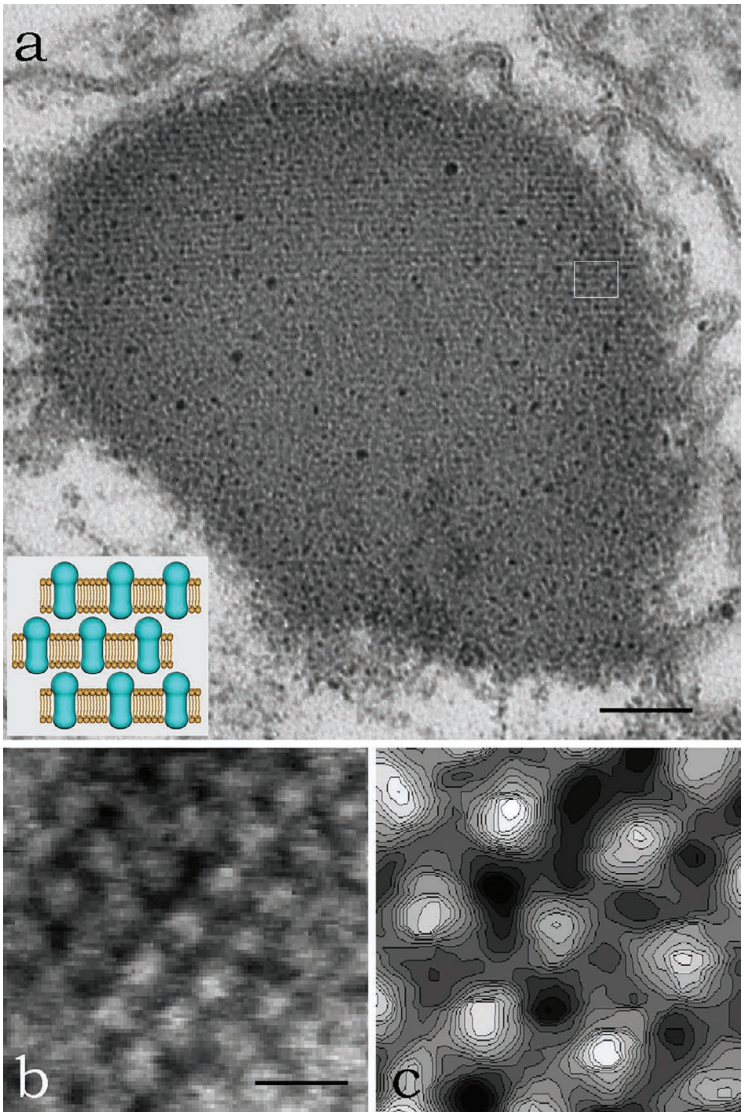


FIGURE 3.76 (a) Transmission electron micrograph of a cross-section of the *Euglena gracilis* photoreceptor showing the fine structure of the organelle. Scale bar: 15 nm. Inset of Figure 3.76a: Disposition of the photoreceptive proteins within the membrane layers of the *Euglena gracilis* photoreceptor. (b) Surface of a lamella showing the ordered pattern of protein oligomers. Scale bar: 10 nm. (c) Grayscale contour plot of the central hexagon of Figure 3.76b.

have been detected in Cyanophyceae (*Anabaena* sp., *Gloeobacter violaceous*) and Cryptophyceae (*Guillarda theta*), Glaucophyceae (*Cyanophora paradoxa*), Chlorophyceae (*Chlamydomonas reinhardtii, Gonium pectorale, Dunaliella salina, Volvox carteri*), Ulvophyceae (*Acetabularia acetabulum*), Mesostigmatophyceae (*Mesostigma viride*), Mamiellophyceae (*Micromonas pusilla, Ostreococcus* sp.), Trebouxiophyceae (*Chlorella vulgaris, Asterochloris* sp.), Chlorarachniophyceae (*Bigelowiella natans*), Pavlovophyceae (*Pavlova lutheri*), Chlorodendrophyceae (*Tetraselmis subcordiformis*), and Dinophyceae (*Oxyrrhis marina, Prorocentrum donghaiense, Pyrocystis lunula, Symbiodinium* sp.). The presence of an integral membrane protein in the membrane of the muroplast

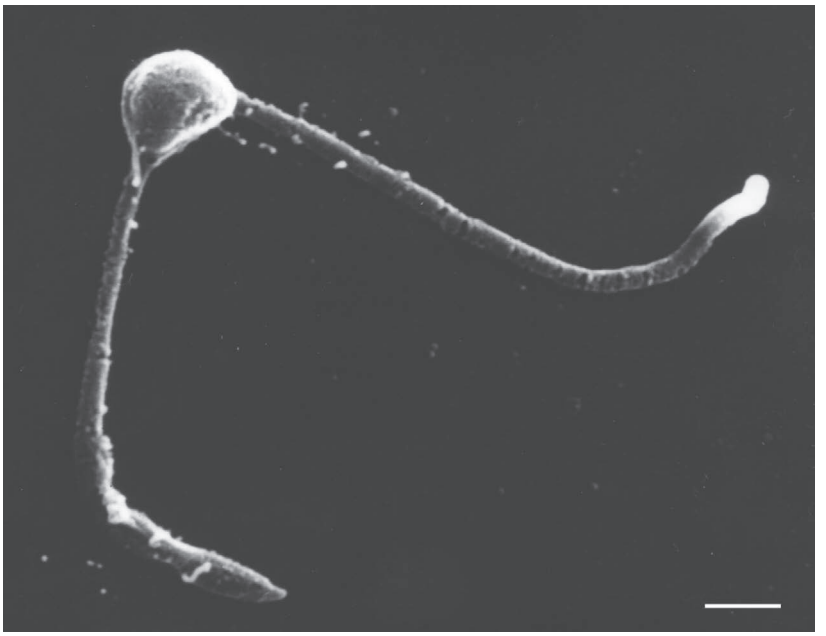


FIGURE 3.77 Scanning electron microscopy image of the isolated photoreceptor-PFR complex of *Euglena gracilis*. Scale bar 0.50 μm.

of *Cyanophora paradoxa*, a glaucophyte, the most primitive of all plastids, could indicate that the common primordial rhodopsin existed in pre-eukaryotic cells before the appearance of the first photosynthetic eukaryotic cell about 1.55×10^9 years ago (Figure 3.78). Retinal has been extracted from cells of *Ochromonas danica* (Chrysophyceae) (Figure 3.74); as already noted, a rhodopsin-like protein has been localized by immunofluorescence microscopy in the membrane of the egg of *Silvetia compressa* (Phaeophyceae) using an anti-rhodopsin antibody (Figure 3.73). In the case of *Euglena gracilis* (Euglenophyceae), a 27 kD protein with an absorption spectrum center at 510 nm was purified from isolated photoreceptors and used to raise antibodies, which labeled the photoreceptor of *Euglena* cells (Figure 3.79a, b, c, and e). From the same preparation, retinal has been extracted from isolated photoreceptors (Figure 3.79d). All these data strongly support the presence of a rhodopsin-like protein in *Euglena* photoreceptors, though no strong evidence of this protein exists in the recently assembled transcriptome of this alga.

All rhodopsins consist of a proteic part, the opsin, organized in seven transmembrane α-helices, and a light-absorbing group, the retinal (i.e. the chromophore). The retinal is located inside a pocket of the opsin, approximately in its center. These proteins can be considered special for many reasons. First, retinal-opsin complex has an intense absorption band whose maximum can be shifted into the visible region of the spectrum, over the entire range from 380 to 640 nm. Second, light isomerizes the retinal inside the protein very efficiently and rapidly. This one-molecule isomerization, that is, the event initiating the vision reaction cascade, can be triggered almost exclusively by light. In the dark, it occurs only about once in a thousand years. Third, remarkable structural changes (movements of a single α-helix) are produced by isomerization of retinal. Light is converted into atomic motion of sufficient magnitude to trigger a signal reliably and reproducibly. Fourth, the photocycle (the photoreceptive protein upon light excitation undergoes a series of conformational changes which can be driven back to the original conformational state) is very fast, so the intracellular photoreceptive machinery is immediately reset for a new response. Fifth, retinal is derived from β-carotene, a precursor with a widespread biological distribution.

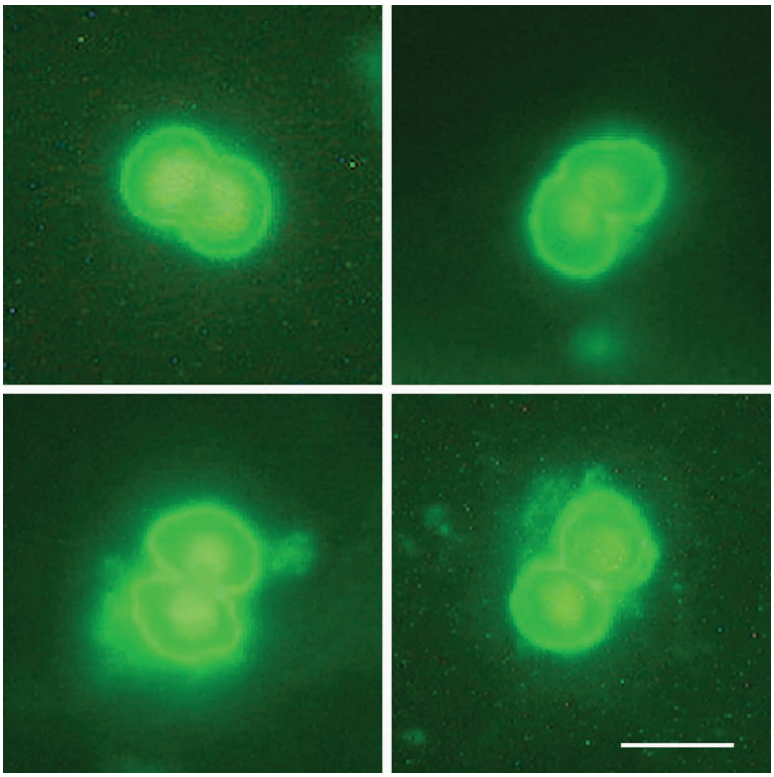


FIGURE 3.78 Immunofluorescence localization of the rhodopsin-like protein in *Cyanophora paradoxa* muroplasts. Scale bar 5 μm.

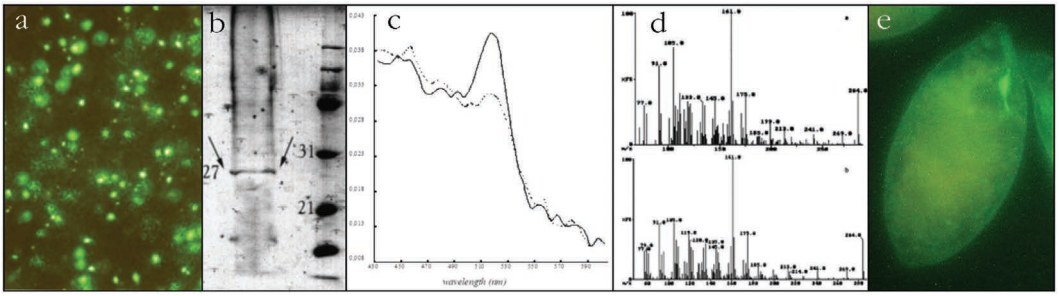


FIGURE 3.79 Isolated photoreceptors of *Euglena gracilis* (a) used to purify a 27 kD protein (b) with an absorption spectrum center at 510 nm (c). Mass spectrum of retinal extracted from the same preparation (d). The protein was used to raise antibodies, which labeled the photoreceptor of *Euglena* cells (e).

BEHAVIORAL AND PHYSIOLOGICAL FEATURES

The structural features described previously should be accompanied by efficient sampling strategies, trajectory control mechanisms, and signal transmission.

Sampling Strategies

To determine the orientation of a stimulus field, an organism has to measure the stimulus intensity at different positions; that is, it should detect either spatial or temporal patterns of light. Femtoplankton (0.02–0.2 μm) is too small compared to the wavelength of light to create differential light intensity; hence, it cannot determine the direction of a light source. Still, femtoplankton microorganisms can use light but can only measure its intensity and move in a light-intensity gradient. In contrast, phytoplankton dimensions are large enough to determine light direction and allow the scanning of the environment by means of their directionally sensitive receptor.

Two fundamental and alternative strategies exist for obtaining information on light direction: parallel sampling and sequential sampling. In parallel sampling, the stimulus is detected by multiple separated receptors positioned on different parts of the organism surface. In this case the organism directly measures the spatial gradient by simultaneous comparison of light intensities at two different part of its body (one instant mechanism). This strategy is present in the zygote of the brown alga *Silvetia compressa*; the photoreceptive system of the zygote is presumably the same as the egg before fertilization, which was described in the previous section. The zygote absorbs or scatters more than 95% of the effective blue wavelengths within one cell diameter, thus creating a steep light gradient across the cells. Photoreceptors in or near the plasma membrane are activated differentially, and the cellular response to this gradient of photoreceptor activation is to organize an axis and germinate from the darkest point. Photopolarization is an early event, which has been observed 4 hours after fertilization. The zygote produces a rhizoidal bulge at about 10 h after fertilization. Initially, any point on the cell surface is capable of becoming the germination site. The bulge elongates by tip growth (i.e. addition of new cell membrane and wall material by localized vesicle secretion), and about 18 h after fertilization, the first cell division occurs. The plane of division is perpendicular to the growth axis, resulting in the formation of two highly asymmetrical cells with different developmental fates. The cell bearing the bulge will form the rhizoid, which will show negative phototaxis, while the other cell will form the thallus. Figure 3.80 shows the first steps of development of a *Silvetia* zygote from fertilization to rhizoid formation: changing of light direction causes a change in the rhizoid growth axis.

In sequential sampling, the stimulus is detected by a single receptor as the cell changes its position in relation to the light source. In this situation, the organism measures a temporal gradient directly and then infers the spatial gradient from the information on the movements of the receptor (two instant mechanisms). This strategy is present in all algae with a single photoreceptor. These algae have only a limited vision of the three-dimensional world in which they navigate and cannot detect light directions by measuring light intensity at two different positions in the cell body. An example is *Leptolyngbya* sp., whose photoreceptor system was described previously. This cyanobacterium characterized by quite inflexible trichomes uses light to grow towards optimal light intensities, with a sort of oriented movement with respect to the stimulus direction. It changes the direction of the trichome by turning towards the light source at the level of the apical cell (Figures 3.81a and 3.81b), where both the photoreceptor and the eyespot are located (Figure 3.2). When the photoreceptor system is impaired, the movement becomes unguided, and the trichomes appear disordered (Figure

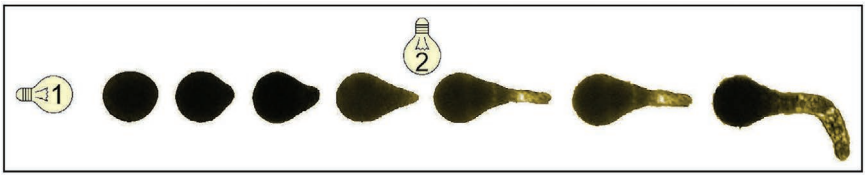


FIGURE 3.80 Parallel sampling used by *Silvetia* sp. zygote to orientate along the thallus-rhizoid growth direction. Light 2 is turned on after turning off Light 1.

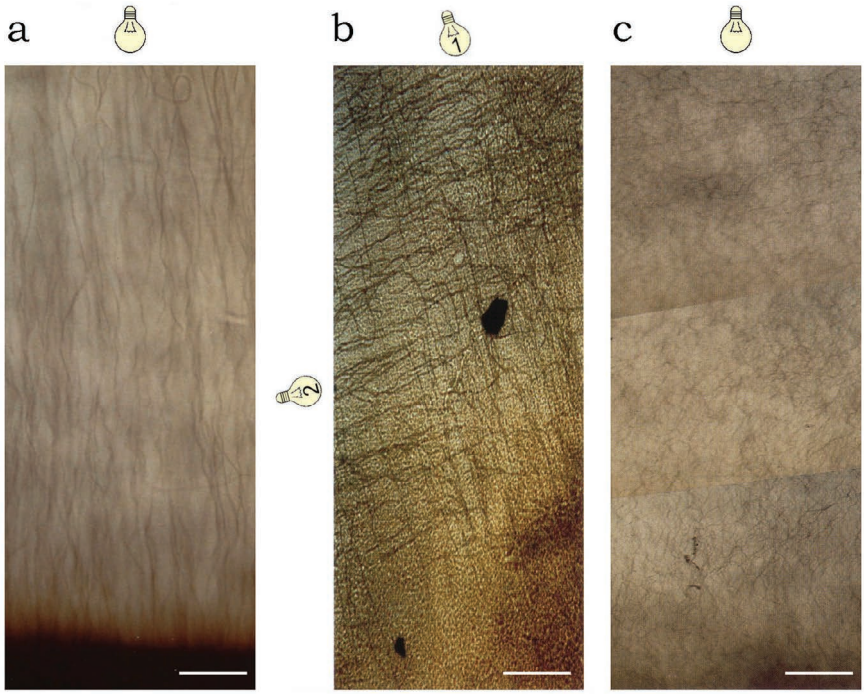


FIGURE 3.81 Sequential sampling by *Leptolyngbya*: refer to text for details. Scale bars: 60 mm.

3.81c). The simultaneous comparison of signals requires widely spaced receptors to detect intensity gradient, which makes a large body size advantageous. On the other hand, sequential sampling requires a coherent pattern of movement. Many algae perform sequential sampling by swimming on helical paths along which their photoreceptor acts as a light antenna continuously searching space for bright spots. Sequential sampling also requires some form of memory to allow the comparison with previously recorded intensities.

Trajectory Control

Another fundamental distinction is based on whether an organism is able to make turns in its motion path, which will direct it toward its destination. Depending on the characteristic of the stimulus and the abilities of the microorganism, guiding may be either direct in the sense of taking a straight-line path to the destination or indirect, as in the case of a biased random walk, to reach the vicinity of the destination. Trajectory control characteristics, and thus behavioral peculiarities, are connected with both the shape of the cell and the functioning of the propelling structure of the algae, that is, the flagellum. If the cell is asymmetric, that is, if it possesses recognizable dorsal and ventral sides, it advances spinning along its axis. It can correct its trajectory by either sudden steering obtained by changing the insertion angle of flagella, like, for example, *Ochromonas danica*, or stiffening of the flagellum via accessory structure of the axoneme, like *Euglena gracilis*. This behavior can be attributed to all heterokont and uniflagellate algae. In the case of a symmetric cell, it can accomplish a gradual smooth correction of its trajectory going forward without spinning (or rotating with a very long period) and displacing the barycenter of the motor pair, as in *Dunaliella salina*. This behavior can be attributed to all isokont cells.

Signal Transmission

Signal transmission in algae is still a poorly investigated topic. Algae are aneural organisms, lacking any system for the transmission of the stimuli received from the outside. The information carried by light has to be translated into an organism-specific swimming control mechanism that allows orientation to the light with high fidelity. Hence, the light signal will be first transduced in an electric signal by mean of electron or ion flux, and this electric signal will be transmit to the algae motor apparatus, that is, the flagellum/a. It has been demonstrated that in *Chlamydomonas reinhardtii*, light absorbed by rhodopsins initiates local photocurrents (a fast photocurrent and a slow photocurrent) in the eyespot region, presumably in the plasma membrane right above the eyespot, where the photosensitive proteins are located. At low intensities, rhodopsins trigger a highly efficient biochemical amplification reaction which involves activation of yet-unknown downstream elements and control of some diffusible messenger, a process analogous to vision in animals. At high light intensities, the second function of rhodopsins, direct channel activity, begins to contribute to depolarization of the plasma membrane, which eventually allows motility responses. Biphasic photocurrents have been shown to exist also in other algae, for example, *Volvox carteri* (Chlorophyta) and *Cryptomonas* sp. (Cryptophyta).

AN EXAMPLE: PHOTORECEPTOR AND PHOTORECEPTION IN *EUGLENA*

As described in the previous section, in order for phototaxis (photoreception) to occur, proper perceiving devices (structural features) satisfying essential requirements are necessary, together with specific behavioral and physiological features. In this section, we will use *Euglena* as example to analyze how these structural, behavioral, and physiological aspects combine to achieve a concerted response to light stimuli. *Euglena* dwells in natural shallow ponds and uses sunlight as a source of energy and information. Its chloroplasts are energy-supplying devices, whereas the simple but sophisticated photoreceptive system already described is used as a light detector.

The photoreceptor ciliary line of evolution, which had its climax in the elaborate and remarkably complex vertebrate eye, originated from the photoreceptor of *Euglena*. According to the definition of the Swiss geneticist Walter Gehring, the prototypical eye, which was presumably the common ancestor of all eyes, is a combination of a photoreceptor cell and a pigment cell, which achieves some directional selectivity by using screening pigment to block light coming from certain directions. The photoreceptor cell is located close to the effector and transmits the information conveyed by the light directly to it (without an intervening information-processing organelle). In the case of *Euglena*, the "eye" is formed within a single cell by the assembly of pigmented and photoreceptive molecules within that cell in two distinct organelles, the eyespot and the photoreceptor. The different components of this primitive eye have been investigated by many different techniques such as electron microscopy, microspectroscopy (cf. Chapter 7), digital microscopy (cf. Chapter 7), molecular biology, and immunofluorescence. We will describe and analyze them to demonstrate how the simple design of *Euglena* photoreceptive system fits Gehring's definition.

As already said, the eyespot consists of a loose collection of globules situated on the dorsal side of the reservoir, always in front of the photoreceptor. The pigments present in the eyespot globules are carotenoids such as β-carotene, diatoxanthin, and diadinoxanthin. The absorption spectrum of the eyespot shows a unique large band centered at 460 nm (Figure 3.82 orange line).

The *Euglena* photoreceptor is located near the base of the locomotory flagellum. Its regular structure has been already described as Type I crystal, that is, an ordered assemblage of stacked membranes formed by 2D crystals of proteins (Figure 3.76a). Each layer contains photoreceptive membrane-spanning proteins arranged in a hexagonal pattern (Figure 3.76b and 3.76c). These proteins are characterized by optical bistability; that is, they possess two isomeric forms, A and B, which interconvert along a photocycling path photochemically but not thermically. This property has been

characterized by both microspectrophotometry (Figure 3.82) and digital microscopy (Figure 3.83) measurements performed on the photoreceptor inside the cell. The absorption spectrum of form A has a band centered at 498 nm (A_{498}) (Figure 3.78, green line). Under physiological conditions, this is the dominant isomeric form of the proteins inside the photoreceptor, which does not fluoresce. The absorption spectrum of form B has a band centered at 462 nm (B_{462}) (Figure 3.78, blue line), which perfectly matches the absorption spectrum of the eyespot. The isomeric form B_{462} is the fluorescent form, energetically lower, which can be considered the signaling state of the protein. Figure 3.83 shows the sequences of the absorbance images of photoreceptor of *Euglena* populated by either the isomeric form A_{498} or the isomeric form B_{462}. The comparison of the sequences highlights the difference between the spectra of the two isomeric forms; the red framed images show the absorption maxima of the photoreceptor.

The absorption difference spectra of the two isomeric forms indicate that UV light (e.g. 365 nm) and green light (e.g. 546 nm) induce the conversion of the non-fluorescent form A_{498} to the fluorescent form B_{462}; the reverse conversion can be induced only by blue light (e.g. 436 nm), which has no effect on the non-fluorescent form A_{498}. Fluorescence microscopy clearly shows the interconversion (i.e. the photocycle) of the two isomeric forms in *Euglena* photoreceptors and isolated photoreceptors (Figure 3.84). The optical bistability of the photoreceptor, together with the experimental evidence of the chromophore and protein isolated from the organelle, strongly support the presence of a rhodopsin-like protein and exclude any other possible photoreceptive pigment.

The functioning of the *Euglena* photoreceptor in nature can be described as the following: the cells normally swim by rotating along a helicoidal path; during this motion, the photoreceptor proteins are in a photodynamic equilibrium in which A_{498} is the dominant isomer. The equilibrium is interrupted when the eyespot comes between the incoming light and the photoreceptor, thus screening the organelle (Figure 3.85). Due to the superimposition of the absorption spectra of the eyespot and the isomer form $B_{462,}$ only UV and green light illuminate the photoreceptor during the screening period, and the only possible transition is that of A_{498} to B_{462}. In details, the photoisomerizable isomeric form A_{498} undergoes an intramolecular photoswitch; that is, A_{498} becomes B_{462} through an excited state, and contemporaneously an intermolecular

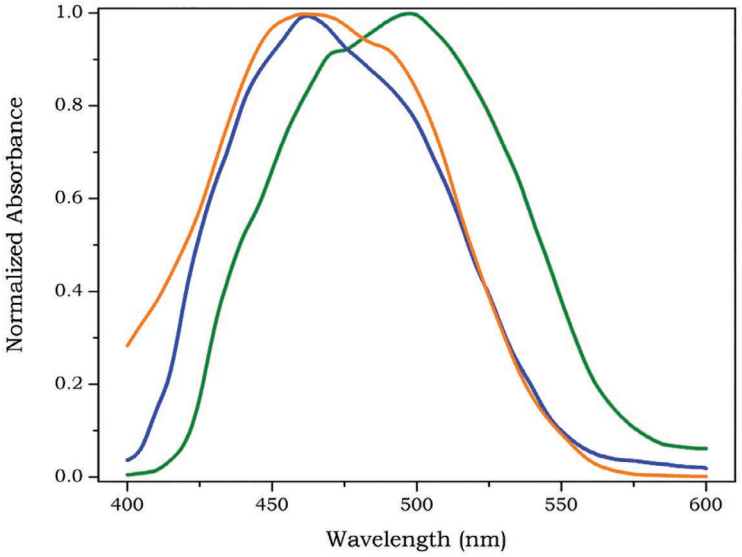


FIGURE 3.82 Absorption spectrum of the eyespot of *Euglena gracilis* (orange line); absorption spectra of the A (green line) and of B (blue line) isomers.

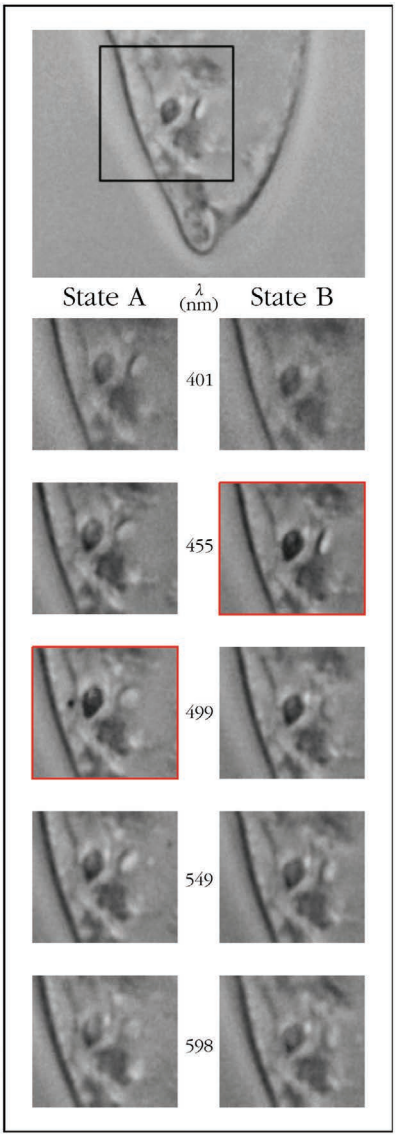


FIGURE 3.83 The sequences of the absorbance images of photoreceptor of *Euglena* populated by either the isomeric form A_{498} or the isomeric form B_{462}. The comparison of the sequences highlights the difference between the spectra of the two isomeric forms; the red-framed images show the absorption maxima of the photoreceptor.

and unidirectional Forster-type energy transfer (FRET) occurs: the newly formed fluorescent B_{462} acts as energy donor for the nearby protein in the A_{498} form, which acts as energy acceptor. The intramolecular switch and the FRET follow each other with a domino progression along the orderly organized and closely packed proteins in the layer(s) of the crystal structure of the photoreceptor (Figure 3.76), modulating the isomeric composition of the photoreceptive protein pool. As a consequence, B_{462}, the signaling state of the protein energetically lower than A_{498}, becomes the dominant isomer. It is worthwhile to highlight that the photoreceptive protein switches from a photoisomerizable device to a fluorescent dye.

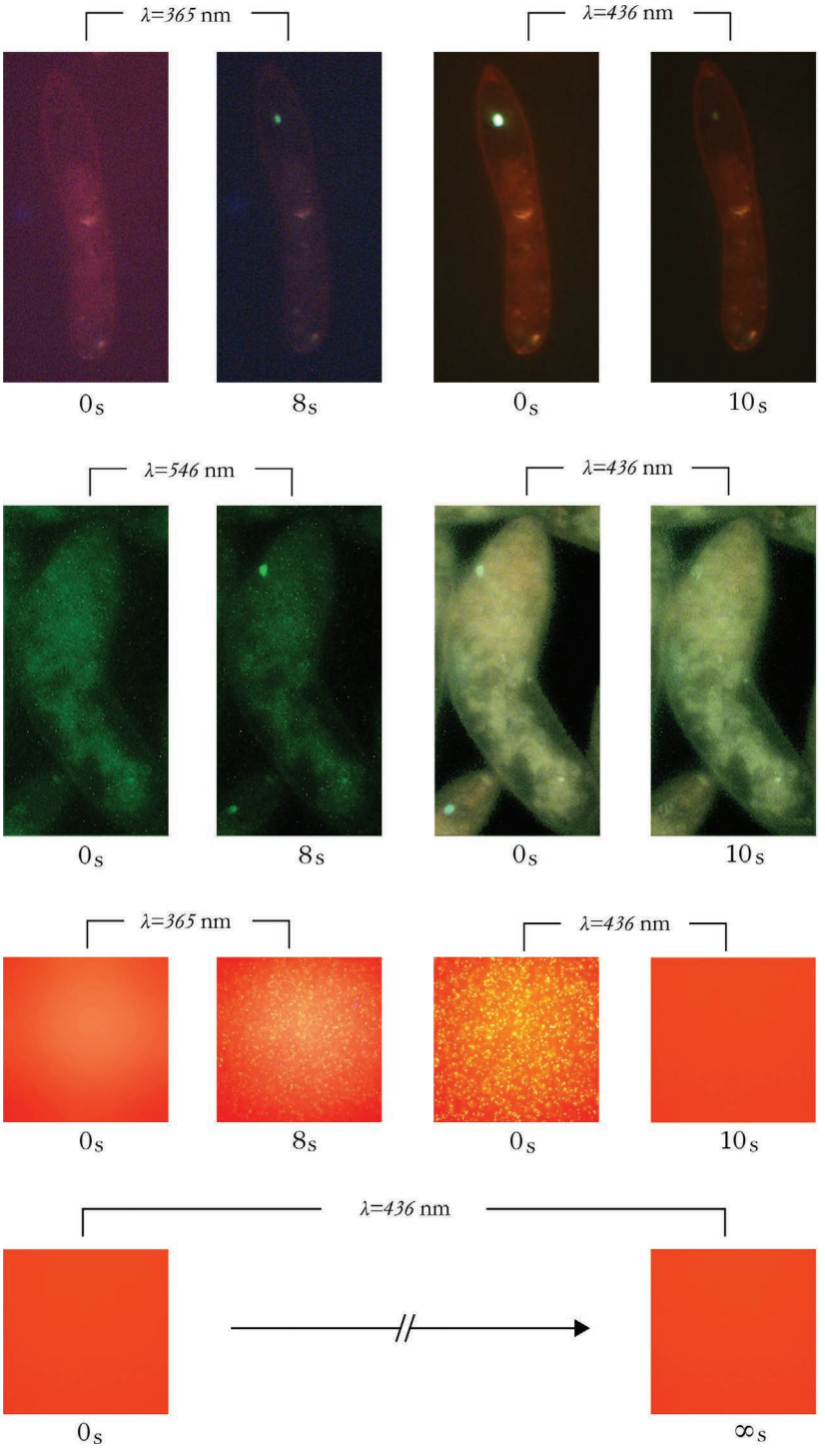


FIGURE 3.84 The photocycle of the two isomeric forms in the photoreceptor of *Euglena gracilis* induced by UV light (top) and green light (center). The reverse conversion is induced by blue light. The photocycle of the two isomeric forms in isolated photoreceptors; blue light cannot induce the photocycle (bottom).

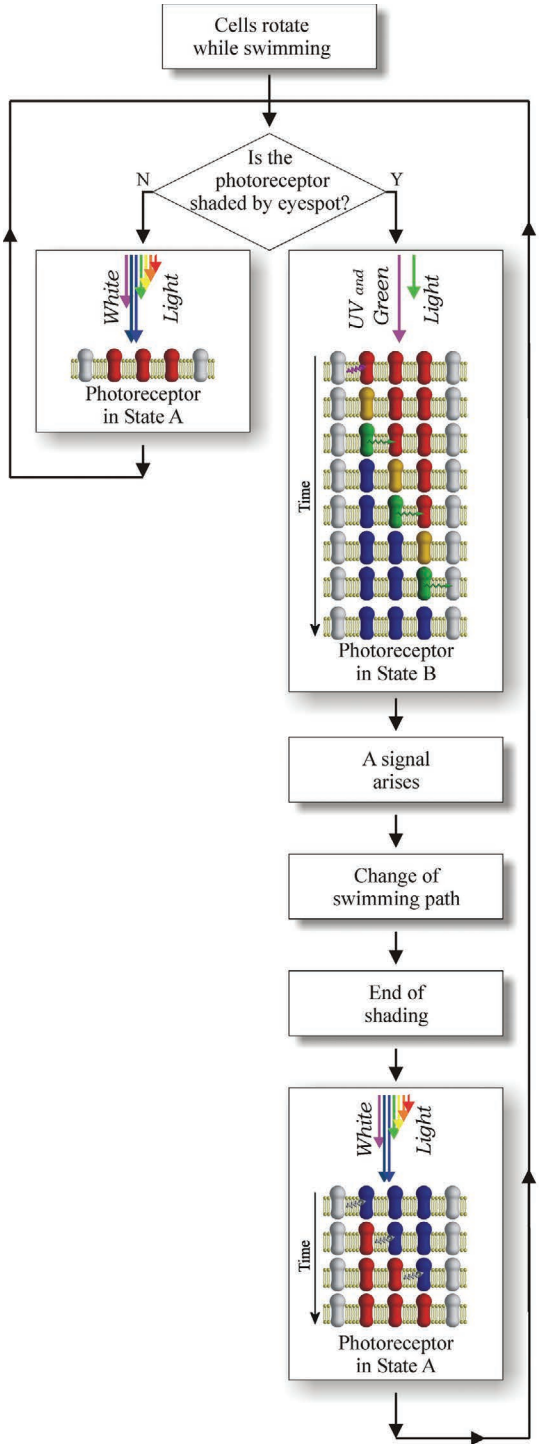


FIGURE 3.85 *Euglena gracilis* phototaxis flow chart.

The energy needed for the transition from A_{498} to B_{462} and the energy transferred from one protein to the nearby protein derive not only from the photons absorbed during the photoreceptor screening by the eyespot but also from the photons absorbed by the photoreceptor during the non-screening period. These photons restore the photoreceptor isomeric composition with A_{498} as dominant isomer. Once the screening by the eyespot is over, the transition from B_{462} to A_{498} can again occur due to the full-spectrum light (natural light) impinging on the photoreceptor, and the isomeric composition with A_{498} as dominant isomer is again restored.

How does the signal generated by the photoreceptor drive *Euglena* movement?

As described, changes in the motion trajectory by bending of the locomotory flagellum are due to the screening of the photoreceptor by the eyespot that changes the electrostatic field. The locomotory flagellum carries the paraxial rod, which is a hollow rod-like structure with a diameter of 90 nm (Figure 3.36a and 3.36b), along its entire length. The PAR is the true effector. When the photoreceptor is screened by the eyespot, the signaling state of the protein becomes the dominant isomer, and a change of the electrostatic field occurs. Since the photoreceptor and the paraxial rod are a structural unit (Figure 3.77), we can hypothesize that the photoelectric signal could be propagated through the paraxial rod filaments via charge transfer between rod proteins, modifying the pitch of its helix, which in turn modifies the distribution of the mass of the rod along the axoneme. This leads to a change in the motion wave running along the flagellum and eventually to a change in the swimming direction.

Chloroplasts

The photosynthetic compartment contains the pigments for absorbing light and channeling the energy of the excited pigment molecules into a series of photochemical and enzymatic reactions. These pigments are organized in proteic complexes embedded in the membrane of sac-like flat compressed vesicles known as the thylakoids. These vesicles are about 24 nm thick and enclose a space, termed lumen, 10 nm wide.

In prokaryotes, the thylakoids are free within the cytoplasm, while in eukaryotes, they are enclosed within bounding membranes to form the chloroplast. The colorless matrix of the chloroplast is known as the stroma. Inside the chloroplast, thylakoids are organized into two different compartments, granal thylakoids, stacked into hollow disks termed grana, and stromal thylakoids forming multiple connections between the grana. All thylakoid surfaces run parallel to the plane of the maximum chloroplast cross-section. Chloroplasts contain nucleic acids and ribosomes. DNA is naked, that is, not associated with proteins, and occurs in two configurations: as scattered but not connected small nucleoids or as a peripheral ring. Chloroplasts are semiautonomous organelles that replicate their own DNA, and this replication is not linked to the division of the organelle. Synthesis of RNA and proteins is possible inside the chloroplast, though they are not strictly autonomous from the nuclear genome. The plastid genes are transcribed and translated within the plastids. The machinery of protein synthesis is, in any case, partially composed of imported nuclear gene products. In this respect, as in others, the chloroplast is no longer independent. Nevertheless, about half of the plastid genome consists of genes that contribute to the machine of gene expression, such as genes for rRNA, tRNAs, RNA polymerase subunits, and ribosomal proteins. Plastids code for, and synthesize, some proteins that are components for photosystems and particular subunits of photosynthetic enzymes. The missing subunits of these complexes are coded in the nucleus and must be imported from the cytoplasm.

Chloroplast development and division (self-replication) may be coordinated with that of the cell or may proceed independently. They divide in mother cells, and they are inherited by daughter cells during vegetative division and usually only from the maternal side in sexual reproduction. The shape and number of chloroplast is extremely variable, from the single cup-shaped chloroplast of *Dunaliella salina* to the ribbon-like chloroplast of *Spirogyra* or the stellate one of *Zygnema* to the numerous (about 10^8) ellipsoidal chloroplasts of the *Acetabularia* giant cell.

The fact that algae of different divisions have different colors, due to the presence of a variety of pigments in the photosynthetic membrane system, might lead to the supposition that the photosynthetic membrane structures are variable. This is true, since the features of photosynthetic membrane system represent a diagnostic important element at the class level. In this chapter, we will consider the structure, composition, and location of the photosynthetic membrane system in each algal division.

Cyanobacteria

The photosynthetic apparatus of these algae is localized on intra-cytoplasmic membranes termed thylakoids. The thylakoid membranes show considerable variations in structure and arrangement depending on the species. Also, the amount of thylakoid membranes per cell is variable due to growth conditions and taxonomic specificity.

In most species, the thylakoids are arranged peripherally in three to six layers running parallel to the cell membrane, forming an anastomosing network of concentric shells. This peripheral region has been called chromatoplast, which is separated from the inner nucleoplasmic region called centroplasm. This type of thylakoid arrangement is characteristic of many unicellular and filamentous cyanobacteria, such as *Synechococcus planctibus* and *Anabaena* sp. In some other organisms such as *Oscillatoria* and *Arthrospira*, the thylakoids are orientated perpendicular to the longitudinal cell wall. A radial arrangement is present in *Phormidium retzi*. Thylakoids are not always restricted to the cell periphery but can be found scattered throughout the cell, as in *Gloeotrichia* sp. However, the arrangement of thylakoids can change from cell to cell and cell type (vegetative cells, heterocyst, akinete) within the same culture, from parallel to a convoluted appearance. Thylakoids can fuse with each other and form an anastomosing network; unlike the chloroplasts of eukaryotic algae, the thylakoids of cyanobacteria form stacking regions only to a very limited extent. During cell division, the thylakoids have to be separated and divided into the daughter cells; generally this division is an active process. Cell division starts by a centripetal growth of the cytoplasmic membrane and peptidoglycan layer to form the septum; the thylakoid cylinder is narrowed at the level of the cross wall by invagination before the septum is formed. Proteins, lipids, carotenoids, and chlorophyll *a* are major components of thylakoids. On the outer surface of the thylakoids, regular rows of electron-dense granular structures are closely attached. These granules, termed phycobilisomes, contain the light-harvesting phycobiliproteins allophycocyanin, phycocyanin, and phycoerythrin (Figure 3.86). The phycobilisome structure consists of a three-cylinder core of four stacked molecules of allophycocyanin, closest to the thylakoid membrane, on which rod-shaped assemblies of coaxially stacked hexameric molecules of only phycocyanin or both phycocyanin and phycoerythrin converge (Figure 3.87). Phycobiliproteins are also accessory pigments for the operation of photosystem II in Glaucophyta, Cryptophyta, and Rhodophyta.

The thylakoid membranes of *Prochloron* are organized into stacked and unstacked regions reminiscent of the grana and stromal lamellae of higher plant chloroplasts. They differ from cyanobacteria in that they contain chlorophyll *a/b* light-harvesting systems rather than phycobiliproteins organized in the phycobilisomes.

Glaucophyta

As already described in Chapter 1, these algae possess inclusion termed cyanelles that are probably symbiotic cyanobacteria functioning as chloroplasts (Figure 3.88). Each cyanelle, surrounded by a reduced peptoglycan cell wall (except in *Glaucosphaera* sp.), is enclosed in a vesicle of the host cytoplasm. Cyanelles do not fix molecular nitrogen in contrast with cyanobacteria; they contain polyphosphate granules and a conspicuous central carboxisome similar to the pyrenoids of other algae. The thylakoid are not stacked but single and equidistant with a concentric arrangement. Cyanelle pigments are chlorophyll *a* and β-carotene, which represents the main carotenoid. Interthylakoidal phycobilisomes contain allophycocyanin and phycocianin. Phycoerythrin is absent from Glaucophyta, but phycoerythrocyanin can be found in some species.

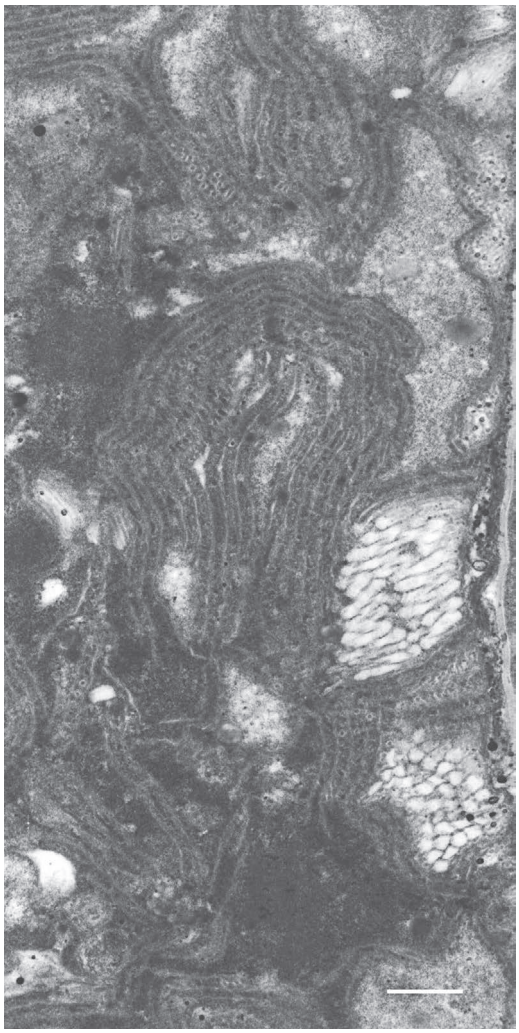


FIGURE 3.86 Transmission electron microscopy image of a cyanobacterium in longitudinal section, showing the thylakoid membranes with phycobilisomes. Scale bar 0.20 μm. Courtesy of Luisa Tomaselli.

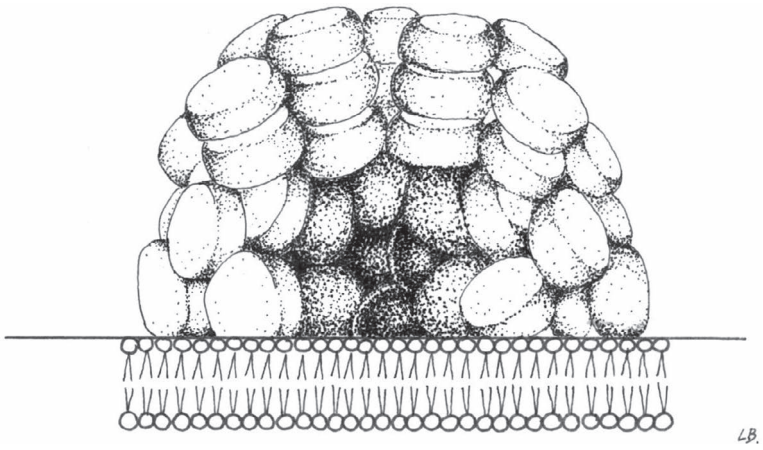


FIGURE 3.87 Schematic drawing of a phycobilisome.



FIGURE 3.88 *Cyanophora paradoxa* isolated cyanelles. Scale bar 5 μm.

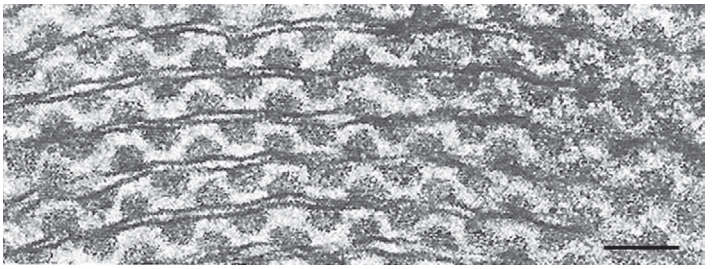


FIGURE 3.89 Transmission electron microscopy image of rhodophyte thylakoid showing the regularly arranged phycobilisomes. Scale bar 0.05 μm.

Rhodophyta

Ultrastructurally, red algal chloroplasts are composed of a double-membraned envelope inside of which are one or more parallel, thylakoidal photosynthetic lamellae. These chloroplasts are not associated with the endoplasmic reticulum, a feature shared with Glaucophyta and Chlorophyta. Encircling thylakoids are present in all Florideophyceae and in some taxa of Bangiophyceae, while the thylakoids in the other red algae lie equidistant and are single, that is, not stacked, unlike any other group of eukaryotic algae (except Glaucophyta), and typically oriented parallel to each other. All thylakoids have phycobilisomes attached to their stromal surface, which contain the accessory phycobiliprotein pigments, that is, allophycocyanin, phycocyanin, and five forms of phycoerythrin (Figure 3.89). Chlorophyll *a* is the only chlorophyll present in the thylakoid membrane, together with carotenoids such as β-carotene and lutein. Plastid number, shape, and position (many, discoid, and parietal) are rather uniform throughout the Florideophyceae, and pyrenoids may or may not be present. A single stellate plastid with a central pyrenoid is commonly associated with porphyridiophyceans, such as *Porphyridium* (Figure 3.90). DNA is organized into numerous nucleoids scattered throughout the chloroplast.

Prasinodermatophyta, Chlorophyta, Charophyta

These algae are not uniform in the ultrastructure of chloroplast; still, some generalizations can be made. The chloroplasts are enclosed only by the double membrane of the chloroplast envelope; there is no additional envelope of endoplasmic reticulum or nuclear membrane. In this respect they resemble Rhodophyta and Glaucophyta in cell compartmentalization. The chloroplasts vary greatly in shape and size. In unicellular forms, it is often cup-shaped with a thick base (*Dunaliella*); in filamentous forms, it is often ring-like or net-like shaped and lies against the cell wall (*Oedogonium*). More massive and elaborate plastids lying along the longitudinal axis of the cell are particularly



FIGURE 3.90 *Porphyridium cruentum* cells with a single stellate plastid. Scale bar: 1μm.

characteristic of members of the Zygnematophyceae. Thylakoids are arranged in stacks of two to six or more; their multilayered arrangement may take on the appearance of grana with membrane interconnections, as in higher plants. Girdle lamellae are absent. One to several pyrenoids embedded within the chloroplast occur in most of the algae of this division, which are often penetrated by thylakoids. The DNA organized in small nucleoids is distributed throughout the chloroplast matrix. Both chlorophyll *a* and *b* are present; accessory pigments include different xanthophylls such as lutein, zeaxanthin, and violaxanthin; β-carotene is always present together with other carotenoids.

Haptophyta

Cells of Haptophyceae species normally possess one or two chloroplasts containing thylakoids stacked in three to form lamellae. There is no girdle lamella. Spindle-shaped pyrenoids are commonly immersed within the chloroplast, penetrated by one or a few pairs of thylakoids, but in some genera, they bulge from the inner face of the organelle. Both the chloroplast and the pyrenoid are surrounded by endoplasmic reticulum confluent with the nuclear envelope, the nucleus itself lying close to the chloroplast. Chlorophylls *a*, c_1, c_2, and in some genera also c_3 are found in the thylakoidal membranes together with carotenes, such as β-carotene, and xanthophylls, the most commonly occurring being fucoxanthin. DNA is organized into numerous nucleoids scattered throughout the chloroplast.

Cryptophyta

The chloroplasts of these algae, one or two per cell, are unusual in both their pigment composition and ultrastructure. Four membranes enclose these organelles: the inner pair forms the plastid envelope, and the outer pair forms the plastid endoplasmic reticulum. This four-membrane configuration is common in chlorophyll *c*–containing algae. An expanded space is present between the plastid endoplasmic reticulum and the plastid envelope on its inward face. This compartment contains 80s ribosomes, starch grains, and the nucleomorph. Thylakoids inside the chloroplast are typically in pairs, although single thylakoids as well as large stacks have been also observed, with no girdle lamella. A pyrenoid is present, projecting from the inner side of the chloroplast. Cryptomonads are characterized by the presence of chlorophylls *a* and c_2; phycoerythrin, phycocyanin, and allophycocyanin; carotenes and several xanthophylls.

The phycobiliproteins differ from those of the red algae and cyanobacteria, since they are of lower molecular weight and do not aggregate to form discrete phycobilisomes, being localized within the lumen of the thylakoids. DNA is organized into numerous nucleoids scattered throughout the chloroplast.

Ochrophyta

Some ultrastructural features of the chloroplast compartments of these algae are common to all seven classes of the division, with few exceptions. Four membranes surround the chloroplasts, the outer two being the chloroplast endoplasmic reticulum and the inner two being the chloroplast envelope. When the chloroplasts are located close to the nucleus, the chloroplast endoplasmic reticulum is continuous with the nuclear envelope. In the Xanthophyceae, this connection is not the rule. Thylakoids are grouped into lamellae of three, or two in some Raphidophyceae, with varying degrees of coherence depending on the species. Thylakoids from adjacent lamellae frequently interconnect across the stroma. In all the classes, with the exception of Eustigmatophyceae and *Chattonella* (Raphidophyceae), one lamella runs around the periphery of the chloroplast beneath the chloroplast envelope, enclosing all the other lamellae. The lamella is called the girdle lamella.

One or more plate-like (Chrysophyceae, Figures 3.91a and 3.91b; Eustigmatophyceae, Figures 3.92a and 3.92b), discoid (Xanthophyceae, Raphidophyceae, Dictyochophyceae), or ribbon-like (Phaeophyceae) plastids are typically present, often lobed, parietal, or located in close connection with the nucleus. In the Bacillariophyceae, chloroplasts are the most conspicuous feature, and their number and shape are consistent features of taxonomic importance. They may be rounded or lobed discs or large and plate-like with or without lobed margins and may range from one to two, four, or more. A typical centric diatom has many disc-shaped plastids, arranged close to the periphery surrounding a large central vacuole or scattered throughout the cell. The raphid diatoms tend to have large chloroplasts (one to four) lying along the girdle, with the central nucleus flanked by two large vacuoles.

The chloroplast DNA is ring shaped and located in the region between the girdle lamella and the others in all classes, with the exception of the Eustigmatophyceae, where it is organized into many dot-like nucleoids, which may be united in a sort of reticulum. The main photosynthetic pigment is chlorophyll *a*, which is the only chlorophyll present in the Eustigmatophyceae. In addition, chlorophylls of the *c* group occur, both c_1 and c_2 (Chrysophyceae, Rhaphidophyceae, Phaeophyceae, and Dictyochophyceae and in only extremely low concentrations in Xanthophyceae) or only c_2 (Bacillariophyceae). The most important accessory pigment is fucoxanthin in Chrysophyceae,

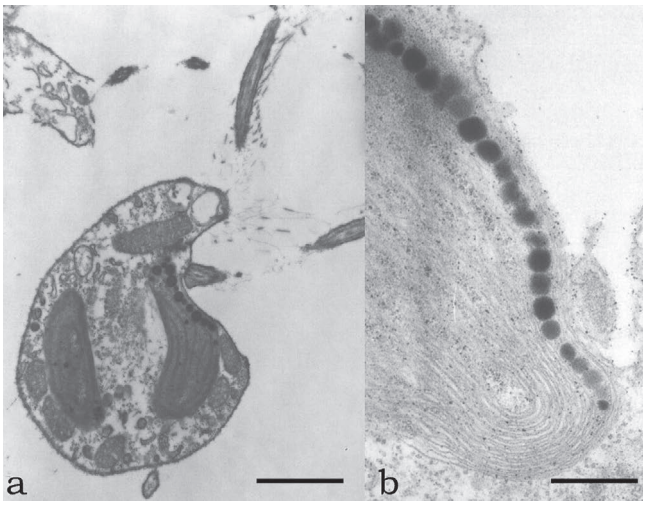


FIGURE 3.91 Transmission electron microscopy image of *Ochromonas danica* in longitudinal section, showing the chloroplast (a). Scale bar 3 μm. Transmission electron microscopy image of a chloroplast at higher magnification showing the thylakoid membrane and the eyespot globules (b). Scale bar 1 μm.

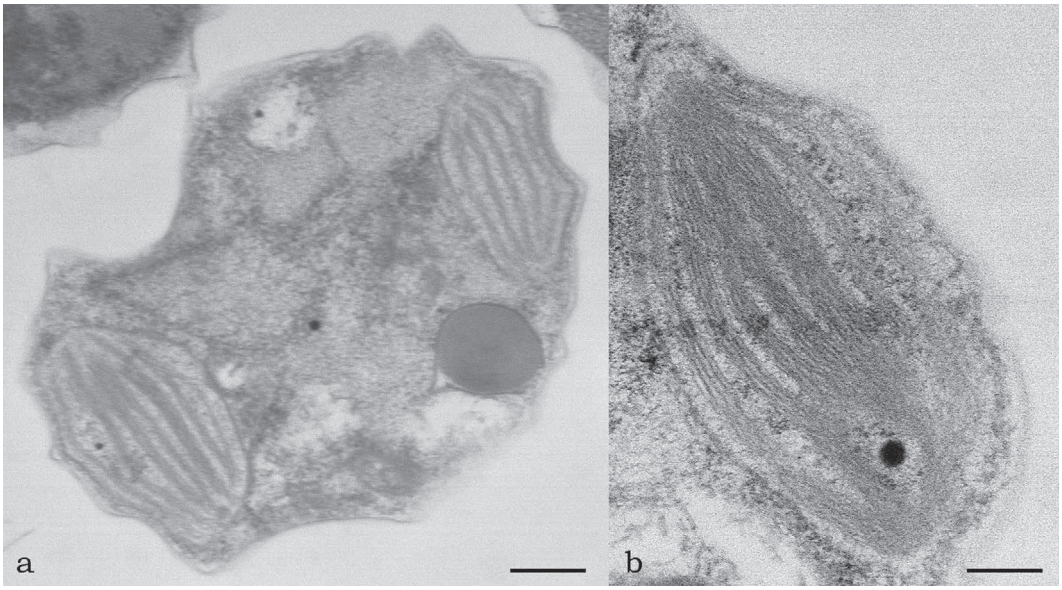


FIGURE 3.92 Transmission electron microscopy image of *Nannochloropsis* sp. in transverse section, showing the chloroplast (a). Scale bar 0.50 μm; chloroplast at higher magnification (b). Scale bar 0.10 μm.

Bacillariophyceae, Dictyochophyceae, and Phaeophyceae; violaxanthin in Eustigmatophyceae; and vaucheriaxanthin in Xanthophyceae. Other accessory pigments are β-carotene and xanthophylls such as diadinoxanthin, heteroxanthin, vaucheriaxanthin, antheraxanthin, and lutein. In the Raphidophyceae, marine and freshwater species differ in their accessory pigments, marine species possessing mainly β-carotene, fucoxanthin, and violaxanthin and freshwater species having β-carotene, diadinoxanthin, heteroxanthin, and vaucheriaxanthin.

Pyrenoids are present in all classes, except in the zoospores of the Eustigmatophyceae and in the freshwater species of Raphidophyceae. They are of a semi-immersed type, attached to the inner face of the chloroplast, pear-shaped in the Phaeophyceae or stalked in the Eustigmatophyceae. They can be one or many (Bacillariophyceae and Phaeophyceae). No storage material or capping vesicles have been found associated with pyrenoids, but lipid or oil droplets, normally distributed randomly in the chloroplast matrix, are often concentrated at the periphery of the pyrenoid.

Cercozoa—Chlorarachniophyceae

Five to seven bi-lobed chloroplasts are present inside these algae in a peripheral position. Each chloroplast is bounded by a system of membranes that may appear either as four separate membranes, as a pair of membranes with a sort of flattened vesicle between them, or as three membranes. Four separate membranes are always found near the proximal end of the pyrenoid and over the pyrenoid itself. The outer pair of membranes, when four are present, is referred to as a type of chloroplast endoplasmic reticulum; however, the inner pair is interpreted as the chloroplast envelope. The thylakoids are often loosely stacked in three, with no girdle lamella. Each chloroplast bears a central, pear-shaped pyrenoid projecting inward. Around the pyrenoid, often tightly associated with it, there are vesicles containing β-1,3-glucan, which is the principal storage carbohydrate. A nucleomorph that contains DNA and a nucleolus-like body is present between the second and third envelope of each chloroplast in a pocket located in the pyrenoid surface. Chloroplasts contain chlorophylls *a* and *b* and xanthophylls.

Miozoa—Dinophyceae

Chloroplasts may be present or absent in these algae, depending upon the nutritional regimen. When present, they are characterized by triple-membrane envelopes not connected with the endoplasmic reticulum; thylakoids are usually in groups of three, unappressed, and girdle lamellae are generally absent. Pyrenoids show various types, stalked or embedded within the chloroplast. DNA is organized into numerous nodules scattered throughout the chloroplast. About 50% of the dinoflagellates with plastids acquired them from a variety of photosynthetic eukaryotes by endosymbiosis (cf. Chapter 1). Hence, pigments other than chlorophyll *a* and c_2 (e.g. carotenoids, xanthophylls) change among the different groups.

The most common chloroplast type is the peridinin-type plastid; an example is *Amphidinium carterae*, probably derived from the red lineage by secondary endosymbiosis, that is, through the uptake of primary plastid-containing endosymbiont. Other groups of dinoflagellates have plastids derived from a tertiary endosymbiotic event, that is, the uptake of a secondary plastid containing endosymbiont. Tertiary plastids are present in the toxic genus *Dinophysis*, characterized by two-membrane, cryptophyte-derived plastids, which contain phycobilin (phycoerythrin) and alloxanthin, a typical cryptophyte carotenoid; in other important species (*Karenia* sp., *Gyrodinium aureolum*, *Gymnodinium galatheanum*) with fucoxanthin as accessory pigment, which possess haptophyte-derived plastids surrounded by two or four membranes; and in *Kryptoperidinium* sp. and close relatives, which have a five-membrane, ochrophyte-derived (diatom) plastid that includes a diatom nucleus of unknown complexity and fucoxanthin as accessory pigment.

A serial secondary endosymbiosis (the uptake of a new primary plastid-containing endosymbiont) occurred in *Lepidodinium* sp. and its close relatives, in which the peridinin plastid has apparently been replaced by a secondary plastid derived from a core chlorophyte alga and surrounded by two membranes.

Noctiluca scintillans presents a completely different plastid situation: this large and conspicuous dinoflagellate, common in coastal areas worldwide, has both a completely heterotrophic form and a green "photosynthetic" form, harboring thousands of free-swimming cells of the pedinophycean *Pedinomonas noctilucae*.

In addition to dinoflagellates with permanent plastids, there are several taxonomic groups of dinoflagellates with kleptoplastids (stolen plastids), which are temporary but functional plastids captured from prey. Table 3.2 shows a list of possible kleptoplastidic dinoflagellates and their possible origins. Most of these dinoflagellates seem to prefer to retain kleptoplastids derived from cryptophytes. Among the most-investigated cases is *Gymnodinium acidotum*; this dinoflagellate is

TABLE 3.2
List of Possible Kleptoplastidic Dinoflagellates and Plastid Origins

Species	Habitat	Species of Plastid Origin	Source of Plastid	Detection
Gymnodinium acidotum	Freshwater	*Chroomonas* spp. (Cryptophyceae)	Direct ingestion	Microspectrophotometry
Amphidinium latum	Marine	Chryptophyceae (Cryptophyceae)	NA	TEM
Amphidinium poeciliochroum	Marine	*Chroomonas* spp. (Cryptophyceae)	Direct ingestion	TEM
Cryptoperidiniopsis sp.	Marine	*Storeatula major* (Cryptophyceae)	Direct ingestion	TEM
Dinophysis acuminata	Marine	*Teleaulax amphioxeia* (Cryptophyceae)	*Myrionecta rubra*	PCR
Dinophysis mitra	Marine	Bacillariophyceae	Unknown ciliate	PCR
Gymnodinium gracilentum	Marine	*Rhodomonas salina* (Cryptophyceae)	Direct ingestion	TEM
Pfiesteria piscicida	Marine	*Rhodomonas* sp. (Cryptophyceae)	Direct ingestion	TEM

characterized by the temporary retention of engulfed chloroplasts of a cryptophyte endosymbiont, *Chroomonas* spp. The exact identification of the prey was performed by microspectrophotometry (cf. Chapter 7). Figure 3.93 shows the absorption spectrum of the chloroplast of *Gymnodinium acidotum* (Figure 3.93a) and the absorption spectra of the chloroplasts of three possible prey, *Chroomonas* sp. (Figure 3.93b), an unknown cryptophyta (Figure 3.93c), and *Cryptomonas* sp.

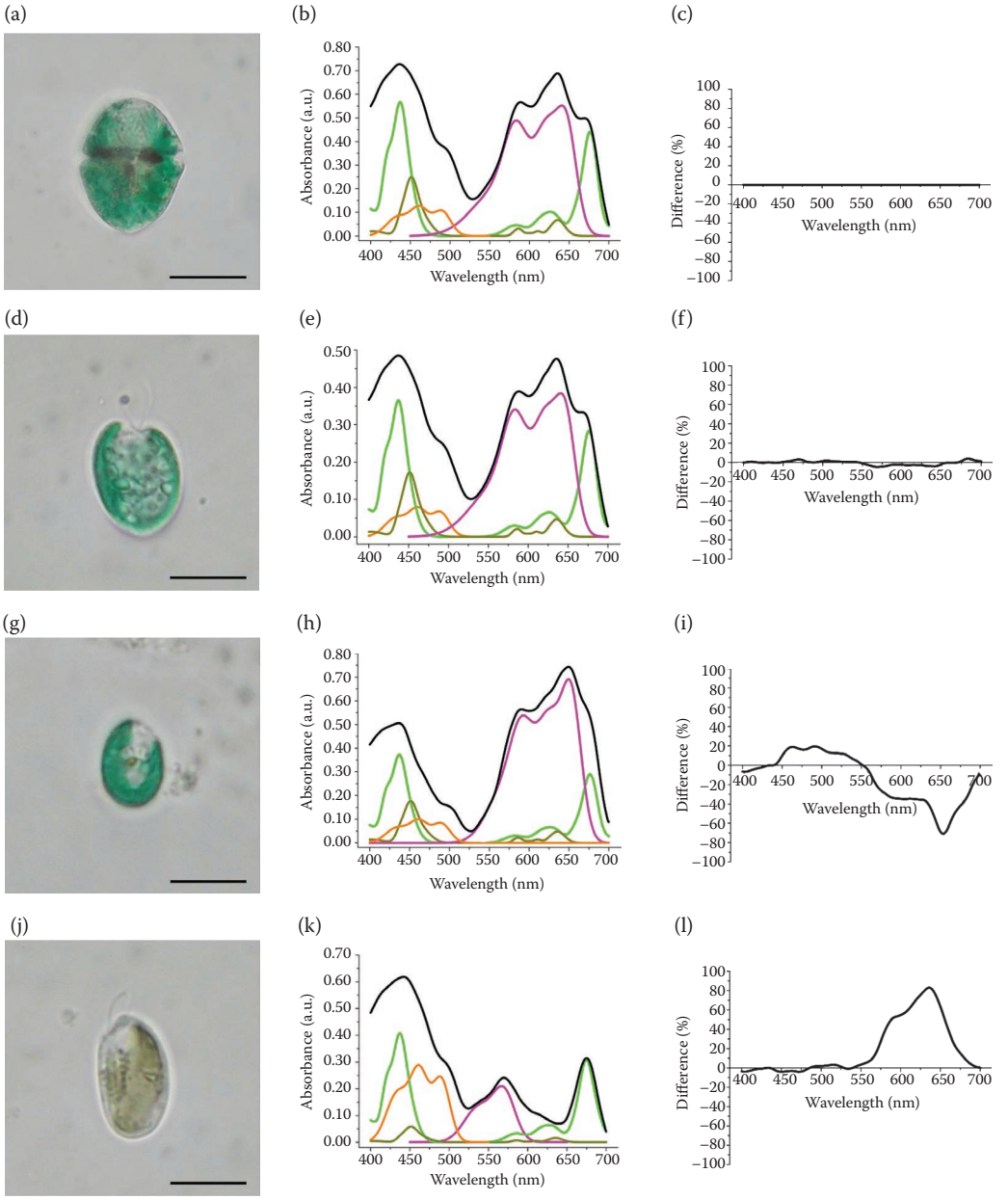


FIGURE 3.93 Absorption spectra of *Gymnodinium acidotum* and its possible prey. See text for details. Scale bar 10 µm. Bright green line: chlorophyll *a;* dark green line: chlorophyll *b;* orange line: carotenoids and xanthophylls; purple lines: phycobiliproteins.

(Figure 3.93d), and the difference spectra calculated between the absorption spectrum of the dinoflagellate and the absorption spectra of the three prey. This analysis confirmed that *Gymnodinium acidotum* preys only upon *Chroomonas* sp.

Euglenozoa—Euglenophyceae

As in the Dinophyta, the chloroplast envelope consists of three membranes. Chloroplasts are typically many per cell and show considerable diversity of size, shape, and morphology (Figures 3.94a and 3.94b).

Five main types can be recognized:

1. discoid chloroplasts with no pyrenoids (*Phacus*);
2. elongated or shield shaped chloroplasts with a central naked pyrenoid (*Trachelomonas*);

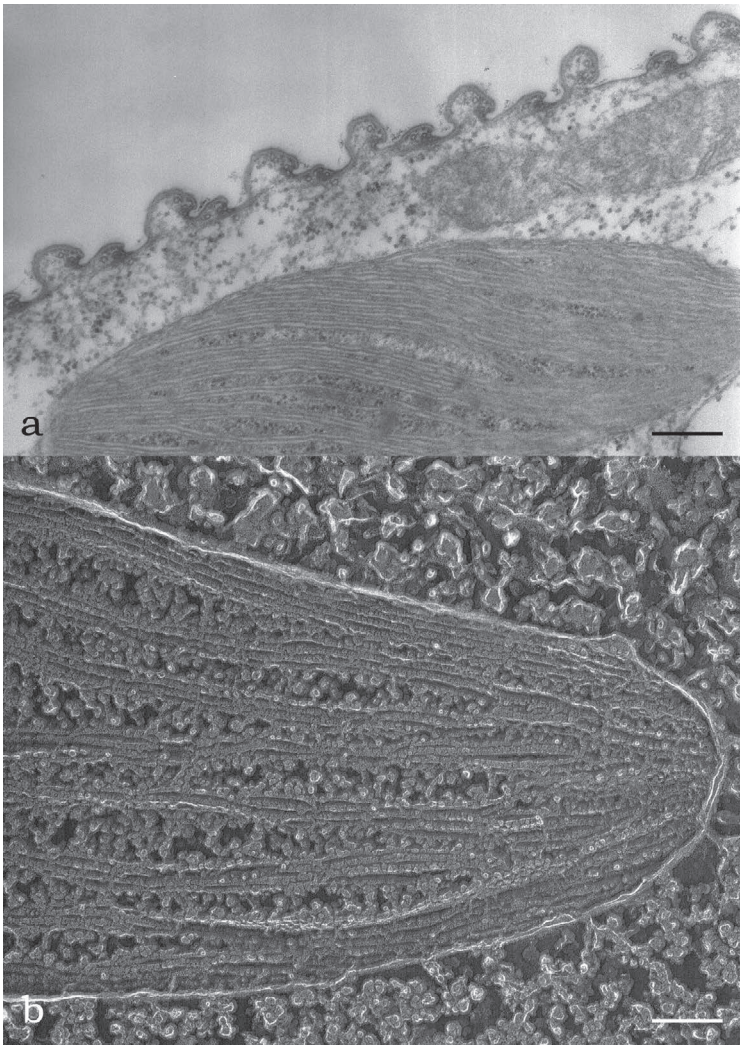


FIGURE 3.94 Transmission electron microscopy image of a chloroplast of *Euglena gracilis* in longitudinal section (a). Scale bar 0.10 µm. Deep-etching image of a chloroplast of *Euglena gracilis* (b). Scale bar 0.05 µm.

3. large plated chloroplasts with the so-called double-sheeted pyrenoid, that is, a pyrenoid that carries on both plastid surfaces a watch glass–shaped cup of paramylon (*Euglena obtusa*);
4. plated chloroplasts with a large pyrenoid projecting from the inner surface, which is covered by a cylindrical or spherical cup of paramylon (*Colacium*);
5. chloroplast ribbons radiating from one to or three paramylon centers (*Eutreptia*).

The chloroplasts are never connected to the nucleus by the endoplasmic reticulum, and thylakoids are usually grouped into threes, forming lamellae as in Ochrophyta and Dinophyta. Girdle lamellae are never found in this group. The photosynthetic pigments are chlorophylls *a* and *b*, with carotenes and xanthophylls as accessory pigments. Chloroplast DNA occurs as tiny granules throughout the whole stroma.

The Nucleus, Nuclear Division, and Cytokinesis

An organized nucleus is absent in Cyanobacteria, where DNA molecules are free in the cytoplasm. The central region of those algae features the naked (without histone proteins) circular DNA, which is not contained within a double membrane and consists of a single unbranched molecule. Transcription and translation processes are accomplished by the assistance of abundant 70s ribosomes located in the centroplasm. These ribosomes are smaller than their counterparts in the eukaryotic cytoplasm but are typical of all prokaryotes, mitochondria, and chloroplasts. Cyanobacteria can only reproduce asexually but appear to have some forms of genetic recombination possible, which are divided into two categories: transformation and conjugation. Transformation occurs when DNA is shed by one cell into the environment, taken up by another cell, and incorporated into its genome, replacing homologous sections of DNA. The ability to be transformed by external DNA is species specific and typically requires special environmental conditions. Conjugation is a "parasexual" process in which one of the partners develops a conjugation tube that connects to the recipient cell. Typically a plasmid (a small circle of DNA) from the donor cell passes through the conjugation tube. It is thought that genes for gas vacuolation, antibiotic resistance, and toxin production are carried on plasmids in cyanobacteria.

In eukaryotic algae, genetic information in the form of DNA, together with the controlling services for its selective expression, occurs in plastids (plastome), mitochondria (chondrome), and the cell nucleus (genome). In the previous section, we described the organization and behavior of chloroplast DNA, which are similar to those of mitochondria. It is worthwhile to recall that plastid and mitochondrial genes and the way in which they are expressed have much in common with the system of gene expression of prokaryotes, and there are many plastid genes with extended introns that are very rare in prokaryotes (genes are mosaics of introns and exons). Introns are DNA sequences of unknown function that are removed in the primary mRNA transcript. Exons are DNA sequences that code for amino acids.

In the nucleus of eukaryotic algae, long, linear, unbranched molecules of DNA are associated with proteins and small amounts of RNA. Two types of proteins are found: the relatively uniform histones (about 20), involved in the structural organization of the DNA, and the very variable proteins involved in gene activity regulation, such as DNA and RNA polymerases. The DNA-protein complex, made up of repeating units termed nucleosomes, is known as chromatin, which is usually highly dispersed in the interphase nucleus. During mitosis and meiosis metaphases, the DNA-protein complexes are more helically condensed around the nucleosome and form the chromosomes, each chromosome consisting of a single DNA molecule.

The nucleus is surrounded by a two-membrane envelope continuous with the endoplasmic reticulum. Between the two membranes, there is a narrow perinuclear space about 20 nm wide. The nuclear envelope is perforated by numerous pores 60–100 nm in diameter. Nuclear pores have a complicated superstructure; they are not simply free openings but are gateways in nuclear envelope

through which the controlled transport of macromolecules (RNA, proteins) takes place. Pores can be arranged in straight lines as in *Bumilleria* (Xanthophyceae), in closely hexagonal groups as in *Prorocentrum* (Dinophyceae), or randomly distributed as in *Glenodinium* (Dinophyceae).

All algal nuclei possess nucleoli that vary in shape, size, and number in the different algal divisions. Nucleoli are dense concentrations of ribonucleoprotein-rich material, which are intimately associated with the specific region of the chromosomal DNA coding for ribosomal RNA. Nucleoli can be single and central as in *Cryptomonas* (Cryptophyceae) or can number more than 20 scattered in the nucleus as in *Euglena acus* (Euglenophyceae).

In eukaryotic algae, the features of the interphase nucleus, DNA replication, and processes of transcription and translation in the expression of genetic information and cytokinesis are comparable to those of all the other eukaryote. Exceptions to this rule will be described.

Rhodophyta

The basic features of mitosis and cytokinesis are the same throughout the division, though some variation may occur. Unlike other groups of eukaryotic algae, where the mitotic spindle is formed between two pairs of centrioles, one at each spindle pole, in red algae, the poles of the spindle are marked by ring-shaped structures or short hollow cylinders named polar rings or nuclear associated organelles (NAOs). The absence of centrioles reflects the complete absence of flagella in the red algae. The chromosomal and interzonal microtubules do not converge towards the polar rings, so the spindle poles are very broad. The nuclear envelope does not break down, though it is perforated by large holes; hence, mitosis is closed. The spindle persists for some time at early telophase, holding daughter nuclei apart; it collapses only at late telophase, when daughter nuclei are kept separated by a vacuole. Cytokinesis is by centripetal furrowing but is typically incomplete; the furrow impinges upon the vacuole but leaves open a cytoplasmic connection between sibling cells. This connection is then filled and blocked by a proteinaceous stopper, named the pit plug; a membrane continuous with the cell membrane generally covers the surfaces of pit plugs, which do not have a translocatory function like plasmodesmata of other algae and plants. The simplest type of pit plug consists only of a proteinaceous core; two- or one-layered caps partly composed of polysaccharides can border the core of both sides with different thicknesses. A cap membrane can be present between the two layers of the cap or bounding the plug core.

Prasinodermatophyta, Chlorophyta, Charophyta

Nuclear and cell division have been intensively and extensively studied in the green algae in light microscopy and at the ultrastructural level, and several different patterns have been recognized. Two basic patterns have emerged from these studies regarding nuclear and cell division in green algae:

1) intranuclear mitosis, with the nuclear envelope closed at metaphase or open at the poles, interrupted by the microtubules of the spindle; other microtubules, transverse to the longitudinal axis of the spindle, are present at telophase and are called the phycoplast; the latter functions somehow in cytokinesis, by furrowing or by cell-plate formation; the daughter nuclei at telophase are in close proximity;
2) the spindle and nuclear envelope are open and a phycoplast is absent; at telophase the microtubules of the intranuclear spindle are persistent, and a phragmoplast-like structure is organized as cytokinesis by furrowing proceeds.

Cylindrocapsa is an example of the first type; the parietal chloroplast divides before mitosis. Two pairs of centrioles are already present at the beginning of the interphase. In early prophase, the nuclear envelope become surrounded by one or two layers of endoplasmic reticulum, which is rough, that is, covered by ribosomes. Perinuclear microtubules appear around the nucleus, and in late prophase they proliferate within the nucleus to form a tilted mitotic spindle between the pairs

of centrioles lying at the spindle poles. At metaphase, the nuclear envelope is still intact and surrounded by the endoplasmic reticulum so that mitosis is closed. The fully condensed chromosomes become aligned to form a distinct metaphase plate and have plate-like layered kinetochores. The non-persistent telophase spindle soon degenerates, though a few microtubules can still be found around the re-formed nuclear envelopes. The pairs of centrioles migrate around the telophase nuclei, away from the former spindle poles and towards the center of the equatorial plane, where they remain until after cytokinesis.

Cisternae of endoplasmic reticulum proliferate in the narrow zone of cytoplasm present between the two daughter nuclei in the center of the cell. They bleb off smooth endoplasmic reticulum vesicles, which become aligned in the equatorial plane to form a cell plate of smooth vesicles. These vesicles coalesce to form a transverse system separating the daughter cells. Here the vesicles accumulate within a phycoplast, that is, a plate of microtubules lying in the future plan of division. After completion of the transverse septum and the resultant separation of the daughter cells, a new cell wall is secreted around each daughter protoplast by exocytosis of Golgi-derived vesicles containing wall material. Each daughter cell thus gains a complete new wall; in the case of *Cylindrocapsa*, daughter cells remain united to form filaments, since the parental walls are persistent. In the case of other green algae with this type of mitosis and cytokinesis, daughter cells are liberated from the parent cell wall as non-flagellate autospores or as zoospores with centrioles ready to form flagella.

Coleochaete possess the second type of nuclear and cell division; the chloroplast begins to cleave at prophase; the single centriolar pair present during the interphase replicates at prophase, and each of the two pairs takes up a position at one pole of the future spindle. Microtubules then form between the centriolar pairs, outside the envelope of the elongate prophase nucleus. The mitosis is open, since the nuclear envelope breaks down during metaphase; endoplasmic reticulum vesicles are present among the spindle microtubules. The chromosomes align in a distinct metaphase plate, but the chromosomal microtubules do not attach to defined kinetochores. At early telophase, daughter nuclei become separated through elongation of the spindle, which is persistent during telophase and holds the nuclei far apart.

By the end of telophase, new microtubules proliferate and surround the spindle microtubules, forming the phragmoplast, which includes also actin filaments. Golgi-derived vesicles appear within the phragmoplast, guided by the microtubules and filaments to the future plane of division, where they become arranged to form a cell plate. The vesicles contain cell wall material, and their coalescence produces a transverse septum consisting of two cell membranes with the new transverse wall between them. Since the coalescence is not complete, connections leading to plasmodesmata are left between the daughter cells. This type of mitosis and cytokinesis is rare in the green algae but is the common mode of division in plants such as bryophytes and tracheophytes.

Cryptophyta

These algae possess a peculiar organelle termed the nucleomorph located in the space between the chloroplast endoplasmic reticulum and the chloroplast envelope. This organelle has a double membrane around it, pierced by pores, and contains both DNA and a nucleolus-like structure where rRNA genes are transcribed. The DNA is organized in three small chromosomes encoding genes for its own maintenance. It possesses the ability to self-replicate without forming a spindle during mitosis. It is considered a vestigial nucleus belonging to a photosynthetic eukaryotic symbiont.

Miozoa—Dinophyceae

The dinoflagellate nucleus, known as dinokaryon, is bounded by a nuclear envelope penetrated by pores in the usual eukaryotic fashion. However, it possesses a number of unusual features, including high amounts of DNA per cell (five to ten times the most common eukaryotic levels, up to a maximum of 200 picograms in *Gonyaulax polyedra*). It is relatively large, often occupying about

one half of the volume of the cell. Nuclear shapes are variable, ranging from spheroid to U-, V-, or Y-shaped configurations. In most dinoflagellates, the chromosomes remain continuously condensed and visible by both light and electron microscopy during interphase and mitosis. Chromosome counts range from 12 to around 400 but may be variable within a species. A prominent nucleolus is also persistent. Each chromosome consists of a tightly super-coiled structure of DNA double helix. The permanent condensed chromosome shows a swirled, fibrillar appearance due to the naked DNA double helices (i.e. no histones are present). The 3–6-nm fibrils are packed in a highly ordered state, up to six levels of coiling. A small amount of basic protein is present in a few species, such as *Oxyrrhis marina*, but none of it corresponds in amino acid content to the histones normally present in eukaryotic chromosomes. A further peculiarity of dinoflagellate chromosomes is the high amount of calcium and other divalent metals, such as iron, nickel, or copper, which may play a role in chromosomal organization. In some dinoflagellates, such as *Noctiluca* and *Blastodinium*, the chromosomes undergo an expanded, decondensed change during interphase and are termed noctikaryotic.

Dinoflagellate mitosis is also unusual. At the time of division, chromosomes divide longitudinally, the split starting at one end of the chromosome and moving along the entire length. The nucleus is invaded by cytoplasmic channels that pass from one pole to the other. Microtubules are present in these channels. The nuclear envelope and the nucleolus are persistent throughout nuclear division. The chromosomes, upon dividing, assume a V or Y configuration, and the apices of such chromosomes are closely associated with the nuclear envelope surrounding a cytoplasmic channel. This association suggests that the cytoplasmic channels serve as a mechanism for the movement of chromosomes.

The nuclear envelope persist during mitosis (closed mitosis), as it does in other algae, such as Euglenophyta and Raphidophyceae. However, with the exception of *Oxyrrhis marina*, where mitotic spindle is intranuclear, the chromosomes do not appear fibrillar, and the mitosis strongly resembles that of *Euglena*, with the mitotic spindle always extranuclear. The spindle microtubules pass through furrows and tunnels that form in the nucleus at prophase. No obvious spindle pole bodies other than concentric aggregation of Golgi bodies are present. Some microtubules contact the nuclear envelope, lining the tunnels at points where the chromosomes also contact. The chromosomes have differentiated dense regions inserted into the envelope.

Dinoflagellate cells undergo binary fission, and each daughter cell can retain half the parent cell wall, which splits along a predetermined fission line. This mode of reproduction is called "desmoschisis," and examples are *Ceratium* and many *Gonyaulax* species. In other dinoflagellates, daughter cells do not share the parent cell wall; this mode of division is called "eleutheroschisis." Binary fission may take place either inside the mother cell (many freshwater *Peridinium* species), or the protoplast may leave the mother cell wall before division through a hole or slit. In thecate species (many marine *Protoperidinium* species), the protoplast escapes, after special thecal plates are dislocated, through a hole. In several species, the protoplast has no flagella and deforms its cell wall during the escape from the mother theca; however, this is not a typical amoeboid stage. After cell division, each daughter cell produces a new cell wall or a new theca in thecate cells.

Euglenozoa—Euglenophyceae

In these algae, the interphase nucleus lies in the central or posterior region of the cell; it is spherical in most spindle-shaped species and ovoid or long and narrow in elongate cells. In the largest species, the nucleus is at least 30 × 15 μm in dimension, but in small species, the spherical nucleus may be less than 2 μm in diameter. The chromosomes retain their condensed condition throughout interphase, appearing as granular or filamentous threads (Figures 3.95a and 3.95b). In some nuclei the chromosomes radiate from the central endosome, while in others (even in the same species), they coil haphazardly throughout the nucleoplasm. Mitosis begins with a forward migration of the nucleus so that it comes to lie immediately posterior to the reservoir. In species with several endosomes in the interphase nucleus, these usually fuse to form a single body. The endosome then

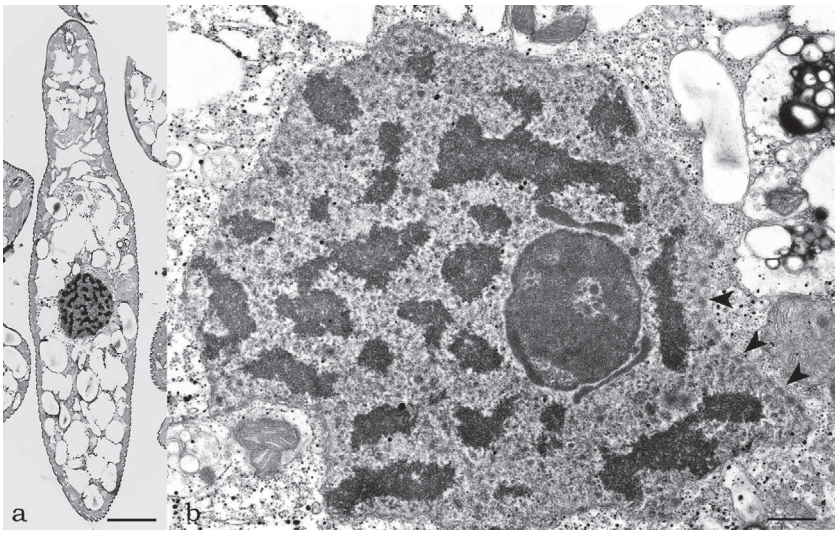


FIGURE 3.95 Transmission electron microscopy image of the WZSL mutant of *Euglena gracilis* in longitudinal section, showing the central nucleus with the condensed chromosomes (a). Scale bar 3 μm. Transmission electron microscopy image of the WZSL mutant of *Euglena gracilis* nucleus, showing the nucleolus, the satellite nucleoli, and the nuclear membrane pores (arrowhead) (b). Scale bar 0.3 μm. Courtesy of Giovanna Rosati.

elongates along the divisions axis, perpendicular to the long axis of the cell, and the chromosomes orient into the metaphase position, following three main types of orientation:

1) pairs of chromatids from late prophase orient into a circlet of single chromatids, separation and segregation having occurred during orientation (*Euglena gracilis*);
2) pairs of chromatids from interphase and/or prophase come to lie along the division axis still as pairs, parallel to one another and to the elongated endosomes (*Euglena communis, Euglena viridis*);
3) single chromosomes from prophase line up along the division axis and there undergo duplication into the pairs of chromatids of that mitosis (*Euglena acus*, *Euglena spirogyra*).

These different types overlap to a certain extent, species differing mainly in the time at which the double structure of the chromosomes first becomes microscopically visible. In all cases, the endosome continues to elongate and the chromatids segregate toward the ends of the endosome into two daughter groups. This stage, with most but not quite all of the daughter chromosomes separated, must be called metaphase in *Euglena*. During this early-to-late metaphase succession, the locomotor apparatus (flagella, photoreceptor, and eyespot) replicates and the reservoir divides. The daughter reservoirs open into the still-single canal, but each now has its own contractile vacuole, eyespot, and flagella. Separation, segregation, and anaphasic movements of the chromatids are irregular, and this, coupled with a very low chromatid velocity, results in an extremely long anaphase. The end of the anaphase is marked by a sudden flowing to the poles of the central region of the elongated endosome, and the persistent nuclear envelope seals around the groups of chromatids and the daughter endosomes to form the telophase nuclei. Once telophase is established, with separate daughter nuclei, one of the two flagella in each daughter reservoir grows to emerge as a locomotory flagellum. A cleavage line is initiated between the now-distinct daughter canals and progresses helically backward to separate the daughter cells.

High chromosome numbers are the rule for species of Euglenophyta, indicating a possible polyploidy.

Ejectile Organelles and Feeding Apparatus

In this section, we will describe organelles that, upon stimulation by contact, heat or chemical, discharge a structure such as a tread or a tube from the surface of the cell. These organelles may serve for defense purpose or as feeding adjuvants.

Prasinodermatophyta, Chlorophyta, Charophyta

Some *Pyramimonas* species (Pyramimonadophyceae) contain ejectile structures similar to the ejectosomes of Cryptophyta. In the undischarged state, they consist of a coiled ribbon, which upon discharge forms a hollow tube tapered at both ends.

Haptophyta

During its motile stage, *Phaeocystis* can eject ribbon-like filaments a few tens of nanometers wide and several tens of micrometers long. Their interconnections form a five-branched star-like configuration (Figure 3.96). The winding of the filaments inside vesicles, as well as their axial twist, are probably the consequences of their biosynthesis within a confined space. As a result, the

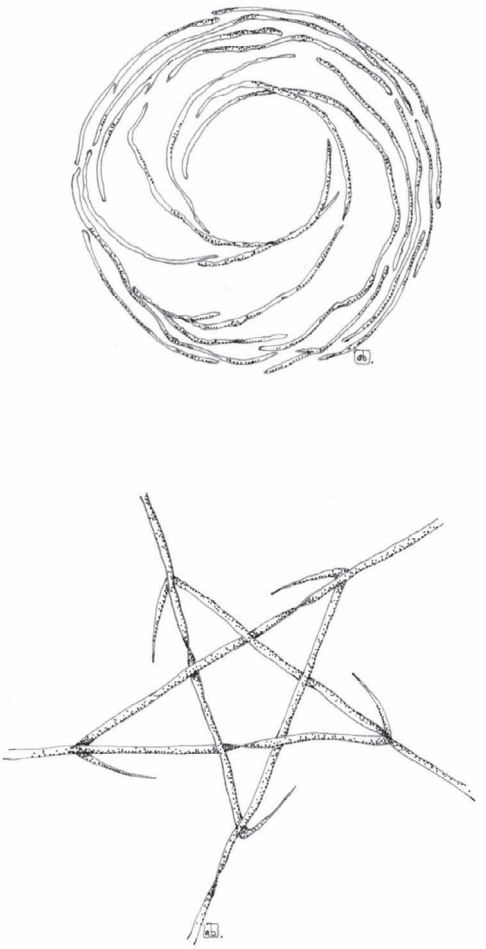


FIGURE 3.96 Ejectile organelles of *Phaeocystis* sp. Coiled filaments before released (top); star-like configuration after release (bottom).

filaments behave like spring-coils whose stored energy is released once the vesicles are broken and the filaments ejected. Using electron diffraction techniques, the filaments have been unambiguously characterized as being made of α-chitin crystals, the polymer chain axis lying along the filament direction. These chains are antiparallel arranged (allomorph), and this arrangement has never been reported before in the algal world.

Cryptophyta

These algae possess large refractile ejectosomes, lining the oral groove, and small ejectosomes scattered around the cell surface at the anterior corners of the periplast plates. An undischarged ejectosome is a tightly coiled, tapered ribbon that is wound with the wider end toward the outside; a smaller coil is attached to it and lies in the depression of the larger one. Prior to release, ejectosomes are enclosed within vesicles. The large ejectosomes are explosive organelles. If cryptophyte cells are irritated by mechanical or chemical stress, they escape the potentially lethal influences by discharging the ejectosomes: the cells jump backwards in fast zigzag movements through the water. When discharged, the ribbon unfurls, with the shorter segment forming a beaklike tip on the longer. The edges of the ribbon tend to curl inwards, producing circular and e-shaped profiles in cross-section (Figure 3.97).

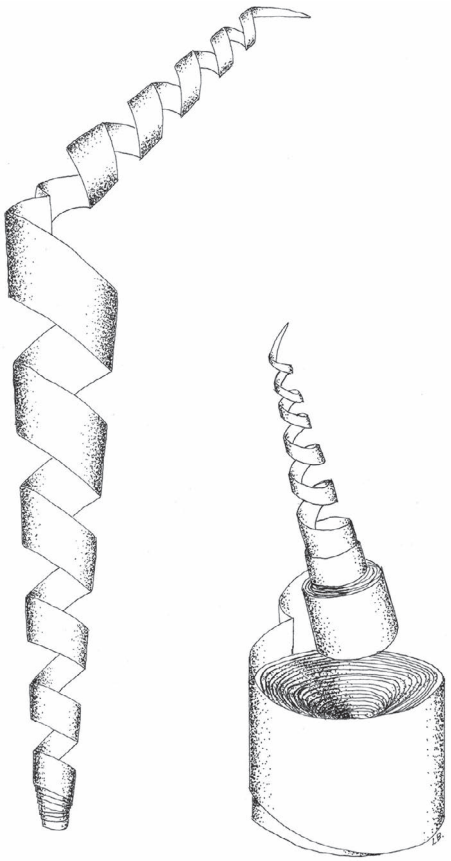


FIGURE 3.97 Ejectile organelles of a cryptophyte. Discharging ejectosome (left) and reel of an undischarged ejectosome just beginning to be pulled out (right).

Ochrophyta

Many species of Raphidophyceae have extrusome organelles that explode on strong stimulation, throwing out up to 200-µm-long slime threads. The material produced may surround a motile individual with mucilage so that it becomes palmelloid.

Cercozoa—Chlorarachiophyceae

Structures interpreted as ejectile organelles (extrusomes) are commonly seen in *Bigelowiella natans*. Each organelle resides in a vesicle and consists of two parts. The anterior part is very short, measuring circa 0.15 µm in length, whereas the posterior part is circa 0.55 µm long. The posterior part has a very distinct substructure, comprising a core surrounded by a less opaque cylinder. The cylinder is lined by a thin membrane-like structure, whereas the core comprises a thinner membranous structure surrounded by a more opaque one. The structure of the anterior part of the ejectile organelle is less well defined. Although it is clear that the membrane of the surrounding vesicle forms an indentation ring that separates the two parts of the ejectile organelle, the path of the membrane in this area is less clear. It appears that only the core of the organelle is discharged, the core apparently turning inside out during discharge. The surrounding cylinder seems to remain in place. The fate of the anterior part of the ejectile organelle after discharge has not been ascertained (Figure 3.98).

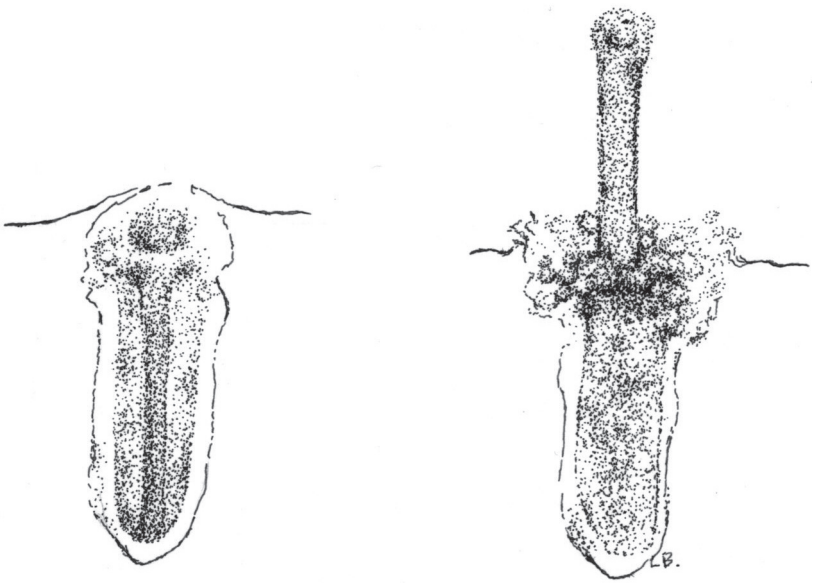


FIGURE 3.98 Ejectile organelle of *Bigelowiella natans* before (left) and during discharge (right).

Miozoa—Dinophyceae

The most common type of extrusomes, with an almost universal occurrence in the motile phase of these algae, are trichocysts, that is, rod-shaped bodies that, when mature, usually lie in the amphiesma perpendicular to the cell membrane (Figure 3.99). The shaft is a paracrystalline, proteinaceous rod a few micrometers in length, rectangular in cross-section. At its distal end, it extends as a group of twisted fibers. The whole is enclosed within a membranous sac, and there is a sheathing material between the rod and the membrane. The tip of the sac is in contact with the cell membrane, passing through the amphiesmal vesicles and the thecal plates, if present. Trichocysts are formed in the vicinity of the Golgi body and move to the cell periphery. They are apparently discharged by a

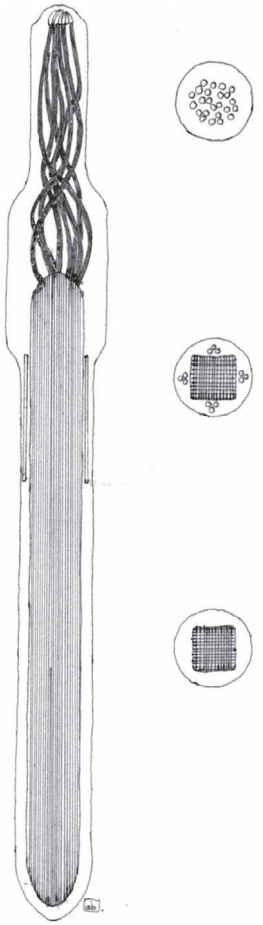


FIGURE 3.99 Undischarged trichocyst of *Gonyaulax poliedra* in longitudinal and transverse sections.

rapid hydration process, the discharged structures measuring up to 200 μm in length. Their function is unknown, but it is assumed to be defensive, excretory, or both.

A less ordered type of extrusomes in dinoflagellates is the mucocyst, a simple sac with granular content, associated with the release of mucoid material. They are located just beneath the cell membrane and are often aggregated in the region of the sulcus; their release in some species is correlated with the psammophilous existence of these algae, facilitating the attachment of the cells to sand grains along the seashore.

More elaborate extrusomes termed nematocysts are found in genera such as *Polykrikos kofoidi* and *Nematodinium*; usually only about 8 to 10 nematocysts are present per cell. These organelles are larger than trichocysts and can reach 20 μm in length. They are conical, fluid-filled sacs with a capitated blunt end. Most of the body consists of a large posterior chamber, from which a smaller anterior chamber is isolated; the whole structure is capped by a lid-like operculum. A sharp stylet in the anterior chamber is connected to a tubular filament in the posterior chamber (Figure 3.100).

Feeding structures are present in dinoflagellates, depending on the type of feeding mechanisms present: feeding tube (peduncle or tentacle) and feeding veil (pallium).

Tube feeding is commonly found among both naked and thecate species of dinoflagellates (e.g. *Dinophysis, Amphidinium, Gyrodinum, Peridinopsis*). Cell membrane is extruded from the

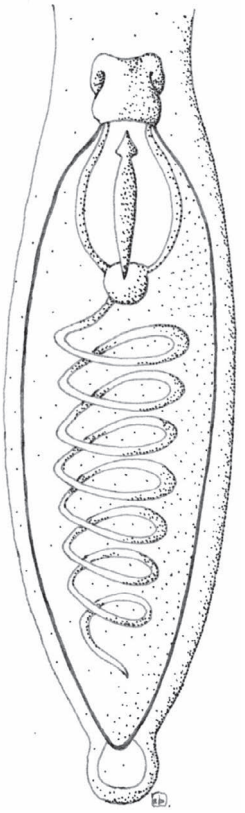


FIGURE 3.100 Nematocysts of *Polykrikos kofoidi*.

cell to form a tube, which can engulf whole cells or penetrate prey cell walls and suck in prey cytoplasm.

Pallium feeding has only been described for heterotrophic thecate species such as *Protoperidinium* and *Diplopsalis*. The prey is captured via a primary attachment filament; an extension of the cytoplasm then emerges from the region of the sulcus-cingulum, which encloses the prey as a veil (pallium). Enzymatical digestion of the prey cytoplasm is brought about inside the veil, and the products are then transported to the predator.

Direct engulfment is mainly found among naked species (e.g. *Gyrodinium, Gymnodinium, Noctiluca*); recently, however, some thecate species have been shown to use this feeding mechanism as well. Feeding behavior in dinoflagellates involves several steps prior to actual ingestion, including precapture, capture, and prey manipulation. As feeding mechanisms allow the ingestion of relatively large prey, or parts thereof, dinoflagellates are regarded as raptorial feeders. While prey size plays an important role in the ability of dinoflagellates to ingest food, this cannot alone explain prey preferences actually found. Some dinoflagellate species can be very selective in their choice of prey, while others show a remarkable versatility.

Euglenozoa—Euglenophyceae

Trichocysts are present only in some phagotrophic species, such as *Entosiphon* and *Peranema trichophorum*. In *Peranema*, ejectile organelles or mucocysts are located beneath the cell surface, often subtending the pellicular articulations. In transverse sections, they appear as hollow tubes of amorphous material, with low electron density, enclosed within a vesicle bounded by

single membrane, often found near the Golgi apparatus, or they show a content of greater density and may subtend the pellicle or protrude through it. Mucocysts subtending the pellicular articulations are ejected from the cell through the grooves. They are characterized by three distinct regions: an inner tube 1.20 μm long and 1.18 μm wide with helical striations, an outer tube 0.77 μm long and 0.21 μm wide with diamond-shaped pattern, and a dense middle band 0.07 μm in width. Often a crown of dense fibrillar material occurs at the tips of the mucocyst. Small slime-extruding mucus bodies are the trichocyst counterparts commonly found in the non-phagotrophs (Figure 3.101).

A feeding apparatus is present in many Euglenophyceae, such as *Diplonema, Ploeotia*, or *Entosiphon*. In the latter (Figure 3.102a), it consists of a cytostome surrounded by four centrally located vanes (series of plicate folds or curved ribbons) and supported by rods composed of closely

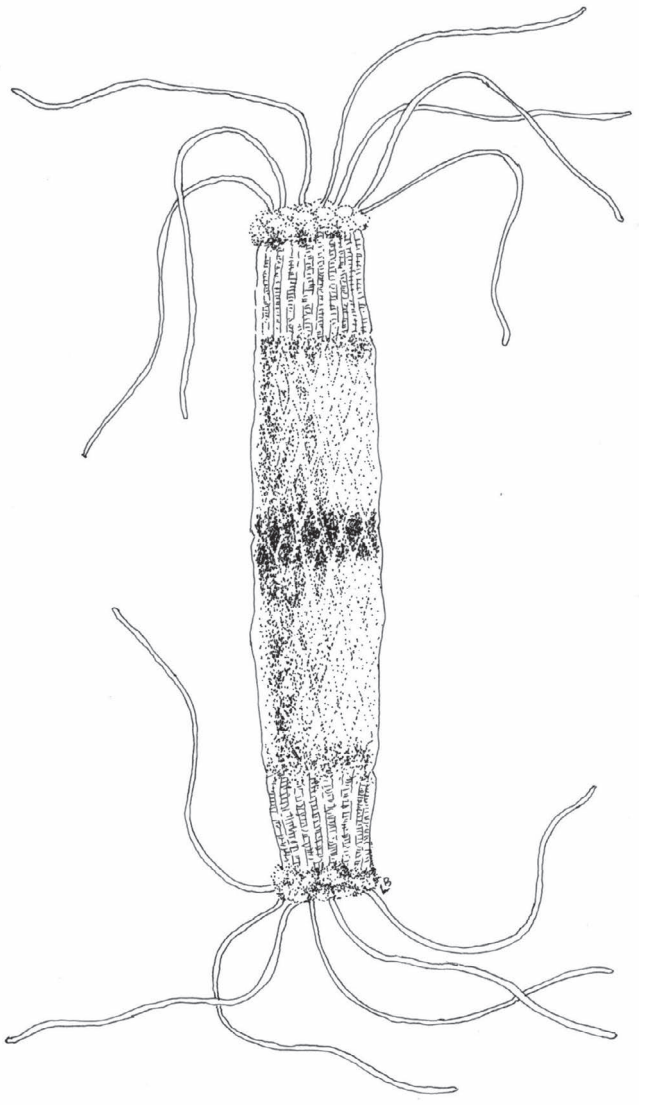


FIGURE 3.101 Ejected mucocyst of *Peranema trichophorum*.

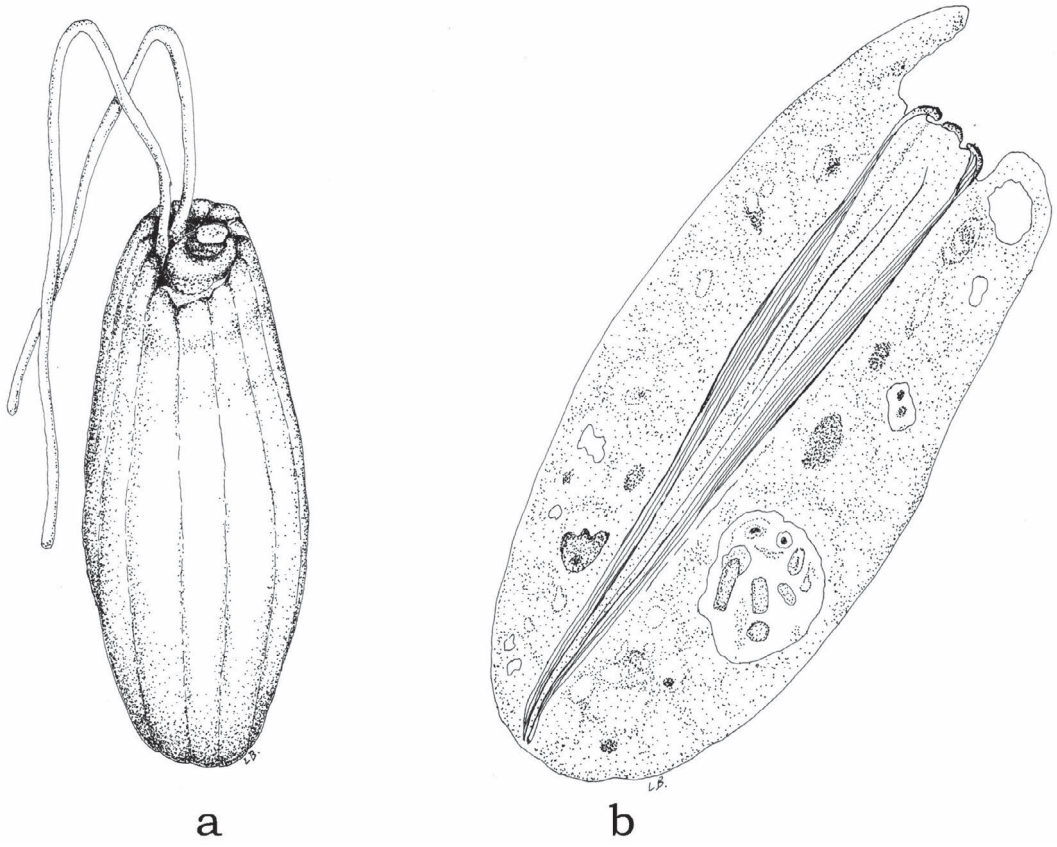


FIGURE 3.102 Cell of *Entosiphon* sp. (a); longitudinal section of the cell, showing the structure of the feeding apparatus (b).

packed microtubules. Near the base of the feeding apparatus, one of the rods splits, giving rise to a total of three stout rods that extend nearly the length of the cell. About one third the distance down the apparatus (from the anterior end), the number of microtubules per rod increases dramatically and then decreases toward the base, giving the apparatus the overall appearance of a cone with one side open (Figure 3.102b). This feeding apparatus can be moved in and out, extending toward the anterior of the cell and then drawing down into the cell for a distance of 3–5 μm. This motion allows food to be drawn into the cell.

SUGGESTED READING

Aihara, Y., Maruyama, S., Baird, A.H., Iguchi, A., Takahashi, S. and Minagawa, J. Green fluorescence from cnidarian hosts attracts symbiotic algae. Proceedings of the National Academy of Sciences, 116, 2118–2123, 2019.

Albertano, P., Barsanti, L., Passarelli, V. and Gualtieri, P. A complex photoreceptive structure in the cyanobacterium *Leptolyngbya* sp. Micron, 31, 27, 2000.

Barlow, H.B. The physical limits of visual discrimination. In: Photophysiology, Giese, A. (Ed.). Academic Press, London, New York, 1964.

Barsanti, L. and Gualtieri, P. Anatomy of *Euglena gracilis*. In: The handbook of algal science, microbiology, technology, and medicine, Konur, O. (Ed.). Elsevier, Amsterdam, 2020.

Barsanti, L., Coltelli, P., Evangelista, V., Passarelli, V., Frassanito, A.M., Gualtieri, P. Low resolution characterization of the 3D structure of the *Euglena gracilis* photoreceptor. Biochem Biophys Research Commun, 375, 471–476, 2008.

Barsanti, L., Evangelista, V. and Passarelli, V. Paolo Gualtieri. In vivo absorption spectra of the two stable states of the *Euglena* photoreceptor photocycle. Photochem Photobiol, 85, 304–309, 2009.

Barsanti, L., Evangelista, V., Passarelli, V., Frassanito, A.M. and Gualtieri, P. Fundamental questions and concepts about photoreception and the case of *Euglena gracilis*. Integrative Biology, 4:1, 22–36, 2012.

Barsanti, L., Evangelista, V., Passarelli, V., Frassanito, A.M., Coltelli, P. and Gualtieri, P. Microspectrophotometry as a method to identify kleptoplastids in the naked freshwater dinoflagellate *Gymnodinium acidotum*. Journal of Phycology, 45:6, 1304–1309, 2009.

Barsanti, L., Frassanito, A.M., Passarelli, V., Evangelista, V., Etebari, M., Paccagnini, E., et al. *Tetraflagellochloris mauritanica* gen. et sp. nov. (Chlorophyceae), a new flagellated alga from the Mauritanian desert: Morphology, ultrastructure, and phylogenetic framing. Journal of Phycology, 49:1, 178–193, 2013.

Barsanti, L., Gualtieri, P. Swimming patterns of the quadriflagellate *Tetraflagellochloris mauritanica* (Chlorophyceae, Chlamydomonadales). Journal of Phycology, 52, 209–218, 2016.

Barsanti, L., Passarelli, V., Walne, P.L. and Gualtieri, P. The protein of *Euglena gracilis* Photoreceptor. FEBS Letters, 482, 247–251, 2000.

Barsanti, V., Passarelli, V., Walne, P.L. and Gualtieri, P. In vivo photocycle of the *Euglena gracilis* photoreceptor. Biophysical Journal, 72, 545, 1997.

Beek, P.L. The long and the short, of flagellar length control. Journal of Phycology, 39, 837–839, 2003.

Bouck, G.B. and Ngo, H. Cortical structure and function in euglenoids with reference to trypanosomes, ciliates, and dinoflagellates. International Review Cytology, 169, 267–318, 1996.

Bouck, G.B. The structure, origin, isolation and composition of the tubular mastigonemes of *Euglena gracilis*. Journal Cell Biology, 50, 362–384, 1971.

Brett, S.J., Perasso, L. and Wetherbee, R. Structure and development of the cryptomonad periplast: A review. Protoplasma, 181, 106–122, 1994.

Buetow, D.E. (Ed.). The biology of *Euglena*. General biology and ultrastructure. Academic Press, New York, 1968.

Buetow, D.E. (Ed.). The biology of *Euglena*. Physiology. Academic Press, New York, 1982.

Buetow, D.E. (Ed.). The biology of *Euglena*. Subcellular biochemistry and molecular biology. Academic Press, New York, 1989.

Cordoba, J., Perez, E., Van Vlierberghe, M., Bertrand, A.R., Lupo, V., Cardol, P. and Baurain, D. De novo transcriptome meta-assembly of the mixotrophic freshwater microalga *Euglena gracilis*. Genes, 12, 842, 2021.

Daugbjerg, N. *Pyramimonas tychotreta*, a new marine species from Antarctica: Light and electron microscopy of the motile stage and notes on growth rates. Journal of Phycology, 36, 160–171, 2000.

Dodge, J. Photosensory systems in eukaryotic algae. In: Evolution of the eye and visual system, Cronly-Dillon, J.R. and Gregory, R.L. (Eds.). Macmillan Press, London, 1991.

Dodge, J.D. and Crawford, R.M. A survey of thecal fine structure in the Dinophyceae. Botanical Journal of Linnean Society, 63, 53–67, 1970.

Dusenbery, D.B. Sensory ecology. Freeman, New York, 1992.

Ehlers, K. and Oster, G. On the mysterious propulsion of *Synechoccoccus*. PLoS One 7:5, e36081, 2012.

Fenchel, T. How dinoflagellate swim. Protist, 152, 329–338, 2001.

Frassanito, A.M., Barsanti, L., Passarelli, V. and Gualtieri, P. A second rhodopsin-like protein in *Cyanophora paradoxa*: Gene sequence and protein expression in a cell-free system. Journal of Photochemistry and P hotobiology B, 125, 188–193, 2013.

Frassanito, A.M., Barsanti, L., Passarelli, V., Evangelista, V. and Gualtieri, P. A rhodopsin-like protein in *Cyanophora paradoxa*: Gene sequence and protein immunolocalization. Cellular and Molecular Life Sciences, 67, 965–971, 2010.

Gilson, P.R. and McFadden, G.I. Molecular, morphological and phylogenetic characterization of six chlorarachniophytes strains. Phycological Research, 47, 7–19, 1999.

Ginger, M.L., Portman, N. and McKean, P.G. Swimming with protists: Perception, motility and flagellum assembly. Nature Reviews Microbiology, 6, 838–850, 2008.

Giometto, A., Altermatt, F., Maritan, A., Stocker, R. and Rinaldo, A. Generalized receptor law governs phototaxis in the phytoplankton Euglena gracilis. PNAS, 112:22, 7045–7050, 2015.

Grain, J., Mignot, J.P. and de Puytorac, P. Ultrastructures and evolutionary modalities of flagellar and cyliary system in protists. Biology of the Cell, 63, 219–237, 1988.

Gregson, A.J., Green, J.C. and Leadbeater, B.S.C. Structure and physiology of haptonema in *Chrisochromulina*. Fine structure of the flagellar/haptonematal root system in *C. acanthi* and *C. simplex*. Journal of Phycology, 29, 674–686, 1993.

Gregson, A.J., Green, J.C. and Leadbeater, B.S.C. Structure and physiology of Haptonema in *Chrisochromulina*. Mechanism of haptonematal coiling and the regeneration process. Journal of Phycology, 29, 686–700, 1993.

Gualtieri, P. and Robinson, K.R. A rhodopsin-like protein in the plasma membrane of *Silvetia compressa* eggs. Photochemistry Photobiology, 75, 76, 2002.

Gualtieri, P. Microspectrophotometry of photoreceptor pigments in flagellated algae. Critical Reviews in Plant Science, 9:6, 475–497, 1991.

Gualtieri, P., Barsanti, L. and Passarelli, V. Absorption spectrum of a single isolated paraflagellar swelling of *Euglena gracilis*. Biochimica et Biophisica Acta, 993, 293–296, 1989.

Gualtieri, P., Ghetti, F., Passarelli, V. and Barsanti, L. Microorganism track reconstruction: An image processing approach. Computers in Biology and Medicine, 18:2, 57–63, 1988.

Gualtieri, P., Pelosi, P., Barsanti, L. and Passarelli, V. Identification of a rhodopsin photoreceptor in *Euglena gracilis*. Biochimica et Biophysica Acta, 117, 55–59, 1992.

Hackett, J.D., Anderson, D.M., Erdner, D.L. and Bhattacharya, D. Dinoflagellates: A remarkable evolutionary experiment. American Journal of Botany, 91, 1523–1534, 2004.

Harrison, F.W. and Corliss, J.O. Microscopy anatomy of invertebrate. Protozoa. Wiley-Liss, New York, 1991.

Hibbed, D.J. and Norris, R.E. Cytology and ultrastructure of *Chlorarachnion reptans* (Chlorarachniophyta divisio nova, Chlorarachniophyceae classis nova). Journal of Phycology, 20, 310–330, 1984.

Hilenski, L.L. and Walne, P.L. Ultrastructure of mucocysts in *Peranema trichophorum*. Journal of Protozoology, 30, 491–496, 1983.

Hoiczyk, E. and Hansel, A. Cyanobacterial cell walls: News from and unusual prokaryotic envelope. Journal of Bacteriology, 182, 1191–1199, 2000.

Honda, D. and Inouye, I. Ultrastructure and taxonomy of a marine photosynthetic stramenopile *Phaemonas parva* with emphasis on the flagellar apparatus architecture. Phycological Reseach, 50, 75–89, 2002.

Horiguchi, T. and Hoppenrath, M. *Haramonas viridis*, a new sand-dwelling raphidophyte from cold temperate waters. Phycological Research, 51, 61–67, 2003.

Hyams, J.S. The *Euglena* paraflagellar rod: Structure, relationship to the other flagellar components and preliminary biochemical characterization. Journal of Cell Science, 55, 199–210, 1982.

Inouye, I. and Hori, T. High-speed video analysis of the flagellar beat and swimming patterns of algae: Possible evolutionary trends in green algae. Protoplasma, 164, 54–69, 1991.

Iomini, C.V., Babaev-Khaimov, M., Sassaroli, D. and Piperno, G. Protein particles in *Chlamydomonas* flagella undergo a transport cycle consisting of four phases. Journal of Cell Biology, 153:1, 13–24, 2001.

Kantsler, V., Dunkel, J., Polin, M. and Goldstein, R.E. Ciliary contact interactions dominate surface scattering of swimming eukaryotes. Proceedings of the National Academy of Sciences, 110:4, 1187–1192, 2013.

Koch, D.L. and Subramanian, G. Collective hydrodynamics of swimming microorganisms: Living fluids. Annual Review of Fluid Mechanics, 43:1, 637–659, 2011.

Lakie, J.M. Cell movement and cell behaviour. Allen and Unwin, London, 1986.

Lauga E. and Powers, T.R. The hydrodynamics of swimming microorganisms. Reports on Progress in Physics, 72, 096601, 2009.

Lavau, S. and Wetherbee, R. Structure and development of the scale case of *Mallomonas adamas*. Protoplasma, 181, 259–268, 1994.

Leadbeater, B.S.C. and Green, J.C. (Eds.). The flagellates. Unit, diversity and evolution. Taylor and Francis, London, 2000.

Leander, B.S. and Farmer, M.A. Comparative morphology of euglenid pellicle. Diversity of strip substructures. Journal of Eukariotic Microbiology, 48, 202–217, 2001.

Lobban, C.S. and Harrison, P.J. Seaweed ecology and physiology. Cambridge University Press, Cambridge (UK), 1997.

Luck, M., Mathes, T., Bruun, S., Fudim, R., Hagedorn, R., Tran Nguyen, T.M., Kateriya, S., Kennis, J.T.M., Hildebrandt, P. and Hegemann, P. A photochromic histidine kinase rhodopsin (HKR1) that is bimodally switched by ultraviolet and blue light. Journal of Biological Chemistry, 287, 40083–40090, 2012.

Maga, J.A. and LeBowitz, J.H. Unravelling the kinetoplastid paraflagellar rod. Trends Cell Biology, 9, 409–413, 1999.

Marian, B. and Melkonian, M. Flagellar hairs in Prasinophytes: Ultrastructure and distribution on the flagellar surface. Journal of Phycology, 30, 659–678, 1994.

Maruyama, T. Fine structure of the longitudinal flagellum in *Ceratium tripos*, a marine dinoflagellate. Journal Cell Science, 58, 109–123, 1982.
Melkonian, M. (Eds.). Algal cell motility. Chapman Hall, New York, 1992.
Melkonian, M. and Robenek, R. The eyespot apparatus of flagellated green algae: A critical review. In: Progress in phycological research, 3, Round, F.E. and Chapman, D.J. (Eds.), 193–268, Biopress Ltd., Bristol (UK), 1984.
Menzel, D. (Ed.). The cytoskeleton of the Algae. CRC Press Inc., Boca Raton (USA), 1992.
Mercatelli, R., Quercioli, F., Barsanti, L., Evangelista, V., Coltelli, P., Gualtieri, P. Intramolecular photo-switching and intermolecular energy transfer as primary photoevents in photoreceptive processes: The case of *Euglena gracilis*. Bichem Biophys Research Commun, 385, 176–18, 2009.
Miyasaka, I., Nanba, K., Furuya, K., Nimura, Y. and Azuma, A. Functional roles of the transverse and longitudinal flagella in the swimming motility of *Prorocentrum minimum*. Journal of Experimental Biology, 207, 3055–3066, 2004.
Moenstrup, Ø. and Sengco, M. Ultrastructural studies on *Bigelowiella natans*, a chlorarachniophyte flagellate. Journal of Phycology, 37, 624–646, 2001.
Moenstrup, Ø. Flagellar structure in Algae: A review, with new observations particularly on the Chrysophyceae, Phaeophyceae, Euglenophyceae, and Reckertia. Phycologia, 21:4, 427–528, 1982.
Niklas, K.J. The cell walls the bind the tree of life. Bioscience, 54, 831–841, 2004.
Nishitani, G., Nagai, S., Hayakawa, S., Kosaka, Y., Sakurada, K., Kamiyama, T., et al. Multiple plastids collected by the dinoflagellate *Dinophysis mitra* through kleptoplastidy. Applied and Environmental Microbiology, 78:3, 813–821, 2012.
Novarino, G. A companion to the identification of cryptomonad flagellates. Hydrobiologia, 502, 225–270, 2003.
O'Malley, S. and Bees, M.A. The orientation of swimming biflagellate in shear flows. Bulletin of Mathematical Biology, 74, 232–255, 2012.
Ooka, H., Ishii, T., Hashimoto, K. and Nakamura, R. Light-induced cell aggregation of *Euglena gracilis* towards economically feasible biofuel production. RSC Advances, 4, 20693–20698, 2014.
Parkinson, P.R. and Ontogeny, V. Phylogeny. The strange case of the silicoflagellates. Constancea, 83, 1–29, 2002.
Patterson, D.J. and Larsen, J. The biology of free-living heterotrophic flagellates. Claredon Press, Oxford, 1991.
Pickett-Heaps, J.D., Carpenter, J. and Koutoulis, A. Valve and seta (spine) morphogenesis in the centric diatom *Chaetoceros peruvianus*. Protoplasma, 181, 269–282, 1994.
Polin, M., Tuval, I., Drescher, K., Gollub, J.P. and Goldstein, R.E. *Chlamydomonas* swims with two "gears" in a eukaryotic version of run-and-tumble locomotion. Science, 325:5939, 487–490, 2009.
Preisig, H.R. Siliceous structure and silicification in flagellate protists. Protoplasma, 181, 29–42, 1994.
Preisig, H.R., Anderson, O.R., Corliss, J.O., Moestrup, Ø., Powell, M.J., Roberson, R.W. and Wetherbee, R. Terminology and nomenclature of protest cell surface structures. Protoplasma, 181, 1–28, 1994.
Purcell, E.M. Life at low Reynolds number. American Journal of Physics, 45:1, 3–11, 1977.
Qiu, T., Lee, T.-C., Mark, A.G., Morozov, K.I., Münster, R., Mierka, O., Turek, S., Leshansky, A.M. and Fischer, P. Swimming by reciprocal motion at low Reynolds number. Nature Communications, 5, 1–8, 2014.
Rafai, S., Jibuti, L. and Peyla, P. Effective viscosity of microswimmer suspension. Physical Review Letters, 104, 098102, 2010.
Rave, J.A. and Brownlee, C. Understanding membrane function. Journal of Phycology, 37, 960–967, 2001.
Rizzo, P.J. Those amazing dinoflagellate chromosomes. Cell Research, 13, 215–217, 2002.
Rosati, G., Verni, F., Barsanti, L., Passarelli, V. and Gualtieri, P. Ultrastructure of the apical zone of *Euglena gracilis*: Photoreceptor and motor apparatus. Electron Microscopy Review, 4, 319–342, 1991.
Sato, H., Greuet, C., Cachon, M. and Cosson, J. Analysis of the contraction of an organelle using its birefringency: The R-fibre of the *Ceratium flagellum*. Cell Biology International, 28, 387–396, 2004.
Solomon, C.M., Evelyn, J. Lessard, Keil, R.G. and Foy, M.S. Characterization of extracellular polymers of *Phaeocystis globosa* and *P. antarctica*. Marine Ecology Progress Series, 250, 81–89, 2003.
Tamaki, S., Tanno, Y., Kato, S., Ozasa, K., Wakazaki, M., Sato, M., Toyooka, K., Maoka, T., Ishikawa, T., Maeda, M. and Shinomura, T. Carotenoid accumulation in the eyespot apparatus required for phototaxis is independent of chloroplast development in *Euglena gracilis*. Plant Science, 298, 110564, 2020.
Taylor Max, F.J.R. Charles Atwood Kofoid and his dinoflagellate tabulation system: An appraisal and evaluation of the phylogenetic value of tabulation. Protist, 150, 213–220, 1999.

Tsang, A.C. H, Lam, A.T. and Riedel-Kruse, I. H. Polygonal motion and adaptable phototaxis via flagellar beat switching in the microswimmer *Euglena gracilis*. Nature Physics, 14, 1216–1222, 2018.

Ueki, N., Matsunaga, S., Inouye, I. and Hallmann, A. How 5000 independent rowers coordinate their strokes in order to row into the sunlight: Phototaxis in the multicellular green alga *Volvox*. BMC Biology, 8:1, 103, 2010.

Ulloa, O., Henríquez-Castillo, C., Ramírez-Flandes, S., Plominsky, A.M., Murillo, A.A., Morgan-Lang, C., Hallam, S.J. and Stepanauskas, R. The cyanobacterium *Prochlorococcus* has divergent light-harvesting antennae and may have evolved in a low-oxygen ocean. Proceedings of the National Academy of Sciences, 118, 2021.

Verni, F. Rosati, G., Lenzi, P., Barsanti, L. and Gualtieri, P. Morphological relationship between paraflagellar swelling and paraxial rod in *Euglena gracilis*. Micron and Microcopica Acta, 23:1/2, 37–44, 1992.

Verspagen, J.M.H., Snelder, E.O.F.M., Visser, P.M., Huisman, J., Mur, L.R. and Ibelings, B.W. Recruitment of benthic microcystis to the water column: Internal buoyance changes or resuspension? Journal of Phycology, 40, 260–270, 2004.

Vikram Singh, A., Kishore, V., Santomauro, G., Yasa, O., Bill, J. and Sitti, M. Mechanical coupling of puller and pusher active microswimmers influences motility. Langmuir, 36, 5435−5443, 2020.

Vismara, R., Barsanti, L., Evangelista, V., Verni, F. and Gualtieri, P. A short flagella mutant of *Dunaliella salina*. Micron, 35, 337–344, 2004.

Westfall, J.A., Bradbury, P.C. and Townsend, J.W. Ultrastructure of the dynoflagellate Polykrikos. Journal of Cell Science, 63, 245–261, 1983.

Xia, S., Zhang, Q., Zhu, H., Cheng, Y., Liu, G. and Hu, Z. Systematics of a kleptoplastidal dinoflagellate, *Gymnodinium eucyaneum* Hu (Dinophyceae), and its cryptomonad endosymbiont. PLoS One, 8:1, e53820, 2013.

Young, J.R., Davis, S.A., Brown, P.R. and Mann, S. Coccolith ultrastructure and biomineralization. Journal of Structural Biology, 126, 195–215, 1999.

Zhang, F., Vierock, J., Yizhar, O., Fenno, L.E., Tsunoda, S., Kianianmomeni, A., Prigge, M., Berndt, A., Cushman, J., Polle, J., Magnuson, J., Hegemann, P. and Deisseroth, K. The microbial opsin family of optogenetic tools. Cell, 147, 1446–1457, 2011.

Zingone, A., Chretiennot-Dinet, M.J., Lange, M. and Medlin, L. Morphological and genetic characterization *Phaeocystis cordata* and *P. jahnii*, two new species from Mediterranean sea. Journal of Phycology, 35, 1322–1337, 1999.

http://ina.tmsoc.org/terminology/3coccoliths.htm


Taylor & Francis
Taylor & Francis Group
http://taylorandfrancis.com

4 Photosynthesis

LIGHT

The sun is the universal source of energy in the biosphere. During the nuclear fusion processes occurring in the sun, matter is changed into energy and emitted into space in the form of electromagnetic radiation, with both wave and particle properties. Almost all light in the natural environment originates from the sun. Its spectral distribution (Figure 4.1, thin black line) is similar to that of an efficient radiant surface known as a black body at a temperature of 5800 K (Figure 4.1, thick black line) and ranges from short wavelengths (10^{-6} nm, γ- and X-rays) to long wavelengths (10^{15} nm, long radio waves) (Figure 4.2).

In passing through the atmosphere, a small portion of this light is absorbed, and some is scattered. Short wavelengths are strongly scattered, and ozone absorption effectively eliminates wavelengths less than 300 nm (Figure 4.1, grey line). At longer wavelengths, water vapor, carbon dioxide, and oxygen absorb light significantly at particular wavelengths, producing sharp dips in the spectrum. At still-longer wavelengths, beyond 4000 nm, all objects in the environment become significant sources of radiation, depending on their temperature, and surpass sunlight in intensity. These environmental characteristics restrict the range of electromagnetic radiation. About 99% of the sun radiation that reaches the surface of the earth has a spectral range from about 300 nm (ultraviolet) to about 4000 nm (infrared), and it is called broadband or total solar radiation.

Three spectral regions exist almost superimposably on broadband radiation, which can be associated with specific phenomena, such as harmful and potentially mutagenic ultraviolet radiation (UV 100–400 nm), sight (visible light 400–700 nm), and heat (infrared radiation 700–4000 nm) (Figure 4.2).

Ultraviolet light is arbitrarily broken down into three bands, according to its anecdotal effects. UV-A (315–400 nm) is the least harmful and most commonly found type of UV light, because it has the least energy. UV-A light is often called black light and is used for its relative harmlessness and its ability to cause fluorescent materials to emit visible light, thus appearing to glow in the dark. Most phototherapy and tanning booths use UV-A lamps. UV-B (280–315 nm) is typically the most destructive form of UV light, because it has enough energy to damage biological tissues yet not quite enough to be completely absorbed by the atmosphere. UV-B is known to cause skin cancer. Since most of the extraterrestrial UV-B light is blocked by the atmosphere, a small change in the ozone layer could dramatically increase the danger of skin cancer. Short-wavelength UV-C (200–280 nm) is almost completely absorbed in air within a few hundred meters. When UV-C photons collide with oxygen molecules, the O-O bond is broken, and the released O atom reacts with O_2 molecule (and for energetic reasons with a collision partner M) and forms ozone (O_3). UV-C is almost never observed in nature, since it is absorbed very quickly. Germicidal UV-C lamps are often used to purify air and water because of their ability to kill bacteria.

The visible range extends from 400 to 700 nm; these wavelengths are utilized for both vision and photosynthesis. The radiation utilized by oxygenic photosynthetic organisms is termed photosynthetic active radiation. We will see in the following that this range has been expanded to 750 nm after the discovery of red-shifted chlorophylls.

Infrared light contains the least amount of energy per photon of any other band. Because of this, an infrared photon often lacks the energy required to pass the threshold of metabolic pathways. Little of the ultraviolet radiation (UV-A and UV-B) and infrared is utilized directly in photosynthesis.

DOI: 10.1201/9781003187707-4

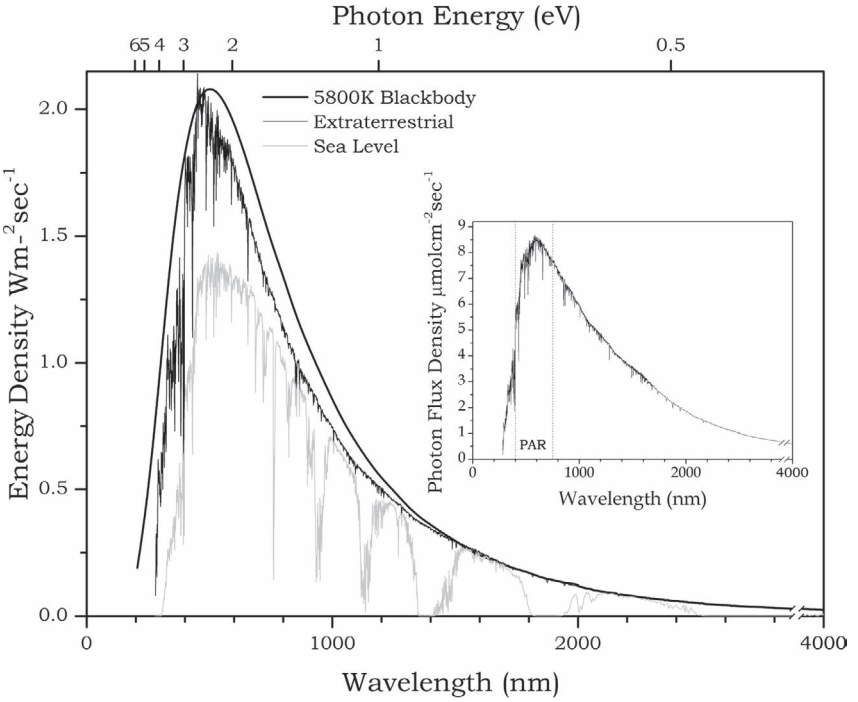


FIGURE 4.1 Spectral irradiance of the incoming sun radiation outside the atmosphere and at sea level compared with that of a perfect black body at 5800 K. The curve in the insert is the photon flux density spectrum.

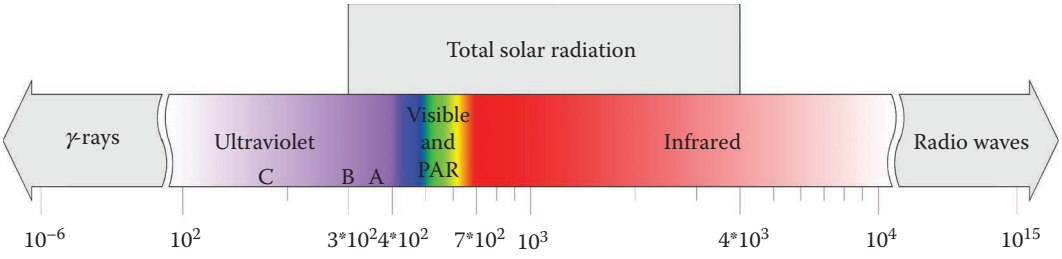


FIGURE 4.2 The electromagnetic spectrum, from γ-rays (10^{-6} nm) to radio waves (10^{15} nm).

The particles producing electromagnetic waves are called photons or quanta. The energy (E) in joules (or watts per second) of a photon (or quantum) can be expressed by Plank's law:

1) $$E = h \times c \times \lambda^{-1}$$

where h is Planck's constant (6.626×10^{-34} $J \times s$); c is the speed of light (3×10^8 m s^{-1}), and λ is the photon wavelength in meters (m).

According to this formula, the shorter the photon wavelength, the higher its energy; for example, the energy of 1 photon of 300-nm light is equal to 6.63×10^{-19} J, the energy of 1 photon of 400-nm light is equal to 4.97×10^{-19} J, the energy of 1 photon of 700-nm light is equal to 2.84×10^{-19} J, and the energy of 1 photon of 4000-nm light is equal to 0.49×10^{-19} J. It takes a larger number of longer wavelength photons to supply a given quantity of energy with respect to shorter wavelength photons.

This relationship has the effect of changing the shape of the curve represented in two different ways: the peak of the energy curve is at approximately 500 nm (Figure 4.1, thin black line), whereas the peak of the photon flux curve is at approximately 700 nm (insert of Figure 4.1).

The energy of photons can also be expressed in terms of electron volts (eV). Absorption of a photon can lead to excitation of an electron and hence of a molecule. This excited electron acquires potential energy (capacity of producing chemical work) measured in eV. An electron volt is the potential energy of 1 V gained by the excited electron, which is equal to 1.60×10^{-19} J. Thus the energy of 1 photon of 300-nm light is equal to 4.14 eV (i.e. 6.63×10^{-19} J divided by 1.60×10^{-19} J), the energy of 1 photon of 400-nm light is equal to 3.11 eV, the energy of 1 photon of 700-nm light is equal to 1.77 eV, and the energy of 1 photon of 4000-nm light is equal to 0.30 eV.

The average intensity of the total solar radiation reaching the upper atmosphere is about 1.4 kW m^{-2} (UV 8%, visible light 41%, infrared radiation 51%). The amount of this energy that reaches any one "spot" on the earth's surface will vary according to atmospheric and meteorological (weather) conditions, the latitude and altitude of the spot, and local landscape features that may block the sun at different times of the day. In fact, as sunlight passes through the atmosphere, some of it is absorbed, scattered, and reflected by air molecules, water vapor, clouds, dust, and pollutants from power plants, forest fires, and volcanoes. Atmospheric conditions can reduce solar radiation by 10% on clear, dry days and by 100% during periods of thick clouds. At sea level, on an ordinary clear day, the average intensity of solar radiation is less than 1.0 kWm^{-2} (UV 3%, visible light 42%, infrared radiation 55%). Penetrating water, much of the incident light is reflected from the water surface, more light being reflected from a ruffled surface than a calm one, and reflection increases as the sun becomes lower in the sky (Table 4.1). As light travels through the water column, it undergoes a decrease in its intensity (attenuation) and a narrowing of the radiation band caused by the combined absorption and scattering of everything in the water column, including water itself. In fact, different wavelengths do not penetrate equally; infrared light (700–4,000 nm) penetrates least, being almost entirely absorbed within the top 2 meters, and ultraviolet light (300–400 nm) is also rapidly absorbed. Within the visible spectrum (400–700 nm), red light is absorbed first, much of it within the first 5 meters. In clear water, the greatest penetration is by the blue-green region of the spectrum (450–550 nm), while under more turbid conditions, the penetration of blue rays is often reduced to a greater extent than that of the yellow-red wavelengths (550–700 nm). Depending on all these conditions, 3–50% of incident light is usually reflected, and the Beer-Lambert law can mathematically describe the way the light decreases as function of depth

$$I_z = I_0 \times e^{-k \times z} \quad (2)$$

where I_z is the intensity of light at depth z; I_0 is the intensity of light at depth 0, that is, at the surface; and k is the attenuation coefficient, which describes how quickly light attenuates in a particular body of water.

TABLE 4.1
Sunlight Reflected by Sea Surface

Angle Between Sun Rays and Zenith	0°	10°	20°	30°	40°	50°	60°	70°	80°	90°
% of reflected light	2	2	2.1	2.1	2.5	3.4	6	13.4	34.8	100

Algae use the light eventually available in two main ways:

- as information in sensing processes, supported by the photoreceptors systems, as already explained in Chapter 3;
- as energy in transduction processes, supported by chloroplasts in photosynthesis.

Both types of processes depend on the absorption of photons by electrons of chromophore molecules with extensive systems of conjugated double bonds. These conjugated double bonds create a distribution of delocalized *pi* electrons over the plane of the molecule. Upon absorption of a photon in the range 400–700 nm, *pi* electrons can be driven to an available electronic "excited state" (an unoccupied orbital of higher energy, higher meaning the electron is less tightly bound). Only absorption of a photon in this range can lead to excitation of the electron and hence of the molecule, since the lower energy of an infrared photon could be confused with the energy derived by molecular collisions, eventually increasing the noise of the system and not its information. Moreover, the higher energy of an UV photon could dislodge the electron from the electronic cloud and destroy the molecular bonds of the chromophore. Charge separation is produced in the chromophore molecule elevated to the excited state by the absorption of a photon, which increases the molecule capability to perform work. In sensing processes, charge separation is produced by the photo-isomerization of the chromophore around a double bond, thus storing electrostatic energy, which triggers a chain of conformational changes in the protein that induces the signal transduction cascade.

In photosynthesis, a charge separation is produced between a photo-excited molecule of a special chlorophyll (electron donor) and an electron-deficient molecule (electron acceptor) located within van der Waals distance, that is, a few Å. The electron acceptor in turn becomes a donor for a second acceptor and so on; this chain ends in an electron-deficient trap. In this way, the free energy of the photon absorbed by the chlorophyll can thereby be used to carry out useful electrochemical work, avoiding its dissipation as heat or fluorescence. The ability to perform electrochemical work for each electron that is transferred is termed redox potential; a negative redox potential indicates a reducing capability of the system (the system possesses available electrons), while a positive redox potential indicates an oxidizing capability of the system (the system lacks available electrons).

Photosynthetic activity of algae, which roughly account for more than 50% of global photosynthesis, make it possible to convert the energy of PAR into biologically usable energy by means of reduction and oxidation reactions; hence, photosynthesis and respiration must be regarded as complex redox processes.

As shown in Equation 3, during photosynthesis, carbon is converted from its maximally oxidized state + 4 in CO_2 to 0 in strongly reduced compounds such as carbohydrates $[CH_2O]_n$, using the light energy.

3) $$nCO_2 + nH_2O + \text{light} \xrightarrow{\textit{Chlorophyll a}} (CH_2O)_n + nO_2$$

In this equation, light is specified as a substrate, chlorophyll *a* is a requisite catalytic agent, and $(CH_2O)_n$ represents organic matter reduced to the level of carbohydrate. These reduced compounds may be re-oxidized to CO_2 during respiration, liberating energy. The process of photosynthetic electron transport takes place at between +0.82 eV (redox potential of the H_2O/O_2 couple) and −0.42 eV (redox potential the CO_2/CH_2O couple).

Approximately half of incident light intensity impinging on the earth surface (0.42 kWm^{-2}) belongs to the PAR. In water, as explained previously, the useful energy for photo-biochemical processes is even lower and distributed within a narrower wavelength range. About 95% of the PAR impinging on algal cells is mainly lost due to the absorption by components other than chloroplasts and to the ineffectiveness of the transduction of light energy into chemical energy. Only 5% of the PAR is used by photosynthetic processes. Despite this high energy waste, photosynthetic energy transformation is the basic energy-supplying process for algae.

PHOTOSYNTHESIS

Photosynthesis encompasses two major groups of reactions. Those in the first group, the light-dependent reactions, involve the capture of the light energy and its conversion to energy currency as NADPH and ATP. These reactions are absorption and transfer of photon energy, trapping of

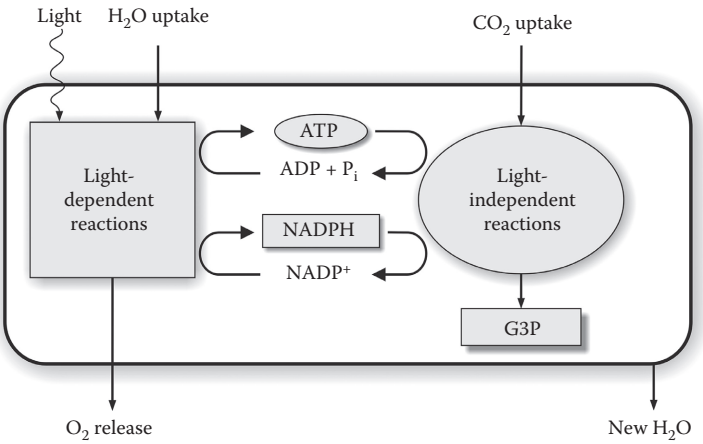


FIGURE 4.3 Schematic drawing of the photosynthetic machinery.

this energy, and generation of a chemical potential. The latter reaction follows two routes: the first one generates NADPH thanks to the falling of the high-energy excited electron along an electron transport system; the second one generates ATP by means of a proton gradient across the thylakoid membrane. Water splitting is the source of both electrons and protons. Oxygen is released as a by-product of the water splitting.

The reactions of the second group are the light-independent reactions and involve the sequence of reactions by which this chemical potential is used to fix and reduce inorganic carbon in triose phosphates (Figure 4.3).

Light-Dependent Reactions

Photosynthetic light reactions take place in thylakoid membranes where chromophore-protein complexes and membrane-bound enzymes are situated (Figure 4.4). The thylakoid membrane cannot be considered a rigid, immutable structure at all. It is rather a highly dynamic system, whose molecular compositions and conformation, including the spatial pattern of its components, can change very rapidly. This flexibility, is, however, combined with a high degree of order necessary for the energy-transforming processes.

Quantitative analysis established that the 7-nm-thick thylakoid membrane consists of approximately 50% lipids and 50% proteins. Galactolipids, a constituent that is specific to thylakoid membranes, make up approximately 40% of the lipid fraction. Chlorophylls, carotenoids, xanthophylls (when present), phycobilins (when present), phospholipids, sulfolipids, quinones, and sterols, all components occurring in a bound form, represent the remaining 10%.

Chlorophylls are the essential pigments of photosynthesis, for which they both harvest light and transduce it into chemical energy. There are five chemically distinct chlorophylls known to date, termed chlorophyll *a*, *b*, c_1, c_2, *d*, and *f*, which are present in light-harvesting complexes of oxygenic photosynthetic organisms (Figures 4.5 and 4.6). Chlorophyll *a* consists of a hydrophilic porphyrin head formed by four linked pyrrole rings with a magnesium atom chelated (Mg^{2+}) at the center and a hydrophobic phytol tail. Chlorophyll *b* possesses the same structure as chlorophyll *a*, but a keto group (-CH=O) is present in the second pyrrole ring instead of a metil group ($-CH_3$). Chlorophyll *c* possesses only the hydrophilic porphyrin head without the phytol tail; chlorophyll c_2 differs from chlorophyll c_1 for possessing two vinyl groups ($-CH=CH_2$) instead of one. Chlorophyll *d* differs from chlorophyll *a* only in the C3 position at ring I, where a formyl

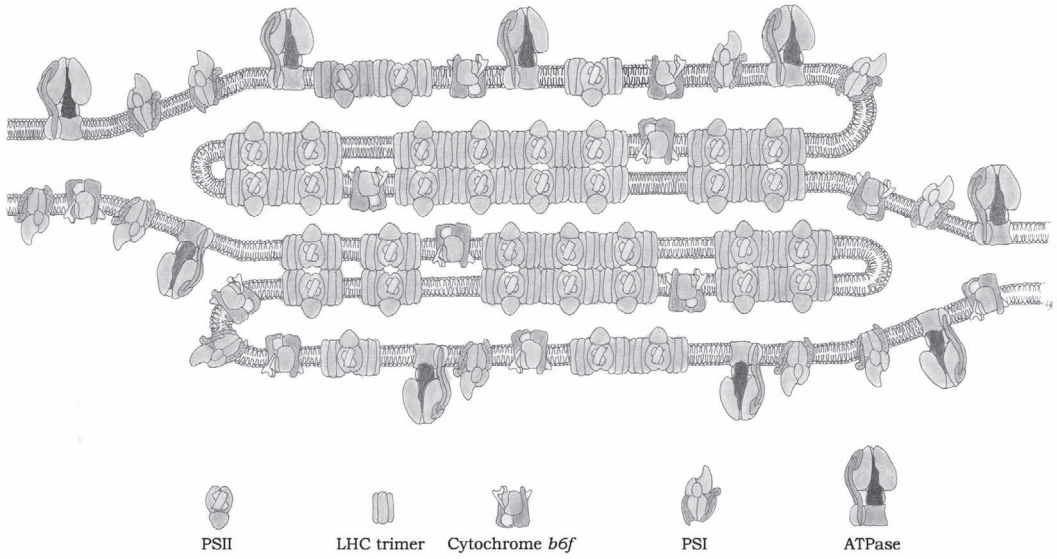


FIGURE 4.4 Model of the topology of chloroplast thylakoid membrane showing the disposition of the major intrinsic protein complexes, PSI, PSII, LHCII trimer, cytochrome b_6f dimer and ATPase, according to Allen and Forsberg (2001).

group in chlorophyll *d* replaces the vinyl group in chlorophyll *a*. Chlorophyll *f* differs from chlorophyll *a* only in the C2 position at ring I, where a formyl group is present. Chlorophylls *a*, *b*, and *c* were identified in the 19th century; chlorophyll *d* was reported in 1943 but recognized only in 1996 in the cyanobacterium *Acaryochloris marina*; chlorophyll *f* was discovered for the first time in 2010 in Shark Bay (Australia) in the stromatolite-forming cyanobacterium *Halomicronema hongdechloris*.

Each chlorophyll has its own absorption spectrum (Figures 4.5 and 4.6). The discovery of the red-shifted chlorophylls *d* and *f* has expanded the portion of solar spectrum available for photosynthesis to 750 nm. This relatively modest increment (about 50 nm) increases the number of available photons by 19%. The far red light (>700 nm) reaching the Earth surface is abundant, containing approximately one fifth of the photons of PAR (400–700 nm). This could be significant in environments where energy sources and light are limited, such as hot spring mats, desert rocks and soil, and lower regions of the canopy.

Carotenoids are C_{40} hydrocarbon chains, strongly hydrophobic, with one or two terminal ionone rings, functioning as accessory pigments for energy capture and transfer and also playing protective roles. Xanthophylls are carotenoid derivatives with a hydroxyl group in the ring; they have a role in non-radiative dissipation of excess absorbed light energy (Figures 4.6 and 4.7). Phycobilins (Figure 4.8) possess four pyrrolic rings, linearly arranged, and unlike the chlorophylls, they are strongly covalently bound to a protein. These are complex proteins, often with more than one subunit, with more than one phycobilin as chromophore. Figure 4.9 shows the most common phycobiliproteins. They are considered accessory pigments for the operations of photosystem II (see next paragraph). The organization of phycobiliproteins in the phycobilisome was described in Chapter 2 (cf. Figures 3.87 and 3.89 of Chapter 3).

The protein complex content consists mainly of highly organized energy-transforming units, enzymes for electron transport and ATP synthesis, more or less integrated into the thylakoid

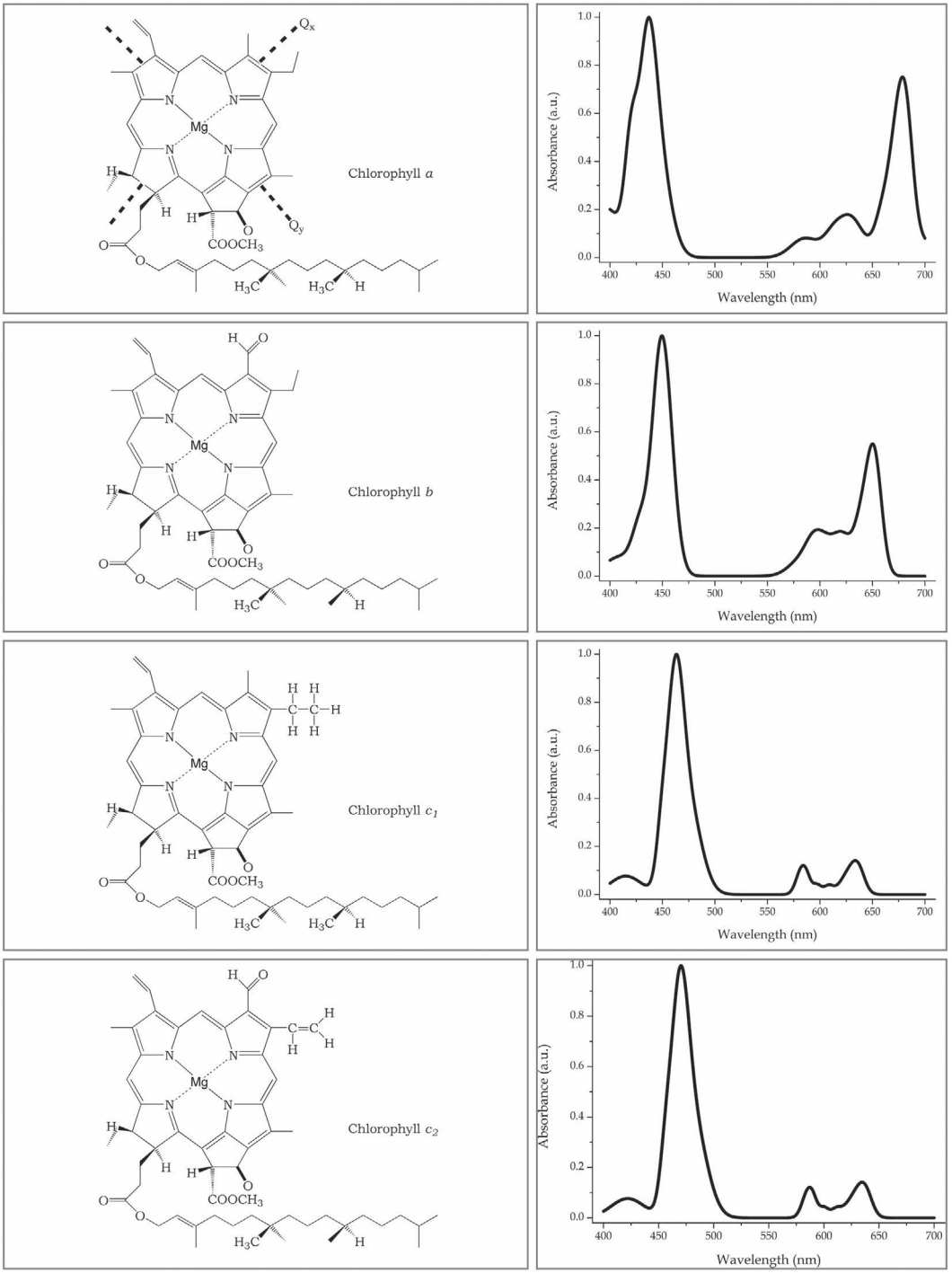


FIGURE 4.5 Structure of chlorophylls *a*, *b*, c_1, c_2.

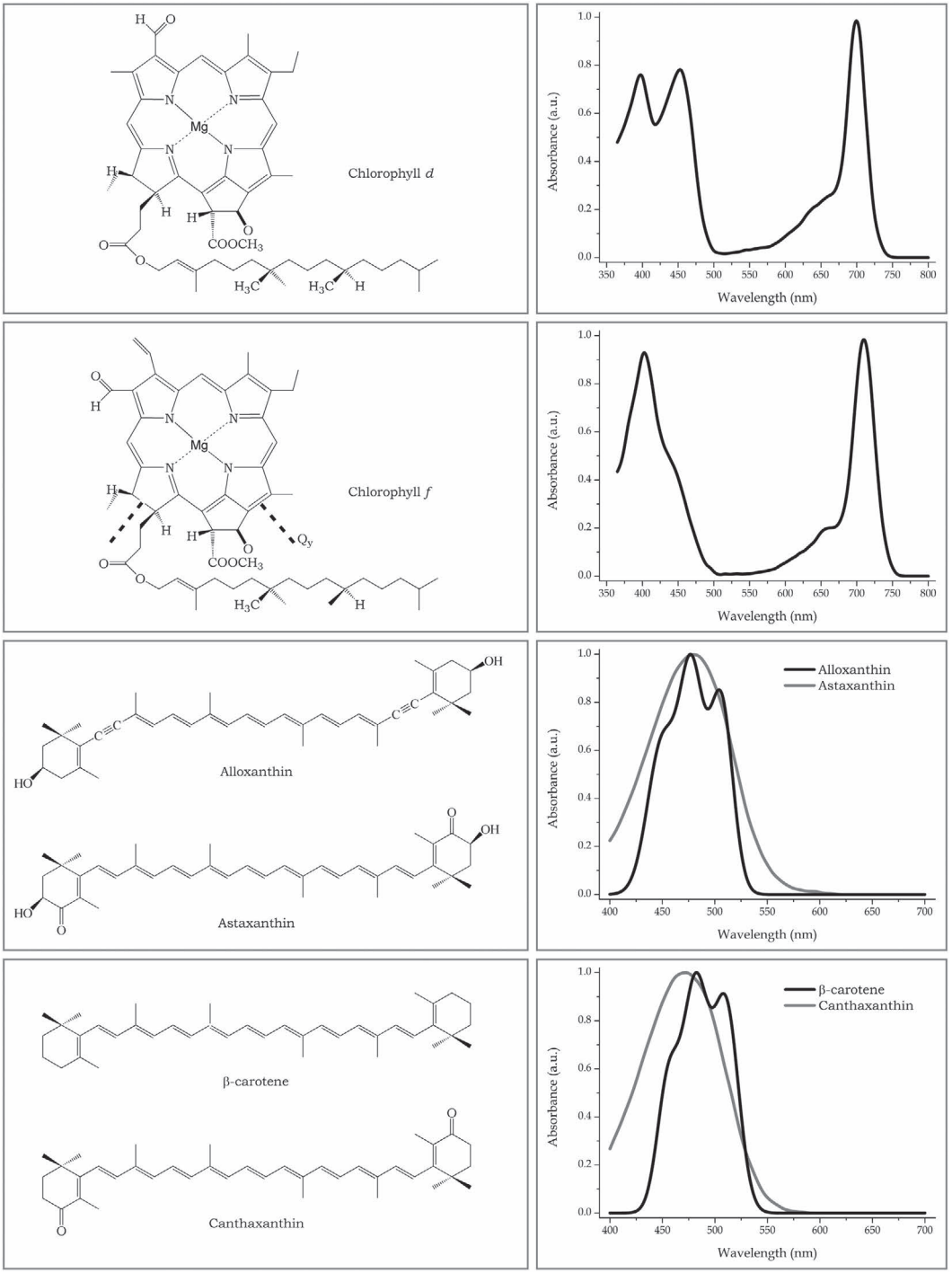


FIGURE 4.6 Structure of chlorophylls *d, f,* alloxanthin, astaxanthin, β-carotene, and cantaxanthin.

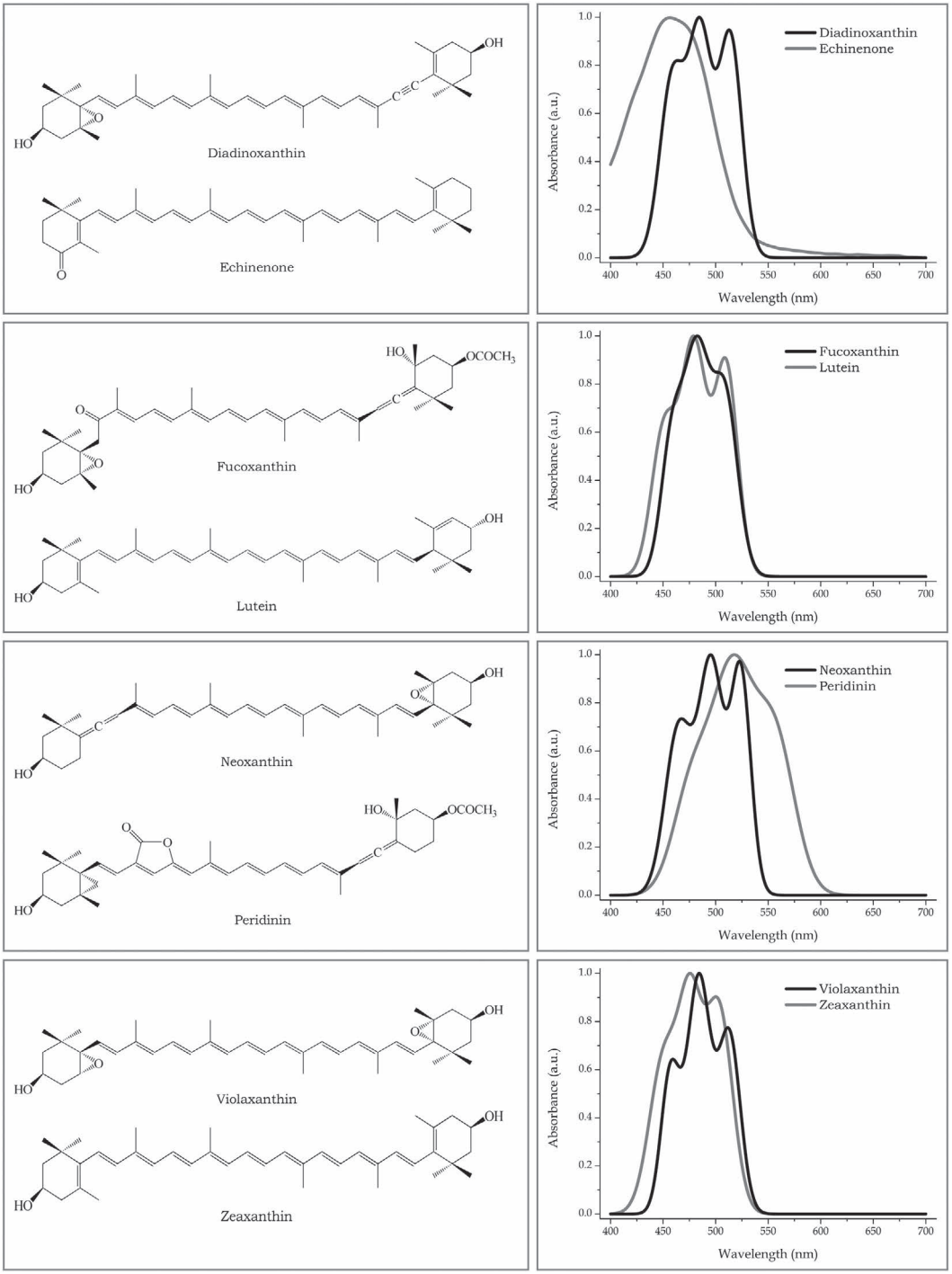


FIGURE 4.7 Structure of diadinoxanthin, echinenone, fucoxanthin, lutein, neoxanthin, peridinin, violaxanthin, zeaxanthin.

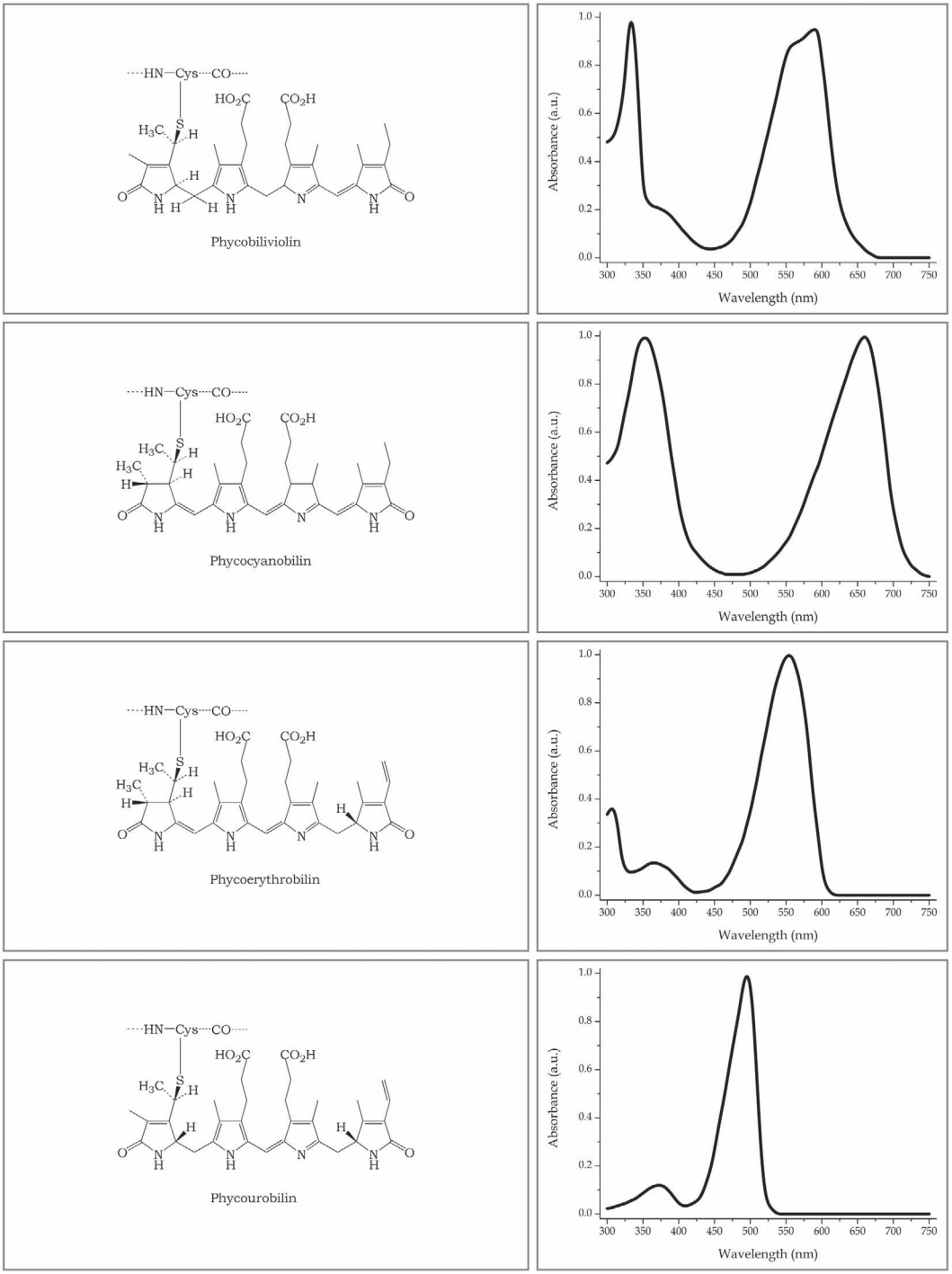


FIGURE 4.8 Structure of polypeptide-bound phycobiliviolin, phycocyanobilin, phycoerythrobilin, phycourobilin.

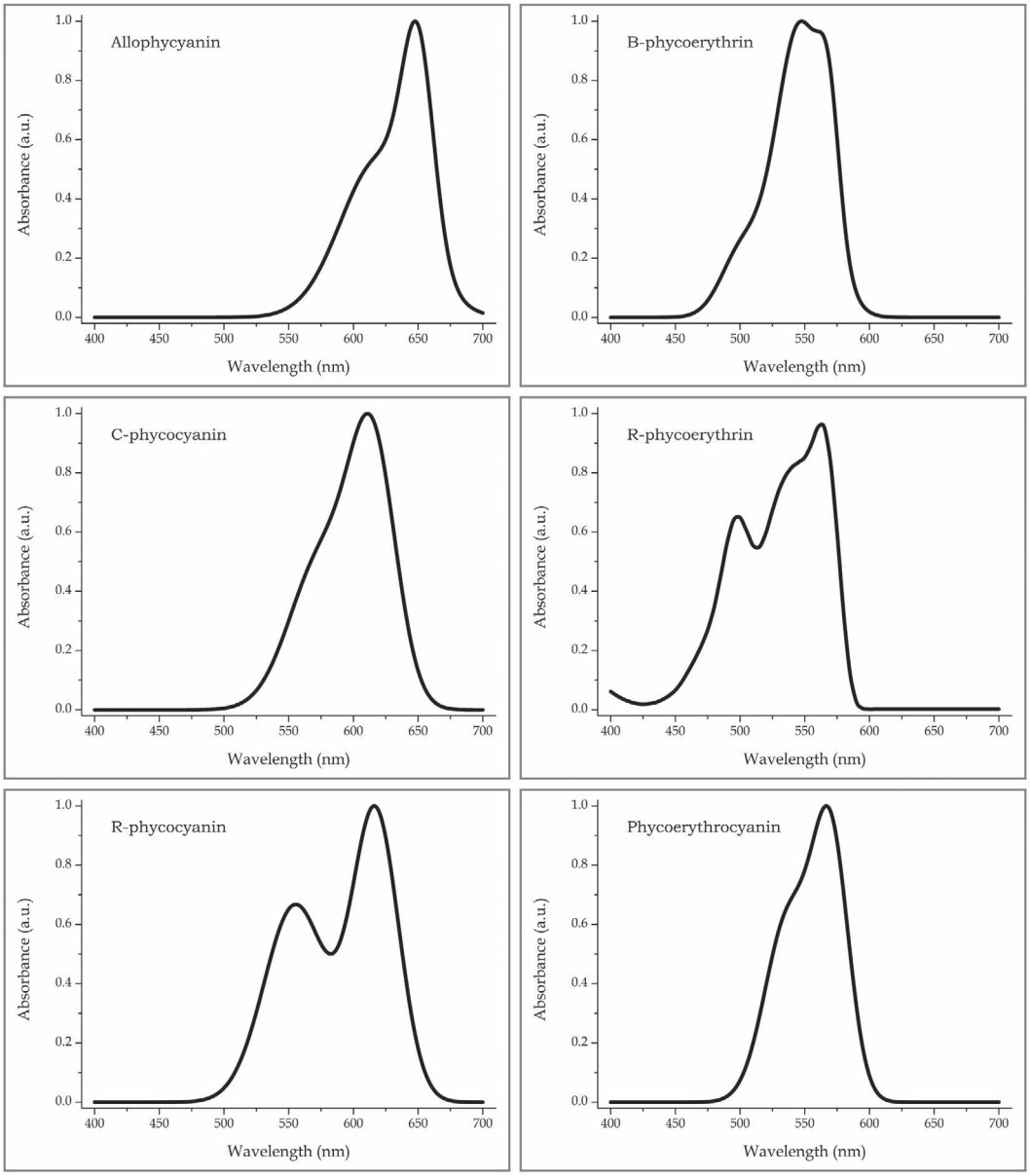


FIGURE 4.9 Structure of the main phycobiliproteins: allophycocyanin, C-phycocyanin, R-phycocyanin, B-phycoerythrin, R-phycoerythrin, phycoerythrocyanin. The prefixes R, C, and B indicate the origins of proteins from Rhodophyta, Cyanobacteria, and Bangiales (Bangiophyceae, Rhodophyta), respectively.

membrane. The energy-transforming units are two large protein complexes termed photosystems I and II, surrounded by light-harvesting complexes. Photons absorbed by PSI and PSII induce excitation of special chlorophylls *a*, P_{700}, and P_{680} (P stands for pigment, while the numbers 700 and 680 stand for the wavelength in nanometer of maximal absorption), initiating translocation of an electron across the thylakoid membrane along organic and inorganic redox couples forming the electron transfer chains (ETCs). The main components of these chains are plastoquinones, cytochromes, and ferredoxin. This electron translocation process eventually leads to a reduction of $NADP^+$ to NADPH

and to a transmembrane difference in the electrical potential and H^+ concentration, which drives ATP synthesis by means of an ATP synthase.

Thylakoid membranes are differentiated into stacked and unstacked regions. Stacking increases the amount of thylakoid membrane in a given volume. Both regions surround a common internal thylakoid space, but only unstacked regions make direct contact with the chloroplast stroma. The two regions differ in their content of photosynthetic assemblies; PSI and ATP synthase are located almost exclusively in unstacked regions, whereas PSII and LCHII are present mostly in stacked regions. This topology derives from protein–protein interactions rather than lipid bi-layer interactions. A common internal thylakoid space enables protons liberated by PSII in stacked membranes to be utilized by ATP synthase molecules that are located far away in unstacked membranes.

What is the functional significance of this lateral differentiation of the thylakoid membrane system? If both photosystems were present at high density in the same membrane region, a high proportion of photons absorbed by PSII would be transferred to PSI because the energy level of the excited state P_{680*} relative to its ground state P_{680} is higher than that of P_{700*} relative to P_{700}. A lateral separation of photosystems solves this problem by placing P_{680*} more than 100 Å from P_{700}. The positioning of PSI in the unstacked membranes gives it direct access to the stroma for the reduction of $NADP^+$. In fact the stroma-exposed surface of PSI, which contains the iron-sulfur proteins that carry electrons to ferredoxin and ultimately to $NADP^+$, protrudes about 50 Å beyond the membrane surface and could not possibly be accommodated within the stacks, where adjacent thylakoids are separated by no more than 40 Å. It seems likely that ATP synthase is also located in unstacked regions to provide space for its large protruding portion and access to ADP. In contrast, the tight quarters of the appressed regions pose no problem for PSII, which interacts with a small polar electron donor (H_2O) and a highly lipid-soluble electron carrier (plastoquinone). According to the model of Allen and Forsberg (2001), the close appression of grana (stacks of thylakoids) membranes arises because the flat stroma-exposed surfaces of LCHII form recognition and contact surfaces for each other, causing opposing surfaces of thylakoids to interact. There is not steric hindrance to this close opposition of stacked grana membranes, because PSII, like LCHII itself, presents a flat surface that protrudes no more than 10–20 Å beyond the membrane surface.

The functional significance of thylakoid stacking is presumably to allow a large, connected, light-harvesting antenna to form both within and between membranes. Within this antenna, excitation energy can pass between chlorophylls located in LCHII complexes that are adjacent to each other within a single membrane and between appressed membranes.

The degree of stacking and the proportion of different photosynthetic assemblies are regulated in response to environmental variables such as the intensity and spectral characters of incident light. The lateral distribution of LHC is controlled by reversible phosphorylation. At low light levels, LHC is bound to PSII. At high light levels, a specific kinase is activated by plastoquinol, and phosphorylation of threonine side chains of LHC leads to its release from PSII. The phosphorylated form of these light-harvesting units diffuses freely in the thylakoid membrane and may become associated with PSI to increase its absorbance coefficient (Figure 4.4).

Central to the photosynthetic process is PSII, which catalyzes one of the most thermodynamically demanding reactions in biology:

4) $$2H_2O \rightarrow 4e^- + 4H^+ + O_2$$

that is, the photo-induced oxidation of water. PSII has the power to split water and use its electrons and protons to drive photosynthesis. The first ancestor bacteria carrying on anoxygenic photosynthesis probably synthesized ATP by oxidation of H_2S and FeS compounds then abundant in the environment. The released energy could have been harnessed via production of a proton gradient, stimulating evolution of electron transport chains and the reducing equivalents (electrons) generated used in CO_2 fixation and thence biosynthesis. This was the precursor of the PSI. About 2800 billion years ago (Ba), the evolutionary pressure to use a less strongly reducing (and therefore more

abundant) source of electrons appears to have culminated in the development of the singularly useful trick of supplying the electrons to the oxidized reaction center from a tyrosine side chain, generating tyrosine cation radicals that are capable of sequential abstraction of electrons from water. Oxygenic photosynthesis, which requires the coupling in series of two distinct types of reaction centers (PSI and PSII), must have depended upon lateral transfer of genes between the evolutionary precursors of the modern sulfur bacteria (whose single reaction center resembles PSI) and those of purple bacteria (whose single reaction center resembles PSII). Thus, the cyanobacteria appeared. They were the first dominant organisms to use photosynthesis. As a by-product of photosynthesis, oxygen gas (O_2) was produced for the first time in abundance; the first rise of oxygen in the atmosphere, known as the Great Oxidation Event (GOE), is dated to 2.3–2.4 Ba, as well as constrained on the basis of geochemical proxies. This event represents the minimum age for the origin of oxygenic photosynthesis and the emergence and diversification of oxygen-requiring metabolic and biosynthetic pathways. Initially, oxygen released by photosynthesis was absorbed by iron (II), then abundant in the sea, thus oxidizing it to insoluble iron (III) oxide (rust). Red "banded iron deposits" of iron (III) oxide are marked in marine sediments of ca. 2500 million years ago. Once most/all iron (II) had been oxidized to iron (III), then oxygen appeared and began to increase in the atmosphere, gradually building up from zero ca. 2500 million years ago to approximately present levels ca. 500 million years ago. This was the "oxygen revolution."

Oxygen is corrosive, so prokaryotic life either became extinct, survived in anaerobic (oxygen-free) environments (and does so to this day), or evolved antioxidant protective mechanisms. The latter could begin to use oxygen to pull electrons from organic molecules, leading to aerobic respiration. The respiratory electron transport chain probably evolved from established photosynthetic electron transport, and the citric acid cycle probably evolved using steps from several biosynthetic pathways.

Hence cyanobacteria marked the planet in a very permanent way and paved the way for the subsequent evolution of oxidative respiratory biochemistry. This change marks the end of the Archaean Era of Precambrian Time.

PSII and PSI: Structure, Function, and Organization

The PSII and PSI photosynthetic complexes are very similar in eukaryotic algae (and plants) and cyanobacteria, as are many elements of the light capture, electron transport, and carbon dioxide (CO_2) fixation systems. The PSI and PSII complexes contain an internal antenna-domain carrying light-harvesting chlorophylls and carotenoids both non-covalently bound to a protein moiety and a central core domain where biochemical reactions occur. In the internal antenna complexes, chlorophylls do most of the light harvesting, whereas carotenoids and xanthophylls mainly protect against excess light energy and possibly transfer the absorbed radiation. In all photosynthetic eukaryotes, PSI and PSII form a super-complex since they are associated with an external antenna termed the light-harvesting complex. The main function of LHCs is the absorption of solar radiation and the efficient transmittance of excitation energy toward reaction center chlorophylls. LHCs are composed of a protein moiety to which chlorophylls and carotenoids are non-covalently bound. In eukaryotic algae, ten distinct light-harvesting apoproteins (Lhc) can be distinguished. Four of them are exclusively associated with PSI (Lhca1–4), another four with PSII (Lhcb3–6), and two (Lhcb1 and Lhcb2) are preferentially but not exclusively associated with PSII; that is, they can shuttle between the two photosystems. The apoproteins are three membrane-spanning α-helices and are nuclear encoded. LHCs are arranged externally with respect to the photosystems. In Cyanobacteria, Glaucophyta, Rhodophyta, and Cryptophyta, no LHCs are present, and the light-harvesting function is performed by phycobiliproteins organized in phycobilisomes (Figure 2.82 of Chapter 2). These structures are peripheral to the thylakoid membranes in Cyanobacteria, Glaucophyta, and Rhodophyta (Figures 2.81 and 2.84 of Chapter 2) and localized within the lumen of thylakoids in Cryptophyta. The phycobilisome structure consists of a three-cylinder core of four stacked molecules of allophycocyanin, closed to the thylakoid membrane, on which rod-shaped assemblies of

coaxially stacked hexameric molecules of only phycocyanin or both phycocyanin and phycoerythrin converge. Phycobilisomes are linked to the PSII, but they can diffuse along the surface of the thylakoids, at a rate sufficient to allow movements from PSII to PSI within 100 ms. Though prokaryotes, *Prochlorococcus* sp., *Prochlorothrix* sp., and *Prochloron* sp. differ from other cyanobacteria in possessing an external chlorophyll *a* and *b* antenna, like eukaryotic algae, instead of the large extrinsic phycobilisomes.

PSII complex can be divided into two main protein super-families differing in the number of membrane-spanning α-helices, that is, the six-helix protein superfamily, which includes the internal antennae CP43 and CP47 (CP stands for chlorophyll-protein complex), and the five-helix proteins of the reaction center core D1 and D2 (so called because they were first identified as two *diffuse* bands by gel electrophoresis and staining) where ETC components are located. External antenna proteins of prochlorophytes belong to the six-helix CP43 and CP47 superfamily and not to the three-helix LHCs superfamily.

PSII is a homodimer, where the two monomers in the dimers are almost identical. The monomer consists of over 20 subunits. All the redox active cofactors involved in the activity of PSII are bound to the reaction center proteins D1 and D2. Closely associated with these two proteins are the chlorophyll *a* binding proteins CP43 and CP47 and the extrinsic luminally bound proteins of the oxygen evolving complex. Each monomer also includes one heme *b*, one heme *c*, two plastoquinones, two pheophytins (a chlorophyll *a* without Mg^{2+}), and one non-heme Fe and contains 36 chlorophylls *a* and 7 *all-trans* carotenoids assumed to be β-carotene molecules. Eukaryotic and cyanobacterial PSII are structurally very similar at the level of both their oligomeric states and organization of the transmembrane helices of their major subunits. The eukaryotic PSII dimer is flanked by two clusters of Lhcb proteins. Each cluster contains two trimers of Lchb1, Lchb2, and Lchb3 and the other three monomers, Lchb4, Lchb5, and Lchb6.

The reactions of PSII are powered by light-driven primary and secondary electron transfer processes across the reaction center (D1 and D2 subunits). Upon illumination, an electron is dislodged from the excited primary electron donor P_{680}, a chlorophyll *a* molecule located towards the luminal surface. The electron is quickly transferred towards the stromal surface to the final electron acceptor, a plastoquinone, via a pheophytin. After accepting two electrons and undergoing protonation, plastoquinone is reduced to plastoquinol, and it is then released from PSII into the membrane matrix. The cation P_{680}^{+} is reduced by a redox active tyrosine, which in turn is reduced by a Mn ion within a cluster of four. When the $(Mn)_4$ cluster accumulates four oxidizing equivalents (electrons), two water molecules are oxidized to yield one molecule of O_2 and four protons. All the redox active cofactors involved in the electron transfer processes are located on the D1 side of the reaction center.

PSI complex possess only an 11-helix PsaA and PsaB protein superfamily. Each 11-transmembrane helix subunit has six-N terminal transmembrane helices that bind light-harvesting chlorophylls and carotenoids and act as internal antennae and five C-terminal transmembrane helices that bind Fe_4S_4 clusters as terminal electron acceptors. The N-terminal parts of the PsaA and PsaB proteins are structurally and functionally homologues to the CP43 and CP47 proteins of PSII; the C-terminal parts of the PsaA and PsaB proteins are structurally and functionally homologues to the D1 and D2 proteins of PSII. Eukaryotic PSI is a monomer that is loosely associated with the Lhca moiety, with a deep cleft between them. The four antenna proteins assemble into two heterodimers composed by Lhca1 and Lhca4 and homodimers composed by Lhca2 and Lhca3. Those dimers create a half-moon–shaped belt that docks to PsaA and PsaB and 12 other proteic subunits of the PSI, termed PsaC to PsaN, that contribute to the coordination of antenna chromophores. On the whole, PSI binds approximately 200 chromophore molecules. The cyanobacterial PSI exists as a trimer. One monomer consists of at least 12 different protein subunits (PsaA, PsaB, PsaC, PsaD, PsaE, PsaF, PsaI, PsaJ, PsaK, PsaL, PsaM, and PsaX) coordinating more than 100 chromophores.

After primary charge separation initiated by excitation of the chlorophyll *a* pair P_{700}, the electron passes along the electron transfer chain consisting of another chlorophyll *a* molecule, a

phylloquinone, and the Fe_4S_4 clusters. At the stromal side, the electron is donated by Fe_4S_4 to ferredoxin and thence transferred to $NADP^+$ reductase. The reaction cycle is completed by re-reduction of P_{700}^+ by plastocyanin (or the interchangeable cytochrome c_6) at the inner (lumenal) side of the membrane. The electron carried by plastocyanin is provided by PSII by way of a pool of plastoquinones and the cytochrome b_6f complex.

Photosynthetic eukaryotes such as Chlorophyta, Rhodophyta, and Glaucophyta have evolved by primary endosymbiosis involving a eukaryotic host and a prokaryotic endosymbiont. All other algae groups have evolved by secondary (or higher-order) endosymbiosis between a simple eukaryotic alga and a non-photosynthetic eukaryotic host. Although the basic photosynthetic machinery is conserved in all these organisms, it should be emphasized that PSI does not necessarily have the same composition and fine-tuning in all of them. The subunits that have only been found in eukaryotes, that is, PsaG, PsaH, and PsaN, have actually only been found in plants and in Chlorophyta. Other groups of algae appear to have a more cyanobacteria-like PSI. PsaM is also peculiar since it has been found in several groups of algae, including green algae; in mosses; and in gymnosperms. Thus, the PsaM subunit appears to be absent only in angiosperms. With respect to the peripheral antenna proteins, algae are in fact very divergent. All photosynthetic eukaryotes have Lhcs that belong to the same class of proteins. However, the Lhc*a* associated with PSI appear to have diverged relatively early, and the stoichiometry and interaction with PSI may well differ significantly between species. Even the green algae do not possess the same set of four Lhc*a* subunits that is found in plants.

Are all those light-harvesting complexes necessary? They substantially increase the light-harvesting capacity of both photosystems by increasing the photon-collecting surface with an associated resonance energy transfer to reaction centers, facilitated by specific pigment–pigment interactions. This process is related to the transition dipole–dipole interactions between the involved donor and acceptor antenna molecules that can be weakly or strongly coupled depending on the distance between and relative orientation of these dipoles. The energy migrates along a spreading wave since the energy of the photon can be found at a given moment in one or another of the many resonating antenna molecules. This wave merely describes the spread of the probability of finding the photon in different chlorophyll antenna molecules. Energy resonance occurs in the chromophores of the antenna molecules at the lowest electronic excited state available for an electron, since only this state has a lifetime (10^{-8} s) long enough to allow energy migration (10^{-12} s). The radiation-less process of energy transfer occurs toward pigments with lower excitation energy (longer-wavelength absorption bands). Within the bulk of pigment-protein complexes forming the external and internal antenna system, the energy transfer is directed to the chlorophyll *a* with an absorption peak at the longest wavelengths. Special chlorophylls *a* (P_{680} at PSII and P_{700} at PSI) located in the reaction center cores represent the final step end of the photon trip, since once excited ($P_{680} + h\nu \rightarrow P_{680}^*$; $P_{700} + h\nu \rightarrow P_{700}^*$), they become redox active species ($P_{680}^* \rightarrow P_{680}^+ + e^-$; $P_{700}^* \rightarrow P_{700}^+ + e^-$); that is, each donor releases one electron per excitation and activates different electron transport chains.

It is worthwhile to emphasize that in the case of *A. marina*, chlorophyll *a* is largely replace by red-shifted chlorophyll *d* (it accounts for about 98% of the total chlorophylls) in the reaction centers and light-harvesting complexes. Hence the special chlorophylls in the case of this cyanobacteria will be P_{713} and P_{740}.

ATP–Synthase

ATP production was probably one of the earliest cellular processes to evolve, and the synthesis of ATP from two precursor molecules is the most prevalent chemical reaction in the world. The enzyme that catalyzes the synthesis of ATP is the ATP synthase or F_0F_1-ATPase, one of the most ubiquitous proteins on earth. The F_1F_0-ATPases comprise a huge family of enzymes with members found not only in the thylakoid membrane of chloroplasts but also in the bacterial cytoplasmic membrane and in the inner membrane of mitochondria. The source of energy for the functioning of

ATP synthase is provided by photosynthetic metabolism in the form of a proton gradient across the thylakoid membrane, that is, a higher concentration of positively charged protons in the thylakoid lumen than in the stroma.

The F_0F_1-ATPase molecule is divided into two portions termed F_1 and F_0. The F_0 portion is embedded in the thylakoid membrane, while the F_1 portion projects into the lumen. Each portion is in turn made up of several different proteins or subunits. In F_0, the subunits are named *a*, *b*, and *c*. There is one *a* subunit, two *b* subunits, and 9–12 *c* subunits. The large *a* subunit provides the channel through which H^+ ions flow back into the stroma. Rotation of the *c* subunits, which form a ring in the membrane, is chemically coupled to this flow of H^+ ions. The *b* subunits are believed to help stabilize the F_0F_1 complex by acting as a tether between the two portions. The subunits of F_1 are called α, β, γ, δ, and ε. F_1 has three copies each of α and β subunits, which are arranged in an alternating configuration to form the catalytic "head" of F_1. The γ and ε subunits form an axis that links the catalytic head of F_1 to the ring of *c* subunits in F_0. When proton translocation in F_0 causes the ring of *c* subunits to spin, the γ-ε axis also spins because it is bound to the ring. The opposite end of the γ subunit rotates within the complex of α and β subunits. This rotation causes important conformational changes in the β subunits, resulting in the synthesis of ATP from ADP and P_i (inorganic phosphate) and its release.

ETC Components

Components of the electron transport system in order are plastoquinone, cytochrome b_6f complex, plastocyanin, and ferredoxin. Each of the components of the electron transport chain has the ability to transfer an electron from a donor to an acceptor, though plastoquinone also transfers a proton. Each of these components undergoes successive rounds of oxidation and reduction, receiving an electron from the PSII and donating the electron to PSI.

Plastoquinone refers to a family of lipid soluble benzoquinone derivatives with an isoprenoid side chain. In chloroplasts, the common form of plastoquinone contains nine repeating isoprenoid units. Plastoquinone possesses varied redox states, which together with its ability to bind protons and its small size enable it to act as a mobile electron carrier shuttling hydrogen atoms from PSII to the cytochrome b_6f complex.

Plastoquinone is present in the thylakoid membrane as a pool of 6–8 molecules per PSII. Plastoquinone exists as quinone A (Q_A) and quinone B (Q_B); Q_A is tightly bound to the reaction center complex of PSII, and it is immovable. It is the primary stable electron acceptor of PSII, and it accepts and transfers one electron at time. Q_B is a loosely bound molecule, which accepts two electrons and then takes on two protons before it detaches and becomes Q_BH_2, the mobile reduced form of plastoquinone (plastoquinol). Q_BH_2 is mobile within the thylakoid membrane, allowing a single PSII reaction center to interact with a number of cytochrome b_6f complexes.

Plastoquinone plays an additional role in the cytochrome b_6f complex, operating in a complicated reaction sequence known as a Q-cycle. When Q_B is reduced in PSII, it not only receives two electrons from Q_A, but it also picks up two protons from the stroma matrix and becomes Q_BH_2. It is able to carry both electrons and protons (e^- and H^+ carrier). At the cytochrome b_6f complex level, it is then oxidized, but FeS and cytochrome b_6 can only accept electrons and not protons, so the two protons are released into the lumen. The Q-cycle of the cytochrome b_6f complex is great because it provides extra protons to the lumen. Here two electrons travel through the two hemes of cytochrome b_6 and reduce Q_B on the stroma side of the membrane. The reduced Q_B takes on two protons from the stroma, becoming Q_BH_2, which migrates to the lumen side of the cytochrome b_6f complex, where it is again oxidized, releasing two more protons into the lumen. Thus the Q-cycle allows formation of more ATP. This Q-cycle links the oxidation of plastoquinol (Q_BH_2) at one site on the cytochrome b_6f complex to the reduction of plastoquinone at a second site on the complex in a process that contributes additional free energy to the electrochemical proton potential.

The cytochrome b_6f complex is the intermediate protein complex in linear photosynthetic electron transport. The cytochrome b_6f complex essentially couples PSII and PSI and also provides

the means of proton gradient formation by using cytochrome groups as redox centers in the electron transport chain, thereby separating the electron/hydrogen equivalent into its electron and proton components. The electrons are transferred to PSI via plastocyanin, and the protons are released into the thylakoid lumen of the chloroplast. The electron transport from PSII to PSI via cytochrome b_6f complex occurs in about 7 msec, representing the rate limiting step of the photosynthetic process.

The cytochrome b_6f exists as a dimmer of 217 kDa. The monomeric complex contains four large subunits (18 to 32 kDa): cytochrome *f*, cytochrome b_6, the Rieske FeS iron-sulfur protein (ISP), and subunit IV, as well as four small hydrophobic subunits, PetG, PetL, PetM, and PetN. The monomeric unit contains 13 transmembrane helices: four in cytochrome b_6 (helices A to D); three in subunit IV (helices E to G); and one each in cytochrome *f*, the ISP, and the four small hydrophobic subunits PetG, PetL, PetM, and PetN. The monomer includes four hemes, one [2Fe-2S] cluster, one chlorophyll *a*, one β-carotene, one plastoquinone. The extrinsic domains of cytochrome *f* and the ISP are on the luminal side of the membrane and are ordered in a crystal structure. Loops and chain termini on the stromal side are less well ordered. The ISP contributes to dimer stability by domain swapping, its transmembrane helix obliquely spans the membrane in one monomer, and its extrinsic domain is part of the other monomer. The two monomers form a protein-free central cavity on each side of the transmembrane interface.

Cytochrome c_6 is a small soluble electron carrier. It is a highly α-helical heme-containing protein. It is located on the luminal side of the thylakoid membrane, where it catalyzes the electron transport from the membrane-bound cytochrome b_6f complex to PSI. It is the sole electron carrier in some cyanobacteria.

Plastocyanin operates in the inner aqueous phase of the photosynthetic vesicle, transferring electrons from cytochrome *f* to PSI, the primary donor of PSI. It is a small protein (10 kDa) composed of a single polypeptide that is coded for in the nuclear genome. Plastocyanin is a β-sheet protein with copper as the central ion that is ligated to four residues of the polypeptide. The copper ion serves as a one-electron carrier with a midpoint redox potential (0.37 eV) near that of cytochrome *f*. Plastocyanin shuttles electrons from the cytochrome b_6f complex to PS I by diffusion. Plastocyanin is more common in green algae and completely substitutes for cytochrome c_6 in the chloroplasts of higher plants. In cyanobacteria and green algae where both cytochrome c_6 and plastocyanin are encoded, the alternative expression of the homologous protein is regulated by the availability of copper.

Ferredoxin is a small protein (11 kDa) and has the distinction of being one of the strongest soluble reductants found in cells (midpoint redox potential = −0.42 eV). The amino acid sequence for ferredoxin from different species is known, as well as the three-dimensional structure. Plants contain different forms of ferredoxin, all of which are encoded in the nuclear genome. In some algae and cyanobacteria, ferredoxin can be replaced by a flavoprotein. Ferredoxin operates in the stromal aqueous phase of the chloroplast, transferring electrons from PSI to a membrane-associated flavoprotein, known as FNR. A 2Fe-2S cluster, ligated by four cysteine residues, serves as a one-electron carrier.

Once an electron reaches ferredoxin, however, the electron pathway becomes branched, enabling redox free energy to enter other metabolic pathways in the chloroplast. For example, ferredoxin can transfer electrons to nitrite reductase, glutamate synthase, and thioredoxin reductase.

Electron Transport: The Z-Scheme

The fate of the released electrons is determined by the sequential arrangement of all the components of PSII and PSI, which are connected by a pool of plastoquinones, the cytochrome b_6f complex, and the soluble proteins cytochrome c_6 and plastocyanin cooperating in series. The electrons from PSII are finally transferred to the stromal side of PSI and used to reduce $NADP^+$ to NADPH, a reaction catalyzed by ferredoxin-$NADP^+$ oxidoreductase (FNR). In this process, water acts as electron donor to the oxidized P_{680} in PSII, and O_2 evolves as a by-product.

Photosystem II uses light energy to drive two chemical reactions: the oxidation of water and the reduction of plastoquinone. Photochemistry in PSII is initiated by charge separation between P_{680} and pheophytin, creating the redox couple P_{680}^{+}/Pheo^{-}. The primary charge separation reaction takes only a few picoseconds. Subsequent electron transfer steps prevent the separated charges from recombining by transferring the electron from pheophytin to a plastoquinone molecule within 200 picoseconds. The electron on Q_A^{-} is then transferred to the Q_B-site. As already stated, plastoquinone at the Q_B-site differs from plastoquinone at the Q_A-site in that it works as a two-electron acceptor and becomes fully reduced and protonated after two photochemical turnovers of the reaction center. The full reduction of plastoquinone at the Q_B-site requires the addition of two electrons and two protons. The reduced plastoquinone (plastoquinol, Q_BH_2) then unbinds from the reaction center and diffuses in the hydrophobic core of the membrane, after which an oxidized plastoquinone molecule finds its way to the Q_B-binding site, and the process is repeated. Because the Q_B-site is near the outer aqueous phase, the protons added to plastoquinone during its reduction are taken from the outside of the membrane. Electrons are passed from Q_BH_2 to a membrane-bound cytochrome, b_6f, concomitant with the release of two protons to the luminal side of the membrane. The cytochrome b_6f then transfers one electron to a mobile carrier in the thylakoid lumen, either plastocyanin or cytochrome c_6. This mobile carrier serves an electron donor to PSI reaction center, the P_{700}. Upon photon absorption by PSI, a charge separation occurs with the electron fed into a bound chain of redox sites, a chlorophyll *a* (A_0), a quinone acceptor (A_1), and then a bound Fe-S cluster, and then on two Fe-S clusters in ferredoxin, a soluble mobile carrier on the stromal side. Two ferredoxin molecules can reduce $NADP^{+}$ to NADPH via the flavoprotein ferredoxin-$NADP^{+}$ oxidoreductase. NADPH is used as redox currency for many biosynthesis reactions such as CO_2 fixation. The energy conserved in a mole of NADPH is about 52.5 Kcal/mol, while in an ATP mole, it is 7.3 Kcal.

The photochemical reaction triggered by P_{700} is a redox process. In its ground state, P_{700} has a redox potential of 0.45 eV and can take up an electron from a suitable donor; hence, it can perform an oxidizing action. In its excited state, it possesses a redox potential of more than −1.0 eV and can perform a reducing action donating an electron to an acceptor and becoming P_{700}^{+}. The couple P_{700}/P_{700}^{+} is thus a light-dependent redox enzyme and possesses the capability to reduce the most electron-negative redox system of the chloroplast, the ferredoxin-$NADP^{+}$ oxidoreductase (redox potential = −0.42 eV). On the other hand, P_{700} in its ground state (redox potential = 0.45 eV) is not able to oxidize, that is, to take electrons from water that has a higher redox potential (0.82 eV). The transfer of electrons from water is driven by the P_{680} at PSII, which in its ground state has a sufficiently positive redox potential (1.22 eV) to oxidize water. In its excited state, P_{680} at PSII reaches a redox potential of about −0.60 eV, which is enough to donate an electron to a plastoquinone (redox potential = 0 eV) and then via cytochrome b_6f complex to P_{700}^{+} at PSI so that it can return to P_{700} and be excited once again. This reaction pathway is called the "Z-scheme of photosynthesis," because the redox diagram from P_{680} to P_{700} looks like a big "Z" (Figure 4.10).

From this scheme, it should be evident that only approximately one third of the energy absorbed by the two primary electron donors P_{680} and P_{700} is turned into chemical form. A 680-nm photon has an energy of 1.82 eV, and a 700-nm photon has an energy of 1.77 eV (total = 3.59 eV), which is three times more than the energy sufficient to change the potential of an electron by 1.24 eV, from the redox potential of the water (0.82 eV) to that of ferredoxin-$NADP^{+}$ oxidoreductase (−0.42 eV).

It is worthwhile to emphasize that any photon that is absorbed by any chlorophyll molecules is energetically equivalent to a red photon since the extra energy of an absorbed photon of shorter wavelength (<680 nm) is lost during the quick fall to the red energy level representing the lowest excited level.

Proton Transport: Mechanism of Photosynthetic Phosphorylation

The interplay of PSI and PSII leads to the transfer of electrons from H_2O to NADPH and the concomitant generation of proton gradient across the thylakoid membrane for ATP synthesis. The

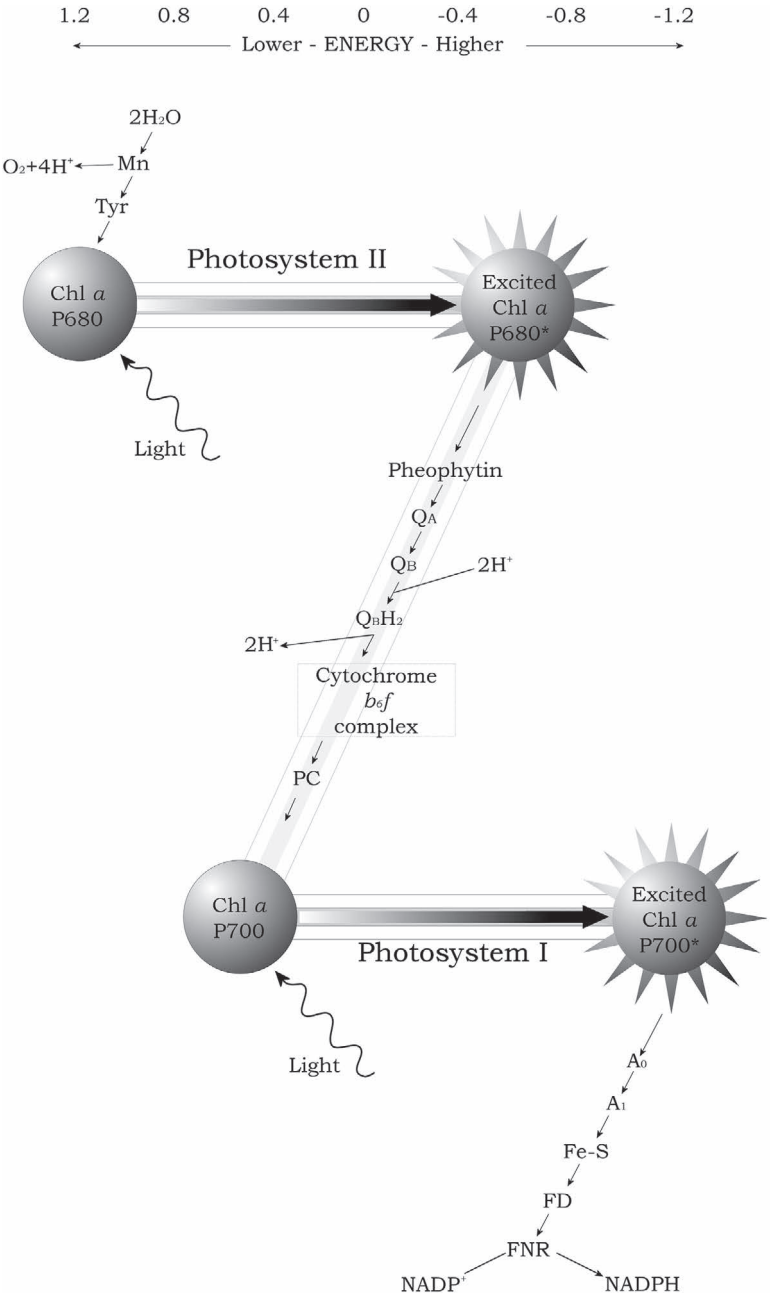


FIGURE 4.10 Schematic drawing of the Z-scheme of photosynthetic electron transport, with the positions of the participants on the oxido-reduction scale.

thylakoid space becomes markedly acidic, approaching pH 4. The light-induced transmembrane proton gradient is about 3.5 pH units. The generation of these protons follows two routes:

- four protons are released for the splitting of two water molecules and the release of one oxygen molecule in the thylakoid space;

- the transport of four electrons through the cytochrome b_6f complex leads to the translocation of eight protons from the stroma to the thylakoid space.

Therefore about 12 protons for each O_2 molecule released are translocated. The proton-motive force Δp, that is, the force created by the accumulation of hydrogen ions on one side of the thylakoid membrane, consists of a pH gradient contribution and a membrane-potential contribution. In chloroplasts, nearly all of Δp arises from the pH gradient, whereas in the mitochondria, the contribution from the membrane potential is larger. This difference is due to the thylakoid membrane permeability to Cl^- and Mg^{2+}. The light-induced transfer of H^+ into the thylakoid space is accompanied by the transfer of either Cl^- in the same direction or Mg^{2+} in the opposite direction (1 per 2 H^+). Consequently electrically neutrality is maintained and no membrane potential is generated. A pH of 3.5 units across the thylakoid membrane corresponds to a Δp of 0.22 V or a ΔG (change in Gibbs free energy) of −4.8 Kcal/mol. The change in Gibbs free energy associated with a chemical reaction is a useful indicator of whether the reaction will proceed spontaneously. This energy is called free energy because it is the energy that will be released or freed up to do work. Since the change in free energy is equal to the maximum useful work that can be accomplished by the reaction, then a negative ΔG associated with a reaction indicates that it can happen spontaneously. About three protons flow through the F_0F_1 ATPase complex per ATP synthesized, which corresponds to a free energy input of 14.4 Kcal per mole of ATP, but only 7.3 Kcal are stored in the ATP molecule, which is a yield of about 50%. No ATP is synthesized if the pH gradient is less than two units because the gradient force is then too small. The newly synthesized ATP is released into the stromal space. Likewise, NADPH formed by PSI is released into the stromal space. Thus ATP and NADPH, the products of light reactions of photosynthesis, are appropriately positioned for the subsequent light-independent reactions, in which CO_2 is converted into carbohydrates. The overall reaction can be expressed as:

5) $$4NADP^+ + 2H_2O + 4ADP + 4P_i \xrightarrow{8\ photons\ and\ 4\ e^-} 4NADPH + 4ATP + O_2$$

This equation implies that each H_2O is split in the thylakoids under the influence of the light to give off $½O_2$ molecule and that the two electrons so freed are then transferred to two molecules of $NADP^+$, along with H^+s, to produce the strong reducing agent NADPH. Two molecules of ATP can be simultaneously formed from two ADP and two inorganic phosphates (P_i) so that the energy is stored in high-energy compounds. NADPH and ATP are the assimilatory power required to reduce CO_2 to carbohydrates in the light-independent phase. The generation of ATP following this route is termed non-cyclic phosphorylation since electrons are just transported from water to $NADP^+$ and do not come back.

An alternative pathway for ATP production is cyclic phosphorylation, in which electrons from PSI cycle in a closed system through the phosphorylation sites and ATP is the only product formed. Electron arising from P_{700} are transferred to ferredoxin and then to the cytochrome b_6f complex. Protons pumped by this complex as electrons return to the oxidized form of reaction center P_{700} through plastocyanine. This cyclic phosphorylation takes place when NADP is unavailable to accept electrons from reduced ferredoxin because of a very high ratio of NADPH to $NADP^+$.

The electrochemical potential of the proton gradient drives the synthesis of ATP through an ATP-synthase situated, as we have seen anisotropically in the thylakoid membrane.

Pigment Distribution in PSII and PSI Super-Complexes of Algal Division

Absorption spectra can give us information about the spectral range in which pigment molecules organized in the thylakoid membranes capture photons. Absorption spectra in the visible range, from 400 to 700 nm, have been measured *in vivo* on photosynthetic compartments (thylakoid membranes, chloroplasts) of single cells belonging to each algal division. Each spectrum represents the envelope of the real absorption data and is coupled to the plot of the fourth-derivative absorption

spectrum. This mathematical tool allows the resolution of absorption maxima relative to the different components of the pigment moiety characterizing the division, which cannot be detected in the envelope spectrum because of the overlapping of their multiple spectra. These components have been grouped and related to the following pigment classes: chlorophylls *a*, *b*, c_1 c_2, *d*, and *f*; carotenoids; xanthophylls; cytochromes; and phycobiliproteins. Each pigment possesses its own distinctive absorption spectrum in the visible range, which has been decomposed in its Gaussian bands and relative absorption maxima. By relating the absorption maxima resolved by means of fourth-derivative analysis with the absorption maxima of the Gaussian bands of the different pigments, it is possible both to predict the presence of a specific pigment in an alga and to give an unknown alga a plausible taxonomic framing.

Chlorophylls and cytochromes always show the same absorption maxima independently of the algal division, though the intensity of their absorption bands may change; phycobiliproteins, carotenoids, and xanthophylls show a variable distribution of their single components, which is characteristic of each algal division. Figures 4.11, 4.12, 4.13, and 4.14 show the absorption spectra of the photosynthetic compartments in all the different algal divisions. The absorption spectrum of the tissue of a higher plant, a lawn daisy (*Bellis perennis*), is shown to highlight the uniformity of the pigment distribution throughout the algal green lineage and plants (Figure 4.15).

It should be stressed that all pigments other than chlorophyll *a* perform two main functions: protection of photosynthetic assemblies from photosensitization processes (mainly carotenoids) and absorption of light at wavelengths other than those absorbed by chlorophyll *a* and transfer of its energy to P_{680} and P_{700}.

Light-Independent Reactions

We have seen that NADPH and ATP are produced in the light phase of photosynthesis. The next phase of photosynthesis involves the fixation of CO_2 into carbohydrates. Although many textbooks state that glucose ($C_6H_{12}O_6$) is the major product of photosynthesis, the actual carbohydrate end-products are those listed in Table 1.2 in Chapter 1 (sucrose, paramylon, starch, etc.). The fixation of CO_2 takes place during the light-independent phase using the assimilatory power of NADPH and ATP in the chloroplast stroma (eukaryotic algae) or in the cytoplasm (prokaryotic algae). Light-independent reactions do not occur in the dark; rather they occur simultaneously with the light reactions. However, light is not directly involved. Light-independent reactions are commonly referred to as the Calvin Benson Bassham cycle (CBB cycle) after the pioneering work of their discoverers (Figure 4.16).

The first metabolite was a three-carbon organic acid known as 3-phosphoglycerate (3-PG). For this reason, the pathway of carbon fixation in algae and most plants is referred to as C3 photosynthesis. Since the first product was a C3 acid, Calvin hypothesized that the CO_2 acceptor would be a C2 compound. However, no such C2 substrate was found. Rather, it was realized that the CO_2 acceptor was a C5 compound, ribulose 1,5-bisphosphate (RuBP), and that the product of carboxylation was two molecules of 3-PG. This crucial insight allowed the pathway of carbon flow to be determined.

While the CBB cycle involves a total of 13 individual enzymatic reactions, only two enzymes are unique to this pathway: ribulose-1,5-bisphosphate carboxylase/oxygenase and phosphoribulokinase (PRK). All other enzymes involved also perform functions in heterotrophic metabolism. PRK catalyzes the phosphorylation of ribulose-monophosphate to ribulose-1,5-bisphosphate. RuBP in turn is the substrate for RuBisCO, which catalyzes the actual carbon fixation reaction.

RuBisCO

The RuBisCO enzyme alone represents the most important pathway by which inorganic carbon enters the biosphere. It has also been described as the most abundant protein on earth. It is thought that as much as 95% of all carbon fixation by C3 organisms (that includes all phytoplankton) occurs through RuBisCO.

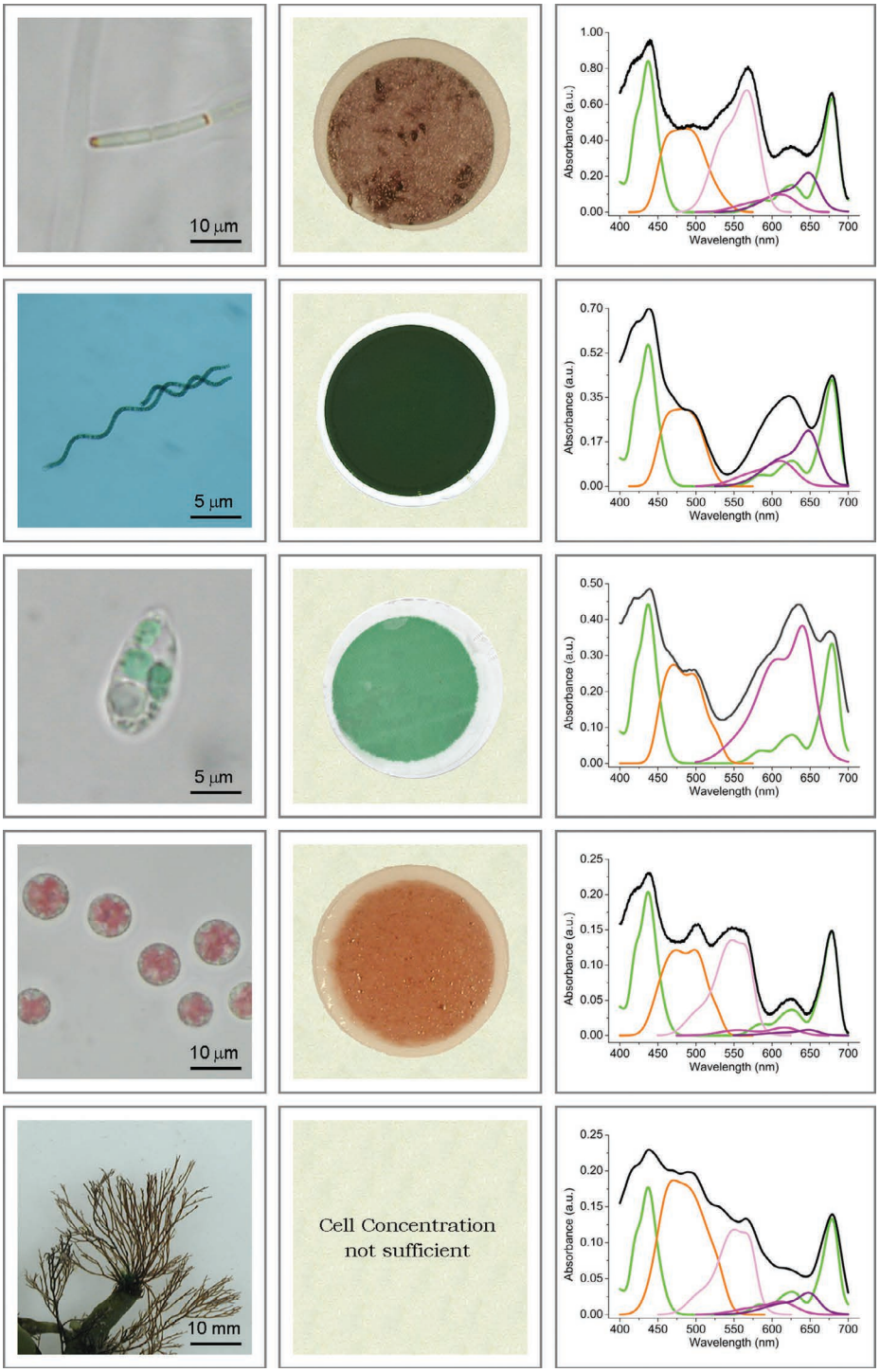


FIGURE 4.11 *In vivo* absorption spectra of photosynthetic compartments of *Leptolyngbya* (Cyanobacteria), *Arthrospira* (Cyanobacteria), *Cyanophora* (Glaucophyta), *Porphyridium* (Rhodophyta), *Polysiphonia lanosa* (Rhodophyta), from top to bottom. Bright green line: chlorophyll *a;* orange line: carotenoids and xanthophylls; purple lines: phycobiliproteins.

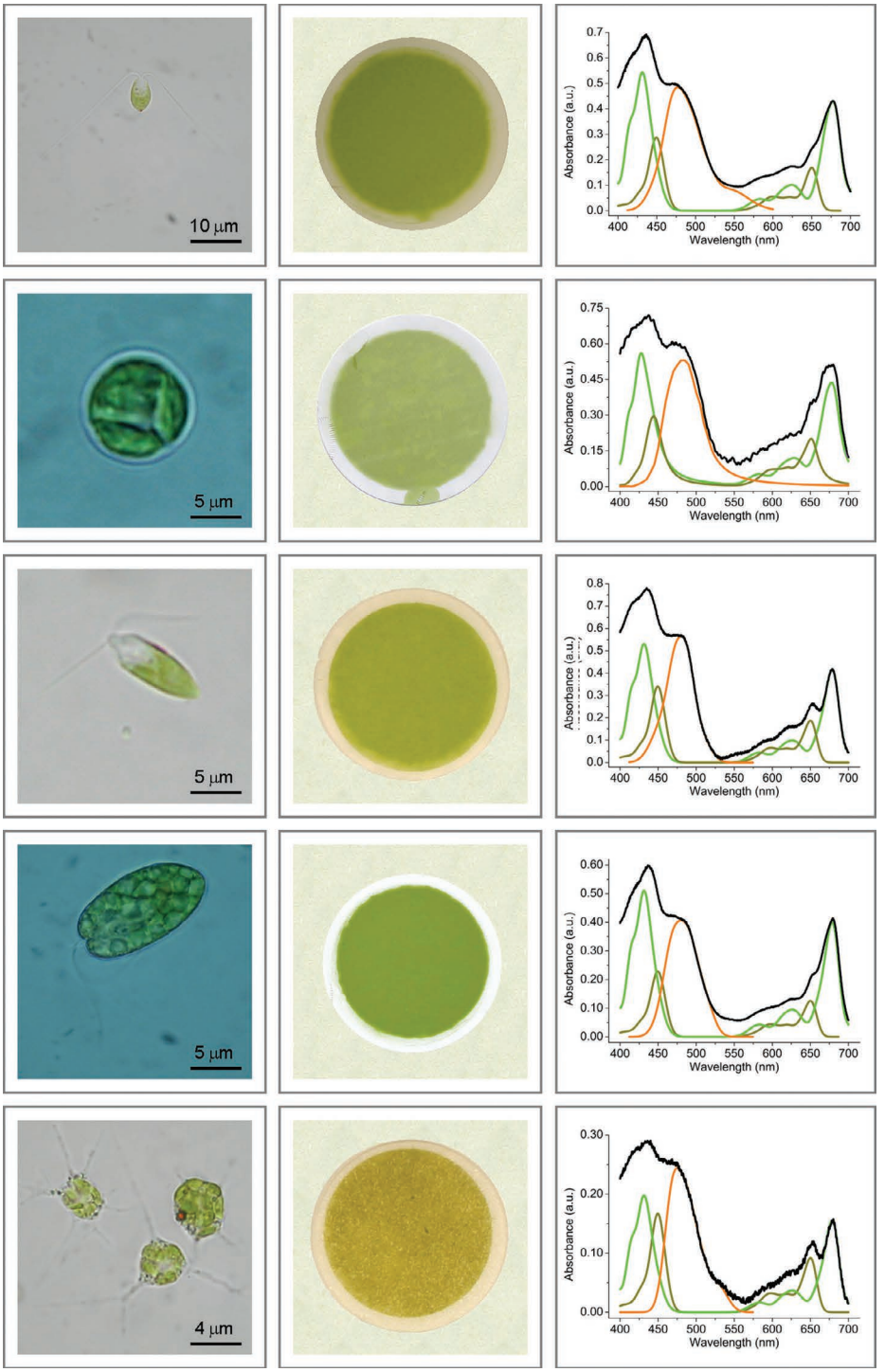


FIGURE 4.12 *In vivo* absorption spectra of photosynthetic compartments of *Tetraflagellochloris mauritanica* (Chlorophyta), *Chlorella* (Chlorophyta), *Dunaliella* (Chlorophyta), *Tetraselmis* (Chlorophyta), and *Gymnochlora* (Chlorarachniophyceae), from top to bottom. Bright green line: chlorophyll *a;* dark green line: chlorophyll *b;* orange line: carotenoids and xanthophylls.

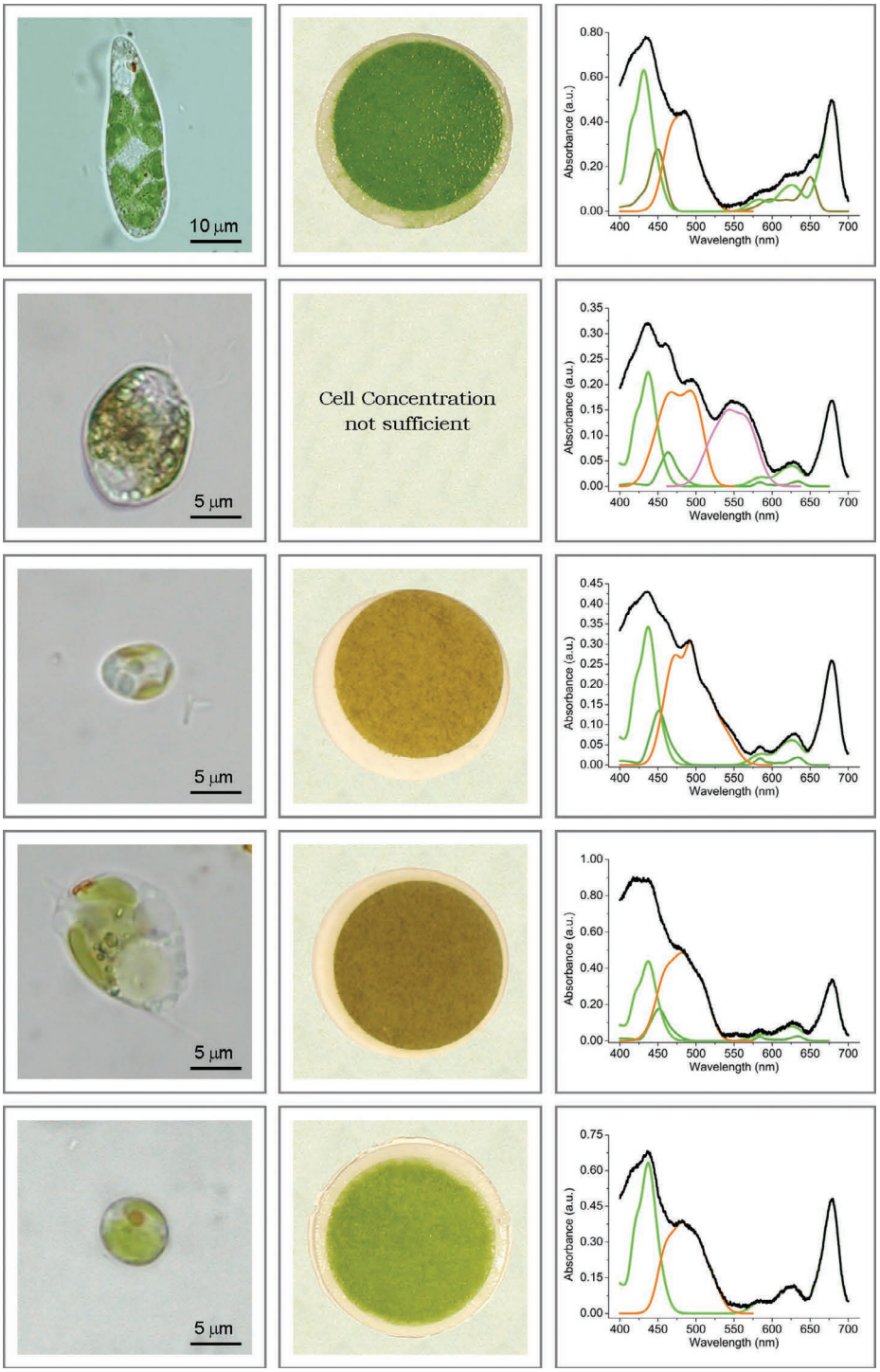


FIGURE 4.13 *In vivo* absorption spectra of photosynthetic compartments of *Euglena* (Euglenophyta), *Rhodomonas* (Cryptophyta), *Pavlova* (Haptophyta), *Ochromonas* (Ochrophyta), and *Nannochloropsis* (Ochrophyta), from top to bottom. Bright green line: chlorophyll *a;* dark green line: chlorophyll *b;* orange line: carotenoids and xanthophylls; purple line: B-phycobiliprotein (545).

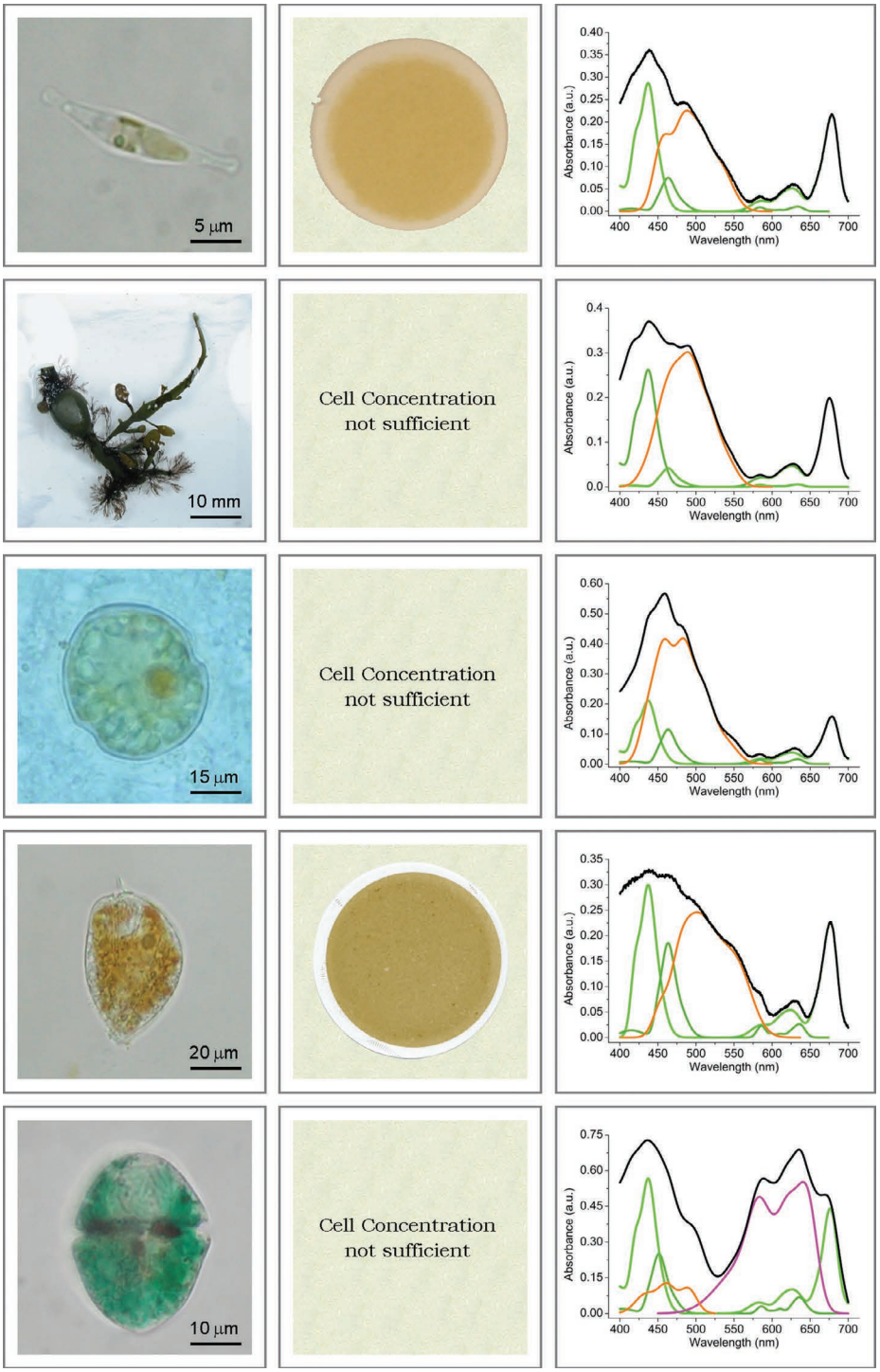


FIGURE 4.14 *In vivo* absorption spectra of photosynthetic compartments of *Phaeodactylum* (Ochrophyta), *Ascophyllum nodosum* (Ochrophyta) *Karenia* (Dinophyceae), *Prorocentrum* (Dinophyceae), *Gymnodinium* (Dinophyceae), from top to bottom. Bright green line: chlorophyll *a;* dark green line: chlorophyll *b;* orange line: carotenoids and xanthophylls; purple line: R-phycocyanin (645).



FIGURE 4.15 *In vivo* absorption spectra of photosynthetic compartments of the lawn daisy *Bellis perennis* shown to highlight the uniformity of pigment distribution throughout the algae green lineage and plants. Bright green line: chlorophyll *a;* dark green line: chlorophyll *b;* orange line: carotenoids and xanthophylls.

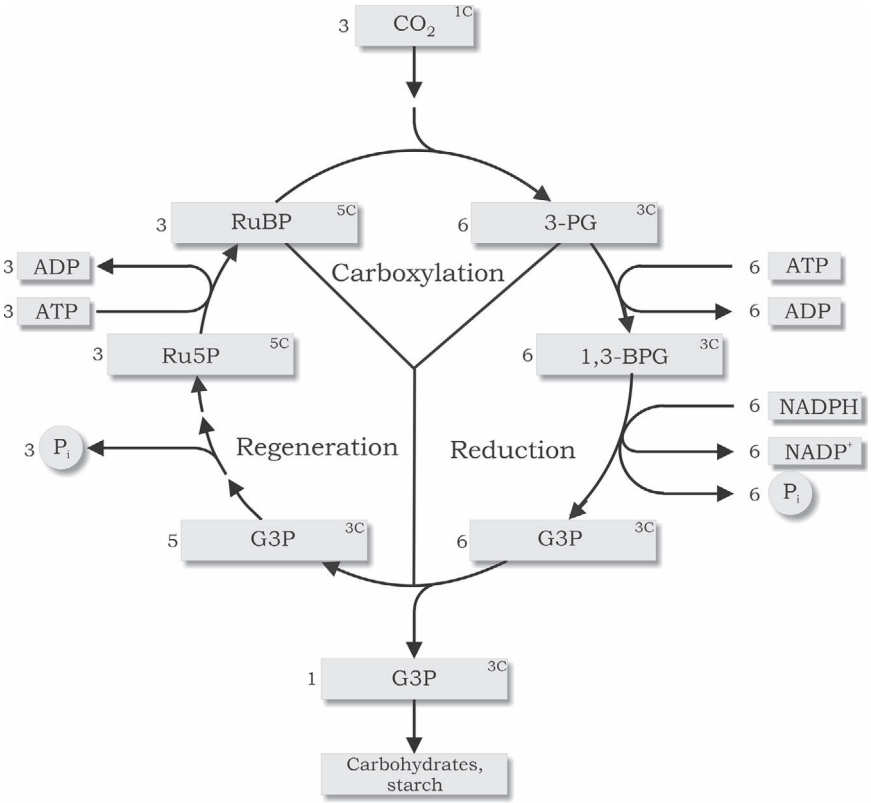


FIGURE 4.16 Schematic drawing of the three phases of Calvin Benson Bassham cycle.

RuBisCO is known to catalyze at least two reactions: the reductive carboxylation of ribulose 1,5-bisphosphate to form two molecules of 3-phosphoglycerate and the oxygenation of RuBP to form one molecule of 3-PG and one molecule of 2-phosphoglycolate.

The oxygenation of RuBP is commonly referred to as photorespiration and has traditionally been seen as a wasteful process, in particular because the regeneration of RuBP in photorespiration

leads to the evolution of CO_2 and requires free energy in the form of ATP. In addition, RuBisCO suffers from several other inefficiencies. Both reactions (carboxylation and oxygenation) occur in the same active site and compete, making the enzyme extremely sensitive to local partial pressures of CO_2 and O_2. RuBisCO makes up 20–50% of the protein in chloroplasts. It acts very slowly, catalyzing three molecules per second. This compares to 1000 molecules per second for typical enzymatic reactions. Large quantities are needed to compensate for its slow speed. It may be the most abundant protein on earth. Last, RuBisCO rarely performs its function at a maximum rate (K_{max}), since the partial pressure of CO_2 in the vicinity of the enzyme is often smaller than its Michaelis-Menten half-saturation constant (K_m). RuBisCO has been shown to occur in two distinct forms in nature, termed Forms I and II. Form I of the enzyme is an assemblage of eight 55-kDa large subunits (rbcL) and eight 15-kDa small subunits (rbcS). These subunits assemble into a 560-kDa hexadecameric protein-complex designated as L8S8. Most photosynthetic prokaryotes that depend on the CBB cycle for carbon assimilation and all eukaryotic algae express a Form I type RuBisCO. The exception to this rule can be found in several marine dinoflagellates, which apparently contain a nuclear-encoded Form II of RuBisCO. Form II of RuBisCO is a dimer of large subunits (L2) and is otherwise found in many photosynthetic and chemoautotrophic bacteria. Phylogenetic analysis of large number of Form I rbcL DNA sequences revealed the division of Form I into four major clades, referred to as IA, IB, IC, and ID. Form IA is commonly found in nitrifying and sulfur-oxidizing chemoautotrophic bacteria as well as some marine *Synechococcus* (marine type A) and all *Prochlorococcus* strains sequenced to date. All other cyanobacteria as well as all green algae possess a Form IB type enzyme. Form IC of rbcL is expressed by some photosynthetic bacteria, such as hydrogen oxidizers. Form ID encompasses a diverse group of eukaryotic lineages, including essentially all chromophytic, eucaryotic algae such as Phaeophyceae, Rhodophyta, Bacillariophyceae, and Raphidophyceae.

The phylogeny of RuBisCO displays several interesting incongruences with phylogenies derived from ribosomal DNA sequences. This has led to the speculation that over evolutionary history, numerous lateral gene transfers may have occurred, transferring RuBisCO among divergent lineages. For example, the dinoflagellate *Gonyaulax polyedra* contains a Form II RuBisCO most similar to sequences found in proteobacteria. Within the Form I clade, as many as six lateral transfers have been suggested to explain the unusual phylogeny observed among the cyanobacteria, proteobacteria, and plastids. Some bacteria may have acquired a green-like cyanobacterial gene, while marine *Synechococcus* and *Prochlorococcus* almost certainly obtained their RuBisCO genes from a purple bacterium.

Three-dimensional structures of the RuBisCO enzyme are now known for a number of species, including *Synechococcus,* the green alga *Chlamydomonas reinhardtii,* and the red alga *Galdieria sulphuraria*. Based on these and other studies, it is now believed that the primary catalytic structure of RuBisCO is a dimer of two large subunits (L2). In Form I RuBisCO, four L2 dimers are cemented to form L8S8 hexadecameric superstructure whereby the major contacts between the L2 dimers are mediated by the small subunits. A Mg^{+2} cofactor as well as the carbamylation of Lys201 is required for the activity of the enzyme. A loop in the beta barrel and two other elements of the large subunit, one in the N- and one in the C-terminus of the protein, form the active site in *Synechococcus*. Small subunits apparently do not contribute to the formation of the active site.

Calvin Benson Bassham Cycle

The reactions of the Calvin cycle can be thought of as occurring in three phases (Figure 4.16):

Carboxylation—fixation of CO_2 into a stable organic intermediate
Reduction—reduction of this intermediate to the level of carbohydrate
Regeneration—regeneration of the CO_2 acceptor

Carboxylation

Carboxylation involves the addition of one molecule of CO_2 to a five-carbon "acceptor" molecule, ribulose biphosphate. This reaction is catalyzed by the enzyme RuBisCO. Plants invest a huge amount of their available nitrogen into making this one protein. As a result, RuBisCO is the most abundant protein in the biosphere. The resulting six-carbon product splits into two identical three-carbon products. These products are 3-phosphoglycerate, or simply 3-PG. At this point in the cycle, CO_2 has been "fixed" into an organic product, but no energy has been added to the molecule.

Reduction

The second step in the Calvin cycle is the reduction of 3-PG to the level of carbohydrate. This reaction occurs in two steps: (a) phosphorylation of 3-PG by ATP to form a 1,3-biphosphoglycerate (1,3-BPG) and (b) reduction of 1,3-BPG by NADPH to form glyceraldehyde-3-phosphate (G3P), a simple three-carbon carbohydrate, its isomers collectively called triose phosphates. This reaction requires both ATP and NADPH, the high-energy chemical intermediates formed in the light reactions.

The NADP+ and ADP formed in this process return to the thylakoids to regenerate NADPH and ATP in the light reactions.

Regeneration

The final stage in the Calvin cycle is the regeneration of the CO_2 acceptor RuBP. This involves a series of reactions that convert triose phosphate first to the five-carbon intermediate Ru5P (ribulose 5-phosphate), then phosphorylation of Ru5P to regenerate RuBP (ribulose-bisphosphate). This final step requires ATP formed in the light reactions.

Overall, for every three turns of the cycle, one molecule of product (triose phosphate) is formed ($3CO_2$:1G3P). The remaining 15 carbon atoms (5 G3P) re-enter the cycle to produce three molecules of RuBP.

The triose phosphate formed in the Calvin cycle can remain in the chloroplast, where it is converted to starch. This is why chloroplasts form starch grains. Alternatively, triose phosphate can be exported from the chloroplast, where it is converted to carbohydrates in the cytoplasm. Both reactions involve the release of phosphate. In the case of carbohydrates, the phosphate must be returned to the chloroplast to support continued photophosphorylation (ATP formation).

The net energy balance of six rounds of the Calvin cycle to produce one mole of hexose is thus:

$$6)\quad 6CO_2 + 18ATP + 12NADPH + 12\ H_2O \rightarrow C_6H_{12}O_6 + 18ADP + 18P_i + 12NADP^+ + 6H^+$$

Photorespiration

Photosynthetic organisms must cope with a competing reaction that inhibits photosynthesis known as photorespiration. Unlike photosynthesis, this process involves the uptake of oxygen and the release of carbon dioxide.

Recall that mitochondrial respiration involves the uptake of O_2 and the evolution of CO_2 and is associated with the burning of cellular fuel to obtain energy in the form of ATP. In contrast, photorespiration starts in the chloroplast and actually wastes energy.

Photorespiration can be defined as the light-dependent uptake of O_2 in the chloroplast. It is caused by a fundamental "inefficiency" of RuBisCO.

During photosynthesis, RuBisCO catalyzes the carboxylation of RuBP to give two molecules of PGA. However, it can also catalyze the oxygenation of RuBP to give one molecule of PGA and one molecule of a two-carbon compound called phosphoglycolate. This reaction occurs because O_2 can compete with CO_2 at the active site of RuBisCO. Since oxygenation of RuBP competes with carboxylation, it lowers the efficiency of photosynthesis. A significant portion (25%) of the carbon in phosphoglycolate is lost as CO_2. Algae must use energy to "recover" the remaining 75% of this carbon, which further limits the efficiency of photosynthesis.

If photorespiration lowers the yield of photosynthesis, why has such a process been maintained throughout the course of evolution? The answer to this intriguing question has to do with the origins of RuBisCO and the CBB cycle. RuBisCO is an ancient enzyme, having evolved over 2.5 billion years ago in cyanobacteria. During this period in earth's history, the atmosphere contained high levels of CO_2 and very little oxygen. Thus, photorespiration did not present a problem for early photosynthetic organisms. By the time oxygen levels accumulated to significant levels in the atmosphere (ironically, by the process of photosynthesis!), the catalytic mechanism of RuBisCO was apparently "fixed." In other words, since O_2 and CO_2 both compete for the same active site of the enzyme, algae could not decrease the efficiency of oxygenation without also decreasing the efficiency of carboxylation. To compensate, algae evolved an elaborate pathway, known as the photo-respiratory pathway, to recover at least some of the carbon that would otherwise be lost. This pathway involved biochemical reactions in the chloroplast, mitochondria, and peroxisome. The importance of photorespiration is easily demonstrated by the fact that nearly all plants grow better under high CO_2 versus low CO_2. Conditions that favor carboxylation (photosynthesis) over oxygenation (photorespiration) include high CO_2, moderate light intensities, and moderate temperatures. Conditions that favor oxygenation over carboxylation include low CO_2 levels, high temperatures, and high light intensities.

THE PHOTOSYNTHESIS-IRRADIANCE RESPONSE CURVE (P-VS-E CURVE)

The P-vs-E curve, or light-response curve, shows how photosynthetic rate varies with increasing irradiance. The rate of photosynthesis can be measured as net O_2 evolution or as carbon fixation per chlorophyll *a* units, measured as mg C × (mg chlorophyll *a*)$^{-1}$ × h^{-1}. This curve describes a complex multi-step process that depends upon several limiting factors. Three regions are present in the curve: a light-limited region, a light-saturated region, a light-inhibited region. The basic description of the P-E curves requires a non-linear mathematical function to account for the light saturation effects. Quite a few such functions have been employed with varying degrees of success, such as rectangular hyperbola, quadratic, exponential, and hyperbolic tangent.

In our opinion, rectangular hyperbolic functions such as the Michaelis-Menten formulation that describe the nutrient uptake kinetics are quite suitable to describe the dynamic relationship between photosynthetic rate and irradiance, though the Michaelis-Menten formulation shows a much less sharp transition from the limited to the saturated region. The P-E curve (without the light-inhibited) region can be described with the following rectangular hyperbolic function:

$$P_E = (P_{max} \times E_\lambda)/(K_{m\,+}\, E_\lambda) \tag{7}$$

where P_E is the photosynthetic rate at any irradiance E, E_λ is the spectral irradiance (in μmol m^{-2} s^{-1}), and K_m is the half saturation constant when $P_E = P_{max}/2$ (Figure 4.17a).

In the light-limited region, that is, at low irradiance levels, the rate of photon absorption determines the rate of steady-state electron transport from H_2O to CO_2. In the light-limited region, the available light is insufficient to support the maximum potential rate of the light-dependent reactions and thus limits the overall rate of photosynthesis. In this region, P_E can be described as:

$$P_E = E_\lambda \times \alpha \tag{8}$$

where E_λ is the spectral irradiance, and α is a measure of "photosynthetic efficiency," or how efficiently solar energy is converted into chemical energy. α represents the slope of the P-vs-E curve at low light levels, that is, the initial linear part of the curve estimated as:

$$(\text{mg chlorophyll } a)^{-1} \times \text{h}^{-1} \times \mu\text{mol m}^{-2}\text{s}^{-1}$$

α takes into account that the light absorbed by the algal cell is proportional to the functional absorption cross-section (σ_{PSII}) of the PSII (the effective area that a molecule presents to an incoming photon and that is proportional to the probability of absorption) and to the number of photosynthetic units (n):

9) $$\alpha = \sigma_{PSII} \times n$$

Equation 8 shows that photosynthetic rate is linearly proportional to irradiance at low irradiance levels. The greater the slope (α), the more efficient the photosynthetic process (Figure 4.17b). Keeping constant the number of photosynthetic units but increasing the functional absorption cross-section, the slope will increase. The slope can be normalized to chlorophyll biomass, and, if so, a superscript "B" is added to denote this normalization: α^B. In this case, the curve dimensions are O_2 evolved (or C fixed) per unit chlorophyll *a* and quanta per unit area.

At very low irradiance levels, the rate of oxygen consumption will be greater than the rate of oxygen evolution; hence, respiration is greater than photosynthesis, and net oxygen evolution will be negative. Therefore, the P-E curve does not pass through the origin. The irradiance value on the X-axis at which photosynthesis balances respiration is called the light compensation point (E_c). Therefore, Equation 7 becomes:

10) $$P_E = P_{max} (E_\lambda - E_c)/(K_m + (E_\lambda - E_c))$$

This phenomenon (chlororespiration) is more pronounced in cyanobacteria, where the photosynthetic and respiratory pathways share common electron carriers (cytochromes). The irradiance levels needed to reach the compensation point (E_c) are about 10 μmol $m^{-2}s^{-1}$ for shallow water but are much lower in dim habitats.

As irradiance increases, more ATP and NADPH are produced, and the overall rate of photosynthesis become increasingly non-linear, rising towards its maximum or saturation level, P_{max} (light-saturated photosynthesis per unit of chlorophyll *a*). This pattern will continue until some other factor becomes limiting. By definition, in the light-saturated region, the rate of photon absorption exceeds the rate of steady-state electron transport from H_2O to CO_2. Saturating irradiance, E_K, is defined at the point at which the extrapolated initial slope crosses P_{max}.

11) $$E_K = P_{max}/\alpha$$

E_K represents an optimum on the photosynthesis irradiance curve.

The light-saturated photosynthetic rate is independent from the functional absorption cross-section of the photosynthetic apparatus and is only related to the number of photosynthetic units (n) and their steady-state electron turnover rate through the PSII reaction center ($1/\tau_{PSII}$):

12) $$P_{max} = n \times (1/\tau_{PSII})$$

This equation says that increasing the number of n photosynthetic units (but not their size) the saturation level P_{max} increases and that P_{max} cannot be derived from measurements of light absorption (Figure 4.17c). In other words, above the saturation point (E_K), light-dependent reactions produce more ATP and NADPH than can be used by the light-independent reaction for CO_2 fixation; that is, increasing irradiance no longer causes any increase in the photosynthetic rate. Above E_K and under normal conditions, the availability of CO_2 is the limiting factor, since the concentration of CO_2 in the atmosphere is very low (0.035% v/v).

Saturating irradiances show some correlation with habitat, but generally, they are low compared with full sun. Intertidal species require 400–600 μmol $m^{-2}s^{-1}$ (ca. 10% of the full sun irradiance),

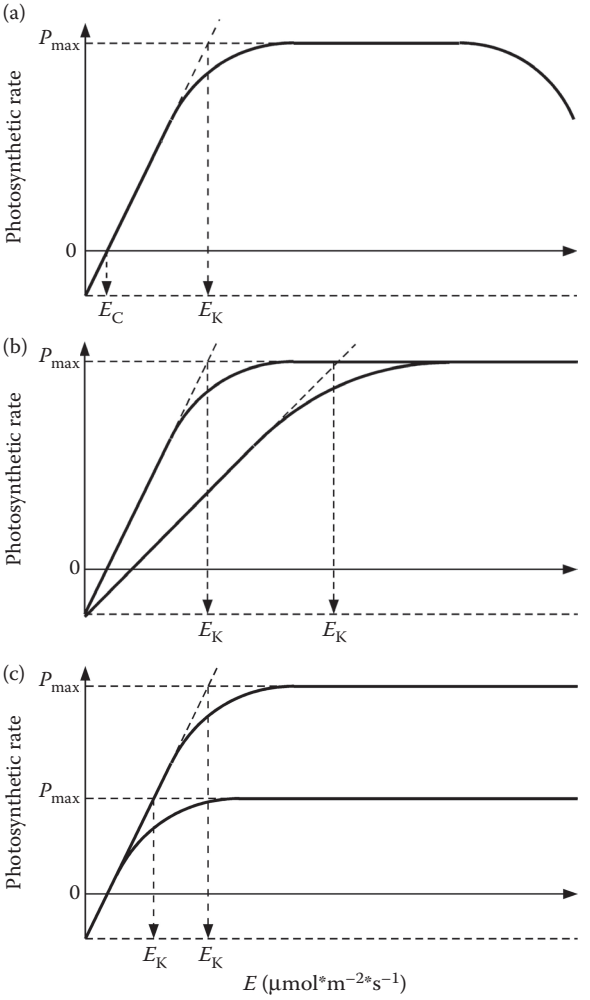


FIGURE 4.17 Photosynthesis-irradiance response curves; E_C: irradiance compensation point; E_K: saturating irradiance; P_{MAX}: maximum photosynthetic rate. typical plot (a); comparison of two curves with different slopes: keeping constant the number of photosynthetic units, but increasing the functional absorption cross-section, the slope increases (b); comparison of two curves with different maximum photosynthetic rate: increasing the number of photosynthetic units, P_{MAX} increases (c).

upper and mid-sublittoral species 150–250 μmol $m^{-2}s^{-1}$, and deep sublittoral species less than 100 μmol $m^{-2}s^{-1}$. Diatoms under ice saturate at 5 μmol $m^{-2}s^{-1}$.

A further increase in irradiance beyond light saturation can lead to a reduction in photosynthetic rate from the maximum saturation level. This reduction, which is dependent on both the irradiance and the duration of the exposure, is often termed photoinhibition. Photoinhibition (PI) occurs when the absorbed light energy exceeds the capacity of the organism to utilize it via electron transfer, photochemical quenching, or non-photochemical quenching pathways. It can be thought as a modification of P_{max} either by a reduction in the number of photosynthetic units or by an increase in the maximum turnover rate (Equation. 12); thus photoinhibition leads to a reduction in the photochemical efficiency of PSII through a reduction in the population of functional (O_2 evolving) reaction centers. Increasing irradiance levels increase the probability that more than one photon, two, for example, will strike the same reaction centers at the same time. The added energies of two blue

photons, for example, could be very harmful, since the resulting energy will correspond to a UV photon and could damage the chromophores.

PSII is the most sensitive complex in the thylakoid to photodamage, while PSI is relatively stable. Excessive light promotes formation of reactive oxygen species (ROS), which in turn react with PSII components. Once PSII proteins are damaged, the complex becomes inactive and a repair cycle is initiated, during which replacement of damaged proteins occurs and PSII activity is restored. If the rate of damage caused by oxidative stress exceeds the rate of PSII repair, then PI occurs.

In many photosynthetic organisms, a first mode of defense against PI is the synthesis of special stress-related light-harvesting II (LHCII) subunits, termed LHCSR, which accumulate in high light conditions and direct the absorbed light to non-photochemical processes that reduce the production of oxygen radicals.

A second mode of defense involves a decrease in PSII antenna size. This is achieved by phosphorylation-activated disconnection of LHCII from PSII, followed by a decline in chlorophyll *b* (chl *b*) content and a reduction of LHCII expression, thereby curbing the uptake of excess light energy. Overall, the change leads to more efficient photosynthetic activity due to reduced generation of ROS, and maintains a high steady-state level of photosynthesis. The latter occurs because the PSII repair cycle is continuously replacing the damaged reaction center (RC) proteins.

The third major mechanism for protection from PI involves the accumulation of carotenoids in the vicinity of the chlorophylls of PSII and LHCII. These carotenoids, such as lutein and β-carotene, quench the energy of the excited chlorophylls, preventing the formation of harmful radicals. In the underlying xanthophyll cycle, violaxanthin is converted in high light (HL) to antheraxanthin, which is further converted to zeaxanthin. Zeaxanthin accumulation in the PSII quenches the photoexcited chlorophyll radicals to produce heat.

Photoacclimation

Photoacclimation is a complex light response that changes cellular activities on many time scales.

The aquatic environment presents a highly variable irradiance (E) field with changes occurring over a wide range of time scales. For example, changes in E on short time scales can result from focusing and defocusing of radiation by waves at the surface. Longer time scale changes can result from variable cloud cover or turbulent motion that transports phytoplankton across the exponential E gradient of the surface mixed layer. In a well-mixed surface layer, phytoplankton experiences long periods of low E interspersed by short periods of saturating or even supersaturating E. The diurnal solar cycle causes changes in E on even longer time scales. To cope with the highly variable radiation environment, phytoplankton has developed numerous strategies to optimize photosynthesis while minimizing susceptibility to photodamage. Photosynthetic acclimation to E over time scales of hours to days proceeds through changes in cellular pigmentation or structural characteristics, such as size and number of photosynthetic units. On shorter time scales, cells adjust photon utilization efficiencies by changing the distribution of harvested energy between photosystems (state transitions) or by dissipating excess energy through non-photochemical processes, for example xanthophyll cycle or photoinhibition.

Therefore, photoacclimation involves change in macromolecular composition in photosynthetic apparatus. It is relatively easy to observe acclimation in unicellular algae and seaweed, where chlorophylls per cell or per unit surface are can increase five- to tenfold as irradiance decreases. The response is not a linear function of irradiance; rather, at extremely low light levels, cells often become a bit chlorotic, and on exposure to slightly higher (but still low) irradiance, chlorophyll reaches a maximum. Increase in irradiance leads to a decrease in the cellular complement of chlorophylls until a minimum value is reached. The absolute irradiance levels that induce this effects are species specific, and chlorotic response is not universal. The changes in pigmentation resulting from photoacclimation have profound consequences for light

absorption properties of the cells. First, cells acclimated to high irradiance levels generally have high carotenoid concentration relative to chlorophyll *a*. Carotenoids such as β-carotene and zeaxanthin do not transfer excitation energy to the reaction centers and consequently act to screen the cell from excess light. Some xanthophylls such as lutein transfer excitation energy, but with reduced efficiency, and therefore effectively reduce the functional absorption cross-section of the associated photosystem. Because these carotenoids absorb light without a concomitant increase in the functional cross-section of PSII, organisms acclimated to high irradiance levels often have lower maximum quantum yield of photosynthetic O_2 evolution. Second, when cells acclimate to low irradiance levels, the subsequent increase in pigmentation is associated with a decrease in functional optical absorption section normalized to chlorophyll *a*. This effect is due primarily to the self-shading of the chromophores between layers of thylakoids membranes and is an inverse function the number of membranes in the chloroplast; that is, the more membranes, the lower the optical cross-section. Thus, as cells accumulate chlorophyll, each chlorophyll molecule becomes less effective in light absorption; a doubling of cellular chlorophyll does not produce a doubling in the rate of light absorption. The reduction in the chlorophyll-specific optical absorption cross-section can be visualized considering the fate of photons incident on two stacks of thylakoid membranes: one is a thin stack from a cell acclimated to high irradiance levels, and the second is a thick stack from a cell acclimated to low irradiance levels. The probability of a photon passing through a thick stack of membranes without being absorbed is small compared with a thin stack of membranes. This so-called "package effect" reduces the effectiveness of increased pigmentation in harvesting light and has important implications for the capital costs of light harvesting, that is, the investments in the physical structures of the organism required for the metabolic processes. The diminution in the optical absorption cross-section with increased chlorophyll is also a function of cell size: the larger the cell, the more important this effect. At some point, a cell is, for most practical purposes, optically black and further increases in pigment levels confer no advantage in light absorption.

There are two basic photoacclimation responses in algae. In one, acclimation is accomplished primarily by changes in the number of photosynthetic reaction centers, while the effective absorption cross-section of the reaction centers remains relatively constant. The second is characterized by relatively large changes in the functional size of the antennae serving the reaction centers, while the number of reaction centers remains relatively constant. Complementary changes in either of the responses produce the same effect on the initial slope of the photosynthesis-irradiance curve. As the functional size of the antenna serving PSII, and not the number of reaction centers, determines the light-saturation parameter, organisms that vary the cross-section would tend to have more control over this parameter, as long as the turnover time remains constant.

PHOTOSYNTHESIS IN LIGHT-LIMITED ENVIRONMENTS

Among the factors that limit the rate of primary production through photosynthesis in aquatic systems (light, nutrients, CO, temperature), light is the one that shows the more extreme variation within the aquatic medium. Light decreases with depth down to levels that cannot support photosynthesis, with a marked change also in spectral distribution. Furthermore, to a much greater extent than the other limiting factors, light availability varies with time: both within the day—from darkness to the full noon sun and as clouds pass across the sun—and with the seasons during the course of the year. Hence, low-light ecosystems are among the most challenging environments for photosynthetic organisms, and relatively few algae thrive at the lower limit of the photic zone. Notwithstanding the constraints that restrict photosynthesis and growth at low photon flux density, deep-water algal populations are far more diverse and extensive than expected, and exploration associated with submersible collection of this diversity is continuously leading to an increase of the number of recorded species.

The depth receiving 1% of surface irradiance has typically been cited as the average compensation depth and the lower limit of the euphotic zone, but we will see that there are many deviations from this figure.

The dependence of benthic primary production on irradiance can be defined by three distinct compensation irradiances:

- $E_{c\,phot}$, compensation irradiance for photosynthesis, the irradiance at which net photosynthesis is zero (0), that is, the rates of gross photosynthesis and autotrophic respiration are equal;
- $E_{c\,growth}$, compensation irradiance for growth, the irradiance at which gross primary production balances the carbon losses (respiration, grazing, exudation of dissolved organic carbon, reproduction) for a particular organism;
- $E_{c\,comm}$, compensation irradiance for community metabolism, the irradiance at which gross community primary production balances the respiratory carbon loss for the entire community.

$E_{c\,phot}$ is by far the most often reported measure of compensation irradiance and is an important physiological trait but does not have a direct translation to the distribution and long-term production of benthic organisms. It approximates $E_{c\,growth}$ only when measurements are obtained from individuals collected close to the depth limit of a particular species or acclimated at an irradiance close to that found at the depth limit. These conditions are not frequently met. $E_{c\,growth}$, for which there is a reasonable empirical basis, is the relevant parameter for estimating the areal extent of benthic primary producers (the area receiving irradiances $\geq E_{c\,growth}$). $E_{c\,comm}$ represents the threshold irradiance above which benthic communities are autotrophic and can contribute to net production of organic carbon in coastal ecosystems.

$E_{c\,growth}$ and $E_{c\,comm}$ are the ecologically and biogeochemically relevant irradiance thresholds for benthic communities. These thresholds respectively delineate the deepest extent of benthic primary producers and the depth over which these communities act as sources of organic carbon to coastal ecosystems.

The maximum depth of distribution of primary producers, both microalgae (planktonic and benthic) and benthic macroalgae, which represents an estimate of $E_{c\,growth}$, ranges from 90 to 268 m, corresponding to 11 to 0.0005% of incident surface radiation.

The first example of oceanic deep-water dwelling microalga is *Prochlorococcus*, the smallest and most abundant photosynthetic organism on Earth (estimated global population $\approx 10^{27}$ cells). This cyanobacterium was recorded in the Arabian Sea, growing at depth of 120 to 160 m, at photon fluxes averaging 0.04% of surface incident radiation.

Together with their closest phylogenetic relatives of the genus *Synechococcus*, *Prochlorococcus* belongs to the group of marine picocyanobacteria (≤2 μm in cell diameter), which are significant contributors to primary production in the modern ocean. *Prochlorococcus* collectively produces an estimate 4 gigatons of fixed carbon each year, approximately the same net primary productivity as global croplands. Distinguishing characteristics of *Prochlorococcus*, vis-à-vis other marine cyanobacteria, include an extremely small size (0.5–0.7 μm in diameter) and the adaptation to extremely low light through increased light absorption capabilities. In fact, *Prochlorococcus* is one of the few cyanobacteria (together with *Prochloron* and *Prochlorothrix*) that lack membrane-bound phycobilisomes; instead, its main light-harvesting antenna complex is made up of prochlorophyte chlorophyll-binding protein (Pcb), which binds divinyl chlorophyll *a* and divinyl chlorophyll *b*. The use of these pigments causes a red shift in its absorption spectra. *Prochlorococcus* also possesses very high levels of accessory pigments (monovinyl chlorophyll *b*) per cell in the antenna complex and high ratios of accessory pigments to chlorophyll *a* (high A480/A450 and A450/A680).

It displays exceptional photosynthetic efficiencies, averaging 0.107 mg C (mg chlorophyll *a*)$^{-1}$h^{-1} (μmol photons m^{-2}s^{-1})$^{-1}$, biomass-normalized photo-synthetic rates, P^B, between 0.48 and 3.84 mg C (mg chlorophyll *a*)$^{-1}$h^{-1}, and saturating irradiance, E_k, as low as 9.2 μmol m^{-2}s^{-1}.

Much less is known about the ecological limits of benthic microalgae, *in situ* light requirements, or maximum depth of distribution. Limited field studies of benthic microalgae distributions and assessments of their photophysiology under low light conditions suggest the potential for depth and light limits similar to those of phytoplankton and benthic macroalgae. Significant concentrations of chemically intact chlorophyll *a* have been reported from sediments in outer shelf and upper slope habitats in several locations globally and, offshore from North Carolina, to depths as great as 222 m, which could suggest the presence of benthic microalgae in these very low-light environments.

Recently, obligate benthic diatoms were discovered living on the upper continental slope offshore from North Carolina in waters as deep as 191 m. A total of 126 species were identified from prepared samples, more than 90% of which are obligate benthic forms. Species of the epipsammic, monoraphid genus *Cocconeis* dominated in samples collected at bottom depths from 67 to 191 m. This discovery substantially extends the known depth range of these primary producers and holds significant implications for oceanic productivity and biogeochemical cycling. Mid-day, near bottom, photosynthetically active radiation values recorded at the 191 m site averaged 0.106 $\mu mol\ m^{-2}s^{-1}$, representing about 0.028% of surface incident radiation and resulting from a water column attenuation coefficient of 0.0446 m^{-1} (cf. Equation 2). The presence of active benthic microalgae in these extremely low light conditions suggests the development of special light-harvesting adaptations, including elevated levels of the blue-light absorbing accessory pigment fucoxanthin.

The maximum depth of macroalgae distribution is 268 m, where dark-purple crustose coralline algae (Rhodophyta) grow on primary basement substratum of San Salvador Island, Bahamas. Crustose corallines have adopted the ideal strategy for life in deep water; they can survive in spite of slow growth, they tolerate a wide range of nutrients, and they are well protected against grazing by herbivores. Their thallus structure represents a horizontal light receiver with no self-shading by a single cell layer, which enhances light absorption. These algae have an increased content of accessory pigments, including carotenoids, xanthophylls, and phycobiliproteins, which absorb light in spectral regions different from those of the green chlorophylls *a* and *b* and channel it to chlorophyll *a*, which is the only molecule able to convert sunlight energy into chemical energy. Moreover, they show an increased photosynthetic antenna size, which in turn increases the chance of photon absorption.

In dependence to the clarity of water and the annual sum of photosynthetic active radiation impinging at the water surface, the lower depth limit of crustose coralline algae shifts with lower latitude from several meters in cold temperate waters (e.g. 15 m on Helgoland Island, North Sea) to several hundred meters in tropical waters (e.g. 268 m in the Bahamas). The annual sum of impinging irradiance must support at least the annual need of energy for maintenance metabolism, measured by the maintenance respiration rate, and guarantee a minimum of energy surplus for establishment of growth and reproduction. Compared to cold-temperate regions, Caribbean algae are able to survive in such extreme depths due to the higher solar irradiance, a 12-hour period of daylight and clear water conditions. For algae with a more complex, even erected thallus and the presence of non-photosynthetic tissue, as typically found in kelps, the need for light energy increases, and the algae have to grow in shallower waters, as the amount of respiration and self-shading areas increase.

At the depth of crustose corallines, the red part of the sunlight spectrum is filtered out from the water, the faint residual light is blue-green, and its amount is approximately 0.0005% of the surface value. Considering that "full sun" (i.e. irradiance in the middle of the day) shines approximately 10^4 $mol\ m^{-2}\ year^{-1}$ on the earth surface, 0.0005% is equivalent to a photon flux of only 5 $mol\ m^{-2}\ year^{-1}$ during full sunlight at its maximum zenith. At this low photon flux density, there are a number of constraints that restrict photosynthesis and growth in the form of energy-consuming processes whose rates are invariant with photon flux density and thus consume a large fraction of adsorbed photons at lower photon flux densities. Among these processes are the redox

back reactions of reaction center II, the leakage of H+ through thylakoid membranes, and the turnover of photosynthetic proteins. The first process limits the rate of linear transport and ADP phosphorylation; the second consumes ATP. These energy-consuming processes are sequential, so that their effects in constraining photosynthetic and growth rates are multiplicative. It is still difficult to explain how these algae that can grow at less than 1 μmol $m^{-2}sec^{-1}$ cope with these energy-consuming reactions which use an increasing fraction of the energy input as the photon flux density decreases.

Also, green and brown algae occur to depths comparable with those of red algae. In San Salvador Island, Bahamas, above the depth of crustose coralline algae, around 210 m, trace amounts of the rock-boring green alga *Ostreobium* sp. have been found, followed at 155 m by *Rhipiliopsis profunda*, another green alga. In the same location, the brown alga *Lobophora variegata* has been collected at 140 m, but many other ochrophytes and chlorophytes have been observed in different locations of coastal oceans between 100 and 157 m (Table 4.1).

Recently, particular attention has been paid to a group of little-known chlorophytes persisting in deep, low-light, benthic marine habitats, where grazing pressure and competition for space are highly reduced. This group forms the early diverging chlorophytic lineage of the Palmophyllales, which includes the three genera of *Palmophyllum*, *Verdigellas*, and *Palmoclathrus. Verdigellas* has mostly been recorded from depths between 60 and 120 m, whereas *Palmophyllum* and *Palmoclathrus* species occur in shallower water, between 40 and 100 m. These algae are characterized by a unique type of multicellularity, forming firm, well-defined microscopic thalli composed of isolated spherical cells morphologically and ultrastructurally identical in a gelatinous matrix (palmelloid organization). Several members have evolved relatively large, erect thalli with specialized gross morphological features. Individuals of the deep-water genus *Verdigellas* attach to substrate by means of one or more distinct holdfast structures, from which thalli expand above, yielding an umbrella-like morphology well adapted to maximally capture the sparse light penetrating from the sea surface and reflected from the underlying substratum. *Palmoclathrus*, a genus from seasonally changing temperate waters, features a stout, perennial holdfast system consisting of a basal disk and one to several cylindrical stalks from which seasonal peltate blades grow. *Palmophyllum* is morphologically simpler, forming irregular lobed crusts that are tightly attached to the substrate. Motile stages and their accompanying basal bodies and flagellar roots have never been observed. These algae lack the green light-harvesting photosynthetic pigments siphonoxanthin and siphonein typically found in other low-light–adapted green algae but adapt to low-light conditions by maintaining high concentration of chlorophyll *b*, which absorbs the blue-green light of deeper water more efficiently than does chlorophyll *a*.

The interest in the Palmophyllales is strictly connected to their deep-branching position, which raises questions about the nature of the green plant ancestor, generally accepted to be a unicellular flagellate. The molecular phylogenetic evidence that the non-flagellate Palmophyllales form a distinct and early diverging lineage of green algae indicates that the green plant ancestor could have been a non-motile unicellular organism, maybe possessing transient motile stages.

A separate mention has to be given to other benthic primary producers, thriving at very dimly lit deep-water habitats, that is, corals, invertebrates in intimate endosymbiosis with photosynthetic dinoflagellates of the genus *Symbiodinium* (zooxanthellae). The deepest known hermatypic coral reefs are mainly located in Jamaica, Bahamas, at depths around 70 m. Recently, a deep-water coral community has been discovered at Pulley Ridge off the southwest coast of Florida, in waters 58 to 75 m deep. At these depths, large areas with up to 60% live coral coverage are present; the zooxanthellate scleractinian coral *Agaricia* sp. is one of the most abundant hermatypic corals in southern Pulley Ridge, forming tan-brown plates up to 50 cm in diameter. The corals generally appear to be healthy, with no obvious evidence of coral bleaching or disease, though they appear to be thriving on 1–2% (5–30 μmol m^{-2} sec^{-1}) of the available surface light (PAR) and about 5% of the light typically available to shallow-water reefs (500–1000 μmol m^{-2} sec^{-1}).

Besides zooxanthellate corals, the deepest portion of the photic zone also hosts antiphatarians, commonly known as black corals. These organisms have been traditionally considered an exclusive azooxanthellate order of anthozoan hexacorals, a trait thought to reflect their preference for low-light environments that do not support photosynthesis. They occur in dimly lit to dark areas in both shallow water, where they are present in shaded microenvironments, and deep water, where they are effectively shaded by light intensities decreasing with depth. ITS2 genotyping and histology performed on antiphatarian species collected from the Hawaiian Islands and Johnston Atoll at depths between 10 and 396 m detected *Symbiodinium* cells in all the samples collected down to below the compensation depth for photosynthesis in Hawaiian waters (approx. 125 m). This study represents the deepest record for *Symbiodinium*, indicating that at least some members of this dinoflagellate genus have incredibly diverse habitat preferences and broad environmental ranges. Moreover, these findings suggest that the carbon demand of these dinoflagellate is either reduced by dormancy or met by means other than photosynthesis, such as by self-digestion or heterotrophic feeding on an external carbon source. Heterotrophic endosymbiont feeding has been suggested in zooxanthellate invertebrates that are seasonally exposed to environmental conditions that do not support photosynthesis, and these modes of nutrition would make sense for *Symbiodinium* populations located below the compensation depth for photosynthesis.

Low-light habitats are not limited to aquatic environments; they are also present in subaerial locations, such as hypogea. The most comprehensive studies of subaerial biofilms have been carried out on the three catacomb sites dedicated to St. Domitilla, St. Callistus, and Priscilla in Rome (Italy) and on Maltese paleo-Christian catacombs situated in Rabat (Malta) and on the Hypogeum of Hal Saflieni in Paola (Malta).

Micro-environmental parameters (light intensity/photoperiod, degree of wetness of the surface, relative humidity, temperature) determine which microorganisms prevail in a specific hypogeum, but the undisputed phototrophic protagonists in sub-aerial biofilms are filamentous cyanobacteria. Different species of terrestrial epilithic cyanobacteria belonging to the genera *Eucapsis* Clements et Shantz 1909, *Leptolyngbya* Anagnostidis et Komárek 1988, *Scytonema* Agardh ex Bornet et Flahault 1887, and *Fischerella* Gomont 1895 occur as dominant organisms in these phototrophic microbial communities.

Some of these taxa have never been recorded outside of these habitats and for this reason are defined as "troglobitic," that is, obligate cavernicole taxa unable to survive outside of caves or other low-light environments. Subaerophytic troglobitic cyanobacteria belonging to the genus *Leptolyngbya* are particularly abundant in phototrophic biofilms present in both Roman and Maltese hypogea. These cyanobacteria live under extremely low photon fluxes, rarely exciding 10 μmol m^{-2} sec^{-1}, similarly to deep-water algae. At this extremely low photon fluxes, these algae can grow because of the presence of phycobiliproteins organized in phycobilisomes in the thylakoid membranes inside the cell that transfer their absorbed extra energy to chlorophylls. They sense the light direction by means of a photoreceptive apparatus that is located in the apical portion of the tip cell, which is composed of a carotenoid-containing screening device and a light detector based on rhodopsin-like proteins (cf. Chapter 3).

THE ENERGY RELATIONSHIPS IN PHOTOSYNTHESIS: THE BALANCE SHEET

The consumption of a mole of glucose releases 686 kcal of energy. This value represents the difference between the energy needed to break the bonds of the reactants (glucose and oxygen) and the energy liberated when the bonds of the products (H_20 and CO_2) form. Conversely, the photosynthesis of a mole of glucose requires the input of 686 kcal of energy. The overall equation for each process is the same; only the direction of the arrow differs:

13) $$C_6H_{12}O_6 + 6O_2 \leftrightarrow 6H_2O + 6\,CO_2$$

The average bond energies between common atoms are the following:

C-H = 98 kcal/mole;
O-H = 110 kcal/mole;
C-C = 80 kcal/mole;
C-O = 78 kcal/mole;
H-H = 103 kcal/mole;
C-N = 65 kcal/mole;
O=O = 116kcal/mole;
C=C = 145 kcal/mole;
C=O (as found in CO_2) = 98 kcal/mole.

The 24 covalent bonds of glucose require a total of 2182 kcal to be broken. The six double bonds of oxygen require another 696. Thus, a grand total of 2878 kcal is needed to break all the bonds of the reactants in cellular respiration.

As for the products, the formation of six molecules of CO_2 involves the formation of 12 double polar covalent bonds each with a bond energy of 187 kcal; total = 2244. The formation of six molecules of H_2O involves the formation of 12 O-H bonds, each with an energy of 110 kcal; total = 1320. Thus, a grand total of 3564 kcal is released as all the bonds of the products form.

Subtracting this from the 2878 kcal needed to break the bonds of the reactants, we arrive at −686 kcal, the free energy change of the oxidation of glucose. This value holds true whether we oxidize glucose quickly by burning it or in the orderly process of cellular respiration in mitochondria. The minus sign indicates that free energy has been removed from the system. The details of the energy budget are just the same. The only difference is that now it takes 3564 kcal to break the bonds of the reactants, and only 2878 kcal are released in forming glucose and oxygen. So we express this change in free energy (+686 kcal) with a plus sign to indicate that energy has been added to the system. The energy came from the sun and now is stored in the form of bond energy that can power the needs of all life.

Photosynthetic reduction of CO_2 can be summarized by the equations:

14) $$2H_2O \rightarrow O_2+4H^+ +4e^-$$

15) $$CO_2+4H^+ +4e^- \rightarrow (CH_2O) + H_2O$$

Four electrons have to be transferred from water, through a redox span of 1.24 eV, to reduce one molecule of CO_2. The energy required for the reduction of 1 mole of CO_2 is therefore:

16) $4 \text{ moles} \times 6.02 \times 10^{23} \text{ moles}^{-1} \times 1.24 \text{ eV} \times 1.60 \times 10^{-19} \text{ JeV}^{-1} = 47.77 \times 10^4 \text{J}$ (115.10 Kcal)

Theoretically, the energy requirement could be satisfied by the capture of 4 moles of photons of PAR light, say, a red photon of 700 nm; the energy content of these photons will be:

17) $4 \text{ moles} \times 6.02 \times 10^{23} \text{ moles}^{-1} \times 2.84 \times 10^{-19} \text{ J} = 68.4 \times 10^4 \text{J}$ (163.40 Kcal)

However, due to the thermodynamic losses during energy conversion, the fraction of absorbed photon energy converted in chemical energy seldom exceeds 0.35. Thus, 8 moles of photons are required for the reduction of 1 mole of CO_2:

18) $8 \text{ moles x } 6.02 \times 10^{23} \text{ moles}^{-1} \text{x } 2.84 \times 10^{-19} \text{ J} = 136.8 \times 10^4 \text{J} \times 0.35 = 47.9 \times 10^4 \text{ J}$ (114.9 Kcal)

A mole of glucose (formed by the addition of six CO_2 molecules) requires:

19) $$6 \times 114.9 \text{ Kcal} = 689.4 \text{ Kcal}$$

That is the value calculated by taking into account the balance of the energy of bonds previously described.

SUGGESTED READING

Adir, N., Zer H., Shochat, S. and Ohad, I. Photoinhibition, a historical perspective. Photosynthetic Research, 76, 343–370, 2003.

Agustí, S., González-Gordillo, J.I., Vaqué, D., Estrada, M., Cerezo, M.I., Salazar, G., Gasol, J.M. and Duarte, C.M. Ubiquitous healthy diatoms in the deep sea confirm deep carbon injection by the biological pump. Nature Communications, 6, 1–8, 2015.

Akutsu, S., Fujinuma, D., Furukawa, H., Watanabe, T., Ohnishi-Kameyama, M., Hiroshi Ono, O., et al. Pigment analysis of a chlorophyll *f*-containing cyanobacterium strain KC1 isolated from Lake Biwa. Photomedicine and Photobiology, 33, 35–40, 2011.

Allen, J.F. and Forsberg, J. Molecular recognition in thylakoid structure and function. Trend in Plant Science, 6, 317–326, 2001.

Antonaru, L.A., Cardona, T., Larkum, A.W. and Nürnberg, D.J. Global distribution of a chlorophyll *f* cyanobacterial marker. The ISME Journal, 14, 2275–2287, 2020.

Bag, P. Light harvesting in fluctuating environments: Evolution and function of antenna proteins across photosynthetic lineage. Plants, 10, 1184, 2021.

Barber, J. Photosystem II: A multisubunit membrane protein that oxidases water. Current Opinion in Structural Biology, 12, 523–530, 2002.

Bassi, R. and Caffarri, S. Lhc proteins and the regulation of photosynthetic light harvesting function by xanthophylls. Photosynthesis Research, 64, 243–256, 2000.

Behrendt, L., Schrameyer, V., Qvortrup, K., Lundin, L., Sørensen, S.J., Larkum, A.W.D., et al. Biofilm growth and near-infrared radiation-driven photosynthesis of the chlorophyll *d*-containing cyanobacterium *Acaryochloris marina*. Applied and Environmental Microbiology, 78:11, 3896–3904, 2012.

Behrenfeld, M.J., Prasil, O., Babin, M. and Bruyant, F. In search of a physiological basis for covariations in light-limited and light-saturated photosynthesis. Journal of Phycology, 40, 4–25, 2004.

Bibby, T.S., Nield, J., Chen, M., Larkum, A.W.D. and Barber, J. Structure of a photosystem II supercomplex isolated from *Prochloron didemni* retaining its chlorophyll *a/b* light-harvesting system. PNAS, 100, 9050–9054, 2003.

Bibby, T.S., Nield, J., Partensky, F. and Barber, J. Antenna ring around photosystem I. Nature, 413, 590, 2001.

Biller, S.J., Berube, P.M., Lindell, D. and Chisholm, S.W. *Prochlorococcus*: The structure and function of collective diversity. Nature Reviews Microbiology, 13, 13–27, 2015.

Blanchard, G.F., Guarini, J.-M., Dang, C. and Richard, P. Characterizing and quantifying photoinhibition in intertidal microphytobenthos. Journal of Phycology, 40, 692–696, 2004.

Brettel, K. and Leibl, W. Electron transfer in photosystem I. Biochimica Biophysica Acta, 1507, 100–114, 2001.

Cardona, T. Early Archean origin of heterodimeric photosystem I. Heliyon, 4, e00548, 2018.

Catling, D.C., Zahnle, K.J. and McKay, C. Biogenic methane, hydrogen escape, and the irreversible oxidation of early earth. Science, 293, 839–843, 2001.

Chen, M. and Blankenship, R.E. Expanding the solar spectrum used by photosynthesis. Trends in Plant Science, 16:8, 427–431, 2011.

Chen, M., Li, Y., Birch, D. and Willows, R.D. A cyanobacterium that contains chlorophyll f—A red-absorbing photopigment. FEBS Letters, 586:19, 3249–3254, 2012.

Chen, M., Schliep, M., Willows, R.D., Cai, Z.L., Neilan, B.A. and Scheer, H. A red-shifted chlorophyll. Science, 329:5997, 1318–1319, 2010.

Chitnis, P.R. Photosystem I: Function and physiology. Annual Review Plant Molecular Biology, 52, 593–626, 2001.

De Martino, A., Douady, D., Quinet-Szely, M., Rousseau, B., Crepineau, F., Kirk Apt and Caron, L. The light harvesting antenna of brown algae. European Journal of Biochemistry, 267, 5540–5549, 2000.

Ferreira, K.N., Iverson, T.M., Maghlaoui, K., Barber, J. and Iwata, S. Architecture of the photosynthetic oxygen-evolving center. Science, 19, 303, 1831–1838, 2004.

Gan, F. and Bryant, D.A. Adaptive and acclimative responses of cyanobacteria to far-red light. Environmental Microbiology, 17, 3450–3465, 2015.

Goudet, M.M.M., Orr, D.J., Melkonian, M., Müller, K.H., Meyer, M.T., Carmo-Silva, E. and Griffiths, H. RuBisCO and carbon-concentrating mechanism co-evolution across chlorophyte and streptophyte green algae. New Phytol, 227, 810–823, 2020. https://doi.org/10.1111/nph.16577

Govindjee, G., Allen, J.F. and Beatty, J.T. Celebrating the millennium: Historical highlights of photosynthesis research, part 3. Photosynthesis Research, 80, 1–13, 2004.

Hall, D.O. and Rao, K.K. Photosynthesis. Cambridge University Press, Cambridge (UK), 1999.

Havelkova-Dousova, H., Prasil, O. and Behrenfeld, M.J. Photoacclimation of *Dunaliella tertiolecta* (Chlorophyceae) under fluctuating irradiance. Photosynthetica, 42, 273–281, 2004.

Heathcote, P., Fyfe, P.K. and Jones, M.R. Reaction centers: The structure and evolution of biological solar power. Trends in Biochemical Sciences, 27, 79–84, 2002.

Hohmann-Marriott, M.F. and Blankenship, R.E. Evolution of photosynthesis. Annual Review of Plant Biology, 62:1, 515–548, 2011.

Jabłońska, J. and Tawfik, D.S. The evolution of oxygen-utilizing enzymes suggests early biosphere oxygenation. Nature Ecology & Evolution, 5, 442–448, 2021.

Jiang, J., Zhang, H., Kang, Y., Bina, D., Lo, C.S. and Blankenship, R.E. Characterization of the peridinin–chlorophyll *a*-protein complex in the dinoflagellate *Symbiodinium*. Biochimica et Biophysica Acta (BBA)—Bioenergetics, 1817:7, 983–989, 2012.

Jordan, P., Fromme, P., Witt, H.T., Klukas, O., Saenger, W. and Krauß, N. Three-dimensional structure of cyanobacterial photosystem I at 2.5 Å resolution. Nature, 411, 909, 917, 2001.

Kamiya, N. and Shen, J.-R. Crystal structure of oxygen-evolving photosystem II from *Thermosynechococcus vulcanus* at 3.7 Å resolution. PNAS, 100, 98–103, 2003.

Kargul, J., Nield, J. and Barber, J. Three dimensional reconstruction of a light-harvesting Complex I–Photosystem I Supercomplex from *Chlamydomonas reinhardtii*. Journal of Biological Chemistry, 278, 16135–16141, 2003.

Kramer, D.M., Avenson, T.J. and Edwards, G.E. Dynamic flexibility in the light reaction of photosynthesis governed by both electron and proton transfer reaction. Trend in Plant Science, 9, 349–357, 2004.

Krause-Jensen, D., Sejr, M.K., Bruhn, A., Rasmussen, M.B., Christensen, P.B., Hansen, J.L., Duarte, C.M., Bruntse, G. and Wegeberg, S. Deep penetration of kelps offshore along the west coast of Greenland. Frontiers in Marine Science, 375, 2019.

Kurisu, G., Zhang, H., Smith, J.L. and Cramer, W.A. Structure of the cytochrome b6f complex of oxygenic photosynthesis: Tuning the cavity. Science, 302, 1009–1014, 2003.

Larkum, A.W.D., Chen, M., Li, Y., Schliep, M., Trampe, E., West, J., Salih, A. and Kühl, M. A novel epiphytic chlorophyll *d*-containing cyanobacterium isolated from a Mangrove-associated red alga. Journal of Phycology, 48, 1320–1327, 2012.

Larkum, A.W.D. and Kühl, M. Chlorophyll *d*: The puzzle resolved. Trends in Plant Science, 10:8, 355–357, 2005.

Larkum, A.W.D., Raven, J. and Douglas, S. (Eds.). Photosynthesis of Algae, Vol. 14, Series Editor: Govindjee. Kluwer Academic Publishers, Dordrecht, 2003.

Laviale, M. and Neveux, J. Relationships between pigment ratios and growth irradiance in 11 marine phytoplankton species. Marine Ecology Progress Series, 425, 63–77, 2011.

Lee, H.W. and Kim, M.S. *Palmophyllum crassum*, a new record of an ancient species in green algae from Korea. Korean Journal of Environmental Biology, 35, 319–328, 2017.

Li, Y., Scales, N., Blankenship, R.E., Willows, R.D. and Chen, M. Extinction coefficient for red-shifted chlorophylls: Chlorophyll *d* and chlorophyll *f*. Biochimica et Biophysica Acta—Bioenergetics, 1817:8, 1292–1298, 2012.

MacIntyre, H.L., Kana, T.M., Anning, T. and Geider, R.J. Photoacclimation of photosynthesis irradiance response curves and photosynthetic pigments in microalgae and cyanobacteria. Journal of Phycology, 38, 17–38, 2002.

Markovic, D. Energy storage in the photosynthetic electron-transport chain. An analogy with Michaelis-Menten kinetics. Journal of Serbian Chemical Society, 68, 615–618, 2003.

Mielke, S.P., Kiang, N.Y., Blankenship, R.E., Gunner, M.R. and Mauzerall, D. Efficiency of photosynthesis in a Chl *d*-utilizing cyanobacterium is comparable to or higher than that in Chl *a*-utilizing oxygenic species. Biochimica et Biophysica Acta—Bioenergetics, 1807:9, 1231–1236, 2011.

Nelson, N. and Ben-Shem, A. The complex architecture of oxygenic photosynthesis. Nature Reviews Molecular Cell Biology, 5, 1–12, 2004.

Nugent, J.H.A. and Evans, M.C.W. Structure of biological solar energy converters—Further revelations. Trends in Plant Sciences, 9, 368–370, 2004.

Ort, D.R., Zhu, X. and Melis, A. Optimizing antenna size to maximize photosynthetic efficiency. Plant Physiology, 155:1, 79–85, 2011.

Perrine, Z., Negi, S. and Sayre, R.T. Optimization of photosynthetic light energy utilization by microalgae. Algal Research, 1:2, 134–142, 2012.

Pfannschmidt, T. Chloroplast redox signal: How photosynthesis controls its own genes. Trends in Plant Sciences, 8, 33–41, 2003.

Rathbone, H.W., Michie, K.A., Landsberg, M.J., Green, B.R. and Curmi, P.M. Scaffolding proteins guide the evolution of algal light harvesting antennas. Nature Communications, 12, 1–9, 2021.

Raven, J.A. and Hurd, C.L. Ecophysiology of photosynthesis in macroalgae. Photosynthesis Research, 113, 105–125, 2012.

Raven, J.A. The cost of photoinhibition. Physiologia Plantarum, 142:1, 87–104, 2011.

Reed, B. ATP synthase: Powering the movement of life. Harvard Science Review, Spring, 8–10, 2002.

Reyes-Gómez, V.P., Velasquez Pomar, H. and Gavio, B. Notes on the marine algae of the International Biosphere Reserve Seaflower, Caribbean Colombia VIII: New records of red algae (Rhodophyta) from San Andres, Old Providence, and Saint Cataline, Colombia. Acta Botánica Mexicana, https://doi.org/10.21829/abm128.2021.1848, 2021.

Saenger, W., Jordan, P. and Krauß, N. The assembly of protein subunits and cofactors in photosystem I. Current Opinion in Structural Biology, 12, 244–254, 2002.

Samsonoff, W.A. and MacColl, N. Biliproteins and phycobilisomes from cyanobacteria and red algae at the extremes of habitat. Archives of Microbiology, 176, 400–405, 2001.

Sánchez-Baracaldo, P. and Cardona, T. On the origin of oxygenic photosynthesis and cyanobacteria. New Phytologist, 225, 1440–1446, 2020.

Schmid, V.H.R., Potthast, S., Wiener, M., Bergauer, V., Paulsen, H. and Storf, S. Pigment binding of photosystem I in light-harvesting proteins. Journal of Biological Chemistry, 277, 37307–37314, 2002.

Stomp, M., Huisman, J., de Jongh, F., Veraart, A.J., Gerla, D., Rijkeboer, M., Ibelings, B.W., Wollenzlen, U.I.A. and Stal, L.J. Adaptive divergence in pigment composition promotes phytoplankton biodiversity. Nature, 432, 104–107, 2004.

Tice, M.M. and Lowe, D.R. Photosynthetic microbial mats in the 3,416-Myr-old ocean. Nature, 431, 549–552, 2004.

Ting, C.S., Rocap, G., King, J. and Chisholm, S.W. Cyanobacterial photosynthesis in the ocean: The origins and significance of divergent light-harvesting strategies. Trend in Microbiology, 10, 134–142, 2002.

Tomo, T., Allakhverdiev, S.I. and Mimuro, M. Constitution and energetics of photosystem I and photosystem II in the chlorophyll *d*-dominated cyanobacterium *Acaryochloris marina*. Journal of Photochemistry and Photobiology B: Biology, 104, 1–2, 333–340, 2011.

Towe, K.M., Catling, D., Zahnle, K., McKay, C. The problematic rise of archean oxygen. Science, 295, 1419a–1419a, 2002.

Treves, H., Küken, A., Arrivault, S., Ishihara, H., Hoppe, I., Erban, A., Höhne, M., Moraes, T.A., Kopka, J. and Szymanski, J. Carbon flux through photosynthesis and central carbon metabolism show distinct patterns between algae, C3 and C4 plants. Nature Plants, 8, 78–91, 2022.

van Grondelle, R. and Boeker, E. Limits on natural photosynthesis. The Journal of Physical Chemistry B, 121, 7229–7234, 2017.

Walker, J.E. (Ed.). The mechanism of F_1F_0-ATPase. Biochimica Biophysica Acta, 1458, 221–510, 2000.

Wynn-Williams, D.D., Edwards, H.G.M., Newton, E.M. and Holder, J.M. Pigmentation as a survival strategy for ancient and modern photosynthetic microbes under high ultraviolet stress on planetary surfaces. International Journal of Astrobiology, 1, 39–49, 2002.

Zhu X.G., Long, S.P. and Ort, D.R. What is the maximum efficiency with which photosynthesis can convert solar energy into biomass? Current Opinion in Biotechnology, 19:2, 153–159, 2008.

Zouni, A., Witt, H.-T., Kern, J., Fromme, P., Krauß, N., Saenger, W. and Orth, P. Crystal structure of photosystem II from *Synechococcus elongates* at 3.8 Å resolution. Nature, 409, 739–743, 2001.

www.life.uiuc.edu/govindjee/


Taylor & Francis
Taylor & Francis Group
http://taylorandfrancis.com

5 Culturing

COLLECTION, STORAGE, AND PRESERVATION

Algae grow in almost every habitat in every part of the world. They can be found on very different natural substrates, from animals (snails, crabs, sloths, and turtles are algal hosts) to plants (tree trunks, branches and leaves, water plants, and macroalgae), from springs and rivers to hypersaline lagoons and salt lakes. They also colonize artificial habitats, such as dams and reservoirs, fountains, and pools, but cans, bottles, plant pots, or dishes all allow algae to extend their natural range. The ubiquity of these organisms together with the plasticity of their metabolic requirements makes many algal species easily available for investigation, collection, or simple observation.

Floating microalgae can be collected with a mesh net (e.g. with 25–30 μm pores) or, if in sufficient quantity (i.e. coloring the water), by simply scooping a jar through the water. A small amount of the bottom sediments will also provide many of the algal species that live in or on these sediments. Some algae live attached to other types of substrate, such as dead leaves, twigs, and any underwater plants which may be growing in the water. Macroalgae and the attached microalgae can be collected by hand or with a knife, including part or all of the substrate (rock, plant, wood, etc.) if possible. Algae growing on soil are difficult to collect and study, many requiring culturing before sufficient and suitable material is available for identification.

Any sample should be labeled with standard information such as the locality, date of collection, and as many as possible of the following features: whether the water is saline, brackish, or fresh; whether the collection site is terrestrial or a river, stream, or lake; whether the alga is submerged during water level fluctuations or floods; whether the water is muddy or polluted; whether the alga is free floating or attached and, if the latter, the type of substrate to which it is attached; and the color, texture, and size of the alga. Algae can be stored initially in a glass jar, plastic bottle, or bag, or in a vial with some water from the collecting site. The container should be left open or only half filled with liquid, and wide shallow containers are better than narrow deep jars. If refrigerated or kept on ice soon after collecting, most algae can be kept alive for short periods (a day or two). If relatively sparse in the sample, some algae can continue to grow in an open dish stored in a cool place with reduced light. For long-term storage, specimens can be preserved in liquid, dried, or made into a permanent microscope mount. Even with ideal preservation, examination of fresh material is sometimes essential for an accurate determination. Motile algae particularly must be examined while flagella and other delicate structures remain intact, since preservation procedures may cause the detachment of the flagella.

Commercial formalin (40% formaldehyde in water), diluted between 1/10 and 1/20 with the collecting medium, is the most commonly used fixative. Since formaldehyde is considered carcinogenic, any contact with skin, eyes, and air passages should be avoided. This compound mixed with other chemicals such as glacial acetic acid and alcohol (FAA 1-1-8 by volume: 40% formaldehyde *1*: glacial acetic acid *1*: 95% alcohol *8*) gives better preservation results for some of the more fragile algae, whereas the standard alcohol and water mix (e.g. 70% ethyl alcohol) will ruin all but the larger algae. However, FAA may cause thin-walled cells to burst.

Color is an important taxonomic characteristic, especially for cyanobacteria, and formalin is a good preservative for green algae, cyanobacteria, and dinoflagellates because cell color remains intact if samples are stored in the dark. Algae can be kept in diluted formalin for a number of years, but best results are achieved if the formalin solution is replaced by 70% ethyl alcohol with 5% glycerin (the latter to prevent accidental drying out).

Lugol's solution is the preferred preservative commonly used for short-term (e.g. a few months, but possibly a year or more) storage of microalgae. It is excellent for preserving chrysophytes, but it

DOI: 10.1201/9781003187707-5

makes the identification of dinoflagellates difficult, if not impossible. Samples can be preserved and kept in dark bottles away from light for as long as 1 year in Lugol's solution (0.05–1% by volume). The solution is prepared by dissolving 20 g potassium iodide and 10 g iodine crystals in 180 ml of distilled water and by adding 20 ml glacial acetic acid. Note that Lugol's solution is affected by light and has a shelf life of about 6 months.

Dried herbarium specimens can be prepared by "floating out" similarly to aquatic flowering plants. Ideally, fresh specimens should be fixed prior to drying. Most algae will adhere to absorbent herbarium paper. Smaller, more fragile specimens or tangled, mat-forming algae may be dried onto mica or cellophane. After "floating out," most freshwater algae should not be pressed but simply left to air dry in a warm dry room. If pressed, they should be covered with a piece of waxed paper, plastic, or muslin cloth so that the specimen does not stick to the drying paper inside the press.

To examine a dried herbarium specimen, a few drops of water are added to the specimen to make it swell and lift slightly from the paper. This makes it possible to remove a small portion of the specimen with forceps or a razor blade.

Observations (preferably including drawings or photographs) based on living material are essential for the identification of some genera and a valuable adjunct to easier observations on preserved material for other genera. The simplest method is to place of drop of the water including the alga onto a microscope slide and carefully lower a coverslip onto it. It is always tempting to put a large amount of the alga onto the slide, but smaller fragments are much easier to view under a microscope. Microalgae may be better observed using the "hanging drop method"; that is, a few drops of the sample liquid are placed on a coverslip, which is turned over onto a ring of paraffin wax, liquid paraffin, or "slide ring."

A permanent slide can be prepared with staining such as aniline blue (1% aqueous solution, pH 2.0–2.5); toluidine blue (0.05% aqueous solution, pH 2.0–2.5); and potassium permanganate, $KMnO_4$ (2% aqueous solution), which are useful stains for macroalgae (different stains suit different species) and India ink, which is a good stain for highlighting mucilage and some flagella-like structures. Staining time ranges from 30 seconds to 5 minutes (depending on the material), after which the sample is rinsed in water. Mounting is achieved by adding a drop or two of glycerin solution (75% glycerin, 25% water) to a small piece of the sample placed on a microscope slide, then carefully lowering the coverslip. Sealing with nail polish is essential. This method is unsuitable for most unicellular algae, which should be examined fresh or in temporary mounts of liquid-preserved material.

Magnifications between 40 and 1000 times are required for the identification of all but a few algal genera. A compound microscope with 10× or 12× eyepiece and 4×, 10×, or 40× objectives is therefore an essential piece of equipment for anyone wishing to discover the world of algal diversity. An oil immersion 100× objective would be a useful addition, particularly when aiming to identify samples to species level. Phase-contrast or interference microscopy (e.g. Nomarski) can improve the contrast for bleached or small specimens. A dissecting microscope providing 20× or 40× up to 60× magnification is a useful aid but is secondary to a compound microscope. A camera lucida attachment is helpful for producing accurate drawings, while an eyepiece micrometer is important for size determinations. Formulas for calculating biomass for various phytoplankton shapes using geometric forms and measurements and shape code for each taxa exist in the literature and are routinely used in procedures for phytoplankton analysis that require biovolume calculations (Table 5.1). Scanning and transmission electron microscopes are beyond the reach of all but specialist institutions; however, they are an essential tool for identifying some of the very small algae and investigating the details of their ultrastructure.

In an attempt to speed up the time-consuming procedure of classification by optical microscopy, several kinds of automatic analysis and microalgae identification methods have been set up. They include, for example, methods based on algal cell morphology identification, absorption spectroscopy, the fluorescence spectroscopy high-performance liquid chromatographic method flow cytometric method, and the gene probe method. Though automated classification of microalgae is a rather active field of research, commercial developments are rather limited.

TABLE 5.1
Shape Codes and Corresponding Dimensions Required for Calculating Biovolumes of Various Phytoplankton Species

Shape	Dimensions Required				
	Code	Length	Width	Depth	Diameter
Cone	CON	L	W		
Cylinder	CYL	L	W	DP	D
Dumbbell box	DBB	L	W	DP	
Dumbbell	DBL	L	W	DP	
Diamond box	DMB	L	W	DP	
Fusiform	FUS	L	W		
Ovoid box	OVB	L	W	DP	
Ovoid	OVO	L	W		
Rectangular box	RTB	L	W	DP	
Sphere	SPH				D
Teardrop	TRP	L	W		

Pioneering attempts in microalgal image automatic classification were able to distinguish between few species of distinct size and shape using simple geometric features. To achieve higher classification accuracy, a hundreds of features such as shape, moments, texture, contours, and several classifiers, such as decision trees, Bayesian statistics, ridge linear regression, neural networks, fuzzy logic, and genetic algorithms were used. Unfortunately, most of the existing research systems are still adapted to identify a few specific types of algae. This is mainly due to the difficulties in choosing the correct feature pattern. The previously described techniques are very complex and limited in their applicability; an innovative software methodology that combines robust image segmentation, shape feature extraction, centroid distance spectrum calculation, and characteristic color (i.e. pigment signature) determination, which can offer a reliable, real-time recognition of multialgal samples, has been recently developed. Introducing a categorization parameter never used before, that is, centroid distance spectrum calculation and the pigment fingerprint of each alga, combined with a very simple technology, this methodology has the capacity to obtain real-time recognition accuracy comparable to that obtained by a phycologist. This methodology needs only a simple hardware platform, which integrates an optical microscope equipped with a color charge-coupled device digital camera, a personal computer, and commercial software such as MATLAB n(cf. Chapters 6 and 7 for details of the methodology). Images are processed according to the following flow of operations:

1. Image Acquisition
For image acquisition, slides from algae samples are prepared without any kind of processing or fixation. All the color images are acquired with the highest accuracy, because image processing can remove unwanted information, not add new information. All the objects present in the microscope field images undergo real-time processing. Those corresponding to objects other than algae, such as debris, particles, detritus, and overlapping cells, are discarded.

2. Contour Detection
The amount of data of the acquired images is reduced by representing the algae by means of descriptors such as lengths and contours.

3. Centroid Distance Spectrum Calculation
To obtain invariant features for translation, rotation, and scaling, the contour is normalized, oriented following maximum Feret diameter, and its points uniformly resampled (Figures 5.1a–1f).

4. Characteristic Color Identification
In order to identify the characteristic color of the algae, the occurrence of each color of the image (histogram) is calculated. The result of this operation is a bimodal distribution of colors, that is, the chloroplast domain and the non-chloroplast domain. The color with the maximal occurrence in the chloroplast domain is defined the characteristic color of the alga, that is, the color that represents the pigment signature of the group the alga belongs to (Figures 5.1g–5.1l).

5. Classification of Images
All the features measured by the operations described so far are used to classify the microalgae according to classifier algorithms usually based on an automatic neural network that assigns the alga to a specific database class. Each database class corresponds to an alga taxonomically recognized by the expert at the genus and/or species level. The classification accuracy achievable by this methodology can be as high as 97%. Figure 5.1 shows the results of the application of the algorithms for contour detection on *Gymnodinium acidotum* (Dinophyceae) (a–f) and characteristic color identification on *Cyanophora paradoxa* (Glaucophyceae) (g–f).

Culture Types

A culture can be defined as an artificial environment in which the algae grow. Theoretically, culture conditions should resemble the alga's natural environment as far as possible; actually, many significant differences exist, most of which are deliberately imposed. In fact, following isolation from the natural environment, algal strains are maintained under largely artificial conditions of media composition, light, and temperature. The imposition of an artificial environment on a cell population previously surviving under complex, fluctuating conditions and following a seasonal life cycle inevitably causes a period of physiological adaptation and/or selection, during which population growth will not occur or is very slow.

While contaminated algal cultures have previously been satisfactory for certain application and experiments, modern experimental methods and application demand contaminants not be present and taxonomy and growth characteristics of the strains be defined. Hence, for most purposes, algal cultures are maintained as unialgal, contaminant-free, or axenic stocks. "Unialgal" cultures contain only one kind of alga, usually a clonal population (but may contain bacteria, fungi, or protozoa), whereas "axenic" cultures should contain only one alga, and no bacteria, fungi, or protozoa are present.

To obtain a unialgal culture, a species must be isolated from all the rest; three major techniques borrowed from microbiology are available for obtaining unialgal isolates: streaking and successive plating on agar media, serial dilution, and single-cell isolations using capillary pipettes. Streaking is useful for single-celled, colonial, or filamentous algae that will grow on an agar surface. Filaments can be grabbed with a slightly curved pipette tip and dragged through soft agar (less than 1%) to remove contaminants. It is best to begin with young branches or filament tips which have not yet been extensively epiphytized. Many flagellates, however, as well as other types of algae must be isolated by single-organism isolations or serial-dilution techniques. A particularly effective means of obtaining unialgal cultures is isolation of zoospores immediately after they have been released from parental cell walls but before they stop swimming and attach to a surface. Recently released zoospores are devoid of contaminants, unlike the surfaces of most algal cells, but catching zoospores requires a steady hand and experience.

Sterile cultures of micro-algae may be obtained from specialized culture collections. Alternatively, axenic cultures can be obtained by treating isolated algae to an extensive washing procedure, which can include also one or more antibiotics. Resistant stages such as zygotes or akinetes can be treated with bleach to kill epiphytes and then planted on agar for germination. It is usually necessary to try several different concentrations of bleach and times of exposure to find a treatment that will kill epiphytes without harming the alga. When diatoms represent the contaminating species, addition of low concentrations (5 mg L^{-1}) of germanium dioxide, GeO_2, to a culture medium can inhibit diatom

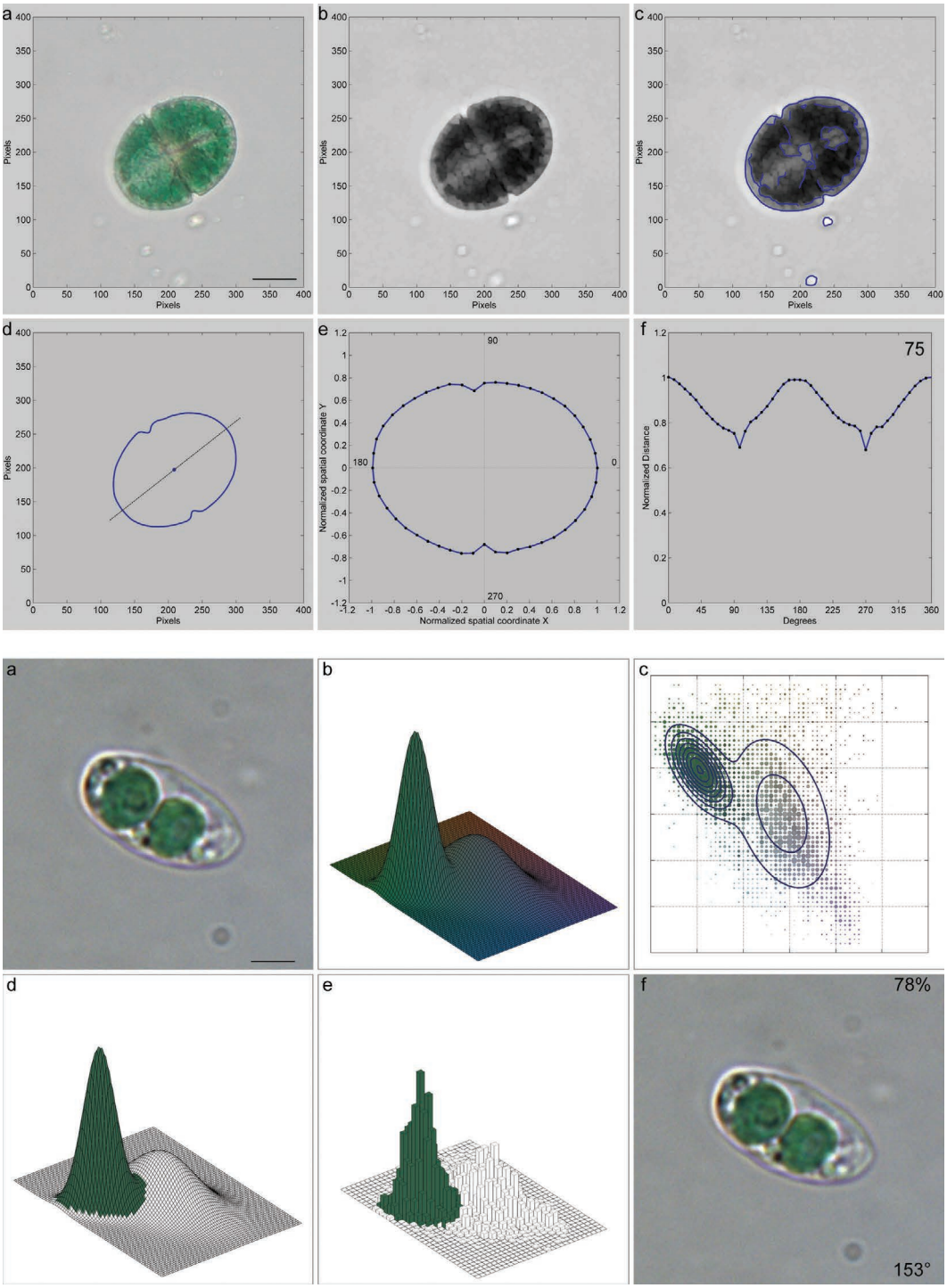


FIGURE 5.1 Results of the application of the algorithm for centroid distance spectrum calculation on *Gymnodinium acidotum* (upper frames) and application of the algorithm for characteristic color calculation on *Cyanophora paradoxa* (lower frames).

growth, since it disrupts silica deposition. "Cleaning" previously contaminated cultures is a time-consuming process that requires skill and could take several years in sizeable collections. Extensive measures must be taken to keep pure unialgal cultures chemically and biologically clean. Chemical contamination may have unquantifiable, often deleterious, and therefore undesirable effects on algal growth. Biological contamination of pure algal cultures by other eukaryotes and prokaryotic organisms in most cases invalidates experimental work and may lead to the extinction of the desired algal species in culture through out-competition or grazing. In practice, it is very difficult to obtain bacteria-free (axenic) cultures, and although measures should be taken to minimize bacterial numbers, a degree of bacterial contamination is often acceptable.

If biological contaminants appear in a culture, the best remedy is to isolate a single cell from the culture with a micropipette and try to establish a new, clean clonal culture. Alternatively the culture can be streaked on an agar plate in hopes of attaining a colony free of contaminants. Neither of these methods works well, however, for eliminating bacteria that attach firmly to the surface of microalgae. Placing a test tube in a low-intensity 90 kHz sec^{-1} ultrasonic water bath for varying lengths of time (a few seconds to tens of minutes) can sometimes physically separate bacteria without killing the algae, making it easier to obtain an axenic culture by micropipette isolation. Often, however, to achieve an axenic culture, antibiotics must be added to the growth medium to discourage growth of contaminating cyanobacteria and other bacteria. Best results appear to occur when an actively growing culture of algae is exposed to a mixture of penicillin, streptomycin, and gentamycin for around 24 hours. This drastically reduces the growth of bacteria while allowing the microalgae to continue to grow, increasing the chances of obtaining an axenic cell when using micropipette or agar streaking isolation. Different algal species tolerate different concentrations of antibiotics, so a range of concentrations should be used (generally 50–500 ‰ w/v). Other antibiotics can be used, such as chloramphenicol, tetracycline, and bacitracin. Antibiotic solutions should be made with distilled water filter-sterilized (0.2 μm filter units) into sterile tubes and stored frozen until use. Another approach is to add a range of antibiotic concentrations to a number of subcultures and then select the culture that has surviving algal cells but no surviving bacteria or other contaminants. Sterility of cultures should be checked by microscopic examination (phase contrast), adding a small amount of microalgal culture to sterile bacterial culture medium (e.g. 0.1% peptone), and observing regularly for bacterial growth. Absence of bacterial growth does not, however, ensure that the microalgal culture is axenic, since the majority of bacteria do not respond to standard enrichments. In reality there is no way of demonstrating that a microalgal culture is completely axenic. In practice, therefore, axenic usually means "without demonstrable unwanted prokaryotes or eukaryotes." Some microalgal cultures may die when made axenic, probably due to the termination of obligate symbiotic relationships with bacteria.

The collection of algal strains should be carefully protected against contamination during handling and poor temperature regulation. To reduce risks, two series of stocks are often retained, one which supplies the starter cultures for the production system and the other which is only subjected to the handling necessary for maintenance. Stock cultures are kept in test tubes at a light intensity of about 1.5 W m^{-2} (about 5 μEinstein $m^{-2}s^{-1}$) and a temperature of 16°C to 19°C. Constant illumination is suitable for the maintenance of flagellates but may result in decreased cell size in diatom stock cultures. Stock cultures are maintained for about a month and then transferred to create a new culture line.

Culture Parameters

A culture has three distinct components: the culture medium contained in a suitable vessel; the algal cells growing in the medium; and air, to allow exchange of carbon dioxide between medium and atmosphere.

For strictly autotrophic alga, all that is needed for growth is light, CO_2, water, nutrients, and trace elements. By means of photosynthesis, the alga will be able to synthesize all the biochemical compounds necessary for growth. Only a minority of algae is, however, autotrophic; many are unable to synthesize certain biochemical compounds (certain vitamins, for example) and will require these to be present in the medium (obligate mixotrophy condition; cf. Chapter 1).

The most important parameters regulating algal growth are nutrient quantity and quality, light, pH, turbulence, salinity, and temperature. Optimal parameters as well as the tolerated ranges are species specific; the different parameters may be interdependent, and a parameter that is optimal for one set of conditions is not necessarily optimal for another.

Temperature

The temperature at which cultures are maintained should ideally be as close as possible to the temperature at which the organisms were collected; for example, polar organisms (<10°C), temperate (10°C–25°C), or tropical (>20°C). Most commonly cultured species of micro-algae tolerate temperatures between 16°C and 27°C, although this may vary with the composition of the culture medium, the species and strain cultured. An intermediate value of 18°C–20°C is most often employed. Temperature controlled incubators usually use constant temperature (transfers to different temperatures should be conducted in steps of 2°C per week), although some models permit temperature cycling. Temperatures lower than 16°C will slow down growth, whereas those higher than 35°C are lethal for a number of species.

Light

As for plants, light is the source of energy which drives photosynthetic reactions in algae, and in this regard intensity, spectral quality, and photoperiod need to be considered. Light intensity plays an important role, but the requirements greatly vary with the culture depth and the density of the algal culture: at higher depths and cell concentrations, the light intensity must be increased to penetrate through the culture. Light intensity (e.g. direct sunlight, small container close to artificial light) that is too high may result in photo-inhibition. The most often employed light intensities range between 100 and 200 $\mu E\ s^{-1}m^{-2}$, which corresponds to about 5–10% of full daylight (2000 $\mu E\ s^{-1}m^{-2}$). Moreover, overheating due to both natural and artificial illumination should be avoided.

Light may be natural or supplied by fluorescent tubes emitting either in the blue or the red light spectrum, as these are the most active portions of the light spectrum for photosynthesis. Light intensity and quality can be manipulated with filters. Many microalgal species do not grow well under constant illumination, although cultivated phytoplankton develops normally under constant illumination, and hence a light/dark (LD) cycle is used (maximum 16:8 LD, usually 14:10 or 12:12).

pH

The pH range for most cultured algal species is between 7 and 9, with the optimum range being 8.2–8.7, though there are species that dwell in more acid/basic environments. Complete culture collapse due to the disruption of many cellular processes can result from a failure to maintain an acceptable pH. The latter is accomplished by aerating the culture. In the case of high-density algal culture, the addition of carbon dioxide allows to correct for increased pH, which may reach limiting values of up to pH 9 during algal growth.

Salinity

Marine algae are extremely tolerant to changes in salinity. Most species grow best at salinity slightly lower than that of their native habitat, which is obtained by diluting sea water with tap water. Salinities of 20–24 $g\ l^{-1}$ are found to be optimal for most marine species.

Mixing

Mixing is necessary to prevent sedimentation of the algae, to ensure that all the cells of the population are equally exposed to the light and nutrients, to avoid thermal stratification (e.g. in outdoor cultures), and to improve gas exchange between the culture medium and the air. The latter is of primary importance, as the air contains the carbon source for photosynthesis in the form of carbon dioxide. For very dense cultures, the CO_2 originating from the air (containing 0.036% CO_2) bubbled through the culture is limiting, and pure carbon dioxide may be supplemented to the air supply (e.g. at a rate

of 1% of the volume of air). CO_2 addition furthermore buffers the water against pH changes as a result of the CO_2/HCO_3^- balance (cf. Chapter 2).

Mixing of microalgal cultures may be necessary under certain circumstances: when cells must be kept in suspension in order to grow (particularly important for heterotrophic dinoflagellates), in concentrated cultures to prevent nutrient limitation effects due to stacking of cells, and to increase gas diffusion. It should be noted that in the ocean, algae cells seldom experience turbulence, and hence mixing should be gentle. Depending on the scale of the culture system, mixing is achieved by gentle manual swirling once a day (test tubes, Erlenmeyer flasks), aerating (bags, tanks), or using paddle wheels and jet pumps (ponds). Not all algal species can tolerate vigorous mixing, and most cultures do well without mixing, particularly when not too concentrated.

Culture Vessels

Culture vessels should have the following properties: non-toxic (chemically inert), reasonably transparent to light, easy to clean and sterilize, and a large surface-to-volume ratio (depending on organism).

Certain materials which could potentially be used for culture vessels may leach chemicals into the medium with a deleterious effect on algal growth. The use of chemically inert materials is particularly important when culturing oceanic plankton and during isolation. Recommended materials for culture vessels and media preparation include:

- Borosilicate glass
- Polycarbonate
- Teflon
- Polystyrene

Culture vessels are usually borosilicate glass conical flasks (narrow- or wide-mouth Erlenmeyer flasks) of various volume (from tens of milliliters to 3–5 liters) or test tubes for liquid culture and agar cultures. Borosilicate glass flasks and tubes, which have been shown to inhibit growth of some species, can be replaced by more expensive transparent polycarbonate vessels, which offer excellent clarity and good physical strength. Like borosilicate, polycarbonate is autoclavable, but it is expensive and becomes cloudy and cracks with repeated autoclaving, undergoing some loss of mechanical strength. Teflon is very expensive, and it is used only for media preparation, while polystyrene, the cheaper alternative to Teflon and polycarbonate, is not autoclavable. Polystyrene tissue culture flasks can be purchased as single-use sterile units and used for transport purposes.

The vessels are capped by non-adsorbent cotton-wool plugs, which will allow gas transfer but prevent entry of microbial contaminants. A more efficient and costly way of capping is to use foam plugs or silicone bubble stoppers (bungs), which also allow efficient gas transfer; these plugs are re-usable and autoclavable. Glass, polypropylene, or metal covers and caps are also used for flasks and tubes.

Materials which should generally be avoided during microalgal culturing include all types of rubber and PVC.

MEDIA CHOICE AND PREPARATION

The correct maintenance of algal strains is dependent on choice of growth media and culture parameters. Two approaches are possible for the selection of media composition:

- theoretically it is better to work on the principle that if the alga does not need the addition of any particular chemical substance to the culture media (i.e. if it has no observable positive effect on growth rate), do not add it;
- in practice it is often easier to follow well-known (and presumably, therefore, well-tested) media recipes and safer to add substances "just in case" (provided they have no observable detrimental affect on algal growth).

When choosing a culture medium, the natural habitat of the species should be considered in order to determine its environmental requirements. It is important to know whether the environment is eutrophic, hence nutrient rich, or oligotrophic, hence nutrient poor, and whether the algae belong to an *r*-selected or *k*-selected species. *R*-selected species are characterized by a rapid growth rate, autotrophic metabolism, and a wide environmental plasticity, whereas *k*-selected species show a slow growth rate, mixotrophic or photoheterotrophic metabolism, and a low environmental tolerance.

The media recipes currently available are not always adequate for many species, and the exact choice for a particular species therefore is dependent on trial and error. It must be remembered that there are (within limits) no right and wrong methods in algal culturing; culture media have only been developed by trying out various additions, usually based on theoretical considerations. Refinement of media composition for laboratory-maintained algal cultures has been the object of research for several decades, resulting in many different media recipes reported in the literature and used in different laboratories.

Media can be classified as defined or undefined. Defined media, which are often essential for nutritional studies, have constituents that are all known and can be assigned a chemical formula. Undefined media, on the other hand, contain one or more natural or complex ingredients, for example, agar or liver extract and seawater, the composition of which is unknown and may vary. Defined and undefined media may be further subdivided into freshwater or marine media.

In choosing or formulating a medium, it may be important to decide whether it is likely to promote heavy bacterial growth. Rich organic media should be avoided unless the algae being cultivated are axenic. For contaminated cultures, mineral media should be used. These may contain small amount of organic constituents, such as vitamins or humic acids and, in either case, provide insufficient carbon for contaminating organisms to outgrow the algae.

Culture collections have attempted to rationalize the number of media recipes and to standardize recipes for algal strain maintenance. In particular, the use of undefined biphasic media (soil/water mixture) is declining due to lack of reproducibility in media batches and occasional contamination of the media by soil samples.

Media may be prepared by combining concentrated stock solutions which are not combined before use, to avoid precipitation and contamination. Reagent-grade chemicals and bidistilled (or purer) water should be used to make stock solutions of enrichments. Gentle heating and/or magnetic stirring of stock solutions can be used to ensure complete dissolution. When preparing a stock solution containing a mixture of compounds, each compound has to be dissolved individually in a minimal volume of water before mixing, then combined with the others and the volume diluted to the needed amount.

Another practical way of preparing artificial defined media is to mix the ingredients together and dry them prior to long-term storage. Constituents are added sequentially to distilled water, smallest quantities first, for obtaining a solution and finally a stiff slurry. Prior to the addition of the major salts, the pH is adjusted to 4–5. The mixture is then transferred to a clean desiccator of suitable size and the final additions are made. The well-stirred slurry is vacuum-dried, and the dry mixture is then stored with calcium chloride as a desiccant. It can be stored for some years if kept dry.

Solid media are usually prepared using 1.0–1.5% w/v agar, tubes being rested at an angle of 30° during agar gelation to form a slope that increases the surface area available for growth.

As noted, media are sterilized either by autoclaving at 126°C (20 minutes, 1 atm pressure) or by filtration, using 0.2 μm pore cellulose nitrate or acetate sterile filters. Generally, subculturing is performed using aseptic microbiological techniques; laminar flow cabinets, equipped with Bunsen flame, microbiological loops and glass, or plastic sterile pipettes are required.

Freshwater Media

Freshwater media are generally selected because they possess characteristics similar to the natural environment or they differentially select for a specific algal component of the habitat. Artificial media, with known chemical composition, are often employed as additives to natural media with an

unknown chemical composition, such as lake water, to enrich them. They are often used to simulate diverse nutritional or physical requirements of a particular species or groups of species, especially when the exact nutritional requirements are unknown.

Media are generally prepared from premixed stock solutions. Aliquots from these stocks are measured and added to a given volume of water. Some, however, must be prepared by weighting or measuring the desired components and adding them directly to a given volume of liquid. Accuracy in measuring liquid aliquots from stock solution or water and weighing of chemicals is essential. Improper procedures may result in precipitation of one or more of the components of the medium, such as nitrates and phosphates, or failure of some of the constituents to go into solutions.

Stock solution can be prepared and stored at low temperature in tightly sealed glassware, since evaporation may alter initial concentrations.

Water generally employed for freshwater media should belong to one of the following types: copper-distilled water, single glass-distilled water, double glass-distilled water, membrane filtered water, or deionized water. In most laboratories, single- or double-distilled water is routinely used, which can be deionized by passing it through a pre-packed deionizing column.

Freshwater media can be "defined" and "undefined." Defined media such as Sueoka's or bold basal medium has been proved successful for many algal classes. Most of these defined media can be used for additional algal groups by adding a variety of other components or modifying the amounts of certain reagents. These "undefined" media often have the advantage of supporting growth of large number of different algal species, but, when highly organic, they have also the disadvantage of encouraging more bacterial growth than strictly inorganic media.

Some of the most commonly used freshwater media, defined and undefined, are listed in Tables 5.2 to 5.12.

TABLE 5.2
BG11 Medium Composition

BG11 Medium	
Reagents	**Per Liter**
$NaNO_3$*	1.5 g
$K_2HPO_4 \cdot 3H_20$	0.004 g
$MgSO_4 \cdot 7H_2O$	0.075 g
$CaCl_2 \cdot 2H_20$	0.027 g
Citric acid ($C_6H_8O_7$)	0.006 g
Ammonium ferric citrate ($C_6H_8O_7 \cdot xFe \cdot yNH_3$)	0.006 g
Na_2Mg–EDTA**	0.001 g
Na_2CO_3	0.02 g
Microelement stock solution	1 ml
Microelement Stock Solution	
H_3BO_3	2.860 g
$MnCl_2 \cdot 4H_2O$	1.810 g
$ZnSO_4 \cdot 7H_2O$	0.222 g
$Na_2MoO_4 \cdot 2H_2O$	0.390 g
$CuSO_4 \cdot 5H_2O$	0.079 g
$Co(NO_3)_2 \cdot 6H_2O$	0.0494 g
pH= 7.4	

* *To be omitted for N_2-fixing cyanobacteria*

** *Ethylenediaminetretaacetic acid*

TABLE 5.3
Diatom Medium Composition

Diatom Medium	
Reagents	**Per Liter**
$Ca(NO_3)_2 \cdot 4H_2O$	20 mg
KH_2PO_4	12.4 mg
$MgSO_4 \cdot 7H_2O$	25 mg
$NaHCO_3$	15.9 mg
FeNa–EDTA	2.25 mg
Na_2–EDTA	2.25 mg
H_3BO_3	2.48 mg
$MnCl_2 \cdot 4H_2O$	1.39 mg
$(NH_4)_6Mo_7O_{24} \cdot 4H_2O$	1.0 mg
Biotin (vitamin B_7)	0.04 mg
Thiamine HCl (vitamin B_1)	0.04 mg
Cobalamin (vitamin B_{12})	0.04 mg
$Na_2SiO_3 \cdot 9H_2O$	57 mg
pH = 6.9	

TABLE 5.4
DY-III Medium Composition

DY–III Modified Medium	
Reagents	**Per Liter**
$MgSO_4 \cdot 7H_2O$	50 mg
KCl	3 mg
NH_4Cl	2.68 mg
$NaNO_3$	20 mg
H_3BO_3	0.8 mg
Na_2 EDTA $\cdot 2H_2O$	8 mg
$Na_2SiO_3 \cdot 9H_2O$	14 mg
$FeCl_3 \cdot 6H_2O$	1 mg
$CaCl_2$	75 mg
MES buffer	200 mg
Microelement stock solution	1 ml
Vitamin solution	1 ml
Microelement Stock Solution	
$MnCl_2 \cdot 4H_2O$	200 mg
$ZnSO_4 \cdot 7H_2O$	40 mg
$CoCl_2 \cdot 6H_2O$	8 mg
$Na_2MoO_4 \cdot 6H_2O$	20 mg
$Na_3VO_4 \cdot nH_2O$	2 mg
H_2SeO_3	2 mg
Vitamin Solution	
Biotin (vitamin B_7)	0.5 µg
Thiamine HCl (vitamin B_1)	100 mg
Cobalamin (vitamin B_{12})	0.5 mg
pH = 6.7	

TABLE 5.5
Aaronson's Medium Composition

Aaronson's Medium	
Reagents	**Per Liter**
NH_4Cl	0.5 g
KH_2PO_4	0.3 g
$MgSO_4 \cdot 7H_2O$	1.0 g
$MgCO_3$	0.4 g
$C_6H_9NO_6$ (nitrilotriacetic acid)	0.2 g
$CaCO_3$	0.05 g
$C_5H_9NO_4$ (glutamic acid)	3.0 g
Glucose	10.0 g
Arginine	0.4 g
Hystidine monocloride	0.4 g
Biotin (vitamin B_7)	0.00001 g
Thiamine HCl (vitamin B_1)	0.001 g
Microelement stock solution	10 ml
Microelement Stock Solution	**Per Liter**
$Fe(NH_4)_2 (SO_4)_2 \cdot 6H_2O$	0.5 g
H_3BO_3	0.025
$MnSO_4 \cdot H_2O$	0.125 g
$CoSO_4 \cdot 7H_2O$	0.025 g
$CuSO_4 \cdot 5H_2O$	0.020 g
$ZnSO_4 \cdot H_2O$	0.25 g
$(NH_4)_6Mo_7O_{24} \cdot 4H_2O$	0.0125 g
$Na_3VO_4 \cdot 16H_2O$	0.025 g
pH = 5.0	

TABLE 5.6
Cramer and Myers Medium Composition

Cramer and Myers Modified Medium	
Reagents	**Per Liter**
$(NH_4)_2HPO_4$	1g
KH_2PO_4	1g
$MgSO_4 \cdot 7H_2O$	0.2 g
$CaCl_2$	0.02g
$Na_3C_6H_5O_7 \cdot 2H_2O$ (sodium citrate)	0.8 g
$Fe_2(SO_4)_3 \cdot nH_2O$	3 mg
$MnCl_2 \cdot 4H_2O$	1.8 mg
$CoSO_4 \cdot 7H_2O$	1.5 mg
$ZnSO_4 \cdot 7H_2O$	0.4 mg
$Na_2MoO_4 \cdot 2H_2O$	0.2 mg
$CuSO_4 \cdot 5H_2O$	0.02 mg
H_3BO_3	2.48 mg

TABLE 5.6 *(Continued)*
Cramer and Myers Medium Composition

Carbon Sources (choose one)	Per Liter
• $C_6H_{12}O_6$ (glucose)[a]	10 g
• $C_4H_6O_4$ (succinic acid)[a]	5 g
• $C_5H_9NO_4$ (glutammic acid)[a]	5 g
• $C_2H_3O_2Na \cdot 5H_2O$ (sodium acetate)[b]	1.64 g
Thiamine HCl (vitamin B_1)	0.5 mg
Cobalamin (vitamin B_{12})	0.02 mg
[a]pH = 3.4	
[b]pH = 6.8	

TABLE 5.7
Sueoka's Medium Composition

Sueoka's Medium	
Reagents	**Per Liter**
Beijerinck's solution	5 ml
Phosphate solution	5 ml
Hutner's trace elements	1 ml
Beijerinck's Solution	
NH_4Cl	100 g
$MgSO_4 \cdot 7H_2O$	4 g
$CaCl_2 \cdot 2H_2O$	2 g
Phosphate Solution	
KH_2PO_4	144 g
K_2HPO_4	288 g
Hutner's Trace Elements	
H_3BO_3	11.4 g
$MnCl_2 \cdot 4H_2O$	5.06 g
Na_2–EDTA	50 g
$CuSO_4 \cdot 5H_2O$	1.57 g
$ZnSO_4 \cdot H_2O$	22 g
$CoCl_2 \cdot 6\ H_2O$	1.61 g
$FeSO_4 \cdot 7H_2O$	4.99 g
$(NH_4)_6Mo_7O_{24} \cdot 4H_2O$	1.10 g
pH= 6.8	

TABLE 5.8
Bold Basal Medium Composition

Bold Basal Medium	
Reagents	**Per Liter**
KH_2PO_4	175 mg

TABLE 5.8 *(Continued)*
Bold Basal Medium Composition

Reagents	Per Liter
$CaCl_2 \cdot 2H_2O$	25 mg
$MgSO_4 \cdot 7H_2O$	75 mg
$NaNO_3$	250 mg
K_2HPO_4	75 mg
NaCl	25 mg
H_3BO_3	11.42 mg
Microelement stock solution	1 ml
Solution1	1 ml
Solution 2	1 ml
Microelement Stock Solution	
$ZnSO_4 \cdot 7H_2O$	8.82 g
$MnCl_2 \cdot 4H_2O$	1.44 g
MoO_3	0.71 g
$CuSO_4 \cdot 5H_2O$	1.57 g
$Co(NO_3)_2 \cdot 6H_2O$	0.49 g
Solution 1	
Na_2–EDTA	50 g
KOH	3.1 g
Solution 2	
$FeSO_4$	4.98 g
H_2SO_4 (conc.)	1 ml
pH = 6.8	

TABLE 5.9
MES–Volvox Medium Composition

MES-Volvox Medium	
Reagents	**Per Liter**
MES buffer	1.95 g
$Ca(NO_3)_2 \cdot 4H_2O$	117.8 mg
$Na_2C_3H_9O_6P \cdot 5H_2O$ (sodium glycerophosphate)	60 mg
$MgSO_4 \cdot 7H_2O$	40 mg
KCl	50 mg
NH_4Cl	26.7 mg
Biotin (vitamin B_7)	0.0025 mg
Cobalamin (vitamin B_{12})	0.0015 mg
Microelement stock solution	6 ml
Microelement Stock Solution	
Na_2–EDTA	750 mg
$FeCl_3 \cdot 6H_2O$	97 mg
$MnCl_2 \cdot 4H_2O$	41 mg
$ZnCl_2$	5 mg

TABLE 5.9 *(Continued)*
MES–Volvox Medium Composition

Reagents	Per Liter
$CoCl_2 \cdot 6H_2O$	2 mg
$Na_2MoO_4 \cdot 2H_2O$	4 mg
pH = 6.7	

TABLE 5.10
Jaworski's Medium Composition

Jaworski's Medium (JM)	
Reagents	**Per Liter**
$MgSO_4 \cdot 7H_2O$	50 mg
$Ca(NO_3)_2 \cdot 4H_2O$	20 mg
$NaNO_3$	80 mg
$Na_2HPO_4 \cdot 12H_2O$	36 mg
$NaHCO_3$	15.9 mg
KH_2PO_4	12.8 mg
H_3BO_3	2.48 mg
FeNa–EDTA	2.25 mg
Na_2 EDTA	2.25 mg
$MnCl_2 \cdot 4H_2O$	1.39 mg
$(NH_4)_6Mo_7O_{24} \cdot 4H_2O$	1 mg
Cobalamin (vitamin B_{12})	0.04 mg
Tiamina HCl (vitamin B_1)	0.04 mg
Biotin (vitamin H)	0.04 mg
pH = 6.5	

TABLE 5.11
CY-II *Cyanophora paradoxa* Medium Composition

CY-II Medium	
Reagents	**Per Liter**
$NH_4C_2O_3H_3$	200 mg
$FeCl_3$	1 mg
$CaCl_2 \cdot 2H_2O$	50 mg
KCl	30 mg
$MgSO_4 \cdot 7H_2O$	100 mg
$Na_2C_3H_9O_6P \cdot 5H_2O$ (sodium glycerophosphate)	50 mg
Tris-base (pH = 7.2)	333 mg
Cobalamin (vitamin B_{12})	1 μg
PII metal mix	10 ml
Vitamin solution	5 ml

TABLE 5.11 ***(Continued)***
CY-II *Cyanophora paradoxa* Medium Composition

Reagents	Per Liter
PII Metal Mix	
Na_2-EDTA · $2H_2O$	10 mg
$MnCl_2$ · H_2O	0.4 mg
$ZnSO_4$ · $7H_2O$	0.05 mg
$FeCl_3$ · $6H_2O$	0.1 mg
H_3BO_3	2 mg
$CoCl_2$ · $7H_2O$	0.01 mg
Vitamin Solution	
Biotin (vitamin B_7)	1 µg
Thiamine HCl (vitamin B_1)	0.5 mg
Folic acid	2 µg
Nicotin acid	0.1 mg
Calcium pantothenate	0.1 mg
PABA (para amino benzoic acid)	10 µg
Thymine	3 mg
Inositol	5 mg
pH = 7.6	

TABLE 5.12
Zarrouk's Medium Composition

Zarrouk's Medium	
Reagents	**Per Liter**
$NaHCO_3$	16.8 g
K_2HPO_4	0.5 g
$NaNO_3$	2.5 g
K_2SO_4	1.0 g
NaCl	1.0 g
$MgSO_4$· $7H_2O$	0.2 g
$CaCl_2$· $2H_2O$	0.04 g
Fe_2SO_4· $7H_2O$	0.01 g
EDTA	0.08 g
Microelement stock solution	1 ml
Microelement Stock Solution	
H_3BO_3	2.86 g
$MnCl_2$ · $4H_2O$	1.81 g
$ZnSO_4$ · $4H_2O$	0.222 g
Na_2MoO_4	0.0177 g
$CuSO_4$ · $5H_2O$	0.079 g
pH = 9	

Marine Media

Seawater is an ideal medium for growth of marine species, but it is an intrinsically complex medium, containing over 50 known elements in addition to a large but variable number of organic compounds. Usually it is necessary to enrich seawater with nutrients such as nitrogen, phosphorus, and iron. Synthetic formulations have been designed primarily to provide simplified, defined media. Marine species generally have fairly wide tolerances, and difficulties attributed to media can frequently be related to problems of isolation, conditions of manipulations and incubation, and the physiological state of the organism. A single medium will generally serve most needs of an investigator. Many media are only major variations of some that are widely applicable and often equally effective. Whatever the choice, a medium should be as simple as possible in composition and preparation.

Media for the culture of marine phytoplankton consist of a seawater base (natural or artificial), which may be supplemented by various substances essential for microalgal growth, including nutrients, trace metals and chelators, vitamins, soil extracts, and buffer compounds.

The salinity of the seawater base should first be checked (30–35‰ for marine phytoplankton) and any necessary adjustments (addition of fresh water/evaporation) made before addition of enrichments.

Seawater, stock solutions of enrichments, and the final media must be sterile in order to prevent (or more realistically minimize) biological contamination of unialgal cultures. Autoclaving is a process which has many effects on seawater and its constituents, potentially altering or destroying inhibitory organic compounds, as well as beneficial organic molecules. Because of the steam atmosphere in an autoclave, CO_2 is driven out of the seawater and the pH is raised to about 10, a level which can cause precipitation of the iron and phosphate added in the medium. Some of this precipitate may disappear upon re-equilibration of CO_2 on cooling, but both the reduced iron and phosphate levels and the direct physical effect of the precipitate may limit algal growth. The presence of EDTA and the use of organic phosphate may reduce precipitation effects. Addition of 5% or more of distilled water may also help to reduce precipitation (but may affect final salinity). The best solution, however, if media are autoclaved, is to sterilize iron and phosphate (or even all media additions) separately and add them aseptically afterwards.

Some marine microalgae grow well on solid substrate. A 3% high-grade agar can be used for the solid substrate. The agar and culture medium should not be autoclaved together, because toxic breakdown products can be generated. The best procedure is to autoclave 30% agar in deionized water in one container and nine times as much seawater base in another. After removing from the autoclave, sterile nutrients are added aseptically to the water, which is then mixed with the molten agar. After mixing, the warm fluid is poured into sterile Petri dishes, where it solidifies when it cools. The plate is inoculated by placing a drop of water containing the algae on the surface of the agar and streaking with a sterile implement. The plates are then maintained under standard culture conditions.

Seawater Base

The quality of water used in media preparation is very important. Natural seawater can be collected near shore, but its salinity and quality are often quite variable and unpredictable, particularly in temperate and polar regions (due to anthropogenic pollution and toxic metabolites released by algal blooms in coastal waters). The quality of coastal water may be improved by ageing for a few months at 4° (allowing bacteria degradation), by autoclaving (heat may denature inhibitory substances), or by filtering through acid-washed charcoal (which absorbs toxic organic compounds). Most coastal waters contain significant quantities of inorganic and organic particulate matter and therefore must be filtered before use (using, for example, Whatman no. 1 filter paper).

The low biomass and continual depletion of many trace elements from the surface waters of the open ocean by biogeochemical processes makes this water much cleaner and therefore preferable for culturing purposes. Seawater can be stored in polyethylene carboys in cool dark conditions.

Artificial seawater, made by mixing various salts with deionized water, has the advantage of being entirely defined from the chemical point of view, but it is very laborious to prepare and often does not support satisfactory algal growth. Trace contaminants in the salts used are at rather high concentrations in artificial seawater because so much salt must be added to achieve the salinity of full strength seawater. Commercial preparations are available which consist of synthetic mixes of the major salts present in natural sea water, such as Tropic Marine Sea Salts produced by Tropic Marin (Germany) and Instant Ocean Sea Salts by Instant Ocean (USA).

Nutrients, Trace Metals, and Chelators

The term "nutrient" is colloquially applied to a chemical required in relatively large quantities but can be used for any element or compound necessary for algal growth.

The average concentrations of constituents of potential biological importance found in typical seawater are shown in Table 5.13. These nutrients can be divided in three groups, I, II, and III; with decreasing concentration.

- Group I: concentrations of these constituents exhibit essentially no variation in seawater, and high algal biomass cannot deplete them in culture media. These constituents do not, therefore, have to be added to culture media using natural seawater but do need to be added to deionized water when making artificial seawater media.
- Group II: these elements also have quite constant concentrations in seawater, or vary by a factor of less than 5. Because microalgal biomass cannot deplete their concentrations significantly, they also do not need to be added to natural seawater media. Standard artificial media (and some natural seawater media) add molybdenum (as molybdate), an essential nutrient for algae; selenium (as selenite), which has been demonstrated to be needed by some algae; and strontium, bromide, and fluoride, all of which occur at relatively high concentrations in seawater but none of which have been shown to be essential for microalgal growth.
- Group III: microalgae need all these elements (silicon is needed only by diatoms and some chrysophytes, and nickel is only known to be needed to form urease when algae are using urea as a nitrogen source). These nutrients are generally present at low concentrations in natural seawater, and since microalgae take up substantial amounts of them, concentrations vary widely (generally by a factor of 10 to 1000). All of these nutrients (except silicon and nickel in some circumstances) generally need to be added to culture media in order to generate significant microalgal biomass.

Nitrate is the nitrogen source most often used in culture media, but ammonium can also be used, and indeed it is the preferential form for many algae since it does not have to be reduced prior to amino acid synthesis, the point of primary intracellular nitrogen assimilation into the organic linkage. Ammonium concentrations greater than 25 μM are, however, often reported to be toxic to phytoplankton; hence, ammonium concentrations should be kept low.

Inorganic (ortho)phosphate, the phosphorus form preferentially used by microalgae, is most often added to culture media, but organic (glycero)phosphate is sometimes used, particularly when precipitation of phosphate is anticipated (when nutrients are autoclaved in the culture media rather than separately, for example). Most microalgae are capable of producing cell surface phosphatases that allow them to utilize this and other forms of organic phosphate as a phosphorus source.

TABLE 5.13
Average Concentration of Typical Seawater Constituents

Element	Average Molar Concentration (range in brackets)
Group I	
Na^+	$4.7 \cdot 10^{-1}$
K^+	$1.02 \cdot 10^{-2}$
Mg^{2+}	$5.3 \cdot 10^{-2}$
Ca^{2+}	$1.03 \cdot 10^{-2}$
Cl^-	$5.5 \cdot 10^{-1}$
SO_4^{2-}	$2.8 \cdot 10^{-2}$
HCO_3^-	$2.3 \cdot 10^{-3}$
BO_3^{3-}	$4.2 \cdot 10^{-4}$
Group II	
Br^-	$8.4 \cdot 10^{-4}$
F^-	$6.8 \cdot 10^{-5}$
$I0_3^-$	$4.4 \cdot 10^{-7}$
Li^+	$2.5 \cdot 10^{-5}$
Rb^+	$1.4 \cdot 10^{-6}$
Sr^{2+}	$8.7 \cdot 10^{-5}$
Ba^{2+}	$1 \cdot 10^{-7}$
MoO_4^{2-}	$1.1 \cdot 10^{-7}$
VO_4^{3-}	$2.3 \cdot 10^{-8}$
CrO_4^{2-}	$4 \cdot 10^{-9}$
AsO_4^{3-}	$2.3 \cdot 10^{-8}$
SeO_4^{2-}	$1.7 \cdot 10^{-9}$
Group III	
NO_3^-	$3 \cdot 10^{-5}$ (10^{-8} to $4.5 \cdot 10^{-5}$)
PO_4^{3-}	$2.3 \cdot 10^{-6}$ (10^{-7} to $3.5 \cdot 10^{-6}$)
Fe^{3+}	$1 \cdot 10^{-9}$ (10^{-10} to 10^{-7})
Zn^{2+}	$6 \cdot 10^{-9}$ ($5 \cdot 10^{-11}$ to 10^{-7})
Mn^{2+}	$5 \cdot 10^{-10}$ ($2 \cdot 10^{-10}$ to 10^{-6})
Cu^{2+}	$4 \cdot 10^{-9}$ ($5 \cdot 10^{-10}$ to $6 \cdot 10^{-9}$)
Co^{2+}	$2 \cdot 10^{-11}$ (10^{-11} to 10^{-10})
SiO_4^{4-}	$1 \cdot 10^{-4}$ (10^{-7} to $1.8 \cdot 10^{-4}$)
Ni^{2+}	$8 \cdot 10^{-9}$ ($2 \cdot 10^{-9}$ to $1.2 \cdot 10^{-8}$)

The trace metals which are essential for microalgal growth are incorporated into essential organic molecules, particularly a variety of coenzyme factors which enter into photosynthetic reactions. The concentrations (or more accurately the biologically available concentrations) of Fe, Mn, Zn, Cu, and Co (and sometimes Mo and Se) in natural waters may be limiting to algal growth. Little is known about the complex relationships between chemical speciation of metals and biological availability. It is thought that molecules complexing with metals (chelators) influence the availability of these elements. Chelators act as trace metal buffers, maintaining constant concentrations of free ionic metal. It is the free ionic metal, not the chelated metal, which influences microalgae, either as a nutrient or as a toxin. Without proper chelation, some metals (such as Cu) are often present at toxic concentrations, and others (such as Fe) tend to precipitate and become unavailable to phytoplankton. In natural seawater, dissolved organic molecules (generally present at concentrations of 1–10 mg l^{-1}) act as chelators.

The most widely used chelator in culture media additions is EDTA, which must be present at high concentrations since it mostly complexes with Ca^{2+} and Mg^{2+}, present in large amounts in seawater. EDTA may have an additional benefit of reducing precipitation during autoclaving. High concentrations of this acid have, however, occasionally been reported to be toxic to microalgae. As an alternative, the organic chelator citrate is sometimes utilized, having the advantage of being less influenced by Ca^{2+} and Mg^{2+}. The ratio of chelator:metal in culture medium ranges from 1:1 in f/2 to 10:1 in K medium. High ratios may result in metal deficiencies for coastal phytoplankton (i.e. too much metal is complexed), and many media therefore use intermediate ratios.

In today's aerobic ocean, iron is present in the oxidized form as various ferric hydroxides, and thus it is rather insoluble in seawater. While concentrations of nitrogen, phosphorus, zinc, and manganese in deep water are similar to plankton elemental composition, there is proportionally 20 times less iron in deep water than is apparently needed, meaning that iron may be the ultimate geochemically limiting nutrient to phytoplankton in the ocean (cf. Chapter 2). Iron availability for algal uptake seems to be largely dependent on levels of chelation. It is highly recommended that iron be added as the chemically prepared chelated iron salt of EDTA rather than as iron chloride or other iron salts; the formation of iron chelates is relatively slow, and iron hydroxides will form first in seawater, leading to precipitation of much of the iron in the culture medium.

Apparently as a result of the extreme scarcity of copper in anaerobic waters, copper was not utilized by organisms until the earth became aerobic and copper increased in abundance. Consequently copper does not seem to be an obligate requirement, algae either not needing it or needing in such a small amount that free ionic copper concentrations in natural seawater are sufficient to maintain maximum growth rates. Copper may indeed be toxic, particularly to more primitive algae, and hence copper, if added to culture media at all, should be kept at low concentrations.

The provision of manganese, zinc, and cobalt in culture medium should not be problematic, since even fairly high concentrations are not known to be toxic to algae.

Vitamins

Many planktonic algae are auxotrophic for one or more vitamins; that is, they lack one or more vitamin biosynthetic pathways and therefore must gather essential vitamins from the environment. Possession of a biosynthetic pathway means independence, at the cost of synthesis. A survey conducted on more than 300 algal species has shown that more than half required cobalamin (vitamin B_{12}); about 20% of microalgal species need thiamine (vitamin B_1), and less than 5% need biotin (vitamin B_7) (Figure 5.2).

Cobalamin (vitamin B_{12}) is a cobalt-containing tetrapyrrole related to chlorophyll and heme. Cobalamin acts as a cofactor for enzymes that catalyze either rearrangement-reduction reactions or methyl transfer reactions. In bacteria, there are more than 20 cobalamin-dependent enzymes, including those important for methanogenesis, but in eukaryotes, there are many fewer. Higher plants have no cobalamin-dependent enzymes and so neither utilize nor synthesize cobalamin.

Cobalamin appears to be important in transferring methyl groups and methylating toxic elements such as arsenic, mercury, tin, thallium, platinum, gold, and tellurium.

Biotin (vitamin B_7) is a cofactor for several essential carboxylase enzymes, including acetyl coenzyme A (*CoA*) carboxylase, which is involved in fatty acid synthesis and so is universally required. The molecule consists of an imidazole ring fused to a sulfur-containing tetrahydrothiophene ring with a fatty acid side chain. In eubacteria, the first precursor for biotin synthesis is pimeloyl-*CoA*, but the source of this differs among different species.

Like biotin, thiamine (vitamin B_1) also plays a pivotal role in intermediary carbon metabolism. The active form of the vitamin is thiamine pyrophosphate (TPP), which is essential for all

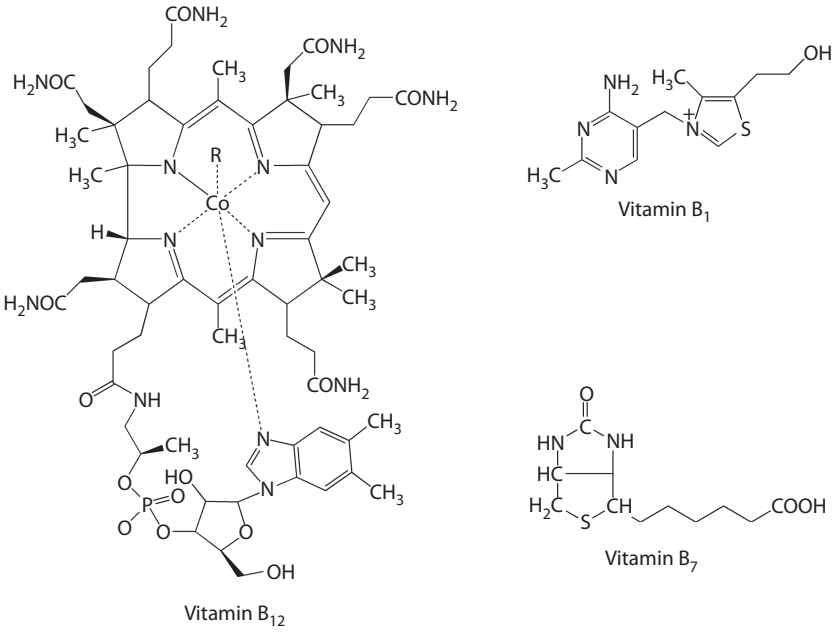


FIGURE 5.2 Structure of cobalamin (vitamin B_{12}), thiamine (vitamin B_1), and biotin (vitamin B_7).

organisms. The cofactor associates with a number of enzymes involved in primary carbohydrate and branched-chain amino acid metabolism, including pyruvate dehydrogenase, transketolase, α-ketoacid decarboxylase, and α-ketoacid oxidase. Thiamine consists of a thiazole and a pyrimidine moiety, which are produced in separate branches of the biosynthetic pathway before being coupled together to produce thiamine phosphate. This is then further phosphorylated to produce the active cofactor TPP.

It is recommended that these vitamins be routinely added to seawater media. No other vitamins have ever been demonstrated to be required by any photosynthetic microalgae.

Soil Extract

Soil extract has historically been an important component of culture media. It is prepared by heating, boiling, or autoclaving a 5 to 30% slurry of soil in fresh water or seawater and subsequently filtering out the soil. The solution provides macronutrients, micronutrients, vitamins, and trace metal chelators in undefined quantities, each batch being different and hence having unpredictable effects on microalgae. With increasing understanding of the importance of various constituents of culture media, soil extract is less frequently used.

Buffers

The control of pH in culture media is important since certain algae grow only within narrowly defined pH ranges, and also to prevent the formation of precipitates. Except under unusual conditions, the pH of natural seawater is around 8. Because of the large buffering capacity of natural seawater due to its bicarbonate buffering system (cf. Chapter 2), it is quite easy to maintain the pH of marine culture media. The buffer system is overwhelmed only during autoclaving, when high temperatures drive CO_2 out of solution and hence cause a shift in the bicarbonate buffer system and

an increase in pH, or in very dense cultures of microalgae, when enough CO_2 is taken up to produce a similar effect.

As culture medium cools after autoclaving, CO_2 reenters solution from the atmosphere, but certain measures must be taken if normal pH is not fully restored:

- the pH of seawater may be lowered prior to autoclaving (adjustment to pH 7–7.5 with 1M HCl) to compensate for subsequent increases;
- certain media recipes include additions of extra buffer, either as bicarbonate, Tris (Tris-hydroxymethyl-aminomethane), or glycylglycine, to supplement the natural buffering system. Tris may also act as a Cu buffer but has occasionally been cited for its toxic properties to microalgae such as *Haematococcus* sp. Glycylglycine is rapidly metabolized by bacteria and hence can only be used with axenic cultures. These additions are generally not necessary if media are filter sterilized, unless very high cell densities are expected.
- the problem of CO_2 depletion in dense cultures may be reduced by having a large surface area of media exposed to the atmosphere relative to the volume of the culture or by bubbling with either air (CO_2 concentration 0.036%) or air with increased CO_2 concentrations (0.5–5%). Unless there is a large amount of biomass taking up the CO_2, the higher concentrations could actually cause a significant decline in pH. When bubbling is employed, the gas must first pass through an inline 0.2-μm filter unit (e.g. Millipore Millex GS) to maintain sterile conditions. For many microalgal species, aeration is not an option, since the physical disturbance may inhibit growth or kill cells.

Some of the most commonly used marine media, defined and undefined, are listed from Tables 5.14 to 5.21. Table 5.22 indicates the algal classes that have been successfully cultured in the media included in this chapter.

TABLE 5.14
Walne's Medium Composition

Walne's Medium	
Reagents	**Per Liter Sea Water**
Solution A	1.0 ml
Solution C	0.1 ml
Solution D (to add for diatoms)	2.0 ml
Solution A	**Per Liter**
$FeCl_3 \cdot 6H_2O$	1.3 g
$MnCl_2 \cdot 4H_2O$	0.4 g
H_3BO_3	33.6 g
Na_2_EDTA	45.0 g
$NaH_2PO_4 \cdot 2H_2O$	20.0 g
$NaNO_3$	100.0 g
Solution B	1 ml
Solution B	**Per 100 ml**
$ZnCl_2$	2.1 g
$CoCl_2 \cdot 6H_2O$	2.0 g
$(NH_4)_6Mo_7O_{24} \cdot 4H_2O$	0.9 g
$CuSO_4 \cdot 5H_2O$	2.0 g

TABLE 5.14 *(Continued)*
Walne's Medium Composition

Solution B	**Per 100 ml**
Concentrated HCl	10 ml
Solution C	**Per 200 ml**
Thiamine HCl (vitamin B_1)	0.2 g
Cobalamin (vitamin B_{12})	10 mg
Solution D	**Per Liter**
$Na_2SiO_3 \cdot 5H_2O$	40.0 g

TABLE 5.15
ASN-III Medium Composition

ASN-III Medium	
Reagents	**Per Liter Sea Water**
NaCl	25 g
$MgCl_2 \cdot 6H_2O$	2 g
$MgSO_4 \cdot 7H_2O$	3.5 g
$NaNO_3$	0.75 g
$K_2HPO_4 \cdot 3H_2O$	0.02 g
KCl	0.5 g
$CaCl_2 \cdot 2H_2O$	0.5 g
$C_6H_8O_7$ (citric acid)	0.003 g
$C_6H_8O_7 \cdot xFe \cdot yNH_3$ (ammonium ferric citrate)	0.003 g
Na_2Mg–EDTA	0.0005 g
Na_2CO_3	0.02 g
Microelement stock solution	1 ml
Microelement Stock Solution	**Per Liter**
H_3BO_3	2.860 g
$MnCl_2 \cdot 4H_2O$	1.810 g
$ZnSO_4 \cdot 7H_2O$	0.222 g
$Na_2MoO_4 \cdot 2H_2O$	0.390 g
$CuSO_4 \cdot 5H_2O$	0.079 g
$Co(NO_3)_2 \cdot 6H_2O$	0.0494 g
pH= 7.5	

TABLE 5.16
CHU-11 Medium Composition

CHU-11 Medium	
Reagents	**Per Liter Sea Water**
$MgSO_4 \cdot 7H_2O$	0.075 g
$CaCl_2 \cdot 2H_2O$	0.036 g

TABLE 5.16 ***(Continued)***
CHU-11 Medium Composition

Reagents	**Per Liter Sea Water**
$NaNO_3$	1.5 g
$K_2HPO_4{\cdot}3H_2O$	0.04 g
Na_2CO_3	0.02 g
$Na_2SiO_3{\cdot}9H_2O$	0.58 g
$C_6H_8O_7$ (citric acid)	0.006 g
$C_6H_8O_7{\cdot}xFe{\cdot}yNH_3$ (ammonium ferric citrate)	0.006 g
Na_2Mg–EDTA	0.001 g
Microelement stock solution	1 ml
Microelement Stock Solution	**Per Liter**
H_3BO_3	0.5 g
$MnCl_2 \cdot 4H_2O$	2 g
$Zn(NO_3)_2 \cdot 6H_2O$	0.5 g
$Na_2MoO_4 \cdot 2H_2O$	0.025 g
$CuCl_2 \cdot 2H_2O$	0.025 g
$Co(NO_3)_2 \cdot 6H_2O$	0.025 g
$VOSO_4 \cdot 6H_2O$	0.025 g
HCl 1 M	3 ml
pH= 7.5	

TABLE 5.17
PCR-S11 Medium Composition

PCR-S11 Medium	
Reagents	**Per Liter Sea Water**
$(NH_4)_2SO_4$	2.68 mg
Na_2_EDTA/$FeCl_3$	8 mg
Na_2PO_4 (pH=7.5)	14 mg
HEPES-NaOH (pH=7.5)	200 mg
Microelement stock solution	0.5 ml
Microelement Stock Solution	**Per Liter**
H_3BO_3	18.549 mg
$MnSO_4 \cdot H_2O$	10.140 mg
$ZnSO_4 \cdot 7H_2O$	1.725 mg
$(NH_4)_6Mo_7O_{24} \cdot 4H_2O$	0.494 mg
$CuSO_4 \cdot 5H_2O$	0.749 mg
$Co(NO_3)_2 \cdot 6H_2O$	0.873 mg
$VSO_5 \cdot 5H_2O$	0.098 mg
$Na_2WO_4 \cdot 2H_2O$	0.198 mg
KBr	0.714 mg
KI	0.498 mg
$Cd(NO_3)_2 \cdot 6H_2O$	0.925 mg
$NiCl_2 \cdot 6H_2O$	0.713 mg
$Cr(NO_3)_3 \cdot 9H_2O$	0.240 mg
SeO_2	0.333 mg

TABLE 5.17 ***(Continued)***
PCR-S11 Medium Composition

Microelement Stock Solution	Per Liter
$KAl(SO_4)_2 \cdot 12H_2O$	2.846 mg
Cobalamin (vitamin B_{12})	10 µg
pH = 7.5	

TABLE 5.18
f/2 Medium Composition

f/2 Medium	
Reagents	**Per Liter Sea Water**
$NaNO_3$	0.075 g
$NaH_2PO4 \cdot H_2O$	0.005 g
Microelement stock solution	1 ml
Vitamin solution	1 ml
Microelement Stock Solution	**Per Liter**
$FeCl_3 \cdot 6H_2O$	3.150 g
Na_2–EDTA	4.160 g
$MnCl_2 \cdot 4H_2O$	0.180 g
$CoCl_2 \cdot 6H_2O$	0.010 g
$CuSO_4 \cdot 5H_2O$	0.010 g
$ZnSO_4 \cdot H_2O$	0.022 g
$Na_2MoO_4 \cdot 2H_2O$	0.006 g
Vitamin Solution	
Biotin (vitamin B_7)	0.5 mg
Thiamine HCl (vitamin B_1)	100 mg
Cobalamin (vitamin B_{12})	0.5 mg
pH= 8.0 adjust with 1 M NAOH or HCl	

TABLE 5.19
K Medium Composition

K Medium	
Reagents	**Per Liter Sea Water**
$NaNO_3$	75 mg
$Na_2C_3H_9O_6P \cdot 5H_2O$ (sodium glycerophosphate)	2.16 mg
NH_4Cl	2.67 mg
Tris-base (pH 7.2)	121.1 mg
Microelement stock solution	1 ml
Vitamin solution	1 ml
Microelement Stock Solution	**Per Liter**
FeNa–EDTA	4.3 g
Na_2–EDTA $\cdot 2H_2O$	37.22 g
$CuSO_4 \cdot 5H_2O$	4.9 mg

TABLE 5.19 *(Continued)*
K Medium Composition

Reagents	Per Liter Sea Water
$MnCl_2 \cdot 4H_2O$	178.2 mg
$ZnSO_4 \cdot 7H_2O$	22 mg
$Na_2MoO_4 \cdot 2H_2O$	6.3 g
H_2SeO_3	1.29 µg
$FeCl_3 \cdot 6H_2O$	3,15 g
$CoCl_2 \cdot 6H_2O$	11.9 mg
Vitamin Solution	**Per Liter**
Biotin (vitamin B_7)	0.1 mg
Thiamine HCl (vitamin B_1)	200 mg
Cobalamin (vitamin B_{12})	1 mg
pH = 7.2	

TABLE 5.20
Johnson's Medium Composition

Johnson's Medium	
Reagents	**Per Liter Sea Water**
$Mg_2Cl_2 \cdot 6H_2O$	1.5 g
$Mg_2SO_4 \cdot 7H_2O$	0.5 g
KCl	0.2 g
$CaCl_2$	0.2 g
KNO_3	1 g
$NaHCO_3$	0.043 g
KH_2PO_4	0.035 mg
$NH_4Mo_7O_{24} \cdot 4H_2O$	0.38 mg
$CuCl_2 \cdot 2H_2O$	0.041 mg
$MnCl_2 \cdot 4H_2O$	0.41 mg
$ZnCl_2$	0.041 mg
VOCl2	0.041 mg
$FeCl_3 \cdot 6H_2O$	2.44 mg
$CoCl_2 \cdot 6H_2O$	0.015 mg
H_3BO_3	0.61 mg
EDTA	1,89 mg
Tris-base (pH 7.5)	2.45 g
pH = 7.5	

TABLE 5.21
ESAW Medium Composition

ESAW Medium	
Reagents	**Per Liter**
NaCl	21.19 g
Na_2SO_4	3.55 g

TABLE 5.21 ***(Continued)***
ESAW Medium Composition

Reagents	Per Liter
KCl	0.599 g
Na_2HCO_3	0.174 g
KBr	0.0863 g
H_3BO_3	0.023 g
NaF	0.0028 g
$MgCl_2{\cdot}6H_2O$	9.592 g
$CaCl_2{\cdot}2H_2O$	1.344
$SrCl_2$	0.0218
$NaNO_3$	46.7 mg
$NaH_2PO_4{\cdot}H_2O$	3.09mg
$Na_2SiO_3{\cdot}9H_2O$	30 mg
Metal stock I	1 ml
Metal stock II	1 ml
Vitamin solution	1 ml
Metal Stock I	
Na_2–EDTA · $2H_2O$	3.09 g
$FeCl_3$· 6 H_2O	1.77 g
Metal Stock II	
Na_2–EDTA · $2H_2O$	2.44 g
$ZnSO_4$ · $7H_2O$	0.073 g
$CoSO_4$ · $7H_2O$	0.016 g
$MnSO_4$ · $4H_2O$	0.54 g
Na_2MoO_4 · $2H_2O$	1.48 mg
Na_2SeO_3	0.173 mg
$NiCl_2{\cdot}6H_2O$	1.49 mg
Vitamin Solution	
Biotin (vitamin B_7)	1 mg
Thiamine HCl (vitamin B_1)	100 mg
Cobalamin (vitamin B_{12})	2 mg
pH = 8.2	

For a full range of possible media, refer to the catalog of strains from culture collections present all over the world, such as:

- EPSAG (Experimentelle Phykologie und Sammlung von Algenkulturen, University of Gottigen, www.epsag.uni-goettingen.de/).
- UTEX (Culture Collection of Algae at the University of Texas at Austin, www.utex.org).
- CCAP (Culture Collection of Algae and Protozoa, Argyll, Scotland, www.ccap.ac.uk).
- CPCC (Canadian Phycological Culture Centre, University of Waterloo Ontario, www.uwaterloo.ca/canadian-phycological-culture/).
- NCMA (National Center for Culture of Marine Microbiota, Bigelow Laboratory, Maine, https://ncma.bigelow.org/).
- CSIROAU (Australian National Algal Culture Collection, Tasmania, www.csiro.au/en/about/facilities-collections/collections/anacc).

TABLE 5.22
Media Listed in This Chapter and the Corresponding Cultured Algal Groups

Medium	Group Cultured
BG11 Medium	Freshwater and soil Cyanophyceae
Diatom Medium	Freshwater Bacillariophyceae
DY-III Medium	Freshwater Chrysophyceae
Aaronson's Medium	*Ochromonas* sp.
Cramer and Myers Medium	Euglenophyceae
Sueoka's Medium	Freshwater Chlorophyceae
Bold Basal Medium	Broad spectrum medium for freshwater Chlorophyceae, Xanthophyceae, Chrysophyceae, Cyanophyceae
MES-Volvox Medium	Broad spectrum medium for freshwater algae
Jaworski's Medium (JM)	Broad spectrum medium for freshwater algae
CY-II-Medium	*Cyanophora paradoxa* (Glaucophyceae)
Zarrouk's Medium	Mass production of *Arthrospira* sp.
Walne's Medium	Broad spectrum medium for marine algae (especially designed for mass culture)
ASN-III Medium	Marine Cyanobacteria
CHU-11 Medium	Marine Cyanobacteria
PCR-S11 Medium	Prochlorophyceae
f/2 Medium	Broad spectrum medium for coastal algae
Johnson's Medium	Halophilic algae (e.g. *Dunaliella* sp.)
K Medium	Broad spectrum medium for oligotrophic marine algae
ESAW Medium	Broad spectrum medium for costal and open ocean algae

- PCC (Pasteur Culture Collection of Cyanobacteria www.pasteur.fr/recherche/banques/PCC/).
- NCCA (Norwegian Culture Collection of Algae, University of Oslo, https://niva-cca.no)

STERILIZATION OF CULTURE MATERIALS

All vessels used for culture purposes should be scrubbed (abrasive brushes are not appropriate for most plastics) and soaked with warm detergent (not domestic detergents, which leave a residual film on cultureware, but phosphate-free laboratory detergent), then rinsed extensively with tap water. After soaking in 10% HCl for 1 day–1 week (not routinely necessary but particularly important for new glass and polycarbonate material), vessels should be rinsed extensively with distilled and finally bidistilled water and left inverted to dry in a clean, dust-free place or in a oven.

Sterilization can be defined as a process which ensures total inactivation of microbial life, and should not be confused with disinfection, which is defined as an arbitrary reduction of bacterial numbers. The primary purpose of sterilization is to prevent contamination by unwanted organisms, but it may also serve to eliminate unwanted chemicals. Sterilization can be obtained by means of several methods, the choice depending on the purpose and material used, either empty glassware/plasticware or medium-containing vessels, but also on the facilities available in a laboratory.

Several methods are available for sterilization of material, some of which can also be used for growth media:

- gases, such as ethylene oxide, EtO, find the best application on heat-sensitive equipment on which steam autoclaving (sterilization with heat) cannot be performed. EtO sterilizes by alkylation; it substitutes for hydrogen atoms on molecules such as proteins and DNA,

and, by attaching to these molecules and disrupting them, EtO stops these molecules' normal life-supporting functions. This method is widely used for the sterilization of medical devices, but it is not a routinely available technique for algology laboratories. Moreover, EtO is a potent carcinogen;

- dry heat; some laboratories use dry heat to sterilize empty vessels, putting the material in a oven for at least 3–4 hours at 160°C; however, only higher temperatures (200°C–250°C) guarantee an effective result. Vessels are covered with aluminum foil to maintain sterility on removal from the oven. This procedure is suitable only for few materials that stand high temperatures, such as glass, Teflon, silicone, metal, and cotton;
- autoclaving (moist heat) is the most widely used technique for sterilizing culture media and vessels and is the ultimate guarantee of sterility (including the destruction of viruses). A commercial autoclave is best, but pressure cookers of various sizes are also suitable. Sterility requires 15 minutes at 1–2 bar pressure and a temperature of 121°C in the entire volume of the liquid (i.e. longer times for larger volumes of liquid; approximately 10 min for 100 ml, 20 min for 2 l, 35 min for 5 l). Flasks containing media should be no more than half full and should be left partially open, plugged with cotton wool, or covered with aluminum foil or paper, since for sterility, the steam must penetrate the material. Autoclave steam may introduce chemical contaminants; empty glass and polycarbonate vessels should be autoclaved containing a small amount of bidistilled water which is poured out (thus diluting contaminants) under sterile conditions immediately prior to use. Vessels should never be closed, because of the risk of implosion, using cotton wool bungs or leaving screw caps slightly open. Ensure the heating elements are covered with distilled water, and the escape valve should not be closed until a steady stream of steam is observed. After autoclaving, the pressure release valve should not be opened until the temperature has cooled to below 80°C. Autoclave steam may contaminate the media (i.e. with trace metals from the autoclave tubing). Autoclaving also produces leaching of chemicals from the medium vessel into the medium (silica from glass bottles, toxic chemicals from plastics). Autoclaving in well-used Teflon or polycarbonate vessels reduces leaching of trace contaminants;
- pasteurization (heating to 90°C–95°C for 30 minutes) of media in Teflon or polycarbonate bottles is a potential alternative, reducing the problems of trace metal contamination and alteration of organic molecules inherent with autoclaving. Pasteurization does not, however, completely sterilize seawater containing media; it kills all eukaryotes and most bacteria, but some bacterial spores probably survive. Heating to 90°C–95°C for at least 30 minutes and cooling, repeated on two or more successive days ("tyndallization") may improve sterilization efficiency; it is assumed that vegetative cells are killed by heat and heat resistant spores will germinate in the following cool periods and be killed by subsequent heating;
- ultraviolet radiation (240–280 nm) is not often used for culture materials, because very high intensities are needed to kill everything in a medium such as seawater (1200 W lamp, 2–4 h for culture media in quartz tubes). Such intense UV light necessarily alters and destroys the organic molecules in seawater and generates many long-lived free radicals and other toxic reactive chemical species. Therefore, seawater exposed to intense UV light must be stored for several days prior to use to allow the level of these highly reactive chemical species to decline;
- sterile filtration is probably the best method of sterilizing certain media, especially seawater-based media, without altering their chemistry, as long as care is taken not to contaminate the seawater with dirty filter apparatus. Sterilization efficiency is, however, to some extent reduced compared with heat sterilization methods. Membrane filters of 0.2 µm porosity are generally considered to yield water free of bacteria, but not viruses. 0.1-µm filters can be used, but the time required for filtration of large volumes of culture media may be excessively long. The filtration unit must be sterile: for small volumes (<50 ml),

pre-sterilized single-use filter units for syringe filtration (e.g. Millipore Millex GS) can be used; for volumes up to 1 liter, reusable autoclavable self-assembly filter units (glass or polycarbonate) with 47-mm cellulose ester sterile membrane filters (e.g. Millipore HA) can be used with suction provided by a vacuum pump; for larger volumes, inline systems with a peristaltic pump and cartridge filters may be the best option. Filter units (particularly disposable plastic systems) and the membrane filters themselves can also leak toxic compounds into the filtrate. The first portion of filtrate (e.g. 5% of volume to be filtered) should be discarded to alleviate this problem.

Most stock solutions of culture medium additions can be sterilized separately by autoclaving, although vitamin stock solutions are routinely filtered through 0.2-μm single-use filter units (e.g. Millipore Millex GS), since heat sterilization will denature these organic compounds. Filter sterilization of all additions may reduce uncertainties about stability of the chemical compounds and contamination from autoclave steam, but absolute sterilization is not guaranteed. Stock solutions can be stored in ultraclean sterile glass, polycarbonate, or Teflon tubes/bottles. In order to minimize effects of any microbial contaminations, all stock solutions should be stored in a refrigerator at 4°C, except vitamin stocks, which are stored frozen at −20°C and thawed immediately prior to use.

CULTURE METHODS

Algae can be produced according to a great variety of methods, from closely controlled laboratory methods especially suited for microalgae to less predictable methods in outdoor tanks for both micro- and macroalgae. Indoor culture allows control over illumination, temperature, nutrient level, pH, O_2 and CO_2 concentration, and contamination with predators and competing algae, whereas outdoor algal systems, though cheaper, may be difficult to monitor for extended periods. Open cultures such as uncovered ponds and tanks (indoors or outdoors) are more readily contaminated than closed culture vessels such as tubes, flasks, carboys, bags, and so on. Axenic cultivation can be also chosen, in the case of microalgae, by using cultures free of any foreign organisms such as bacteria, but this cultivation is expensive and difficult, since it requires a strict sterilization of all glassware, culture media, and vessels to avoid contamination. These constraints make it impractical (and very expensive) for commercial operations. On the other hand, non-axenic cultivation, though cheaper and less laborious, is more prone to crash, less predictable, and often of inconsistent quality.

Different types of culture methods are used worldwide, and they will be presented and discussed separately for micro- and macroalgae.

Microalgae

The most routine culture methods adopted for microalgae include batch, continuous and semi-continuous, ponds and photobioreactors.

Batch Cultures

The most common culture system is the batch culture, due to its simplicity and low cost. This is a closed system, volume limited, in which there is no input or output of materials; that is, resources are finite. The algal population cell density increases constantly until the exhaustion of some limiting factor, while other nutrient components of the culture medium decrease over time. Any products produced by the cells during growth also increase in concentration in the culture medium. Once the resources have been utilized by the cells, the cultures die unless supplied with new medium. In practice this is done by sub-culturing, that is, transferring a small volume of existing culture to a large volume of fresh culture medium at regular intervals. In this method, algal cells are allowed to grow and reproduce in a closed container. A typical batch culture setup can be a 250 ml Erlenmeyer

culture flask with a cotton/gauze bung; in some cases, the bung can be fitted with a Pasteur pipette and air is bubbled into the culture to maintain high levels of O_2 and CO_2 and provide mixing.

Batch culture systems are highly dynamic. The population shows a typical pattern of growth according to a sigmoid curve (Figure 5.3a), consisting of a succession of six phases, characterized by variations in the growth rate (Figure 5.3b); the six phases are summarized in Table 5.23.

The growth curve, relative to phases 3, 4, and 5, without the lag, acceleration, and crash phases, can be described with a rectangular hyperbolic function similar to the Michaelis-Menten formulation that describes the nutrient uptake kinetics and the dynamic relationship between photosynthetic rate and irradiance.

After the inoculum, growth does not necessarily start right away, since most cells may be viable but not in condition to divide. The interval necessary for the transferred cells to adapt to the new situation and start growing is the first phase of the growth curve, the lag phase. This lag or induction phase is relatively long when an algal culture is transferred from a plate to liquid culture. Cultures inoculated with exponentially growing algae have short lag phases, which can seriously reduce the time required for up-scaling. The lag in growth is attributed to the physiological adaptation of the cell metabolism to growth, such as the increase of the levels of enzymes and metabolites involved in cell division and carbon fixation. During this phase, the growth rate is zero.

After a short phase of growth acceleration, characterized by a continuously increasing growth rate, up to its maximum value, which is achieved in the following exponential phase, the cell density increases as a function of time t according to the exponential function:

1) $$N_2 = N_1 * e^{\mu(t_2 - t_1)}$$

where N_2 and N_1 are the number of cells at two successive times (t_2 and t_1), and μ is the growth rate. During this phase, the growth rate reached is kept constant. The growth rate is mainly dependent on algal species and cultivation parameters, such as light intensity, temperature, and nutrient availability.

The exponential growth phase normally lasts for a very short period, since cells start to shade each other as their concentration increases. Hence, the culture enters the phase of retardation, and cell growth rate decreases because mainly light, but also nutrients, pH, carbon dioxide, and other physical and chemical factors, begin to limit growth. Following this phase, the cell population continues to increase, but the growth rate decreases until it reaches zero, at which point the culture enters the stationary phase, during which the cell concentration remains constant at its maximum value. The final stage of the culture is the death or "crash" phase, characterized by a negative growth rate; during this phase, water quality deteriorates, mainly due to catabolite accumulation, and nutrients are depleted to a level incapable to sustain growth. Cell density decreases rapidly, and the culture eventually collapses.

In practice, culture crashes can be caused by a variety of reasons, including the depletion of a nutrient, oxygen deficiency, overheating, pH disturbance, or contamination. The key to the success of algal production is maintaining all cultures in the exponential phase of growth. Also, the nutritional value of the produced algae is lower once the culture is beyond phase 4 due to reduced digestibility, deficient composition, and possible production of toxic metabolites.

In batch cultures, cell properties such as size, internal nutrient composition, and metabolic function vary considerably during the above growth phases. This often makes interpretation of the results difficult. During the exponential growth phase, cell properties tend to be constant. However, this phase usually only lasts for a short period of time, and if one wishes to estimate growth rates of the exponential phase of batch cultures, daily sampling appears to be insufficient to allow a reasonably accurate estimate. Moreover, the accuracy of growth rate determination is highest in artificial, defined media as compared to cells grown in natural surface water media.

A significant advantage of batch culture systems is their operational simplicity. The culture vessels most often consist of an Erlenmeyer flask with a sample-to-flask volume ratio of about 0.2, in

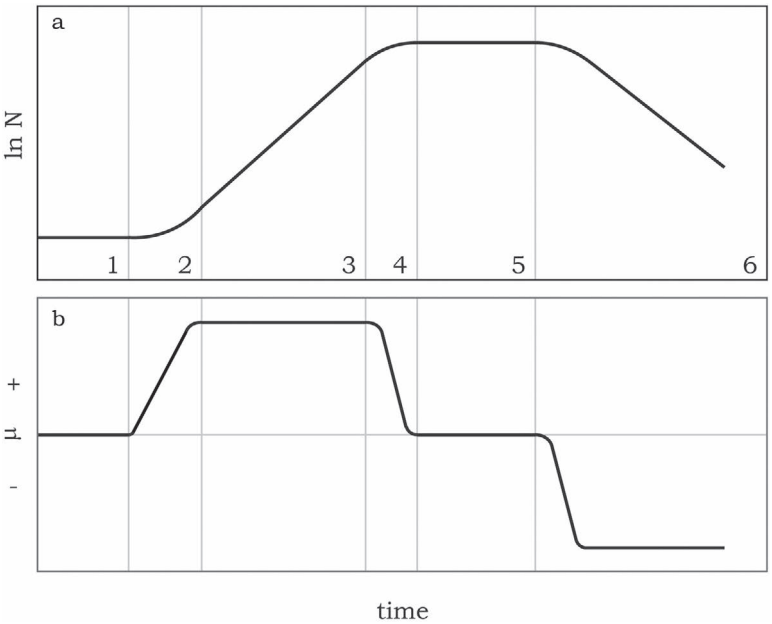


FIGURE 5.3 Growth curve of an algal population under batch culture conditions (a). Corresponding variations of the growth rate (b).

TABLE 5.23
Description of the Six Successive Phases of Growth for an Algal Population Under Batch Culture Conditions

Phase	Growth	Growth Rate Interpretation	Description
1	Lag	Zero	Physiological adaptation of the inoculum to changing conditions
2	Acceleration	Increasing	Trivial
3	Exponential	Constant	Population growth changes the environment of the cells
4	Retardation	Decreasing	Effects of changing conditions appear
5	Stationary	Zero	One or more nutrients (or light) are exhausted down to the threshold level of the cells
6	Decline	Negative	The duration of the stationary phase and the rate of decline are strongly dependent on the kind of organisms

order to prevent carbon dioxide limitation. This volume ratio is only critical if the flasks are shaken by hand once a day during the culturing run. If the flasks are cultured on a rotating shaker table, a sample-to-flask volume ratio of 0.5 is permitted.

Batch culture systems are widely applied because of their simplicity and flexibility, allowing one to change species and to remedy defects in the system rapidly. Although often considered the most reliable method, batch culture is not necessarily the most efficient method. Batch cultures are harvested just prior to the initiation of the stationary phase and must thus always be maintained for a substantial period of time past the maximum specific growth rate. Also, the quality of the harvested cells may be less predictable than that in continuous systems and, for example, vary with the timing of the harvest (time of the day, exact growth phase).

Another disadvantage is the need to prevent contamination during the initial inoculation and early growth period. Because the density of the desired phytoplankton is low and the concentration of nutrients is high, any contaminant with a faster growth rate is capable of outgrowing the culture. Batch cultures also require a lot of labor to harvest, clean, sterilize, refill, and inoculate the containers.

Continuous Cultures

In continuous cultures, resources are potentially infinite: cultures are maintained at a chosen point on the growth curve by the regulated addition of fresh culture medium. In practice, a volume of fresh culture medium is added automatically at a rate proportional to the growth rate of the alga, while an equal volume of culture is removed. This method of culturing algae permits the maintenance of cultures very close to the maximum growth rate, since the culture never runs out of nutrients.

Fresh growth medium is stored in a large vessel. Air is pumped into the airspace in this medium vessel. This air pressure will push the medium through a tube which is connected to the culture vessel. By opening and closing the clamp on this medium line, one can add medium to the culture vessel. Air is also pumped into the culture vessel, passes down a long glass tube to the bottom of the culture, and bubbles up. This keeps the culture well suspended as well as high in oxygen and CO_2. The air flowing into the culture vessel flows out through an outflow tube. As fresh medium is added, the level of the liquid in the culture vessel rises; when the level reaches the bottom of the outflow tube, old medium and cells flow out of the culture vessel into a waste flask. There is a second glass tube in the culture vessel, the sample port. When a sample of cells from the culture vessel is needed, the clamp on the sample port can be opened up, and medium and cells flow out.

Continuous culture systems have been widely used to culture microbes for industrial and research purposes. The early development of a continuous culture system can be traced back to the 50s, when the first chemostat, also called bactogen, was developed.

Batch and continuous culture systems differ in that in a continuous culture system, nutrients are supplied to the cell culture at a constant rate, and in order to maintain a constant volume, an equal volume of cell culture is removed. This allows the cell population to reach a "steady state" (i.e. growth rate and the total number of cells per milliliter of culture remain constant).

Two categories of continuous cultures can be distinguished *sensu* Fogg and Thake (1987):

- turbidostat culture, in which fresh medium is delivered only when the cell density of the culture reaches some predetermined point, as measured by the extinction of light passing through the culture. At this point, fresh medium is added to the culture and an equal volume of culture is removed. The diluted culture increases in cell density until the process is repeated.
- chemostat culture, in which a flow of fresh medium is introduced into the culture at a steady, predetermined rate. The latter adds a limiting vital nutrient (e.g. nitrate) at a fixed rate; in this way, the growth rate and not the cell density is kept constant. In a chemostat, the medium addition ultimately determines growth rate and cell density.

In many chemostat continuous culture systems, the nutrient medium is delivered to the culture at a constant rate by a peristaltic pump or solenoid gate system. The rate of media flow can be adjusted and is often set at approximately 20% of culture volume per day. Air is pumped into the culture vessel through a sterile filter. This bubbling air has three effects: it supplies CO_2 and O_2 to the culture, aids in circulation and agitation of the cultures, and pressurizes the head space of the culture vessel so as to provide the force to "remove" an amount of media (and cells) equal to the volume of inflowing media. The culture may be aseptically sampled by opening the clamp on a sample port. The magnetic stirrer and aeration help to prevent the cells from collecting in the bottom of the culture vessel. A truly continuous culture will have the medium delivered at a constant volume per unit time. However, delivery systems such as peristaltic pumps or solenoid gates are inherently

unreliable. In order to deliver exactly the same amounts of medium to several cultures growing at once, a "semi-continuous" approach can be taken.

The rate of flow of medium into a continuous culture system is known as the "dilution rate." When the number of cells in the culture vessel remains constant over time, the dilution rate is said to equal the rate of cell division in the culture, since the cells removed by the outflow of medium are replaced by an equal number of cells through cell division in the culture. The principal advantage of continuous culture is that the rate of dilution controls the rate of microbial growth via the concentration of the growth-limiting nutrient in the medium. As long as the dilution rate is lower than the maximum growth rate attainable by the algal species, the cell density will increase to a point at which the cell division rate ("birth rate") exactly balances the cell washout rate ("death rate"). This steady-state cell density is also characterized by a constancy of all metabolic and growth parameters. On the other hand, if the dilution rate exceeds the maximum cell division rate, then cells are removed faster than they are produced and total washout of the entire cell population eventually occurs.

The disadvantages of the continuous system are its relatively high cost and complexity. The requirements for constant illumination and temperature mostly restrict continuous systems to indoors, and this is only feasible for relatively small production scales. Continuous cultures have the advantages of producing algae of more predictable quality. Furthermore, they are amenable to technological control and automation, which in turn increases the reliability of the system and reduces the need for labor.

Semi-Continuous Cultures

In a semi-continuous system, the fresh medium is delivered to the culture all at once, by simply opening a valve in the medium delivery line. Fresh medium flows into the culture vessel, and spent culture flows out into a collecting vessel. Once the required medium has entered the culture, the valve is closed, and the culture is allowed to grow for 24 hours, when the procedure is repeated. The semi-continuous technique prolongs the use of large tank cultures by partial periodic harvesting followed immediately by topping up to the original volume and supplementing with nutrients to achieve the original level of enrichment. The culture is grown up again, partially harvested, and so on. Semi-continuous cultures may be indoors or outdoors, but usually their duration is unpredictable. Competitors, predators, and/or contaminants and metabolites eventually build up, rendering the culture unsuitable for further use. Since the culture is not harvested completely, the semi-continuous method yields more algae than the batch method for a given tank size.

Commercial-Scale Cultures

Existing commercial microalgae culture systems range in volume from about 10^2 L to more than 10^9 L. However, aside from the specialized small-scale culture systems (<1000 L), other types of culture systems predominate: large open ponds, circular ponds with a rotating arm to mix the cultures, raceway ponds, or large bags.

There are several factors to be considered for choosing the proper culture system: the biology of the alga, the cost of land, labor, energy, water, nutrients, climate (if the culture is outdoors), and the type of final product. The various large-scale culture systems also need to be compared on their basic properties such as their light utilization efficiency, ability to control temperature, hydrodynamic stress placed on the algae, ability to maintain the culture as unialgal and/or axenic, and how easy they are to scale up from laboratory scale to large scale. The final choice of system is almost always a compromise between all of these considerations to achieve an economically acceptable outcome.

A common feature of most of the algal species currently produced commercially (i.e. *Chlorella, Spirulina*, and *Dunaliella*) is that they grow in highly selective environments, which means that they can be grown in open-air cultures and still remain relatively free of contamination by other algae and protozoa. Thus, *Chlorella* grows well in nutrient-rich media, *Spirulina* requires a high pH

and bicarbonate concentration, and *Dunaliella salina* grows at very high salinity. Those species of algae that do not have this selective advantage must be grown in closed systems. This includes most of the marine algae grown as aquaculture feeds (e.g. *Skeletonema, Chaetoceros, Thalassiosira, Tetraselmis*, and *Isochrysis*) and the dinoflagellate *Crypthecodinium cohnii*, grown as a source of long-chain polyunsaturated fatty acids, as well as almost all other species being considered for commercial mass culture. In the particular case of *Crypthecodinium cohnii,* a large scale fermentation plant is operated by Martek Biosciences, a fully owned subsidiary of the Dutch chemical company Royal DSM, based in Columbia, Maryland. Martek's "life'sDHA" is the only US Food and Drug Administration (FDA)–approved docosahexaenoic acid (DHA) additive for infant formula produced from *Crypthecodinium cohnii*.

Outdoor Ponds

Different types of ponds have been designed and experimented with for microalgae cultivation, which vary in size, shape, materials used for construction, and mixing device. Large outdoor ponds can be unlined; with a natural bottom; or lined with inexpensive materials such as clay, brick, or cement or expensive plastics such as polyethylene, PVC sheets, glass fiber, or polyurethane. Unlined ponds suffer from silt suspension, percolation, and heavy contamination, and their use is limited to a few algal species and to particular soil and environmental conditions.

Also, natural systems such as eutrophic lakes or small natural basins can be exploited for microalgal production, provided suitable climatic conditions and sufficient nutrients. Examples are the numerous temporary or permanent soda lakes such as Lake Kossorom, along the northeast border of Lake Chad, where *Arthrospira* sp. grows almost as monoculture and is collected for human consumption by the Kanembou people inhabiting those areas. *Arthrospira* sp. naturally blooms also in two adjacent maar crater lakes, Twin Ma and Taung Pyauk, formed through early quaternary alkali basaltic phreatomagmatic eruptions in the central Myanmar region. The lakes are filled with highly alkaline waters (pH 10–11). Production began in 1988 and by 1999 increased to 100 tons per year. About 60% is harvested from boats on the surface of the lake, and about 40% is grown in outdoor ponds alongside the lake. During the dry season between February and April, the cyanobacterium forms thick mats on the lakes, and people in boats collect a dense concentration of *Arthrospira* in buckets. *Arthrospira* is harvested on parallel inclined filters, washed with fresh water, dewatered, and pressed again. This paste is extruded into noodle-like filaments which are dried in the sun on transparent plastic sheets. Dried filaments are taken to a pharmaceutical factory in Yangon, pasteurized, and pressed into tablets ready to be sold.

Another cyanobacterium used as a food and health supplement is *Aphanizomenon flos-aquae*, which since 1987 has been harvested from Upper Klamath Lake, Oregon, by Klamath Valley Botanicals, LLC, and marketed by registered trademark Klamath's Best. *A. flos-aquae* blooms are often biphasic, with a first peak in late June to early July and a second peak late in September to mid-October. The alga undergoes a dormancy phase in winter. The harvested biomass is screened and centrifuged to remove small extraneous material. The algal concentrate is then gravity-fed into a vertical centrifuge that applies high centrifugal force to separate cells and colonies, removing about 90% of the remaining water. At this stage, the algal product is 6–7% solids. Once concentrated, the product is chilled to 2°C and stored before being pumped to the freezers. The frozen algae is then put into storage boxes and shipped to the freezer facility for storage. When needed, the frozen product is shipped to an external commercial freeze-drying facility to be freeze-dried into a powder containing 3 to 5% water content. This final product is processed into consumable products such as capsules or tablets.

Natural ponds that do not necessitate mixing and need only minimal environmental control represent other extensive cultivation systems. The largest natural ponds used for commercial production of microalgae are *Dunaliella salina* lagoons located in Australia, operated by BASF: Whyalla (South Australia) has extensive cultivation in 460 ha unmixed ponds and Hutt Lagoon (Western Australia) semi-intensive cultivation in 740 ha ponds. Both facilities produce biomass

for extraction of pro-vitamin A and β-carotene, along with other naturally occurring mixed carotenoids. Currently BASF is the world's largest producer of algal β-carotene, all of which is grown in Australia.

Mass algal cultures in outdoor ponds are applied also in Taiwanese shrimp hatcheries where *Skeletonema costatum* is produced successfully in rectangular outdoor concrete ponds of 10–40 tons of water volume and a water depth of 1.5–2 m.

Circular ponds were the first artificial ponds used in large-scale cultivation of microalgae. These are the largest types of open ponds, getting their name from the circular shape of the culture tank, with a center pivot that rotates to provide circular motion to the water. They have a typical depth of 25–30 cm and a diameter of 45 m; a rotating agitator located at the center of the pond provides efficient mixing and prevents sedimentation of algae biomass. The design of these cultivation systems is limited by the size (bigger ponds introduce stronger water resistance and strain on the mechanical parts of agitator), the high energy usage in the agitation process, and the high construction costs. Currently, this cultivation system is used in Japan by Chlorella Industry Co., LTD, in the Kyushu Chikugo factory (Fukuoka prefecture, Japan) for the production of high-quality *Chlorella* biomass. This facility consists of 16 outdoor circular ponds with a total area of more than 13,000 m^2, and it is unique in the depth of its ponds, about 10–15 cm, shallower with respect to other circular ponds but necessary to ensure sunlight penetration to the bottom of the pond.

Raceway ponds are one of the most frequently used open pond types for the cultivation of microalgae. They consist of a series of closed-loop channels around 30 cm deep and a paddlewheel which enables recirculation of microalgae biomass to ensure equal distribution of nutrients and prevent sedimentation of microalgae biomass. Raceway ponds are one of the best open pond cultivation designs available due to their energy efficiency, as a single paddlewheel is sufficient enough to properly agitate a 50,000 m^2 raceway pond. One successful raceway pond cultivation was operated by Sapphire Energy's Columbus Algal Biomass Farm located in Columbus (New Mexico), United States, which successfully produced 520 metric tonnes of dried microalgae biomass during 2 years of its operation without any technical issues. In addition, the same company built a 130-ha raceway pond named Green Crude Farm in Luna Country, near Columbus, the world's first commercial demonstration algae-to-energy facility (also known as the Integrated Algal BioRefinery or IABR), aimed at producing algal biomass to turn into renewable, low-carbon "green crude" oil.

Other facilities use raceway culture ponds, such as those operated by Cyanotech Co. in Hawaii; Cyanotech has built a plant that encompasses 45 ha of algae cultivation ponds on the Kailua-Kona Coast for *Haematococcus* astaxanthin and *Artrosphira* biomass for tablets and powder. Raceway ponds from 1,000 to 5,000 m^2 are adopted, with stirring accomplished by one large paddle wheel per pond. The location was chosen to take advantage of the relatively consistent warm temperatures, sunshine, and low levels of rainfall needed for optimal cultivation of microalgae. The facility includes a processing plant, an onsite extraction plant, and office and research buildings. The company continues to be a world leader in microalgae cultivation and, in line with the goal of sustainability, uses solar to power the farm.

Earthrise Nutritionals, now wholly owned by Dainippon Ink and Chemicals (the present DIC corporation), is today the largest *Arthrospira* producer globally and the world's largest *Arthrospira* farm, located in the Sonoran Desert of southeastern California on a 50-ha site. It operates 37 ponds with food-grade liners, each 5,000 m^2, which are harvested every day during the growing season from April through October. Clean, fresh water and nutrients are added daily to feed the algae, mixed by 50-foot paddlewheels in each pond.

Raceway ponds are also used for intensive cultivation of *Dunaliella salina* by Nature Beta Technologies Ltd. in Eilat, Israel. Nature Beta Technologies currently produces about 25 t ash free dry weight (AFDW) *D. salina var. bardawil* biomass each year from 10 ha of raceways and represents one of the largest reliable sources of *D. salina* powder in the world.

Algal production in outdoor ponds is relatively inexpensive, but it cannot be maintained for prolonged periods and is only suitable for a few fast-growing species due to problems with contamination

by predators, parasites, and more opportunistic algae that tend to dominate regardless of the species used as inoculum. Furthermore, outdoor production is often characterized by a poor batch-to-batch consistency and unpredictable culture crashes caused by changes in weather, sunlight, or water quality. As already noted, the current available way to circumvent this problem is by cultivating algae that are capable of surviving extreme alkaline or saline conditions, due to the few contaminants able to thrive under these conditions. At present, large-scale commercial production of microalgae biomass is limited to *Dunaliella*, *Haematococcus*, *Arthrospira*, and *Chlorella*, which are cultivated in open ponds at farms located around the world.

Photobioreactors

An alternative to open ponds for large-scale production of microalgal biomass are photobioreactors. The term "photobioreactor" is used to indicate only closed systems that do not allow direct exchange of gases or contaminants between the algal culture they contain and the atmosphere. These devices provide a protected environment for cultivated species, relatively safe from contamination by other microorganisms, in which culture parameters such as pH, oxygen and carbonic dioxide concentration, and temperature can be better controlled and provided in known amounts. Moreover, they prevent evaporation and reduce water use, lower CO_2 losses due to outgassing, and permit higher cell concentration, thus reducing operating costs, and attain higher productivity. However, these systems are more expensive to build and operate than ponds, due to the need of cooling, strict control of oxygen accumulation, and biofouling, and their use must be limited to the production of very high-value compounds from algae that cannot be cultivated in open ponds. Different categories of photobioreactors exist, such as axenic photobioreactors; tubular or flat photobioreactors; horizontal, inclined, vertical, or spiral; manifold or serpentine photobioreactors; air or pump mixed; and single phase, filled with culture suspension, with gas exchange taking place in a separate gas exchanger, or two-phase, with both the gas and the liquid phase contained in the photostage.

The simplest photobioreactor is an illuminated bag containing the microalgal suspension, mixed by a stream of CO_2-enriched air. Evolution of this basic device leads to tubular photobioreactors, consisting of an array of transparent tubes. They come in multiple reactor geometries, including horizontal, helical (biocoils), and conical, and can be made from a variety of materials ranging from glass capillaries to plastic bags. Gas exchange and addition of nutrients to the culture normally takes place in a separate vessel (single phase). Tubular reactors are widely available because of the ease of manufacture, process scale-up, and suitability for outdoor use due to their large illumination surface area. Large surface areas are obtained by using thin tubes with a diameter of no more than 10 cm and illuminating the reactor from multiple directions. A pump or airlift is used for the circulation of the gas and nutrients throughout the culture. A tubular solar collector is applied to maximize the light penetration to the growing cultures. The arrangement of the tube depends on the area and the mode of cultivation: tubes are sometimes placed parallel to each other and flat above the ground (serpentine or manifold photobioreactors) or arranged like a fence (fence-like photobioreactor). In the photostage, the pH can be adjusted by supplying CO_2. The main disadvantage of tubular reactors is their poor axial mass transfer; long reactors are characterized by significant gas gradients along the tubes.

Flat-panel photobioreactors with a short light path, with a horizontal, inclined, or vertical orientation, have a high surface-to-volume ratio. These photobioreactors are made from Plexiglas or polycarbonate alveolar sheets, 2–4 cm thick, with flexible polyethylene bags enclosed in a rigid framework. Flat photobioreactors have also been developed as transparent flat panels connected in series, vertically arranged 20 cm apart. Compared with tubular systems, flat-panel photobioreactors have one serious disadvantage: a fouling of the channels due to reduced turbulence in their narrow, rectangular shape channels (Figure 5.4).

Despite their much higher initial construction and operation/maintenance costs, which make them uncompetitive for the industrial production of microalgal biomass, photobioreactors have some advantages compared to open ponds (i.e. higher attainable yields) and therefore could be of

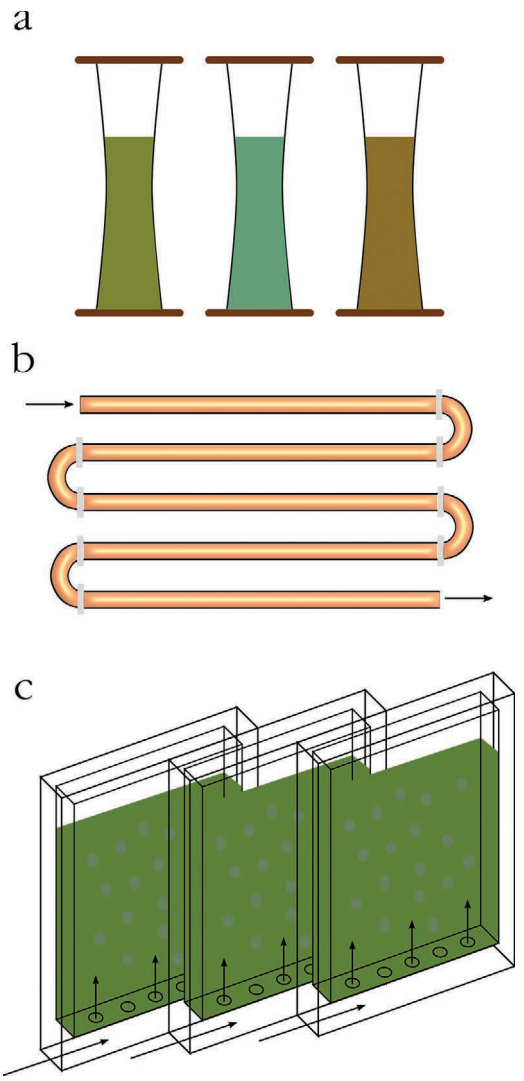


FIGURE 5.4 Photobioreactors: bags (a), tubular system (b), flat panels (c).

choice when the target is to produce high-value bioactive substances which require the adoption of sterile conditions.

The use of photobioreactors dates back to the late 1940s, as a consequence of the investigation on the fundamentals of photosynthesis carried out with *Chlorella*. Open systems were considered inappropriate to guarantee the necessary degree of control and optimization of the continuous cultivation process. Since the first vertical tubular reactors set up in the 1950s for the culture of *Chlorella* under both artificial light and sunlight, several types of photobioreactors have been designed and experimented with. Most of these are small-scale systems, for which experimentation has been conducted mainly indoors, and only a few have been scaled up to a commercial level. Significantly higher photosynthetic efficiencies and a higher degree of system reliability have been achieved in recent years, thanks in particular to the progress in understanding the growth dynamic and requirements of microalgae under mass cultivation conditions. Notwithstanding these advances, there are only a few examples of photobioreactor technology that have expanded from the laboratory to the

market, proving commercially successful. In fact, the main obstacle remains the scaling-up phase, due to the difficulties of transferring a process developed at the laboratory scale to industrial scale in a reliable and efficient way.

Two of the largest commercial systems in operation at present are the Algomed plant located in Klötze, Germany, for the production of *Chlorella vulgaris* biomass and the Algatech plant in Arava Desert, Israel, for the production of *Haematococcus pluvialis* and *Phaeodactylum tricornutum* biomass. Both plants utilize tubular, pump-mixed, single-phase photobioreactors. The Klötze plant, at present fully owned by the Roquette Group (Roquette Klotze GmbH & Co. KG), consists of compact and vertically arranged horizontal running glass tubes of a total length of 500 km and a total PBR volume of 700 m^3. In a glasshouse requiring an area of only 1.2 ha, the plant is the world's first and largest production plant for microalgae and achieves an annual production of 130–150 tonnes dry biomass, demonstrating it is economically feasible under Central European conditions.

Founded in 1998, Algatech is a world leader in the production and supply of AstaPure, natural astaxanthin from *Haematococcus pluvialis* (Figure 5.5), and FucoVital, an innovative proprietary composition for liver health derived from *Phaeodactylum tricornutum* fucoxanthin. The company operates one of the world's largest photobioreactor facilities; it is a patented closed system consisting of a modular array of tubular photobioreactors based on glass tubes 600 km long, set on 10 ha of arid desert land.

Another commercial-scale algae facility is the Ecoduna, housed in a giant 1-ha greenhouse located at Bruck an der Leitha, Austria. The plant has operated at an industrial level since 2018 for the production of *Chlorella* and *Arthrospira* biomass. Schott AG from Germany is the supplier of 43,000 DURAN glass tubes (6 cm diameter, 6 m height) for the installation of the plant tubular photobioreactors divided into 32 units for a total length of 230 km. This fully automated glass and steel plant is characterized by an upright algae flow (mixing is achieved by air + CO_2 bubbling up from the bottom) and 800 m^3 of photoactive volume, which produces up to 100 t of dry biomass per year.

In 2019, the GICON Octagon photobioreactor, part of the EU-funded project Space@Sea, was put into operation in Cottbus, Germany, and was intended to be used on floating work platforms in the oceans as producers of food. The plant consisted of a modular construction of so called "Christmas tree reactors," truncated cone-shaped basic structures, which function as mounting brackets for a flexible double-wall tube system. The biomimetic design is reminiscent of a pine tree (pine tree light collector module, PLM) and provides an optimum light supply due to its geometry. Self-shading of algae is prevented, and light incidence is maximized by allowing variable angles of radiation.

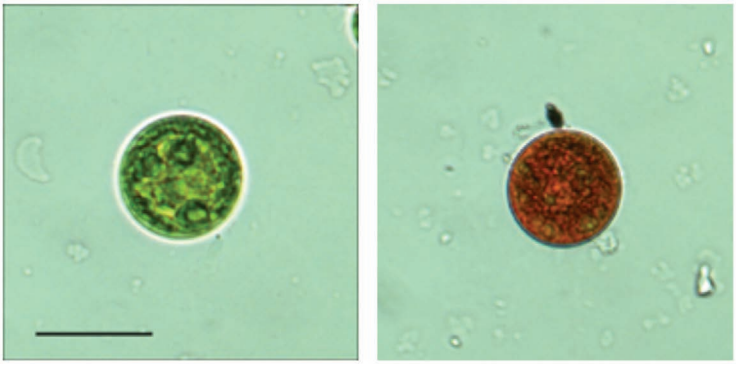


FIGURE 5.5 Green stage and red stage of *Haematococcus pluvialis*. Bar 20 µm.

Another large industrial project is Algafarm, designed, built, and operated between 2011 and 2015 by A4F in Pataias, Portugal, consisting of a series of outdoor tubular photobioreactors scaled up to the largest size in the world, 1,300 m³ on a 1 ha area.

Other industrial plants actually operating are the plant built in Maui, Hawaii (USA), by MicroGaia Ltd. (now BioReal, Inc. a subsidiary of Fuji Chemical Industry Co., Ltd.), which is based on a rather complex design, called BioDome, for the cultivation of *Haematococcus*; the rigid, plastic tube photobioreactor of AAPS (Addavita Ltd., UK); and the flexible, plastic tube photobioreactor of the Mera Growth Module (Mera Pharmaceuticals, Inc. USA).

Culture of Sessile Micro-Algae

Farmers of abalone (*Haliotis* sp.) have developed special techniques to provide food for the juvenile stages which feed in nature by scraping coralline algae and slime off the surface of rocks using their radulae. In culture operations, sessile micro-algae are grown on plates of corrugated roofing plastic, which serve as a substrate for settlement of abalone larvae. After metamorphosis, the spat graze on the micro-algae until they become large enough to feed on macro-algae. The most common species of micro-algae used on the feeder plates are pennate diatoms (e.g. *Nitzchia, Navicula*). The plates are inoculated by placing them in a current of sand-filtered seawater. Depending on local conditions, the micro-algae cultures on the plates take between 1 and 3 weeks to grow to a density suitable for settling of the larvae. As the spat grow, their consumption rate increases and becomes greater than the natural production of the micro-algae. At this stage, the animals are too fragile to be transferred to another plate, and algal growth may be enhanced by increasing illumination intensity and/or the addition of fertilizer.

Macroalgae

Harvesting or collection of macroalgae from the natural environment (wild harvest, including beach cast collection) is an ancient human practice in many regions of the world, like China and Europe, while their cultivation began to grow only in the mid-20th century, particularly in Japan and China, surpassing wild harvest in tonnage about 40 years ago.

Macroalgae cultivation can be performed onshore, offshore, nearshore, and even in aquaculture integrated systems. The cultivation method is chosen according to the species and location of the farm and facilities.

Onshore Cultivation

This type of production takes place in closed systems (e.g. tanks, raceways, ponds, or lagoons) in which water is retained under agitation to keep seaweed suspended and exposed to the light. Tanks of different dimensions and numerous species can all be located together in one place, where they are easy to access, and specialized equipment is not required. The main advantage of land-based cultivation is the monitoring and the opportunity of real-time adjustment of the conditions. Inflows and outflows can be easily monitored, as seawater is pumped onshore and renewed depending on the cultivar needs. In addition, nutrients can be added efficiently to maximize the production of the bioactive compounds of interest while minimizing harmful discharge to the environment, and therefore the composition of the media is under tight control. Light quantity can be manipulated (by shading tanks or by handling the tank depth and seaweed density), and light quality can be controlled artificially by the use of greenhouse coverings and light sources. There is also easy control of pH, CO_2, and salinity, which can be adjusted by mixing fresh/seawater into the on-land tanks.

Land-based cultivation methods have the advantage over ocean-based cultivation systems of adapting to a broad range of macroalgae genera and forms, being suitable for all (except the largest) macroalgae. Farms are not so affected by adverse conditions such as tides, waves, and wind. The main disadvantages of this type of cultivation are the high costs of infrastructure building and maintenance of farm conditions (for instance, in operative work and energy). Land availability

along with suitable water for land-based production is limited, and when available, it is normally expensive.

Offshore Cultivation

The production of seaweed compounds for commercial products (such as polysaccharides) is not profitable in pond systems because of its high cost, and so the use of seaweed produced in these systems is limited to high-value products. Offshore production is an alternative to land-based systems because of the lack of coastal space and its environmental impacts. This type of cultivation is practiced in near-shore areas, including near-farm concepts for kelp growth, tidal flat farms, floating cultivation, ring cultivation, and wind-farm integrated systems. Harvesting techniques include hand-picking, cutting subtidal thalli to bulldoze and tractor, or boat harvesting, while skimmer boats harvest seaweed distant from the coast. Seaweed can either be produced on the sea floor (attached to hard substrate) or on long-lines (anchored lines or nets that are either seeded or have individuals tied to them for grow-out). Due to installation and maintenance cost being very low, attaching seaweed to ropes, lines, or nets is a popular method of cultivation. The cultivation can be carried out attaching the seedlings immediately to the ropes or via transplantation: seedlings are grown indoors, then cultured in greenhouse tanks to the size of small fronds that are later transplanted onto ropes in the sea. These cultivation methods are less costly and labor intensive for the maintenance of the seaweed than land-based ones. In these farming systems, major issues are that the structures and seaweed are susceptible to the most extreme effects of ocean and adverse environmental conditions. Farms have to be extensive and sited in numerous places to mitigate the environmental risk to the crop and be economically viable. Hence, there is a need to invest in structural design and materials that can last in rough sea states. There are also additional costs and energy use involved in transporting the crops and operators to the farms. Normally, these culture systems are placed in coastal waters which have strong water movement and are abundant in inorganic nutrient concentrations. Seaweed cultivation can suffer fouling by macroscopic organisms such as bryozoans, epiphytic seaweed, hydroids, snails, and mussels, inducing deterioration of the algal tissue and causing high biomass loss. In this kind of cultivation, epiphyte overgrowth is a considerable challenge. The impact of such biofouling means that biomass must be harvested at late spring or early summer, limiting the cultivation period and the opportunities for accumulation of storage polysaccharides throughout the summer months. For these reasons, seaweed species selected for open-water farming must be robust and resist both epiphyte growth throughout the season and the local conditions. The adequate maritime area is currently not a limiting factor for expanding offshore agriculture, but climate change, with the consequent changes in water temperature and chemistry, could lead to the reduction of suitable oceanic cultivation areas. In the last years, offshore aquaculture has become an innovative research field due to the growing interest in moving large-scale aquaculture operations further out into the open ocean, demanding original solutions to tackle the challenges of the harsh and/or exposed environment. Various programs to develop kelp offshore systems have been conducted worldwide in the last decade, with a small selection of cultivation systems surviving the harsh oceanic conditions, which improved the economic feasibility of offshore cultivation and can be critical solutions to surpass the problems that inhibit the development of this type of cultivation. However, the results of the cultivation trials showed significant differences in the productivity related to the kelp species selected to cultivate and the farm structure design; hence, it is very important to perform further work to ensure the durability and sustainability of these cultivation procedures.

Nearshore Cultivation

Nearshore cultivation is the most known and used seaweed aquaculture technique, developed in estuarine and near-coast locations. This technique has the advantages of not competing for arable land (the problem of onshore aquaculture) and being protected by the land from mechanical

aggression and damage provoked by sea agitation, sea storms, and currents (the main problem of the offshore aquaculture). Moreover, this technique facilitates the bioremediation of river basins that are anthropogenically polluted with nutrients derived mainly from agriculture activity. In addition, it is less costly and labor intensive with respect to inshore and onshore cultivation. Even though it is near the land, there is low interaction with it; the land is normally used as protection and land base for equipment. The most-used cultivation techniques are line and net cultivation.

Integrated Multitrophic Aquaculture

Macroalgae cultivation can be combined in an integrated multitrophic aquaculture (IMTA) in order to solve some environmental issues of animal aquaculture, such as the eutrophication of the water because of feed supplementation and excretion. The IMTA model is characterized by raising species from different trophic levels in proximity to one and other. Thus, the co-products (organic and inorganic wastes) of one cultured species are recycled to serve as nutritional input for others. This type of cultivation brings benefits due to the interconnected cultivation: there is no need to add fertilizers to promote seaweed growth, and the sustainability and profit are not in risk.

In IMTA systems, the animal's (e.g. fish or mollusk) nutrient output, which is rich in dissolved ammonia and phosphate, is incorporated into the water, converting these compounds into a valuable biomass while stabilizing the levels of oxygen, pH and CO_2. Species with higher productivity in summer, higher rates of nutrient uptake (hence, high growth rates), economic value and that are easy to grow have been identified as the most suitable for IMTA. The environmental benefits and positive externalities offered by seaweed aquaculture are both local, such as reduction of eutrophication and increased habitat for marine biodiversity, and global, by carbon sequestration and "blue" biofuel production. Besides IMTA systems being able to reduce the ecological impacts of aquaculture, the production of algae can also bring financial benefits for the producers through the diversification of products they can commercialize and explore. Thus, seaweed cultivation on an industrial scale, particularly within an IMTA framework, can mitigate general pressure on the environment.

QUANTITATIVE DETERMINATIONS OF ALGAL DENSITY AND GROWTH

Although tedious, time-consuming, and requiring excellence in taxonomic identifications, the traditional counting of phytoplankton is still unsurpassed for quantifying plankton, especially at low limits of detection. The examination and counting of preserved material also allows for direct observation and assessment of cell condition. The fundamental issue that must be addressed prior to choosing a counting technique is whether samples must be concentrated. The three routine methods used to concentrate phytoplankton samples are centrifugation and filtration for live samples and sedimentation (gravitational settling) for preserved samples. Centrifugation and sedimentation are the most commonly used, although filtration onto membrane filters is an effective procedure for fluorescence microscopic enumerations. If the cell density is less than 10^5 cells L^{-1}, the sample needs to be concentrated; if cell density is too high to allow direct counting, the sample will be diluted. Dilution or concentration factors need to be taken into account for calculating the final cell concentration.

Species containing gas vacuoles (cyanobacteria) are unlikely to fully sediment despite Lugol's fixation. Two methods are available for collapsing vacuoles to assist sedimentation. Samples can either be exposed to brief ultrasonication (<1 minute, but may vary for different species), or alternatively, pressure can be applied to the sample by forcing it through a syringe with a fine needle; this will collapse the vacuoles and the cells will then settle through gravity.

If the water sample contains sufficient number of algae and concentration is not required, a direct count can be undertaken. The sample is thoroughly mixed, treated with a few drops of Lugol's solution, mixed again, and allowed to stand for 30 to 60 minutes. The sample is mixed again and subsamples of it used for direct counting and taxonomic identification.

When concentration is required, a simple procedure for gravitational settling is to pour a well-mixed volume of the sample of water containing the microalgae in a measuring cylinder (100 mL), add Lugol's solution to it (1% by volume), and either allow the sample to stand overnight or use a centrifuge so that the cells sink. The iodine in Lugol's solution not only preserves and stains the cells but also increases their density. When the column of water appears clear, the top 90 ml will be gently siphoned off without disturbing the sediment at the base of the cylinder. This leaves the cells concentrated in the bottom 10 ml. Subsamples of this sedimented fraction can be used for the counting procedure and examined under the microscope for identification, keeping in mind that the cells of the original sample have been concentrated 10 times.

At present, there are many kinds of counting procedures available for enumerating phytoplankton, depending on whether counting algae in mixtures, such as from field sampling, or unialgal samples, such as in growth or bioassay experiments in a laboratory. Some techniques are relatively "low-tech" and can be used also in remote locations; others are "high-tech" and require expensive instruments.

The Sedgewick-Rafter counting chamber (Figure 5.6) is a low-tech device routinely used for counting algae in mixed assemblages.

This cell limits the volume and area of the sample to enable easier counting and calculation of phytoplankton numbers. It consists of a brass or polystyrene rectangular frame mounted on a heavy glass slide from which a precise internal chamber has been cut; its dimensions are $50 \times 20 \times 1$ mm, with an area of 1000 mm^2 and a volume of 1 ml. The base is ruled in a 1-mm grid. When the liquid sample is held in the cell by its large, rectangular glass cover slips, the grid subdivides 1 ml volume into microliters.

To fill the Sedgewick-Rafter chamber, the cover slip is placed on top of the chamber, diagonally across the cell, so that the chamber is only partially covered. This helps prevent formation of air bubbles in the cell corners. The cover slip will rotate slowly and cover the inner portion of the cell during filling. The cover slip should not float, nor should there be any air bubbles; the former results from over-filling, the latter from under-filling the chamber. In both cases, the depth of the chamber will be different from 1 mm, and the calculations will be invalidated. A large-bore pipette should be used to transfer the sample into the chamber; after filling, the cover slip is gently pushed to cover the chamber completely. The phytoplankton sample placed into the Sedgwick-Rafter counting chamber is allowed to stand on a flat surface for 20 minutes to enable the phytoplankton to settle. It is then transferred to the stage of an upright light microscope and securely positioned, ready for counting.

Counts are done with the 4× or (more usually) the 10× objective of the compound microscope (depth of field and lens length preclude the use of higher magnification objectives). A Whipple disk

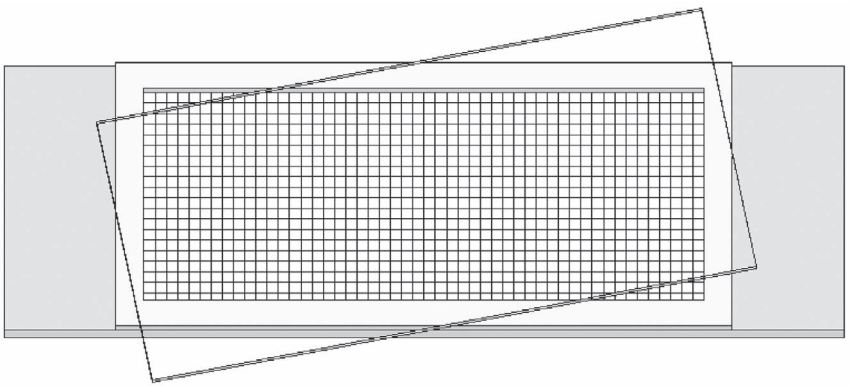


FIGURE 5.6 Schematic drawing of the Sedgewick-Rafter counting chamber.

is inserted into one of the ocular lenses in order to provide a sample grid. It is necessary to first determine the area (A) of the Whipple field for each set of ocular and objective lenses used. This is accomplished with a stage micrometer.

There are 50 fields in the length and 20 fields in the width of the chamber, for a total of 1000 fields. A horizontal strip corresponds to 50 fields. All cells within randomly selected fields are counted. A convention needs to be followed for cells or units lying on a boundary line or field, such as all cells or units overlapping the right-hand and top boundary being counted but not those overlapping the bottom and left-hand boundary. The number of units per milliliter for each taxon is calculated according to following formula:

$$\text{Number of cells} \times \text{ml}^{-1} = (C \times 1000\ \text{mm}^3)/(A \times D \times F) \quad (2)$$

where C is the number of cells counted, A is the area of field in mm^2, D is the depth of a field (Sedgewick-Rafter chamber depth) in mm, and F is the number of fields counted.

For colonial taxa, multiply the count of units by the average number of cells per unit and use the resulting value as C in Equation 2. To adjust for sample concentration or dilution, the result is divided or multiplied by the appropriate factor. To obtain total cell density per milliliter, sum all counts of individual taxa.

If cell density is low (<10 units per field), counting of long transects to cover a large proportion of the chamber floor is more appropriate. Several transects with a width of a chamber field are counted. The number of strips depends on the required precision and the phytoplankton density. The number of cells per mm^3 is calculated according to the following formula:

$$\text{Number of cells} \times \text{ml}^{-1} = (C \times 1000\ \text{mm}^3)/(L \times D \times W \times S) \quad (3)$$

where C is the number of cells counted, L is the length of strip in mm, D is the depth of a field (Sedgewick-Rafter chamber depth) in mm, W is the width of strip in mm, and S is the number of strips counted.

To adjust for sample concentration or dilution, the result is divided or multiplied by the appropriate factor.

A "high-tech" alternative to counting algae in mixed assemblages with the Sedgewick-Rafter cell is the inverted microscope method. The expensive component here is the inverted microscope, whose great advantage is that settling chamber depth does not preclude use of high magnification objective lenses. In 1931, Utermöhl solved the problem of concentrating and enumerating algae in mixed populations when he described a one-step settling and enumeration technique using the inverted microscope. The procedure involved the gravitational sedimentation of preserved phytoplankton into a counting chamber. This counting technique correctly assumed that phytoplankton would fall randomly to the bottom of the chamber and that counts would then be made on random fields or transects. The inverted microscope counting technique has gained broad popularity for phytoplankton enumeration. One of the advantages of this randomized counting technique is the capability of calculating error estimates to verify the accuracy of the enumeration. Through the years, many modified chambers have been designed and used with the inverted microscope.

Special expensive "Utermöhl" chambers can be purchased, but cheaper ones can be constructed from large cover slips and plastic syringe barrels. If a long focal-length lens is available, chambers may be constructed from glass slides.

A measured volume of preserved sample is added to the settling chamber and allowed to settle for at least an hour. Time periods as long as 24–48 hours are preferred, especially if small algae are present in the sample (these will settle only very slowly). Upon settling, the upper portion of the chamber is removed and replaced with a glass plate. The sample is then transferred to an inverted microscope (condenser numerical aperture 0.70; objectives 25× and 40×; oculars 12.5×) with phase contrast optics.

The sample is initially enumerated at 500× (objectives 40× and oculars 12.5×) using a random fields technique. A minimum of 20 random fields and 200 individual cells are enumerated. Additional fields are counted until the minimum count is attained. When there are a large number of cells of a particular taxon in a sample, fewer than 20 random fields are enumerated, with a minimum of 5 random fields examined for this taxon. Individual cells are enumerated, whether in chains, filaments, or colonies. This allows for a more accurate estimate of biomass, which is determined from the cell densities. Upon achieving 20 random fields and 200 individual cells, a low magnification scan (25×) of 20 random fields is used to estimate the rarer, larger forms within the sample.

In the case of unialgal samples (unicells, small colonies, or relatively short filaments) chambers such as the hemacytometer, the Thoma chamber (Figure 5.7), and the Fuchs-Rosenthal or Burker chambers are effective and commonly used for estimating the densities of cultures. The hematocytometer was developed for counting cells in blood samples (now this is mostly done with electronic particle counters). Most of these counting chambers have delicate, mirrored surfaces that must not be scratched. Each mirrored surface has a grid etched upon the surface. In the case of a Thoma chamber, each grid is composed by 16 fields of 0.2-mm sides, separated by three boundary lines (Figure 5.8). These 16 fields are further subdivided into 16 smaller areas each, for a total of 256 counting fields. The chamber is 0.1 mm deep; hence each grid holds exactly 64×10^{-3} ml of sample. You have the choice of counting the algae in the entire grid; counting algae in only one of the 16 squares, then multiplying by 16; or counting algae in an even smaller area and multiplying accordingly.

When counting cells in the entire grid, that is, 16 fields, the cell concentration is calculated according to the following formula:

4) $$\text{Number of cells ml}^{-1} = (C \times 10^3)/64$$

where C is the number of cells counted.

Counts of about 30 cells per field are desirable for accuracy. If there are more than 30 cells per field, dilute the sample or count algae in a lower number of fields and multiply. As for the Sedgewick-Rafter chamber, a convention needs to be followed for cells lying on a boundary line or field, such as all cells overlapping the right-hand and top boundary being counted but not those overlapping the bottom and left-hand boundary (Figure 5.9). The counting process has to be repeated at least ten times to determine an accurate mean.

"High-tech" methods for counting unialgal samples are the electronic particle counter (e.g. Coulter counter) and digital microscopy. In spite of relatively high cost, an electronic particle counter is highly

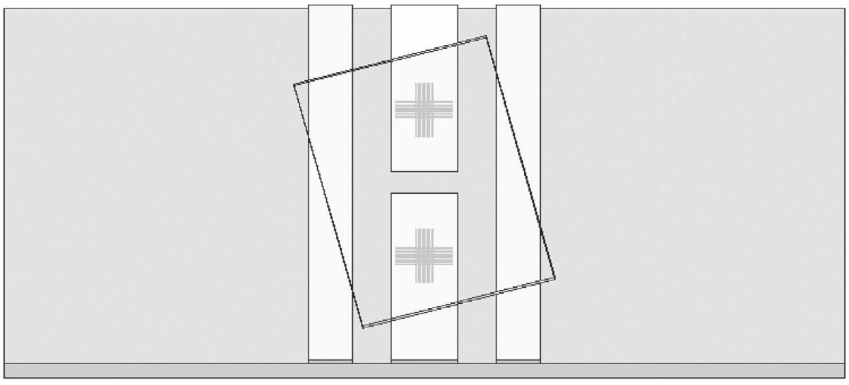


FIGURE 5.7 Schematic drawing of the Thoma counting chamber.

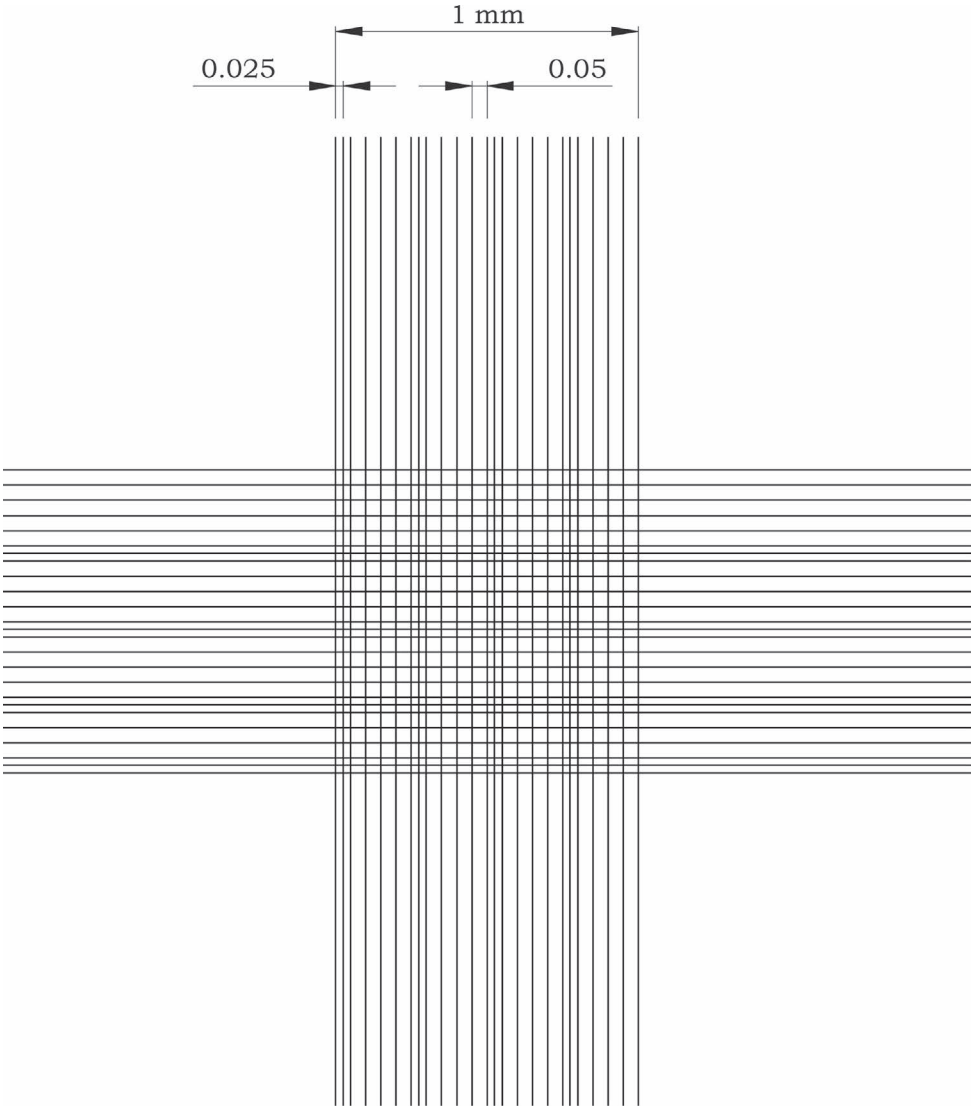


FIGURE 5.8 Schematic drawing of the Thoma chamber ruling.

recommended for doing growth or bioassay studies that require many counts and high accuracy. In addition, the instrument will provide particle size/biovolume distributions. The principle of operation is that particles, suspended in an electrolyte solution, are sized and counted by passing them though an aperture with a particular path of current flow for a given length of time. As the particles displace an equal volume of electrolyte in the aperture, they place resistance in the path of the current, resulting in current and voltage changes. The magnitude of the change is directly proportional to the volume of the particle; the number of changes per unit time is proportional to the number of particles in the sample. When opened, the stopcock introduces vacuum into the system, draws sample through the aperture, and unbalances the mercury in the manometer. The mercury flows past the "start" contact and resets the counter to zero. When the stopcock is closed, the mercury starts to return to its balanced position and draws sample through the aperture. Variously sized aperture tubes are available for use in counting variously sized particles; the aperture size is chosen to match that of particles.

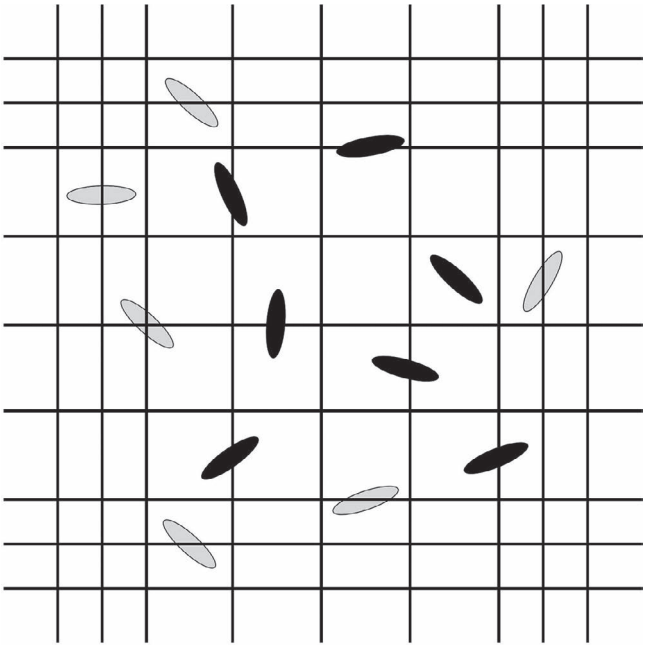


FIGURE 5.9 Schematic drawing of the counting convention: all cells overlapping the right-hand and top boundary are counted (black cells), but those overlapping the bottom and left-hand boundary are not (gray cells).

Digital microscopy represents an automatic, reliable, and very fast approach to cell counting and hence growth determination (cf. Chapter 7).

Growth Rate and Generation Time Determinations

Growth curves are prepared from cell density data obtained with a hemacytometer or electronic particle counter on cultures sampled at intervals, such as once a day, depending upon the growth rate of the alga. Plots of number of cells against time (in days) can be made, and from these curves, specific growth rate or growth constant (μ) and division or generation time (T_g) can be calculated.

A typical growth curve will show a lag phase, an exponential or log phase, and a stationary or plateau phase, where increase in density has leveled off (Figure 5.3a). In the stationary phase, growth is likely limited by resources such as light or nutrients. Growth rate (μ) is calculated with the following equation:

5) $$\mu = \ln(N_2/N_1)/(t_2 - t_1)$$

where N_2 and N_1 are the number of cells at times t_1 and t_2.

When N_2 is twice N_1, that is, the population has undergone a doubling, the growth rate can be expressed as

6) $$\mu = \ln(2)/T_g$$

where T_g is the generation time (Figure 5.3b).

Since ln(2) is equal to 0.6931, generation time can be calculated with the following equation

7) $$T_g = 0.6931\ \mu^{-1}$$

SUGGESTED READING

Alverson, A.J, Manoylov, K.M. and Stevenson, R.J. Laboratory sources of error for algal community attributes during sample preparation and counting. Journal of Applied Phycology, 39, 1–13, 2003.

Andersen, P. and Throndsen, J. Estimating cell numbers. In: Manual on harmful marine algae. IOC Manuals and Guides, Hallegraeff, GM., Anderson, D.M. and Cembella, A.D. (Eds.), 99–129. N0 33, UNESCO Publishing Paris, France, 2003.

Andersen, R.A. (Ed.). Algal culturing techniques. Elsevier Academic Press, Burlington (USA), 2005.

Bello, A.S., Saadaoui, I. and Ben-Hamadou, R. "Beyond the source of bioenergy": Microalgae in modern agriculture as a biostimulant, biofertilizer, and anti-abiotic stress, Agronomy, 11, 1610, 2021.

Berges, J.A., Franklin, D.J. and Harrison, P.J. Evolution of an artificial seawater medium: Improvements in enriched seawater, artificial water over the last two decades. Journal of Phycology, 37, 1138–1145, 2001.

Bertrand, E.M. and Allen, A.E. Influence of vitamin B auxotrophy on nitrogen metabolism in eukaryotic phytoplankton. Frontiers in Microbiology, 3, 2012.

Buck, B.H., Nevejan, N., Wille, M., Chambers, M.D. and Chopin, T. Offshore and multi-use aquaculture with extractive species: seaweeds and bivalves, Springer, Cham, 23–69, 2017.

Buschmann, A.H., Camus, C., Infante, J., Neori, A., Israel, Á., Hernández-González, M.C., Pereda, S.V., Gomez-Pinchetti, J.L., Golberg, A. and Tadmor-Shalev, N. Seaweed production: Overview of the global state of exploitation, farming and emerging research activity. European Journal of Phycology, 52, 391–406, 2017.

Chauton, M.S., Forbord, S., Mäkinen, S., Sarno, A., Slizyte, R., Mozurait yte, R., Standal, I.B. and Skjermo, J. Sustainable resource production for manufacturing bioactives from micro-and macroalgae: Examples from harvesting and cultivation in the Nordic region. Physiologia Plantarum, 173, 495–506, 2021.

Chen, C.-Y., Yeh, K.-L., Aisyah, R., Lee, D.-J. and Chang, J.-S. Cultivation, photobioreactor design and harvesting of microalgae for biodiesel production: A critical review. Bioresource Technology, 102:1, 71–81, 2011.

Chilsholm, S.W. Temporal patterns of cell division in unicellular algae. Canadian Bulletin of Fishery and Aquatic Science, 210, 150–181, 1981.

Clippinger, J.N. and Davis, R.E. Techno-economic analysis for the production of algal biomass via closed photobioreactors: Future cost potential evaluated across a range of cultivation system designs. National Renewable Energy Lab.(NREL), Golden, CO (United States), 2019.

Coltelli, P., Barsanti, L., Evangelista, V., Frassanito, A.M., Passarelli, V. and Gualtieri, P. Automatic and real time recognition of microalgae by means of pigment signature and shape. Environmental Science Progress and Impact, 15:7, 1397–1410, 2013.

Croft, M.T., Warren, M.J. and Smith, A.G. Algae need their vitamins. Eukaryotic Cell, 5:8, 1175–1183, 2006.

Day, J.G. Conservation strategies for algae. In: Plant conservation biotechnology, Benson E.E. (Ed.), 111–124. Taylor and Francis Ltd., London, 1999.

De Vree, J.H., Bosma, R., Janssen, M., Barbosa, M.J. and Wijffels, R.H. Comparison of four outdoor pilot-scale photobioreactors. Biotechnology for Biofuels, 8, 1–12, 2015.

Fogg, G.E, and Thake, B. Algal cultures and phytoplankton ecology. University of Wisconsin Press, Madison (USA), 1987.

García-Poza, S., Leandro, A., Cotas, C., Cotas, J., Marques, J.C., Pereira, L. and Gonçalves, A.M. The evolution road of seaweed aquaculture: Cultivation technologies and the industry 4.0. International Journal of Environmental Research and Public Health, 17, 6528, 2020.

Giovannoni, S.J. Vitamins in the sea. Proceedings of the National Academy of Sciences, 109:35, 13888–13889, 2012.

Gualtieri, P. and Barsanti, L. Identification of cellular and subcellular features by means of digital microscopy. International Journal of Biomedical Computing, 20:79–86, 1987.

Guillard, R.R.L. Culture methods. In: Manual on harmful marine algae. IOC Manuals and Guides, N0 33, Hallegraeff, G.M., Anderson, D.M. and Cembella, A.D. (Eds.), 45–62. UNESCO Publishing Paris, France, 2003.

Hamilton, P.B., Proulx, M. and Earle, C. Enumerating phytoplankton with an upright compound microscope using a modified settling chamber. Hydrobiologia, 444, 171–175, 2001.

Hirooka, S., Tomita, R., Fujiwara, T., Ohnuma, M., Kuroiwa, H., Kuroiwa, T. and Miyagishima, S.-y. Efficient open cultivation of cyanidialean red algae in acidified seawater. Scientific Reports, 10, 1–12, 2020.

Hoffman, J., Pate, R.C., Drennen, T. and Quinn, J.C. Techno-economic assessment of open microalgae production systems. Algal Research, 23, 51–57, 2017.

Johnson, M.K., Johnson, E.J., MacElroy, R.D., Spencer, H.L. and Bruff, B.S. Effect of salt on the halophilic alga *Dunaliella viridis*. Journal of Bacteriology 95:4, 1461–1468, 1968.

Labeda, D.P. (Ed.). Isolation of Biotechnological organisms from nature. McGraw-Hill Publishing Company, New York, 1990.

Legrand, J., Artu, A. and Pruvost, J. A review on photobioreactor design and modelling for microalgae production. Reaction Chemistry & Engineering, 6, 1134–1151, 2021.

Luo Q., Gao, Y., Luo, J., Chen, C., Liang, J. and Yang, C. Automatic identification of diatoms with circular shape using texture analysis. Journal of Software, 6:3, 2011.

Mansoor, H., Sorayya, M., Aishah, S. and Mogeeb, A.A.M. Automatic recognition system for some cyanobacteria using image processing techniques and ANN approach. International Conference on Environmental and Computer Science. 19. IACSIT Press, Singapore, 2011.

Masojídek, J. and Torzillo, G. Mass cultivation of freshwater microalgae. In: Encyclopedia of ecology, Fath, B.D. (Ed.). Elsevier, Amsterdam, 2226–2235, 2008.

Mooney-McAuley, K., Edwards, M., Champenois, J. and Gorman, E. Best practice guidelines for seaweed cultivation and analysis: Public output report [WP1A5. 01] of the EnAlgae Project. http://dx.doi.org/10.25607/OBP-792, 2016.

Mosleh, M., Manssor, H., Malek, S., Milow, P. and Salleh, A. A preliminary study on automated freshwater algae recognition and classification system. BMC Bioinformatics, 13:Suppl 17, S25, 2012.

Osama, A., Hosney, H. and Moussa, M. Potential of household photobioreactor for algae cultivation. Journal of Water and Climate Change, 12, 2147–2180, 2021.

Paxinos, R. and Mitchell, J.G. A rapid Utermohl method for estimating algal numbers. Journal of Planktonic Research, 22, 2255–2262, 2000.

Peteiro, C., Sánchez, N. and Martínez, B. Mariculture of the Asian kelp *Undaria pinnatifida* and the native kelp *Saccharina latissima* along the Atlantic coast of Southern Europe: An overview. Algal Research, 15, 9–23, 2016.

Posten, C. Design and performance parameters of photobioreactors. TATuP-Zeitschrift für Technikfolgenabschätzung in Theorie und Praxis, 21, 38–45, 2012.

Rahman, K.M. Food and high value products from microalgae: Market opportunities and challenges. Springer, 3–27, 2020.

Raoof, B., Kaushik, B.D. and Prasanna, R. Formulation of a low-cost medium for mass production of Spirulina. Biomass and Bioenergy, 30:6, 537–542, 2006.

Richmond, A. (Ed.). Handbook of microalgae mass culture and biotechnology and applied phycology. Blackwell Publishing, Malden (USA), 2004.

Sañudo-Wilhelmy, S.A., Cutter, L.S., Durazo, R., Smail, E.A., Gómez-Consarnau, L., Webb, E.A., et al. Multiple B-vitamin depletion in large areas of the coastal ocean. PNAS, 109:35, 14041–14045, 2012.

Sukačová, K., Lošák, P., Brummer, V., Máša, V., Vícha, D. and Zavřel, T. Perspective design of algae photobioreactor for greenhouses—A comparative study. Energies, 14, 1338, 2021.

Sunda, W.G. and Huntsman, S.A. Effects of pH, light, and temperature on Fe-EDTA chelation and Fe hydrolysis in seawater. Marine Chemistry, 84, 35–47, 2003.

Sunda, W.G. and Huntsman, S.A. Relationship among photoperiod, carbon fixation, growth, chlorophylla, and cellular iron and zinc in a costal diatom. Limnology Oceanography, 49, 1742–1753, 2004.

Thomas, J.-B., Sodré Ribeiro, M., Potting, J., Cervin, G., Nylund, G.M., Olsson, J., Albers, E., Undeland, I., Pavia, H. and Gröndahl, F. A comparative environmental life cycle assessment of hatchery, cultivation, and preservation of the kelp *Saccharina latissima*. ICES Journal of Marine Science, 78, 451–467, 2021.

Tredici, M.R. Photobioreactors. In: Encyclopedia of bioprocess technology: Fermentation, biocatalysis and bioseparation, Flinckinger, M.C. and Drew, S.W. (Eds.), 395–419, Wiley and Sons, New York, 1999.

Umdu, E. and Univ, Y. Building integrated photobioreactor. Elsevier, 243–258, 2020.

Valdovinos-García, E.M., Petriz-Prieto, M.A., Olán-Acosta, M.d.l.Á., Barajas-Fernández, J., Guzmán-López, A. and Bravo-Sánchez, M.G. Production of microalgal biomass in photobioreactors as feedstock for bioenergy and other uses: A techno-economic study of harvesting stage. Applied Sciences, 11, 4386, 2021.

van den Burg, S., Wakenge, C. and Berkhout, P. Economic prospects for large-scale seaweed cultivation in the North Sea. Wageningen Economic Research, 19, 2019.

van Oirschot, R., Thomas, J.-B.E., Gröndahl, F., Fortuin, K.P., Brandenburg, W. and Potting, J. Explorative environmental life cycle assessment for system design of seaweed cultivation and drying. Algal Research, 27, 43–54, 2017.

Verikas, A., Gelzinis, A., Bacauskiene, M., Olenina, I., Olenin, S. and Vaiciukynas, E. Automated image analysis- and soft computing-based detection of the invasive dinoflagellate *Prorocentrum minimum* (Pavillard) schiller. Expert Systems with Applications, 39:5, 6069–6077, 2012.

Warren, A., Day, J.G. and Brown, S. Cultivation of protozoa and algae. In: Manual of Environmental Microbiology, Hurtst C.J., Crawford R.L., Knudsen G.R., McInerney, M.J. and Stenzenbach, L.D. (Eds.), 71–83. ASM Press, Washington, 2002.

Zhang, L., Luo, Z., Wang, B. and Zhang, J. Comparative study of C-V active contour model and subdivision for micro alga image segmentation. International Conference on Electric Information and Control Engineering (ICEICE), 1241–1244. https://doi.org/10.1109/ICEICE.2011.5778135, 2011.

Zittelli, G.C., Rodolfi, L. and Tredici, M.R. Industrial production of microalgal cell-mass and secondary products–species of high potential. In: Handbook of microalgal culture: Biotechnology and applied phycology, 298–303. Richmond, A. (Ed.). Blackwell Science, Oxford, 2004.

6 Utilization

Microalgae and macroalgae have been utilized by man for hundreds of years as food, fodder, remedies, and fertilizers. The earliest record of seaweed utilization dates to 13,000 years ago at a late Pleistocene settlement in Chile; remains of marine algae belonging to the genera *Durvillaea* (Ochrophyta, Phaeophyceae), *Porphyra* (Rhodophyta, Bangiophyceae), *Mazzaella* (Rhodophyta, Florideophyceae), *Sarcothalia* (Rhodophyta, Florideophyceae), *Gracilaria* (Rhodophyta, Florideophyceae), *Gigartina* (Rhodophyta, Florideophyceae), *Macrocystis* (Ochrophyta, Phaeophyceae), *Sargassum* (Ochrophyta, Phaeophyceae), and *Trentepohlia* (Chlorophyta, Ulvophyceae) were recovered from hearths and stone artifacts located in the remains of domestic huts at the archeological site of Monte Verde in southern Chile. All of the algae are edible and have important medicinal properties; hence, these findings suggest a strong reliance on coastal resources for food and medicine by early humans in the Americas.

Other records show that people collected macroalgae for food starting in 500 BC in China and a thousand years later in Europe. Here the earliest recorded account of seaweed use is in a poem dating back to 563 AD dealing with the collection of seaweed by the monks of Iona, in the west of Scotland, to provide food for themselves and the poor.

Microalgae such as *Arthrospira* (Cyanobacteria, Cyanophyceae) have a history of human consumption in Mexico and Africa. In the 14th century, the Aztecs harvested *Arthrospira* from Lake Texcoco and used it to make a sort of dry cake called *tecuitlatl*, and very likely the use of this cyanobacterium as food in Chad dates back to the same period, or even earlier, to the Kanem Empire (9th century).

People migrated from countries such as China, Japan, and Korea, but also from Indonesia and Malaysia, where algae have always been used as food, and brought this custom with them, so that today there are many more countries all over the world where the consumption of algae is not unusual, including in Europe.

Nowadays, on the east and west coasts of the United States and Canada, around Maine, New Brunswick, Nova Scotia, and British Columbia, there are companies that cultivate macroalgae onshore in tanks specifically for human consumption, and their markets are growing, both in those two countries and with exports to Japan. Ireland, Northern Ireland, and Scotland are showing a renewed interest in macroalgae that were once a traditional part of the diet, especially for Irish people during the potato famine of 1846. Macroalgae are also collected from the wild or farmed along the Atlantic coast of Europe from Portugal, France, and the Netherlands, up north to the Scandinavian region.

In addition to direct consumption, agars and carrageenans extracted from red macroalgae and alginates from brown macroalgae and microalgae have been included in a remarkable array of prepared food products, serving mostly to modify viscosity or texture. Global utilization of macroalgae is on the increase, and, in terms of harvested biomass per year, macroalgae are among the most important cultivated marine organisms.

As we will see in detail in "Algae in a Bio-Based Economy" (this chapter), global production of algae is dominated by marine macroalgae, grown in both marine and brackish waters, and cultivation has overshadowed production of algae collected from the wild, which accounted for about 3% of the total in 2019. A few species belonging to eight genera of red and brown algae dominate world seaweed production: *Eucheuma* spp., *Kappaphycus alvarezii, Gracilaria* spp., *Porphyra* spp., *Pyropia* spp., *Saccharina japonica* syn. *Laminaria japonica, Undaria pinnatifida,* and *Sargassum fusiforme*. The small production of green macroalgae is due primarily to five genera: *Caulerpa*, *Monostroma*, *Enteromorpha*, *Capsosiphon*, and *Codium*. Large-scale commercial production of microalgae biomass is limited to *Arthrospira, Dunaliella* (Chlorophyta, Chlorophyceae),

DOI: 10.1201/9781003187707-6

Haematococcus (Chlorophyta, Chlorophyceae), and *Chlorella* (Chlorophyta, Trebouxiophyceae), which are cultivated in open ponds and/or closed systems at farms located around the world.

These algae are a source of viable and inexpensive carotenoids, pigments, proteins, and vitamins that can be used for the production of nutraceuticals, pharmaceuticals, animal feed additives, and cosmetics.

HUMAN FOOD

Cyanobacteria

Some *Nostoc* species are regionally being used as food and herbal ingredients. *Ge-xian-mi* has been regarded as *Nostoc sphaeroides*; however, its taxonomic identity remains controversial. This *Nostoc* species has been used as a delicacy for hundreds of years and is found in rice fields from December to May in Hubei, China. Colonies of *ge-xian-mi* are dark green and pearl-shaped, develop from hormogonia, and can reach 2.5 cm in diameter. Dried *Nostoc* spp. balls are sold in Asian markets; they are stir-fried, sautéed with oysters, and used in soups and as thickeners for other foods.

Another species is *Nostoc flagelliforme* Bornet et Flahault, a terrestrial cyanobacterium that naturally grows on arid and semi-arid steppes in the northern and northwestern parts of China, where it is considered an edible delicacy with special medical value and great economic value. The Chinese have used it as food for about 2000 years, as described in an old text dating back to the Jin Dynasty (265–316 AD). Its herbal value was recognized more than 400 years ago, as recorded with other economic *Nostoc* species in the *Compendium of Materia Medica* of 1578. *N. flagelliforme* is called *fah tsai* (hair vegetable) in Chinese because of its hair-like appearance. However, the pronunciation of *fah tsai* sounds like another Chinese word that means to be fortunate and get rich. Therefore, it also symbolizes good luck. *N. flagelliforme* has been consumed in China, especially Guangdong, and among the overseas Chinese on account of its food and herbal values as well as its spiritual image.

Since this cyanobacterium has been collected and traded from old times, there is less and less of it as market demand increases with economic growth. People gather it with tools that more or less destroy the vegetation, and in addition to this loss by harvesting, pasturing of cattle is rapidly diminishing the resource. On the other hand, exploitation of land has greatly reduced the area producing *Nostoc flagelliforme*, and the quality of the product is degrading. Hence, recently the Chinese government has prohibited further collection for the sake of environmental protection.

Arthrospira also has a history of human consumption, which can be traced to Mexico and in Africa. About 1300 AD, the Aztecs harvested *Arthrospira* from Lake Texcoco, near Tenochtitlan (today Mexico City), and used it to make a sort of dry cake called *tecuitlatl*, which was sold in markets all over Mexico and commonly eaten with maize and other cereals or in a sauce called *chilmolli* made with tomatoes, chili peppers and spices. Very likely the use of *Arthrospira* as food in Chad dates back to the same period, or even earlier, to the Kanem Empire (9th century AD), indicating that two very different and very distant populations independently discovered the food properties of *Arthrospira*. Human consumption of this cyanobacterium in Chad was reported for the first time in 1940 by the French phycologist Dangeard in the little-known *Journal of the Linnean Society of Bordeaux*. He wrote about an unusual food called *dihé* eaten by the Kanembu of Chad and concluded that it was a purée of the filamentous cyanobacterium *Arthrospira platensis*. However, at that time, his report failed to capture the attention it deserved because of the war. In 1966, the botanist Leonard, member of the 1964–1965 Belgian Trans-Saharan Expedition, confirmed the observations of Dangeard. He reported finding a greenish, edible substance being sold as dry cakes in the market of Fort-Lamy (today N'Djamena, the capital of Chad). His investigation revealed that these greenish cakes, called *dihé*, were a common component of the diet of the Kanembu populations of Chad and Niger and that they were almost entirely composed of *Arthrospira*, blooming naturally in the saline-soda lakes of the region. Like *tecuitlatl, dihé* was commonly eaten as a thick, pungent sauce made of chili peppers and spices poured over millet, the staple of the region. In 1976, Delpeuch and

his collaborators at Office de la Recherche Scientifique et Technique Outre-mer [ORSTOM], Paris, France) carried out a study on the nutritional and economic importance of *dihé* for the populations of the prefectures of Kanem and Lac in Chad. The use of *Arthrospira* by Kanembu was mentioned again in 1991 in a Canadian survey of food consumption and nutritional adequacy in wadi zones of Chad, which suggested that *dihé* makes a substantial contribution to vitamin A intake.

Arthrospira is still harvested and consumed by the Kanembu who live around Lake Kossorom, a soda lake at the irregular northeast fringe of Lake Chad in the prefecture of Lac. *Arthrospira* is harvested from Lake Kossorom throughout the year, with a minimum yield in December and January and a maximum in the period between June and September during the rainy season. The bloom is present as a thick blue-green mat floating onto the surface of the lake only few hours a day, early in the morning. When the sun is high, the temperature of the water rises, and the bloom disperses; therefore, harvesting begins at sunrise and is over in about 2 hours.

Only Kanembu women carry out the harvesting; men are banned from entering the water, since it is a deep-rooted belief that they would make the lake barren. The harvesting begins early in the morning, and the work is coordinated by an old woman (the captain) who is responsible for guarding the lake even when the harvesting is over. Just before harvesting begins, the women form a line along the shore at positions assigned to them by the captain according to the village they come from, so as to avoid overcrowding in areas where the alga bloom is more abundant and where trampling and muddying of the water would reduce the quality of *dihé*. The harvesting is carried on according to rules and procedures handed down from mother to daughter from time immemorial. With their basins, the women skim off the blue-green mat that floats at the surface of the water, especially along the shore, and pour it into twine baskets, which act as primary filters, or directly into jars (Figures 6.1a and 6.1b). In about 2 hours, the harvesting is over, and the women move to sandy areas close to the lake for the filtration and drying of the alga. The women dig round holes in the sand, 40–50 cm in diameter and about 5 cm deep, and line them with clean sand, which is patted to obtain a smooth, firm surface. The algal suspension is then carefully poured into the holes, and the surface of the biomass is smoothed with the palm of the hand. Within a few minutes, almost all of the extracellular water will have seeped out of the biomass, and the *dihé* is then cut into 8–10-cm squares, 1–1.5 cm thick, and removed from the holes as soon as it is firm enough for the squares to be handled without breaking (Figures 6.1c, 6.1d, 6.1e, and 6.1f). The drying is completed on mats in the sun. *Dihé* is traded in the local markets and in the markets of the main towns of Chad, from where it can also taken across the borders of Chad to Nigeria, Cameroon, and other countries. It is estimated that about 40 tons of *dihé* are harvested from Lake Kossorom every year, corresponding to a local trading value of more than US $100,000, which represents an important contribution to the economy of one of the poorest nations in the world.

Dihé is mainly used to prepare *la souce*, a kind of vegetable broth served with corn, millet, or sorghum meal, which occasionally can have fish or meat as additional ingredients. Well-dried *dihé* is crumbled in a bowl either by hand or with a mortar and pestle; cold water is then added to disperse the lumps, and the suspension is strained through a fine sieve to remove such solid impurities as sticks, grass, and leaves. The suspension is poured away from most of the sand that settles to the bottom of the bowl. The cleaned *dihé* is cooked for 1–1.5 h, which further disperse the lumps, yielding a blue-green broth that still contains small amounts of plant debris and sand. This broth is transferred into a bowl, left to settle for 5–10 minutes to allow sedimentation of any residual sand, strained very carefully once more, and then poured over sautéed onions. Salt, chili peppers, bouillon cubes, and *gombo* (*Hibiscus esculentus,* Malvaceae) are added, and *la souce* is then simmered and occasionally stirred until cooked.

A minor utilization of *dihé* is as a remedy applied to wounds to speed up the healing process or as a poultice to soothe the pain and reduce the swelling of mumps.

Arthrospira biomass has a high content of protein, about 55–60% of the dry matter; with respect to other food (milk, eggs, etc.), the proteins are low in lysine and sulfured amino acids such as methionine and cysteine, but their amount is much higher than in other vegetables, including



FIGURE 6.1 Harvesting of *Artrosphyra* bloom from Lake Kossorom (a, b). Drying of *Artrosphyra* and preparation of *dihé* on the shore of Lake Kossorom (c, d, e, f). Courtesy of Dr. Gatuger Abdulqader.

legumes. Phycobiliproteins represent a major portion of proteins, and among them phycocyanin can reach 7–13% of the dry matter; carbohydrates reach 10–20% of the dry weight and consist mainly of reserve products, while lipids account for 9–14% of the dry weight. The mineral fraction represents 6–9% of the dry biomass, rich in K, P, Na, Ca, Mn, and Fe. Group A, B, and C vitamins are also present, with an average β-carotene content of 1.5 mg per gram of *Arthrospira*, corresponding to 0.25 µg of vitamin *A*. Considering a Recommended Dietary Allowance (RDA) of vitamin A of about 800 µg, and taking into account a natural 20–30% decrease in β-carotene level due to *dihé* storing conditions, we can say that a daily consumption of 5 g of *dihé* would provide about 100% of the RDA.

Rhodophyta

Foliose algae belonging to the genera *Porphyra* and *Pyropia* (Bangiophyceae) are popularly known as *nori* in Japan, *kim* in Korea, *zicai* in China, and *laver* in Europe (Brittany, Ireland) (cf. Figures

1.1d and 1.33 of Chapter 1). They are among the most nutritious macroalgae, with a protein content of 25–50%, and about 75% of that is digestible. They are also an excellent source of iodine, trace minerals, and dietary fibers. Sugars are low (0.1%) and the vitamin content very high, with significant amounts of vitamins A, complex B, and C, but the shelf life of vitamin C can be short in the dried product. During processing to produce the sheets of *nori*, most salt is washed away, so the sodium content is low. The characteristic taste of *nori* is caused by the large amounts of three amino acids: alanine, glutamic acid, and glycine. It also contains taurine, which controls blood cholesterol levels. *Pyropia tenera* and *P. yezoensis* are preferred industrial sources of the red pigment R-phycoerythrin, which is utilized as a fluorescent "tag" in the medical diagnostic industry.

Algae of the genus *Porphyra*, many species of which have been reclassified as *Pyropia* on the basis of wide taxon sampling and molecular analysis, have been cultivated in Japan and the Republic of Korea since the 17th century, because even at that time, natural stocks were insufficient to meet demand. Today *Porphyra/Pyropia* is one of the largest aquaculture industries in Japan, Korea, and China, expanding to other countries because of its economic importance and health benefits.

Species that are included in the genus *Porphyra* are primarily intertidal and widely distributed in mostly temperate areas of the world's oceans, including a large group of southern hemisphere species, mostly as yet undescribed, from South America, the South Atlantic, South Africa, Australia, New Zealand, and the subantarctic islands. As for *Pyropia*, this genus is not only the most speciose of the Bangiales, but it also displays the greatest morphological variation and has the widest geographic distribution. Species range from tropical to cold, temperate waters and are reported from all major land masses.

Porphyra/Pyropia species have a history of consumption by the indigenous peoples of northwest America (Alaska) and Canada, Hawaii, New Zealand, and parts of the British Isles. *Pyropia abbottae* Krishnamurthy is a nutritionally and culturally important species of red alga used by First Peoples of coastal British Columbia and neighboring areas, down to northern California. This species, along with *P. torta* and possibly others, is a highly nutritious food, still gathered in quantity today by the Coast Tsimshian, Haida, Heiltsuk, Kwakwaka'wakw, and other coastal peoples from wild populations in large quantities, dried and processed, and served in a variety of ways: toasted as a snack; cooked with clams, salmon eggs, or fish in soup; or sprinkled on other foods as a condiment. The common linguistic origin of the majority of names for this species among some 16 language groups in five language families indicates widespread exchange of knowledge about this seaweed from southern Vancouver Island north to Alaska. The harvesting and preparation of this seaweed is exacting and time intensive. It necessitates a wide range of knowledge and skills, including an understanding of weather patterns, tides, and currents; an appreciation of the growth and usable life stages of the seaweed; and a knowledge of the optimum drying locations and techniques and the procedures for secondary moistening, chopping, and drying to achieve the best flavors and greatest nutritional value. *P. abbottiae* is generally harvested in May. Though formerly a women's activity, like *dihé* harvesting by Kanembu women, both genders now participate in seaweed gathering. The postharvest preparation and handling of the seaweed are fairly labor intensive and detailed. Once processed, seaweed is considered "an expensive and prestigious food" and is valued as a gift or trade item that is often exchanged for equally valuable products from other groups, especially on the central and northern coasts of British Columbia and Alaska. *P. abbottiae* is valued also for its medicinal properties as gastrointestinal aid, taken as decoction or applied as a poultice for any kind of sickness in the stomach and as an orthopedic aid applied on broken collarbones.

Nearly 188 species of *Porphyra* and 77 of *Pyropia* have been reported from all over the world, from Japan to the North Atlantic coasts of Europe and America, from the Pacific coast of Canada and United States to the Indian coast.

Porphyra grows as a very thin, flat blade, which can be yellow, olive, pink, or purple. It can be either round, round to ovate, obovate, linear, or linear lanceolate, from 5 to 35 cm in length. The thalli are either one or two cells thick, and each cell has one or two stellate chloroplasts with a

pyrenoid. *Porphyra* has a heteromorphic life cycle with an alternation between an aploid gametophyte consisting of a macroscopic foliose thallus, which is eaten, and a filamentous diploid sporophyte called the conchocelis phase (cf. Figure 1.33 of Chapter 1). This diploid conchocelis phase in the life cycle was earlier thought to be *Conchocelis rosea*, a shell-boring independent organism. Understanding that these two phases were connected was a major research advance made in 1949 in Britain, when the British phycologist Kathleen Mary Drew-Baker demonstrated in culture that *P. umbilicalis* (L.) Kütz had a diploid conchocelis phase. Until this landmark work, cultivation of *Porphyra* was developed intuitively, by observing the seasonal appearance of spores, but nobody knew where the spores came from, so there was little control over the whole cultivation process. Drew's findings completely revolutionized and transformed the *Porphyra* industry in Japan and subsequently throughout Asia, allowing indoor mass cultivation of the filamentous form in sterilized oyster shells and the seeding of conchospores directly onto nets for outplanting in the sea. All Japanese species of *Porphyra* investigated so far produce the conchocelis phase, which can be maintained for long periods of time in free culture. It grows vegetatively under a wide range of temperatures, irradiances, and photoperiods, and it is probably a perennial persistent stage in the life history in many species in nature as well.

Since Drew's time, cultivation has flourished and now accounts for virtually all the production in China, Japan, and the Republic of Korea. Processing of wet blades into dried sheets of *nori* has become highly mechanized by an adaptation of the paper-making process. Wet blades are rinsed, chopped into small pieces, and stirred in a slurry, which is then poured onto mats or frames for most of the water to drain away. The mats are run through a dryer to complete the drying process. The sheets are peeled from the mats and packed in bundles of ten for sale. This product is called *hoshi-nori,* which distinguishes it from *yaki-nori*, which is toasted. *Nori* is used mainly as a luxury food. It is often wrapped around a rice ball of sushi, a typical Japanese food consisting of a small handful of boiled rice with a slice of raw fish on the top. It can be incorporated into soy sauce and boiled down to give an appetizing luxury sauce. It is also used as a raw material for jam and wine. In China, it is mostly used in soups and for seasoning fried foods. In the Republic of Korea, it has similar uses as in Japan.

Dried *nori* is in constant oversupply in Japan, and producers and dealers are trying to encourage its use in United States and other countries. Production and markets in China are expanding, although the quality of the product is not always as good as that from the Republic of Korea and Japan.

The fronds of the red alga *Palmaria* (*Rhodymenia*) *palmata* (Florideophyceae) are known as *dulce*, *dulse*, or *dillisk* (cf. Figure 1.21 of Chapter 1); they are eaten raw as a vegetable substitute or dried and eaten as a condiment in North America and Europe (Brittany, Ireland, and Iceland). Alaska natives consume the fronds fresh or seared on a hot stove or add the air-dried fronds to soups and fish head stews. *Palmaria* is found in the eulittoral zone and sometimes the upper sublittoral. It is collected by hand by harvesters plucking it from the rocks at low tide. It is perennial, and when either plucked or cut, new growth appears from the edge of the previous season's leaf. It is harvested mainly in Ireland and the shores of the Bay of Fundy in eastern Canada and is especially abundant around Grand Manan Island, situated in the Bay of Fundy, in line with the Canadian-United States border between New Brunswick and Maine. The harvest season here is from mid-May to mid-October. After picking, fronds are laid out to sun dry for 6–8 hours; if the weather is not suitable, it can be stored in seawater for a few days, but it soon deteriorates. Whole dulse is packed for sale in plastic bags, 50 g per bag. Inferior dulse, usually because of poor drying, is broken into flakes or ground into powder for use as a seasoning. In Ireland, it is sold in packages and looks like dark-red bundles of flat leaves. It is eaten raw in Ireland, like chewing tobacco, or is cooked with potatoes in soups and fish dishes.

Dulse is a good source of minerals, being very high in iron and containing all the trace elements needed in human nutrition, and has also high vitamin content. In Canada, one company has cultivated it in land-based systems (tanks) and promotes it as a sea vegetable with the trade name "Sea

Parsley." It is a variant of normal dulse plants, but with small frilly outgrowths from the normally flat plant. It was found by staff at the National Research Council of Canada's laboratories in Halifax, Nova Scotia, among samples from a commercial dulse harvester.

Chondrus crispus (Florideophyceae), the Irish moss, carrageenan moss or pioca, has a long history of use in foods in Ireland and some parts of Europe (Figure 6.2). It is not eaten as such but used for its thickening powers when boiled in water, a result of its carrageenan content. One example is its use in making blancmange, a traditional vanilla-flavored pudding. In eastern Canada, the Acadian Seaplants company is cultivating a strain of *Chondrus crispus* and marketing it in Japan as hana nori (flower seaweed), a yellow macroalgae that resembles the more traditional Japanese nori that is in limited supply from natural resources because of overharvesting and pollution. First introduced to the Japanese market in 1996, the dried product, to be reconstituted by the user, was reported to be selling well at the end of 1999, with forecasts of a market valued at tens of millions of US dollars. It is used in macroalgae salads, as a sashimi garnish, and as a soup ingredient.

Fresh *Gracilaria* (Florideophyceae) has been collected and sold as a salad vegetable in Hawaii (USA) for several decades. It is known as *ogo*, *ogonori*, or *sea moss*. The mixture of ethnic groups in Hawaii (Hawaiians, Filipinos, Koreans, Japanese, Chinese) creates an unusual demand, and supply

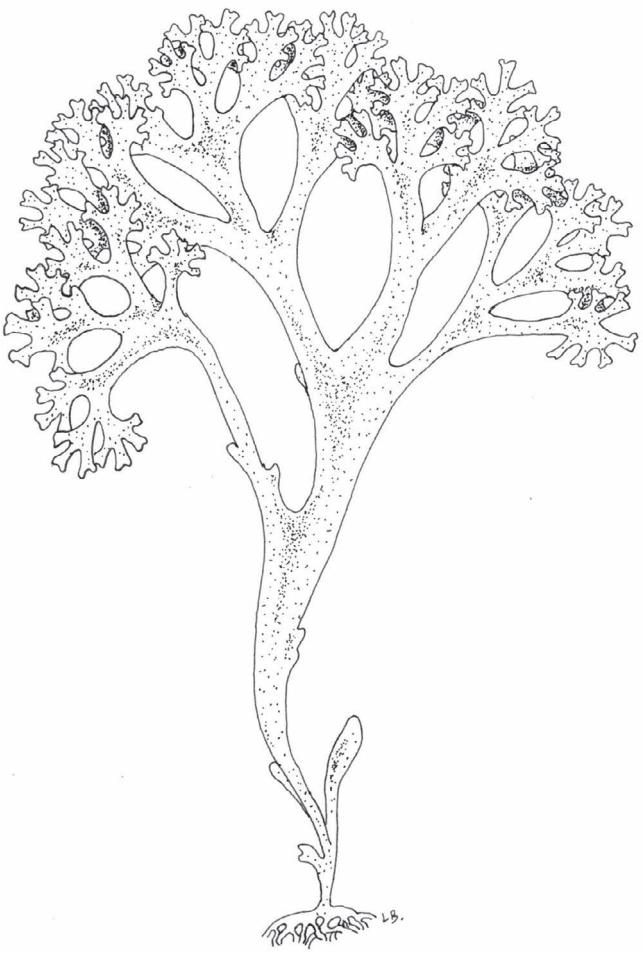


FIGURE 6.2 Frond of *Chondrus crispus*.

has at times been limited by the stocks available from natural sources. Now it is being successfully cultivated in Hawaii using an aerated tank system, producing up to 6 tons fresh weight per week. *Limu manauea* and *limu ogo* are both sold as fresh vegetables, the latter usually mixed with raw fish. In Indonesia, Malaysia, the Philippines and Vietnam, species of *Gracilaria* are collected by coastal people for food. In southern Thailand, an education program was undertaken to show people how it could be used to make jellies by boiling and making use of the extracted agar. In the West Indies, *Gracilaria* is sold in markets as sea moss; it is reputed to have aphrodisiac properties and is also used as a base for a non-alcoholic drink. *Gracilaria* sp. contains (wet weight basis) 6.9 ± 0.1% total protein, 24.7 ± 0.7% crude fiber, 3.3 ± 0.2% total lipid, and 22.7 ± 0.6% ash. It contains of 28.5 ± 0.1 mg of vitamin C per 100 g of wet biomass and 5.2 ± 0.4% mg of β-carotene per 100 g of dry weight, which corresponds to vitamin A activity of 865 μg. According to standard classification adopted by the Association of Official Analytical Chemists (AOAC), this can be considered a very high value of vitamin A activity for a food item, which makes *Gracilaria* a potential source of β-carotene for human consumption.

In Chile, the demand for edible macroalgae has increased, and *Gracilaria chilensis* and *Callophyllis variegata* (*carola*) (Florideophyceae) are among the most popular (Figure 6.3). *Gracilaria chilensis* farming is profitable, which has stimulated research activity in recent years. Several planting techniques have been developed to fasten *Gracilaria* to the substratum, which are commonly used by commercial farms in Chile. As *C. variegata*, this red macroalga has a promising future due to its high commercial value. However, knowledge of its biology is limited, and research projects have been funded for the management of the natural resources and opportunities for cultivation. Carpospores are available during winter, whereas tetraspores are available during spring. Natural populations of *C. variegata* are also being studied to develop management recommendations. From this perspective, it has been demonstrated that the holdfast of this species has a high regeneration capacity, which enables the harvested population to recover.

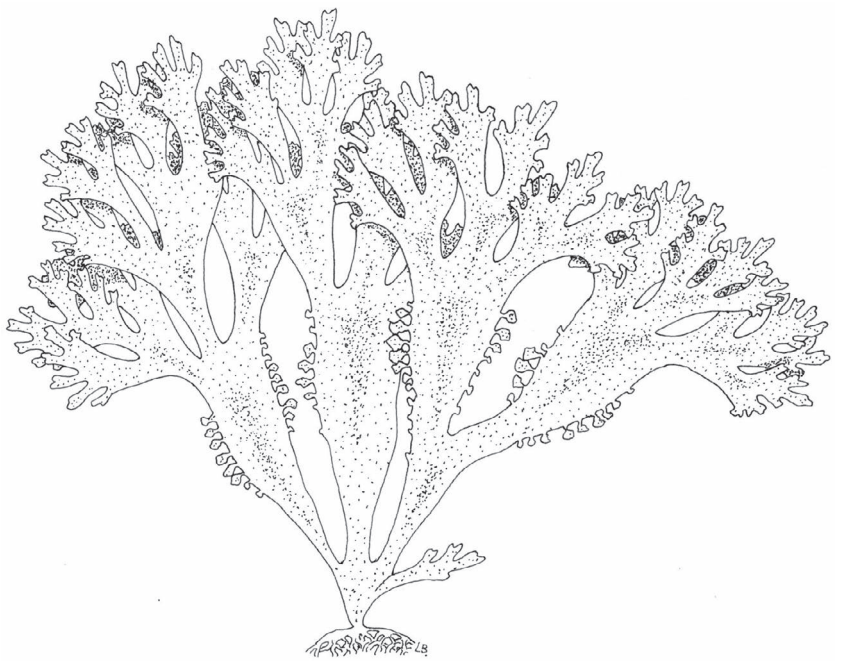


FIGURE 6.3 Frond of *Callophyllis variegata*.

Ochrophyta—Phaeophyceae

Alaria esculenta is a large brown kelp that grows in the upper limit of the sublittoral zone (Figure 6.4). It is known as winged kelp. It has a wide distribution in cold waters and does not survive above 16°C. Presumably due to this factor and rising sea temperatures, the genus has largely disappeared from the English Channel within the past 100 years. It is found in areas such as the coasts of the North Atlantic (France, Scotland, Ireland, Greenland, Iceland, northeastern United States, northeastern Canada), the North Sea (England, Norway, Netherlands), the Arctic Sea (Novaya Zemlya), and the North Pacific (Sakhalin and northern Hokkaido). *Alaria esculenta* is a colonizing species and can form the main canopy in the exposed rocky areas where it grows. Although it is typically not found at a depth more than 8–10 meters, it has been recorded at depths over 20 meters. Its highest seasonal growth rate can reach 20–25 centimeters per month. As with all kelps, *Alaria* demonstrates a heteromorphic, sporic life history, with a macroscopic, dominant sporophyte and a microscopic gametophyte. The sporophyte comprises a ramified holdfast; an unbranched stipe; and a blade with a percurrent, cartilaginous midrib. Unique to the genus *Alaria* is that the sori of the unilocular sporangia are restricted to certain blades, the sporophylls. Most species, such as *Alaria esculenta*, are perennial and can live up to 7 years in some locations; after reproduction, the blade sloughs off, leaving the stipe and meristem. The persisting meristem produces a new blade at the beginning of the next growing season.

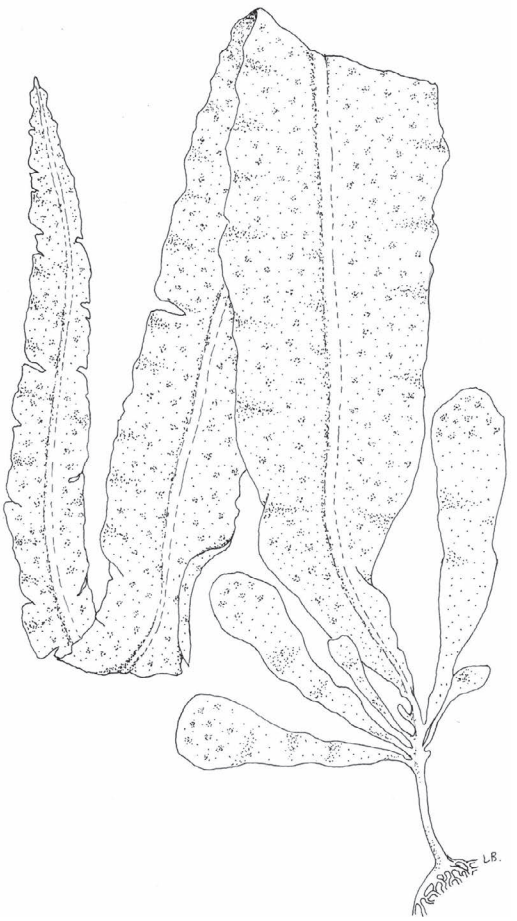


FIGURE 6.4 Frond of *Alaria esculenta*.

Eaten in Ireland, where it is called Atlantic wakame or murlins, and Scotland and Iceland either fresh or cooked, it is said to have the best protein among the kelps and is also rich in trace metals and vitamins, especially niacin. It is usually collected from the wild and eaten by local people, and while it has been successfully cultivated, this has not been extended to a commercial scale.

China is the largest producer of edible macroalgae, contributing to about 90% of global figures. The greater part of this is for *haidai*, produced from hundreds of hectares of the brown macroalga *Saccharina japonica* (Figure 6.5). It is a large macroalga, usually 2–5 m long, but it can grow up to 10 m in favorable conditions. It requires water temperatures below 20°C. *Saccharina* was originally native to Japan and the Republic of Korea, where it has been cultivated since 1730. It was introduced accidentally to China in 1927, probably by the importation of logs from Hokkaido in Japan. Prior to that, China had imported its needs from the naturally growing resources in Japan and the Republic of Korea. In the 1950s, China developed a method for cultivating *Saccharina*; sporelings ("seedlings") are grown in cooled water in greenhouses and later planted out in long ropes suspended in the ocean. This activity became a widespread source of income for large numbers of coastal families and made China self-sufficient in *Saccharina*, also leading to a strong export market.

In Japan, people consume a dried mixture of *Saccharina* species: *S. longissima, S. japonica, S. angustata, S. coriacea*, and *S. ochotensis.* These algae are all harvested from natural sources, mainly on the northern island of Hokkaido, with about 10% coming from the northern shores of Honshu. The plants grow on rocks and reefs in the sublittoral zone, from 2–15 m deep. They prefer calm water at temperatures between 3°C and 20°C. The naturally growing plants are biennial and are ready for harvesting after 20 months. Harvesting is from June to October from boats. Hooks of various types are attached to long poles and used to twist and break the macroalgae from the rocky

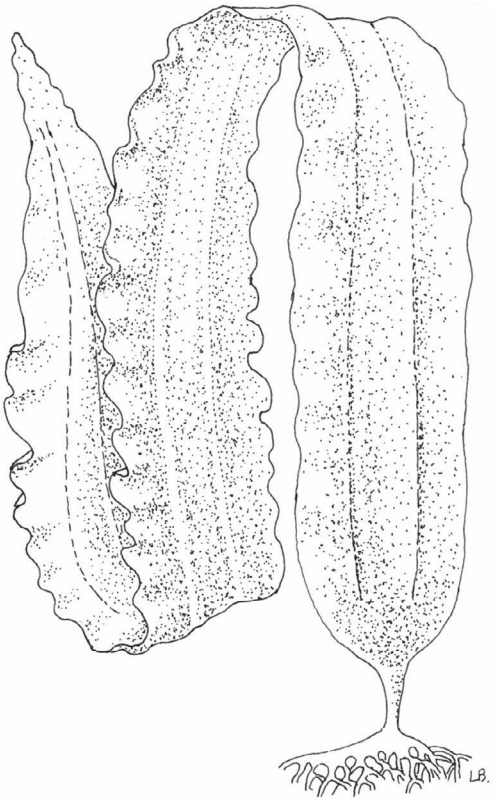


FIGURE 6.5 Frond of *Saccharina japonica*.

bottom. In the 1970s, forced cultivation was introduced, similar to the system developed in China in the early 1950s. Today, about one third of Japan's requirements come from cultivation, with the remaining two thirds still coming from natural resources.

For cultivation, *Saccharina* must go through its life cycle, involving an alternation of generations (see Figure 1.32 of Chapter 1). Seedstock is produced from meiospores released from wild or cultivated sporophytes, incubated in a cool, dark place for up to 24 hours. The spores attach to a substratum within 24 hours and develop into gametophytes. In 2 months, gametophytes release gametes, fertilization occurs, and sporophytes grow about 6 mm long. Seedstock is reared on horizontal or vertical strings, placed in sheltered waters for about 10 days; after this period, the strings are cut into small pieces that are inserted into the warp of the culture rope. The ropes with the young sporophytes are attached to floating rafts, which can be vertical-line or horizontal-line rafts. The first type consists of a large-diameter rope, 60 m long, whose ends are anchored to a wooden peg driven into the sea bottom. Buoys fixed every 2–3 m keep the rope floating. The ropes with the young sporophytes attached hang down from this rope at 50 cm intervals. The second consists of three ropes laid out parallel, 5 m apart. The ropes with the young sporophytes are tied across two ropes so that they are more or less horizontal, and each of them has equal access to light.

In China, the largest region for *Saccharina* cultivation is in the Yellow Sea, where yields are increased by spray application of nitrogen fertilizer directly on the floating raft areas. In Japan, the cultivation is mainly in the waters between Honshu and Hokkaido islands, rich in nitrogen fertilizers. Harvesting takes place in the summer, from mid-June to early July, when the fronds are laid out in the sun to dry and then packed.

Saccharina species contain about 10% protein, 2% fat, and useful amounts of minerals and vitamins, though generally lower than those found in *nori*. For example, it has one tenth the amounts of vitamins but three times the amount of iron compared with *nori*. Brown macroalgae also contain iodine, which is lacking in *nori* and other red macroalgae. In China, *haidai* is regarded as a health vegetable because of its mineral and vitamin content, especially in the north, where green vegetables are scarce in winter. It is usually cooked in soups with other ingredients. In Japan, it is used in everyday food, such as a seasoned and cooked *kombu* that is served with herring or sliced salmon.

Another exploited kelp is *Undaria* sp., which together with *Saccharina* sp. is one of the two most economically important edible algae. This alga has been a food item of high value and importance in Japan since 700 AD. Cultivation began in Japan at the beginning of the 19th century, when the demand exceeded the wild stock harvest, and was followed later in China. The Republic of Korea began the cultivation around the 70s and today is the largest producer of *wakame/quandai-cai* from *Undaria pinnatifida, t*he main species cultivated (Figure 6.6). *U. pinnatifida* grows on rocky shores and bays in the sublittoral zone, down to about 7 m, indigenous to the northwest Pacific Ocean and the cold temperate coastal regions of Japan, China, Korea, and southeast Russia. It grows best between 5°C and 15°C and stops growing if the water temperature rises above 25°C. *Undaria pinnatifida* has been spread around the world by international shipping and mariculture and has extended its range to include four continents since the 1980s. It is now growing in the temperate Pacific Ocean (Australia and New Zealand), the southeastern temperate Indian ocean, the Mediterranean (France, Spain, Italy), and the temperate north and south Atlantic Ocean (United States, Mexico, Argentina, Great Britain, Belgium, France).

Undaria is an annual plant with a life cycle similar to *Saccharina*. It has an alternation of generations with a large sporophyte and a microscopic gametophyte, and its cultivation method its similar to that of *Saccharina*.

The ropes are immersed in seawater tanks containing fertile sporophytes in April–May, when the water temperature is 17°C–20°C, to let spores attach to them. The ropes are then lashed to frames submerged in seawater tanks until September–November. When the young plants are 1–2 cm long and the temperature falls below 15°C, the ropes are removed from the frames and wound around a rope that is suspended by floats and anchored to the bottom at each end. Harvesting begins

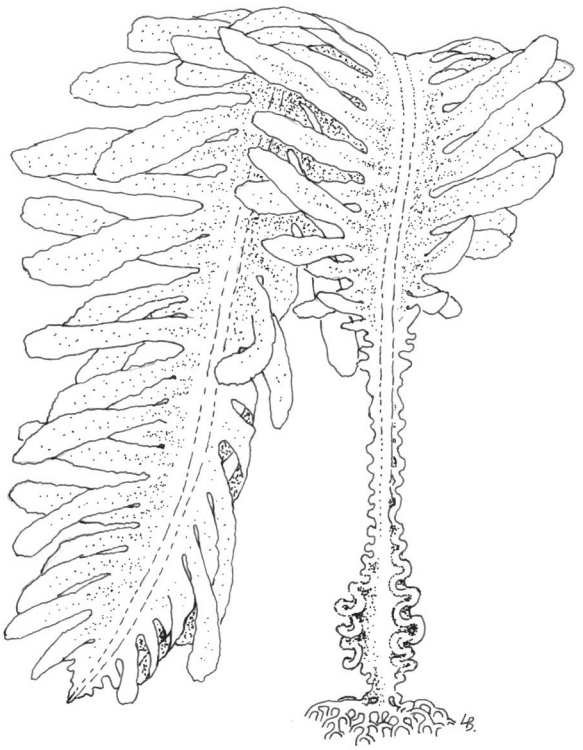


FIGURE 6.6 Frond of *Undaria pinnatifida*.

by thinning out the plants by cutting them off at a point close to the rope. The remaining plants on the rope have plenty of space and continue to grow. Harvesting finishes in April.

After its accidental introduction, cultivation of *Undaria* has also been undertaken in France, where a new technique has been developed and applied. Once the spores have been collected in spring, they are cultivated in laboratories using techniques close to those used for the microalgae. Through precisely controlled light and temperature, the reproducing elements (gametes) are blocked, to the benefit of the cells that give them life (gametophytes). One month before outplanting, the gametophytes are brought to maturation. After fertilization, the solution with the suspended zygotes is sprayed onto a nylon line that is wound around a frame. The zygotes germinate and young sporophytes begin to grow on the frames and are eventually outplanted on floating ropes in the usual way. It is then possible to produce large quantities of reproducing cells which can then be brought to maturity—any time of the year—to form gametes.

Undaria is processed into a variety of food products. After harvesting, the algae are washed (seawater and then freshwater), the central midrib is removed, and the pieces are dried; this is *suboshi wakame*. To avoid fading of the color during, the fresh fronds are mixed with ash from wood or straw so that the alkalinity of the ash deactivates the enzymes responsible for fading. After 2–3 days in the dark, the algae are washed to remove salt and ash (seawater and then freshwater), the midrib is removed, and the pieces are dried. This is *haiboshi wakame,* which keeps its deep green color for a long time and retains the elasticity of the fresh fronds.

The major *wakame* product is salted *wakame*. Fresh fronds are heated in water at 80°C for 1 minute, quickly cooled, dehydrated by 24-hour incubation with salt (30% w/w) and then stored at −10°C. When ready for packaging, the midribs are removed and the pieces placed in plastic bags for sale. It is a fresh green color and can be preserved for long periods when stored at low temperatures.

The crude protein content of *wakame* and *kombu* is 16.3 g% and 6.2 g%, respectively, and both algae contain all essential amino acids, which account for 47.1% of the total amino acid content in *wakame* and for 50.7% in *kombu*. *Wakame* and *kombu* have high contents of β-carotene, 1.30 and 2.99 mg/100 g d.w. or 217 and 481 μg retinol/100 g d.w., respectively. The basic component in sea vegetables is iodine, an essential trace element and an integral part of two hormones released by the thyroid gland. *Wakame* and *kombu* contain 26 and 170 mg/100 g d.w. of iodine, respectively. The recommended daily dose for adults is 150 μg, meaning that the consumption of 557 mg of *wakame* and 88 mg of *kombu* would satisfy the daily requirement for iodine. The toxic dose of iodine for adults is thought to be over 2000 μg per day. The intake of the recommended amount of *wakame* and *kombu* per day would supply 0.94 and 6.29 mg of iodine, respectively, meaning that 1.18 g of *kombu* a day would not exceed the recommended safe dose of iodine. However, it is claimed that iodine supplements can be toxic only if taken in excess, while eating sea vegetables should cause no concern.

Sargassum fusiforme is another brown algae popular as food in Japan and the Republic of Korea, known as *hiziki* (Figure 6.7). It grows at the bottom of the eulittoral and top of the sublittoral zones, on the southern shore of Hokkaido, all around Honshu, on the Korean peninsula, and on most coasts of the China Sea. Up to 20,000 wet tons were harvested from natural beds in the Republic of Korea in 1984, when cultivation began. Since then, cultivation has steadily increased on the southwest coast. This medium-dark brown macroalga grows to about 20–30 cm. in length; the many branches along central stipes give an appearance slightly reminiscent of conifer leaves, with a finer frond structure than *wakame* and *kombu*. The protein, fat, carbohydrate, and vitamin contents are similar



FIGURE 6.7 Frond of *Sargassum fusiforme*.

to those found in *kombu*, although most of the vitamins are destroyed in the processing of the raw macroalgae. The iron, copper, and manganese contents are relatively high, certainly higher than in *kombu*. Like most brown macroalgae, its fat content is low (1.5%), but 20–25% of the fatty acid is eicosapentaenoic acid (EPA).

The cultivation process is very similar to that of *Undaria* and *Saccharina*. Young fronds collected from natural beds are inserted in a rope at 10 cm intervals. Seeding ropes are attached to the main cultivation rope, kept at a depth of 2–3 m using flotation buoys along the rope anchored to the seabed at each end. Cultivation is from November to May, and harvesting is in May–June.

The harvested fronds are washed with seawater, dried in the sun, and boiled with the addition of other brown macroalgae such as *Eisenia bicyclis* or *Ecklonia cava* (Figure 6.8), which helps remove phlorotannin, which gives *Sargassum* its astringent bitter taste. The resulting product is cut into

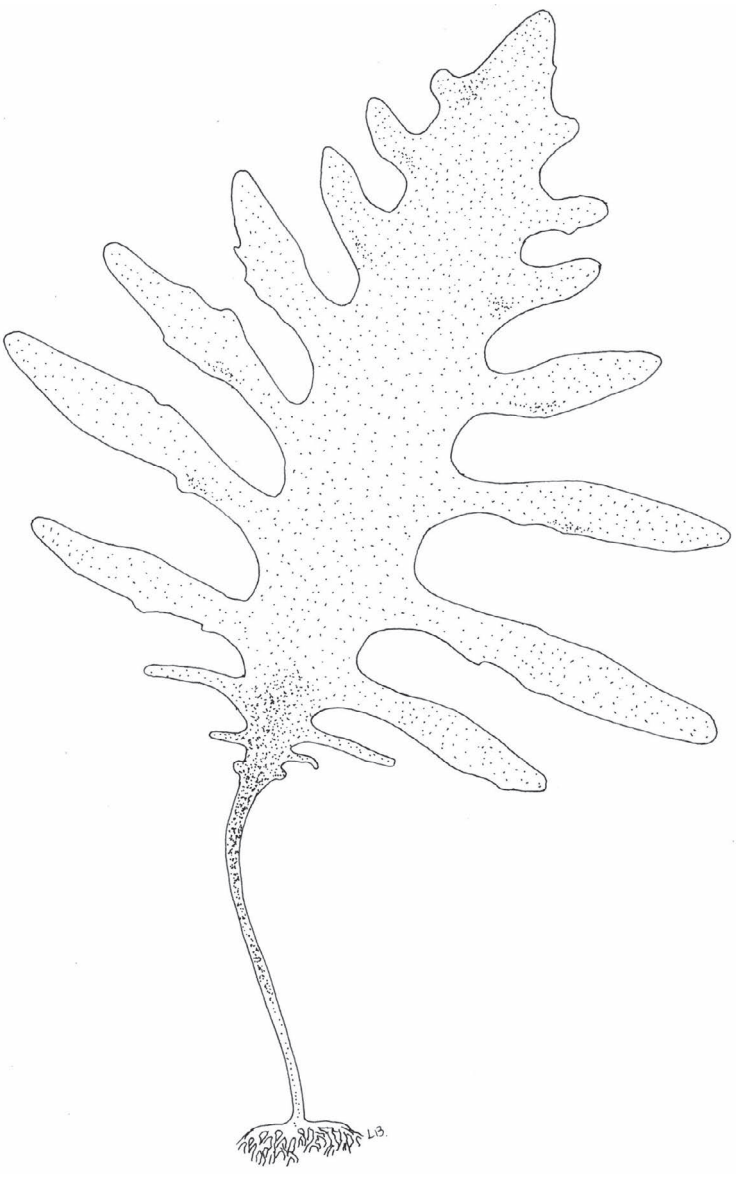


FIGURE 6.8 Frond of *Ecklonia cava*.

short pieces, sun-dried, and sold packaged as *hoshi hiziki*. Typically it is cooked in stir fries, with fried bean curd and vegetables such as carrot, or it may be simmered with other vegetables.

Japan produces also *Cladosiphon okamuranus* cultivated around Okinawa Island. This brown macroalga is also harvested from natural populations around the southern islands of Japan and consumed as *mozuku*. It is characterized by a thallus with stringy, not turgid, fronds, and it can exceed 50 cm in length. *Cladosiphon* grows in the sublittoral zone, mainly at depths of 1–3 m. As *Undaria* and *Saccharina*, its life history involves an alternation of generations. Spores collected from the sporophytes are stored during the summer and used for seeding nets in fall. When young sporophytes have grown to 2–5 cm, the nets are moved to the main cultivation sites. The fronds are harvested after about 90 days, when they have grown to 50 cm. Harvesting is done by divers using a suction pump that draws the macroalgae up and into a floating basket beside the attending boat. The harvested macroalgae are washed, salted with 20–25% salt, and left to dehydrate for about 15 days. Drained fronds are sold in wet, salted form in packages.

Chlorophyta

Monostroma (Ulvophyceae) (Figure 6.9) and *Ulva* (Ulvophyceae) (Figure 6.10) are two green macroalgae cultivated in Japan, known as *aonori* or *green laver.*

Monostroma latissimum occurs naturally in the bays and gulfs of southern areas of Japan, usually in the upper eulittoral zone. The fronds are bright green in color, flat, and leafy, consisting of a single cell layer. They are slender at the holdfast and grow wider toward the apex, often with

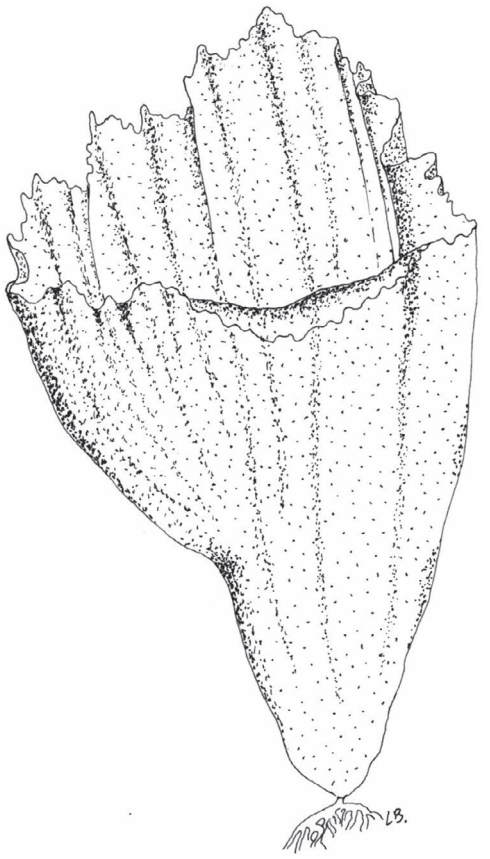


FIGURE 6.9 Frond of *Monostroma latissimum*.

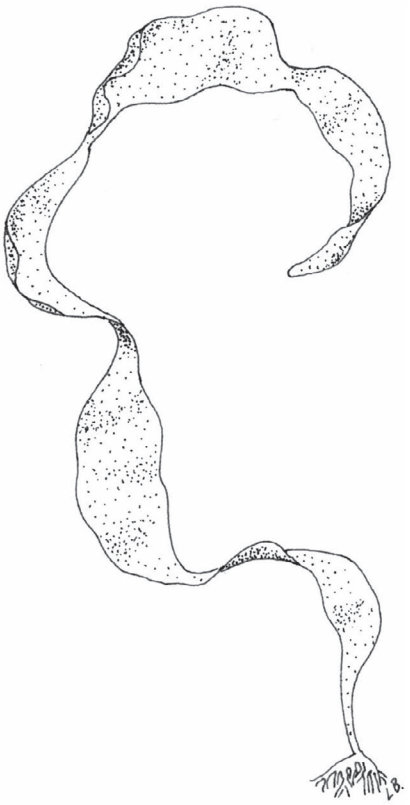


FIGURE 6.10 Frond of *Ulva* sp.

a slight funnel shape that has splits down the side. *Monostroma* reproduces seasonally, usually during the tropical dry season or temperate spring. It is found in shallow sea water usually less than 1 m in depth; generally grows on rocks, coral, mollusk shells, or other hard substrate but also grows as an epiphyte on sea plants, including crops such as *Kappaphycus* and *Eucheuma*. It averages 20% protein and has a useful vitamin and mineral content. It has a life cycle involving an alternation of generations, one generation being the familiar leafy plant, the other microscopic and approximately spherical. It is this latter generation that releases spores that germinate into the leafy frond. For cultivation, these spores are collected on rope nets by submerging the nets in areas where natural *Monostroma* populations grow. The seeded nets are then placed in the bay or estuary, fixed to poles so that they are underwater at high tide, and exposed for about 4 hours at low tide or using floating rafts in deeper water. The nets are harvested every 3–4 weeks, and the growing season allows about three to four harvests. The harvested macroalga is washed well in seawater and freshwater. It can then either be processed into sheets and dried, for sale in shops, or dried, either outside or in dryers, and then boiled with sugar, soy sauce, and other ingredients to make "*nori*-jam."

Ulva prolifera and *Ulva intestinalis* are found in bays and river mouths around Japan and are also found in many other parts of the world, including Europe, North America, and Hawaii. They can thrive in both salt and brackish waters and are usually found at the top of the sublittoral zone. Fronds can be attached to firm substrate in clear, shallow waters and also occur as epiphyte on cultured red seaweed such as *Kappaphycus, Eucheuma, Gracilaria, Gelidiella*, and others. They contains about 20% protein, little fat, low sodium, high iron and calcium, and vitamin B-group content

generally higher than most vegetables. The life history involves an alternation of generations with the same appearance of long, tubular filaments.

As for *Monostroma*, rope nets are seeded with spores by submerging them in areas where *Ulva* is growing naturally. Seed collection is from June to September, depending on the country, and young plants are visible by early November. Harvesting, by hand or by machine, can be done two to three times during the growing period, and harvested fronds are washed in freshwater and dried in large trays.

Ulva sp. (cf. Figure 1.31 of Chapter 1) is known as sea lettuce, since fronds are usually flat, narrow, and bright green; may be convoluted; and have an appearance rather like lettuce. It is slender at the holdfast and grows wider toward the apex. It is naturally found in shallow sea water usually less than 1 m in depth, where it grows on rocks, coral, mollusk shells, or other hard substrate but also as an epiphyte on other sea macroalgae. It reproduces seasonally, during the tropical dry season or temperate spring. It can be collected from the wild and added to *Monostroma* as part of *aonori*.

Caulerpa lentillifera (Figure 6.11) and *C. racemosa* (cf. Figure 1.20 of Chapter 1) are two edible green algae used in fresh salads and known as sea grapes or green caviar because of their appearance, like bunches of green grapes. These algae often produce "runners" under the substrate, which can produce several vertical branches extending above the substrate. They naturally grow on sandy or muddy bottom in shallow protected waters. *C. lentillifera* has been very successfully cultivated in enclosures similar to prawn ponds in the central Philippines, with water temperature ranging between 25°C and 30°C. Pond depth should be about 0.5 m, and areas of about 0.5 ha are usual. Also, some strains of *C. racemosa* give good yields under pond cultivation conditions.

Planting is done by hand, pushing the small plants into the soft bottom of the pond at 0.5–1 m intervals. Two months after, fronds are harvested, leaving about 25% of the plants as seed for the next harvest. Depending on growth rates, harvesting can then be done every 2 weeks. The harvested plants are washed thoroughly in seawater to remove all sand and mud, then sorted and placed in 100–200 g packages; these will stay fresh for 7 days if chilled and kept moist.

Table 6.1 summarizes edible algae and the corresponding food items.

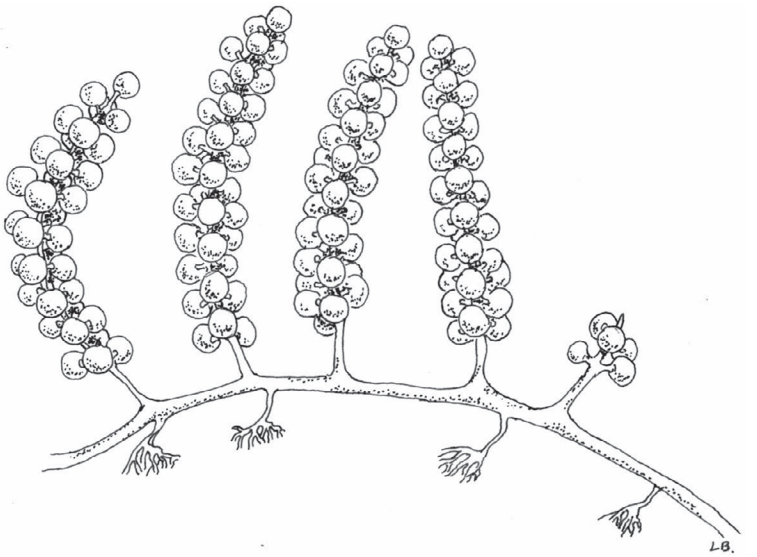


FIGURE 6.11 Frond of *Caulerpa lentillifera*.

TABLE 6.1
Summary of Edible Algae and the Corresponding Food Items

Scientific Name	Common Name	Class
Nostoc flagelliforme	*facai*	Cyanophyceae
Arthrospira sp.	*dihé/tecuitlatl*	Cyanophyceae
Porphyra spp.	*nori/laber/zicai*	Bangiophyceae
Porphyra yezoensis	*kim/purple laver*	Bangiophyceae
Chondrus crispus	*pioca/Irish moss*	Florideophyceae
Palmaria (Rhodymenia) palmata	*dulce*	Florideophyceae
Callophyllis variegata	*carola*	Florideophyceae
Asparagopsis taxiformis	*limu kohu*	Florideophyceae
Gigartina spp.	*botelhas*	Florideophyceae
Gracilaria coronopifolia	*manauea*	Florideophyceae
Gracilaria parvispora	*ogo*	Florideophyceae
Gracilaria verrucosa	*ogo-nori/sea moss*	Florideophyceae
Ahnfeltiopsis concinna	*aki aki*	Florideophyceae
Sargassum echinocarpum	*kala*	Phaeophyceae
Dictyopteris plagiogramma	*lipoa*	Phaeophyceae
Undaria pinnatifida	*wakame/sea mustard/miyeok*	Phaeophyceae
Saccharina spp.	*kombu*	Phaeophyceae
Nereocystis spp.	*black kelp*	Phaeophyceae
Sargassum fusiforme	*hiziki/hijiki*	Phaeophyceae
Alaria esculenta	*oni-wakame*	Phaeophyceae
Cladosiphon okamuranus	*mozuku*	Phaeophyceae
Codium edule	*wawale'iole*	Ulvophyceae
Ulva prolifera	*'ele'ele/green laver*	Ulvophyceae
Ulva fasciata	*palahalaha*	Ulvophyceae
Caulerpa lentillifera	*eka*	Ulvophyceae
Monostroma nitidum	*aonori*	Ulvophyceae

ANIMAL FEED

Microalgae are utilized in aquaculture as live feeds for all growth stages of bivalve mollusks (e.g. oysters, scallops, clams and mussels); for the larval/early juvenile stages of abalone, crustaceans, and some fish species; and for zooplankton used in aquaculture food chains. Over the last four decades, several hundred microalgae species have been tested as food, but probably fewer than 20 have gained widespread use in aquaculture. Microalgae must possess a number of key attributes to be useful aquaculture species. They must be of an appropriate size for ingestion, from 1 to 15 μm for filter feeders and 10 to 100 μm for grazers and readily digested. They must have rapid growth rates, be amenable to mass culture, and also be stable in culture to any fluctuations in temperature, light, and nutrients that may occur in hatchery systems. Finally, they must have a good nutrient composition, including an absence of toxins that might be transferred up the food chain.

Successful strains for bivalve culture included *Isochrysis galbana* (Haptophyta, Coccolithophyceae), *Isochrysis* sp. (T.ISO) (Haptophyta, Coccolithophyceae), *Diacronema lutheri* (Haptophyta, Pavlovophyceae) (cf. Figure 1.1ah of Chapter 1), *Tetraselmis suecica* (Chlorophyta, Chlorodendrophyceae) (cf. Figure 1.1n of Chapter 1), *Pseudoisochrysis paradoxa* (Haptophyta, Coccolithophyceae), *Chaetoceros calcitrans* (Ochrophyta, Bacillariophyceae), and *Skeletonema costatum* (Ochrophyta, Bacillariophyceae).

Isochrysis sp. (T.ISO), *Diacronema lutheri*, and *Chaetoceros calcitrans* are the most common species used to feed the larval, early juvenile, and broodstock (during hatchery conditioning) stages

of bivalve mollusks; these are usually fed together as a mixed diet. Many of the strains successfully used for bivalves are also used as direct feed for crustaceans (especially shrimp) during the early larval stages, especially diatoms such as *Skeletonema* spp. and *Chaetoceros* spp. Benthic diatoms such as *Navicula* spp. and *Nitzschia* are commonly mass-cultured and then settled onto plates as a diet for grazing juvenile abalone. *Isochrysis* sp. (T.ISO), *Pavlova lutheri*, *T. suecica*, or *Nannochloropsis* spp. (cf. Figure 1.1ar of Chapter 1) are commonly fed to the brine shrimp *Artemia* or rotifers, which are then fed on to later larval stages of crustacean and fish larvae.

Microalgal species can vary significantly in their nutritional value, and this may also change under different culture conditions. Nevertheless, a carefully selected mixture of microalgae can offer an excellent nutritional package for larval animals, either directly or indirectly (through enrichment of zooplankton). Microalgae that have been found to have good nutritional properties—either as monospecies or within a mixed diet—include *C. calcitrans*, *C. muelleri, D. lutheri, Isochrysis* sp. (T.ISO), *T. suecica, S. costatum*, and *Thalassiosira pseudonana* (Ochrophyta, Bacillariophyceae). Several factors can contribute to the nutritional value of a microalga, including its size and shape, digestibility (related to cell wall structure and composition), biochemical composition (e.g. nutrients, enzymes, toxins if present), and the requirements of the animal feeding on the alga. Since the early reports that demonstrated biochemical differences in gross composition between microalgae and fatty acids, many studies have attempted to correlate the nutritional value of microalgae with their biochemical profile. However, results from feeding experiments that have tested microalgae differing in a specific nutrient are often difficult to interpret because of the confounding effects of other microalgal nutrients. Nevertheless, from examining all the literature data, including experiments where algal diets have been supplemented with compounded diets or emulsions, some general conclusions can be reached.

Microalgae grown to the late-logarithmic growth phase typically contain 30 to 40% protein, 10 to 20% lipid and 5 to 15% carbohydrate. When cultured through to the stationary phase, the proximate composition of microalgae can change significantly; for example, when nitrate is limiting, carbohydrate levels can double at the expense of protein. There does not appear to be a strong correlation between the proximate composition of microalgae and nutritional value, though algal diets with high levels of carbohydrate are reported to produce the best growth for juvenile oysters (*Ostrea edulis*) and larval scallops (*Patinopecten yessoensis*), provided polyunsaturated fatty acids (PUFAs) are also present in adequate proportions. In contrast, high dietary protein provided the best growth for juvenile mussels (*Mytilus trossulus*) and Pacific oysters (*Crassostrea gigas*). PUFAs derived from microalgae, that is, docosahexaenoic acid (DHA), eicosapentaenoic acid, and arachidonic acid (AA), are known to be essential for various larvae.

The fatty acid content showed systematic differences according to taxonomic group, although there were examples of significant differences between microalgae from the same class. Most microalgal species have moderate to high percentages of EPA (7 to 34%). Haptophytes (e.g. *Pavlova* spp. and *Isochrysis* sp. [T.ISO]) and cryptomonads are relatively rich in DHA (0.2 to 11%), whereas eustigmatophytes (*Nannochloropsis* spp.) and diatoms have the highest percentages of AA (0 to 4%). Chlorophytes (*Dunaliella* spp. and *Chlorella* spp.) are deficient in both C20 and C22 PUFAs, although some species have small amounts of EPA (up to 3.2%). Because of this PUFA deficiency, chlorophytes generally have low nutritional value and are not suitable as a single-species diet. Chlorodendrophyceae such as *Tetraselmis* spp. and Mamiellophyceae such as *Micromonas* spp. contain significant proportions of C20 or C22, respectively. In the late-logarithmic phase, prymnesiophytes, on average, contain the highest percentages of saturated fats (33% of total fatty acids), followed by diatoms and eustigmatophytes (27%), prasinophytes and chlorophytes (23%), and cryptomonads (18%). The content of saturated fats in microalgae can also be improved by culturing under high light conditions.

The content of vitamins can vary between microalgae. Ascorbic acid shows the greatest variation, that is, 16-fold (1 to 16 mg g^{-1} dw). Concentrations of other vitamins typically show a two- to fourfold difference between species, that is, β-carotene 0.5 to 1.1 mg g^{-1}, niacin 0.11 to 0.47 mg g^{-1}, α-tocopherol 0.07 to 0.29 mg g^{-1}, thiamin 29 to 109 μg g^{-1}, riboflavin 25 to 50 μg g^{-1}, pantothenic

acid 14 to 38 μg g^{-1}, folates 17 to 24 μg g^{-1}, pyridoxine 3.6 to 17 μg g^{-1}, cobalamin 1.8 to 7.4 μg g^{-1}, biotin 1.1 to 1.9 μg g^{-1}, retinol ≤ 2.2 μg g^{-1}, and vitamin D < 0.45 μg g^{-1}. To put the vitamin content of the microalgae into context, data should be compared with the nutritional requirements of the consuming animal. Unfortunately, nutritional requirements of larval or juvenile animals that feed directly on microalgae are, at best, poorly understood. However, the requirements of the adult are far better known and, in the absence of information to the contrary, will have to serve as a guide for the larval animal. These data suggest that a carefully selected, mixed-algal diet should provide adequate concentrations of the vitamins for aquaculture food chains.

The amino acid composition of the protein of microalgae is very similar between species and relatively unaffected by the growth phase and light conditions. Further, the composition of essential amino acids in microalgae is very similar to that of protein from oyster larvae (*C. gigas*). This indicates that it is unlikely the protein quality is a factor contributing to the differences in nutritional value of microalgal species.

Sterols, minerals, and pigments also may contribute to nutritional differences of microalgae.

A common procedure during the culture of both larval fish and prawns is to add microalgae (i.e. "green water") to intensive culture systems together with the zooplankton prey. Addition of microalgae to larval tanks can improve the production of larvae, though the exact mechanism of action is unclear. Theories advanced include (a) light attenuation (i.e. shading effects), which have a beneficial effect on larvae; (b) maintenance of the nutritional quality of the zooplankton; (c) excretion of vitamins or other growth-promoting substances by algae; and (d) a probiotic effect of the algae. Most likely, the mechanism may be a combination of several of these possibilities. Maintenance of NH_3 and O_2 balance has also been proposed, though this has not been supported by experimental evidence. The most popular algae species used for green water applications are *N. oculata* and *T. suecica*. More research is needed on the application of other microalgae, especially those species rich in DHA, to green water systems. Green water may also be applied to extensive outdoor production systems by fertilizing ponds to stimulate microalgal growth and correspondingly zooplankton production as food for larvae introduced into the ponds.

For a long time, animals such as sheep, cattle, and horses that lived in coastal areas have eaten macroalgae, especially in those European countries where large brown macroalgae were washed ashore. Today the availability of macroalgae for animals has been increased with the production of macroalgae meal: dried macroalgae that has been milled to a fine powder. In the early 1960s, Norway was among the early producers of macroalgae meal, using *Ascophyllum nodosum* (Ochrophyta, Phaeophyceae), a macroalgae that grows in the eulittoral zone so that it can be cut and collected when exposed at low tide. France has used *Saccharina digitata*, Iceland both *Ascophyllum* and *Saccharina* species, and the United Kingdom *Ascophyllum*.

Because *Ascophyllum* is so accessible, it is the main raw material for macroalgae meal, and most experimental work to measure the effectiveness of macroalgae meal has been done on this macroalgae. The macroalgae used for meal must be freshly cut, as drift macroalgae is low in minerals and usually becomes infected with mold. The wet macroalgae is passed through hammer mills with progressively smaller screens to reduce it to fine particles. These are passed through a drum dryer starting at 700°C–800°C and exiting at no more than 70°C. It should have a moisture level of about 15%. It is milled and stored in sealed bags because it picks up moisture if exposed to air. It can be stored for about a year.

Analysis shows that it contains useful amounts of minerals (potassium, phosphorus, magnesium, calcium, sodium, chlorine, and sulfur), trace elements and vitamins. Trace elements are essential elements needed by humans and other mammals in smaller quantities than iron (approximately 50 mg kg^{-1} body weight), and include zinc, cobalt, chromium, molybdenum, nickel, tin, vanadium, fluorine, and iodine. Because most of the carbohydrates and proteins are not digestible, the nutritional value of macroalgae has traditionally been assumed to be in its contribution of minerals, trace elements, and vitamins to the diet of animals. In Norway, it has been assessed as having only 30% of the feeding value of grains.

Ascophyllum is a very dark macroalga due to a high content of phenolic compounds. It is likely that the protein is bound to the phenols, giving insoluble compounds that are not attacked by bacteria in the stomach or enzymes in the intestine. *Alaria esculenta* is another large brown macroalgae but much lighter in color, and in some experimental trials, it has been found to be more effective than *Ascophyllum* meal. It is this lack of protein digestibility that is a distinct drawback to *Ascophyllum* meal providing useful energy content. In preparing compound foodstuffs, farmers may be less concerned about the price per kilogram of an additive; the decisive factor is more likely to be the digestibility and nutritive value of the additive.

In feeding trials with poultry, adding *Ascophyllum* meal had no benefit except to increase the iodine content of the eggs. With pigs, addition of 3% *Ascophyllum* meal had no effect on the meat yield. However, there have been some positive results reported with cattle and sheep. An experiment for 7 years with dairy cows (seven pairs of identical twins) showed an average increase in milk production of 6.8% that lead to 13% more income. A trial involving two groups each of 900 ewes showed that those fed macroalgae meal over a 2-year period maintained their weight much better during winter feeding and also gave greater wool production.

The results of trials reported previously and in the following suggested reading leave the impression that macroalgae meal is probably only really beneficial to sheep and cattle. Certainly the size of the industry has diminished since the late 1960s and early 1970s, when Norway alone was producing about 15,000 t of macroalgae meal annually. Australia, Canada, Ireland, Norway, the United Kingdom, and the United States use macroalgae meal as a feed additive for sheep, cattle, horses, poultry, goats, dogs, cats, emus, and alpacas. In fish farming, wet feed usually consists of meat waste and fish waste mixed with dry additives containing extra nutrients, all formed together in a doughy mass. When thrown into the fish ponds or cages it must hold together and not disintegrate or dissolve in the water. A binder is needed; sometimes a technical grade of alginate is used. It has also been used to bind formulated feeds for shrimp and abalone. However, cheaper still is the use of finely ground macroalgae meal made from brown macroalgae; the alginate in the macroalgae acts as the binder. The binder may be a significant proportion of the price of the feed, so macroalgae meal is a much better choice. However, since the trend is to move to dry feed rather than wet, this market is not expected to expand.

There is also a market for fresh macroalgae as a feed for abalone. In Australia, the brown macroalgae *Macrocystis pyrifera* (Ochrophyta, Phaeophyceae) (Figure 6.12) and the red macroalgae *Hydropuntia edulis* (Rhodophyta, Florideophyceae) have been used. In South Africa, *Porphyra* (Rhodophyta, Bangiophyceae) is in demand for abalone feed, and recommendations have been made for the management of the wild population of the macroalgae. Pacific *dulse* (*Devaleraea mollis* Rhodophyta, Florideophyceae) has been found to be a valuable food for the red abalone, *Haliotis rufescens*, and development of land-based cultivation has been undertaken with a view to producing commercial quantities of the macroalgae. The green macroalgae, *Ulva lactuca* (Chlorophyta, Ulvophyceae), has been fed to *Haliotis tuberculata* and *H. discus*. Feeding trials showed that abalone growth is greatly improved by high protein content, and this is attained by culturing the macroalgae with high levels of ammonia present.

Hydrocolloids

The principal commercial seaweed extracts continue to be the three hydrocolloids: agar, alginates (derivative of alginic acid), and carrageenans, which are extracted from various red and brown macroalgae. A hydrocolloid is a non-crystalline substance with very large molecules, which dissolves in water to give a thickened (viscous) solution. The processed food industry is still the primary market for the seaweed hydrocolloids, where they serve as texturing agents and stabilizers of certain products, such as ice cream (they inhibit the formation of large ice crystals, allowing the ice cream to retain a smooth texture); agar and its derivative products agarose and bacteriological agar have long enjoyed attractive markets as microbiological and electrophoresis media, respectively. Alginates

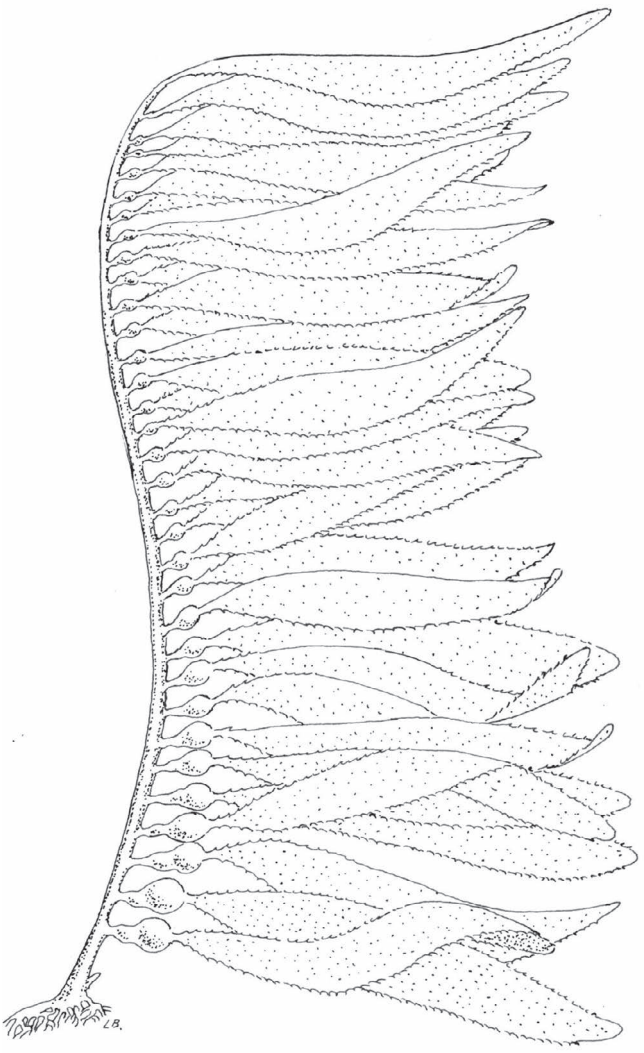


FIGURE 6.12 Frond of *Macrocystis pyrifera*.

continue to be used in textile printing, paper coating, and other relatively low-margin industrial applications, but their use in restructured meat products for pet and human foods offer better profit margins. Interest is growing in the use of alginate beads for controlled drug release, and this could develop into a profitable niche market. Carrageenan has long enjoyed a small share of the personal care toothpaste binder market and has started to make inroads into cosmetics and pharmaceuticals, such as drug capsules and excipient formulations.

The use of macroalgae as a source of these hydrocolloids dates back to 1658, when the gelling properties of agar, extracted with hot water from a red macroalgae, were first discovered in Japan. Extracts of Irish moss (*Chondrus crispus*; Figure 6.2), another red macroalgae, contain carrageenan and were popular as thickening agents in the 19th century. It was not until the 1930s that extracts of brown macroalgae containing alginate were produced commercially and sold as thickening and gelling agents. Industrial uses of macroalgae extracts expanded rapidly after the Second World War but were sometimes limited by the availability of raw materials. Once again, research into life cycles has led to the development of cultivation industries that now supply a high proportion of the

raw materials for some hydrocolloids. Today, approximately 1 million tons of wet macroalgae are harvested annually and extracted to produce the above three hydrocolloids. In 2009, total hydrocolloid sales volume was about 87,000 tons for a value of more than 1000 million US dollars.

There are a number of artificial products reputed to be suitable replacements for macroalgae gums, but none have the exact gelling and viscosity properties of macroalgae gums, and it is very unlikely that macroalgae will be replaced as the source of these polysaccharides in the near future.

Agar

Agar, a general name for polysaccharides extracted from some red algae, is built of alternating D- and L-galactopyranose units. The name agar is derived from a Malaysian word *agar-agar*, which literally means "macroalgae." As the gelling agent *kanten*, it has been known from Japan since the 17th century; extracts from red macroalgae were carried up the mountains to freeze overnight so that water and other impurities could be extracted from the material. Agar finds its widest use as a solid microbiological culture substrate. Modern agar is a purified form consisting largely of the neutral fraction known as agarose; the non-ionic nature of the latter makes it more suitable for a range of laboratory applications. Agar in a crude or purified form also finds wide usage in the food industry, where it is used in various kinds of ices, canned foods, and bakery products.

The higher-quality agar (bacteriological-grade agar) is extracted from species of the red algal genera *Pterocladiella* (Florideophyceae) and *Gelidium* (Florideophyceae) (Figure 6.13), which are harvested by hand from natural populations in Spain, France, Portugal, Morocco, the Azores, California, Mexico, New Zealand, South Africa, India, Indonesia, the Republic of Korea, Chile, and Japan. Agars of lesser quality (food-grade agar) are extracted from *Gracilaria* and *Hypnea* (Florideophyceae) species. *Gelidium* is a small, slow-growing alga, and, while efforts to cultivate it in tanks and ponds have been biologically successful, they have generally proved uneconomic. *Gracilaria* species were once considered unsuitable for agar production because the quality of the agar was poor. In the 1950s, it was found that pre-treatment of the macroalgae with alkali before extraction lowered the yield but gave a good-quality agar. This allowed expansion of the agar industry, which had been previously limited by the available supply of *Gelidium*, and led to the harvesting of a variety of wild species of *Gracilaria* in countries such as Argentina, Chile, Indonesia, and Namibia. Chilean *Gracilaria* was especially useful, but evidence of over-harvesting of the wild crop soon emerged. Cultivation methods were then developed both in ponds and in the open waters of protected bays. These methods have since spread beyond Chile to other countries, such as China, Indonesia, the Republic of Korea, Namibia, the Philippines, and Vietnam, usually using species of *Gracilaria* native to each particular country. *Gracilaria* species can be grown in both cold and warm waters. Today, the supply of *Gracilaria* still derives mainly from the wild, with the extent of cultivation depending on price fluctuations.

Strong-gelling agar is extracted directly from *Gelidium* with a dilute acid solution to break down cell walls in a pressure cooker; whereas extracting strong-gelling agar from *Gracilaria* requires the use of a boiling alkali solution. The alkali treatment converts the galactose 6-SO_4 to 3, 6 anhydrogalactose, well-known chemistry that "de-links" the polygalactose molecules and enhances the gelling process. These process differences explain why it is difficult to optimize the production of agar from both seaweeds in the same process line.

Currently, two companies have emerged as undisputed leaders within the industry: Algas Marinas in Chile and Agarindo Bogatama in Indonesia; between them, they are producing about 3600 t y^{-1}, or about 38% of current production. Other strong producers are Setexam in Morocco, MSC Co. in Korea, Hispanagar in Spain and Huey Shyang Seaweed Industrial Company in China. These six companies account for about 5500 t y^{-1} of production/sales, or 57% of current total market. Some European producers have also chosen to expand production outside their home country. B & V from Italy has production interests in Indonesia and Morocco (although production there has been recently curtailed). Hispanagar, with some existing overseas operations, has started up activities in China as well.

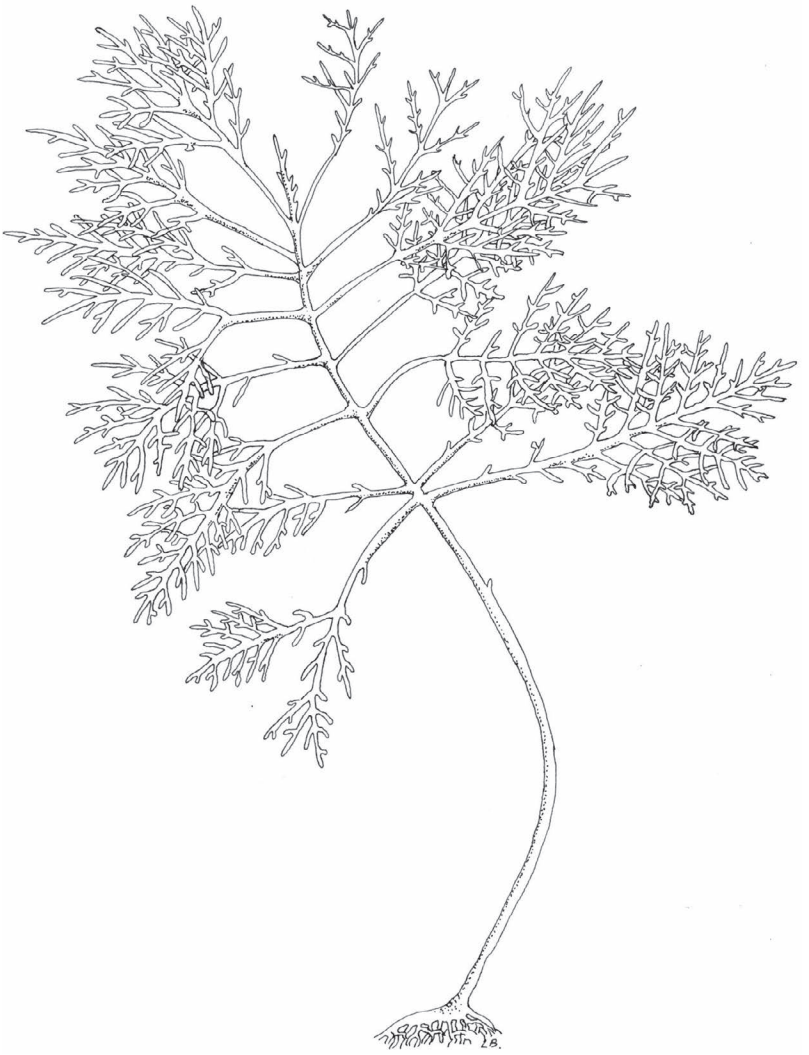


FIGURE 6.13 Frond of *Gelidium* sp.

Alginates

Alginates are cell-wall constituents of brown algae (Phaeophyceae). They are chain-forming heteropolysaccharides made up of blocks of mannuronic acid and guluronic acid. Composition of the blocks depends on the species being used for extraction and the part of the thallus from which extraction is made. Extraction procedures probably also affect alginate quality. Alginates of one kind or another seem to be present in most species of brown algae, but they occur in exploitable quantities (30–45% dry weight) only in the larger kelps and wracks (Laminariales and Fucales). The more useful brown macroalgae grow in cold waters, thriving best in waters up to about 20°C. Brown macroalgae are also found in warmer waters, but these are less suitable for alginate production and are rarely used as food. A wide variety of species are used, harvested in both the northern and southern hemispheres.

Alginates of commerce are primarily the alkali or alkaline earth salts of alginic acid, the sodium salt being the most widely used in foods. The only other derivative of alginic acid that is used in the food industry is propylene glycol alginate (PGA). The ammonia and alkali metal salts of alginic

acid readily dissolve in cold water at low concentrations to produce viscous solutions. Alginates, especially sodium alginate, are widely used in the textile industry because they form an excellent dressing and polishing material. Calcium alginate, which is insoluble in water, has been used in the manufacture of a medical dressing very suitable for burns and extensive wounds where a normal dressing would be extremely difficult to remove; the calcium alginate is extruded to make a fiber which is then woven into a gauze-like product; alginates with a high proportion of guluronic acid blocks are most suitable for this purpose. When applied to either a wound or burn, a network is formed around which a healthy scab may form; the bandage may be removed with a sodium chloride solution, which renders the alginate soluble in water. Alginates are also used as a thickening paste for colors in printing textiles and as a hardener and thickener for joining threads in weaving; the alginates may subsequently be dissolved away, giving special effects to the material. Other uses include glazing and sizing paper, special printers' inks, paints, cosmetics, insecticides, and pharmaceutical preparations. In the United States, alginates are frequently used as stabilizers in ice cream, giving a smooth texture and body, and also as a suspending agent in milkshakes. Alginates take up atomically heavy metals in a series of affinities; for example, lead and other heavy metals will be taken up in preference to sodium, potassium, and other "lighter" metals; accordingly, alginates are useful in lead and strontium-90 poisoning.

Twenty-five to 30 years ago, almost all extraction of alginates took place in Europe, the United States, and Japan. The major change in the alginates industry over the last decade has been the emergence of producers in China in the 1980s. Initially, production was limited to low-cost, low-quality alginate for the local industrial markets produced from locally cultivated *Laminaria* (Saccharina) *japonica*. By the 1990s, China producers were competing in western industrial markets for alginates, primarily based on low cost.

Some 35,000 tons of alginates per annum are extracted worldwide. Alginate manufacturing in the United States has ceased to exist; whereas Europe (mainly Scotland and Norway) is still able to maintain a fairly substantial part of its alginate industry even though Europe is a high-cost production region. This is primarily due to the FMC company's ability to increase their market share of high-quality, specialty grades of alginates being sold in developed countries. Of the 8900 tons y^{-1} of alginates still being produced in Europe, two thirds is being produced by FMC in its Norway facility. Asia-Pacific, on the other hand, is where the real capacity growth has taken place, but at the same time, markets for this capacity are mostly in the Asia-Pacific region.

About 15 years ago, *Ascophyllum nodosum* and *Macrocystis pyrifera* accounted for 58% of the harvest, while today *Laminaria* and *Lessonia* species are dominant, accounting for 81% of the world harvest. Ireland, Scotland, Iceland, France, and Canada possess substantial resources of *Ascophyllum nodosum* seaweed, but this species is now relatively costly to harvest, and the extract quality is not competitive with other species, so hardly any is being used today. In addition, special *A. nodosum* extracts are finding new, more profitable markets as a source of animal and plant nutrients and growth promoters. The giant kelp *Macrocystis pyrifera* was in the past an important raw material for the alginate industry, particularly Kelco in San Diego (Figure 6.12); it was harvested from large offshore beds off the coasts of California and Mexico. *Macrocystis* has the distinction of being the largest macroalgae in the world; the largest attached plant recorded was 65 m long, and the plants are capable of growing at up to 50 cm per day.

Ascophyllum nodosum and *Laminaria hyperborea* are used in Norway and Scotland. *Ascophyllum* is sustainably harvested in Ireland to produce macroalgae meal that is exported to Scotland for alginate extraction. Norway processes *Laminaria hyperborea*, manufacturing high-quality alginates.

Carrageenan

Of the three categories of hydrocolloids under consideration, carrageenan is the most difficult to characterize, mainly because of its chemical complexity. This polysaccharide built up from D-galactopyranose units only has many chemical forms: the brittle gel-forming kappa, the elastic gel-forming iota, and the non-gelling but commercially unavailable lambda. To replace lambda

in cold soluble applications, the mu/nu hybrids obtained from Chilean *Gigartina* (Rhodophyta, Florideophyceae) and *Sarcothalia* (Rhodophyta, Florideophyceae) species are used. Alkali treating of these extracts yields kappa/iota hybrids that find use in dairy and toothpaste products. Kappa carrageenan today is almost exclusively obtained from farmed *Kappaphycus alvarezii* (Rhodophyta, Florideophyceae) and iota from farmed *Eucheuma denticulatum* (Rhodophyta, Florideophyceae).

The word carrageenan is derived from the colloquial Irish name for this macroalgae, carrageen (from the Irish placename, probably Carrigeen Head in Co. Donegal, Carraigín; "little rock") the use of this macroalgae to extract a gel has been known in Ireland since 1810. *Chondrus crispus* (Irish moss; Figure 6.2) used to be the sole source of carrageenan, but species of *Eucheuma, Ahnfeltia* (Rhodophyta, Florideophyceae), and *Gigartina* are now commonly used. About 50,000 t of carrageenan are manufactured worldwide, and although *Chondrus* is no longer the unique source, it is still the principal one. Modern carrageenan is a branded product designed, by mixing various types of carrageenan, to give a gel with particular qualities. Most of the *Chondrus* that is used in the carrageenan industry comes from the Maritime Provinces of Canada (Nova Scotia, etc.), where *C. crispus* is harvested from natural populations. The bulk of the harvest is collected using long-handled rakes and dredges from small boats. The macroalgae is then dried, either by spreading and air-drying or by using rotary dryers, and exported to the United States and Denmark for processing.

Carrageenan production was originally dependent on wild macroalgae, especially *Chondrus crispus*, with a limited resource base in France, Ireland, Portugal, Spain, and the east coast provinces of Canada. As the carrageenan industry expanded, the demand for raw material began to strain the supply from natural resources. However, since the early 1970s, the industry has expanded rapidly, following the availability of other carrageenan-containing macroalgae that have been successfully cultivated in warm-water countries with low labor costs.

The seaweed for production of carrageenan are dominated by the warm-water species *K. alvarezii* (*cottonii*) and *Eucheuma denticulatum* (*spinosum*). Both are being cultivated by vegetative growth, primarily in the Philippines and Indonesia, with smaller amounts from Tanzania. The other seaweed being used are cold water species: *Sarcothalia crispata* and *Gigartina skottsbergii* (*Gigartina radula* of commerce), coming mainly from Chile, with smaller amounts from Mexico. *Chondrus crispus*, another cold-water carrageenophyte, comes predominantly from Maritime Canada, with smaller amounts from France, but is declining in availability and use. None of these cold-water weeds are cultivated, so supply depends entirely on the natural harvest. These cold-water weeds are needed to supply specific types of carrageenan that cannot be obtained from the cultivated warm-water weeds.

Twenty-five years ago, almost all carrageenan extraction took place in Western Europe and the United States, with the remainder taking place in Asia-Pacific and Latin America. Since then, the situation has changed considerably, in particular with the introduction of human food-grade semi-refined carrageenan (PES). From its start in the mid-1970s, PES has progressively reconfigured the geographic distribution of production facilities as well as increasing the percent of PES being produced.

Table 6.2 summarizes commercially exploited algae and the corresponding extracts.

Fertilizers

There is a long history of coastal people using macroalgae, especially the large brown macroalgae, to fertilize nearby land. Wet macroalgae is heavy, so it was not usually carried very far inland, although on the west coast of Ireland, enthusiasm was such that it was transported several kilometers from the shore. Generally, drift macroalgae or beach-washed macroalgae is collected, although in Scotland, farmers sometimes cut *Ascophyllum* exposed at low tide. In Cornwall (UK), the practice was to mix the macroalgae with sand, let it rot, and then dig it in. For over a few hundred kilometers of the coastline around Brittany (France), beach-cast brown macroalgae is regularly collected by farmers and used on fields up to a kilometer inland. Similar practices are reported for

TABLE 6.2
Summary of Commercially Exploited Algae and the Corresponding Extracts

Scientific Name	Class	Extracts
*Gracilaria chilensis (*syn. of *Agarophyton chilense)*	Florideophyceae	Agar
Gelidium lingulatum	Florideophyceae	Agar
Pterocladiella spp.	Florideophyceae	Agar
Hypnea spp.	Florideophyceae	Agar
Saccharina hyperborea	Phaeophyceae	Alginates
Saccharina digitata	Phaeophyceae	Alginates
Saccharina japonica	Phaeophyceae	Alginates
Saccharina saccharina	Phaeophyceae	Alginates
Macrocystis pyrifera	Phaeophyceae	Alginates
Ascophyllum nodosum	Phaeophyceae	Alginates
Durvillaea potatorum	Phaeophyceae	Alginates
Ecklonia spp.	Phaeophyceae	Alginates
Lessonia nigrescens	Phaeophyceae	Alginates
Lessonia trabiculata	Phaeophyceae	Alginates
Ahnfeltia spp.	Florideophyceae	Carrageenan
Chondrus crispus	Florideophyceae	Carrageenan
*Gigartina skottsbergii (*syn. of *Sarcopeltis skottsbergii)*	Florideophyceae	Carrageenan
*Gigartina canaliculata (*syn. of *Chondracanthus canaliculatus)*	Florideophyceae	Carrageenan
Mazzaella laminaroides	Florideophyceae	Carrageenan
Sarcothalia crispata	Florideophyceae	Carrageenan
Kappaphycus alvarezii	Florideophyceae	Carrageenan
Eucheuma denticulatum	Florideophyceae	Carrageenan
Iridaea spp.	Florideophyceae	Carrageenan

many countries around the world. For example, in a more tropical climate like the Philippines, large quantities of *Sargassum* have been collected and used wet locally but also sun dried and transported to other areas. In Puerto Madryn (Argentina), large quantities of green macroalgae are cast ashore every summer and interfere with recreational uses of beaches. Part of this algal mass has been composted and then used in trials for growing tomato plants in various types of soil. In all cases, the addition of the compost increased water holding capacity and plant growth, so composting simultaneously solved environmental pollution problems and produced a useful organic fertilizer.

Macroalgae meal is dried, milled macroalgae, and again it is usually based on the brown macroalgae because they are the most readily available in large quantities. Species of *Ascophyllum*, *Ecklonia*, and *Fucus* (Ochrophyta, Phaeophyceae) are the common ones. They are sold as soil additives and function as both fertilizer and soil conditioner. They have a suitable content of nitrogen and potassium but are much lower in phosphorus than traditional animal manures and the typical N:P:K ratios in chemical fertilizers. The large amounts of insoluble carbohydrates in brown macroalgae act as soil conditioners (improve aeration and soil structure, especially in clay soils) and have good moisture retention properties. Their effectiveness as fertilizers is also sometimes attributed to the trace elements they contain, but the actual contribution they make is very small compared to normal plant requirements. One company in Ireland that produces milled macroalgae for the alginate industry is developing applications for macroalgae meal in Mediterranean fruit and vegetable cultivation. Afrikelp is another example of a commercially available dried macroalgae sold as a fertilizer and soil conditioner; it is based on the brown macroalgae *Ecklonia maxima* that is washed up on the beaches of the west coast of Africa and Namibia. Like all brown macroalgae, *Ascophyllum* contains alginate, a carbohydrate composed of long chains. When calcium is added to alginate, it

forms strong gels. By composting the dried, powdered *Ascophyllum* under controlled conditions for 11–12 days, the alginate chains are broken into smaller chains, and these chains still form gels with calcium but they are weaker. The composted product is a dark brown, granular material containing 20–25% water, and it can be easily stored and used in this form. Steep slopes are difficult to cultivate with conventional equipment and are likely to suffer soil loss by runoff. Spraying such slopes with composted *Ascophyllum*, clay, fertilizer, seed, mulch, and water has given good results, even on bare rock. Plants quickly grow, and topsoil forms after a few years. The spray is thixotropic, that is, it is fluid when a force is applied to spread it, but it sets to a weak gel when standing for a time and sticks to the sloping surface. It holds any soil in place and retains enough moisture to allow the seeds to germinate. Composted *Ascophyllum* has been used after the construction of roads in a number of countries and has found other uses as well.

Maerl is the common name of a fertilizer derived from calcareous red algae; *maerl* beds are characterized by accumulations of living and dead unattached non-geniculate calcareous Florideophyceae (mostly Corallinales such as *Phymatolithon calcareum* and *Lithothamnion corallioides*). Also known as rhodolith beds, these habitats occur in tropical, temperate, and polar environments. In Europe they are known from throughout the Mediterranean and along most of the Western Atlantic coast from Portugal to Norway, although they are rare in the English Channel, Irish Sea, North Sea, and Baltic Sea. *Maerl* beds are often found in subdued light conditions, and their depth limit depends primarily on the degree of light penetration. In the northeast Atlantic, *maerl* beds occur from low in the intertidal to about 30 m depth; in the West Mediterranean, they are found down to 90–100 m, while in the East, they occur down to depths of about 180 m. *Maerl* beds in subtidal waters have been utilized over a long period in Britain, with early references dating back to 1690. In France, *maerl* has been used as a soil fertilizer for several centuries. Extraction of *maerl*, either from beds where live thalli are present or where the *maerl* is dead or semi-fossilized, has been carried out in Europe for hundreds of years. Initially, the quantities extracted were small, being dug by hand from intertidal banks, but in the 70s, about 600,000 tons of *maerl* was extracted per annum in France alone. Amounts have declined to about 500,000 tons p.a. since then, though *maerl* extraction still forms a major part of the French seaweed industry both in terms of tonnage and value of harvest. Live *maerl* extraction is obviously very problematic with regard to growth rates for replacement. Dead *maerl* extraction is liable to lead to muddy plumes and excessive sediment load in water that later settles out and smothers surrounding communities.

Maerl is marketed mainly for use as an agricultural fertilizer for soil improvement in horticulture, mainly to replace lime as an agricultural soil conditioner. There are conflicting reports on the benefits of *maerl* use as opposed to the use of dolomite or calcium carbonate limestone. Other uses include as an animal food additive, for biological de-nitrification and in neutralization of acidic water in the production of drinking water, and as aquarium gravel, as well as in the pharmaceutical, cosmetics, nuclear, and medical industries. These uses are all related to the chemical composition of *maerl*, which is primarily composed of calcium and magnesium carbonates. It is occasionally used for miscellaneous other purposes such as hardcore for filling roads and surfacing garden paths.

Maerl beds are analogous to the sea-grass beds or kelp forests in that they are structurally and functionally complex perennial habitats formed by marine algae that support a very rich biodiversity. The high biodiversity associated with *maerl* grounds is generally attributed to their complex architecture. Long-lived *maerl* thalli and their dead remains build up on underlying sediments to produce deposits with a three-dimensional structure that is intermediate in character between hard and soft grounds. *Maerl* thalli grow very slowly, such that *maerl* deposits may take hundreds of years to develop, especially in high latitudes. One of the most obvious threats is commercial extraction, as this has led to the wholesale removal of *maerl* habitats (e.g. from five sites around the coasts of Brittany), whilst areas adjacent to extraction sites show significant reductions in diversity and abundance. Even if the proportion of living *maerl* in commercially collected material is low, extraction has major effects on the wide range of species present in both live and dead *maerl* deposits. Brittany is the main area for *maerl* extraction, with about 500,000 tons extracted annually; smaller

amounts are extracted in SW England and southwest Ireland. *Maerl* beds represent a non-renewable resource as extraction, and disruption far outstrips their slow rate of accumulation. In France, *maerl* extraction is now considered mining, which implies more constraints for the extractors and more controls on the impact of extraction. Scientists, managers, and policy makers have been slow to react to an escalating degradation of these habitats, such that there is now an urgent need to protect these systems from severe human impacts.

Macroalgae extracts and suspensions have achieved a broader use and market than macroalgae and macroalgae meal. They are sold in concentrated form; are easy to transport, dilute, and apply; and act more rapidly. They are all made from brown macroalgae, although the species vary between countries. Some are made by alkaline extraction of the macroalgae, and anything that does not dissolve is removed by filtration; others are suspensions of very fine particles of macroalgae.

Macroalgae extracts have given positive results in many applications. There are probably other applications where they have not made significant improvements, but these receive less, if any, publicity. However, there is no doubt that macroalgae extracts are now widely accepted in the horticultural industry. When applied to fruit, vegetable, and flower crops, some improvements have included higher yields, increased uptake of soil nutrients, increased resistance to some pests such as red spider mite and aphids, improved seed germination, and more resistance to frost. There have been many, many controlled studies to show the value of using macroalgae extracts, with mixed results. For example, they may improve the yield of one cultivar of potato but not another grown under the same conditions. No one is really sure about why they are effective, despite many studies having being done. The trace element content is insufficient to account for the improved yields and other effects. It has been shown that most of the extracts contain several types of plant growth regulators such as cytokinins, auxins, and betaines, but even here there is no clear evidence that these alone are responsible for the improvements. Finally there is the question: Are macroalgae extracts an economically attractive alternative to NPK fertilizers? Perhaps not when used on their own, but when used with NPK fertilizers, they improve the effectiveness of the fertilizers, so less can be used, with a lowering of costs. Then there are always those who prefer an "organic" or "natural" fertilizer, especially in horticulture, so macroalgae extracts probably have a bright future.

The use of macroalgae as fertilizers dates back at least to the 19th century. Early usage was by coastal dwellers, who collected storm-cast macroalgae, usually large brown macroalgae, and dug it into local soils. The high fiber content of the macroalgae acts as a soil conditioner and assists moisture retention, while the mineral content is a useful fertilizer and source of trace elements. In the early 20th century, a small industry developed based on the drying and milling of mainly storm-cast material, but it dwindled with the advent of synthetic chemical fertilizers. Today, with the rising popularity of organic farming, there has been some revival of the industry but not yet on a large scale; the combined costs of drying and transportation have confined usage to sunnier climates where the buyers are not too distant from the coast. Liquid macroalgae extracts are the growth area in macroalgae fertilizers. These can be produced in concentrated form for dilution by the user. Several can be applied directly onto plants, or they can be watered in around the root areas. In 1991, it was estimated that about 10,000 t of wet macroalgae were used annually to make 1000 t of macroalgae extracts with a value of US $5 million. However, since that time, the market has probably doubled as the usefulness of these products has become more widely recognized and organic farming has increased in popularity.

Cosmetics

To date, microalgal extracts can be found in many face and skin care products, such as anti-aging cream, refreshing or regenerative care products, sun creams, emollients and anti-irritants in peelers. Dermochlorella is actually extracted from *Chlorella vulgaris*, which can stimulate collagen synthesis in skin, supporting tissue regeneration and wrinkle reduction. Protulines is a protein-rich extract

from *Arthrospira* (*Spirulina*), which helps combat early skin aging, exerting a tightening effect and preventing wrinkle formation.

More generally, extracts of algae are often found on the list of ingredients on cosmetic packages, particularly in face, hand, and body creams or lotions, but the use of algae themselves in cosmetics, rather than extracts of them, is rather limited.

Milled macroalgae, packed in sachets, is sold as an additive to bath water, sometimes with essential oils added. Bath salts with macroalgae meal are also sold. Thalassotherapy has come into fashion in recent years, especially in France. In thalassotherapy, macroalgae pastes, made by cold-grinding or freeze-crushing, are applied to the person's body and then warmed under infrared radiation. This treatment, in conjunction with seawater hydrotherapy, is said to provide relief for rheumatism and osteoporosis. Mineral-rich seawater is used in a range of therapies, including hydrotherapy, massage, and a variety of marine mud and algae treatments. One of the treatments is to cover a person's body with a paste of fine particles of macroalgae, sometimes wrap them in cling wrap, and warm the body with infrared lamps. It is said to be useful in various ways, including relief of rheumatic pain or the removal of cellulite. Paste mixtures are also used in massage creams, with promises to rapidly restore elasticity and suppleness to the skin. Macroalgae pastes are made by freeze grinding or crushing. The macroalgae is washed, cleaned, and then frozen in slabs. The slabs are either pressed against a grinding wheel or crushed, sometimes with additional freezing with liquid nitrogen that makes the frozen material more brittle and easier to grind or crush. The result is a fine green paste of macroalgae.

There appears to be no shortage of products with ingredients and claims linked to macroalgae: creams, face masks, shampoos, body gels, bath salts, and even a do-it-yourself body wrap kit. The efficacy of these products must be judged by the user. One company recently pointed out that the lifetime of cosmetic products has reduced over the years and now rarely exceeds 3 or 4 years. Perhaps the macroalgae products that are really effective will live longer than this.

Cosmetic products, such as creams and lotions, sometimes indicate on their labels that the contents include "marine extract," "extract of alga," "macroalgae extract," or similar. This usually means that one of the hydrocolloids extracted from macroalgae has been added. Alginate or carrageenan could improve the skin moisture retention properties of the product.

Functional Foods and Nutraceuticals

There is a strong body of science underpinning health benefits from foods, and new, different, natural sources of so-called "functional foods" and "nutraceuticals" are continuously investigated and tested for their applicability in improving health and reducing risk through prevention. A working definition of functional food was proposed by the EC Concerted Action on Functional Food Science in Europe (FUFOSE): a food that beneficially affects one or more target functions in the body beyond adequate nutritional effects in a way that is relevant to either an improved state of health and well-being and/or reduction of risk of disease. It is consumed as part of a normal food pattern. It is not a pill, a capsule, or any form of dietary supplement. A working definition has also been recently suggested for the portmanteau word "nutraceutical," coined in 1989 by Dr. S. De Felice from the terms "nutrition" and "pharmaceutical": a nutraceutical is a food or a part of a food for oral administration with demonstrated safety and health benefits beyond the basic nutritional functions to supplement diet, presented in a nonfood matrix or nonconventional food formats, in such a quantity that exceeds those that could be obtained from normal foods and with such frequency as required to realize such properties, and is labeled a "nutraceutical." Despite the different definitions, the boundary between functional foods and nutraceuticals is not always clear, and the main difference is the format in which they are consumed: functional foods are always consumed as ordinary foods, while nutraceuticals are consumed as pills, tablets, and so on.

From this perspective, algae, both micro- and macroalgae (seaweed), are a largely untapped reservoir still to be explored. As already noted in the introduction, algae have a history of consumption

all over the world and have been used in the diets of eastern countries, like Japan, Korea, China, the Philippines, and Indonesia, since the pre-historical period, with the earliest recorded use dating back to 2700 B.C. In Japan, about 50 species of algae are used as foods, with an estimated annual consumption per person of 1.4 kg. This ancient tradition and everyday habit have made possible a large amount of epidemiological research showing the health benefits linked to algae consumption. Observational data collected in Southeast Asian populations give a strong indication of the association between algae intake, reduced disease risk, and health outcomes. The Japanese in particular have one of the lowest rates of obesity in the world, a very long life expectancy (83 years), a low rate of heart-related deaths, and an extraordinarily low rate of certain types of cancer. In contrast, highly caloric diets typical of western developed countries, together with a decrease in physical activity due to a modified sedentary lifestyle, have caused an increase of the incidence of obesity and associated comorbidities at an epidemic rate.

Algae can be considered both a functional food because of their high-quality nutritional value (protein content, presence of all of the essential amino acids in levels sufficient to meet normal nutritional requirements) and a nutraceutical because of their content in bioactive ingredients, such as ω-3 essential PUFA (e.g. DHA, EPA), sterols, minerals (e.g. Na, K, Ca, Mg and iodine), carotenoids (e.g. β-carotene, astaxanthin), essential vitamins (e.g. A, B_1, B_2, C, D, E), polyphenols, polysaccharides (e.g. alginate, fucoidan, β-glucan). Many of these bioactive ingredients have been tested in clinical trials or are under validation to assess their efficacy in tackling vitality issues, especially in the field of lipid metabolism, oxidative cellular stress, cancer, and neurological and cardiovascular diseases. For example, some of the general effects of algal PUFAs include anti-arteriosclerosis, antihypertension, anti-inflammation, and immunoregulation. Pigments and polyphenols have shown bioactivity effect toward cancer, as antioxidants and anti-inflammatories; algal polysaccharides, most of which cannot be digested in the human gastrointestinal tract, act as a good source of dietary fibers, which stimulate human health by creating a better intestinal environment or because of their hypocholesterolemic and hypolipidemic properties. Because of their precious content of high-value compounds, algae are systematically screened for these substances as exploitable functional food and nutraceuticals. Many of these compounds have also been tested as therapeutic supplements.

Table 6.3 shows the main bioactive compounds present in algae, with the corresponding health effects.

In the following, details will be given on some of these algal compounds.

Among prokaryotic microalgae, the cyanobacterium *Arthrospira* sp. has undergone numerous rigorous toxicological studies that have highlighted its potential therapeutic applications in the area of immunomodulation, anticancer, antiviral, and cholesterol reduction effects. A number of extracts were found to be remarkably active in protecting human lymphoblastoid T-cells from the cytopathic effects of HIV infection.

Active agents consisting of sulfolipids with different fatty acid esters were isolated also from *Lyngbya lagerheimii* and *Phormidium tenue*. Additional cultured cyanobacterial extracts with inhibitory properties were also found in *Phormidium cebennse, Oscillatoria raciborskii, Scytonema burmanicum, Calothrix elenkinii,* and *Anabaena variabilis.* A protein called cyanovirin isolated from an aqueous cellular extract of *Nostoc ellipsosporum* prevents the *in vitro* replication and cytopathicity of primate retroviruses. Cryptophycin 1, an active compound isolated from *Nostoc* strain GSV224, exerts antiproliferative and antimitotic activity by binding to the ends of the microtubules, thus blocking the cell cycle at the metaphase of mitosis. Cryptophycin 1 is the most potent suppressor of microtubule dynamics yet described. It belongs to the family of cryptophycins, potent anticancer agents at picomolar concentrations, which exert their cytotoxic effects in both alkaloid- and taxol-resistant cancer cells that contribute to the proliferation of drug-resistant tumors.

Other studies using water soluble extracts of cyanobacteria have found a novel sulfated polysaccharide, calcium spirulan, to be an antiviral agent. This compound appears to be selectively inhibiting the penetration of enveloped viruses into host cells, thereby preventing replication. Using specific assays for the quantification of viral replication *in vitro*, spirulan exhibited strong inhibition

TABLE 6.3
Example of Bioactive Compounds Present in Algae, With the Corresponding Health Effects

Category	Specific Product	Source	Effects
Carotenoids	astaxanthin	*Haematococcus* sp.	Antioxidant/Antihypertensive
	β-carotene	*Dunaliella* sp. *Porphyra tenera* (syn. of *Neopyropia tenera)*	Antioxidant/Antimutagenic
	fucoxanthin	*Sargassum fusiforme* *Fucus serratus* *Padina tetrastomatica* *Saccharina japonica*	Antiangiogenic/ Retinol deficiency protection/ Antioxidant/ Photoprotective
	zeaxanthin	*Ascophyllum nodosum*	Eye disease remediation
	lutein	*Porphyra tenera*	Antimutagenic
	siphonoxanthin	*Codium fragile*	Anticancer/Antiangiogenic
PUFA	ARA	*Parietochloris incisa* *Porphyridium cruentum* *Rhodomella subfusca* *Gracilaria sp*. *Ceramium rubrum*	
	DHA	*Crypthecodinium cohnii*	
	EPA	*Phaeodactylum tricornutum* *Nannochloropsis* sp.	
Polyphenols	flavonoids	*Palmaria palmata*	Antioxidant
	catechins	*Halimeda* sp.	Antimicrobial
	phlorotannins	*Ecklonia cava*	Anti-inflammatory/Lipid metabolism control
Polysaccharides	alginic acid	*Undaria pinnatifida* *Saccharina latissima*	Anticancer/Antibacterial
	carrageenan	*Chondrus crispus* *Eucheuma cottonii* *Gigartina skottsbergii*	Anticoagulant/Antiviral/ Stimulation collagen biosynthesis
	fucoidan	*Macrocystis* sp. *Saccarina japonica* *Undaria pinnatifida*	Anti-HIV/Anti-arteriosclerosis Lipid metabolism control/ Reduction of interleukin production
	β-glucan	*Euglena gracilis*	Immunostimulant/Antiviral
	laminaran	*Saccharina* sp. *Fucus vesicolotus*	Antihypertensive/Anticoagulant/ Dietary fiber/Wound repair
	ulvan	*Ulva lactuca* *Monostroma* sp.	Gastric ulcer repair
	phorphyran	*Porphyra* sp.	Anticoagulant/ Antihypercholesterolemic
Vitamins	tocopherol	*Fucus* sp. *Saccharina* sp. *Kappaphycus* sp.	Antioxidant
	ascorbic acid	*Chondrus crispus* *Sargassum* sp.	Antioxidant
Extracts	Methanolic extract	*Hypnea valentiae* *Padina pavonia*	Acetylcholinesterase inhibition/Cytotoxic activity

of human cytomegalovirus, herpes simplex virus type 1, human herpes virus type 6, and human immunodeficiency virus type 1.

Among eukaryotic microalgae, a polypeptide has been separated from *Chlorella pyrenoidosa* that exhibited inhibitory activity on human liver cancer HepG2 cells. It has been named CPAP (*C. pyrenoidosa* antitumor polypeptide).

Apart from these very specific compounds, as already stated, the general beneficial effect of microalgae is attributed to their content in pigments, carotenoids in particular, PUFA and polysaccharides. Carotenoids (both carotenes and xanthophylls) are tetraterpenoid organic pigments that serve two key roles in algae: they absorb light energy for use in photosynthesis, and they protect chlorophyll from photodamage. There has been much interest in carotenoids, especially their effect on human health, because they have a market value of several hundred million Euros. Their chemical synthesis is still a demanding challenge for chemists. The major dietary source of vitamin A (essential for cell growth, embryonic development, vision, and immune system functioning) for mammals, including humans, is derived from carotenoids.

Carotenoids, by their quenching action on reactive oxygen species, carry intrinsic anti-inflammatory properties, whereas PUFA exhibit antioxidant activity and polysaccharides act as immunostimulators.

A major bottleneck in the exploitation of microalgal biomass for the production of high-value compounds is low productivity of the culture, both in terms of biomass and product formation. One fundamental reason for this is slow cell growth rates owing to inefficient use of strong light. Furthermore, most microalgal products are secondary metabolites that are produced when growth is limited. One solution to this bottleneck could be to milk the secondary metabolites from the microalgae. This involves continuous removal of secondary metabolites from cells, thereby enabling the biomass to be reused for the continuous production of high-value compounds.

Recently, a new method was developed for milking β-carotene from *Dunaliella salina* in a two-phase bioreactor. In this technique, cells are first grown under normal growth conditions and then stressed by excess light to produce larger amounts of β-carotene. At this stage, the second, biocompatible organic phase is added and the β-carotene is extracted selectively via continuous recirculation of a biocompatible organic solvent (lipophylic compound) through the aqueous phase containing the cells. Because the cells continue to produce β-carotene, the extracted product is continuously replaced by newly produced molecules. Therefore, the cells are continuously reused and do not need to be grown again. In contrast to existing commercial processes, this method does not require the harvesting, concentrating, and destroying of cells for extraction of the desired product. Furthermore, purification of the product is simple owing to the selectivity of the extraction process. The general application of this process would facilitate the commercialization of microalgal biotechnology and development of microalgal products.

The properties of the cell membrane play an important role in the contact between biocompatible lipophilic solvents and hydrophobic parts of the cell membrane, since this contact might be prevented by the presence of a cell wall and/or hydrophilic parts of the outer membrane. Physiological properties of the cells, such as their capacity for continuous endo- and exo-cytosis, might also play a role in the milking process. Other considerations are the location and way in which the product accumulates inside the cells and the function of that product inside the cells. A product like chlorophyll would be difficult to extract owing to its location in thylakoid membranes and because it is bound strongly to other cell components. The extraction of a product with a protective effect on the cells (e.g. β-carotene) will enhance its synthesis. The milking process can also be applied to other algae and other products besides *D. salina*, for example, in *Haematococcus pluvialis* for the recovery of astaxanthin and marine microalgae for PUFA.

As well as its use in aquaculture (e.g. to give salmon a pink color), astaxanthin has also been described as having nutraceutical importance related to free-radical scavenging, immunomodulation, and cancer prevention. *Haematococcus pluvialis* can produce and accumulate astaxanthin to concentrations of 1–8% of the dry weight. This concentration within the cell would make milking of *H. pluvialis* more successful compared with *D. salina*. However, cultivation of *H. pluvialis* is more complex than *D. salina*, and productivity is lower. Furthermore, extraction, purification, and concentration are a heavy burden on the production cost. As the final product cost is also sensitive to algal productivity and duration of the growth period, this process is not economically feasible at present.

Polyunsaturated fatty acids are gaining increasing importance as valuable pharmaceutical products and ingredients of food owing to their beneficial effect on human health. Docosahexaenoic acid (22:6 ω3) and eicosapentaenoic acid (20:5 ω3), in particular, are important in the development and functioning of brain, retina, and reproductive tissues both in adults and infants. They can also be used in the treatment of various diseases and disorders, including cardiovascular problems, a variety of cancers, and inflammatory disease. At present, PUFAs are produced commercially from fish oil, but this is an insufficient source of these products, and microalgae provide an optimal lipid source of PUFAs. Microalgal-derived PUFA, such as arachidonic acid and DHA are added as fortifications to infant formulae—an industry that is worth $10 billion per annum alone.

Microalgae are the primary producers of EPA and DHA, which are eventually accumulated through the various trophic levels. Changes in microalgal lipid content are carried on up the food chain, impacting the growth and dietary make-up of zooplankton, crustacean larvae, mollusks, and some fish. This subsequently affects the accumulation of EPA and DHA fatty acids in higher organisms and humans. Consequently, lipid profiles in microalgae play a vital role in maintaining the integrity of the world's aquatic food webs.

Several heterotrophic microalgae and mycetes have been used as biofactories for omega-3 fatty acids commercially, but a strong interest also in autotrophic microalgae has emerged in recent years. To date, the ω-3 fatty acid content of numerous microalgae strains have been studied. *Phaeodactylum tricornutum* and *Nannochloropsis* sp. demonstrated an EPA content of up to 39% of total fatty acids, while Labyrinthulomycetes such as *Thraustochytrium* and *Schizochytrium limacinum* contained a DHA percentage of between 30 and 40% of total fatty acids when grown heterotrophically. High biomass and commercially acceptable EPA and DHA productivities are achieved with microalgae grown in media with optimized carbon and nitrogen concentrations and controlled pH and temperature conditions. High oil production, including DHA from *Schizochytrium* (50% w/w), can be obtained as a result of high growth rate by controlling of nutrients such as glucose, nitrogen, sodium, and some other environmental factors, such as oxygen concentrations, as well as temperature and pH, achieving high cell densities and DHA productivities.

The heterotrophic marine dinoflagellate *Crypthecodinium cohnii* has a lipid content greater than 20% dry weight and is known for its ability to accumulate fatty acids that have a high fraction (30–50%) of DHA. Lipids are important components of algal cell membranes but also accumulate in globules in other parts of the cells. Microalga growth and fatty acid formation are affected by medium composition and environmental conditions (e.g. carbon sources). Lipid production occurs under growth-limiting conditions; during linear growth, the cells are stressed owing to nutrient limitation and therefore produce more lipids. Also, the concentration of DHA, hence the lipid quality, is negatively affected by increases in lipid concentration. The highest-quality lipid is obtained when glucose is used as the carbon source and when the cell concentration and lipid content of the cells are the lowest.

Milking can be used also for DHA production by *C. cohnii*. In this process, cells are first grown under the correct conditions for growth, after which they are stressed to produce higher concentrations of DHA. A biocompatible organic solvent is added during the DHA production stage to extract the product. This process enables the production of high-quality lipid, thereby reducing extraction and purification costs. Furthermore, higher amounts of DHA are produced by substitution of extracted lipids by newly synthesized lipid, increasing the productivity of the system.

EPA production potential has been found also in the genus *Nitzschia* (especially *N. alba* and *N. laevis*). It was reported that the oil content of *N. alba* was as high as 50% of cell dry weight and the EPA constituted 4–5% of the oil. *N. laevis* could utilize glucose or glutamate as single substrate for heterotrophic growth, and the cellular EPA content of the alga in heterotrophic conditions was also higher than that in photoautotrophic conditions, suggesting that this diatom is a good heterotrophic EPA producer.

From a production point of view, an increase in microalgal lipid content can be induced by a sudden change of growth conditions. The accumulation of starch and/or lipid reserves is considered a

survival mechanism in response to growth-limiting stresses, such as UV radiation, temperature and shock, or nutrient deprivation, as long as light conditions are present that still allow efficient photosynthesis. For example, during nutritional deprivation (e.g. nitrogen) and under the provision of light, cellular division of many marine or brackish microalgae is put on hold and cells begin to accumulate lipids, leading to a two- to threefold increase in lipid content. Both total lipid and omega-3 fatty acid production can be adjusted by varying growth conditions. The diatom *Phaeodactylum tricornutum* can be induced to increase its lipid level from 81.2 mg/g of culture dry weight to 168.5 mg/g dry weight, and *Nannochloropsis* sp. and *Dunaliella* sp., can achieve a total lipid content of up to 47% and 60% of dry ash weight by modifying the light intensity, temperature, and salinity levels.

ω3 fatty acid biosynthesis can be stimulated by a number of environmental stresses, such as low temperature, change of salinity, or UV radiation. For example, *Pavlova lutheri* increased its relative EPA content from 20.3 to 30.3 M% when the culture temperature is reduced to 15°C. Similarly, *Phaeodactylum tricornutum* had a higher EPA content when the temperature was shifted from 25°C to 10°C for 12 h.

Salinity may also regulate PUFA biosynthesis; for example, *Crypthecodinium cohnii* increases its total DHA content up to 56.9% of total fatty acids when cultured in 9 g/L NaCl. Other treatments that cause the generation of reactive oxygen species and lipid peroxidation also result in higher PUFA contents. For example, *Phaeodactylum tricornutum* increased its EPA content up to 19.84% when stressed with UV light. Some of the increased PUFAs are used to repair membrane damage, but as PUFAs contain many double bonds, these also act as an antioxidant by scavenging free radicals.

Apart for external stresses, metabolic engineering is another promising approach to increase the production of fatty acids in microalgae. Genes encoding key enzymes involved in the fatty acid biosynthesis have been identified in *Ostreococcus tauri, Thalassiosira pseudonana, Phaeodactylum tricornutum*, and *Chlamydomonas reinhardtii*.

As for macroalgae, extracts from several species may prove to be a source of effective antiviral agents, although the tests have been either in vitro (in test tubes or similar) or on animals, with few advancing to trials involving people. A notable exception is Carraguard, a mixture of carrageenans similar to those extracted from Irish moss. Carraguard has been shown to be effective against human immunodeficiency virus (HIV) in vitro and against herpes simplex virus in animals. Testing advanced to Phase 3 clinical trial in South Africa, with the contribution of Bill and Melinda Gates Foundation. This was the first Phase 3 trial of a novel candidate microbicide to be conducted among a general population of 6000 women and was completed as planned in 4 years without any safety concerns. The trial did not show that Carraguard is effective in preventing HIV transmission during vaginal sex but confirmed its safety, which could make it a potentially useful vehicle for future microbicides.

Extracts from the brown macroalga *Undaria pinnatifida* have also shown antiviral activity; an Australian company is involved in several clinical trials in Australia and the United States of such an extract against HIV and cancer. Because antiviral substances in macroalgae are composed of very large molecules, it was thought they would not be absorbed by eating macroalgae. However, it has been found in one survey that the rate of HIV infection in macroalgae-eating communities can be markedly lower than it is elsewhere. This has led to some small-scale trials in which people infected with HIV ate powdered *Undaria*, with a resulting decrease of 25% in the viral load.

Fucoxanthin, a carotenoid commonly distributed in brown algae, such as *Undaria pinnatifida, Scytosiphon lomentaria*, *Petalonia binghamiae,* and *Laminaria religiosa,* is a potent drug candidate and can be utilized as an excellent supplement like astaxanthin, since it acts as an antioxidant and inhibits GOTO cells of neuroblastoma and colon cancer cells. Recently, apoptosis activity of fucoxanthin against HL-60 (human leukemia) and Caco-2 (cancer colon) cells has been reported.

Algae, especially marine algae, contain large amount of structural polysaccharides (e.g. cellulose, hemicellulose, and lignin), storage polysaccharides (e.g. glucan, fucoidan, agar, carrageenan), and mucopolysaccharides (e.g. porphyran). Most of these polysaccharides are not digested by humans

and therefore can be defined as dietary fiber, that is, physiologically beneficial non-digestible carbohydrates. Dietary fiber included in algae is classified into two types, insoluble, such as cellulose, mannans, and xylan, and water-soluble, such as agars, alginic acids, furonans, laminaran, and phorphyran. The proportion of these two fractions determines the properties of the fiber. Soluble fiber is characterized by its ability to form viscous gels in contact with water in the intestinal tract; it is fermented in high proportions, and its main properties are related to the decrease of cholesterol and glucose in blood and the development of intestinal microbiota. Insoluble fiber does not form gels in contact with water but is capable of retaining water in its structural matrix, producing an increase in fecal mass that accelerates intestinal transit; it is sparsely fermented and has a marked laxative and intestinal regulating effect. In algae, the proportion of dietary fiber is considerable, ranging from 36 to 60% of the dry matter, with soluble dietary fiber being very high (approximately 55–70%) compared to terrestrial vegetables. For example, in red algae such as *Chondrus* and *Porphyra* (nori), the soluble fiber content is about 15–22% dw, higher than that of insoluble fiber. On the other hand, brown algae such as *Fucus* or *Saccharina* have a higher insoluble fiber content (27–40% dw) with respect to soluble fiber.

In unicellular Rhodophyta such as *Porphyridium* sp. and *Rhodella* sp., these polysaccharides are a constituent of the cell wall; they are highly sulfated and consist mainly of xylose, glucose, and galactose. These compounds selectively inhibit the reverse transcriptase (RT) enzyme of human immunodeficiency virus and its replication *in vitro*. Sulfated polysaccharides produced by *Porphyridium aerugineum* act as a coating material on the surface of sanitary items to prevent infection from epidemic diseases such as COVID-19.

Rodents fed with a diet supplemented with biomass and polysaccharide derived from *Porphyridium* results in a decrease in blood cholesterol concentration (by 22 and 29%, respectively) and triglyceride levels, increased feces weight (by 130 and 196%, respectively) and bile acid excretion (5.1- and 3.2-fold more). Moreover, algal biomass or polysaccharide increased the length of both the small intestine (by 17 and 30%, respectively) and the colon (by 8.5 and 32%, respectively).

Among the polysaccharides, β-glucans are present inside the algae as storage compounds or wall components. These polysaccharides consist of linked glucopyranosyl units. They differ in structure, size, branching frequency, and conformation, and all these features influence their physiological functions and biological activity.

The simplest structure consists of a linear chain of glucopyranosyl units linked by β-(1,3)-D-glycosidic bonds; this structure is presents in Euglenophyceae, such as *Euglena* sp., *Astasia* sp., and *Peranema* sp., and haptophytes, such as *Rebecca salina*. Another simple structure, consisting of a chain of glucopyranosyl units linked by alternate β-(1,3)- and β-(1,4)-D-glycosidic bonds, is present in Chlorophyceae, such as *Ulva lactuca*, Xanthophyceae such as *Monodus subterraneum*, Rhodophyceae such as *Kappaphycus alvaretzii*, and Dinophyceae such as *Peridinium gatunense*. A more complex structure consisting of a linear β-(1,3) chain with β-(1,6) side chain branches is present in Phaeophyceae such as *Laminaria* sp. and *Eicenia* sp., Chrysophyceae such as *Ochromonas* sp., Raphidophyceae such as *Haramonas dimorpha,* and Bacillariophyceae such as *Chaetoceros muelleri* and *Pheaodactylum tricornutum*. Linear β-(1,3)- and β-(1,3;1,4)-glucans are mainly insoluble compounds, while side chain–branched β-(1,6;1,3)-glucans are mainly soluble.

β-glucans function as pathogen-associated molecular patterns (PAMPs) and can be non-specifically recognized by pattern recognition receptors (PRRs) present on the surface of the innate immune system cells. β-glucans have a potent immunomodulating activity, and their action is mediated through receptors such as Dectin-1 (a C-type lectin receptor), Toll-like receptors, complement receptor 3, scavenger receptors, and lactosylceramide. Dectin-1 is indicated as the preferential receptor for β-1-3 linked linear glucans. Upon linkage of the glucan effector with Dectin-1, the innate immune response is activated, which leads to production of both ROS and inflammatory cytokines through the activation of transcription factors such as nuclear factor kappa-light-chain-enhancer of activated B cell (NF-kB), enzymes such as phospholipase C, and mitogen-activated protein kinases. This ability to enhance defense mechanisms against infection and simultaneously

down-regulate inflammations makes β-glucans a promising alternative to the mainstream use of immunosuppressive drugs for inflammatory diseases.

Among the insoluble β-glucans, those present in *Euglena* sp. and euglenoids in general deserve to be mentioned. This linear β-(1,3)-glucan, termed paramylon, is present in granular form in various locations inside the cell (Figure 6.14a); in some species, the granules are scattered throughout the cytoplasm, while in others, they can be massed together. In some other species, there are only a few granules, but they are large and located in a fairly constant position (Figure 6.1bi). The shape and size of granules differ markedly and, together with their distribution inside the cell, represent a taxonomic feature. Paramylon has an unusually high crystallinity as a natural macromolecule. This high crystallinity is an advantage, in that paramylon granules can be isolated in a very low-cost and efficient manner by simply disrupting the cells and purifying the granules by successive washing with a low concentration of detergent (Figures 6.14b and 6.14c). Paramylon crystallinity is due to higher order aggregates of nanofibrils, measuring 4–10 nm (Figure 6.14d), composed of unbranched triple helices of β-(1,3)-D-glucan chains (Figures 6.14e and 6.14f).

Paramylon either in granules or as nanofibers has been used to assess the beneficial potential of β-glucans in different experimental models involving plants, animals, and humans and investigate the structure-function relationship and mechanism of action.

In its granular form, paramylon was tested on *Artemia* shrimp upon addition to the culture medium. It proved effective in mitigating negative effects of stressors (e.g. deteriorated environmental

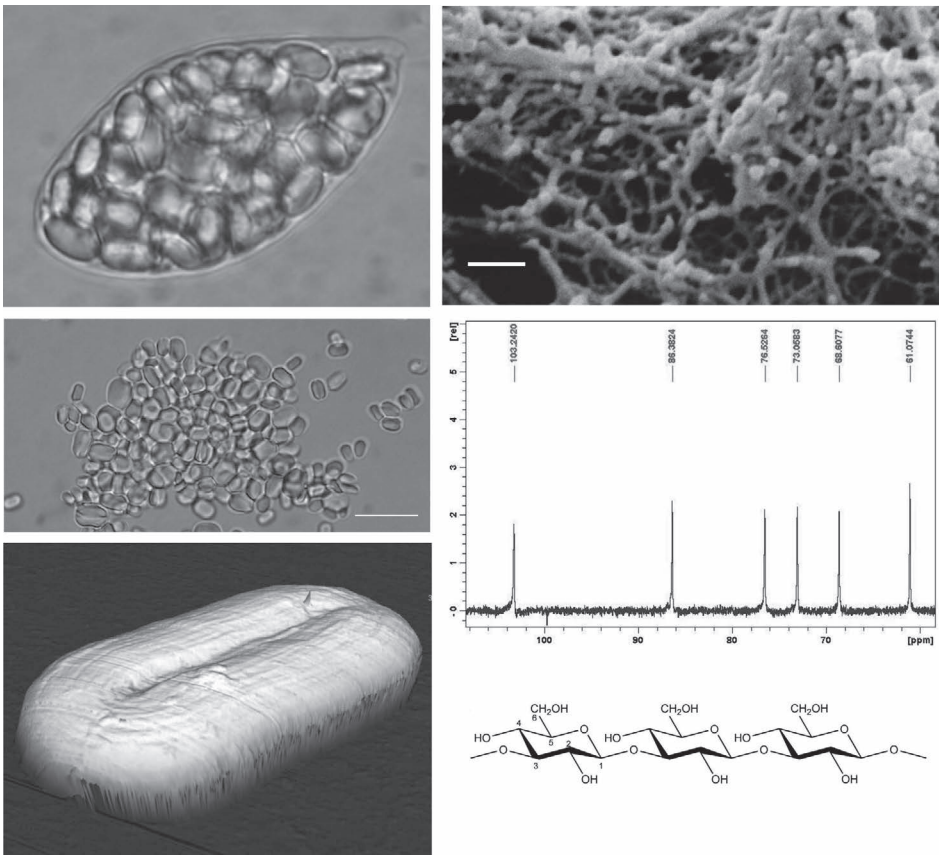


FIGURE 6.14 *Euglena gracilis* non-photosynthetic WZSL mutant full of paramylon granules (a); extracted paramylon granules (b); single paramylon granule viewed by AFM (c); paramylon nanofibers (d); NMR spectrum of paramylon (e); paramylon molecular structure (f). Scale bar 8μm.

conditions), enhancing the survival performance of both adults and offspring, and increasing the number of offspring and hence the reproductive success of the population. The effect of the glucan may be due to the entry of paramylon granules into the digestive tract of the shrimp, which enhances the production of cell-activating factors in the hemocytes, increasing the phagocytic activity of the granulocytes, thus providing defense against diseases. Paramylon could be used as non-specific dietary additive in aquaculture feed, improving its nutritional value, mitigating negative effects of stressors when they occur, and promoting innate immunity of the animals.

Paramylon nanofibers were tested in human peripheral blood mononuclear cells (PBMCs) to verify the β-glucan capacity to activate the innate immune system response.

Paramylon nanofibers increased transactivation of the nuclear factor k-light-chain-enhancer of activated B cells, which is the rapid acting primary transcription factor, that is, the first responder to harmful stimuli, as shown by the evident immunofluorescence nuclear labelling of treated PBMC (Figures 6.15a and 6.15b). NF-kB in turn increases the expression of pro-inflammatory mediators (TNF-α, IL-6, COX-2, and iNOS). These mediators are highly inflammatory and are indispensable when priming immune responses and licensing dendritic cells. Paramylon nanofibers also induced the production of high level of NO, which increased from 4h to 24h and exerted an inhibitory effect on cytokine expression via inhibition of NF-kB transactivation, thus preventing a dangerous cytokine storm. This signaling cascade guarantees a safe activation of the innate immune system, as demonstrated by the presence of newly differentiated dendritic cells (Figure 6.15c, arrowheads).

Paramylon nanofibers have also an anti-fibrotic effect, as demonstrated in mice with liver fibrosis induced by 4 weeks of treatment of CCl_4 administered via intraperitoneal injection. The administration of paramylon nanofibers ameliorated the overall clinical picture of the animals, dampening the CCl_4-induced loss of weight and preventing the increase of aspartate aminotransferase (AST) typical of hepatocyte damage. It also restored the normal tissue consistency and appearance; in fact, CCl_4-treated liver had a trabecular "fishnet" texture typical of mild to severe edema, while normal color and consistency was restored in paramylon-treated livers, indicating a relieved hepatic injury (Figures 6.16a, 6.16b, 6.16c). Collagen deposition in liver of paramylon treated animals was lower than in CCl_4-treated animals (Figures 6.16d, 6.16e, 6.16f). Moreover, nanofiber treatment greatly reduced the overall alteration of tissue parenchyma and the lobular architecture was like that of a non-damaged liver, with mild hepatocyte ballooning with respect to CCl_4-damaged livers and almost no necrosis regions nor infiltration of inflammatory cells (Figures 6.16e, 6.16g, 6.16f). Reduction of inflammation and collagen production by liver stellate cells is due to the inhibiting action of hepatic γδT cells upon Dectin-1 ligation by paramylon nanofibers, which promotes hepatocyte regeneration. This important protective effect of paramylon in sterile inflammation could be exploited for experimental therapeutics in hepatic fibrosis and inflammation.

Paramylon nanofibers proved effective in counteracting low water availability (i.e. drought) stress in tomato plants (Figures 6.17a, 6.17b, 6.17c). Flowering and fruit ripening of stressed paramylon-treated plants were about 2 weeks precocious with respect to untreated well-watered plants, whereas fruits of stressed untreated plants did not move beyond the green ripening stage (Figures 6.17a and 6.17c).

Thanks to paramylon action, the optimal water regimen of about 8.64 L $plant^{-1}$ day^{-1} could be lowered to 0.36 L $plant^{-1}$ day^{-1}. Ecophysiological parameters (i.e. leaf water potential, stomatal conductance, and photosynthetic yield), were dramatically influenced by water stress, all of them undergoing a continuous decrease to saturation. Root treatment with paramylon nanofibers allowed all the parameters to recover to the values of well-watered plants. These results indicate an effective action of paramylon nanofibers on stomatal behavior, whose control improves water use efficiency and hence prevents dehydration. This action is associated with a transient modification of the content of main plant hormones, that is, abscissic acid, jasmonic acid, and salicylic acid.

The great increase of physical-chemical and quality parameters such as the antioxidant compounds (vitamin A/C/E, lycopene, β-carotene, and phenols), together with the increase of carbohydrates (glucose, fructose, and sucrose), in fruits of paramylon-treated plants improve their

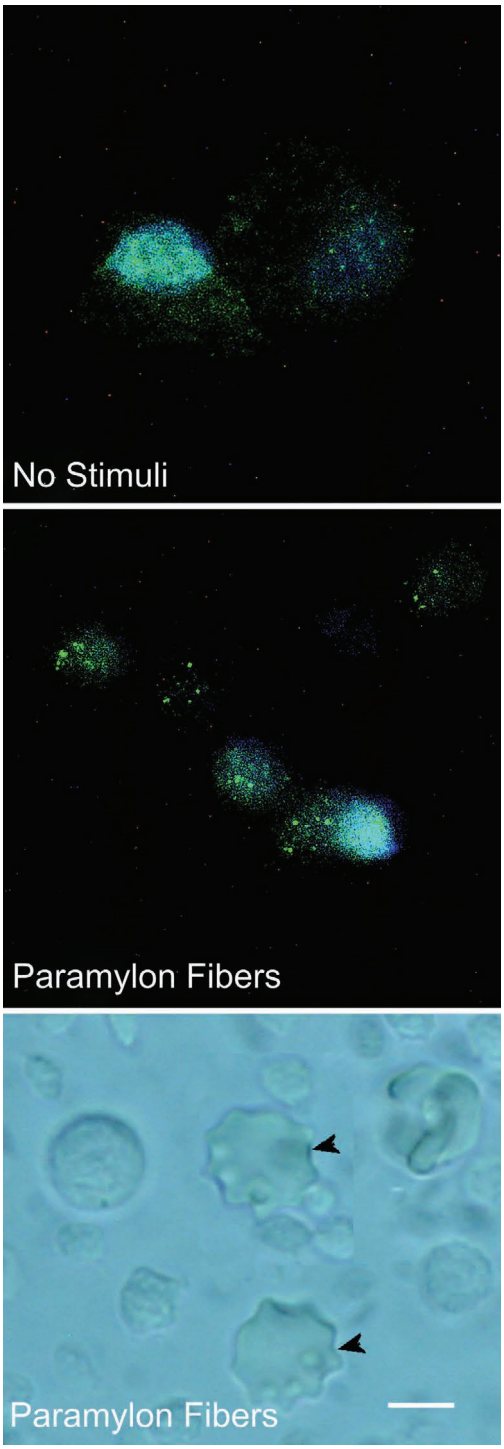


FIGURE 6.15 Immunofluorescence evidence of NF-kB trans-activation after paramylon nanofibers treatment (top and center). Differentiation of new dendritic cells (arrowheads) induced by paramylon nanofibers treatment (bottom). Scale bar 10μm.

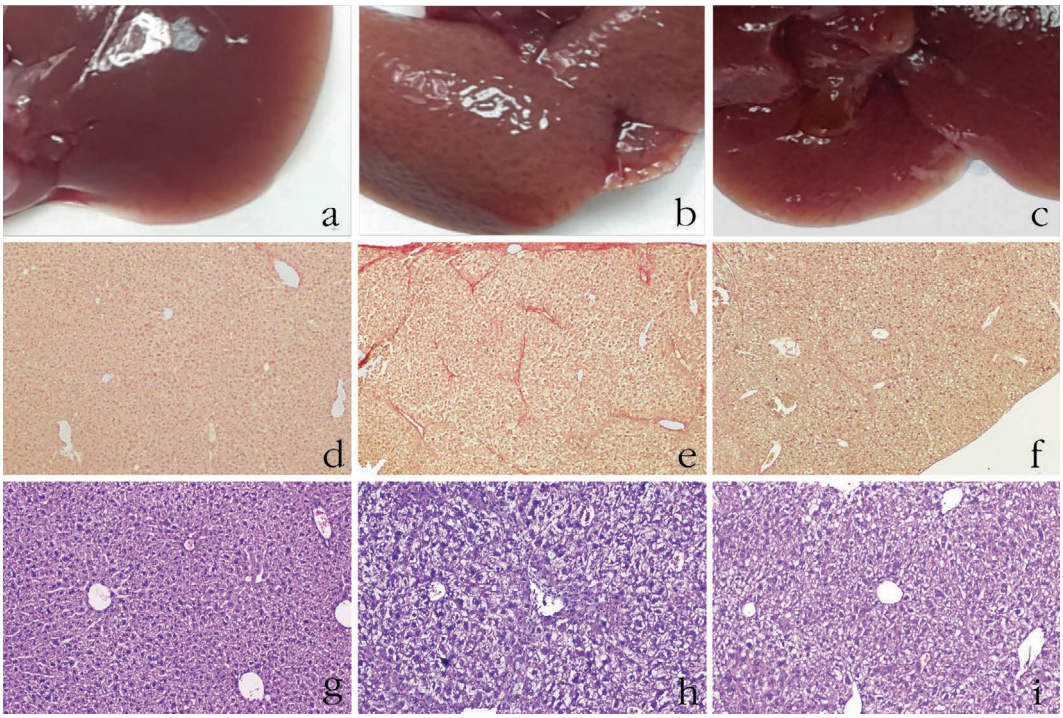


FIGURE 6.16 Liver consistency and appearance in non-treated mice (a), CCl_4 treated mice (b) and CCl_4 + paramylon treated mice (c). Collagen deposition in non treated mice (d), CCl_4 treated mice (e) and CCl_4 + paramylon treated mice (f). Liver parenchima aspect and globular architecture in non treated mice (g), CCl4 treated mice (h) and CCl4 coupled with paramylon treated mice (i).

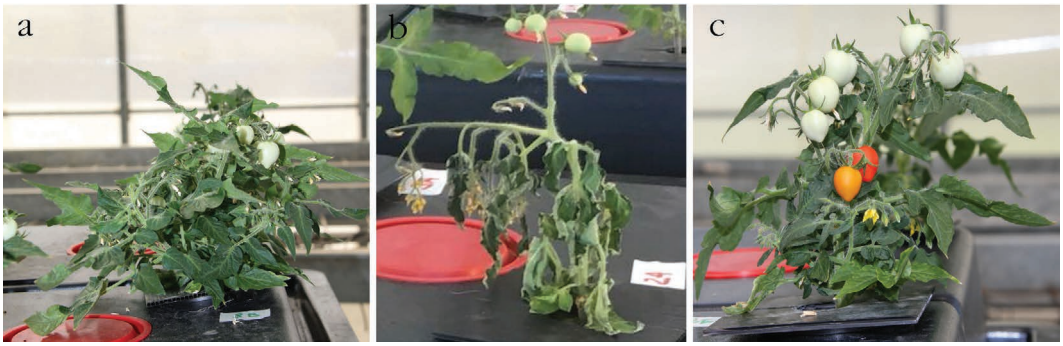


FIGURE 6.17 Effects of paramylon nanofiber treatment on water-stressed tomato plants. Optimal water regimen (a); water scarcity regimen (b); water scarcity regimen coupled with paramylon nanofiber root treatment (c).

nutritional value and sensory quality. Moreover, the higher dry matter content (i.e. lower moisture) allows a better post-harvest storage capability, extending the commercial period and increasing the commercial product value.

HARMFUL ALGAL BLOOMS AND TOXINS

Harmful algal blooms (HABs) occur when marine and freshwater micro- or macroalgae grow beyond normal concentration, becoming a major threat to the ecology of many ecosystems either

through the enormous increase of their biomass or through the production of potent toxins, and bioactive compounds. The consequences of these sometimes dramatic phenomena can have enormous economic impacts for example on exploited marine resources and their markets or become a challenging sanitary problem with harmful effects on either aquatic organisms (mortality, delayed growth, impaired reproduction) or human health, whether through direct contact exposure or through bioaccumulation of toxic compounds in edible products.

The frequency and extent of these phenomena are globally increasing across the freshwater-to-marine boundaries within estuaries and coastal waters, pointing to a complexity of interplaying causes, such as ongoing eutrophication, new introductions of harmful species, increasing temperature, ecosystem disruption by human-caused nutrient over-enrichment, and global climate changes. There is evidence that increased CO_2 (and reduced pH) in marine and freshwater ecosystems can also exacerbate blooms and increase toxicity of some species, especially when combined with changes in nutrient availability.

The success of a HAB is the result of the interplay between the physiological adaptation of the harmful algal species or population, the environmental conditions, the interaction with co-occurring organisms, and physical dynamics that alter abiotic conditions and aggregate or disperse cells.

Transfer of species and their introduction to new areas are often due to ballast water transport, which has been linked to the proliferation of previously rare or undetected harmful algae in the discharge location but also to migratory animals or winds. Entire ecosystems have been completely changed by non-indigenous species introduction by human activities, such as the expansion of aquaculture worldwide, which has created another mechanism whereby species can be transported (aquaculture products and seed stocks are often shipped worldwide) and introduced to new areas. Once harmful species have been introduced, many site-specific factors in concert will control whether the species can successfully establish and thrive in the new area.

Anthropogenically introduced nutrients play a major role in the success of harmful species. Over-enrichment of coastal waters by nutrients is the result of increasing human population growth and density and consequent increasing food production activities (agriculture, animal production, aquaculture), which in turn increase sewage discharge and run-off from farmed and populated areas. The global production and use of chemical N fertilizers has undergone an enormous expansion in the last 70 years, while the use of P fertilizers has undergone a much smaller increase. This is mainly due to the lack of anthropogenic synthesis of P, which comes exclusively from mined sources (cf. Chapter 2). Of these two major agricultural nutrients, only 10–30% reach consumers, and more than half is lost to the environment (direct runoff, atmospheric volatilization, eventual deposition). Nowadays about 60% of all N fertilizers and feed additives used worldwide are in the form of urea ($CO[NH_2]_2$), whose consumption is projected to increase more than 200-fold by 2050. Urea can be a significant contributor both to total N and to the fraction used by phytoplankton in estuarine and coastal waters and preferentially by many harmful species. Moreover, urea rapidly hydrolyzes to NH^{4+} in water, which is another important N form used by algae, including HAB-forming species.

Other major sources of nutrient pollution are increasing intensive animal production and aquaculture, both producing dense animal populations per unit area with consequent high concentration of wastes. Both activities causes contamination of adjacent waters, which eventually leads to extreme habitat degradation; in the case of aquaculture, which in many countries is expanding at an unsustainable pace, various toxin-producing HABs and high-biomass HABs have been linked to this activity.

Many data are available about the increase of some micro- and macroalgae harmful blooms in relation to the increase in N and/or P loading. The dinoflagellate *Prorocentrum minimum*, for example, a high-biomass bloom former, has been found to track anthropogenic nitrogen and phosphorus input such as sewage outfalls, agriculture runoff, or aquaculture facilities on a global basis. Other dinoflagellate blooms along the coast of China, where the annual use of N fertilizers, especially urea, increased during to past decades to reach about 42 million tonnes around 2010, has followed this trend of nutrient loading, expanding their geographic extent in virtually all waters of the

country, increasing the duration of the bloom from days to months, increasing the number of species and consequently their harmful impact. As for macroalgae, the green tides of *Ulva prolifera* that completely covered the water of the Qingdao Sailing Center during the 2008 Olympics Games were caused by the nutrient loading of the local river basin. These massive green tides are more and more frequent along the Yellow Sea, where they can last for 2 months and affect an area up to thousands of square kilometers, with a total floating biomass sometimes exceeding 1 million tonnes in a single green tide outbreak. This enormous biomass has been estimated to correspond to about 360,000 tonnes of carbon, 23,000 tonnes of nitrogen, and 400 tonnes of phosphorus. Once the bloom is over, the floating biomass settles to the bottom and decomposes, leading to environmental and ecological perturbations in the settlement region due to the release into the sea of biogenetic elements, mainly in the form of reduced nitrogen (ammonium) and phosphate that are then mixed up in the water column and interfere with nutrient recycling and distribution. A very recent study investigated the impact of one of the largest *Ulva* green tides (2016) in the Yellow Sea on the phytoplankton assemblage of that area; the most remarkable change was an increase in abundance and proportion of the pelagophyte *Aureococcus anophagefferens* (Ochrophyta, Pelagophyceae), in turn responsible for harmful brown tide blooms with densities exceeding 10^6 cells mL^{-1}.

The unique gene complement of *A. anophagefferens* encodes a very much greater number of proteins involved in light harvesting and organic matter use as well as metal- and selenium-requiring enzymes relative to competing phytoplankton. These genes allow the alga to thrive in a very peculiar niche characterized by conditions (low light, high organic matter, and elevated metal levels) that have become increasingly prevalent in anthropogenically modified habitats (estuaries, cost lines). Because of its unique adaptability, this unicellular alga can use organic forms of carbon, nitrogen, and phosphorus for growth and has the capacity to survive in the darkness. Although not known to produce compounds toxic to humans, *A. anophagefferens* have decimated multiple fisheries because of toxicity to bivalves and impacted seagrass habitats, which provide valuable nurseries and refuge for fish, because of extreme light attenuation. While these blooms were once thought to be constrained to the coasts of the United States, where they were documented for the first time in 1985, they are now becoming a global problem, with *A. anophagefferens* blooming in shallow, anthropogenically modified habitats with low levels of light and inorganic nutrients and elevated organic carbon and nitrogen concentrations and spreading to many other countries, like Africa and China, possibly via transport in ballast water of ships.

Apart from the examples of HAB species cited previously, the inventory of the micro- and macroalgae recognized as HAB species or associated with harmful effects on either other aquatic organisms or humans is quite extensive and expanding as new species are detected and identified.

Harmful algal bloom species belong to seven classes of microalgae: Cyanophyceae, Prymnesiophyceae (Coccolithophyceae), Chrysophyceae, Bacillariophyceae, Raphidophyceae, Dictyochophyceae, and Dinophyceae, and five classes of macroalgae: Florideophyceae, Ulvophyceae, Charophyceae, Zygnematophyceae, and Phaeophyceae. According to a recent publication, the different impacts of HABs upon the environment, food chains, and human health can be classified into five categories:

1) Non-toxic but high-biomass blooming species that can directly or indirectly kill aquatic organisms (fish and invertebrates) by depletion of dissolved oxygen of water bodies or by their physical effects and can also prevent or outcompete the growth of other algae. Examples are the green tides due to *Ulva* and other Ulvophyceae (e.g. *Cladophora, Chaetomorpha, Caulerpa*) and the brown tides due to *Sargassum* and other Phaeophyceae (e.g. *Dictyota, Cladosiphon*) or to *Aureococcus* (Pelagophyceae) or the massive nuisance blooms of the diatom *Dydimosphenia geminata* (Bacillariophyceae), commonly called "dydimo," typical of high-light, shallow waters, which attaches by a mucopolysaccaride stalk to benthic substrates in flowing waters and splash zones of lakes. The production of stalks can be so large that river bottoms may become covered by a thick felt. The stalks

may become long and stringy, forming white strands up to 1 meter long, covering water surfaces with a thick felt, which can adversely affect freshwater fish, plant and invertebrate species, such as by reducing the number of suitable habitats and excluding the growth of other diatoms, but it also impacts the tourism industry, especially along the coasts of Chile and Argentina (Figure 6.18). Red tides are due to *Gracilaria* and other Florideophyceae (e.g. *Hypnea, Acanthophora, Laurencia*), whose thick biomass canopies foul beaches and shorelines, cause light limitation, and severely impact seagrass and coral habitats. In this category we can also include the cyanobacterium *Planktothrix perornata*, which is common in the phytoplankton communities that grow in channel catfish (*Ictalurus punctatus*) production ponds in the southeastern United States, which assimilate and reduce ammonia-nitrogen concentrations. These cyanobacteria, which produce the common "earthy" and "musty" compounds geosmin and 2-methylisoborneol (MIB), can bloom and dominate the other phytoplankton species, leading to the accumulation of these compounds in the flesh of the catfish, thereby rendering the fish unpalatable and unmarketable.

2) Species producing toxins involved in food poisoning in humans with either neurological or gastrointestinal symptoms. In this category can be found species producing toxins associated with paralytic shellfish poisoning (PSP), diarrheic shellfish poisoning (DSP), azaspiracid shellfish poisoning (AZP), amnesic shellfish poisoning (ASP), neurotoxic shellfish poisoning (NSP), ciguatera fishfood poisoning (CFP), and cyanotoxin poisoning (hepatotoxins). All these different poisonings will be dealt with later in the chapter.
3) Species causing no damage to humans but harmful to fish and marine invertebrates by mechanical effects (lesions or gill clogging) or secretion of fatty acids or galactolipids that damage the epithelium of gill tissues and destroy blood cells (hemolysins). Examples of the first organisms are the chain-forming diatoms bearing barbed setae, *Chaetoceros convolutus* and *C. concavicornis*. These setae, when breaking, remain stuck in fish gill tissues and cause bleeding of capillaries, dysfunction of gas exchange and suffocation by mucus overproduction. Examples of hemolysin-producing organisms are the raphidophytes *Heterosigma akashiwo* and *Chattonella antiqua*, the haptophytes *Prymnesium polylepis* and *Prymnesium parvum*, and the dinoflagellates *Karenia mikimotoi* and *Amphidinium*.



FIGURE 6.18 Warning sign for the presence of *Dydimosphenia geminata* (dydimo) along the cost of Patagonia.

4) Toxin-producing species affecting humans through exposure to bloom waters or aerosols (impact on respiratory systems), such as *Ostreopsis ovata*.
5) Species not listed as toxic to man but found to produce toxins when using bioassays and therefore likely to represent a potential danger.

Toxicity is a trait peculiar to microalgae, an intrinsic characteristic of these organisms which directly synthesize toxic compounds or form them by the composition of metabolic products.

Of the millions of species of existing microalgae, those that produce specific toxins scarcely exceed 100, occurring in both salt and freshwaters. As already noted, toxin production is often linked to HABs, which bio-accumulate these dangerous compounds and bio-amplify them throughout the food web to affect humans and other organisms, either following the consumption of contaminated seafood or via direct exposure to bloom waters and aerosols. Shellfish, mainly filter-feeding bivalves of commercial interest (mussels, scallops, oysters, clams, etc.) are the most exposed to these toxic blooms and the major vectors of human intoxication associated with the toxins of HABs at a global scale, though gastropods, crustaceans, cephalopods and echinoderms can also accumulate toxic compounds.

Algae which seem to be direct producers of toxic substances mostly belong to these classes: Cyanophyceae, Prymnesiophyceae, Raphidophyceae, Bacillariophyceae, and Dinophyceae.

Cyanophyceae

Among the 50 freshwater existing cyanobacteria genera, 12 are capable of producing toxins. While blue-green algae have significant taste and odor constituents, representing a moldy smell, their toxic metabolites have no taste, odor, or color. The risk of exposure to algal toxins may come from drinking water, recreational water, dietary supplements, or residue on produce irrigated with contaminated water and consumption of animal tissue. Avoiding cyanobacteria toxins is not as easy as avoiding a harmful algal bloom, as toxins may be present in fish, shellfish, and water even after the bloom has dissipated. Cyanobacterial toxins are responsible for a variety of health effects such as skin irritations, respiratory ailments, neurological effects, and carcinogenic effects. The three major classes of these compounds are:

- Hepatotoxic cyclic pentapeptides. The most frequently occurring and widespread toxins of this group are nodularins and microcystins. *Nodularia spumigena,* a well-known cyanobacterium, produces nodularins and is primarily a concern in marine and brackish waters, where it creates a risk to recreational swimmers. It is known to cause liver hemorrhages to cattle drinking *Nodularia*-containing pond water. Nodularin's structure is similar to microcystin, an inhibitor of liver PP1 and PP2 protein phosphatases and a tumor promoter. Microcystins and their more than 60 variants are isolated from freshwaters worldwide and are produced by *Microcystis* sp. (the most commonly identified cyanobacteria in human and animal poisonings), *Anabaena* sp., and other cyanobacteria. These toxins are very stable in the environment; are resistant to heat, hydrolysis, and oxidation; and have a strong affinity for the liver. Among the symptoms of exposure to microcystins are weakness, loss of appetite, vomiting, diarrhea, and eventually cancer.
- Neurotoxic alkaloids. These toxins are divided in two main classes, anatoxins and saxitoxins, produced by the genera *Anabaena*, *Planktothrix*, and *Aphanizomenon.* Anatoxins may affect the nervous system, skin, liver, or gastrointestinal tract. These neurotoxins can cause symptoms of diarrhea, shortness of breath, convulsions, and death in high doses due to respiratory failure. Saxitoxins are the cause of paralytic shellfish poisoning in humans consuming contaminated shellfish. There are no reports of similar poisonings via the drinking water route. Another alkaloid toxin is cylindrospermopsin produced by the filamentous cyanobacteria *Cylindrospermopsis raciborskii*, *Anabaena bergii*, and *Aphanizomenon flos-aquae*.

- Neurotoxic amino acid. B-N-methylamino-L-alanina (BMAA) is a neurotoxic amino acid produced by cyanobacterial symbionts belonging to the genus *Nostoc*, *Nodularia spumigena*, *Aphanizomenon* spp., and other cyanobacteria. This toxin is likely to undergo bioaccumulation in the ecosystem, from zooplankton up to fish, through bivalves. It is considered a possible cause of amyothrophic lateral sclerosis (ALS) and Parkinson's and Alzheimer's dementia.
- Endotoxic lipopolysaccharides (LPSs). These compounds are common constituents of the outer cell walls of Cyanobacteria, similar to the cell wall toxin found in *Salmonella* bacteria but less toxic. LPSs are contact irritants and inflammatory agents.

Prymnesiophyceae

This class contain a few toxic species. Among them, *Prymnesium parvum* produces a mixture of toxins collectively named prymnesins, which exhibit potent cytotoxic, hemolytic, neurotoxic, and ichthyotoxic effects. Prymnesins can be used also as defense against grazers and herbivorous organisms (allelopathic role). *Prymnesium polylepis* produces and excretes at least four different compounds with hemolytic and ichthyotoxic effects. The major hemolytic compound is a galactolipid, 1-acyl-3-digalacto-glycerol. These toxins cause osmoregolatory failure similar to that brought about by *Prymnesium parvum*.

Another widely distributed marine haptophyte, *Phaeocystis* sp., is familiar to fishermen in the form of extensive blooms of mucilaginous colonies, which are avoided by herring. It produces large quantities of acrylic acid, which has strong bactericidal properties. Already 70 years ago, *Phaeocystis pouchetii* was suspected to cause avoidance of herring; it was demonstrated that food intake and growth were reduced in sea cage–cultivated salmon during the spring bloom of *P. pouchetii*, and water from *P. pouchetii* cultures was toxic towards cod larvae.

Species belonging to the genus *Phaeocystis* are important in all oceans, and *P. pouchetii* is an important common component of northern and temperate spring blooms of phytoplankton; it is grazed by zooplankton at normal rates, and it also can be a diet preferable to diatoms. Its life cycle is known to be polymorphic, with at least two different stages: the colony-forming stage, which is the most conspicuous, with colonies up to several millimeters consisting of aflagellate cells embedded in mucilage, and the motile stage, with unicellular biflagellate cells.

Phaeocystis pouchetii has been reported to produce a polyunsaturated aldehyde (PUA) as diatoms, the 2-*trans*-4-*trans*-decadienal. This compound is known to interfere with the proliferation of different cell types, both prokaryotic and eukaryotic. As mechanical stress is known to induce the release of PUAs in other phytoplankton species, the release of 2-*trans*-4-*trans*-decadienal has been suggested to be a mean of deterring grazers, such as zooplankton or fish larvae. Since copepods avoid grazing on healthy colonies of *P. pouchetii*, the production and excretion of PUAs seem to depend on the state of the cells, environmental factors, or both. This PUA can be released into the sea in the absence of grazers, indicating that it may serve as an allelochemical, that is, a compound which gives *P. pouchetii* a competitive advantage over phytoplankton species blooming at the same time by inhibiting their growth. This haptophyte also produces acrylic acid, an antibiotic that kills bacteria inside and around the colonies, and dimethylsuphide (DMS).

Bacillariophyceae

Species belonging to the genus *Pseudo-nitzschia* are responsible of blooms with proven toxic effects due to the production of domoic acid (DA), the cause of ASP. DA was first isolated in Japan from the red macroalga *Chondria armata* (Florideophyceae) in 1958 and was consequently named after the Japanese word for macroalgae, which is *domoi*. The production of DA by species of the genus *Pseudo-nitzschia* was discovered only in 1987 and was first treated with skepticism, because this water-soluble three carboxylic amino acid was known as a folk medicine in Japan to treat intestinal

pinworm infestations when used in very small doses. Domoic acid can enter the marine food chain via uptake by shellfish such as mussels that filter their food out of the water. This water can contain both diatoms themselves and the toxin, which is released to the water column (although there is no evidence yet that the toxin can be taken up directly). The toxin accumulates in the digestive gland and certain tissues of shellfish, and it appears to have no effect on the animals. Domoic acid may be metabolized by bacteria (e.g. of the genera *Alteromonas* and *Pseudomonas*) present in tissue of blue mussels (*M. edulis*). Scallops are reported not to contain these elimination bacteria. Anchovies can also contain domoic acid in their guts by feeding on toxic *Pseudo-nitzschia* spp.; this toxin affects their behavior and survival. Effects are also seen in seals. In humans, consumption of contaminated seafood mostly affects the elderly or infirm. Heat does not destroy domoic acid, although shellfish toxicity can decrease during cooking or freezing via domoic acid transfer from the meat to the surrounding liquid. The sea otter is the only animal known to be able to avoid intoxication, probably recognizing toxic prey by their odor. The mechanism of domoic acid toxicity is explained by its structural similarity with the excitatory neurotransmitter glutamic acid and its analogues, but with a much stronger receptor affinity. Domoic acid is three times more potent than its analogue kainic acid and up to 100 times more potent than glutamic acid itself. After exposure, domoic acid binds predominately to *N*-methyl-*D*-aspartate (NMDA) receptors in the central nervous system, causing depolarization of the neurones. Subsequently, the intercellular calcium concentration increases, resulting in sustained activation of calcium-sensitive enzymes, eventually leading to depletion of energy, neuronal swelling, and cell death. The affected neurones are mainly located in the hippocampus, explaining the most striking effect of domoic acid poisoning, which is short-term memory loss, observed in 25% of the affected persons in the 1987 contaminated mussel event. Other symptoms are confusion, nausea, vomiting, gastro-enteritis, cramps and diarrhea, all within 24 h. Neurological complaints, including ataxia, headaches, disorientation, difficulty in breathing, and coma, develop 48 h after consumption. Permanent brain damage can also be caused by domoic acid intoxication. Effects of chronic low-level ingestion are unknown. Domoic acid from mussels is more neurotoxic than the chemically pure compound. This increase is due to domoic acid potentiation, caused by high concentrations of glutamic and aspartic acids present in mussel tissue. This neurotoxic synergism occurs through a reduction in the voltage-dependent Mg_2 block at the receptor-associated channel, following activation of non-NMDA receptors, in addition to the NMDA receptor activation by domoic acid itself.

Intensive research over the last years has revealed a new class of phytotoxins produced by diatoms with more subtle and less specific effects, a discovery that has drawn a lot of attention since the diatoms have traditionally been regarded a key component of the food chain. Three closely related polyunsaturated aldehydes have been isolated from *Thalassiosira rotula*, *Skeletonema costatum*, and *Pseudo-nitzschia delicatissima*: 2-*trans*-4-*cis*-7-*cis*-decatrienal, 2-*trans*-4-*trans*-7-*cis*-decatrienal and 2-*trans*-4-*trans*-decadienal. In the same study, these aldehydes were found to inhibit cleavage of sea urchin embryos and reduce growth of $CaCO_2$ cells and hatching of copepod eggs. The structural element shared by these compounds, the unsaturated aldehyde group, is able to form adducts with nucleophiles and is thus capable of inducing reactions that are toxic to the cell. The harmful effects of PUAs have been demonstrated at the organism level as inducers of apoptosis in sea urchin embryos, at the cell level as cytotoxicity in human cell lines, and at the protein level by deactivation of enzymes.

Raphidophyceae

This class includes at least two toxic genera: *Chattonella* and *Heterosigma,* which are known for toxic red tides, especially in Japanese waters, related to extensive mortalities of farmed fish. *Chattonella marina* produces free fatty acids responsible for the destruction of fish gills at very low concentration; 500 cells mL^{-1} are sufficient to cause toxic effects. Three neurotoxic compounds have been isolated from this alga, which could correspond to brevetoxins. *Heterosigma akashiwo* produces allelophatic substances that clogs fish gills by mucus over-production and cause hemolysis of gill cells.

Dinophyceae

This class includes about a dozen genera, with at least 30 species, producing water- and lipid-soluble, low molecular weight, neuroactive secondary metabolites that are among the most potent non-proteinaceous poisons known. In general, these toxins have been shown to block the influx of sodium through excitable nerve membranes, thus preventing the formation of action potentials. The toxins are accumulated and sometimes metabolized by the shellfish which feed upon these dinoflagellates, causing different types of shellfish poisoning, such as paralytic shellfish poisoning, diarrheic shellfish poisoning, neurotoxic shellfish poisoning, ciguatera fish poisoning, and amnesic shellfish poisoning.

Ingestion of contaminated shellfish results in a wide variety of symptoms, depending upon the toxins(s) present, their concentrations in the shellfish, and the amount of contaminated shellfish consumed.

In the case of PSP, the poisoning is caused by saxitoxin and its analogs produced mainly by *Alexandrium* spp. but also by other genera such as *Gymnodinium* and *Pyrodinium*. The effects are predominantly neurological and include tingling, burning, numbness, drowsiness, incoherent speech, and at high doses complete respiratory paralysis and death.

Less well characterized are the symptoms associated with DSP and NSP. DSP is caused by okadaic acid (OA), a lyposoluble cyclic polyether with a carboxylic function, and its analogs, especially dinophysystoxins. OA and its analogs are diarrheic shellfish toxins and tumor promoters found in many dinoflagellates of the genera *Dinophysis* and to a lesser extent in a few species of *Phalachroma* and *Prorocentrum*. DSP is primarily observed as a generally mild gastrointestinal disorder, that is, nausea, vomiting, diarrhea, and abdominal pain accompanied by chills, headache, and fever.

Both gastrointestinal and neurological symptoms characterize NSP, including tingling and numbness of lips, tongue, and throat, muscular aches, dizziness, reversal of the sensations of hot and cold, diarrhea, and vomiting. The NSP toxins are brevetoxins, a family of polycyclic ether toxins produced mainly by *Karenia brevis*.

Another syndrome caused by dinoflagellate toxins is ciguatera fish poisoning, connected with eating contaminated tropical reef fish. These toxins are produced by *Gambierdiscus toxicus,* a photosynthetic benthic dinoflagellate that normally grows as an epiphyte and has a relatively slow growth rate of approximately one division every 3 days. In its coral reef habitat, *G. toxicus* is biflagellate and swims if disturbed but is usually motionless and attached to certain macroalgae. The dinoflagellate may also be associated with macroalgal detritus on the sea floor.

G. toxicus produces two classes of polyether toxins, ciguatoxins (CTX) and maitotoxins (MTX). The CTX are lipophilic and are accumulated in fish through food web transfer. More than 20 CTX congeners have been isolated; however, only a few have been fully characterized structurally. The maitotoxins are transfused ladder-like polyether toxins but are somewhat more polar, due to the presence of multiple sulfate groups. MTX was originally identified as a water-soluble toxin in the viscera of surgeon fish and later found to be the principal toxin produced by *Gambierdiscus toxicus*. MTX have not been demonstrated to bioaccumulate in fish tissues, possibly due to their more polar structure. Thus, if MTX is involved in ciguatera poisoning, it may be implicated only in ciguatera poisonings derived from herbivorous fishes.

The toxic potency of MTX exceeds that of CTX (respectively 10 and 50 ng kg^{-1} in mice). Its biological activity is strictly calcium dependent and causes both membrane depolarization and calcium influx in many different cell types.

These toxins are bioaccumulated in shellfish and become progressively concentrated as they move up the food chain from small fish to large fish that eat them and reach particularly high concentrations in large predatory tropical reef fish. Barracuda are commonly associated with ciguatoxin poisoning, but eating grouper, sea bass, snapper, mullet, and a number of other fish that live in oceans between latitude 35°N and 35°S has caused the disease. These fish are typically caught by sport fishermen on reefs in Hawaii, Guam and other South Pacific islands, the Virgin Islands, and Puerto Rico. Ciguatoxin usually causes symptoms within a few minutes to 30 hours after eating

contaminated fish, and occasionally it may take up to 6 hours. In its typical form, CFP is characterized initially by the onset of intense vomiting, diarrhea, and abdominal pain within hours of ingestion of toxic fish. Within 12–14 h of onset, a prominent neurological disturbance develops, characterized by intense paresthesia (tingling, crawling, or burning sensation of the skin) and dysesthesia (painful sensation) in the arms, legs, and perioral region; myalgia; muscle cramping; and weakness. During this stage of the illness, pruritus and sweating are commonly experienced. Ciguatera poisoning is rarely fatal. Symptoms usually clear in 1 to 4 weeks.

Another dinoflagellate causing blooms associated with human illness and faunal damage is *Ostreopsis ovata*. This organism is known as a potential producer of palytoxin and its analogues. Palytoxin is the most potent proteinaceous compound reported so far that causes fatal illness to humans following consumption of shellfish and bottom-feeding fish that have accumulated the toxins. It has been shown that these toxins are released by the cells at the end of the stationary phase of growth, suggesting that long-term blooms may lead to an increase of water-soluble toxins and increase in harmful effects of aerosols.

Unlike toxic microalgae blooms, macroalgal blooms usually lack direct chemical toxicity but typically have a broader range of distribution and ecological impacts. In aquatic ecosystems, macroalgae are largely beneficial by providing an important structural habitat for invertebrates and fishes and a source of nutrition for herbivore and detrital food webs. Macroalgae are a natural, common feature of inland waters as well as estuaries, coastal waters, and (to a limited extent) oceanic waters, particularly the Gulf of Mexico, North Atlantic Ocean, and Caribbean Sea where pelagic *Sargassum* is distributed.

Causes and effects of macroalgal blooms are similar in many ways to those associated with harmful phytoplankton species; they can result in the displacement of indigenous species, oxygen depletion (hypoxia/anoxia), noxious and toxic odors (hydrogen sulfide, dimethyl sulfide, and dimethyl disulfide), habitat loss, alterations of biogeochemical cycles and food webs, alterations in grazing, and die-offs of seagrasses and coral reefs. From a socioeconomic perspective, the excessive biomass also causes undesirable effects for humans, such as decreased recreational uses of beaches and waterways; increased fouling of pumps, filters, and intake pipes; taste and odor problems in drinking water supplies; increased costs of water treatment; increased costs of managing aquatic resources and losses of commercially important finfish and shellfish due to habitat loss and fouling of fishing gear; and increasingly expensive biomass removal programs.

The frequency and extent of macroalgal HAB have increased in estuaries and coastal waters throughout North America during the past five decades to now include all coastal states as well as Hawaii; in addition, macroalgal HAB have become common in inland freshwater systems, including lakes, streams, rivers, springs, and reservoirs. As for microalgae, the increasing trend of macroalgal HABs results primarily from increased nutrient loading and eutrophication.

Macroalgae produce a great number of secondary metabolites, including terpenes, aromatic compounds, acetogenins, polyphenols and fluorotannins, substances derived from amino acids, and various alkaloids that are ecologically useful to algae. Substances synthesized by species of the Phaeophyceae, like the Dictyoles (dictyol B, dictyol acetate A, B, H, and pachydictyol), act against herbivores and are also used as a defense against epiphytes and epibionts that invade algal surfaces. Many members of the Rhodophyceae synthesize biologically active metabolites that vary from simple brominated aromatic acetones and brominated phenols to mono, diterpene, and sesquiterpene complexes. Algae of the division Chlorophyta mainly synthesize di- and sesquiterpenes that have a variety of biological activities including antiherbivory, bactericidal, antifungal, and spermicidal.

As already mentioned, macroalgae HAB species belong to five classes: Florideophyceae, Ulvophyceae, Charophyceae, Zygnematophyceae, and Phaeophyceae, with freshwater, estuarine, coastal, and marine species.

Among the red algae forming bloom in sea water, *Gracilaria* spp. (Florideophyceae) can develop thick canopies that overgrow seagrasses because of the light limitation they cause. Similar blooms fouling beaches and shore, especially along the east coast of the United States, are due to other

Florideophyceae, such as *Laurencia* spp., *Hypnea*, *Acanthophora*, *Spyridia filamentosa*, and *Wrightiella blodgettii*. All these macroalgae tolerate a wide range of environmental conditions, can free float, or are attached to the benthos.

The class Ulvophyceae contains genera forming blooms in many alkaline freshwater and brackish lakes and rivers, such as *Cladophora*, the most widely distributed genus throughout the world freshwater ecosystems, or *Phitophora oedogonia*, which, similarly to *Spirogyra* spp. (Zygnematophyceae), can rapidly grow in shallow littoral areas of eutrophic habitats. Among the Ulvophyceae, the genus *Ulva* is responsible for 52% of all algal blooms recorded between 1976 and 2018; this alga can grow in habitats spanning freshwater to salt springs and brackish lakes, and even in the Great Salt Lake, where the salinity is higher than 50. It can be found globally in tropical, temperate, and polar climates, where it colonizes urbanized bays and harbors. Its blooms form thick mats that overgrow the benthos, causing hypoxia and anoxia, offensive odors, and loss of biodiversity, such as the blooms of *Chaetomorpha* and *Cladophora* (Ulvophyceae), which occur in the same shallow urbanized estuaries and coastal lagoons.

Charophyceae as *Chara* and *Nitella* can become problematic in shallow waters when their excessive growth reaches the water surface and impedes human recreational uses.

Of the blooming Phaeophyceae, the genus *Sargassum* exhibits the most blooming tendencies, often leading to wide-scale events. The two species *Sargassum natans* and *Sargassum fluitans* are repeatedly known to bloom in the Atlantic Ocean and Gulf of Mexico. In 2018, this free-floating algae bloomed across a stretch of 8850 km of the Atlantic Ocean from West Africa to the Gulf of Mexico, equating to more than 20 million metric tonnes of biomass and creating the world's largest macroalgal bloom. Three other blooming brown algae are *Pilayella littoralis*, which forms sludge-like masses that strand and accumulate on beaches, and *Cladosiphon* spp. and *Dictyota* spp., which typically affect the Florida Keys as a consequence of nutrient enrichment and eutrophication, overgrowing seagrasses and corals.

Table 6.4 summarizes toxic algae and the corresponding metabolites.

TABLE 6.4
Summary of Toxic Algae and the Corresponding Metabolites

Scientific Name	Class	Toxin
Nodularia spumigena	Cyanophyceae	Nodularins
Microcystis spp., *Anabaena spp.*	Cyanophyceae	Microcystins
Anabaena spp., *Planktothrix* spp., *Aphanizomenon* spp.	Cyanophyceae	Anatoxins, saxitoxins
Cylindrospermopsis raciborskii, Anabaena bergii, Aphanizomenon flos-aquae	Cyanophyceae	Cylindrospermopsins
Nostoc, Nodularia spumigena, Aphanizomenon spp.	Cyanophyceae	BMAA
Chondria armata domoi	Florideophyceae	Domoic acid
Prymnesium parvum	Haptophyceae	Prymnesins
Prymnesium polylepis	Haptophyceae	Toxic galactolipids
Phaeocystis pouchetii	Haptophyceae	Acrilic acid, PUA
Pseudo-nitzschia spp.	Bacillariophyceae	Domoic acid
Thalassiosira rotula	Bacillariophyceae	PUA
Skeletonema costatum	Bacillariophyceae	PUA
Pseudo-nitzschia delicatissima	Bacillariophyceae	PUA
Chattonella marina	Raphidophyceae	Brevetoxins
Heterosigma akashiwo	Raphidophyceae	Hemolytic substances
Alexandrium spp., *Gymnodinium* spp., *Pyrodinium* spp.	Dinophyceae	Saxitoxins
Dinophysis spp., *Phalachroma* spp., *Prorocentrum* spp.	Dinophyceae	Okadaic acid, dinophysystoxins
Karenia brevis	Dinophyceae	Brevetoxins
Gambierdiscus toxicus	Dinophyceae	Ciguatoxins, maitotoxins
Ostreopsis ovata	Dinophyceae	Palytoxins

ALGAE AS TOOLS FOR ENVIRONMENTAL MONITORING

The monitoring of environmental water quality is essential for the proper management of inland waters, for their governing and repair by taking prompt actions in case of alert events. Physical-chemical water quality parameters, such as pH, chlorine, temperature, flow, and turbidity, are routinely measured using in situ online instrumentation. However, an effective water management procedure should also take into consideration the organisms present in the water samples, because they do reflect the overall water quality, integrating in their metabolism the effects of physical and chemical changes over time. Blooming of potentially toxic species should be monitored to prevent intoxication of humans and animals through the consumption of contaminated organisms along the food chain as well as to protect them from toxins delivered via water spray or direct contact. The damage of living resources, such as shellfish and fish, together with all the organisms feeding on them, as well as the economic losses to fisherman, aqua-culturists, and tourist industry, should not be minimized.

Microalgae, thanks to their short lifespan (a few weeks) and generation times (about 1 day), are capable of fast, strong, and predictable responses to different ecological and toxicological factors by modifying the composition and density of their population.

Microalgae are routinely examined by means of bright field optical microscopy because of the micrometric dimensions of the cells and the color they possess due to the presence of photosynthetic pigments. This first analytical step could be sped up by making it as automated as possible to improve its reproducibility and effectiveness for water monitoring and protection purposes.

Identification of microalgae can achieve 67–83% accuracy for trained but not routinely engaged personnel, which increases to 84–95% for routinely engaged personnel. This variation is due to the lack of unanimity in the classification, even when the inspected microalgae possess a very distinct morphology. The goal of automated systems is to combine a level of accuracy and precision comparable to or higher than that of an expert taxonomist with the minimum analysis time.

Four different methodologies are currently available to implement systems for automated and real-time analysis of microalgae: flow cytometry, metagenomics, remote sensing, and digital microscopy. These systems are effective in assessing the condition of water bodies even if they have to deal with hindering factors such as the very different size and morphological and physiological features of the thousands of existing species of microalgae.

Almost all these methodologies require a preliminary sampling procedure, which should be as extensive as possible since statistical difference between sample devices and locations produces not accurate and imprecise measurements, counteracting the monitoring purpose. For quantitative studies, the minimum requirement is to take an integrated sample from 0 to 10 m depth using a net or hose sampler (which can collect a volume of about 5 L) or by pooling equal amounts of water volume from fixed depths. An alternative method for sampling is the use of in-situ imaging devices, consisting of submersible digital cameras. These submersed systems are capable of acquiring and storing microalgae images in the field of view of the camera for a preset time.

We will briefly describe these methodologies and analyze their pros and cons.

Flow Cytometry

This methodology analyzes the microalgae suspended in an environmental sample. The analysis is fast, provides rapid extraction of single cell multi-features, and separates collection of microalgae from extraneous materials for further analysis. Flow cytometers combine three units: fluidics, optics, and electronics. The fluidics unit pressurizes the water sample and focuses microalgae cells in an interrogation point where every cell is analyzed by the optics unit. This unit consists of excitation optics (multiple lasers) producing visible forward scatter, side scatter, and up to 18 fluorescent signals, which will be read by the detection optics (photomultiplier tubes and photodiodes). The forward scatter, which indicates the relative size of the cell, is measured in the direction of the light path, while

the side scatter, which indicates the internal complexity of the cell, is measured perpendicularly to the light path. A series of dichroic filters, transmitting selected wavelengths and reflecting all the others, steer the fluorescent light at different angles in different paths toward the photomultiplier tubes. Band-pass filters, inserted in each optical path, select a small window of a specific wavelength of light and allow the measure of the fluorescence signal produced by the pigments, that is, chlorophylls and phycobilins, present in the photosynthetic membranes of microalgae. The electronics unit converts the analogic signals from the detectors into digital signals that can be processed by a computer. The strongest drawback of this approach is that cells can be differentiated only on the basis of their optical features as a whole (i.e. at "zero" resolution), and the system is unable to classify the microalgae at the level of species. Therefore, toxic species cannot be identified, and the occurrence and distribution of each algal species cannot be measured with accuracy.

Automated submersible equipment exists, such as the Imaging FlowCytoBot, which combines flow cytometry and hydrodynamic focusing. This system can work underwater for months, acquiring in-situ high-frequency microalgae images at an image rate of 3×10^4 high-resolution images/hr. This setup provides a desirable improvement of flow cytometry methodologies.

Metagenomic Analysis

This methodology performs parallel analysis of the genomes of the microalgae community present in an environmental sample. Metagenomic analysis begins with the isolation and selection of the cells from the environmental sample by means of size fractionation using filters with different porosities or by flow cytometry. DNA is then extracted for sequencing by shotgun metagenomics (i.e. random sequencing of the whole DNA) or by barcoding gene amplification (i.e. the search for ubiquitous genes such as 16S ribosomal DNA for prokaryotic algae and 18S ribosomal DNA for eukaryotic algae). Due to the high target number of these RNA molecules in the cells, it is possible to design 18–25 base pair length probes with a very high taxonomic specificity. This specificity must be tested by comparing nucleotide sequences to sequence databases and calculating the statistical significance (BLAST) in order to find regions of similarity.

For shotgun metagenomics or barcoding gene amplification, DNA fragments (up to 800 nucleotides) can be directly sequenced using next-generation sequencing technologies or cloned in a vector for amplification and subsequent sequencing. Taxonomic assignation of shotgun metagenomic sequences is a challenging task because of the highly fragmented nature of the sequences and the unbalanced set of reference genomes. Bioinformatics analysis is the main bottleneck for metagenomic projects. Annotation is a time-consuming task requiring comprehensive bioinformatics skills and soundly trained experts.

Rapid target identification of single toxic algal species such as the dinoflagellates *Alexandrium minutum* and *Gymnodinium catenatum* can be performed by means of sandwich hybridization, which is another barcoding analysis technique. A capture probe bound to a solid surface immobilizes the target ribosomal RNA and forms a hybrid complex with a second signal probe. When the solid surface is an electrochemical biosensor, the detection event is transformed into a measurable electrical current.

Genomic analysis possesses high taxonomic resolution and can be applied also to preserved environmental samples. High taxonomic resolution is mandatory when toxic and non-toxic strains are morphotypes of a same species and hence very difficult to identify by optical microscopy (e.g. *Alexandrium tamarense* species complex). Quantitative real-time PCR-based assay, which simultaneously amplifies and quantifies the DNA, is a more sophisticated technique that increases the accuracy of metagenomic analysis.

Composition and densities of microalgae population by metagenomic analysis is difficult to estimate because this methodology quantifies DNA and/or RNA, not single cells. Nucleic acids are specie-specific traits and can vary depending on the growth phase. Moreover, DNA can properly identify only species already studied, whose sequenced reference genome has been deposited in

a database. Generally, only a single species or strain at the time can be analyzed in a quantitative approach; multiple and parallel reactions can be performed, but the parallel determination of specific taxa of algae requires difficult, time consuming and expensive validation.

From an economic point of view, real-time PCR instruments are becoming affordable also for small research groups and are now quite common in molecular biology-equipped laboratories, thanks also to the low cost of consumable per sample (duplicate reactions about $20), which makes real-time PCR a potential routine method for monitoring applications.

Remote Sensing

The use of satellite color imagery, such as Terra/Aqua MODIS, Landsat 8 OLI imagery, or Sentinel-2A/B MSI, has proven an effective tool for detecting harmful algal blooms in water bodies globally around the world because of its high temporal and spectral resolution. Algorithms for the detection of massive blooms of toxic species from these images are mainly based on the absorption and reflection band characteristics of algal pigments in water.

Algae possess high absorption in the blue and red bands and high reflectance in the green and near-infrared bands. To produce an image that highlights the HAB, reflectance in the red and near-infrared bands has been used for long time to create normalized difference vegetation index (NDVI) images. Nowadays, other algorithms are used to improve these images, such as the floating algae index (FAI), which processes spectral information of the red, infrared, and short-wave infrared bands to correct for the atmospheric effect. Moreover, to evaluate the concentration of the HAB biomass, the chlorophyll reflection peak intensity algorithm is used, which is based on the reflectance of the blue, green, and red bands and utilizes the correlation between algae concentration and chlorophyll content.

Remotely monitoring HABs could be complicated by the presence of multiple co-occurring species, optically complex waters and cloud gaps, and in general by the variable atmospheric conditions. Hence, original satellite images are usually preprocessed to eliminate influences by aerosol and water vapor scattering, and cloud covering.

New hyperspectral sensors currently being studied, designed, and built for satellites, such as the NASA Plankton, Aerosol, Cloud, Ocean Ecosystem (PACE) mission, scheduled to launch by 2023, which hopefully will change the way of monitoring water quality from space with increased spectral, temporal, and spatial resolution. The sensitivity of this system will improve the limits of the previous systems, allowing the identification of phytoplankton community composition and separation of phytoplankton pigment absorption from that of colored dissolved organic matter.

Digital Microscopy

This methodology needs a hardware platform, consisting of an optical microscope equipped with a color CCD digital camera used for image acquisition and a personal computer, the more sophisticated the better. The PC should possess specific designed software algorithms for microalgae analysis. From a general point of view, the automatic microalgae image classification process by means of digital microscopy (DM) consists of a preliminary sampling step followed by four phases: image acquisition, image processing, feature extraction and selection, and microalgae classification by artificial neural network (Figure 6.19). A more extensive description of DM is given in Chapter 7.

The way images are acquired decides which kind of features can be extracted for classification. Microalgae morphological features (i.e. contours, sizes, etc.), universally used for their identification, require digital images with high spatial resolution (full HD CCD camera with complementary metal-oxide-semiconductor sensors). Microalgae taxonomists usually base their analysis on algal cell morphological and hue features; therefore, digital microscope systems equipped with a spectrophotometric unit, which possesses sub-micrometric lateral spatial resolution, nanometric spectral

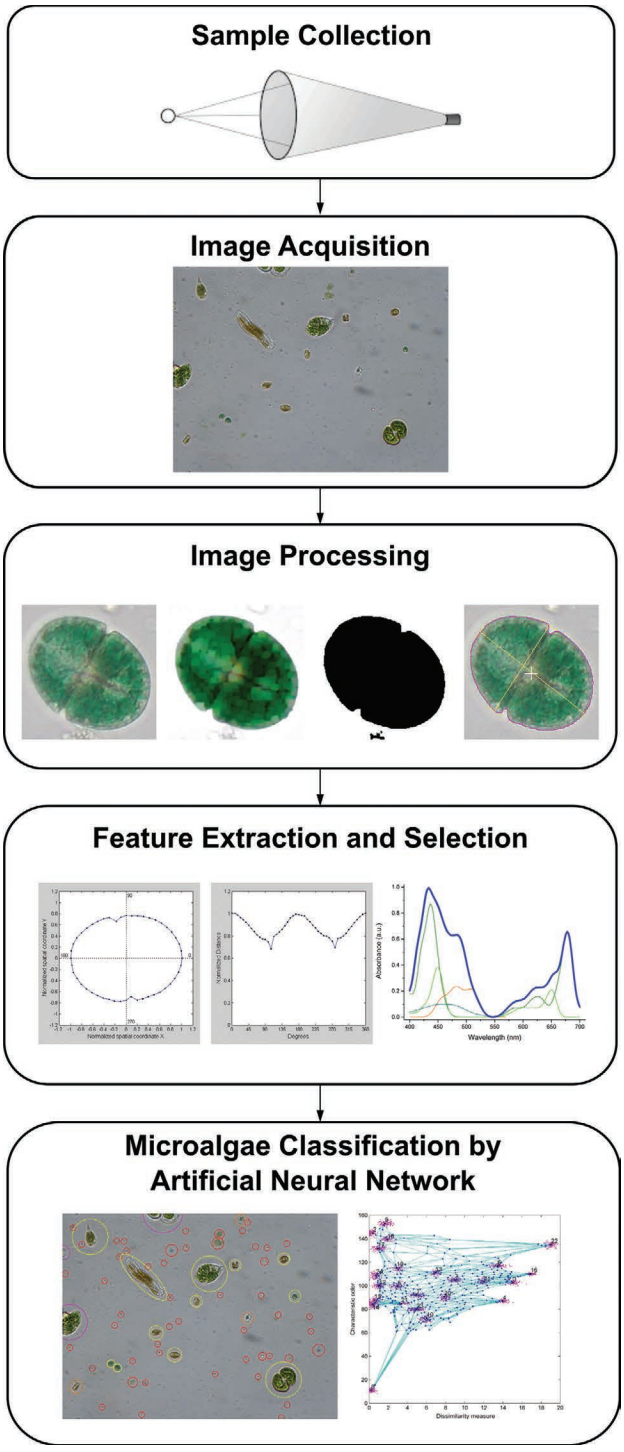


FIGURE 6.19 Flow chart of the automatic microalgae image classification process.

resolution, and detection of very low photon fluxes are the most adequate systems for microalgae classification.

Algae color features (i.e. pigment composition) require a color camera or microspectrophotometers (cf. Chapter 7). If the comparative standard for the automatic analysis is the judgment of an

expert taxonomist, all the images should be acquired at the highest spatial (14 Mpixels with 1080 lines of 1920 pixels) and color resolution (24 bits with more than 16 million colors) to achieve a reliable understanding of algal shape and pigment composition. As consequence, slides from field samples should be prepared without any kind of processing or fixation to avoid unpleasant manipulation of algae shape and color. It is very important to be aware that biological images are often far more difficult to process and recognize than daily-life images. The acquisition process should produce well-focused images with the highest information content to exploit in the successive steps. The microscope, a traditional one or a bench-mounted one, should be set at the best performance of Koehler illumination, as we describe in Chapter 7. The illumination should be even and uniform to avoid shadows, and the flux emitted from the tungsten lamp should be set so that the dark noise of the CCD camera has no influence and camera saturation does not occur. The lamp color temperature should be set at about 3200 K for color balance, while the selection of the optimal aperture diaphragm is made by inserting gray filters in the light path.

Black-and-white (B/W) digital or color cameras placed in the optical tube by means of a c-mount adapter ring are used for spatial information acquisition. The cameras must undergo calibration in three steps: white balancing, gamma correction, and matrix correction. The camera is interfaced with the computer by means of a Firewire or USB port. The standard time for digitalization and quantization is 40 ms. Up-to-date high storage disks (terabytes) eliminate storage problems.

Slides from environmental samples are prepared in the laboratory and acquired by the digital microscope station. To obtain a higher density of cells for slide, some preliminary sedimentation procedure of the environmental samples may be necessary. Using a bright field microscope, the slide is entirely scanned following a boustrophedonic path by means of a motorized microscope stage. One thousand images can be acquired from a slide containing about 15 microliters of environmental sample (400 μm^2 coverslip surface, ~30 μm sample height).

The goal of image processing algorithms is to identify microalgae in the acquired images for extracting their morphological and spectral features. The standard algorithms used by most of the research groups consist of several phases: denoising (enhancing object connectivity by means of morphological and statistical operations), thresholding (finding the correct boundaries between regions on the basis of their discontinuities in a grayscale or color space), segmentation (partitioning the images in a set of regions that collectively cover the entire image), and contour detection (identifying the closed boundary that delineates intensity transitions between the algae and the background). Different features are calculated for each processed image, which describe the characteristics of the different microalgae and enable their classification. The outcome of the whole procedure is the identification of the objects recognized as microalgae, which are represented as vectors containing morphological and spectroscopic features.

For clustering the microalgae in taxonomic groups, these calculated vectors are used as input for artificial neural networks (ANNs). ANN models are used because they can solve problems of classification of raw data with remarkable success. ANNs are non-linear statistical data models that consist of artificial neurons, that is, equations that simulate the functioning of biological neurons, with forward and backward connections in a hierarchy of layers.

At the present stage of development, DM is not yet ready for field analysis applications, though it is very promising for automatic environmental monitoring and protection of public water supplies. So far, digital microscopy achieved satisfactory results only for a limited number of species. Even if hundreds of morphological features can be calculated from each microalga, they do not always allow a reliable affiliation to a systematic group. The absorption spectrum of the pigments present inside the photosynthetic compartment of each alga, or its shortcut, that is, the characteristic color that can be obtained with a simple color camera, should to be considered an essential feature for algal recognition.

Automatic classification procedures produce satisfactory results if compared with those obtained by an expert taxonomist, irrespective of the different hardware architectures and software strategies, though a comparison of the different automatic classification systems is difficult mainly

because they have been trained, tested, and validated on different taxonomic groups. The main misjudgments are mainly caused by cell groups, in which the microalgae do not show their typical morphological features or are out of focus, or by a wrong classification of non-plankton particles and unidentified objects. These errors are about 10% of the examined cells.

To give an idea of the time necessary for a complete analysis of an environmental sample (from image acquisition to result validation), the digital microscope system we developed can be used as an example. The hardware setup is based on a high-quality transmission microscope equipped with a CCD color camera and a polychromator-based spectrophotometer (cf. Figure 7.14 in Chapter 7). The cell features used are morphological and spectroscopic features, with major weights for the dissimilarity measure of the cell contours and the characteristic colors of the segmented microalgae. The database contains 53,869 algal images divided into 24 taxonomic groups; the time necessary for scanning a slide (1000 microscope fields) and building the input dataset is about 4.5 minutes. Most of this time is spent in removing the out-of-focus-cells. The ANN training process takes about 3.5 minutes. The resulting average accuracy is 98.6%, verified by a phycology expert.

Though this overview is over-simplified, we can draw a pros and cons list of the presented methodologies. Flow cytometry is the fastest but less accurate; metagenomics is the most accurate, but it needs sound knowledge and a lot of patience; remote sensing can be used mainly for macro-scale analysis; digital microscopy has very good accuracy, but lab systems so far available are mainly limited to relatively narrow taxonomic groups. Still, it is the best compromise up to now.

The average price for the setups of all these methodologies is over $100,000. Leasing lab equipment is becoming a possible solution for accessing all the machines need in a lab, especially the most expensive ones.

ALGAE AS TOOLS FOR BIOREMEDIATION

Heavy Metals

Heavy metals such as copper and zinc can be essential trace elements for photosynthetic organisms. In higher concentrations, however, these metals, as well as other nonessential metals such as chromium, lead, mercury, and cadmium, have severe toxic effects.

All these metals, ultimately derived from a growing number of diverse anthropogenic sources (industrial effluents and wastes, urban runoff, sewage treatment plants, boating activities, agricultural fungicide runoff, domestic garbage dumps, and mining operations), have progressively affected an increasing number of terrestrial and aquatic ecosystems. Toxicity may result in diverse effects, which depend on the type of algae, the nature and concentration of the metal, and the environmental conditions accompanying heavy metal stress. Interestingly, nutrient availability (in particular nitrogen) dramatically increases the ability of algae to accumulate heavy metals, suggesting that agricultural runoff into fresh water and coastal areas will greatly increase the entry and the consequent concentration of heavy metals into the food chain. The concentration may occur through the action of chelators, which directly bind and store the metal ions, as well as by induction of defense mechanisms that allow the cell to reduce the toxic effects of the metals. Generally, heavy metal toxicity is related to the oxidative damage induced in living systems, which can be promoted by both directly increasing the cellular concentration of reactive oxygen species and reducing the cellular antioxidant capacity. At high concentrations, ROS can be extremely harmful to organisms, since they can oxidize proteins, lipids, and nucleic acids, often leading to alterations in cell structure and mutagenesis. Potential targets for peroxidation are the chloroplasts, which have a complex system of membranes rich in polyunsaturated fatty acids. Therefore, modulation of chloroplastic antioxidants seems to be a particularly important strategy, allowing algae to acclimate to environmental stress. Under acute conditions, however, the toxic effects of the pollutants may overwhelm the antioxidant defenses. This may result in cell death or the shutdown of all cellular machinery. Growth inhibition

and chlorosis are common symptoms of metal phytotoxicity in several algae, in which photosynthesis is probably the most affected metabolic process.

Algae are able to tolerate certain concentrations of heavy metals by adsorption (physical sequestration at the cell surface) or absorption (metabolic uptake). Algal surfaces (cell wall and mucilage) contain different functional groups such as carboxyl, hydroxyl, amine, sulfate, and other charged groups which are created by their carbohydrate, protein, and lipid components and differ in affinity and specificity towards heavy metals. In some algae, adsorption occurs directly onto the cell wall; in others, the presence of various amounts of mucilage or extracellular polymeric substances may play a key role in metal binding. Absorption of heavy metal ions via intracellular transport and chelation may follow surface adsorption. Once inside the cell, heavy metals undergo detoxification by means of binding with metal-binding peptides and proteins, binding and precipitation within the cytoplasm and/or vacuole, and sequestration with electron-dense polyphosphate granules.

Chromium (Cr) is among the most investigated heavy metal because of the high toxicity of one of its ionic forms. This metal, which is not essential for any metabolic process, is the 7th most abundant element on earth and 21st in crustal rocks. It does not occur freely in nature but as chromite $(Fe, Mg)Cr_2O_4$, an oxide mineral formed with oxygen, iron, and magnesium. Chromium concentrations in non-polluted waters vary from 2 to 10 μM in fresh waters and 0.2 to 1 μM in oceanic waters, although levels as high as 20 mM have been reported for paper mill effluents and tanning wastewaters. In natural environments, Cr occurs in several oxidation states from Cr^{2+} to Cr^{6+}, with trivalent and hexavalent states being the most stable and frequent in the terrestrial environment. Cr^{3+} and Cr^{6+} differ in terms of mobility, bioavailability, and toxicity.

Cr^{3+} is an essential trace element for humans; together with insulin, it removes glucose from blood and plays a vital role in fat metabolism. Cr^{3+} compounds are water insoluble because they are largely bound to floating particles in water and therefore are relatively innocuous and immobile. Cr^{6+} compounds are toxic and are among the causes of lung cancer. Cr^{6+} moves readily through soil and aquatic environments due to its high solubility in water (1680 g L^{-1}) and is a strong oxidizing agent capable of being absorbed through the membranes. In oxygen-saturated environment Cr^{3+} oxidizes to Cr^{6+}, which can easily cross cell membranes, with highly toxic effects due to the increase of reactive oxygen species and reduction of cell antioxidant capacity. In algae and plants, Cr^{6+} affects mainly the photosynthetic machinery extremely sensitive to peroxidation.

The presence of chromium in aquatic environments leads to the selection of specific algal populations, which can play the role of either indicators or bioremediators, thanks to a bio concentration factor (i.e. the ratio of the concentration of the chemical inside the organism to the concentration of the chemical in the surrounding environment) up to 10^4. An impressive and deterministic discrimination between these two roles can be obtained by microspectroscopy (cf. Chapter 7), as demonstrated by the analysis of the effects of increasing concentration of Cr^{6+} on three different fresh water microalgae: *Chlamydomonas reinhardtii, Eudorina unicocca*, and *Chlorella kessleri*.

These algae differ in their covering: *Chlamydomonas* is a naked cell; *Eudorina* possesses a mucilage cover, whereas *Chlorella* is surrounded by a cell wall. In vivo microspectroscopy allowed the monitoring of chlorophyll degradation with the consequent formation of phaeophytins, the magnesium-free derivative of chlorophylls, inside the chloroplasts. The results of this procedure showed that the differences in cell coverings correspond to different exclusion mechanisms for heavy metals (chromium in this case). Figure 6.20 shows the toxic effect of Cr^{6+} on the three algae, comparing the absorption spectra before and after the chromium treatment.

The spectroscopic contribution of phaeophytins and chlorophylls to the chloroplasts absorption spectrum was calculated using an unsupervised statistical estimation in a fully Bayesian setting that extract these spectra from the chloroplast absorption spectrum (cf. Chapter 7).

In *Chlamydomonas*, the toxic effect is dramatically rapid, and the complete pheophinitization of both chlorophyll *a* and *b* is obtained at Cr^{6+} concentration ≥ 10 μmM. Because *Chlamydomonas* cells lack a protective wall, they cannot cope with the Cr^{6+} damage of their photosynthetic machinery; hence they can be considered an effective bioindicator (Figure 6.20, top). In *Eudorina*, the toxic effect is gradual, and the complete pheophinitization of both chlorophyll *a* and *b* is reached

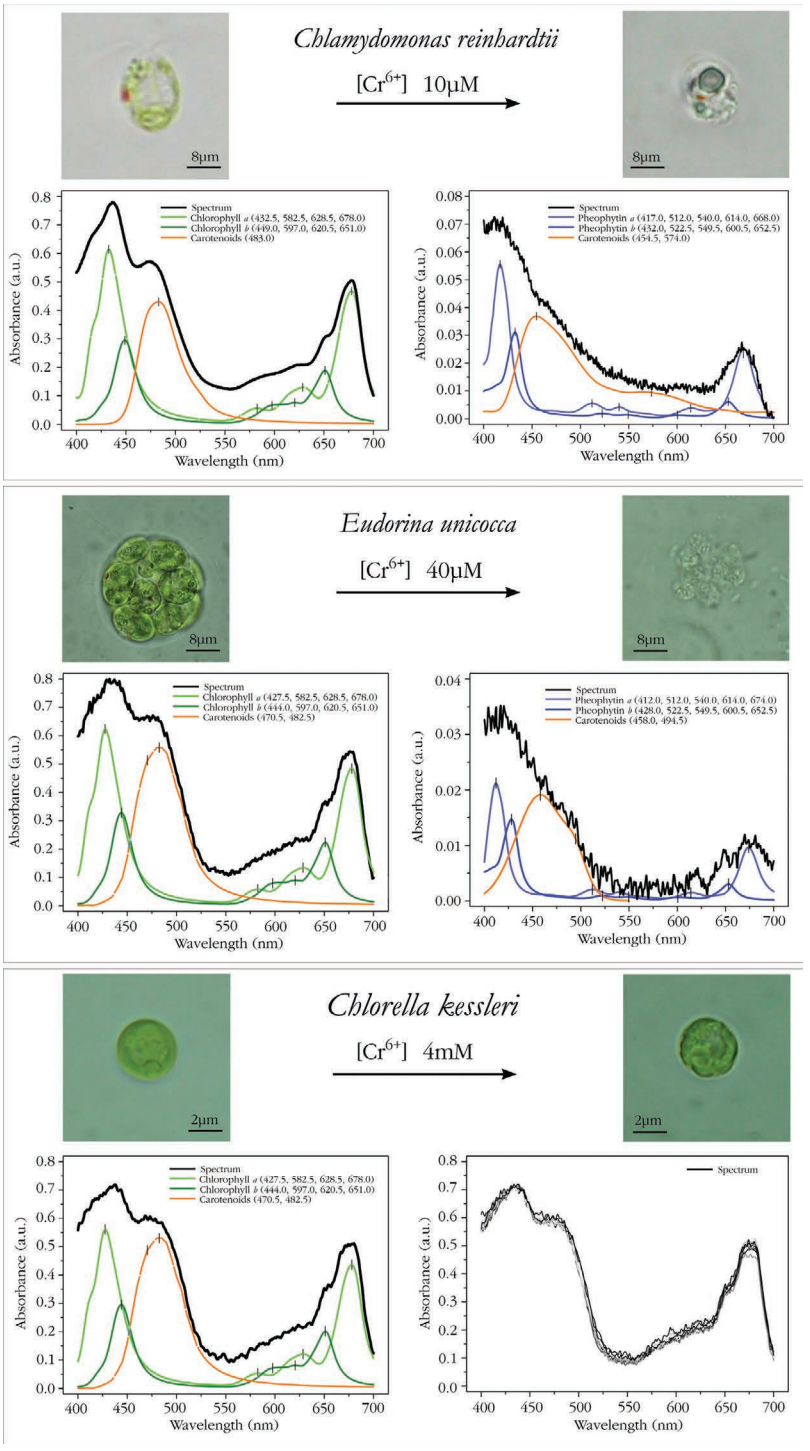


FIGURE 6.20 The toxic effect of Cr^{6+} on *Chlamydomonas, Eudorina*, and *Chlorella*.

at concentration ≥ 40 µmM. Because *Eudorina* cells are embedded in a mucilage covering, the Cr^{6+} effect is attenuated due to the difficulty of the ions to cross the mucilage barrier (Figure 6.20, center).

In *Chlorella*, Cr^{6+} up to 4 mM has almost no effect on the chloroplasts, and no pheophinitization is observed. Because *Chlorella* is protected by a robust cell wall, Cr^{6+} entrance in the cell is

completely hindered. This wall gives *Chlorella* a high removal capacity of toxic ions and allows it to survive in highly contaminated environment; hence, *Chlorella* can be considered a useful sorption tool to detoxify contaminated waste water (Figure 6.20, bottom). Once the biomass is separated by the wastewater, the metal adsorbed on the cell surface can be easily recovered with deionized water and solution of various acids, such as EDTA.

Food Industry Wastewater

According to the World Water Assessment Program of UNESCO, wastewater should be considered an untapped, valuable resource instead of a costly problem. Hence, a circular economic approach is needed to foster both innovative technologies and cost-effective solutions to manage and exploit this resource, with the aim of reducing the amount of untreated wastewater (more than 80% of the wastewater produced) and increasing its safe re-cycling and re-use but also up-cycling this waste by converting it to high-value products. In the industrial food sector, dairy enterprises are among the greatest consumers of water (from 1 to 10 m^3 of water per every cubic meter of milk processed) and therefore the largest food industry wastewater source, especially in Europe. Dairy effluents usually contain suspended and dissolved solids, soluble and trace organics, fats, chlorides, and lactose and colloidal proteins and are characterized by a high biological oxygen demand (BOD) and chemical oxygen demand (COD), high pH, and high ammonia nitrogen. Given the quantities of wastewater generated and their high load of pollutants, dairy wastewater is particularly challenging from an environmental point of view, and treatment is necessary prior to either direct (to waters such as streams, lakes, or sea) or indirect (to publicly owned treatment works) discharge. Biological treatments, which apply the metabolism of microorganisms to achieve absorption and digestion of organic matter, are preferred due to the highly biodegradable contaminants present in this type of waste.

The capability of microalgae to grow under mixotrophic conditions allows them to grow and effectively remove many pollutants (nitrogen, phosphates, organic carbon, etc.) in a wide variety of wastewater such as sewage, agricultural runoff, and food industrial effluents. This characteristic make them a promising tool for recycling and valorization of food industry wastewater, which can be exploited to reduce the high costs of their cultivation by coupling high-value biomass production with environmental bioremediation.

The filamentous cyanobacterium *Arthrospira platensis*, a promising bioethanol producer, has been successfully tested for its growing capacity on cheese whey, producing a biomass with an increased carbohydrate content compared to control. Eukaryotic algae such as *Chlorella vulgaris*, *Scenedesmus* sp., and *Chlamydomonas polypyrenoideum* have been tested for their tolerance to high nutrient loads of raw dairy wastewater, showing great potential for efficient phytoremediation and biodiesel production.

Among the tested algae for their bioremediation capacity, the spontaneous, non-photosynthetic WZSL mutant of *Euglena gracilis* proved to act as a bio-remediating organism for the tertiary treatment of dairy wastewater and simultaneously provide a source of a high-value polysaccharide, a linear β-1-3-linked glucan (paramylon), which plays the role of energy reserve for the cells. A description of the immune-activating characteristics of this glucan can be found in the section "Functional Foods and Nutraceuticals" of this chapter.

The bio-remediating capacity of this algae was tested on the raw wastewater (i.e. without any previous mechanical or chemical treatment) produced by a small dairy facility (50 t y^{-1} average cheese production) by monitoring the variation of the commonly controlled key waster parameters, that is, biochemical oxygen demand (BOD_5), soluble chemical oxygen demand, total suspended solids (TSS), ammonia nitrogen (NH_3-N), nitrate nitrogen (NO_3-N), orthophosphate (PO_4^{3-}-P), electric conductivity (EC), and pH.

The wastewater consisted of second cheese whey, generated after the production of cottage cheese, mixed with other wastewater streams. It contained mainly lactose (about 4% w/w), together

with lipids, organic acids used as technological coadjutants (i.e. lactic or citric acid), salts (i.e. $CaCl_2$), and the detergents and disinfectants used in the process.

The initial values of BOD_5, COD, NH_3-N, PO_4^{3-}-P, NO_3-N, TSS, EC, and pH in the wastewater were outside the permissible ranges for indirect discharge (Italian regulation), except for the nitrates, whose initial concentration was lower than the limit. The BOD_5/COD ratio, also known as the biodegradability index (BI), was 0.6, indicating that the waste was thoroughly biodegradable and could be effectively treated biologically. The test was conducted in a small bench scale fermenter, allowing the algae to grow inside dialysis tubing immersed in the wastewater.

The alga treatment began its remediating action after only 3 days, lowering the value of the parameters close to the limit for indirect discharge. After 4 days, the treatment produced its most dramatic effect, causing a 90% reduction of the measured parameters. At the end, after 11 days, only residual amounts of the pollutants were present in the wastewater (Figure 6.21a and 6.21b). The WZSL mutant seems particularly suitable to remediate dairy wastewater, commonly containing concentrations of NO_3-N lower than the permissible limit and concentrations of NH_3-N higher than the permissible limit, because this cell can use NH_4^+ as sole nitrogen source for growing, due to the lack of nitrite reductase, nitrate reductase, and urease for assimilating nitrogen from other sources. Moreover, since the mutant grows well in the dark, there is no need to illuminate the fermenter to foster the growth of the cells, since the mutant, unlike the photosynthetic wild type, grows well in the dark.

Figure 6.21, bottom, shows the *Euglena* mutant cell at the beginning of the experiment: paramylon granules are small and scattered within the cytoplasm, accounting for about 20% of the cell dry weight (Figure 6.21c). After 5 days, cells appear filled up with big paramylon granules, which account for about 85% of the cell dry weight (Figure 6.21d) and reach the value of about 2.6 g L^{-1}. This paramylon concentration is almost identical to that obtained with glucose, which is the optimal carbon source for the synthesis of the cell reserve. For all these features, this wastewater treatment can be considered a short-term process, which could be stopped after 5 days, obtaining the best remediating effect coupled with the highest amount of valuable polysaccharide production.

Biomass amount and BOD_5, COD, NH_3-N, and PO_4^{3-}-P concentrations are negatively correlated; that is, as the biomass increases, the pollutant concentrations decrease, meaning that the microalgae consumed the organic and inorganic load of the dairy effluent. In the case of NO_3-N and TSS, biomass increase had no influence on the concentration of these parameters because of the inability of the cells to utilize nitrite and nitrate as N source and to the lack of a direct interaction of the cells with the effluent because of the dialysis membrane.

These results demonstrate the circular sustainability of this data, which, thanks to the bioremediating capacity of the non-photosynthetic WSZL mutant, can up-cycle raw dairy wastewater by recovering the major contaminants present and transform them into a biomass consisting of about 85% dw of a high-value polysaccharide (high-value, low-impact process). This bench-scale setup could be scaled up by exploiting the design of tubular photobioreactors commonly used to grow a wide variety of microalgae; in the case of treatment plants, the dialysis tubes, either in rows or in spiral arrangement, would be immersed in the wastewater effluent circulating around them.

ALGAE IN A BIO-BASED ECONOMY

Environmental protection and energy production are among the greatest challenges facing mankind in the 21st century, while sustainability is becoming more and more a central topic in the future strategies of a bio-based economy, whose accomplishment is entirely dependent on the utilization of renewable resources, especially biomass, to produce multi-functional applications (food, feed, chemicals, fuel, power, and heat). Hence, the mandatory transition to a sustainable economy has to balance the growth of economic activities, the protection of natural resources and biodiversity, and the needs of a growing world population, expected to reach 9 billion by 2050, which is going to put enormous pressure on environmental resources. Moreover, the growth rate of agriculture will

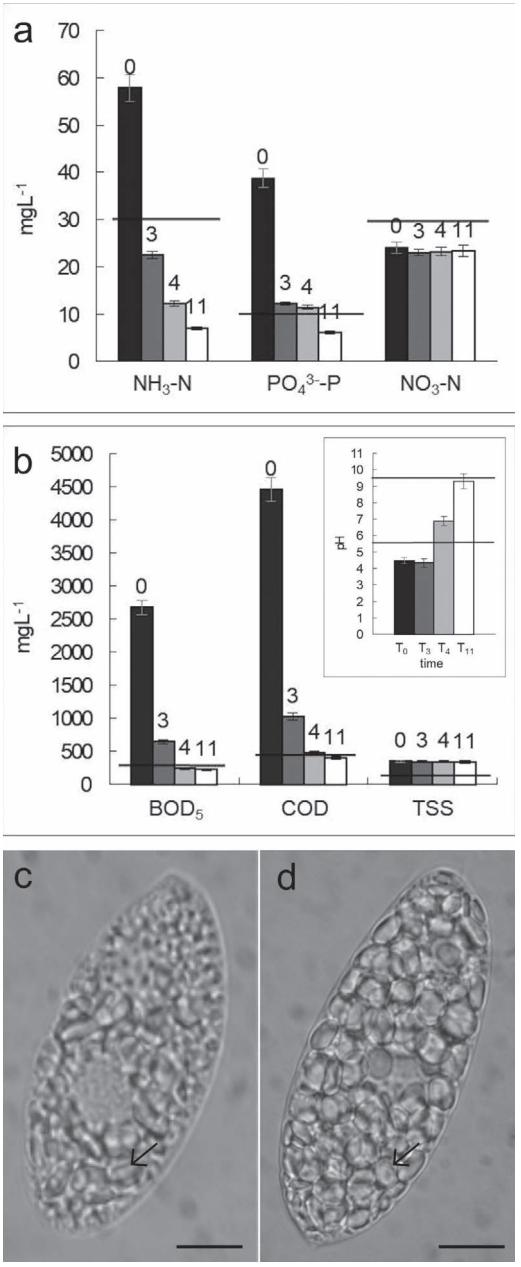


FIGURE 6.21 Remediation action of *Euglena* WZSL mutant on dairy wastewater parameters (a, b). The *Euglena* WZSL mutant cell at the beginning of the experiment (c) and after 5 days of growth in the dairy waste (d).

be limited by arable land and freshwater supply and that of fisheries by the need to lower catches to maintain healthy wild fish stocks. The new bio-economy vision will necessarily focus on the development of new kinds of bio-based products to substitute and replace old fossil-based products, aiming at opening up new markets and creating new value chains in the attempt to synchronize sustainability and economic growth.

In this panorama, algae, both micro and macro, have been gaining increasing attention for their huge potential for biorefinery processing within a circular economy framework, where they are no

longer wastes and by-products but co-products, which can also be marketed. A wide range of bio-based, high-value compounds and products can be manufactured from algal biomass together with lower-value commodity energy compounds.

As all the organisms that perform oxygenic photosynthesis (the only biological process funneling solar energy into the biosphere), algae and cyanobacteria store into their biomass the solar energy that reaches the Earth's surface at a rate of 120,000 TW y^{-1}. The current global energy demand of 15 TW y^{-1}, projected to increase to 23 TW y^{-1} by 2030, yet it falls greater than three orders of magnitude behind the solar energy on Earth. Therefore, exploitation of this potential by culturing photoautotrophs could satisfy at least part of the energy required for anthropic activities.

Microalgae (cyanobacteria plus many phyla of eukaryotes) and macroalgae span a wide variety of habitats worldwide and have high photosynthetic rates and efficiency. Under natural condition, the photosynthetic efficiency, that is, the ratio of conversion of photosynthetically active radiation to biomass free energy, can be as high as 3% in microalgae and 6–8% in macroalgae, while the efficiency of C3 plants is only about 0.2%. Higher values in the range 10–20% have been already attained for microalgae in near-optimal growing conditions, and substantially higher values are estimated possible, which are far from the theoretical maximum of photosynthetic efficiency of C3 (4.6%) and C4 plants (6%).

Algae use sunlight to grow as a completely exploitable feedstock, consisting of raw biomass, primary metabolites, and secondary metabolites. Primary metabolites (e.g. carbohydrates, most amino acids and proteins, lipids, nucleic acids, vitamins and cofactors, chlorophylls and plastidial carotenoids, minerals) are necessary for basic survival and are used for energy and tissue construction. High-value secondary metabolites, such as most polymeric carbohydrates, terpenes, diterpenes and terpenoids, phlorotannins, phenolic compounds, fucosterols, halogenated compounds, lutein, astaxanthin, fucoxanthin, lectins, and most polyunsaturated fatty acids, are assembled from primary metabolite fragments and often have vital functions but are not involved in the development or maintenance of the organism. They are limited in their biological distribution, often species-specific, and most often produced for intervention in ecological interactions. Many of these metabolites exhibit important activities such as anti-oxidative, anti-inflammatory, antifungal, antibiotic, antiviral, immune-stimulant, and antitumor factors and have the generally regarded as safe (GRAS) designation, which allows their use for human and animal consumption.

The metabolic plasticity of algae allows qualitative and quantitative tailoring of product synthesis. The production of these compounds can be integrated with bio-remediation, such as CO_2 mitigation and the removal of nutrients (N, P, NH_4^+, NO_3^-, and PO_4^{3-}), metals and heavy metals (Cr^{6+}, Cd^{2+}, Cu^{2+}, Zn^{2+}, Pb^{2+}, Hg^{2+}) from waste effluents. Microalgae are capable of enormous CO_2 capture and sequestration; theoretically, a maximum of 2350 Tg CO_2 can be sequestrated in a 100,000-km^2 microalgae culture area, accounting for 5–8% of global CO_2 emission reductions. On average, annual 539 Tg CO_2 sequestration and 324×10^6 t of microalgal-biomass yields would be achieved using a 53,000-km^2 culture area. In other words, microalgae with both open and closed culture modes could convert, in theoretical terms, 513 t of CO_2 into 280 tons of dry biomass per hectare per year using about 9% light energy to sequestrate. Microalgae can also fix CO_2 from exhaust fumes and soluble carbonates if cultivated near CO_2 point sources, such as coal or natural gas power plants or factories. As for macroalgae, they represent an important conduit for CO_2 removal from the atmosphere, with the global wild seaweed CO_2 capture estimated at 173 Tg C y^{-1} and the CO_2 capture potential of seaweed aquaculture counted as 0.68 Tg C y^{-1}.

One of the main concerns for biomass production is the life cycle extent, since shorter life feed stocks are more sustainable than longer-lived ones. Microalgae have the shortest life cycle in all biomass feedstock, ranging from 1 to 4 days, while food crops, such as rice and maize, need between 90 and 180 days. Hence, microalgae can grow very, rapidly leading to higher productivity (per unit area per year) in comparison to conventional crops. As an example, *Phaeodactylum tricornutum* cultivated in small-scale vertical tubular photobioreactors in Almeria (Spain) reached biomass productivity of about 100 t dw ha^{-1} y^{-1} (32 g m^2 d^{-1}), while soybean crops in the United States can reach biomass productivity of 2.6 t dw ha^{-1} y^{-1}.

In the case of macroalgae, most of them have complex, biphasic life cycles, involving free-living haploid gametophyte and diploid sporophyte generations. Either phase of the life cycle can be exploited, depending on the seaweed species. The harvestable biomass of kelp consists of sporophytes up to several meters long (45 m in *Macrocystis*), while in nori (*Pyropia* and *Porphyra*), the life stage of interest is the haploid gametophyte. Other exploited seaweed types, for example, *Gracilaria* and *Chondrus*, have isomorphic life cycles, with both sporophyte and gametophyte developing macroscopic exploitable thalli. The complexity of these life cycles clearly extends their length, which very often lasts months, and makes the exploitation of seaweed biomass more challenging with respect to microalgae.

For biorefinery purposes, the primary factor to consider is the chemical composition of the algal biomass, which greatly differs between micro- and macroalgae. Carbohydrates (especially sulfated and non-sulfated polysaccharides) dominate macroalgal biomass, making more than half of their dry mass (up to 84% in *Gelidium* spp.), leaving to the lipid fraction only a very low percentage (seldom more than 5% dry mass). This composition is due to the fact that macroalgae need substantially more compounds with a mechanical function for supporting the structure of the thallus, which consequently reduce the amount of lipids. The major components of microalgal biomass are proteins (up to 70% in *Arthrospira*) and lipids (more than 70% in *Botryococcus* and *Schizochytrium*). Microalgae have a higher surface-to-volume ratio with respect to macroalgae and a higher proportion of chloroplasts and hence of thylakoid membranes over the total cell volume. Since phospholipids are the main component of cell membranes, this leads to a higher content of lipids. On the other hand, both micro- and macroalgae cells contain large amounts of water, with important effects regarding post-harvest processing and quality conservation. Cell metabolism and enzyme activities continue after harvesting if the raw material is not stabilized, causing biomass deterioration. A further challenge is microbial activity in the harvested biomass, which can be faced only by adopting appropriate conservation techniques, ensuring a supply of high-quality products or processing.

Table 6.5 lists some algae biotechnology companies, products, target markets, and locations. Clearly most of the producers focus their efforts on high-value products, with returns high enough to counterbalance the economic disadvantage connected to the production/exploitation of the biomass.

Algae-Based Products: Use and Market Scenarios

The global microalgae market was valued around $900 million in 2021 and is projected to reach $1.8 billion by 2028, at a compound annual growth rate of 10.3% during the forecast period 2021 to 2028 and prevalence of the food/feed market. The growth of this market is mainly attributed to the inclination towards health and wellness trends and growing dietary supplement industry, growing demand for natural food colors, growing vegetarianism, growing nutraceutical industry, and increasing preference for microalgae-sourced products. Geographically, North America is estimated to account for the largest share of the global microalgae market in 2021, followed by Asia-Pacific and Europe. The large share of North America is primarily attributed to the huge consumption of health supplements, strict regulations against the use of synthetic colors, growth of subsidiary industries like cosmetics and biofertilizers, increasing preference for natural protein sources, and presence of key algae biomass manufacturers with huge production capacities, especially in the United States. However, Europe is expected to witness significant growth in the near future, mainly due to the increased adoption of microalgae, especially *Arthrospira* and *Chlorella*, in the manufacturing of therapeutic and nutritional products, growing reluctance towards the usage of synthetic colors, rising demand for natural blue colorants, and investments from leading color stakeholders in the phycocyanin space.

According to FAO statistics (2021), 56,546 t of microalgae were produced worldwide in 2019, supplied primarily by 56,208 t of *Arthrospira* cultivated in 10 countries and 248 t of microalgae (*Haematococcus pluvialis*, *Chlorella vulgaris*, *Tetraselmis* spp., *Dunaliella salina*) cultivated in four countries. China is the leading producer of both *Spirulina* (54,650 t, ≥97% of the global

TABLE 6.5
Some Algal Biotechnology Companies, Indicating Their Locations, Main Products, and Target Markets. All web links were accessed in April 2022.

Algae	Location	Products	Target Market	Link
Microalgae				
Aphanizomenon	USA	Bulk Biomass	Feed & Food	www.klamathafa.com
Arthrospira	USA	Micronutrients	Pharma & Personal Care	www.earthrise.com
Arthrospira/ Chlorella	Canada	EPA/DHA	Pharma & Personal Care	www.florahealth.com
Arthrospira/Chlorella	India	β-carotene/Dry Biomass	Pharma & Personal Care	www.parrynutraceuticals.com
Arthrospira	USA	Dry Biomass	Feed & Food	www.earthrise.com
Arthrospira	Japan	Dry Biomass/ Pigments	Feed & Food/Chemicals	www.dlt-spl.co.jp
Arthrospira	France	Dry Biomass	Feed & Food	www.algazur.fr
Arthrospira	The Netherlands	DHA/Cosmetics	Pharma & Personal Care	www.corbion.com
Arthrospira/Chlorella	Taiwan	Dry Biomass	Feed & Food	www.wilson-groups.com
Arthrospira/ Nannochloropsis	Germany	Dry Biomass	Feed & Food	www.bluebiotech.de
Chlorella	USA	Micronutrients	Pharma & Personal Care	www.sunchlorellausa.com
Chlorella	Germany	Micronutrients	Pharma & Personal Care	www.algomed.de
Chlorella	Japan	Micronutrients	Pharma & Personal Care	www.dlt-spl.co.jp
Chlorella	France	Micronutrients	Pharma & Personal Care	www.roquette.com
Chlorella	Germany	Micronutrients	Pharma & Personal Care	www.bluebiotech.de
Chlorella	USA	Dry Biomass	Feed & Food	www.phycom.eu
Crypthecodinium	USA/The Netherlands	EPA/DHA	Pharma & Personal Care	www.dsm.com
Cyanobacteria	USA	Micronutrient/ Bioethanol	Pharma & Personal Care/Bio-Energy	http://algenol.com/
Dunaliella	Japan	Micronutrients	Pharma & Personal Care	www.nikken-miho.com
Euglena	USA	Prebiotic β-1,3-glucan	Pharma & Personal Care	www.algaeon-inc.com
Euglena	Japan	Micronutrients/ Prebiotic/Biofuel	Pharma & Personal Care/Bio-Energy	www.euglena.jp
Euglena	USA	Micronutrients/β-1,3-glucan	Pharma & Personal Care	http://valensa.com/
Haematococcus	Sweden	Astaxanthin	Pharma & Personal Care	www.astareal.se/
Haematococcus	Israel	Astaxanthin	Pharma & Personal Care	www.algatech.com
Haematococcus	Germany	Astaxanthin	Pharma & Personal Care	www.bluebiotech.de
Haematococcus	New Zealand	Astaxanthin	Pharma & Personal Care	https://astasupreme.co.nz
Haematococcus/ Arthrospira	USA	Astaxanthin/Dry Biomass	Pharma & Personal Care	www.cyanotech.com/
Schizochytrium	China	EPA/DHA	Pharma & Personal Care	www.chinahuison.com
Microalgae	France	Micronutrients	Pharma & Personal Care	www.thalgo.com
Microalgae	France	Anti-oxidant	Pharma & Personal Care	www.algosud.com
Microalgae	USA	EPA/DHA	Pharma & Personal Care	www.cellana.com
Microalgae	USA	Biofuel/Fertilizer	Bio-Energy/Chemicals	www.algaesystems.com
Microalgae	France	Cosmetics	Pharma & Personal Care	www.greensea.fr
Macroalgae				
Chondracanthus chamissoi	Peru	Human food	Feed & Food/Pharma	algaex.pe/en/about-us/
Codium fragile	France	Cosmetics	Pharma & Personal Care	www.gelyma.com
Ulva clathrata	China	Bioactive molecules	Pharma & Personal Care	www.seawin-bio.com

TABLE 6.5 ***(Continued)***
Some Algal Biotechnology Companies, Indicating Their Locations, Main Products, and Target Markets. All web links were accessed in April 2022.

Algae	Location	Products	Target Market	Link
Eucheuma spp.	Tunisia	Carrageenans	Feed & Food/Pharma	www.seltmg.com/
Gracilaria spp.	Tunisia	Agar	Feed & Food/Pharma	www.seltmg.com/
Kappaphycus spp.	USA	Carrageenans	Feed & Food/Pharma	www.cargill.com/
Macrocystis pyrifera	France	Alginate	Feed & Food/Pharma	www.cosmetics.specialchem.com/
Monostroma nitidum	Japan	Human food	Feed & Food/Pharma	www.konanchemical.com/
Porphyra/Pyropia spp.	Spain	Human food	Feed & Food/Pharma	www.portomuinos.com/
Saccharina japonica	Germany	Human food	Feed & Food	www.la-mer.com/
Sargassum spp.	Germany	Human food	Feed & Food	www.la-mer.com/
Undaria pinnatifida	China	Human food	Feed & Food	https://en.judayang.com/

production) and *Haematococcus* (200 t, about 80% of the global production), followed by Chile and France. Most commercial microalgae cultivation is focused on the production of dried biomass destined to direct bulk purchasing by manufacturers from various industries (e.g. nutraceuticals, food and feed) for the extraction of high-value compounds (primary and secondary metabolites) and further product development.

Again according to FAO figures (2021), overall world cultivation production of macroalgae for various food and non-food uses reached 34.7 Mt in 2019 (about 96.9% of the global amount) corresponding to a market value of $14.7 billion, projected to grow to more than 24 billion in 2028. In contrast, the harvesting of seaweed from wild stocks remained at 1.1 Mt in 2019 (about 3%). Seaweed accounted for nearly 30% of the world aquaculture production in terms of wet weight and arise the fastest growing component of food production (≥7% y^{-1}), far exceeding the growth rates of agriculture (2.6% y^{-1}), livestock production (2.6% y^{-1}), and wild fisheries (0.1%y^{-1}); sustaining this high growth rate has been proposed to play a critical role in developing the capacity of feeding the more than 9 billion people populating Earth by 2050.

The growth of the seaweed market is expected to be driven by factors such as the increase of seaweed in food products, increasing consumption of seaweed-based products as a source of high nutrients and minerals (direct human consumption still representing the largest segment of the market), rising consumer adoption of plant-based products, and growing government initiatives to boost seaweed cultivation. Also, the growing demand for biofuels and technological advancements is expected to create lucrative opportunities for manufacturers in the seaweed market. The Asia-Pacific region is estimated to command the largest share of the seaweed market in 2021, followed by Europe and North America. In 2019, seaweed production in Asia contributed 97.4% of world production, and seven of the top ten seaweed producing countries were from Eastern or Southeastern Asia: China, Indonesia, Republic of Korea, Philippines, North Korea, Chile, Japan, Malaysia, Norway, and United Republic of Tanzania. The large share of the Asia-Pacific regional market is mainly attributed to the presence of several local and regional players, various government initiatives to promote the cultivation and usage of seaweed in several industries, growing demand for organic food products, and increasing applications of commercial sea vegetables, especially in food. Moreover, large-scale production and huge consumption of seaweed in the region, owing to the availability of the raw materials, favorable climatic conditions for the production of seaweed, and cheap labor availability, further support the growth of the seaweed market in the region. The Americas and Europe contributed 1.4 and 0.8%, respectively, of the world seaweed production, which was primarily fulfilled by wild collection, cultivation still being in its infancy, and limited to 4.7 and 3.9%, respectively, of total seaweed production. As for Africa and Oceania, their

contribution to the world seaweed production was only 0.4 and 0.05% respectively, cultivation being the main source of seaweed production (81.3% in Africa, 85.3% in Oceania).

Currently, more than 500 species of seaweed, belonging to 100 genera, are collected and utilized, although only 33 genera of seaweed (mainly red and brown) are harvested and/or farmed commercially worldwide. Among these, the eight genera providing the majority of the world seaweed production are red and brown macroalgae, namely *Eucheuma* spp.*, Kappaphycus alvarezii, Gracilaria* spp.*, Porphyra* spp.*, Pyropia spp., Saccharina japonica, Undaria pinnatifida,* and *Sargassum fusiforme*. In 2019 brown seaweed accounted for 47.3% of world seaweed cultivation in terms of tonnage and 52% in terms of value, while red seaweed accounted for 52.6% in terms of tonnage and 47.6% in terms of value. Green seaweed cultivation accounted for only 0.05% of all seaweed, with a world production of about 17 Kt in 2019, primarily comprising five species: *Caulerpa* spp., *Monostroma nitidum, Ulva prolifera, Capsosiphon fulvescens,* and *Codium fragile*.

Overall, the vast majority of seaweed biomass produced (about 87%) is used for direct human consumption in both fresh and dried staple food; the rest is further processed, mainly for the production of thickening ingredients (hydrocolloids such as alginate, agar, and carrageenan), used in many food and non-food products.

All the algae-based commodities can be allocated into four broad market scenarios, energy, feed and food, chemicals and materials, and pharmaceuticals and personal care. Within these markets, offer and demand for these products are growing and could grow substantially in the future. The scenarios, listed in order of decreasing value, are divided into main sectors. When no other way is specified, the data refer to the European situation.

Energy is a high-volume commodity market with fluctuating fossil fuel prices and homogenous products which are easily substituted for each other. The overall world energy consumption in 2019 was about 14,000 Mtoe (tons of oil equivalents), corresponding to about $6800 billion, with the three main sectors of electricity (50%), heating (21%), and transport (29%).

The European feed and food market is worth about 113 billion €. The feed sector is preponderant (about 111 billion €), especially due to the growth of aquaculture fish production, which covers 90% of this sector (about 100 billion €). The chemicals and materials market is worth about 13 billion € globally. Biopolymer products, mostly attributed to the packing industries, dominate the entire chemical and materials market (86%). The pharmaceuticals and personal care market is a low-volume high-value market, equally divided into the two main sectors of beauty-related products and nutraceutical/therapeutic compounds, worth 1.2 billion € each.

A large number of potential products can be identified, which break out in their use, projected markets, and selling prices.

The target markets differ for the different products; biomass is mainly funneled to the chemical and materials market and bio-energy, while primary metabolites are used in all markets. Secondary metabolites are mainly funneled into the pharmaceuticals and personal care market, with an important role as micronutrients in the feed and food market. Selling prices greatly differ between the three product groups, increasing from biomass to secondary metabolites.

Raw biomass can be used as slow-releasing fertilizer for agricultural crops and plants to improve the soil organic matter and its water holding-capacity. In case of macroalgae, their high content of polysaccharides and low amount of lignin with respect to first-generation feedstock such as sugar cane and corn make their biomass suitable for ethanol fermentation. The defatted biomass resulting from biodiesel extraction, mixed with water, can be sent to anaerobic digestion to produce biogas; it can be also a source of pigments or other bioactive compounds or a source of proteins. Residual lipids in the defatted biomass could be upcycled as supplement for animal feed. Glycerol, a byproduct of the transesterification of lipids to biodiesel, can be converted to polymers, solvents, or aliphatic polyesters or used to generate electricity directly in biofuel cells. The digestate resulting from biogas production is only used as a soil fertilizer and conditioner, similarly to animal manure.

At European level, microalgae biomass is mainly used for food supplements and nutraceuticals (24%), cosmetics (24%), and feed (19%), which together contribute to 67% of the total uses. As for

macroalgae biomass, the production is mainly used for food (36%), food-related uses (supplements, nutraceuticals, hydrocolloid production) (15%), and feed (10%), while cosmetics and well-being products contribute a 17% share of the biomass. Other applications such as fertilizers and biostimulants contribute less than 11% of the total share, and commercial application such as biofuels, bioremediation, biomaterials, and pharmaceuticals have only a small share at the European scale.

There are differences between the value of microalgae and macroalgae raw biomass, which mainly depend on the scale of production, production costs, geographical origin, applications and type of facilities, processing costs, and step of the value chain (business to business, B2B, or business to consumer, B2C). In the case of microalgae, cultivation costs are highly variable and range \$220–5,940 t^{-1} dry weight mass in large facilities using open pond cultivation up to more than \$7000 t^{-1} for sophisticated photobioreactors. At the European level, B2B values on a dry weight basis of *Arthrospira* and *Chlorella* (the two main species marketed for food and food supplements) vary between 25–50 and 30–70 € Kg^{-1}, respectively, which increases to 150–280 € Kg^{-1} for both algae in the case of B2C values. In the case of macroalgae, the minimum selling price of raw biomass at world level range between \$280 and 560 t^{-1} dry weight mass depending on the cultivation system configuration and economics (aquaculture biomass having higher production costs with respect to biomass harvested from wild stocks) but can undergo great variation depending on the applications and their added value. In the case of biomass used for direct consumption, the retail price varies mainly according to the product formulation (fresh or dry) and species identity. In Europe, the price on average is more than 100 € Kg^{-1} for dried and flaked edible seaweed, with the highest average value of 251 € Kg^{-1} belonging to *Porphyra* (nori) and the lowest average value of 25 € Kg^{-1} belonging to *Fucus*.

Primary metabolites are processed into many different bioenergy and bio-based products. Lipids (including waxes) are extracted for biofuel conversion, while polysaccharides can be converted through anaerobic fermentation to hydrogen, ethanol, butanol, and organic acids.

Glycolipids and phospholipids, soluble proteins, starches, and oligomeric sugars are converted into personal care products and pharmaceutical ingredients. Chlorophylls and thylakoid isoprenoids (sterols and primary carotenoids, such as β-carotene, lutein, and phycocyanin) are used as pigments for paints and polymers. The highest wholesale prices are those of glycolipids/phospholipids and chlorophylls, 10,000 and 15,000 € t^{-1}, respectively, while biofuels (biodiesel, bioalcohol and biohydrogen) have the lowest price <1,000 € t^{-1}.

Due to the small quantities produced, only high-value secondary metabolites such as PUFAs and secondary carotenoids are economically viable. PUFAs (especially DHA an EPA) and oxylipins are used as nutritional supplements for both human and animal consumption because of their cardiovascular health-promoting properties and pro- and anti-inflammatory activity. Secondary carotenoids, such astaxanthin, zeaxanthin, and canthaxanthin, are only accumulated after exposure to specific environmental stimuli. They are of primary importance in the pharmaceutical and personal care market because of their antioxidant capacity. They are also used as pigments in food and feed, especially for aquaculture and poultry. Sterols are used as cholesterol-lowering products and anti-inflammatory compounds. Antibiotic substances and polyketides mainly have antibacterial and antifungal activity. Heterogeneous β-glucans are very important immune stimulants for humans and bio-stimulants for plants. The highest selling prices are those of isoprenoids such as antioxidants (\$$10^6$ t^{-1}), immune-stimulant polysaccharides (\$$5 \times 10^5$ t^{-1}), and PUFAs and oxylipins sold as micronutrients and anti-inflammatory compounds (up to \$$5 \times 10^6$ t^{-1}). The other secondary metabolites have lower prices.

The overall economic turnover resulting from the exploitation of the algal biomass changes with market application. The lowest value is the of bioenergy market; biogas, bioethanol, and biodiesel have an average selling price lower than \$1 kg^{-1}, which can be considered low but still exceeded by their high downstream process costs, which average \$27 kg^{-1}. For biogas, costs cover digestion and separation of CO_2; for bioethanol, costs cover milling (wet or dry), enzymatic hydrolysis, fermentation, and distillation; for biodiesel, costs cover dry milling, CO_2 lipid extraction, transesterification,

and purification. The chemical and materials market reaches higher selling prices ($1–5 kg^{-1}) but much lower than the feed and food and personal care markets, which range from $20 to 200 kg^{-1}. These two markets sell biomass products with the highest commercial values and lowest volumes.

Exploitation of the Algae Potential for Different Target Markets

The exploitation of microalgae and macroalgae involves two stages: cultivation/production of biomass and refinery of biomass to produce bio-based products for different applications.

Cultivation/production of biomass can be divided into: (a) for microalgae, cultivation is carried in open-air systems such as ponds, raceway/circular ponds, or closed systems such as photobioreactors (PBRs) (tubular or flat panels) or fermenters; for macroalgae, the worldwide production has reached the "farming more than catching" milestone; hence, most of the biomass is mainly based on aquaculture, performed in closed systems onshore (tanks, raceways, ponds, or lagoons), in installations offshore (lines, nets, floating rafts), and even in aquaculture integrated systems, while just a minimum percentage is harvested from wild stocks. (b) For microalgae, biomass recovery is done by harvesting to separate cells from the growth media and concentrating them in a wet paste (80% moisture); it can be done using various techniques (flocculation, flotation, sedimentation, filtration, centrifugation); for macroalgae, harvesting can be manual or mechanical. Manual harvesting is used in the case of wild stocks, it includes foraging and hand harvesting (cutting by hand using a sickle or similar tool), and while it is more labor intensive, it has less impact on the environment. Mechanical harvesting can be achieved using boats with a hook-like structure that uproots seaweed or by custom-built devices (cutting dredge, suction cutter) in the case of aquaculture setups.

Biomass refining includes: (a) mechanical or chemical post-harvest of the microalgal biomass by either dewatering by drying to avoid possible deterioration of the biomass quality and stabilize it for either further processing or direct use or mechanical or chemical disruption to directly liberate the cell metabolites and improve subsequent extraction efficiency. In the case of macroalgae, the harvested biomass is washed using seawater or fresh water in order to reduce the levels of contaminating material and then dried to reduce water activity, which in turn restricts microbial growth as well as chemical and enzymatic degradation. (b) Selective extraction of products and co-products, including any of the processing routes that extract primary and secondary metabolites for the different target markets; the choice of the route depends upon both the end products and the planned use.

Cost-effective and efficient cultivation methods and systems are a major hurdle for the commercialization of microalgae as bio-feedstock, since biomass production costs are still very high compared to conventional crops. Similarly, harvesting and concentration of microalgae biomass are the most time- and energy-intensive and least scalable steps in the production process. The economic impact of these procedures depends upon both the cultivation system used, since cultures grown in open pond are more dilute than cultures grown in PBR, and the techniques used, which in turn are dependent on many factors including cell type and size, density, downstream processing required, and value of the end products. Cultivation/production yield of the biomass is highly dependent on the cultivation system and plant location, which influences the cultivation/production yield via climate: radiation, day length, temperature, and rainfall. Useful data in this regard can be gathered by the comparison of two facilities using the same three different cultivation systems (open ponds, tubular PBR, flat panel PBR) of the same area (1000 m^2) and located in two geographically and climate different countrysides. The first facility was located in in Lelystad (the Netherlands) on a 12,000-m^2 area, connected to 200 m^2 extra land for infrastructure and associated equipment. In 2015, this facility reported the following productivities: about 1.5 t for open ponds, about 3 t for tubular PBR, and about 5 t for flat panel PBR; that is, biomass production per area in flat panel PBR is more than three times and in tubular PBR twice as much as in open pond. These differences can be fully attributed to differences in the photosynthetic efficiency of the systems, 1.5% for open ponds, 3% for tubular PBR, and 5% for flat panel PBR. The second facility, located in Willemstad (Curacao), with a geographical position (13°N Lat) considered optimal for microalgae

cultivation, recorded higher annual productivity for all cultivation systems: 3.7 t for open ponds, 7.5 t for tubular panels, and 12.5 t for flat panels. Geographical position also influenced the biomass production cost; facilities located in Lelystad had the following costs: open raceway ponds produced biomass at about 35 € Kg^{-1}, while tubular and flat panel PBR produced biomass at about 19 and 12 € Kg^{-1}, respectively. In Willemstad, the prices were about half. Increasing production capacity from 1000m^2 to 100 ha reduces the price to about 6 € Kg^{-1} for open systems and 4.50 € Kg^{-1} for PBRs. This price level is still too high for bulk markets but could make high-value niche markets more profitable. Though significant reduction in cost will be difficult to achieve, biomass production cost in flat panel PBR is expected to decrease to 0.50 € Kg^{-1}.

Comparison between the different cultivation/production systems does not result in a single best solution. Each system has its own pros and cons. Open systems are simple and need a lower initial investment with respect to closed systems but at the expense of lower efficiency of CO_2 use, which leads to lower productivities, since cultures grown in these systems are about one order of magnitude more dilute than in closed systems (low volumetric productivity), and consequently greater volumes need to be processed. Moreover, open system have high risk of contamination by other algae, grazers, or bacteria and high consumption of water because of losses through evaporation. Although closed systems need a greater initial investment, they provide excellent reproducibility due to operational control, and, as already stated, they offer higher productivities and flexibility in design, construction, and operation, offering higher potential for improvement. According to a bio-economic production model, the total investment cost of a 1-ha cultivation system, either open or closed, is about 10^6 €. Upscaling to 100 ha will result in a 50×10^6 € investment for both types of systems, with superimposable breakdown of the costs, that is, the same categories and same cost percentages for each cultivation system.

In the case of macroalgae-based biorefineries, economic viability assessment of large-scale cultivation operation may be difficult, because very often a disconnect exists between the location of the macroalgae source and the conversion facility, and this generates a long list of additional costs, such as biomass transportation, facility upscaling, and biomass drying, which adds to the baseline costs relative to hatchery facility, inoculation, seeding method, and grow out. Moreover, off-shore and in-shore systems, unlike on-shore systems, cannot function year-round, due to uncontrollable environmental parameters. Reliable techno-economic data are provided by a modular process model estimating the performance of a system designed to simultaneously grow two species, *Saccharina latissima* and *Nereocystis luetkeana*, deployed off the western coast of United States in the form of a long-line released in 30 km segments. The model included the evaluation of five sub-processes: spore production in a macroalgae hatchery; line deployment and inoculation; growth; harvesting and conversion into fuel by hydrothermal liquefaction (HTL); and recovery of nitrogen and phosphorus from the aqueous phase yielded by the HTL process. For the baseline pathway of the system configuration, the minimum biomass selling price assuming a yield of 30 kg m^{-1} and 100 operational days y^{-1} was calculated to about $280 t of dry mass, quite low with respect to the price of microalgae biomass.

Figure 6.22 shows the breakdown of the costs for micro- and macroalgae biomass production in different cultivation systems. Capital cost includes the initial investment for the capital goods (land, buildings, infrastructure, cultivation and production system construction, insurance; in the case of macroalgae, also seeding vessels and machines, cranes, buoys, lines). Equipment includes the technical facilities for functioning and harvesting the biomass. Energy mostly consists of electricity consumption. Labor consists of the salary of all the people working in the plant. Consumables includes raw material and utilities such as water and CO_2 supply, fertilizers (mainly N and P), tubing, cleaning devices and chemical cleaning, and all the disposable materials. Wastewater treatment includes collection, proper delivery, and levy. The influence of the different factors changes according to the different cultivation systems. In the case of open systems, such as raceway ponds and onshore tanks, the most influential factors appear to be wastewater treatment (34 and 25%), followed by capital cost (21 and 25%), consumables (12 and 15%), and energy (12 and 15%). In the case of closed systems such as PBRs, the wastewater treatment decreases drastically (7% for tubular PBR; 8% for flat panel PBR), while the consumable factor rises up to about 36% for tubular PBR and

32% for flat panel PBR. The capital cost is slightly higher (29 and 26%, respectively), like the energy consumption (13 and 18%, respectively). For macroalgae off-shore cultivation systems and IMTA, the most influential factors are consumables for both systems (43 and 33%), followed by labor (30 and 35%), and equipment (10 and 15%). Wastewater treatments have only a minimum impact (2%), as well as energy (5%), while capital costs are limited to 10% for both systems.

Currently, there is not a complete biorefinery process developed and operating at commercial scale aiming at the exploitation of micro- and macroalgae biomass in all its possible components, that is, raw biomass, lipids, polysaccharides, pigments, proteins, and so on. Therefore, refinery of the biomass for the production of bulk commodities such as biofuel, chemical, or feed and food differs from the production of high-value compounds used as food additives or cosmetics. Processing costs are lower for bulk commodities and mainly involve drying and cell disruption steps; they result in biorefinery cost of about 1.0–2.0 € kg^{-1}. Drying microalgae, whatever the method used, has a high energy cost and is one of the constraints on commercial development. Solar drying is still problematic with current technology owing to the time and space required, and it is not recommended for microalgae products intended for human consumption. In the case of macroalgae, their high water content, commonly ranging between 63 and 92%, not only implies the need for large amounts of biomass for biorefinery but also poses a challenge for product preservation and transport, since macroalgae are characterized by rapid microbial decomposition after harvesting and are susceptible to contamination by heat-tolerant, spore-forming pathogenic bacteria that are often resistant to prolonged freezing, drying, or anaerobic conditions. Though process technologies exist that effectively stabilize macroalgae biomass, large investment costs and potentially negative impact on the quality of the product may challenge industrial implementation. Moreover, the availability of the required equipment may be limited in the proximity to harvesting sites, and investments in this equipment

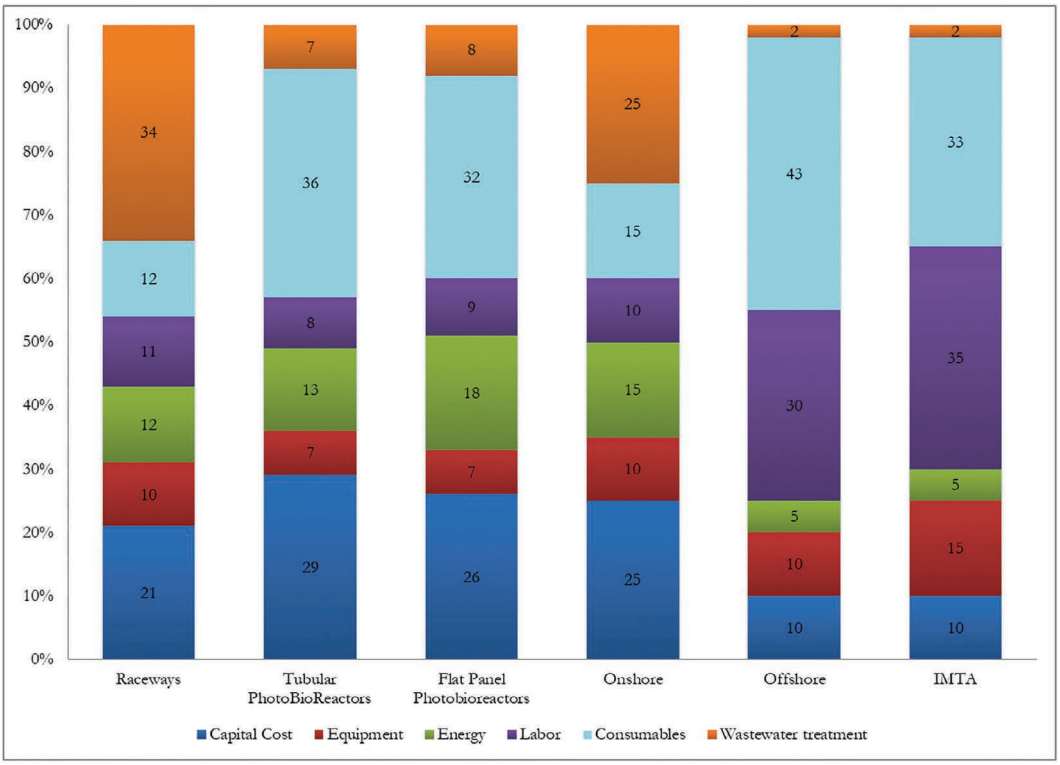


FIGURE 6.22 Cost breakdown analysis for micro- and macroalgae biomass production in different cultivation systems.

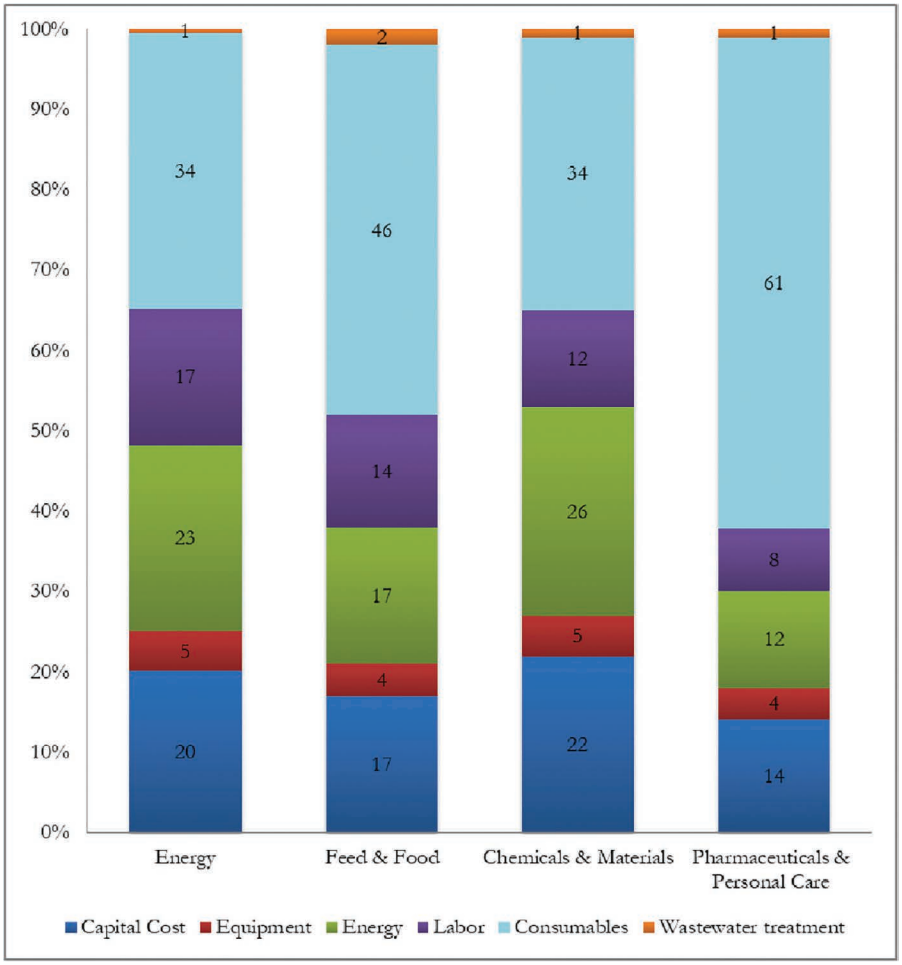


FIGURE 6.23 Cost breakdown analysis for micro- and macroalgae biomass biorefinery analyzed by four markets: energy, feed and food, chemical and materials, and pharmaceutical and personal care.

may be held back by the low use during the off season. In the case of high-value compounds, the biorefinery costs rise to 3.0–5.0 € kg^{-1}, due to the very expensive processing steps involving high amounts of consumables.

Figure 6.23 shows the detailed breakdown of the costs for biomass biorefinery. The factors considered are the same as in Figure 6.22, analyzed by the four market scenarios identified. The influence of the different factors changes according to the different markets. In the case of bio-energy, the most influential factor appears to be consumables (34%), followed by energy (23%) and capital cost (20%), while the wastewater treatment influence can be considered negligible for all the markets. The chemical and materials market has almost the same cost distribution as the bio-energy market. In the case of the feed and food market, the major cost factor is consumables (46%), which reach about 61% in the pharmaceuticals and personal care market. In these latter markets, energy is a minor cost compared to the other two markets.

Sustainability

The sustainability criteria for biomass present an opportunity for algae because algae are classified as a non-food biofuel feedstock and therefore more in line with the sustainability criteria. The

outlook for biofuels based on algae is promising. The biggest hurdle is to produce algae biofuels at a competitive price level. Another bottleneck is the required production capacity to produce huge volumes of biofuels, if algae biofuels are to be a meaningful substitute for oil. In this respect, validated and reliable assessment of economics, energetics, and environmental impact of all the processes involved in algae cultivation/production and refinery is necessary to achieve an integrative concept of sustainability. Life cycle assessment (LCA) is considered an effective tool for environmental sustainability analysis for algae production within well-defined system boundaries. This method quantifies all the relevant emissions and the resources consumed, the related environmental impacts, and the resource depletions associated with the life cycle of a product (e.g. greenhouse gas emissions, eutrophication, land occupation, pollutant emissions). LCA seeks to identify opportunities to improve the environmental footprint of products at different phases of their life cycle and should be performed for each algae-based production system. For an accurate LCA, system boundaries, which can include all the different steps of biomass exploitation (cultivation, harvesting, transformation in products, delivery of the products, and their final use), or just some of them, and functional units (i.e. a reference to which all the input and output can be related) have to be clearly defined to allow comparison of the different results. LCA uses two indicators, the net energy ratio (NER) and the global warming potential (GWP). The NER evaluates the overall energetic effectiveness (i.e. the relation between the energy demand for all the processes needed to obtain algal products and the energy stored in those products) of all the sub-processes in the analyzed system, while GWP, calculated through equivalent CO_2 emission per energy units, measures the climate impact of the emissions of all sub-processes.

The NER value is fundamental when algae are cultivated for bioenergy or as sources of feed and food to be competitive with fossil fuel– and crop-based food commodities, but up to now, LCAs have been performed mostly on algae production for biofuel. In detail, the NER, expressed as the ratio between the energy output and input (without solar energy), indicates the sustainability of the processes; when its value is lower than 1, it means that the fossil energy required for the production process is more than the energy produced by the system; that is, the system is not productive.

Data relative to the cultivation and biomass production of *Nannochloropsis* sp. in three different systems reported NER values of 8.34 in raceway ponds, 4.5 for flat reactors, and 0.2 for tubular reactors. In this case, the LCA did not include the energy required for preparation of the culture medium, inoculation, oil extraction, and subsequent production of biofuels, limiting the energy consumption terms to air pumping and costs of all the equipment and construction. Within the same system boundaries, cultivation and production, but with a different microalga, *Scenedesmus obliquus*, NER was shown to vary (from 0.39 to 7.81) as a function of the reactor light-path (2–16 cm) and power input (20 or 50 Wm^{-3}).

More precise NER calculations are those for two 1-ha plants for cultivation, biomass production, and harvesting (wet biomass 70–80% moisture) of *Tetraselmis suecica* in central Italy (Europe); one plant was made of flat panel bioreactors, and the other plant was made of flat panel bioreactors integrated with photovoltaic panels. The first plant had a productivity of 66.0 t ha^{-1} y^{-1} (330 operation days) and a biomass energy content (i.e. the potential energy content) of 22.2 MJ kg^{-1}; the product of these two figures gave the energy output of the system, which was 1465 GJ ha^{-1} y^{-1}. Since the energy inputs (energy consumed for construction; all the equipment, fertilizers, and chemicals; electricity consumption of the electromechanical equipment for mixing, cooling, and harvesting) were 1781 GJ ha^{-1} y^{-1}, the NER was 0.82. In the second plant, with the same productivity, the same biomass energy content, and the same energy output (1465 GJ ha^{-1} y^{-1}), the energy inputs decrease to 848 GJ ha^{-1} y^{-1}, resulting in a NER of 1.73. This empirically accurate analysis indicates that microalgae biomass production is still not economically sustainable when compared to traditional crops such as soybean, corn, or cassava, which reach NERs of 3.71, 4.11, and 7.57, respectively, within the same system boundaries. By comparing NER data for microalgae to biofuel present in the literature, with boundaries including all the steps from biomass cultivation to biofuel transportation to a gas station (well to pump, WtP), values range from 0.44 to 2, which are far from being competitive with the

5.55 NER value of fossil fuel production. As for LCA, the variability of NER values is mainly due to the fact that the boundaries of the analyzed systems are not comparable and not all the energy input factors are evaluated (e.g. consumption and recycling of high-cost nutrients such as inorganic N and P), which can positively alter the figures.

As for macroalgae, LCA can quantify the direct and indirect environmental impacts of their cultivation, that is, the overall environmental performance of product (and production) systems, especially nutrient (N and P) and carbon (C) equivalent emissions, by quantifying their cradle to grave (or gate) contribution to a range of impact categories. Some LCA studies have been conducted with a focus on specific aspects of seaweed supply chains, for instance wild harvests and valorization strategies, photobioreactor cultivation and oil extraction, macroalgae biorefinery, and production of biofuels from cultivated seaweed biomass. Few studies have chosen to concentrate solely on cultivation, instead including cultivation within the context of a biorefinery system (e.g. for biofuel production), with several studies also addressing sustainability in the context of high-value compounds and bioplastics. Recently, LCA was used to evaluate potential environmental impacts associated with using *Saccharina latissima* as a feedstock for single cell oil (SCO) production through yeast fermentation as part of a biorefinery concept, also including in the assessment the energy and resource consumption associated with the system. SCOs can be used for food, biochemicals, and biodiesel, replacing existing terrestrial oils or higher-value oils and fats such as coconut oil or cocoa butter depending on the molecular composition. This LCA was also expanded to coproducts: protein production and the fragrance chemical 2-phenylethanol. This analysis yielded a climate change impact between 2.5 and 9.9 kg CO_2 eq kg^{-1}, where both variations in seaweed carbohydrate composition and fermentation productivity were taken into account. At the higher end, this is comparable to other single cell oil production processes and at the lower end comparable with terrestrial oil production.

GWP evaluates the net emissions of the greenhouse gases, such as CO_2, CH_4, N_2O, and NH_3, from algae production systems, though data present in literature are mainly limited to CO_2. Carbon credits have been calculated for a WtP system based on the cultivation of *Scenedesmus dimorphus*, with emissions partitioned among the sub-processes such as growth, dewatering, and biooil recovery, through either hydrothermal liquefaction (HTL) or pyrolysis. In both cases, the production systems benefit from a carbon credit due to the CO_2 uptake by the growing microalgae (−220 g CO_2 eq MJ^{-1}). When compared to conventional diesel (+15 g CO2 eq MJ^{-1}), only the microalgae biodiesel obtained through the HTL process produces fewer emissions and does not consume all the CO_2 credit (−10 g CO2 eq MJ^{-1}). Emissions from biodiesel obtained by pyrolysis are much higher than those of the conventional diesel due to the very energy intense steps of biomass drying and heating inside the reactor (+210 g CO_2 eq MJ^{-1}). However, both these values are still higher than that of biodiesel obtained by soybeans (−80 g CO_2 eq MJ^{-1}).

In the case of macroalgae cultivation systems, the model already cited, designed to simultaneously grow two species, that is, *Saccharina latissima* and *Nereocystis luetkeana*, yields extremely favorable results in terms of GWP. These data suggest that macroalgae fuel systems are environmentally favorable over petroleum-based fuel systems and have lower process emissions than biodiesel from canola oil (45.6 g CO2 eq MJ^{-1}) and soybean oil (51.5 g CO2 eq MJ^{-1}).

SELECTED READINGS

Abdulquader, G. Barsanti, L. and Tredici, M.R. Harvest of *Arthrospira platensis* from Lake Kossorom (Chad) and its household usage among the Nanembu. Journal of Applied Phycology, 12, 493–498, 2000.

Adams, J.M., Morris, S.M., Steege, L., Robinson, J. and Bavington, C. Food-grade biorefinery processing of macroalgae at scale: Considerations, observations and recommendations. Journal of Marine Science and Engineering, 9, 1082, 2021.

Amador-Castro, F., García-Cayuela, T., Alper, H.S., Rodriguez-Martinez, V. and Carrillo-Nieves, D. Valorization of pelagic sargassum biomass into sustainable applications: Current trends and challenges. Journal of Environmental Management, 283, 112013, 2021.

Amin, I. and Hong, T.S.S. Antioxidant activity of selected commercial seaweeds. Malaysian Journal of Nutrition, 8, 167–177, 2002.

Araújo, R., Vázquez Calderón, F., Sánchez López, J., Azevedo, I.C., Bruhn, A., Fluch, S., Garcia Tasende, M., Ghaderiardakani, F., Ilmjärv, T. and Laurans, M. Current status of the algae production industry in Europe: an emerging sector of the blue bioeconomy. Frontiers in Marine Science, 7, 1247, 2021.

Arumugam, N., Chelliapan, S., Kamyab, H., Thirugnana, S., Othman, N. and Nasri, N.S. Treatment of wastewater using seaweed: A review. International Journal of Environmental Research and Public Health, 15, 2851, 2018.

Barinova, S., Klochenko, P. and Belous, Y.P. Algae as indicators of the ecological state of water bodies: methods and prospects. Hydrobiological Journal, 51, 2015.

Barsanti, L. and Gualtieri, P. Is exploitation of microalgae economically and energetically sustainable? Algal Research, 31, 107–115, 2018.

Barsanti, L., Bastianini, A., Passarelli, V., Tredici, M.R. and Gualtieri, P. Fatty acid content in wild type and WZSL mutant of *Euglena gracilis*. Journal Applied Phycology, 12, 515–520, 2000.

Barsanti, L., Birindelli, L., Gualtieri, P. Water monitoring by means of digital microscopy identification and classification of microalgae. Environmental Science: Processes & Impacts, 23, 1443–1457, 2021.

Barsanti L, Birindelli L, Gualtieri P. Paramylon and Other Bioactive Molecules in Micro and Macroalgae. *International Journal of Molecular Sciences*. 2022; 23(15):8301. https://doi.org/10.3390/ijms23158301

Barsanti, L., Ciurli, A., Birindelli, L., Gualtieri, P. Remediation of dairy wastewater by *Euglena gracilis* WZSL mutant and β-glucan production. Journal Applied Phycology 33:1, 431–441 2021.

Barsanti, L., Coltelli, P., Evangelista, V. and Gualtieri, P. Swimming patterns of the quadriflagellate *Tetraflagellochloris mauritanica* (Chlorophyceae, Chlamydomonadales). Journal Phycology, 52, 209–218, 2016

Barsanti, L., Coltelli, P., Evangelista, V., Gualtieri, P. Water monitoring. Environment Science Progress & Impact, 16, 2656–2666, 2014.

Barsanti, L., Gualtieri, P. Paramylon treatment improves quality profile and drought resistance in *Solanum lycopersicum* L. cv. Micro-Tom. Agronomy, 9, 394, 2019.

Barsanti, L., Gualtieri, P. Paramylon, a potent immunomodulator from WZSL mutant of *Euglena gracilis*. Molecules, 24, 3114, 2019.

Barsanti, L., Passarelli, V., Evangelista, V., Frassanito, A.M. and Gualtieri, P. Chemistry, physico-chemistry and applications linked to biological activities of β-glucans. Natural Products Reports 28:3, 457–466, 2011.

Barsanti, L., Vismara, R., Passarelli, V. and Gualtieri, P. Paramylon (β-1,3-glucan) content in wild type and WZSL mutant of *Euglena gracilis*. Effects of growth conditions. Journal Applied Phycology, 13, 59–65, 2001.

Basti, L., Hégaret, H. and Shumway, S.E. Harmful algal blooms and shellfish. Harmful Algal Blooms: A Compendium Desk Reference, 135–190, 2018.

Bauenova, M.O., Sadvakasova, A.K., Mustapayeva, Z.O., Kokociński, M., Zayadan, B.K., Wojciechowicz, M.K., Balouch, H., Akmukhanova, N.R., Alwasel, S. and Allakhverdiev, S.I. Potential of microalgae *Parachlorella kessleri* Bh-2 as bioremediation agent of heavy metals cadmium and chromium. Algal Research, 59, 102463, 2021.

Baumeister, T.U., Vallet, M., Kaftan, F., Guillou, L., Svatoš, A. and Pohnert, G. Identification to species level of live single microalgal cells from plankton samples with matrix-free laser/desorption ionization mass spectrometry. Metabolomics, 16, 1–10, 2020.

Beaumont, M., Tran, R., Vera, G., Niedrist, D., Rousset, A., Pierre, R., Shastri, V.P. and Forget, A. Hydrogel-forming algae polysaccharides: From seaweed to biomedical applications. Biomacromolecules, 22, 1027–1052, 2021.

Becker, W. Microalgae in human and animal nutrition. In: Handbook of microalgae mass culture and biotechnology and applied phycology, Richmond, A. (Ed.). Blackwell Publishing, Malden (USA), 2004.

Bhattad, T., Koradiya, A. and Prakash, G. Prebiotic activity of paramylon isolated from heterotrophically grown Euglena gracilis. Heliyon, 7, e07884, 2021.

Binding, C., Pizzolato, L. and Zeng, C. EOLakeWatch; delivering a comprehensive suite of remote sensing algal bloom indices for enhanced monitoring of Canadian eutrophic lakes. Ecological Indicators, 121, 106999, 2021.

Bizzaro, G., Vatland, A.K. and Pampanin, D.M. The One-Health approach in seaweed food production. Environment International, 158, 106948, 2022.

Blas-Valdivia, V., Ortiz-Butron, R., Rodriguez-Sanchez, R., Torres-Manzo, P., Hernandez-Garcia, A. and Cano-Europa, E. Microalgae of the Chlorophyceae class: Potential nutraceuticals reducing oxidative stress intensity and cellular damage. In: Oxidative Stress and Diseases, Lushchak, V. (Ed.). InTech, Rijeka (Croatia), 2012.

Blikra, M.J., Altintzoglou, T., Løvdal, T., Rognså, G., Skipnes, D., Skåra, T., Sivertsvik, M. and Fernández, E.N. Seaweed products for the future: Using current tools to develop a sustainable food industry. Trends in Food Science & Technology, 118, 765–776, 2021.

Blouin, N.A., Brodie, J.A., Grossman, A.C., Xu, P. and Brawley, S.H. *Porphyra*: A marine crop shaped by stress. Trends in Plant Science, 16:1, 29–37, 2011.

Buchholz, C.M., Krause, G. and Buck, B.H. Seaweed and man. In: Seaweed biology, ecological studies, Wiencke, C. and Bischof, K. (Eds.). Springer-Verlag, Berlin Heidelberg, 2012.

Cai, J. Global status of seaweed production, trade and utilization. Seaweed Innovation Forum, Belize, 2021.

Cai, J., Lovatelli, A., Aguilar-Manjarrez, J., Comish, L., Dabbadie, L., Desrochers, A., Diffey, S., Garrido Gamarro, E. Geehan, J. and Hurtado, A. Seaweeds and microalgae: An overview for unlocking their potential in global aquaculture development. FAO Fisheries and Aquaculture Circular, Rome, 2021.

Camacho, F., Macedo, A. and Malcata, F. Potential industrial applications and commercialization of microalgae in the functional food and feed industries: A short review. Marine Drugs, 17, 312, 2019.

Catanesi, M., Caioni, G., Castelli, V., Benedetti, E., d'Angelo, M. and Cimini, A. Benefits under the sea: The role of marine compounds in neurodegenerative disorders. Marine Drugs, 19, 24, 2021.

Chini-Zittelli, G., Rodolfi, L. and Tredici, M.R. Mass cultivation of *Nannochloropsis* sp. in annular reactors. Journal of Applied Phycology, 15, 107–114, 2003.

Cho, T.J. and Rhee, M.S. Health functionality and quality control of laver (*Porphyra, Pyropia*): Current issues and future perspectives as an edible seaweed. Marine Drugs, 18, 14, 2019.

Chopin, T. and Tacon, A.G. Importance of seaweeds and extractive species in global aquaculture production. Reviews in Fisheries Science & Aquaculture, 29, 139–148, 2021.

Choudhary, B., Chauhan, O. and Mishra, A. Edible seaweeds: A potential novel source of bioactive metabolites and nutraceuticals with human health benefits. Frontiers in Marine Science, 8, 740054, 2021.

Cohen, Z. (Ed.). Chemical from microalgae. Taylor and Francis, London, 1999.

Coltelli, P., Barsanti, L. Evangelista, V., Gualtieri, P. Algae through the looking glass. Microscope Research and Techniques, 80, 486–494, 2017.

Coltelli, P., Barsanti, L., Evangelista, V., Frassanito, A.M. and Gualtieri, P. Water monitoring: Automated and real time identification and classification of algae using digital microscopy. Environmental Science: Processes & Impacts, 16, 2656–2665, 2014.

Coltelli, P., Barsanti, L., Evangelista, V., Frassanito, A.M., Passarelli, V. and Gualtieri, P. Automatic and real time recognition of microalgae by means of pigment signature and shape. Environmental Science: Processes & Impacts, 15, 1397–1410, 2013.

Coltelli, P., Barsanti, L., Evangelista, V., Gualtieri, P. Algae through the looking glass. Microscope Research and Techniques, 80, 486–494, 2017.

Coltelli, P., Barsanti, L., Evangelista, V., Gualtieri, P. Reconstruction of the absorption spectrum of an object spot from the color values of the corresponding pixel(s) in its digital image: The challenge of algal colors. Journal of Microscopy, 264, 31–320, 2016.

Cornish, M.L. and Garbary, D.J. Antioxidants from macroalgae: Potential applications in human health and nutrition. Algae, 25:4, 155–171, 2010.

Cotas, J., Leandro, A., Pacheco, D., Gonçalves, A.M. and Pereira, L. A comprehensive review of the nutraceutical and therapeutic applications of red seaweeds (Rhodophyta). Life, 10, 19, 2020.

Dettmar, P.W., Strugala, V. and Craig Richardson, J. The key role alginates play in health. Food Hydrocolloids, 25:2, 263–266, 2011.

di Cicco, M.R., Iovinella, M., Palmieri, M., Lubritto, C. and Ciniglia, C. Extremophilic microalgae *Galdieria* gen. for urban wastewater treatment: Current state, the case of "POWER" system, and future prospects. Plants, 10, 2343, 2021.

Dillehay, T.D., Ramírez, C., Pino, M., Collins, M.B., Rossen, J. and Pino-Navarro, J.D. Monte Verde: Seaweed, food, medicine, and the peopling of South America. Science, 320:5877, 784–786, 2008.

Doucette, G.J., Medlin, L.K., McCarron, P. and Hess, P. Detection and surveillance of harmful algal bloom species and toxins. Harmful Algal Blooms: A Compendium Desk Reference, 39–114, 2018.

Duarte, C.M., Bruhn, A. and Krause-Jensen, D. A seaweed aquaculture imperative to meet global sustainability targets. Nature Sustainability, 5, 185–193, 2022.

Evangelista, V., Barsanti, L., Frassanito, A.M., Passarelli, V. and Gualtieri, P. (Eds.). Algal toxins: Nature, occurrence, effect and detection. NATO Series A: Chemistry and Biology, Springer Science (Dordrecht, The Nederland), 2008.

Fei, C., Zou, S., Wang, T., Wang, C., Kemuma, N.D., He, M., Amin, S.A. and Wang, C. A quick method for obtaining high-quality DNA barcodes without DNA extraction in microalgae. Journal of Applied Phycology, 32, 1165–1175, 2020.

Ferdouse, F., Holdt, S.L., Smith, R., Murúa, P. and Yang, Z. The global status of seaweed production, trade and utilization. Globefish Research Programme, 124, I, 2018.
Fernández, F.G.A., Reis, A., Wijffels, R.H., Barbosa, M., Verdelho, V. and Llamas, B. The role of microalgae in the bioeconomy. New Biotechnology, 61, 99–107, 2021.
Filote, C., Santos, S.C., Popa, V.I., Botelho, C. and Volf, I. Biorefinery of marine macroalgae into high-tech bioproducts: A review. Environmental Chemistry Letters, 19, 969–1000, 2021.
Freile-Pelegrín, Y. and Tasdemir, D. Seaweeds to the rescue of forgotten diseases: A review, Botanica Marina, 62, 211–226, 2019.
Funaki, M., Nishizawa, M., Sawaya, T., Inoue, S. and Yamagishi, T. Mineral composition in the holdfast of three brown algae of the genus *Laminaria*. Fisheries Science, 67, 295–300, 2001.
Gao, G., Burgess, J.G., Wu, M., Wang, S. and Gao, K. Using macroalgae as biofuel: Current opportunities and challenges. Botanica Marina, 63, 355–370, 2020.
Georg Jensen, M., Pedersen, C., Kristensen, M., Frost, G. and Astrup, A. Review: Efficacy of alginate supplementation in relation to appetite regulation and metabolic risk factors: Evidence from animal and human studies. Obesity Reviews, 14:2, 129–144, 2013.
Glibert, P.M. and Burkholder, J.M. Causes of harmful algal blooms. Harmful Algal Blooms: A Compendium Desk Reference, 1–38, 2018.
Godvin Sharmila, V., Kumar, D., Pugazhendi, A. and Kumar, A. Biofuel production from macroalgae: Present scenario and future scope. Bioengineered 12:2, 9216–9238, 2021.
González-Pleiter, M., Cirés, S., Hurtado-Gallego, J., Leganés, F., Fernández-Piñas, F. and Velázquez, D. Ecotoxicological assessment of antibiotics in freshwater using cyanobacteria. Elsevier, 399–417, 2019.
Greene, J.M., Gulden, J., Wood, G., Huesemann, M. and Quinn, J.C. Techno-economic analysis and global warming potential of a novel offshore macroalgae biorefinery. Algal Research, 51, 102032, 2020.
Griffiths, G., Hossain, A.K., Sharma, V. and Duraisamy, G. Key targets for improving algal biofuel production. Clean Technologies, 3, 711–742, 2021.
Harel, M., Koven, W., Lein, I., Bar, Y., Behrens, P., Stubblefield, J., Zohar, Y. and Place, A.R. Advanced DHA, EPA and ARA enrichment materials for marine aquaculture using single cell heterotrophs. Aquaculture, 213, 347–362, 2002.
Hentati, F., Tounsi, L., Djomdi, D., Pierre, G., Delattre, C., Ursu, A.V., Fendri, I., Abdelkafi, S. and Michaud, P. Bioactive polysaccharides from seaweeds. Molecules, 25, 3152, 2020.
Holdt, S. and Kraan, S. Bioactive compounds in seaweed: functional food applications and legislation. Journal of Applied Phycology, 23:3, 543–597, 2011.
Hotaling, L. and Spinrad, R.W. Preparing a workforce for the new blue economy: People, products and policies. Elsevier, 2021.
Hurtado, A.Q., Neish, I.C., Ali, M.K.M., Norrie, J., Pereira, L., Michalak, I., Shukla, P.S. and Critchley, A.T. Extracts of seaweeds used as biostimulants on land and sea crops—an efficacious, phyconomic, circular blue economy: With special reference to *Ascophyllum* (brown) and *Kappaphycus* (red) seaweeds. Elsevier, 263–288, 2021.
Irianto, A. and Austin, B. Probiotics in aquaculture. Journal of Fish Diseases, 25, 633–642, 2002.
Ismail, M.M., Alotaibi, B.S. and El-Sheekh, M.M. Therapeutic uses of red macroalgae. Molecules, 25, 4411, 2020.
Jacobson, T.A., Glickstein, S.B., Rowe, J.D. and Soni, P.N. Effects of eicosapentaenoic acid and docosahexaenoic acid on low-density lipoprotein cholesterol and other lipids: A review. Journal of Clinical Lipidology, 6:1, 5–18, 2012.
Joniver, C.F., Photiades, A., Moore, P.J., Winters, A.L., Woolmer, A. and Adams, J.M. The global problem of nuisance macroalgal blooms and pathways to its use in the circular economy. Algal Research, 58, 102407, 2021.
Juarez, A.B., Barsanti, L., Passarelli, V., Evangelista, V., Vesentini, N., Conforti, V. and Gualtieri, P. In vivo microspectroscopy monitoring of chromium effects on the photosynthetic and photoreceptive apparatus of *Eudorina unicocca* and *Chlorella kessleri*. Journal of Environmental Monitoring, 10, 1313–1318, 2008.
Kiran, B.R. and Venkata Mohan, S. Microalgal cell biofactory—Therapeutic, nutraceutical and functional food applications. Plants, 10, 836, 2021.
Kumar, S., Kumar, R., Diksha, Kumari, A. and Panwar, A. Astaxanthin: A super antioxidant from microalgae and its therapeutic potential. Journal of Basic Microbiology, 61, 1–19, 2021.
Kusmic, C., Barsacchi, R., Barsanti, L., Gualtieri, P. and Passarelli, V. *Euglena gracilis* as source of the antioxidant vitamin E. Effects of culture conditions in the wild type strain in the *Euglena* natural mutant WZSL. Journal of Applied Phycology, 10, 555–559, 1999.

Kusmic, C., Barsanti, L., Di Lascio, N., Faita, F., Evangelista, V., Gualtieri, P. Anti-fibrotic effect of paramylon nanofibers from the WZSL mutant of *Euglena gracilis* on liver damage induced by CCl4 in mice. Journal of Functional Foods, 46, 538–545, 2018.

Lange, L., Connor, K.O., Arason, S., Bundgård-Jørgensen, U., Canalis, A., Carrez, D., Gallagher, J., Gøtke, N., Huyghe, C., Jarry, B., Llorente, P., Marinova, M., Martins, L.O., Mengal, P., Paiano, P., Panoutsou, C., Rodrigues, L., Stengel, D.B., van der Meer, Y. and Vieira, H. Developing a sustainable and circular bio-based economy in EU: By partnering across sectors, upscaling and using new knowledge faster, and for the benefit of climate. Environment & Biodiversity, and People & Business, Frontiers in Bioengineering and Biotechnology, 8, 2021.

Lapointe, B.E., Burkholder, J.M. and Van Alstyne, K.L. Harmful macroalgal blooms in a changing world: Causes, impacts, and management. Harmful Algal Blooms: A Compendium Desk Reference, 515–560, 2018.

Lassus, P.N.C., Hess, P. and Nézan, E. Toxic and harmful microalgae of the world ocean, international society for the study of harmful algae/intergovernmental oceanographic commission of UNESCO. IOC Manuals and Guides, 68 (Bilingual English/French), 2016.

Leandro, A., Pacheco, D., Cotas, J., Marques, J.C., Pereira, L. and Gonçalves, A.M. Seaweed's bioactive candidate compounds to food industry and global food security. Life, 10, 140, 2020.

Lee, Y. Microalgal mass culture systems and methods: Their limitation and potential. Journal of Applied Phycology, 13, 307–315, 2001.

Levasseur, W., Perré, P. and Pozzobon, V. A review of high value-added molecules production by microalgae in light of the classification. Biotechnology Advances, 41, 107545, 2020.

Lordan, S., Ross, R.P. and Stanton, C. Marine bioactives as functional food ingredients: Potential to reduce the incidence of chronic diseases. Marine Drugs, 9:6, 1056–1100, 2011.

Lourenço, S.O., Barbarino, E., De-Paula, J.C., da S. Pereira, L.O. and Marquez, U.M.L. Amino acid composition, protein content and calculation of nitrogen-to-protein conversion factors for 19 tropical seaweeds. Phycological Research, 50, 233–241, 2002.

Lu, C., Rao, K., Hall, D. and Vonshak, A. Production of eicosapentaenoic acid (EPA) in *Monodus subterraneus* grown in a helical tubular photobioreactor as affected by cell density and light intensity. Journal of Applied Phycology, 13, 517–522, 2001.

Lu, M.-M., Gao, F., Li, C. and Yang, H.-L. Response of microalgae *Chlorella vulgaris* to Cr stress and continuous Cr removal in a membrane photobioreactor. Chemosphere, 262, 128422, 2021.

Lyons, D.A., Mant, R.C., Bulleri, F., Kotta, J., Rilov, G. and Crowe, T.P. What are the effects of macroalgal blooms on the structure and functioning of marine ecosystems? A systematic review protocol. Environmental Evidence, 1, 1–6, 2012.

Malloch, S. Marine plant management and opportunities in British Columbia. Fisheries, Sustainable Economic Development Branch, Victoria (British Columbia), 2000.

Menaa, F., Wijesinghe, U., Thiripuranathar, G., Althobaiti, N.A., Albalawi, A.E., Khan, B.A. and Menaa, B. Marine algae-derived bioactive compounds: A new wave of nanodrugs? Marine Drugs, 19, 484, 2021.

Merlo, S., Gabarrell Durany, X., Pedroso Tonon, A. and Rossi, S. Marine microalgae contribution to sustainable development. Water, 13, 1373, 2021.

Mhadhebi, L., Laroche-Clary, A., Robert, J. and Bouraoui, A. Anti-inflammatory, anti-proliferative and anti-oxidant activities of organic extracts from the Mediterranean seaweed, *Cystoseira crinita*. African Journal of Biotechnology, 10:73, 1682–16690, 2011.

Moreira, A., Cruz, S., Marques, R. and Cartaxana, P. The underexplored potential of green macroalgae in aquaculture. Reviews in Aquaculture, 14, 5–26, 2022.

Murakami, T., Ogawa, H., Hayashi, M. and Yoshizumi, H. Effect of *Euglena* cells on blood pressure, cerebral peripheral vascular changes and life-span in stroke-prone spontaneously hypertensive rats. Journal Japanese Society Nutrition Food Science, 41, 115–125, 1998.

Nagai, T. and Yukimoto, T. Preparation and functional properties of beverages made from sea algae. Food Chemistry, 81, 327–332, 2003.

Nakashima, A., Sasaki, K., Sasaki, D., Yasuda, K., Suzuki, K. and Kondo, A. The alga *Euglena gracilis* stimulates Faecalibacterium in the gut and contributes to increased defecation. Scientific Reports, 11, 1–8, 2021.

Nakhate, P. and van der Meer, Y. A systematic review on seaweed functionality: A sustainable bio-based material. Sustainability, 13, 6174, 2021.

Natarajan, L., Omer, S., Jetly, N., Jenifer, M.A., Chandrasekaran, N., Suraishkumar, G. and Mukherjee, A. Eco-corona formation lessens the toxic effects of polystyrene nanoplastics towards marine microalgae Chlorella sp. Environmental Research, 188, 109842, 2020.

Neff, L.M., Culiner, J., Cunningham-Rundles, S., Seidman, C., Meehan, D., Maturi, J., et al. Algal docosahexaenoic acid affects plasma lipoprotein particle size distribution in overweight and obese adults. The Journal of Nutrition, 141:2, 207–213, 2011.

Niccolai, A., Venturi, M., Galli, V., Pini, N., Rodolfi, L., Biondi, N., D'Ottavio, M., Batista, A.P., Raymundo, A. and Granchi, L. Development of new microalgae-based sourdough "crostini": Functional effects of Arthrospira platensis (spirulina) addition. Scientific Reports, 9, 1–12, 2019.

Niccolai, A., Zittelli, G.C., Rodolfi, L., Biondi, N. and Tredici, M.R. Microalgae of interest as food source: Biochemical composition and digestibility. Algal Research, 42, 101617, 2019.

Olasehinde, T.A., Olaniran, A.O. and Okoh, A.I. Macroalgae as a valuable source of naturally occurring bioactive compounds for the treatment of Alzheimer's disease. Marine Drugs, 17, 609, 2019.

Onyeaka, H., Miri, T., Obileke, K., Hart, A., Anumudu, C. and Al-Sharify, Z.T. Minimizing carbon footprint via microalgae as a biological capture. Carbon Capture Science & Technology, 1, 100007, 2021.

Palthur, M.P., Palthur, S.S. and Chitta, S.K. Nutraceuticals: A conceptual definition. International Journal of Pharmacy and Pharmaceutical Sciences, 2:3, 19–27, 2010.

Pangestuti, R. and Kim, S.K. Neuroprotective effects of marine algae. Marine Drugs, 9:5, 803–818, 2011.

Park, E.Y., Kim, E.H., Kim, M.H., Seo, Y.W., Lee, J.I. and Jun, H.S. Polyphenol-rich fraction of brown alga *Ecklonia cava* collected from Gijang, Korea, reduces obesity and glucose levels in high-fat diet-induced obese Mice. Evidence-Based Complementary and Alternative Medicine: eCAM, 2012.

Pereira, H., Barreira, L., Figueiredo, F., Custódio, L., Vizetto-Duarte, C., Polo, C., et al. Polyunsaturated fatty acids of marine macroalgae: Potential for nutritional and pharmaceutical applications. Marine Drugs, 10:9, 1920–1935, 2012.

Perveen, S., Yang, L., Zhou, S., Feng, B., Xie, X., Zhou, Q., Qian, D., Wang, C. and Yin, F. β-1, 3-Glucan from *Euglena gracilis* as an immunostimulant mediates the antiparasitic effect against *Mesanophrys* sp. on hemocytes in marine swimming crab (*Portunus trituberculatus*). Fish & Shellfish Immunology, 114, 28–35, 2021.

Piconi, P. Edible seaweed market analysis. The Island Institute, Rockland, ME, 2020.

Richmond, A. Microalgal biotechnology at the turn of the millennium: A personal view. Journal of Applied Phycology, 12, 441–451, 2000.

Ridolfi, L., Chini-Zitelli, G., Barsanti, L., Rosati, G. and Tredici, M.R. Growth medium recycling in *Nannochloropsis* sp. mass cultivation. Biomolecular Engineering, 20, 243–248, 2003.

Rodríguez, M.C., Barsanti, L., Passarelli, V., Evangelista, V., Conforti, V. and Gualtieri, P. Effects of chromium on photosynthetic and photoreceptive apparatus of the alga *Chlamydomonas reinhardtii*. Environmental Research, 105, 234–239, 2007.

Roles, J., Yarnold, J., Hussey, K. and Hankamer, B. Techno-economic evaluation of microalgae high-density liquid fuel production at 12 international locations. Biotechnology for Biofuels, 14, 1–19, 2021.

Rosati, G., Barsanti, L., Passarelli, V., Giambelluca, T. and Gualtieri, P. Ultrastructure of a novel non-photosyntheic *Euglena* mutant. Micron, 27:5, 367–375, 1996.

Russo, R., Barsanti, L., Evangelista, V., Longo, V., Pucci, L., Penno, G., Gualtieri, P. *Euglena gracilis* paramylon activates human lymphocytes by upregulating pro-inflammatory factors. Food Science & Nutrition, 5, 2, 205–214, 2017.

Salehi, B., Sharifi-Rad, J., Seca, A.M., Pinto, D.C., Michalak, I., Trincone, A., Mishra, A.P., Nigam, M., Zam, W. and Martins, N. Current trends on seaweeds: Looking at chemical composition, phytopharmacology, and cosmetic applications. Molecules, 24, 4182, 2019.

Sathasivam, R., Radhakrishnan, R., Hashem, A. and Abd_Allah, E.F. Microalgae metabolites: A rich source for food and medicine. Saudi Journal of Biological Sciences, 26, 709–722, 2019.

Scartazza, A., Picciarelli, P., Mariotti, L., Curadi, M., Barsanti, L. and Gualtieri, P. The role of *Euglena gracilis* paramylon in modulating xylem hormone levels, photosynthesis and water-use efficiency in *Solanum lycopersicum* L. Physiologia Plantarum, 161, 486–502, 2017.

Schade, S. and Meier, T. Techno-economic assessment of microalgae cultivation in a tubular photobioreactor for food in a humid continental climate. Clean Technologies and Environmental Policy, 23, 1475–1492, 2021.

Shields, R.J. and Lupatsch, I. Algae for aquaculture and animal feeds. Technikfolgenabschätzung—Theorie und Praxis, 21, 23–37, 2012.

Stauffer, B.A., Bowers, H.A., Buckley, E., Davis, T.W., Johengen, T.H., Kudela, R., McManus, M.A., Purcell, H., Smith, G.J. and Vander Woude, A. Considerations in harmful algal bloom research and monitoring: Perspectives from a consensus-building workshop and technology testing. Frontiers in Marine Science, 6, 399, 2019.

Steneck, R.S., Graham, M.H., Bourque, B.J., Corbett, D., Erlandson, J.M., Estes, J.A. and Tegner, M.J. Kelp forest ecosystems: Biodiversity, stability, resilience and future. Environmental Conservation, 29, 436–459, 2002.

Stepp, J.R. and Moerman, D.E. The importance of weed in ethnopharmacology. Journal of Etnopharmacology, 75, 19–23, 2001.

Steven, A.D. Managing the societal uses of phytoplankton: Technology applications and needs. Advances in Phytoplankton Ecology, 265–297, 2022.

Takaichi, S. Carotenoids in Algae: Distributions, biosyntheses and functions. Marine Drugs, 9:6, 1101–1118, 2011.

Talyshinsky, M.M., Souprun, Y.Y. and Huleihel, M.M. Anti-viral activity of red microalgal polysaccharides against retroviruses. Cancer Cell International, 2, 8–15, 2002.

Tang, W., Llort, J., Weis, J., Perron, M.M., Basart, S., Li, Z., Sathyendranath, S., Jackson, T., Sanz Rodriguez, E. and Proemse, B.C. Widespread phytoplankton blooms triggered by 2019–2020 Australian wildfires. Nature, 597, 370–375, 2021.

Tani, Y. and Tsumura, H. Screening for tocopherol-producing microorganisms and α-tocopherol production by *Euglena gracilis* Z. Agriculture Biological Chemistry, 53, 305–312, 1989.

Toranzo, R., Ferraro, G., Beligni, M.V., Perez, G.L., Castiglioni, D., Pasquevich, D. and Bagnato, C. Natural and acquired mechanisms of tolerance to chromium in a Scenedesmus dimorphus strain. Algal Research, 52, 102100, 2020.

Turner, N.J. The ethnobotany of edible seaweeds (*Porphyra abbotae*) and its use by First Nations on the Pacific Coast of Canada. Canadian Journal of Botany, 81, 283–293, 2003.

Van den Burg, S., Dagevos, H. and Helmes, R. Towards sustainable European seaweed value chains: A triple P perspective. ICES Journal of Marine Science, 78, 443–450, 2021.

van den Burg, S., Wakenge, C. and Berkhout, P. Economic prospects for large-scale seaweed cultivation in the North Sea. Wageningen Economic Research Memorandum, 19, 2019.

van Dijk, W., van der Schoot, J.R., Edwards, M., Queguineur, B., Champenois, J., Mooney, K. and Barrento, S. An economic model for offshore cultivation of macroalgae. Swansea University, 2015. https://edepot.wur.nl/424022

Vismara, R., Vestri, S., Barsanti, L. and Gualtieri, P. Diet-induced variations in fatty acid content and composition of two on-grown stages of *Artemia* sp. Journal Applied Phycology, 15, 477–483, 2003.

Vismara, R., Vestri, S., Frassanito, A.M., Barsanti, L. and Gualtieri, P. Stress resistance induced by paramylon treatment in *Artemia* sp. Journal of Applied Phycology, 16, 61–67, 2004.

Vismara, R., Vestri, S., Kusmic, C., Barsanti, L. and Gualtieri, P. Natural Vitamin E enrichment of *Artemia salina* fed freshwater and marine microalgae. Journal of Applied Phycology, 15, 75–80, 2003.

Wilson, S., Blake, C., Berges, J.A. and Maggs, C.A. Environmental tolerances of free-living coralline algae (maerl): Implication for European marine conservation. Biological Conservation, 120, 283–293, 2004.

Zhao, C., Yang, C., Liu, B., Lin, L., Sarker, S.D., Nahar, L., Yu, H., Cao, H. and Xiao, J. Bioactive compounds from marine macroalgae and their hypoglycemic benefits. Trends in Food Science & Technology, 72, 1–12, 2018.

Zhao, J.-Y., Geng, H.-X., Zhang, Q.-C., Li, Y.-F., Kong, F.-Z., Yan, T., Zhou, M.-J., Yang, D., Yuan, Y. and Yu, R.-C. Green tides in the yellow sea promoted the proliferation of pelagophyte *Aureococcus anophagefferens*. Environmental Science & Technology, 56, 3056–3064, 2022.

Zhu, X., Zhao, W., Chen, X., Zhao, T., Tan, L. and Wang, J. Growth inhibition of the microalgae *Skeletonema costatum* under copper nanoparticles with microplastic exposure. Marine Environmental Research, 158, 105005, 2020.

www.aqua-in-tech.com

www.epa.gov/awma/monitoring/

www.fao.org/aquaculture/en/

www.fuelseurope.eu/publication/sustainable-biomass-availability-in-the-eu-to-2050/

www.marlin.ac.uk/habitats/detail/255/maerl_beds

7 Working With Light

HOW LIGHT BEHAVES

In Chapter 4 ("Photosynthesis"), we described the dual nature of light, defining it as electromagnetic radiation with particle and wave properties. Light consists of tiny packets or particles termed photons that propagate through space as electromagnetic waves. Whether transmitted to a radio from the broadcast station; heat radiating from the oven, furnace, or fireplace; X-rays of teeth; or the visible and ultraviolet light emanating from the sun, all the various forms of electromagnetic radiation share fundamental wave-like properties. Every form, including visible light, oscillates in a periodic fashion with peaks and valleys and displays its characteristic amplitude, wavelength, and frequency.

The standard unit of measure for all electromagnetic radiation is the magnitude of the wavelength (λ) and is measured by the distance between one wave crest to the next. Wavelength is usually measured in nanometers (nm) for the visible light portion of the spectrum. Each nanometer represents one-thousandth of a micrometer. The corresponding frequency (v) of the radiation wave, that is, the number of complete wavelengths that passes a given point per second, is proportional to the reciprocal of the wavelength. Frequency is usually measured in cycles per second or Hertz (Hz). Thus, longer wavelengths correspond to lower-frequency radiation and shorter wavelengths correspond to higher-frequency radiation. A wave is characterized by velocity (the speed of light) and phase. If two waves arrive at their crests and troughs at the same time, they are said to be in phase.

An electromagnetic wave, although it carries no mass, does carry energy. The amount of energy carried by a wave is related to the amplitude of the wave (how high the crest is). A high-energy wave is characterized by high amplitude; a low-energy wave is characterized by low amplitude. The energy transported by a wave is directly proportional to the square of the amplitude of the wave. The electromagnetic wave needs no medium to sustain it; unlike sound, light can travel in a vacuum.

During travel, light waves interact with matter. As a consequence of this interaction, waves are scattered or absorbed. In the following, we describe the principal behaviors of light.

Scattering

Scattering is the process by which small particles suspended in a medium of a different density diffuse a portion of the incident radiation in all directions. In scattering, there is no energy transformation but only a change in the spatial distribution of the radiation (Figure 7.1).

In the case of solar radiation, scattering is due to its interaction with gas molecules and suspended particles present in the atmosphere. Scattering reduces the amount of incoming radiation reaching the Earth's surface, since a significant portion of solar radiation is redirected back to space. The amount of scattering that takes place depends upon two factors: wavelength of the incoming radiation and size of the scattering particle or gas molecule. If particles are small compared to the visible radiation, Rayleigh scattering theory holds. It states that the intensity of scattered waves roughly in the same direction of the incoming radiation is inversely proportional to the fourth power of the wavelength. In the Earth's atmosphere, the presence of a large number of small particles compared to the visible radiation (with a size of about 0.5 μm) causes the shorter wavelengths of the visible range to be more intensely diffused. This factor causes the sky to look blue because this color corresponds to the shorter wavelengths of the sun radiation. When the scattering particles are very much larger than the wavelength, the intensity of scattered waves roughly in the same direction of the incoming radiation become independent of the wavelength, and for this reason, the clouds, made of large raindrops, are white. If there were no scattering in the atmosphere, the daylight sky would be black.

DOI: 10.1201/9781003187707-7

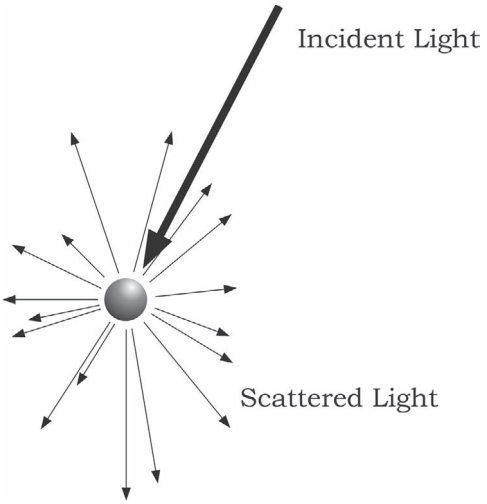


FIGURE 7.1 Light interaction with matter: the scattering process.

Absorption

Some molecules have the ability to absorb incoming light. Absorption is defined as a process in which light is retained by a molecule. As a result, the free energy of the photon absorbed by the molecule can be used to carry out work, can be emitted as fluorescence, or can be dissipated as heat.

The Beer-Lambert law is the basis for measuring the amount of radiation absorbed by a molecule; a sub-cellular compartment, such as a chloroplast or a photoreceptive apparatus; or a cell, such as a unicellular alga (Figure 7.2). The plot of the amount of radiation absorbed (absorbance, A_λ) as a function of wavelengths is called absorption spectrum. The Beer-Lambert law states that the attenuation of the intensity of the incident beam as it passes through a sample is proportional to the concentration of that sample and its thickness (path length). We have adopted this law to measure the absorption spectra of all the algal photosynthetic compartments presented in Chapter 4.

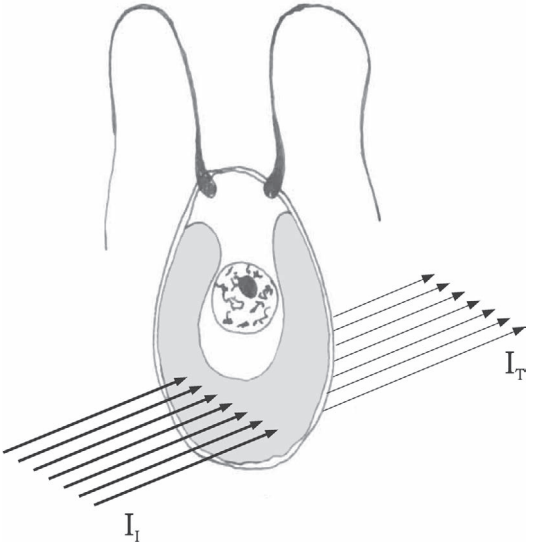


FIGURE 7.2 Light absorption by an unicellular alga; I_I: light incident on the cell; I_T: light transmitted by the cell.

The Beer-Lambert law establishes the logarithmic relationship between absorbance and the ratio between the incident (I_I) and transmitted light (I_T). In turn, absorbance is linearly related to the pigment concentration C (mol L^{-1}), the path length l (cm), and the molar extinction coefficient ε_λ, which is an intrinsic property for each chemical species at a specific wavelength.

1) $$A_\lambda = \log (I_I/I_T) = \varepsilon_\lambda Cl$$

Table 7.1 shows the comparison between transmitted light and absorbance values.

TABLE 7.1
Relationship Between Transmitted Light Percentage and Absorbance Value

Transmittance	Absorbance
100	0.000
90	0.045
80	0.096
70	0.154
60	0.221
50	0.301
40	0.397
30	0.522
20	0.698
10	1.000
1	2.000
0.1	3.000

Fluorescence

Fluorescence is the property of some molecules called fluorochromes to absorb light at a particular wavelength and consequently emit light of longer wavelength. In contrast to bright field microscopy, fluorescence microscopy is capable of imaging the precise location and/or distribution of intracellular molecules (down to a single molecular species). Because of its high specificity, sensitivity, and spatial resolution, fluorescence microscopy is an important tool especially to investigate algal cell biology (e.g. intracellular dynamics in time-resolved measurements), as we show in the book.

Fluorochromes are generally planar molecules, contain aromatic groups, and possess a specific absorption spectrum and a corresponding emission spectrum, which depend on the internal structure of the molecule and the environmental surroundings.

To understand fluorescence, we have to introduce some elementary concepts of molecular spectroscopy. In a molecule, electrons can exist in different electronic energy states. The electronic ground state (S_0) represents the most stable electronic configuration; it has the lowest energy and is the state where the electron spends most of the time. The electronic excited states ($S_{1\ldots n}$) have higher energy than the ground states and possess many vibrational energy levels. The lifetime of an electron in an excited state is short. When a fluorochrome is struck by a photon of an appropriate amount of energy (excitation wavelength), its electrons are elevated from the ground state to an excited state. This phenomenon occurs in femtoseconds (10^{-15} s). After the electrons are excited, they can dwell in this high energy state for a very short time only and decay afterwards to the lowest level of the first excited state (S_1) by vibrational relaxation in picoseconds (10^{-12} s), wasting a part of the absorbed energy. The fluorochrome then emits a photon of longer wavelength and returns to

its ground state S_0 in nanoseconds (10^{-9} s). The transition S_1–S_0 is termed molecular fluorescence. As some of the energy is lost during relaxation, the fluorochrome will emit light with an increased wavelength and lower energy compared to the absorbed light. The emitted light is non-coherent and is emitted over a spherical volume around the fluorochrome. Other de-excitation routes are possible, such as emission of a phosphorescence photon (10^{-3} s); quenching, which is due to the interaction/collision of different molecules; and dispersion of the energy as heat (infrared photon).

Fluorescence is characterized by intrinsic properties such as fluorescence spectrum, defined as the plot of the fluorescence intensity as a function of excitation wavelength; molar extinction coefficient (ε); quantum yield (Φ), and fluorescence lifetime (τ). The ε value measures the capacity of absorption of a fluorochrome, and it is the constant expressed in M^{-1} cm^{-1} in the Beer-Lambert law (cf. Equation 1). The Φ is the ratio of photons absorbed to photons emitted, expressed as a percentage. The τ measures the average time a fluorochrome spends in the excited state before returning to the ground state by emitting a photon. The lifetimes of fluorochromes can range from picoseconds to hundreds of nanoseconds.

A very simple and useful diagram that illustrates the electronic states of a molecule (ground and excited) and the transitions between them (absorption, non-radiative decay, and fluorescence) is the Jablonski diagram, in which the electronic molecular states are arranged vertically according to their energy level (Figure 7.3). The electronic states are indicated with thick lines, the vibrational

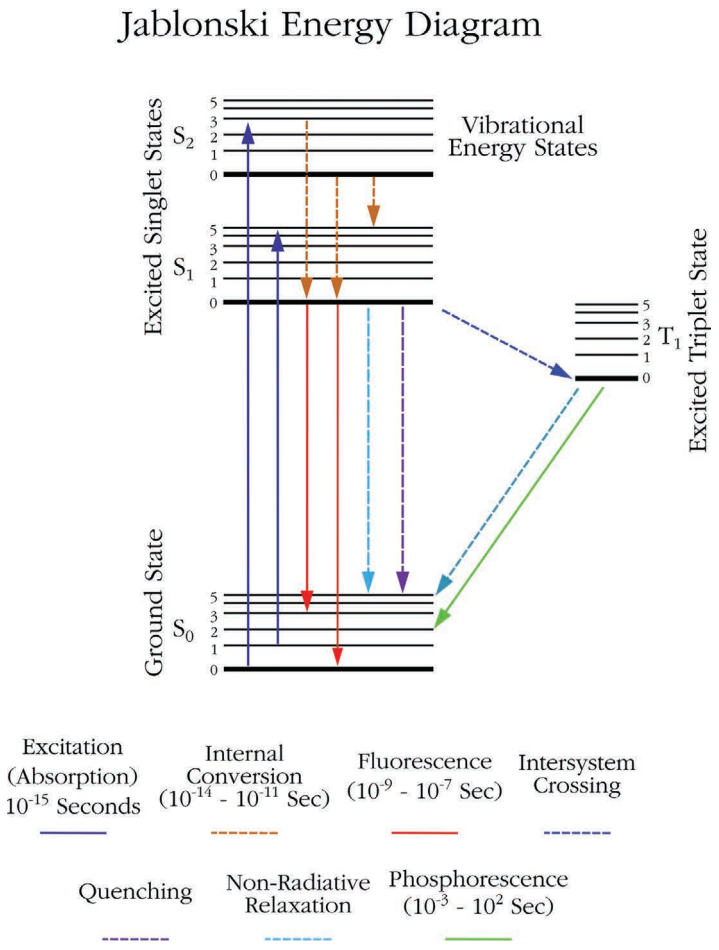


FIGURE 7.3 Jablonski diagram that illustrates the electronic states of a molecule and the transitions between them.

states with thinner lines. Non-radiative transitions are indicated by squiggly arrows and radiative transitions by straight arrows.

Interference

Electromagnetic waves can superimpose. Scattered waves, which usually have the same frequency, are particularly susceptible to the phenomenon of interference, in which waves can add constructively or destructively. When two waves, vibrating in the same plane, meet and the crest of one wave coincide with the crests of the other wave, that is, they are in phase, constructive interference occurs. Therefore, the amplitude of the wave has been increased, and this results in the light appearing brighter. If the two waves are out of phase, that is, if the crests of one wave encounter the troughs of the other, then destructive interference occurs. The two waves cancel each other out, resulting in a dark area (Figure 7.4). The interference of scattered waves gives rise to reflection, refraction, diffusion, and diffraction phenomena.

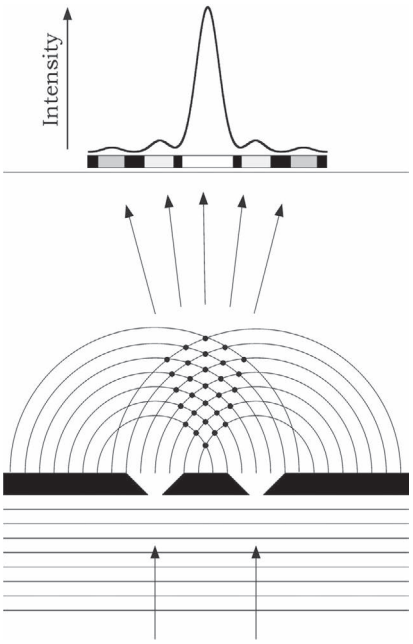


FIGURE 7.4 Interference of light passing through two narrow slits, each acting as a source of waves. The superimposition of waves produces a pattern of alternating bright and dark bands. When crest meets crest or trough meets trough, constructive interference occurs, which makes bright bands; when crest meets trough, destructive interference occurs, which makes dark bands. The dots indicate the points of constructive interference. The light intensity distribution shows a maximum that corresponds to the highest number of dots.

Reflection

Reflection occurs when light is scattered in the direction opposite of that of incident light. Light reflecting off a polished or mirrored flat surface obeys the law of reflection: the angle between the incident ray and the normal to the surface (θ_I) is equal to the angle between the reflected ray and the normal to the surface (θ_R). This kind of reflection is termed specular reflection. Most hard polished (shiny) surfaces are primarily specular in nature. Even transparent glass specularly reflects a portion of incoming light. Diffuse reflection is typical of particulate substances like powders. If you shine a light on baking flour, for example, you will not see a directionally shiny component. The

powder will appear uniformly bright from every direction. Many reflections are a combination of both diffuse and specular components and are termed spread (Figure 7.5), such as that performed by *Emiliana* blooms (cf. Chapter 2).

Now we will turn our attention to the topic of curved mirrors, specifically curved mirrors that have the shape of spheres, spherical mirrors. Spherical mirrors can be thought of as a portion of a sphere that was sliced away and then silvered on one of the sides to form a reflecting surface. Concave mirrors were silvered on the inside of the sphere, and convex mirrors were silvered on the outside of the sphere (Figure 7.6). If a concave mirror were thought of as being a slice of a sphere, then there would be a line passing through the center of the sphere and attaching to the mirror exactly in its center. This line is known as the principal axis. The center of the sphere from which the mirror was sliced is known as the center of curvature of the mirror. The point on the mirror's surface where the principal axis meets the mirror is known as the vertex. The vertex is the geometric center of the mirror. Midway between the vertex and the center of curvature is the focal point. The distance from the vertex to the center of curvature is known as the radius of curvature. The radius of curvature is the radius of the sphere from which the mirror was cut. Finally, the distance from the mirror to the focal point is known as the focal length. The focal point is the point in space at which light incident towards the mirror and traveling parallel to the principal axis will meet after reflection. In fact, if some light from the sun were collected by a concave mirror, then it would converge at the focal point. Because the sun is at such a large distance from the Earth, any light ray from the sun that strikes the mirror will essentially be traveling parallel to the principal axis. As such, this light should be reflected through the focal point.

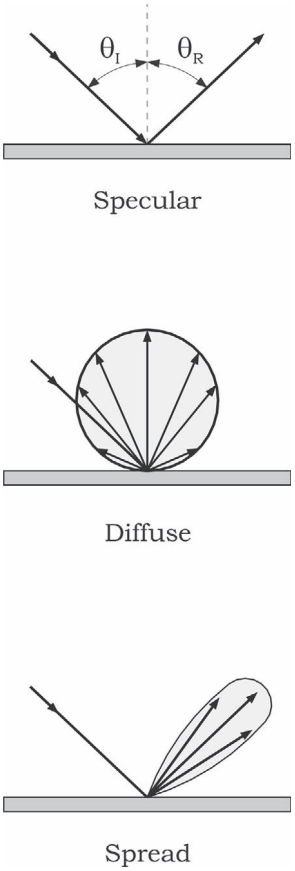


FIGURE 7.5 Different types of reflection; θ_I, angle of incidence; θ_R, angle of reflection.

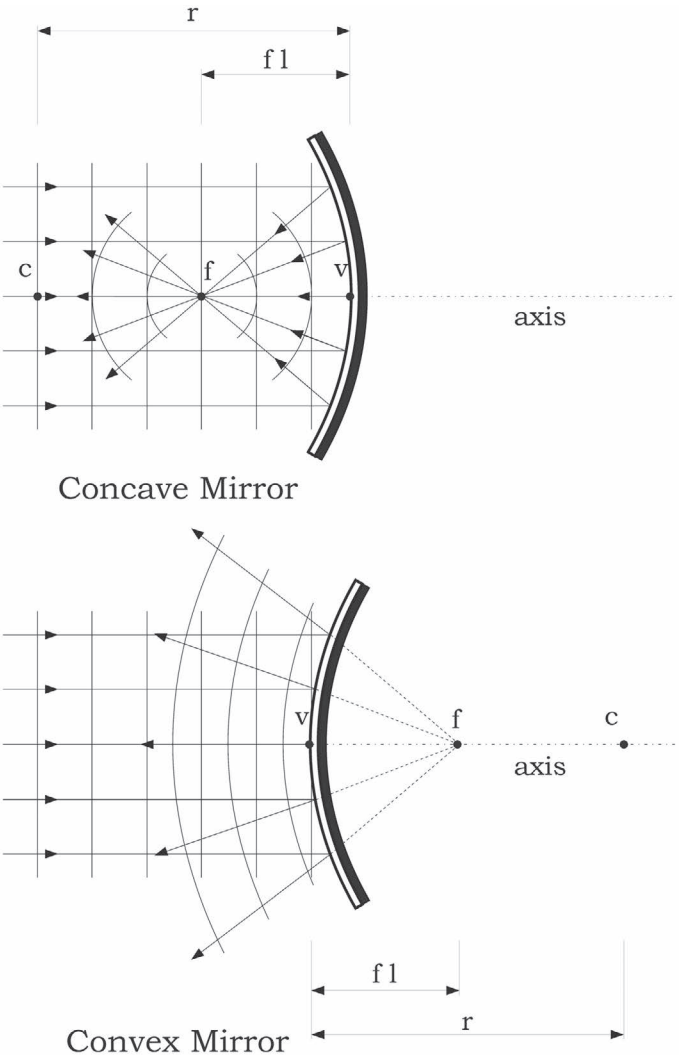


FIGURE 7.6 Curved mirrors; c: center of curvature of the mirror; v: vertex or geometric center of the mirror; f: focal point; r: radius of curvature; fl: focal length.

Unlike concave mirrors, a convex mirror can be described as a spherical mirror silvered on the outside of the sphere. In convex mirrors, the focal point is located behind the convex mirror, and such a mirror is said to have a negative focal length value. A convex mirror is sometimes referred to as a diverging mirror due to its ability to take light from a point and diverge it. Any incident ray traveling parallel to the principal axis on the way to a convex mirror will be reflected in a manner that its extension will pass through the focal point. Any incident ray traveling towards a convex mirror such that its extension passes through the focal point will be reflected and travel parallel to the principal axis.

Refraction

Refraction occurs when light is scattered in the same direction of the incident light, but, passing between dissimilar materials, its rays bend and undergo a slight velocity change. Refraction is dependent on two factors: the incident angle θ, that is, the angle between the incident light and the

normal to the surface, and the refractive index, n, of the material, defined as the ratio between the velocity of the wave in vacuum (c_v) and the velocity of the wave in the medium (c_s):

2) $$n = c_v/c_s$$

Refraction is regulated by the following relationship, termed Snell's law:

3) $$_1n_2 = \sin(\theta_1)/\sin(\theta_2)$$

where $_1n_2$ is the refractive index in passing from medium 1 to medium 2, and θ_1 and θ_2 are the angles made between the direction of the propagated waves and the normal to the surface separating the two media.

For a typical air-water boundary (n_{air} =1, n_{water} = 1.333), a light ray entering the water at 45° from normal travels through the water at 32.11° (Figure 7.7). The refractive index itself decreases with increasing the wavelength. Table 7.2 shows the refractive indices of some common materials.

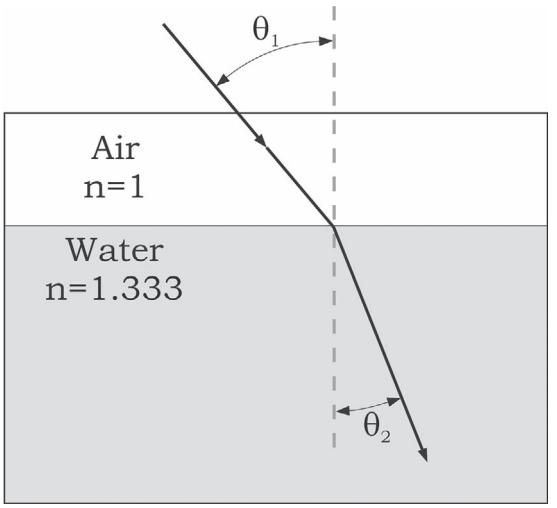


FIGURE 7.7 Refraction of a light ray passing from a medium with lower refractive index (air) to a medium with higher refractive index (water). θ_1, angle of incidence; θ_2, angle of refraction.

Dispersion

Dispersion is a phenomenon that causes the separation of light into components with different wavelengths (e.g. a rainbow) due to their different velocities in a medium other than vacuum. As a consequence, the white light traveling through a triangular prism is separated in its color components, the *spectrum* of light. The red portion of the spectrum deviates less than the violet from the direction of propagation of the white light (Figure 7.8).

Diffraction

Light waves change the propagation direction when they encounter an obstruction or edge, such as a narrow aperture or a slit (Figure 7.9). Diffraction depends upon both the wavelength of incoming radiation (λ) and obstruction or edge dimensions (a). It is negligible when the ratio a/λ is sufficiently large and becomes more and more important when the ratio tends to zero. This effect is

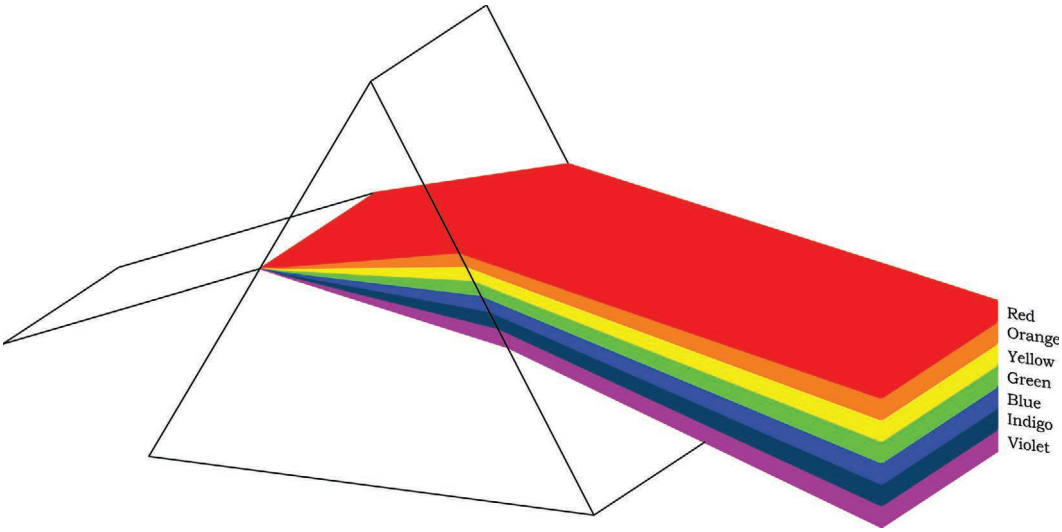


FIGURE 7.8 Dispersion of white light trough a prism: the red portion of the spectrum deviates less than the violet from the direction of propagation of white light.

TABLE 7.2
Refractive Indices of Some Common Materials

Material	Index
Vacuum	1.000
Air at STP	1.00029
Water at 0°	1.333
Water at 20°	1.332
Ice	1.309
Glycerin	1.473
Oil	1.466–1.535
Fluorite	1.434
Quartz	1.544
Glass, Fused Silica	1.459
Glass, Pyrex	1.474
Glass, Crown (common)	1.520
Glass, Flint 29% lead	1.569
Glass, Flint 55% lead	1.669
Glass, Flint 71% lead	1.805
Glass, Arsenic Trisulfide	2.040
Polypropylene	0.900
Polycarbonate	1.200
Plexiglas	1.488
Plastic	1.460–1.55
Nylon	1.530
Teflon	2.200
Salt	1.516

almost absent in most optical systems, such as photographic and video cameras, with a large a/λ; but it is very important in all microscopes, where diffraction limits the resolution a microscope can ultimately achieve (a/λ tends to zero). The resolution is the smallest distance between two points to discriminate them as separate.

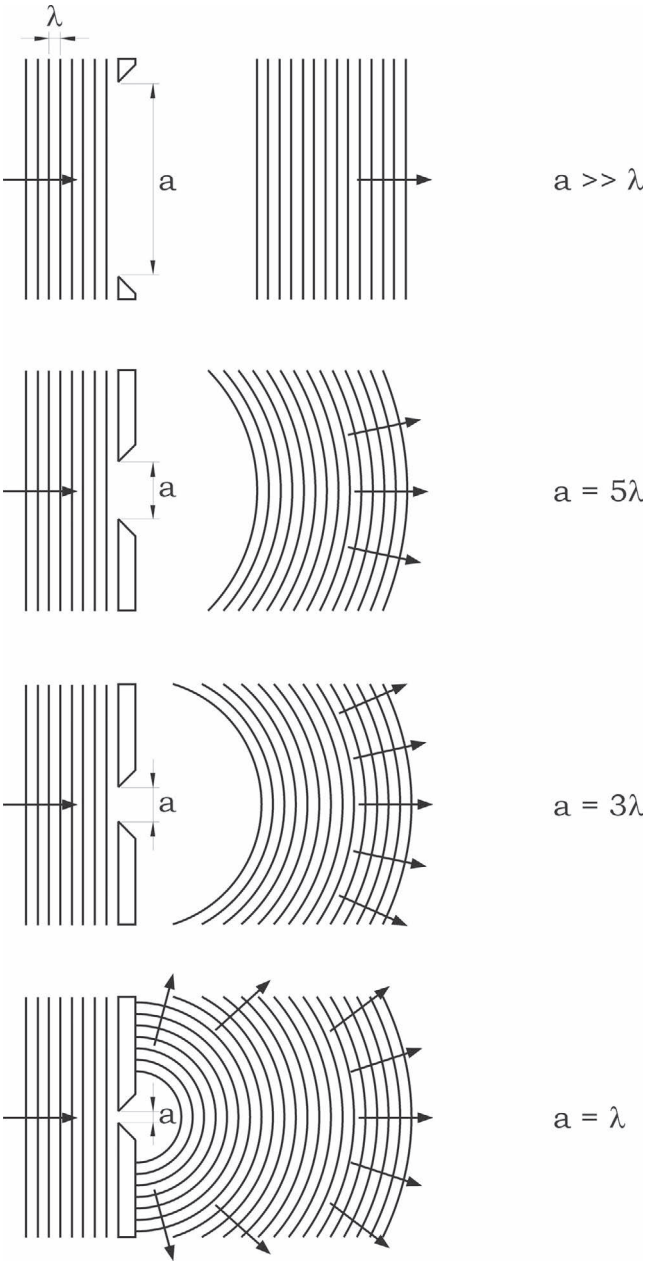


FIGURE 7.9 Diffraction of light from different width aperture; the effect increases with decreasing aperture width.

LAB INSTRUMENTS

The Microscope

In this section, we describe the very basic principles underlying the procedure for the best setting of the microscope setups mainly used in phycology. These setups are the same we used for the images of this book, that is, bright field and fluorescence microscopes.

Fundamental to the understanding of image formation in the microscope is the role of the individual lenses that make up the components along the optical path. To evaluate the action of the lenses, the wave-like properties of light can often be ignored, and we can assume that light travels in straight rays. The converging (positive) or diverging (negative) lenses are the simplest imaging elements. Lenses are typically made up of a transparent dielectric material such as fused silica or optical glass, with the front and back surfaces having the same spherical curvature. Since the surfaces are curved, each ray of light that travels in parallel to the optical axis has a different angle of incidence θ_{inc} on the lens and is refracted according to Snell's law (Equation 3) (Figure 7.10). Therefore, for a converging lens, a parallel paraxial beam of light (beam of rays traveling very close to the optical axis) coming from one side of the lens converges toward its focal point on the other side of the lens. If the light source is located in one of the two focal points, then the beam will emerge from the other side of the lens in a parallel paraxial way.

For a diverging lens, the same type of beam originating from one side of the lens will diverge with an angle determined by the position of the focal point located on the same side; that is, the projected extensions of the diverged rays will converge in this focal point. As for the converging lens, the light behavior is the same on the other side of the lens.

The space between the light source and the entrance surface of the lens is referred to as the object space, while the region between the lens exit surface and the image is known as the image space. Image formation as well as collection and collimation of the incident light inside the microscope rely on the combination of different diverging and converging lenses.

Formed images can be either real or virtual; a real image is the collection of focus points made by converging rays, while a virtual image is the collection of focus points made by extensions of diverging rays. Real images form when objects are place beyond the focal length of a converging lens; if the object is located between f and 2f, the resulting image is magnified and inverted. If the object is located beyond 2f, the resulting image will still be inverted, but smaller than the object. If the object is located between the lens and its focal point (i.e. within f), the image becomes virtual, magnified but upright. Diverging lenses form only virtual images, upright and shrunken, which are located in the object space, and result from the intersection of the projected extensions of the refracted light rays (Figure 7.10).

A real image can be visualized when projected onto a screen, captured on photographic film emulsion or a digital camera (usually a charge-couple device). Conversely, a virtual image requires the assistance of another lens or lens system to be seen by an observer, as in the case of the microscope. In normal or orthoscopic mode (see later), the microscope produces virtual images, and the crystalline lenses of the eyes form the real image on the retina.

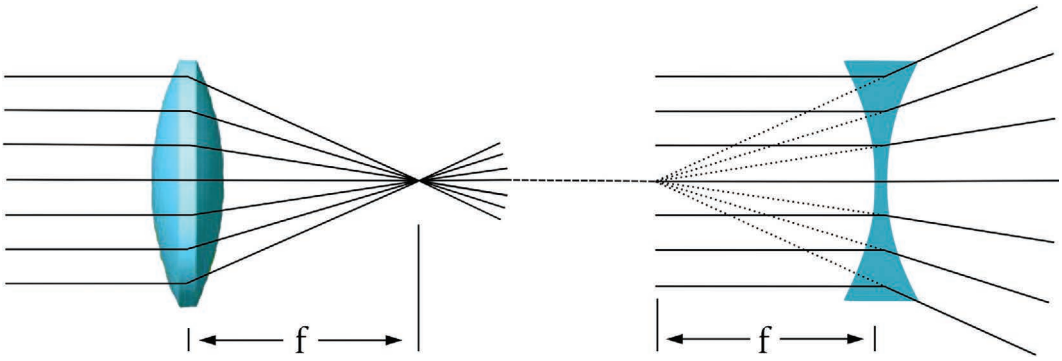


FIGURE 7.10 Converging lens (a) and diverging lens (b).

Bright Field Microscopy

We will now describe the bright field microscope optical path. The first stage is the lamp house, which contains a tungsten-halide lamp and a collector lens and is responsible for establishing the primary illumination conditions for the microscope. The light emitted by the lamp first passes through a collector lens and then into the microscope base, where it is reflected by a mirror and passes through the field diaphragm and the sub-stage condenser. The condenser forms a cone of illumination that bathes the specimen, located on the microscope stage, and subsequently enters the objective. Light leaving the objective is in turn diverted by a beam splitter/prism combination either into the eyepieces to form a virtual image or straight through the projection lens mounted onto an extension tube, where it can then form an image on a CCD camera or photo-camera targets. Filtering and conditioning devices (a.k.a. auxiliary devices) can be inserted along the optical path. The auxiliary device(s) work together to modify image contrast as a function of spatial frequency, phase, polarization, absorption, fluorescence, off-axis illumination, and/or other properties of the specimen and illumination technique.

Illumination is perhaps the most critical factor in determining the overall performance of the bright field microscope, and illumination of the specimen is the most important variable in achieving high-quality images in microscopy and photomicrography or digital imaging.

Köhler illumination is the most common optical illumination scheme for transmitted light microscopy because it serves to illuminate uniformly the image field. However, Köhler illumination has a poor photon efficiency because it fails to take advantage of using the full surface of the source or the full angular distribution of the emitted light. The basic requirements of Köhler illumination are very simple. A collector lens on the lamp housing is required to focus the light emitted by the various points of the lamp filament on the condenser aperture while completely filling the aperture. Simultaneously, the condenser should be focused to bring the sets of conjugate focal planes (a conjugate focal plane of a given plane P is the plane P′ such that points on P are imaged on P′) into specific locations along the optical axis of the microscope.

In a properly focused and aligned optical microscope under Köhler principles, there are two sets of principal conjugate planes that alternate along the optical pathway from the light source filament to the final microscope image produced on either the retina or the image plane of an electronic sensor. One set consists of four field planes (field diaphragm, specimen plan, intermediate image plan located in the eyepiece back focal plane, retina) and is referred to as the field or image-forming conjugate set; the other set consists of four aperture planes (lamp filament, condenser aperture diaphragm, objective rear focal plane, iris diaphragm) and is referred to as the illumination conjugate set. All the planes within a conjugate set are simultaneously in focus. Using the oculars, the planes of the field conjugate set can all be simultaneously viewed when the specimen is in focus (orthoscopic mode). Using a telescope eyepiece in place of an ocular and focusing the rear aperture of the objective, the planes of the illumination conjugate set can be observed (conoscopic mode). A thorough understanding of the relationships between these conjugate plane sets, and their location within the microscope, is essential to understand image formation, carry out correct adjustment of illumination, and place the optical auxiliary components. Meeting these conditions will result in a bright, evenly illuminated specimen plane, even if the light source is inherently uneven, as in the case of a tungsten-halogen lamp filament (the filament will not be in focus in the specimen plane). With the specimen and condenser both in focus, all the planes of the two-conjugate set will be in the correct position so that resolution and contrast can be optimized by adjusting the field and condenser aperture diaphragms.

The existence of two interrelated optical paths and two sets of image planes characterize Köhler illumination and is the basis that allows the various adjustable diaphragms and aperture stops in the microscope to be used to control the cone angles of illumination, and the size, brightness, and uniformity of illumination of the field of view.

Light rays that are focused in one set of conjugate planes are nearly parallel when passing through the other set of conjugate planes. Therefore, whatever appears in focus in one plane of a conjugate

set will appear in focus in all the other planes belonging to the same set and will be out of focus in the other set. This reciprocal relationship between the two sets of conjugate planes determines the way in which the two ray paths fundamentally interact to form an image in the microscope, and it has practical consequences for operating the microscope.

Figure 7.11 shows the image forming (blue rays) and illumination ray paths (red rays) through a microscope adjusted for Köhler illumination.

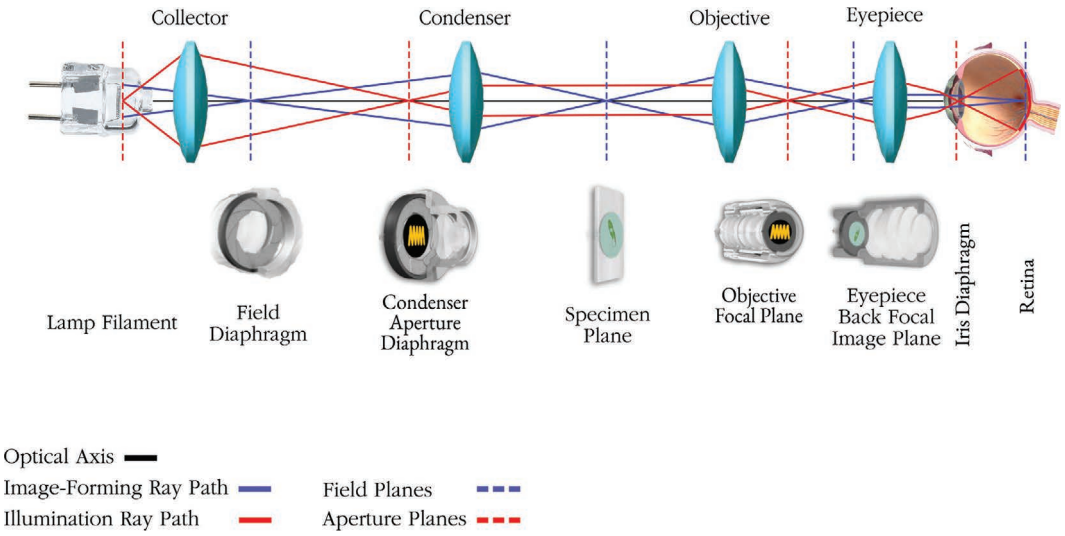


FIGURE 7.11 Image forming (blue rays) and illumination ray paths (red rays) through a microscope adjusted for Köhler illumination. All the planes of the two-conjugate set are shown.

One of the most common ways in which the conjugate nature of the two set planes is exploited is for the placement of auxiliary optical components. These optical elements are likely to be contaminated with dust or fingerprints due to frequent handling. Therefore, auxiliary components should never be placed in the illumination conjugate set planes, because any defects, dust, or debris may appear in the final image of the specimen formed at the level of either the retina or the camera imaging plane. In contrast, measurement reticules, scales, pointers, and other devices that are intended to be in focus and registered on the specimen must be placed in one of the field conjugate planes in order to be imaged together with the specimen.

Steps in Establishing Köhler Illumination

Once the light source is switched on, hold a small sheet of paper directly above the luminous field diaphragm collector lens in the base of the microscope to check whether the light source is properly functioning and projects light into the microscope. When the microscope is operating normally, a small spot of light will be visible on the paper. Otherwise, the electrical components of the illuminating unit should be checked.

The next step is to move the sheet of paper and place it between the specimen and the objective. The opening or closing of the field diaphragm by turning the knurled knob located on the base of the microscope, and of the condenser aperture diaphragm by means of the levers located on the condenser housing, will increase or reduce both the diameter of the spot of light projected onto the paper sheet and its intensity. Select the field diaphragm at half diameter, and set a small aperture field.

The condenser height can be adjusted using the drive knob that moves it up and down along the microscope optical axis. Set the condenser height so that the front lens does not touch the slide (approximately 2 millimeters beneath the lower surface of the slide). Light should now be

discernable in the microscope eyepieces. Next, set the inter-pupillary distance via the folding bridge of the binocular tubes. Squeeze or pull together the tubes to decrease or increase the separation between them until a single large circle of light (instead of two) can be easily visualized through the eyepieces. If the microscope is equipped with focusing eyepieces, turn the movable eyepiece to the zero setting, so eyeglass wearers can leave their glasses on. Peer into the microscope and carefully move the stage, including the specimen, up and down until you see the image details as sharply as possible. Usually, the condenser is not yet focused and centered and the view field will contain elements of the field diaphragm leaves; therefore, narrow the size of the field diaphragm and move the condenser up and down via the adjustment knob until you see a sharp image of the edges of the field diaphragm. When the field diaphragm is in sharp focus, close it down to its smallest opening and use the two centering screws, located on the condenser, to move the bright opening to the center of the view field (a crosshair reticule is very useful for determining the center of the view field). Once the condenser is centered, open the field diaphragm just beyond the view field. The illuminated area of the specimen plane must be at least as large as the field of view for any given objective. Set the light source to its highest power; if the light is too bright, do not reduce the intensity of the lamp but insert a gray filter in the optical path (cf. "Light Source for Microscopy").

At this point in the procedure, you should almost have a suitable image in the view field. The only remaining task is to optimize the resolution. The aperture diaphragm size must now be corrected in order to improve contrast and to seek a suitable balance with resolution. A condenser aperture that is too small will seriously degrade resolution and significantly darken the image, while a condenser aperture that is too large will significantly increase the glare and the light scattering from the specimen, thus hindering vision.

The best set of the aperture diaphragm can be performed by checking the imaged aperture diaphragm located at the level of the rear focal plane of the objective. This is done by removing an eyepiece and inserting a telescopic eyepiece (conoscopic mode) to look down the tube with the eye 10 centimeters away from it. Open and close the condenser aperture diaphragm until you can clearly recognize the image in the objective pupil. Finally, set the diameter of the diaphragm in such a manner that it illuminates about 80% of the pupil diameter, providing nearly full resolution and optimum contrast. Once the condenser aperture diaphragm has been adjusted, insert the eyepiece back into the binocular observation tube mount. The correct setting will produce light of uniform intensity with the numerical aperture equal to that of the objective.

When another objective is rotated into the optical path, you should again adjust the condenser aperture and field diaphragms for optimum illumination conditions.

Numerical Aperture, Airy Disk, and Microscope Resolution

The numerical aperture (NA) of a microscope objective is the measure of its ability to gather light and resolve fine specimen details while working at a fixed specimen distance. The incident light waves passing through the specimen are diffracted by the minute structures present in it, as in Figure 7.8. The diffracted light forms an inverted cone of half-angle (α) with the optical axis. The smaller the structures, the greater α will be. The NA of an objective is the measure of the angle of the inverted cone of diffracted light that the objective can intercept:

4) $$\mathrm{NA} = n \bullet \sin(\alpha)$$

where α is the half angle of intercepted light cone, and η is the refractive index of the immersion medium present between the objective and the cover slip protecting the specimen (see Table 7.2). Theoretically, the highest value of α could be 90°; the routinely used highest-quality objectives commonly have α value of 70°.

The higher the value of NA, the higher the value of α and the more resolved the image, with fine structures visualized with higher clarity. Therefore, NA determines the resolution of a microscope

objective. The limit distance up to which two small structures can be seen as separate entities is used as a measure of the effective resolution of the microscope.

The incident light diffracted by the specimen structure enters through the objective and is reconstituted as an image, which is a degraded representation of the specimen, since not all the diffracted light is collected by the objective. This representation results from the combination of many small elementary diffraction patterns (Airy disk), and it is not a combination of elementary points (Figure 7.12, top). The principal maximum of each Airy disk corresponds to approximately 84% of the luminous energy.

The microscope resolution, that is, the image sharpness, can be calculated according to Abbe's formula:

5) $$Resolution_{x,\ y} = \lambda/2NA$$

6) $$Resolution_{z} = 2\lambda/NA^2$$

where λ is the wavelength of light, and x, y, and z are the spatial coordinates.

The theoretical resolution limit at the shortest practical wavelength (approximately 400 nm) with an α value of 70° and an η value of 1.50 is around 180 nm in the lateral dimension and around 590 nm in the axial dimension. Thus, structures that lie closer than these distances cannot be resolved.

Practically, the most-used formula to calculate resolution is:

7) $$Resolution_{x,\ y} = 1.22\lambda/[NA_{Obj} + NA_{Con}]$$

where λ is the imaging wavelength of light, NA_{Con} is the condenser numerical aperture, and NA_{Obj} is the objective numerical aperture. This means that for maximal resolution, the NA of the condenser should be the same of that of the objective. The factor 1.22 results from experimental calculations.

The Rayleigh criterion states the distance limit between two close image points for them to be recognized as separate (Figure 7.12 bottom). If two image points are far away from each other, so their diffraction pattern, that is, the Airy disk, does not overlap, the points are easy to recognize as separate objects. When the distance between the Airy disks is increasingly reduced, the points are difficult to recognize as separate. The limit distance between two points to recognize two objects as separate is reached when the principal maximum of the second Airy disk coincides with the first minimum of the first Airy disk. The superimposed profiles display two brightness maxima that are separated by a valley. The intensity in the valley is reduced by approximately 20% compared with the two maxima. Fine image structures smaller than the resolving power of the human eye (a situation that is typical at low magnifications and high numerical apertures) will be missed.

The phenomenon of empty magnification will occur if an image is enlarged beyond the physical resolution power of the images. For these reasons, the useful overall combined magnification (magnification of the objective × magnification of eyepiece) of the microscope should be 500 times the numerical aperture of the objective but not greater than 1000 times the numerical aperture. However, since the numerical aperture of an objective is also dependent, to a certain degree, upon the amount of correction for optical aberration, highly corrected objectives tend to have much larger numerical apertures for the respective magnification (examples: 100× planachromat NA = 1.25; 100× planfluorite NA = 1.30; 100× planapochromat NA = 1.40).

CCD Cameras for Optical Microscopy

As stated, virtual images produced by the microscope can be visualized by a CCD camera using a lens-equipped adaptor. The sensor of a CCD camera consists of a large number of squared light-sensing elements called photodiodes, regularly arranged in a two-dimensional array of rows and columns. When photodiodes receive photons, a photoelectric conversion produces an amount of electrons equal to the amount of photons, which are then converted into an output voltage.

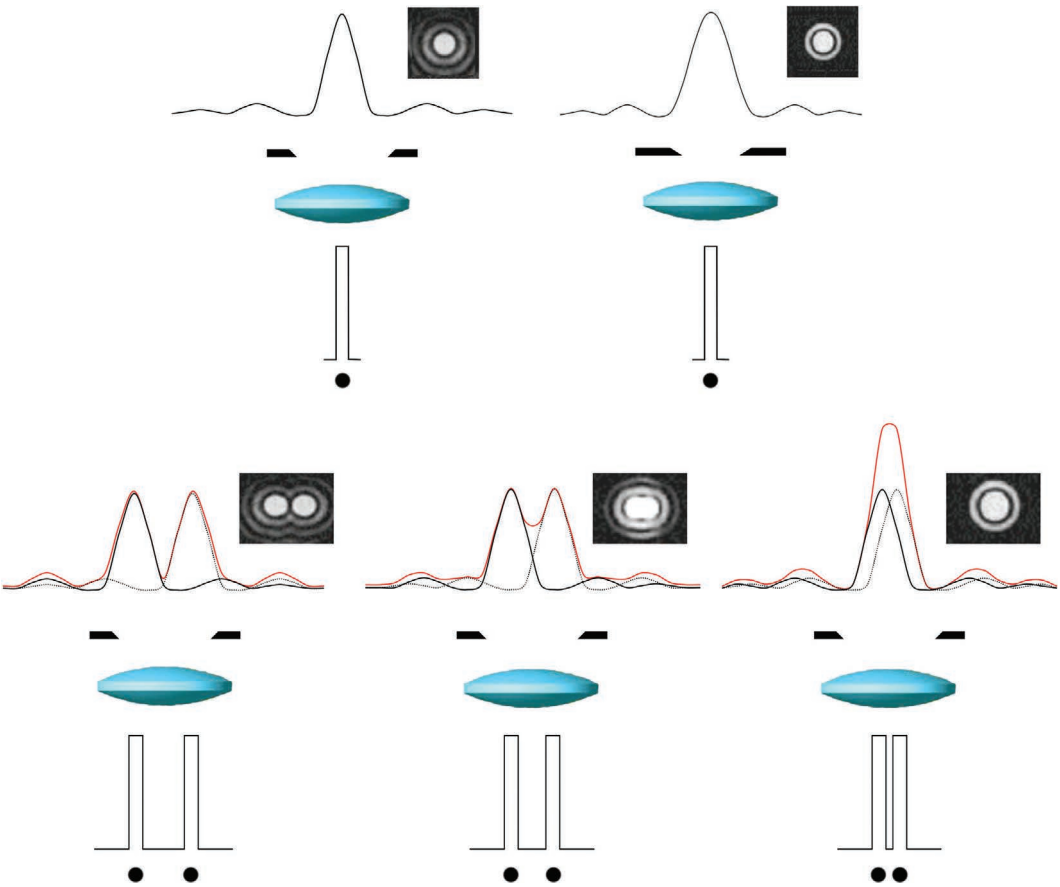


FIGURE 7.12 The incident light diffracted by an aperture is reconstructed as an image, which is a degraded representation of a point (Airy disk), since not all the diffracted light is collected by the lens. The narrower the aperture, the more degraded the Airy disk (top). Rayleigh criterion (bottom).

To simplify the description, we can consider an ideal CCD camera equipped with a squared sensor of 1 cm side. Though ideal, this CCD camera sensor cannot acquire the whole image projected by the microscope, since the diameter of the typical image field is about 2 cm. Therefore, the digital image produced by the camera will correspond to only a portion of the full image field.

The performance of our ideal CCD camera depends on the number of photodiodes: as their count increases, and as a consequence their size decreases, the more resolved the image becomes, and finer image features can be captured. However, a small photodiode has a reduced photon capacity (i.e. the number of photons it can acquire before becoming saturated). Thus, smaller photodiodes have lower signal-to-noise ratios and lower intensity range and produce highly resolved images; larger photodiodes have higher signal-to-noise ratios and higher intensity range and produce poorly resolved images. Therefore, the choice of a CCD camera should be based on the type of application.

To determine the amount of photodiodes necessary to adequately capture all the information contained in the image produced by the microscope and to match the microscope optical resolution to our ideal CCD camera, Equation 7 should be used.

According to this formula, the optical resolution for a typical microscope setup, with a 100× plan apochromatic objective with NA = 1.40 and a condenser with NA = 0.95 and using light at 580 nm (0.58 μm), is 0.3 μm.

The image spot projected onto the surface of the CCD equals the optical resolution multiplied by the objective magnification. Hence, in our example, it will be 30 μm.

The Nyquist-Shannon sampling theorem, which establishes the necessary sampling frequency to convert an analog signal in a digital signal without loss of information, indicates that this 30 µm spot should be sampled at least twice in both the *X* and *Y* direction, but three times is routinely used. A photodiode size of 10 µm × 10 µm or less would be necessary to adequately sample the analog microscope image. Therefore, our ideal camera sensor should have at least $10^3 \times 10^3$ photodiodes (1 megapixel).

This number of photodiodes is valid for a B/W acquisition; to acquire full-color images, CCD color cameras are necessary, which use four photodiodes (two green, one red, one blue) for each pixel. In this case, the sensor resolution should be increased four times (4 megapixel). For a faithful display of the acquired images, a monitor with the same or higher resolution should be used.

Fluorescence Microscopes

At the heart of the modern fluorescence microscope are the epi-illuminator and the filter cube, both sandwiched between the oculars and the nosepiece carrying the objectives (Figure 7.13). The photon flux generated by a high-intensity source is focalized onto a restricted area of the specimen by the microscope objective, and then the same objective is used to capture the light emitted by the excited molecules of the same area of the specimen. With this configuration, the microscope's correctly aligned objective gathers only a solid angle of the 360° image-forming fluorescence emission and transmits it to the detection system.

The essential requirement of any fluorescence microscope is to provide a mechanism for excitation of the specimen with selectively filtered illumination, followed by isolation of the much weaker

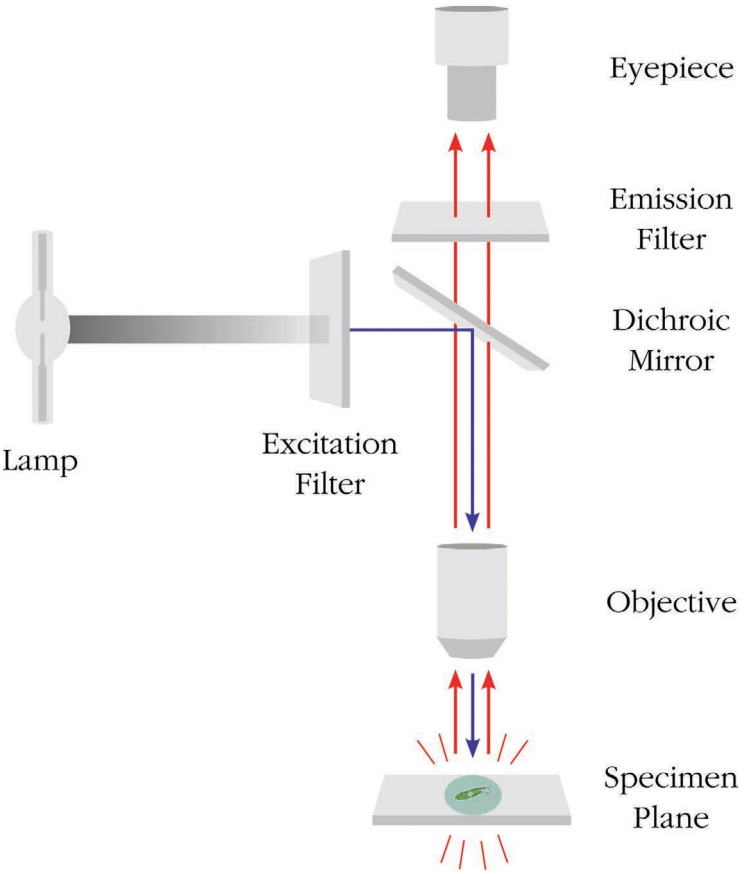


FIGURE 7.13 Schematic drawing of fluorescence microscopy setup.

fluorescence emission using a second filter. This configuration enables image formation on a dark background with the highest sensitivity. The brightness level of the fluorescence emission will be three and six orders of magnitude lower than that of the illumination. Therefore, fluorescence illumination requires approximately up to a million times more light than bright field illumination. The fundamental problem of fluorescence microscopy is to produce high-efficiency illumination of the specimen and simultaneously capture weak fluorescence emission that is effectively separated from the much more intense illumination band.

In fluorescence microscopy, two basic classes of filters regulate transmission of specific wavelengths. Band pass filters transmit just a range of wavelengths and block all light above and below this range. These filters are characterized by their center wavelength and bandwidth, also referred to as the full width at half of maximum transmission. Long-pass filters transmit long wavelengths and block short wavelengths, while short-pass filters have the opposite properties of transmitting short wavelengths while blocking others.

The hallmark optical element in fluorescence is the dichromatic mirror, which is designed to be positioned at a 45-degree angle with respect to both the incident illumination and the optical axis of the microscope. Light from the source passes through the epi-illumination optical path, reaches the fluorescence filter cube, and travels through a band pass excitation filter. The light is then reflected down by the dichromatic mirror into the objective to be focused onto the specimen plane, where it will excite fluorochromes whose spectral properties enable them to absorb light within the region allowed by the band pass excitation filter. Fluorescence emission is captured by the objective and directed back through the dichromatic mirror, which in turn reflects most of the contaminating excitation light back toward the light source. Emission wavelengths passing through the dichromatic mirror are further purified by defined band pass emission filter before traveling to either the eyepieces or the camera image plane.

Practical hints exist for performing successful fluorescence microscopy, such as the reduction of room lighting, since room lights can enter the objective and generate noise in the images. In addition, when the specimen is not being viewed or imaged, the excitation light should be blocked with a shutter or filter to avoid unnecessary photo-bleaching (degradation of the molecules due to high light intensity) by the illumination system. If the immersion medium is autofluorescent, the background becomes noticeably brighter and image contrast is reduced.

Light Sources for Microscopy

Under the stringent conditions of Köhler illumination, the light emanating from each point of the source uniformly illuminates the field diaphragm to produce a similarly uniform field of view. The field brightness is determined primarily by the irradiance of the light source and the square of the condenser (or objective) numerical aperture (the size of the field diaphragm affects only the diameter of the illuminated field and not its brightness).

The irradiance of a light source designed for optical microscopy is one of the most important characteristics to be considered because the brightness of an image is inversely proportional to the square of the magnification. As the objective magnification increases, image brightness proportionally decreases according to the numerical aperture. This means that, even if the optical system were perfect, using a 100× objective with NA 1.40, only a region of 100 μm^2 of specimen would be illuminated. Moreover, only a small fraction of the incident light from the epi-illumination system is transported, since the fluorescence emission intensity due to the small numbers of fluorochromes could be up to six orders of magnitude lower than that of the illumination.

Several illumination sources for optical microscopy are available, with different optical and physical properties. The most common sources used are tungsten-halogen lamps (100 W), arc-discharge mercury HBO lamps (100 W), and arc-discharge xenon XBO lamps (75 W). The light output from arc-discharge lamps is between 10 and 100 times brighter than the halogen lamps; the former are used for fluorescence microscopy, while the latter are typically used for transmitted light microscopy. More precisely, the mercury HBO 100-watt lamp has the highest irradiance

(30 mW m^{-2} nm^{-1}) compared with the xenon (7 mW m^{-2} nm^{-1}) and tungsten lamps (<1 mW m^{-2} nm^{-1}). Quasi-monochromatic LEDs (4.5 mW m^{-2} nm^{-1}) and lasers are used for special spectroscopic investigations.

The emission spectral profiles of the different lamps can be continuous, such as halogen and xenon sources, or have a line profile, such as LED and laser, or be a mix of lines and continuous spectra, as in the mercury lamp.

The xenon lamp has a low, but continuous, power output in the visible region, whereas most of the power output is concentrated at wavelengths above 800 nanometers. Xenon lamps lack the spectral fingerprint found in mercury lamps, yet they are perhaps even more useful because their continuous spectrum can effectively be used to simultaneously excite multiple fluorochromes with near-equal efficiency. The tungsten-halogen lamp exhibits a broad continuous spectral profile that produces relatively little output in the ultraviolet wavelengths but gradually increases before leveling off in the near-infrared region. Like the sun, incandescent lamps also produce essentially blackbody radiation with a spectral distribution that depends on the filament temperature. The spectral output of a tungsten-halogen lamp depends upon the voltage applied to the lamp by means of the power supply potentiometer. At higher voltages, the luminous flux increases with color temperature (3200 K to 3400 K), thus increasing the brightness of wavelengths in the visible spectral region. The mercury lamp has a low continuous emission in the visible range with distinct peaks at 365, 405, 436, 546, and 579 nanometers.

Spectra profile confirm that the requirements of wide-field fluorescence microscopy are fulfilled by arc-discharge sources or LED in some specific cases, while confocal, total internal reflection, and multi-photon microscopy require the adaptation of various laser systems. When choosing a light source for fluorescence, it is important to remember that most fluorochromes are excited by ultraviolet, blue, and green wavelengths.

Digital Microscopy

Digital microscopy consists of coupling microscopes with digital cameras, special hardware setups, and sophisticated image processing algorithms. Providing spatial, spectroscopic, and time coordinates, DM produces a deterministic and augmented real-time image of the *in vivo* metabolic processes dynamics under physiological conditions and/or in response to environmental stressors. Algae are an elective subject for DM due to the micrometric size of their cells, the pigments that characterize them, and their physiology.

Hardware

The hardware platform used to perform *in vivo* spectroscopic and real-time measurements is based on a bright field transmitted light microscope equipped with a tungsten lamp regulated at 100 W (color temperature 3200 K), an oil immersion condenser, and plan apochromatic objectives. An epi-fluorescent system, consisting of a 100 W mercury lamp and different combinations of filters, is mounted onto the microscope together with a manual/motorized mechanical scanning stage driven by a stepper motor controller. A two-port binocular tube mounted onto the microscope houses a color CCD camera connected to a PC via a Firewire interface (IEEE 1394) at the front port; this camera is used to digitalize microscope images for further processing. A high-quality inspection probe is mounted in the back focal plane of the rear port for microspectrophotometric measurements. The probe consists of a bundle of light guides mounted at the level of the entrance pupil in the back focal plane of the microscope. The bundle is vertically aligned at the level of the exit pupil. Each light guide acquires the light transmitted by the cell region of interest (ROI) and images it onto a diffraction grating, that is, a polychromator, which disperses the impinging light into separate wavelengths. The flat dispersed image of the probe is in turn focused onto a second digital CCD camera also interfaced to the computer (Figure 7.14). The personal computer is an Intel Core i7 with 16 GB 1600-MHz DDR3 RAM memory and 2 TB HD.

All the images presented in the book were recorded using this microscope setup and a color camera with a resolution of 4 million pixels necessary to match the optical resolution of the immersion plan-apochromatic objective (100×) and 8 bits for each of the three colors (red, blue, and green) for a correct color quantization. For the presented integrated density images, quasi-monochromatic images were acquired by means of interferential filters with 10 nm bandwidth at about 10 nm wavelength interval from 400 to 700 nm. For selecting the cell region of interest on which the integrated absorbance had to be calculated, each image underwent denoising, thresholding, and segmentation operations.

All the absorption spectra presented in the book were recorded using the polychromator setup (microspectroscopy); the inspection probe was centered on the ROI, such as the chloroplast, in such a way that at least one or two light guides were positioned on an empty microscope field. The light guides positioned on the ROI measured the transmitted light intensity (I_t), while those positioned on the empty field measured the incident light intensity (I_i). The spectra were generally recorded from 400 to 700 nm by measuring absorbance according the Beer-Lambert law (Equation 1).

Software

In the following, we will briefly describe the image processing algorithms used to identify algal cells in the acquired images and further analyze the variations in time of their spatial and spectral features.

1) Denoising: this algorithm enhances the quality of the images, removing the noise always present in them without reducing the image information content. Denoising implements morphological operations such as erode and dilate. The erode operation is useful for removing small debris or detaching two erroneously connected cells or subcellular regions. The dilate operation is the opposite of erosion: it is useful to join broken parts of a cell or a subcellular region.
2) Thresholding: the thresholding algorithm finds the correct boundaries between regions on the basis of their discontinuities in grayscale or color space.
3) Segmentation: this algorithm uses the calculated threshold to partition the image in a set of regions (i.e. the objects and the background) that collectively cover the entire image. At the end of the segmentation procedure, particles, debris, detritus, bacteria, empty dead cells, cells partly overlapping the slide border (or other algae), and out-of-focus cells that are always present in a slide and possess morphological and densitometric features not consistent with algae (a priori knowledge) are discarded as non-algal cells.
4) Detection of contours: this algorithm identifies the contour of each cell (or part of it), that is, the closed curve that delineates intensity transitions (above and over the calculated threshold) in the boundary between the cell (or part of it) and the background. The contour can be standardized, that is, uniformly resampled with $2n$ points, and oriented in a preset direction in order to obtain invariant features necessary for translation, rotation and scaling operations.

An Alternative "Simple" Method for Obtaining Algae Absorption Spectra

As already described in Chapter 4, chromophores are a very limited number of molecules evolved to absorb certain wavelengths of visible light and reflect others. The paucity of these molecules is due to the difficulty in fulfilling the task of absorbing and utilizing sunlight. The number of chromophores present inside algae is finite; they are different type(s) of chlorophylls, carotenoids, and phycobilins. Chromophores can be present, with varying relative abundances, or absent. Colors of all algae are the result of the infinite combinations of these chromophores, which are organized in supra-molecular structures of chromophore-protein complexes inside the photosynthetic compartment.

Detection of colors by the human eye is assigned to only three types of cones: the first one absorbs in the blue region (peak at 420 nm), the second absorbs in the green region (peak at 531

nm), and the third absorbs in the red region (peak at 558 nm). Upon absorption, no matter the λ of the photon, each of the three types of cones always produces the same electrical analogical signal. Digital CCD cameras work in a similar way, producing three digital values for each image pixel corresponding to the blue, green, and red sensors. If these digital values are known, would it be possible to use them to calculate the absorption spectrum of the chromophores responsible for these colors? Using just a CCD camera and available software packages, it is possible to reconstruct the absorption spectrum of an alga region using the color values of the corresponding pixel(s) with high accuracy and processing speed. The reconstructed absorption spectrum would be perfectly superimposable onto the absorption spectrum recorded by microspectroscopy.

The reconstruction consists of determining the set of the absorption spectra of the chromophores inside the photosynthetic compartment (Figures 4.5–4.9), knowing their solvent extracted absorption spectra and the absorption spectra of the photosynthetic compartment (Figures 4.11–4.15).

The reconstruction can be formalized as:

$$MS = W \times CC + N \tag{8}$$

where *MS* is the matrix whose lines represent the average of all the absorption spectra measured on either the same cell or cells belonging to the same species (Figures 4.11–4.15), and *CC* is the matrix whose lines represent the absorption spectra of the component chromophores. The starting values of the lines are the spectra of solvent-extracted chromophores (e.g. the hexane-extracted chlorophyll spectrum), present in the literature. These spectra differ in shape from the spectra of the chromophores in photosynthetic compartment because the extraction process produces unknown displacements, amplification, and contraction/dilatation of the spectral bands. Each of these chromophore spectra is modeled with a mixture of Gaussian curves with known parameters (position, bandwidth, weights). *W* is the matrix whose columns represent the spectra weights of each single chromophore component, and *N* is the noise or measurement error matrix.

By minimizing Equation 8 (i.e. choosing the result with the minimum error matrix), Gaussian curves of all the component chromophores extracted in organic solvents (CC matrix) are modified by means of factors of displacement, contraction/dilatation, and amplification to obtain the ending values, that is, the spectrum of the same component chromophore inside the cell (e.g. the chlorophyll-protein complex in the thylakoid membrane spectrum).

In order to obtain the spectrum that corresponds to the color of the input pixel(s), Equation 8 should be minimized:

$$Color\ Difference = |R_{calc} - R_{input}t| + |G_{calc} - G_{input}| + |B_{calc} - B_{input}| \tag{9}$$

This equation calculates the differences between the color values of the input pixel(s) R_{input}, G_{input}, and B_{input} and the calculated color values (R_{calc}, G_{calc}, and B_{calc}) resulting from the reconstructed chromophore spectra, the microscope tungsten lamp spectral distribution, and the CCD camera responses for its red, green, and blue channels (product data).

The minimization procedure selects type and weight of those reconstructed chromophores spectra that in combination produce the absorption spectrum to the color of the input pixel(s). The absorption spectrum reconstructed from the color values of a region extracted from a digital image of *Euglena gracilis* is compared with the absorption spectrum measured on the same area by microspectroscopy. The microscope setup of Figure 7.14 simultaneously performs the two measurements. The red contoured square in Figure 7.15a shows the position of the entrance pupil of the probe. The light guide used to measure the transmitted light intensity is red, while the guide used to measure the incident light intensity is blue. The blue contoured square shows the region (magenta) of the input color pixels. Figure 7.15b shows the absorption spectrum measured by microspectroscopy (top) and the absorption spectrum reconstructed after the identification of the four component chromophores, that is, chlorophylls *a* and *b*, β-carotene, and echinenone, which are shown inside the

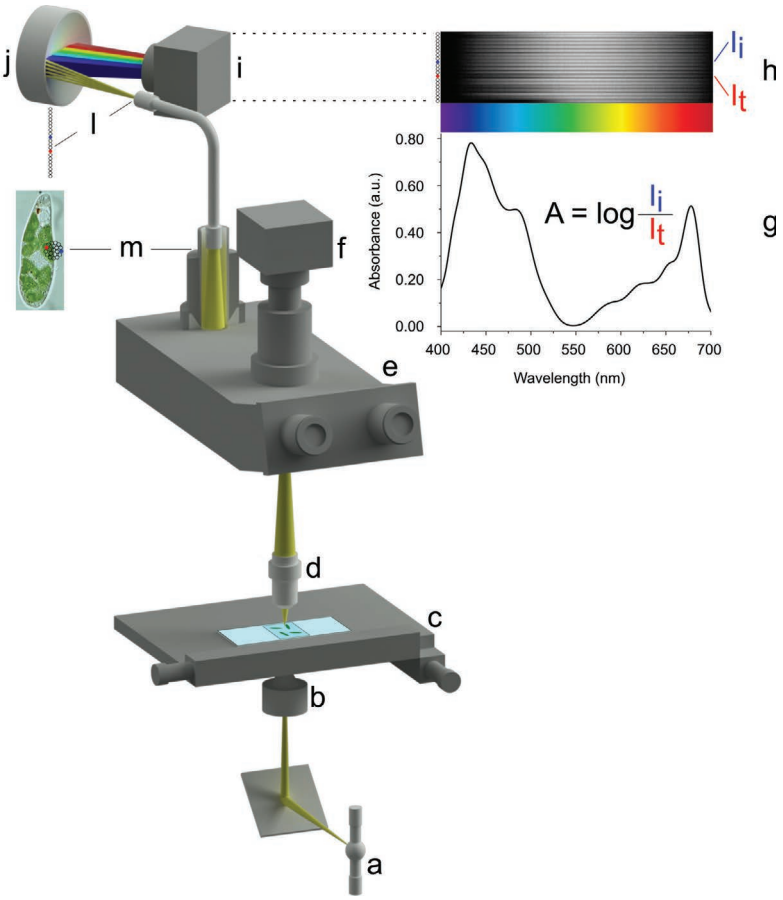


FIGURE 7.14 The hardware platform used for microspectroscopy and a recorded sample spectrum. Lamp (a), condenser (b), microscope stage (c), objective (d), two-port binocular tube (e), CCD camera (f), absorption spectrum of *Euglena gracilis* chloroplast (g), magnified camera target showing the image dispersed by the polychromator from 400 to 700 nm (h), CCD camera (i), polychromator (j), exit pupil of the optical fiber showing the 19 aligned light-guides (l), entrance pupil of the optical fiber showing the bundle of 19 light-guides (m).

spectrum (center). The normalized spectra of these chromophores are drawn in Figure 7.15c. The two absorption spectra are perfectly superimposable, as can be seen from the residual line in Figure 7.15b (bottom). The two colors identified by these spectra are not perceptible as different by the human eye.

FIELD INSTRUMENTS

Almost all light in the natural environment originates from the sun. Its spectral distribution is similar to that of an efficient radiant surface known as a black body at a temperature of 5800°C, which ranges from 100 to 4000 nm (cf. Figure 4.1 of Chapter 4).

In passing through the atmosphere, a small portion of this light is absorbed, and some is scattered. Short wavelengths are strongly scattered, and ozone absorption effectively eliminates wavelengths less than 300 nm. At longer wavelengths, water vapor, carbon dioxide, and oxygen absorb light significantly at particular wavelengths, producing sharp dips in the spectrum. At still-longer

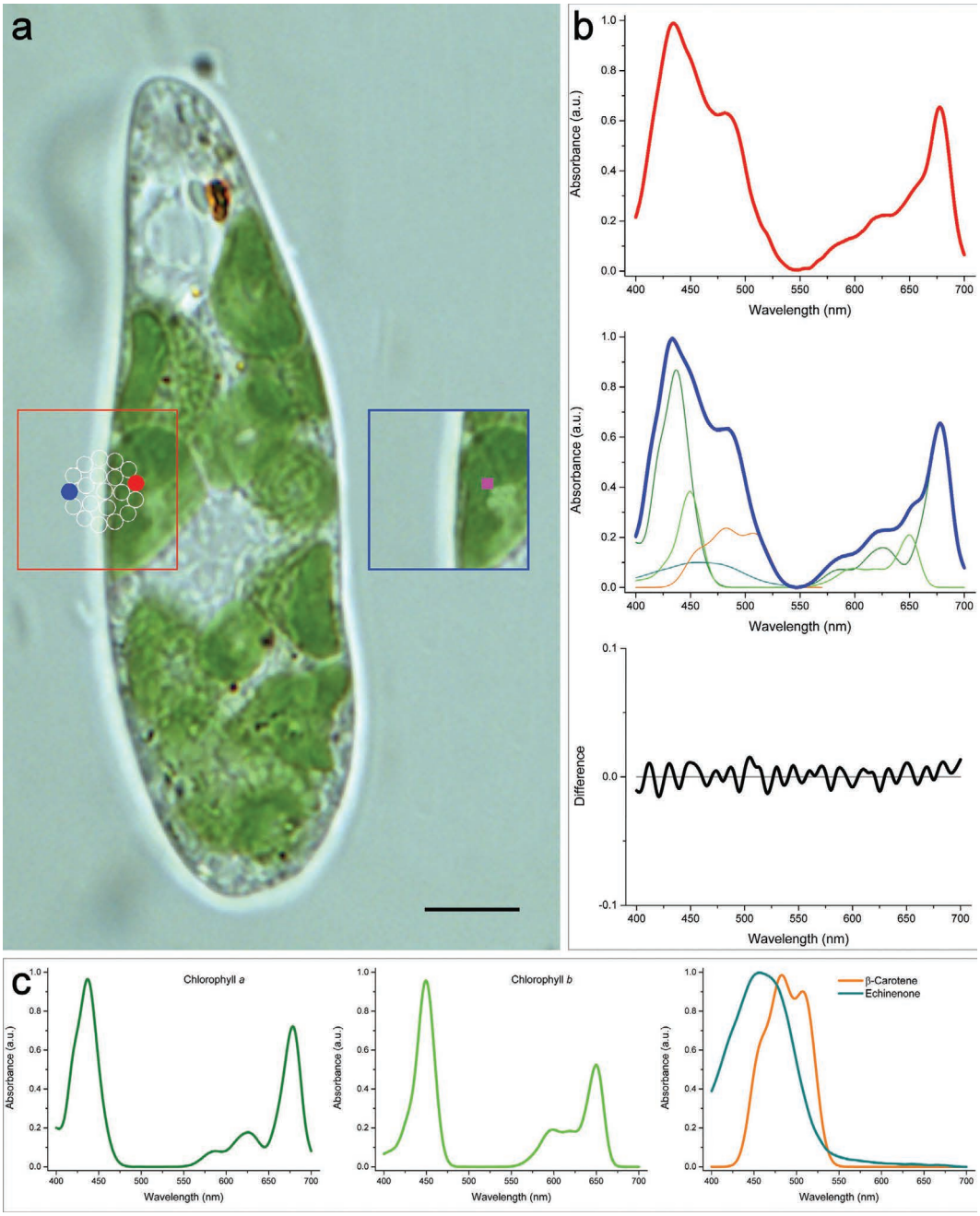


FIGURE 7.15 Comparison between the *in vivo* absorption spectrum of *Euglena gracilis* chloroplast and the corresponding reconstructed spectrum. Digital image of *Euglena gracilis*: the red contoured square shows the position of the entrance pupil of the probe; the blue contoured square shows the region (magenta) of the input color pixels (a). Bar 5 μm. In vivo absorption spectrum of *Euglena* chloroplast (b, top); reconstructed spectrum with the four component chromophores (center); residual line (b, bottom). Normalized spectra of the four component chromophores: chlorophyll *a*, chlorophyll *b*, β-carotene, echinenone (c). Scale bar = 5 μm.

wavelengths, beyond 4000 nm, all objects in the environment become significant sources of radiation, depending on their temperature, and surpass sunlight in intensity. These characteristics of the environment restrict the range of electromagnetic radiation. Solar radiant energy that reaches the surface of the earth has a spectral range from about 300 (ultraviolet) to about 4000 nm (infrared). Photosynthetically active radiation occurs between approximately 400 and 750 nm and is less than 50% of the total energy impinging on the earth's surface (cf. Figure 4.2 of Chapter 4).

Before describing the detectors used in the field application, a short lexicon of the terms and conversion units of light measurements would be very useful because of the plethora of confusing terminology and units.

Radiometry

Radiometry is the science of measuring light in any portion of the electromagnetic spectrum. In practice, the term is usually limited to the measurement of infrared, visible, and ultraviolet light using optical instruments, such as radiation thermocouples, bolometers, photodiodes, photosensitive dyes and emulsions, vacuum phototubes, charge-coupled devices, and so on.

Measurement Geometries: Solid Angles

One of the key concepts to understanding the relationships between measurement geometries is that of the solid angle ω. This can be defined as the angle that, seen from the center of the sphere, includes a given area on the surface of that sphere. The value of a solid angle is numerically equal to the size of the area on the surface of the sphere (A) divided by the square of the radius (r) of that sphere:

$$\omega = A/r^2 \tag{10}$$

The value of a solid angle is given in steradian. A sphere of radius r and surface of $4\pi r^2$ will contain 4π steradians. The steradian is a dimensionless quantity.

A surface can be described as a continuum of infinitesimal points, each occupying an infinitesimal area dA,

$$\mathrm{d}\omega = \mathrm{d}A/r^2 \tag{11}$$

where dω is the differential solid angle of the elemental cone containing a ray of light that is arriving at or leaving a infinitesimal surface dA. The symbol d stands for differential, the operator that reduces the applied variable to an infinitesimal quantity.

Most radiometric measurements do not require an accurate calculation of the spherical surface area. Flat area estimates can be substituted for spherical area when the solid angle is less than 0.03 steradians, resulting in less than 1% error. This roughly translates to a distance at least five times greater than the largest dimension of the detector. When the light source is the sun, flat area estimates can be substituted for spherical area.

Radiant Energy

Light is radiant energy. When light is absorbed by a physical object, its energy is converted into some other form. Visible light causes an electric current to flow in a light detector when its radiant energy is transferred to the electrons as kinetic energy.

Radiant energy (denoted as Q) is measured in joules (J).

Spectral Radiant Energy

A broadband source such as the sun emits electromagnetic radiation throughout most of the electromagnetic spectrum. However, most of its radiant energy is concentrated within the PAR. A

single-wavelength laser, on the other hand, is a monochromatic source; all of its radiant energy is emitted at one specific wavelength.

From this, we can define spectral radiant energy, which is the amount of radiant energy per unit wavelength interval at wavelength λ. It is defined as:

12) $$Q_\lambda = dQ/d\lambda$$

Spectral radiant energy is measured in joules per nanometer (J nm^{-1}).

Radiant Flux (Radiant Power)

Energy per unit time is power, which is measured in joules per second (J sec^{-1}) or watts (W). Light "flows" through space, so radiant power is more commonly referred to as the flow rate of radiant energy with respect to time, or radiant flux. It is defined as:

13) $$\Phi = dQ/dt$$

where Q is radiant energy and t is time.

In terms of a light detector measuring PAR, the instantaneous magnitude of the electric current is directly proportional to the radiant flux. The total amount of current measured over a period of time is directly proportional to the radiant energy absorbed by the light detector during that time.

For phycological purposes, the radiant flux also is expressed as µmol of photons per second.

Spectral Radiant Flux (Spectral Radiant Power)

Spectral radiant flux at wavelength λ is radiant flux per unit wavelength interval. It is defined as:

14) $$\Phi_\lambda = d\Phi/d\lambda$$

and is measured in watts per nanometer (W nm^{-1}).

Radiant Flux Density (Irradiance and Radiant Exitance)

Radiant flux density is the radiant flux per unit area at a point on a surface. Radiant flux density is measured in watts per square meter (W m^{-2}).

There are two possible conditions. The flux can be arriving at the surface, in which case the radiant flux density is referred to as irradiance. Irradiance is defined as:

15) $$E = d\Phi/dA$$

where Φ is the radiant flux arriving at the infinitesimal area dA.

Since irradiance is the radiant flux per unit area, it can be expressed as a mole of photons per area per unit time (µmol $m^{-2}s^{-1}$). Modern instruments measure in situ irradiance directly in these units.

The flux can also be leaving the surface due to emission and/or reflection. The radiant flux density is then referred to as radiant exitance. As with irradiance, the flux can leave in any direction above the surface. The definition of radiant exitance is:

16) $$M = d\Phi/dA$$

where Φ is the radiant flux leaving the infinitesimal area dA.

Typical values for irradiance are (in W m^{-2}):

- Sunlight 1000
- Skylight 100
- Overcast daylight 10

- Moonlight 0.001
- Starlight 0.0001

Spectral Radiant Flux Density

Spectral radiant flux density is radiant flux per unit wavelength interval at wavelength λ. When the radiant flux is arriving at the surface, it is called spectral irradiance and is defined as:

17) $$E_{\lambda} = \mathrm{d}E/\mathrm{d}\lambda$$

When the radiant flux is leaving the surface, it is called spectral radiant exitance and is defined as:

18) $$M_{\lambda} = \mathrm{d}M/\mathrm{d}\lambda$$

Spectral radiant flux density is measured in watts per square meter per nanometer (W m^{-2} nm^{-1}).

Radiance

Imagine a ray of light arriving at or leaving a point on a surface in a given direction. Radiance is simply the amount of radiant flux contained in this ray (a cone of solid angle $\mathrm{d}\omega$). If the ray intersects a surface at an angle θ with the normal to that surface, and the area of intersection with the surface has an infinitesimal cross-sectional area $\mathrm{d}A$, the cross-sectional area of the ray is $\mathrm{d}A\cos\theta$. The radiance of this ray is:

19) $$L = d2\Phi/(\mathrm{d}A \times \mathrm{d}\omega \times \cos\theta)$$

Radiance is measured in watts per square meter per steradian (W m^{-2} sr^{-1}).

Unlike radiant flux density, the definition of radiance does not distinguish between flux arriving at or leaving a surface.

Another way of looking at radiance is to note that the radiant flux density at a point on a surface is due to a single ray of light arriving (or leaving) at an angle θ to the normal to that surface is $\mathrm{d}\Phi/\mathrm{d}A \times \cos\theta$. The radiance at that point for the same angle is then $\mathrm{d}^2\Phi/(\mathrm{d}A \times \mathrm{d}\omega \times \cos\theta)$, or radiant flux density per unit solid angle.

The irradiance, E, at any distance from a uniform extended area source is related to the radiance, L, of the source by the following relationship, which depends only on the subtended central viewing angle, θ, of the radiance detector:

20) $$E = \pi \times L \times \sin^2(\theta/2)$$

Radiance is independent of distance for an extended area source, because the sampled area increases with distance, cancelling inverse square losses. The inverse square law defines the relationship between the irradiance from a point source and distance (d). It states that the intensity per unit area varies in inverse proportion to the square of the distance. In other words, if you measure 16 W m^{-2} at 1 meter, you will measure 4 W m^{-2} at 2 meters and can calculate the irradiance at any other distance. An alternative form is often more convenient:

21) $$E_1 \times d_1^2 = E_2 \times d_2^2$$

Spectral Radiance

Spectral radiance is radiance per unit wavelength interval at wavelength λ. It is defined as:

22) $$L_\lambda = d^3\Phi/(dA \times d\omega \times \cos\theta \times d\lambda)$$

and is measured in watts per square meter per steradian per nanometer (W m^{-2} sr^{-1} nm^{-1}).

Radiant Intensity

We can imagine a small point source of light that emits radiant flux in every direction. The amount of radiant flux emitted in a given direction can be represented by a ray of light contained in an elemental cone. This gives us the definition of radiant intensity:

23) $$I = d\Phi/d\omega$$

where $d\omega$ is the infinitesimal solid angle of the elemental cone containing the given direction. From the definition of a infinitesimal solid angle, we get:

24) $$I = r^2 \times (d\Phi/dA) \text{ or } I = r^2 \times E \text{ or } E = I/r^2$$

where the infinitesimal surface area dA is on the surface of a sphere centered on the source and at a distance r from the source and E is the irradiance of that surface. More generally, the radiant flux will intercept dA at an angle θ from the surface normal. This gives us the inverse square law for point sources:

25) $$E = I_\theta \times \cos\theta/d^2$$

where I_θ is the intensity of the source in the θ direction, and d is the distance from the source to the surface element dA.

Radiant intensity is measured in watts per steradian (W sr^{-1}).

Combining the definitions of radiance (Equation 19) and radiant intensity (Equation 23) gives us an alternative definition of radiance:

26) $$L = dI_\theta/(dA \times \cos\theta)$$

where dI_θ is the infinitesimal intensity of the point source in the θ direction with the surface normal.

Spectral Radiant Intensity

Spectral radiant intensity is radiant intensity per unit wavelength interval at wavelength λ. It is defined as:

27) $$I_\lambda = dI/d\lambda$$

and is measured in watts per steradian per nanometer (W sr^{-1} nm^{-1}).

Photometry

Photometry is the science of measuring visible light in units that are weighted according to the sensitivity of the human eye. It is a quantitative science based on a statistical model of the human visual response to light under carefully controlled conditions. We cannot apply this model to the "perception" of light by algae, since we should substitute the sensitivity of the algal photoreception systems for that of the human eye.

For human perception, the Commission International d'Eclairage (CIE) photometric curves (scotopic and photopic) provide a weighting function that can be used to convert radiometric into

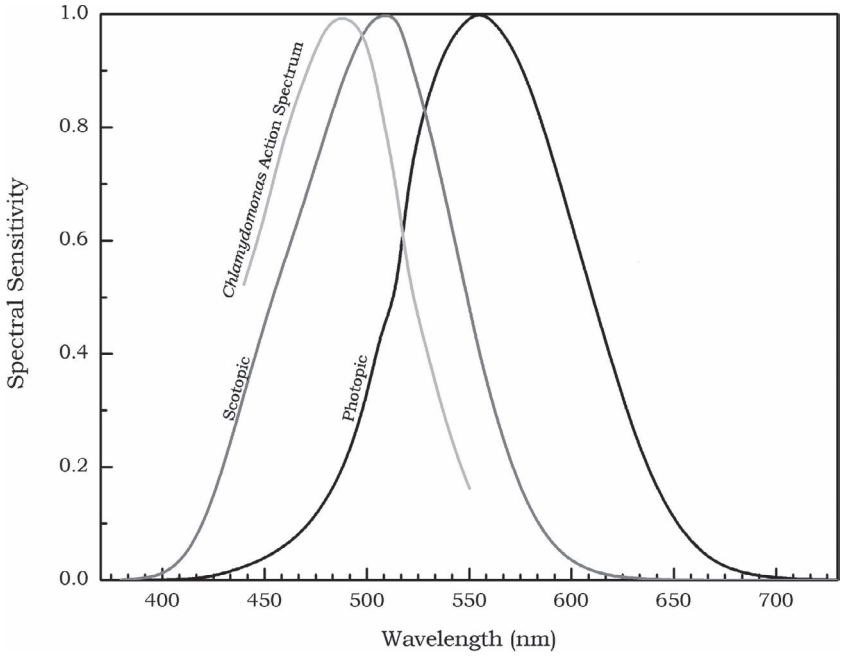


FIGURE 7.16 Curves of spectral sensitivity for the scotopic (dark-adapted) and photopic (light-adapted) human vision compared with the action spectrum of *Chlamydomonas*.

photometric measurements. In a scotopic curve, yellowish-green light receives the greatest weight because it stimulates the eye more than blue or red light of equal radiant power (λ_{max} = 555 nm) (Figure 7.16, Table 7.3); in a photopic curve, blue-green light receives the greatest weight because it stimulates the eye more than other lights of equal radiant power (λ_{max} = 507 nm) (Figure 7.16, Table 7.3). For algae, action spectroscopy may be used for a similar purpose even though the spectra so far measured are contradictory, not very accurate, and very often difficult to interpret (Figure 7.16).

Luminous Flux (Luminous Power)

Luminous flux is radiant flux weighted to match the eye response of the "standard observer." Its unit of measurement is the lumen. The lumen (lm) is the photometric equivalent of the watt, and it is defined as 1/683 watts of radiant power at a frequency of 540×10^{12} Hertz or better at a wavelength of 555 nm.

Luminous Intensity

The luminous intensity is the *luminous flux* emitted from a point source per unit *solid angle* into a given direction. The luminous intensity is measured in candela (the Latin word for "candle"). Together with the CIE photometric curve, the candela provides the weighting factor needed to convert radiometric to photometric measurements. The candela (cd) is the luminous intensity, in a given direction, of a source that emits monochromatic radiation with a frequency of 540×10^{12} Hz (λ = 555 nm) and has a radiant intensity of 1/683 W sr^{-1} in that direction.

If a light source is isotropic, that is, its intensity does not vary with direction, the relationship between lumens and candelas is 1 cd = 4π lm. In other words, an isotropic source with a luminous intensity of 1 candela emits 4π lumens into space, which just happens to be 4π steradians. We can also state that 1 cd = 1 lm sr, analogous to the equivalent radiometric definition. If a source is not isotropic, the relationship between candelas and lumens is empirical. A fundamental method used

TABLE 7.3
Luminous Efficacy of the Eye at Different Wavelengths Has Been Tabulated for Both Light-Adapted (Photopic) Vision and Dark-Adapted (Scotopic) Vision.

λ nm	Photopic Luminous Sensitivity	Photopic lm/W Conversion	Scotopic Luminous Sensitivity	Scotopic lm/W Conversion
380	0.000039	0.027	0.000589	1.001
390	0.000120	0.082	0.002209	3.755
400	0.000396	0.270	0.009290	15.793
410	0.001210	0.826	0.034840	59.228
420	0.004000	2.732	0.096600	164.220
430	0.011600	7.923	0.199800	339.660
440	0.023000	15.709	0.328100	557.770
450	0.038000	25.954	0.455000	773.500
460	0.060000	40.980	0.567000	963.900
470	0.090980	62.139	0.676000	1149.200
480	0.139020	94.951	0.793000	1348.100
490	0.208020	142.078	0.904000	1536.800
500	0.323000	220.609	0.982000	1669.400
507	0.444310	303.464	**1.000000**	**1700.000**
510	0.503000	343.549	0.997000	1694.900
520	0.710000	484.930	0.935000	1589.500
530	0.862000	588.746	0.811000	1378.700
540	0.954000	651.582	0.650000	1105.000
550	0.994950	679.551	0.481000	817.700
555	**1.000000**	**683.000**	0.402000	683.000
560	0.995000	679.585	0.328800	558.960
570	0.952000	650.216	0.207600	352.920
580	0.870000	594.210	0.121200	206.040
590	0.757000	517.031	0.065500	111.350
600	0.631000	430.973	0.033150	56.355
610	0.503000	343.549	0.015930	27.081
620	0.381000	260.223	0.007370	12.529
630	0.265000	180.995	0.003335	5.670
640	0.175000	119.525	0.001497	2.545
650	0.107000	73.081	0.000677	1.151
660	0.061000	41.663	0.000313	0.532
670	0.032000	21.856	0.000148	0.252
680	0.017000	11.611	0.000072	0.122
690	0.008210	5.607	0.000035	0.060
700	0.004102	2.802	0.000018	0.030
710	0.002091	1.428	0.000009	0.016
720	0.001047	0.715	0.000005	0.008
730	0.000520	0.355	0.000003	0.004
740	0.000249	0.170	0.000001	0.002
750	0.000120	0.082	0.000001	0.001
760	0.000060	0.041	0.000001	0.001
770	0.000030	0.020	0.000001	0.001

Note: The table also shows the conversion factors to use when reporting the photometric units (luminous flux) in radiometric units (radiant flux). See text for details.

to determine the total flux (lumens) is to measure the luminous intensity (candelas) in many directions using a goniophotometer and then numerically integrate over the entire sphere. Since 1 steradian has a projected area of 1 square meter at a distance of 1 meter, a 1-candela light source will similarly produce 1 lumen per square meter (Figure 7.17).

Typical values for luminous intensity are (in candelas):

- Flashtube 1,000,000
- Automobile headlamp 100,000
- 100 watt incandescent bulb 100
- Light-emitting diode 0.0001

Luminous Energy

Luminous energy is photometrically weighted radiant energy. It is measured in lumens per seconds (lm s^{-1}).

Luminous Flux Density (Illuminance and Luminous Exitance)

Luminous flux density is photometrically weighted radiant flux density. Illuminance is the photometric equivalent of irradiance, whereas luminous exitance is the photometric equivalent of radiant exitance.

Luminous flux density is measured in lux (lx) or lumens per square meter (lm m^{-2}).

Typical values for illuminance are (in lux):

- Sunlight 100,000
- Skylight 10,000
- Overcast daylight 1,000
- Moonlight 0.1
- Starlight 0.01

Luminance

Luminance is photometrically weighted radiance. In terms of visual perception, we perceive luminance. It is an approximate measure of how "bright" a surface appears when we view it from a given direction. Luminance used to be called "photometric brightness." Luminance is measured in lumens per square meter per steradian (lm m^{-2} sr^{-1}).

Lambertian Surfaces

A Lambertian surface is referred to as a perfectly diffusing surface, which follows Lambert's cosine law. This law states that the reflected or transmitted luminous intensity in any direction from an element of a Lambertian surface varies according to the cosine of the angle between that direction and the normal of the surface. The intensity I_θ of each ray leaving the surface at an angle θ from the ray in a direction perpendicular to the surface (I_n) is given by:

28) $$I_\theta = I_n \times \cos\theta$$

Therefore, even if the luminous intensity decreases by a factor of $\cos\theta$ from the normal, the projected surface decreases by the same factor; as a consequence, the radiance (luminance) of a Lambertian surface is the same regardless of the viewing angle and is given by:

29) $$L = \mathrm{d}I_n \times \cos\theta/(\mathrm{d}A \times \cos\theta) = \mathrm{d}I_n/\mathrm{d}A$$

It is worthwhile to note that in a Lambertian surface, the ratio between the radiant exitance and the radiance is π and not 2π:

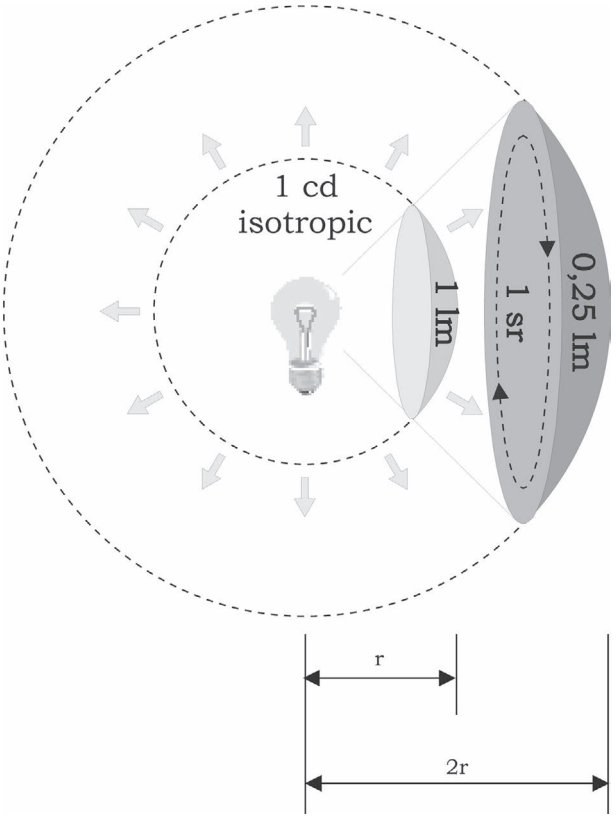


FIGURE 7.17 Luminous intensity: a 1-candela light source emits 1 lumen per steradian in all directions (isotropically). According to the inverse square law, the intensity varies in inverse proportion to the square of the distance; that is, at a distance of 2*r* from the source, the intensity will be equal to ¼ lm per steradian.

30) $$M/L = \pi$$

This equation can be easily derived. Suppose we place an infinitesimal Lambertian emitter d*A* on the inside surface of an imaginary sphere *S*. The inverse square law (Equation 21) provides the irradiance *E* at any point *P* on the inside surface of the sphere. However, $d = D \times \cos\theta$, where *D* is the diameter of the sphere. Thus:

31) $$E = I_\theta/(D^2 \times \cos\theta)$$

and from Lambert's cosine law (Equation 28), we have:

32) $$E = I_n/D^2$$

which simply says that the irradiance (radiant flux density) of any point *P* on the inside surface of *S* is a constant.

This is interesting. From the definition of irradiance (Equation 15), we know that $\Phi = E \times A$ for constant flux density across a finite surface area *A*. Since the area *A* of the surface of a sphere with radius *r* is given by:

33) $$A = 4\pi r^2 = \pi D^2$$

we have:

34) $$\Phi = E \times A = \pi I_n$$

Given the definition of radiant exitance (Equation 16) and radiance for a Lambertian surface (Equation 29), we have:

35) $$M = \mathrm{d}\Phi/\mathrm{d}A = \pi L$$

This explains, clearly and without resorting to integral calculus, where the factor π comes from.

UNIT CONVERSION

Radiant and Luminous Flux (Radiant and Luminous Power)

- 1 J (joule) = 1 W s (watt × second)
- 1 W (watt) = 683.0 lm (photopic) at 555 nm = 1700.0 lm (scotopic) at 507 nm
- 1 lm = 1.464×10^{-3} W at 555 nm = $1/(4\pi)$ candela (cd) (only if isotropic)
- 1 lm s^{-1} (lumen × $seconds^{-1}$) = 1.464×10^{-3} J at 555 nm

A monochromatic point source with a wavelength of 510 nm with a radiant intensity of 1/683 W sr^{-1} has a luminous intensity of 0.503 cd, since the photopic luminous efficiency at 510 nm is 0.503.

A 680-nm laser pointer with the power of 5 mW produces 0.005 W × 0.017 × 683 lm W^{-1} = 0.058 lm, while a 630-nm laser pointer with a power of 5 mW at produces 0.905 lm, a significantly greater power output.

Determining the luminous flux from a source radiating over a spectrum is more difficult. It is necessary to determine the spectral power distribution for the particular source. Once that is done, it is necessary to calculate the luminous flux at each wavelength or at regular intervals for continuous spectra. Adding up the flux at each wavelength gives a total flux produced by a source in the visible spectrum.

Some sources are easier to do this with than others. A standard incandescent lamp produces a continuous spectrum in the visible, and various intervals must be used to determine the luminous flux. For sources like a mercury vapor lamp, however, it is slightly easier. Mercury emits light primarily in a line spectrum. It emits radiant flux at six primary wavelengths. This makes it easier to determine the luminous flux of this lamp with respect to the incandescent.

Generally, it is not necessary to determine the luminous flux, since it is commonly given for each lamp on the basis of laboratory testing during manufacture. For instance, the luminous flux for a 100-W incandescent lamp is approximately 1700 lm. We can use this information to extrapolate to similar lamps. Thus, the average luminous efficiency for an incandescent lamp is about 17 lm W^{-1}. We can now use this as an approximation for similar incandescent sources at various wattages.

Irradiance (Flux Density)

- 1 W m^{-2} = 10^{-4} W cm^{-2} = 6.83×10^2 lux (lx) at 555 nm
- 1 lm m^{-2} = 1 lux = 10^{-4} lm cm^{-2}
- 1 photon at 400 nm = 4.96×10^{-19} J
- 1 W m^{-2} at 400 nm = 1 J m^{-2} s^{-1} = 3.3 μmol $m^{-2}s^{-1}$ = 3.3 μEinstein m^{-2} s^{-1}
- 1 photon at 500 nm = 3.97×10^{-19} J
- 1 W m^{-2} at 500 nm = 1 J × $m^{-2}s^{-1}$ = 4.2 μmol m^{-2} s^{-1} = 4.2 μEinstein m^{-2} s^{-1}
- 1 photon at 600 nm = 3.31×10^{-19} J
- 1 W m^{-2} at 600 nm = 1 J $m^{-2}s^{-1}$ = 5.0 μmol m^{-2} s^{-1} =5.0 μEinstein m^{-2} s^{-1}

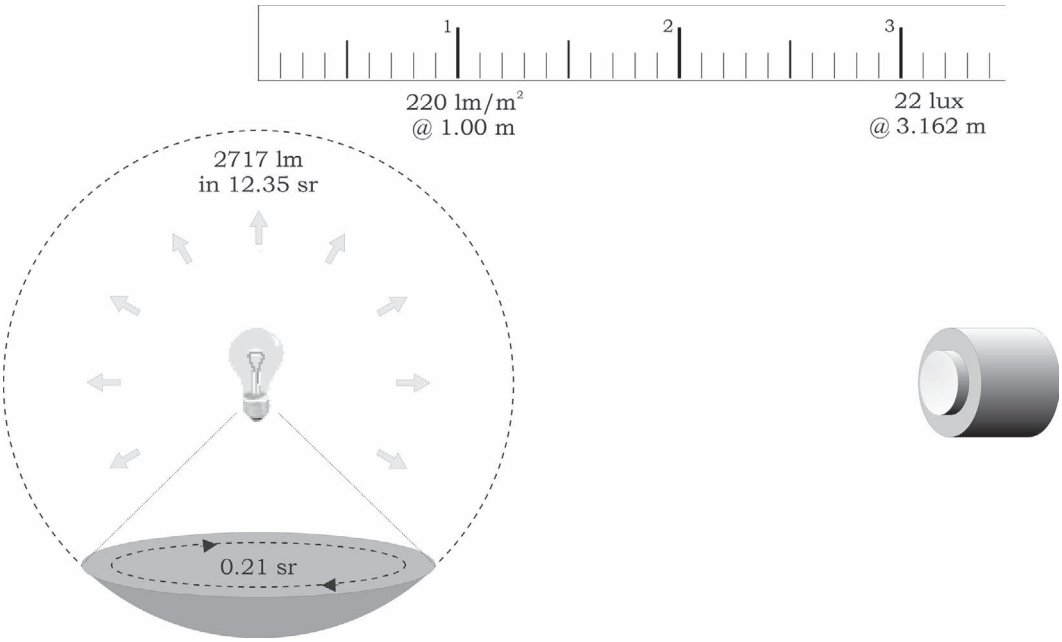


FIGURE 7.18 Example of conversion between lux and lumens.

- 1 photon at 700 nm = 2.83×10^{-19} J
- 1 W m^{-2} at 700 nm = 1 J $m^{-2}s^{-1}$ = 5.9 µmol m^{-2} s^{-1} =5.9 µEinstein m^{-2} s^{-1}

Radiance

- 1 W m^{-2} sr^{-1} = 6.83×10^{2} lm m^{-2} sr^{-1} at 555 nm = 683 cd cm^{-2} at 555 nm

Radiant Intensity

- 1 W sr^{-1} = 12.566 watts (isotropic) = 4π W = 683 cd at 555 nm

Luminous Intensity

- 1 lm sr = 1 cd = 4π lumens (isotropic) = 1.464×10^{-3} W sr^{-1} at 555 nm

Luminance

- 1 lm m^{-2} sr^{-1} = 1 cd m^{-2} = 10^{-4} lm cm^{-2} sr^{-1} = 10^{-4} cd cm^{-2}

Geometries

Converting between geometry-based measurement units is difficult and should only be attempted when it is impossible to measure in the actual desired units. You must be aware of what each of the measurement geometries implicitly assumes before you can convert. The following example shows the conversion between lux and lumens.

If you measure 22.0 lux from a light bulb at a distance of 3.162 meters, how much light, in lumens, is the bulb producing? Assume that the lamp is an isotropic point source, with the exception that the base blocks a 30° solid angle.

Using Equation 21, the irradiance at 1.0 meter is:

$$E_{1.0\ m} = (3.162/1.0)^2 \times 22.0 = 219.96 \text{ lm m}^{-2}$$

Based on the steradiant definition (Equation 10), we know that 1 sr cuts off a spherical surface area of 1 m^2 at a distance of 1 m from the source. Therefore, 220 lm m^{-2} corresponds to 220 lm sr^{-1}. The solid angle of the lamp is equal to $2\pi\ h\ r^{-1}$ (Equation 10), where h is the height of the spherical calotte and corresponds to $2\pi \times [1 - \cos(360 - 30/2)] = 12.35$ sr, while the shadowed solid angle corresponds to 0.21 sr. Therefore, the total lumen output will be 220 lm $sr^{-1} \times 12.35$ sr = 2717 lm (Figure 7.18).

PAR DETECTORS

Photosynthetic irradiance is the radiant flux density of PAR and is expressed as the radiant energy (400–700 nm) incident on a unit of surface per unit time. A PAR detector is typically an irradiance detector that is equally sensitive to light between 400 and 750 nm and insensitive to light outside this region. Irradiance is now internationally expressed in moles of photons per unit area and per unit time as μmol m^{-2} s^{-1} (formerly μEinstein m^{-2} s^{-1}), where 1 μmol (μEinstein) corresponds to 1 micromole of photons, that is, 6.02×10^{17} photons, at a given wavelength. Modern instruments measure in situ irradiance flux densities directly in μmol m^{-2} s^{-1}.

In terms of collector geometry, a PAR detector is usually equipped with either a planar (cosine) or a spherical (scalar) collector. A planar or 2π collector measures PAR in a 180° arc, while a spherical or 4π collectors measures the light impinging from all directions on a single point (Figure 7.19).

The irradiance impinging on the surface of the water or sediment is commonly measured with a planar detector. Spherical detectors provide a measurement of the amount of light available for photosynthesis by phytoplankton suspended in the water column. A leaf resembles a small planar collector whereas algae resemble small spherical collectors.

Direct solar radiation reaching the water surface varies with the angular height of the radiation and therefore, with time of day, season, and latitude. The quantity and quality of light also vary with the molecular transparency of the atmosphere and the distance the light must travel through

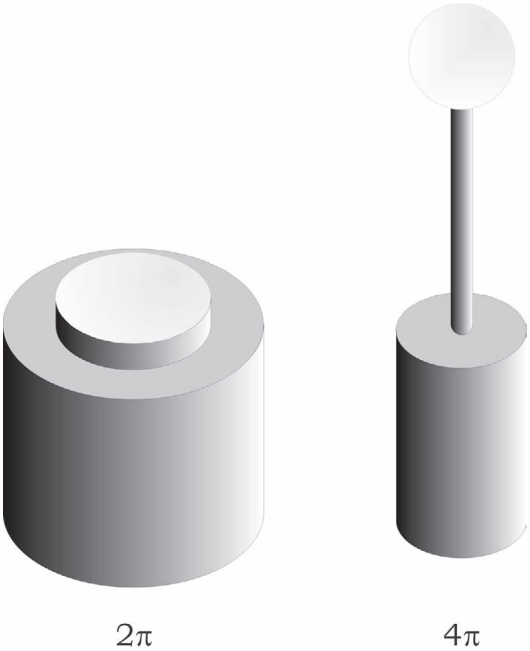


FIGURE 7.19 Examples of PAR detectors equipped with a planar 2π collector or with a spherical 4π collector.

it; therefore, it varies with altitude and meteorological conditions. In water, upwelling (bottom reflected radiance) and down-welling (depth attenuated radiance) irradiance are usually quantified using paired cosine collectors mounted on a frame that is lowered in the water column. Spherical collectors are also mounted on a frame and lowered in the water to obtain light profiles. For photophysiological studies, spherical collectors provide a realistic measure of the total amount of PAR available for photosynthesis in a water body.

Accurate measurement of photosynthetic radiation is essential for controlled environmental research. The most common method of measuring PAR gives equal value, that is, equal energy content, to all photons with wavelength between 400 and 750 nm and is referred to as the photosynthetic photon flux (PPF) measured in $\mu mol\ m^{-2}\ s^{-1}$. The ideal PPF sensor would respond equally to all photons between 400 and 750 nm. However, photosynthesis is driven also by photons with wavelength below 400 and above 750 nm, and photons of different wavelength induce unequal amount of photosynthesis. For these reasons, an accurate measurement of PAR should follow the relative quantum efficiency (RQE) curve, which weights the photosynthetic value of all photons with wavelength from 360 to 760 nm. The RQE resembles the absorption spectrum of the absorbing algal structures. A sensor that responds according to this curve measures yield photon flux (YPF) in micromoles per square meter per second, the same unit of PPF.

Detectors designed to measure YPF or PPF are commercially available. Both types consist of an optical diffuser collector (planar or spherical) and multiple-spectral filters in front of a broad-spectrum photovoltaic detector.

Planar detectors measure only non-reflected sunlight. They should possess cosine-corrected response; since the light impinging on the measurement plane is proportional to the cosine of the angle at which the light is incident, the response of the detector should also be proportional to the cosine of the incidence angle (see Equation 22). An integrating sphere measures both non-reflected and scattered sunlight; it needs no corrections since it is the ideal cosine detector, responding equally to light coming from all direction.

The peak responsivity and bandwidth of a detector can be controlled through the use of filters. Filters can suppress out-of-band light but cannot boost signal and restrict the spatial responsivity of the detector. Filters operate by absorption or interference. Colored glass filters are doped with materials that selectively absorb light by wavelength and obey the Beer-Lambert law. The peak transmission is inherent to the additives, while bandwidth depends on the thickness. Interference filters that select very narrow bandwidths rely on thin layers of dielectric to cause constructive interference between the wave fronts of the incident white light. Therefore, by varying filter thickness, we can selectively modify the spectral responsivity of a detector to match a particular function. Pass band filters are often used to select a specific wavelength radiation. Any of these filter types can be combined to form a composite filter that matches a particular photobiological process. Multiple filters cemented in layers give a net transmission equal to the product of the individual transmissions. The detector's overall spectral sensitivity is equal to the product of the responsivity of the detector and the transmission of the filters. Given a desired overall sensitivity and known detector responsivity, we can then solve for the ideal filter transmission curve.

Different measurement geometries necessitate specialized input optics. Radiance and luminance measurements require a narrow viewing angle (<4°) in order to satisfy the conditions underlying the measurement units. Power measurements, on the other hand, require a uniform response to radiation regardless of input angle to capture all the light.

SUGGESTED READING

Barnes, C., Tibbitts, T., Sager, J., Deitzer, G., Bubenheim, D., Koerner, G. and Bugbee, B. Accuracy of quantum sensor measuring yield photon flux and photosynthetic photon flux. HortScience, 28, 1197–1200, 1993.

Barsanti, L., Evangelista, V. and Gualtieri, P. Absorption microspectroscopy, theory and application in the case of photosynthetic compartment. Micron, 38, 197–213, 2006.

Buhrer, H. Light within algal cultures; implications from light intensity within a lens. Aquatic Science, 62, 91–103, 2000.
Coltelli, P., Barsanti, L., Evangelista, V. and Gualtieri, P. Algae through the looking glass. Microscope Research and Techniques, 80, 486–494, 2017.
Coltelli, P., Barsanti, L., Evangelista, V. and Gualtieri, P. Reconstruction of the absorption spectrum of an object spot from the color values of the corresponding pixel(s) in its digital image: The challenge of algal colors. Journal of Microscopy, 264, 31–320, 2016.
Dusenbery, D.B. Sensory ecology—How an organism acquires and responds to information. W.H. Freeman and Co., New York, 1992.
Evangelista, V., Barsanti, L., Passatelli, V., Frassanito, A. and Gualtieri, P. Microspectroscopy of the photosynthetic compartment of algae. Photochem Photobiol, 82, 139–146, 2006.
Evangelista, V., Evangelisti, M., Barsanti, L. Frassanito, A.M. and Gualtieri, P. A polychromator-based microspectrophotometer. International Journal Biological Science 3, 251–256, 2007.
Falkowski, P.G. and Raven, J.A. Aquatic phoyosynthesis. Volume 49, 621–621. Blackwell Science, Malden, 1997.
Jones, H.G., Archer, N., Rotenberg, E. and Casa, R. Radiation measurement for plant ecophysiology. Journal of Experimental Botany, 54, 879–889, 2003.
Levi, L. Applied Optics—A guide to optical system design. Volume I and Volume II. John Wiley and Sons, Inc., New York, 1980.
Lobban, C.S. and Harrison, P.J. Seaweed ecology and physiology. Cambridge University Press, New York, 1994.
Singsaas, E.L., Ort D.R. and De Lucia, E.H. Variation in measured values of photosynthetic quantum yield in ecophysiological studies. Oecologia, 128, 15–23, 2001.
http://hyperphysics.phy-astr.gsu.edu/hbase/hframe.html
http://intl-lighttech.com
https://coledge.files.wordpress.com/2015/03/thinking-photometrically.pdf
www.biospherical.com/Index.htm
www.cvrl.org/
www.konicaminolta.com/instruments/knowledge/light/index.html
www.licor.com/
www.microscopyu.com/
www.microscopyu.com/microscopy-basics/components
www.optics.arizona.edu/
www.plantphys.net/
www.rp-photonics.com/luminosity.html
www.zeiss.com/microscopy/int/home.html

Subject Index

Note: Page numbers in *italics* indicate illustrations and page numbers in **bold** indicate tables on the corresponding page.

A

absorbance
  spectra, isomeric form, *185*
absorption, *see* light
absorption spectra/um, 234–235, 386
  alternative method, 404
  chloroplast, *196*, 362, *363*, *407*
  eyespot, *184*
  heterocyst, akinete, *80*
  in vivo recording, 404
  normalized, 406
  photosynthetic compartments, *236–240*
  prey chloroplast, *196–197*
  reconstruction, 405
  red shift, 248
accessory pigments, 8, 14, 17, 19, 67
  carotenoids, 7, 194, 198, 220, 249
  monovinyl chlorophyll b, 248
  phycobilins, 7
  phycobiliproteins, 189, 249
  xanthophylls, 192, 194, 249
aerobic photosynthesis, 63
aerobic respiration, 72, 79, 227
akinete, *see* resting stages
albedo
  cloud, 94
  ocean, 75
  surface, 58
algae
  collection, 257, 260, 262, 296, 307–308, 323, 370
  hanging drop method, 258
  identification, 19, 101, 258, 298–299, 356, 358, 360
  mounting, 258
  observation, 19, 258, 298, 398
  permanent slide, 258
  preservation, 257
  shape codes, 258, **259**
  staining, 258
  storage, 257
algae-based products, 368
  biorefinery, 292, 366, 368, 374–376, *376*, 378
  business to business (B2B), 272
  business to consumer (B2C), 272
  exploitation, 339, 368, 372–373, 375, 377
  markets, 307–309, 312, 314, 327, 331, 347, 368, **369**, **370**, 371, 373
  market scenarios, 371, 376
  sustainability, 292, 297–298, 365–366, 376–378
  value chain, 366, 372
algaenans, 72
algal quantitative determination, 298
  Burker chamber, 301
  Coulter Counter, 301
  counting chamber, 300, 301, *301*
  Fuchs-Rosenthal chamber, 301
  Sedgewick-Rafter chamber, 299, *299*
  Thoma chamber, 301
  Utermöhl chamber, 300
Alzheimer's dementia, *see* Harmful Algal Blooms
Amphibia, 51–52
  Anura, 51–52
  critical thermal maximum (CTM), 52–53
  cutaneos respiration, 53
  egg capsule, 51–52
  facultative symbiosis, 53
  intracapsular algae, 52
  mutualism, 52
  tadpoles, 52–53
  Urodela, 51
amphiesma, 114, *115*, 116, 205, *see also* cell membrane type, 3
  athecate taxa, unarmored, naked, 114
  categories, 114, *115*
  Dodge and Crawford system, 114
  thecate taxa, armored, 114, 201, 206–207
amyothrophic lateral sclerosis (ALS), *see* Harmful Algal Blooms
Arachnida, 50
  arthropods, 50, 56
  camouflaging, 43
  epizoic algae, 50
  harvestman, 43, 50
  Opiliones, 50
  spider webs, 50
artificial neural networks (ANNs), 360
Aurearenales, 19
autocolony, *see* reproduction
axoneme, 123, 128–132, 136, 138, 158, 170–171, 176, 182, 188
  9+0 pattern, 128
  9+1 pattern, 128
  9+2 pattern, 128–129
  central doublet, 132–134
  microtubules, 126
  nexin links, 128
  outer/inner dynein arms (ODA IDA), 128
  outer/peripheral doublets, 126, 128, 130, 132, 135–136, 138, 171
  proteins, 128
azaspiracid shellfish poisoning (AZP), 349

B

Bacillariophyceae, **4**, 19, 48–49, 57, 61, 87–88, 93, 101, 107, 149, 193–194, **195**, 241, **284**, 324–325, 342, 348, 350–351, **355**
bacteria, 37, 48–50, 76–78, 82, 92–94, 101, 226–227, 241, 262, 286, 341, 351–352
  anaerobic, 63
  indole-3-acetic acid (IAA) production, 49
  interaction, 49, 86, 167

marine, 49, 92
micronutrients, 49
p-coumaric acid, 49
phycosphere, 48–49
protease, 49
Bangiales, 10, 311, *225*
Bangiophyceae, **3**, 10, 191, 225, 307, 310, **324**, 327
basal bodies, 12, 128, 136–151, 153, 158, 250
1 o'clock–7 o'clock configuration, 137–138, *137*
11 o'clock–5 o'clock configuration, 137–138, *137*
12 o'clock–6 o'clock configuration, 137–138, *137*
cartwheel, 136, 138, 151
clockwise/counterclockwise (CW) (CCW), 12, 137, 162, 165
cruciate, 12, *137*, 139–141
directly opposed (DO), 12
primordial pair, 2A 137–138
root system, 138–141, *140*, *141*, 145, *146*, 147, *147*, 148, *148*, 149, *149*, 150, *150*, *151*, *152*, *153*
transitional plate, 138
binary fission, *see* reproduction
bioactive compounds, 72, 296, 337, **338**, 347, 371
carotenoids, 292, 308, 337, **338**, 339, 367, 372
extracts, 327–329, 331–332, **333**, 335–337, **338**, 341
polyphenols, 337, **338**, 354
polysaccharides, 297, 329–330, 337, **338**, 339, 341–342, 368, 371–372, 375
polyunsaturated fatty acids (PUFA), 21, 291, 325, 340, 367
vitamins, 308, 310–311, 316–317, 325–326, 337, **338**
bio-based economy, 365
biorefinery, 292, 366, 368, 374–376, *376*, 378
biotechnology companies, 368, **369**, **370**
circular economy framework, 366
feedstock, 367, 371, 373, 376, 378
processing, 292, 311–312, 320, 332, 366, 368, 372–373, 375–376
products, 291, 297–298, 307, 310–311, 318, 327, 335–336, 339–340, 364, 367–368, **369**, **370**, 371–373, 377
sustainability, 292, 297–298, 365–365, 376–378
target markets, 368, **369**, **370**, 371, 373
biogeochemistry, 63, 71, 88, 91
atmosphere, 57, 62, 71–76, 78, 81, 85, 88–89, 92, 94, 227, 243–244, 367
biogeochemical cycling, 49, 71–72, 86, 89, 249
biological availability, 71, 275
biosphere, 71–73, 76, 83, 90, 215, 235, 242, 367
hydrosphere, 71, 73, 76
lithosphere, 71, 73, 74, 76, 88
bioluminescence, 26
bioremediation, 298, 361, 364, 372
chlorophyll degradation/chlorosis/pheophinitization, 362–363
exclusion mechanisms, 362
growth inhibition, 361
heavy metals, 10, 331, 361–362, 367
indicators/bioremediators, 58, 362
sorption tool, 364
toxicity, 361–362
biotic interactions, 44
amphibians, 50–53, 56
arthropods, 50, 56
bacteria, 48–50, 58, 60, 86, 262
epiphytism, 15, 43, 297, 322–323, 353
humans, 43, 53, 55
mollusks, 43, 53, 323
polar bears, 55
sloths, 43, 54
turtles, 43, 53
viruses, 44–48
blue-green algae, *see* Cyanobacteria
Bolidophyceae, **4**, 19, 88
brown algae, 1, 35, 128, 150, 168, 250, 307, 319, 330, 341–342, 355
brown tides, *see* Harmful Algal Blooms
business to business (B2B), *see* algae-based products
business to consumer (B2C), *see* algae-based products

C

calcareous macroalgae/microalgae, 74
calcareous red algae, *see* fertilizers
calcified walls, *see* cell membrane type, 2
Calvin Benson Bassham cycle (CBB cycle), 96, 235, *240*, 241
carboxylation, 242
reduction, 242
regeneration, 242
carbonation reaction (Urey reaction), 88
carbon cycle, see oxygen and carbon cycles
carboxysomes, *see* ribulose-1, 5-bisphosphate carboxylase/oxygenase (RuBisCO)
carotenoids **6**, 7, 8, 19, 26, 57–58, 61, 65, 172, 183, 189, 191–192, *196*, 219, 220, 227–228, 235, *236*, *237*, *238*, *239*, *240*, 246–247, 249, 292, 308, 337, **338**, 339, 367, 372, 404
α-carotene, **6**
β-carotene, **6**, 8, 14, 17, 19, 179, 183, 189, 191–192, 194, *222*, 228, 231, 246–247, 292, 310, 314, 319, 325, 337, **338**, 339, 344, **369**, 372, 405, *407*
γ-carotene, **6**
CCD cameras, 358, 360–361, 396, 399, 400–401, 403, 405–406
cell membrane, 21, 23
type, 1 simple, 101, *102*
type, 2 with additional extracellular material, 101, 102, 105, 107, 110
type, 3 with additional intracellular material in vesicles, 101, 114
type, 4 with additional intracellular and extracellular material, 101, 116, 119, *121*
cellular bisection, *see* reproduction, asexual, vegetative
cell walls, *see* cell membrane type, 2
Cercozoa, **4**, **6**, 26, **29**, 64, 65, 194, 205
chloroplasts, 194
ejectile organelle, 205
root system, 150, *151*
Charophyceae, **3**, 15, 110–111, 123, 145, 348, 354–355
Charophyta, **3**, **6**, 15, **29**, 110–111, 203
chloroplasts, 191
phycoplast, 199
root system, 139
Charophytes, 15
Chlorarachniophyceae, **4**, **6**, 26, **29**, 65, 101, 150, 157, 178, 194, *237*, *see also* Cercozoa
net-like plasmodium, 26, 101

Chlorodendrophyceae, **3**, 12, 104, 124–126, 138, 140, 178, 324–325
Chlorokybophyceae, **3**, 15
Chlorophyceae, **3**, 12, 49, 50–52, 58, 61–62, 65, 72, 93, 101, 103, 110–111, 119, 122–123, 128, 138, 140, *141*, 160, 169, 178, **284**, 307–308, 342
chlorophylls, **6**, 14, 19, 23, 26, 76, 215, 219, 226–229, 235, 246, 251, 362, 367, 372, 404
  chlorophyll *a*, 23, 63–65, 67, 192–194, 198, 219–220, *221*, 225, 228–229, 235, 249, 405
  chlorophyll *b*, 14, 63–64, 67, 198, 219–220, *221*, 235, 249, 405
  chlorophyll c_1 19, 192–193, 219–220, *221*, 235
  chlorophyll c_2 19, 65, 192–193, 219–220, *221*, 235
  chlorophyll *d,* 219, 220, *222*
  chlorophyll *f,* 219, 220, *222*
Chlorophyta, **3**, **6**, 9, 11–12, 14, 26, 28, **29**, 31–32, 35–38, 40–42, 53–54, 58, 63–64, 74, 101, 104, 110–111, 123–124, 128, *136*, 136–137, *137*, 159, 162, 165, 167–168, 173–174, 177, 183, 229, *237*, 307–308, 321, 324, 327, 354
  chloroplasts, 191
  nucleus, 199
  root system, 139, *141*
chloroplasts, 9, 10–12, 14, 19, 23, 26, 32, 41, 55, 59, 63, 67, 81, 89, 138, 171, 183, 188–189, 191–192, 194–197, 217–218, 229–231, 234, 241–242, 361–363, 368
  cup-shaped, 191
  discoid, 197
  disc-shaped, 193
  ellipsoidal, 188
  elongated, 197
  lobed, 193–194
  net-like, 191
  plated, 198
  prey, *196*, *197*, 37
  ribbon-like, 188, 193
  shield shaped, 197
  stellate, 9, 188, *192*, 311
Chromista, **3**, 177
chromophore, 173, 179, 184, 218–220, 228–229, 246–247, 404–406, *407*
Chrysophyceae, **4**, 19, 41, 93, 101, 107, 111, 119, 124, *135*, 135, 137, 147–148, 154, 169, 176, 179, 193, **284**, 342, 348
ciguatera fish-food poisoning (CFP), 349, 353–354
cloud condensation nuclei (CCN), 94, *see also* sulfur cycle
coccolith light scattering, 75
coccolithophorid blooms, 74–75
Coccolithophyceae, **3**, 17, 49, 74, 93, 105, 123, 128, 136, 324, 348
Coccoliths, 75–76, 104–105, 154, *see also* cell membrane type, 2
  coccosphere, 105
  heterococcoliths, 105–106, *106*
  holococcoliths, 105, *106*
  nannolith, 105
coenobium, 28, 38, *see also* thallus, structure of
  motile, *30*, *31*
  non-motile, *31*, *40*
Coleochaetophyceae, **3**, 15, 145
collections, *see* culturing
compound eye, 26
Compsopogonophyceae, **3**, 11
Corallinales, 74, 334
coralline algae, 10, 249–250, 296
corals, 23, 43, 107, 322, 349, 353–355
  antiphatarians, 251
  endosymbiosis, 250
  zooxanthellae, 18, 23, 250, 251
cosmetics, 308, 328, 331, 334–336, 368, **369**, 371–372, 275
cruciate root system, 12, *137*, 139–141
crusts, 10, 35, 60–61
  biological sand crusts (BSCs), 60
  CO_2 concentrating mechanism (CCM), 60
  protective carotenoids, 61
  UV-screening pigments, 61
Cryptophyta, **3**, **6**, 18, **29**, 116, 132–133, *134*, 169, 173–175, 177, 183, 189, 227, *238*
  chloroplasts, 192, 196
  ejectile organelle, 204
  gullet, 18, 146
  nucleomorph, 26, 200
  periplast, 116
  polygonal plates, 19
  root system, 145, *148*
  trichocystis, 146
cultures macroalgae, 296
  Integrated Multitrophic Aquaculture (IMTA), 298
  nearshore cultivation, 297
  offshore cultivation, 297
  onshore cultivation, 296
cultures microalgae, 286
  batch, 286–287, **288**, *288*, 289
  closed systems, 291, 308, 373–374
  commercial-scale, 290
  continuous, 289–290
  open systems, 294, 374
  outdoor ponds, 291
  photobioreactor, 293–296, *294*
  semi-continuous, 290
culturing, 257
  collections, 260, 265, 283–284
  methods, 286
  parameters, 287, 290, 293
  sterilization, 284
Cyanidiophyceae, 10, 59, **3**
Cyanobacteria, 2, **3**, **6**, 9, 28, **29**, 307–308, **369**
  blue-green algae, 2, 8–9, 41, 89, 309, 350
  conjugation, 198
  non-diazotroph, 85
  non-heterocystous, 78–79, 86
  thylakoids, 7, 228
  transformation, 198
Cyanophyceae, **3**, 59, 61, 178, **284**, 307, **324**, 348, 350, **355**
Cyanophyta, 41, 65
cytoplasmic bridges, 28

D

diarrheic shellfish poisoning (DSP), 349, 353
diatom, 7, 19, 42, *43*, 48–49, 57, 59–61, 64–65, 67, 74–75, 87–91, 95–97, 102, 325, 340–341, 348–349, 351–352
  centric, *108*, 149, 193
  freshwater, *20*

marine, *20*
oozes, 72, 91
pennate, 107, 109, *109*, 296
sedimentation, 74
diazotrophs, 77–78, 80, 83, 85–87
Dictyochophyceae, **4**, 19, 88, 91, 112, 130, 193–194, 348
digital microscopy, 161–165, 183–184, 301, 303, 356, 358, 360–361, 403
characteristic color, 259–260, *261*, 360
color features, 359
contour detection, 259–260, 360
denoising, 360, 404
hardware, 259, 358, 361, 403, *406*
image acquisition, 259
image classification, 260
image processing, 259, 358, 360, 403–404
image segmentation, 259
pigment signature, 259–260
software, 404
spectroscopic features, 360–361
dimethyl sulfide (DMS), 74, 93–94, 351, *see also* sulfur cycle
dimethylsulfonium propionate (DMSP), 93–94, *see also* sulfur cycle
dinoflagellates, 23, 26, 114, 156
desmochisis, 201
desmokont/dinokont type, 23, 157, *159*, *160*
eleutheroschisis, 201
noctikaryotic chromosomes, 201
temporary cysts, 114
dinokaryon, *see* Dinophyceae
Dinophyceae, **4**, **6**, 23, 26, 40, 48, 72, 93, 103, 114, 127, 130, 137–138, 173–174, 178, 199, 348, 350, 353, **355**
chloroplasts, 195, *196*, *239*
cingulum, 23, 116, 151, 157, 207
cryptophyte-derived plastid, 195
dinokaryon/nucleus, 200
ejectile organelle, 205
girdling flagellum, 23
haptophyte-derived plastid, 195
longitudinal flagellum, 23, 127
ochrophyte-derived plastid, 195
root system, 151, *152*
rotatory swimming, 23
sulcus, 207
transversal flagellum, 23
trichocystis, 26, 205–206
dinotoms, 67, *see also* endosymbiosis
DNA, 41, 198–201, 241, 357
chloroplast, 9, 14, 17, 19, 26, 198
exons, 198
genome, 56, 64–65, 87, 89, 96, 177, 188, 198, 231, 357
introns, 198
nucleoids, 17, 19, 188, 191–193
Donnan equilibrium, 89, *see also* silicon cycle

E

edible algae, 307–308, 314, 316–317, 323, **324**, 372
animal feed, 324–327
human food, 308–327
endoplasmic reticulum, 10, 107, 128, 174–175, 191–195, 198–200, *see also* chloroplasts
endosymbiosis, *66*
α-cyanobacterium, 64
β-cyanobacterium, 63
cryptophyte endosymbiont, 67, 196
cyanobacterial symbiont, 63
cyanobacterium-eukaryote endosymbiosis, 64
diatom endosymbiont, 67
eukaryote-to-eukaryote gene transfer, 65
green algal endosymbiont, 26, 65, 67, 89
green lineage, 63–64, 235, *240*
kleptoplastids, 67, 195, **195**
ochrophyte-derived plastid, 195
primary endosymbiosis, 63–64, *66*
primary plastids, 63, 195
red algal endosymbiont, 89
secondary endosymbiosis, 64, *66*, 89
secondary plastids, 195
second lineage, 63
serial secondary endosymbiosis, *66*
tertiary endosymbiosis, 64–65, *66*, 195
tertiary plastids, 195
testate amoeba, 64
third lineage, 64
endosymbiotic gene transfer (EGT), 2
energy-transfer molecules, *see* photosynthesis
environmental monitoring, 356, 360
digital microscopy, 358–361
flow cytometry, 356
metagenomic analysis, 357
remote sensing, 358
water monitoring, 356
epiphytism, *see* biotic interactions
Erythropeltidales, 11
Eubacteria, 2, **3**, 49, 177, 276
euglenoid movement, *see* metaboly
Euglenophyceae, **4**, **6**, 26, 28, **29**, 61, 103, 116, 127, 130, 132, 136, 176, 179, 342
chloroplast, 197
ejectile organelle, 207
endosome, 201–202
feeding apparatus, 208
nucleus, 199–201
reservoir, 122, 130, *134*, 153, 176, 183, 201–202
root system, 152, *153*
trichocystis, 207
Euglenozoa, **4**, **6**, 26, **29**, 36, 38, 64–65, 116, 152, 175, 197, 201, 207
Eustigmatophyceae, **4**, 19, 21, 72, 101, 110, 135, *135*, 137, 149, 175, 193–194
eutrophication, 95, 298, 347, 354–355, 377
extreme habitats, 37, 43, 51, 347
cold environments, 56–58
desert, 61
dry environments, 60–61
exopolysaccharides (EPSs), 50
geothermal activities, 58–59
hot environments, 58–60
space, 62
UV-screening pigments, 61
eyespot, 15, 17, 19–20, 26, 50, *103*, 162, 165, *172*, 172–177, *177*, 181, 183–184, *184*, 188, *193*, 202

F

facultative anaerobic bacteria, 77
fertilizers, 82, 95, 307, 332–333, 335
  calcareous red algae, 334
  maerl, 334–335
  soil conditioner, 335
fiber
  anchoring, 138, 146
  connecting, 142
  cross-banded, 138
  cross-sectioned, 142, *144*
  non-striated, 140, 143, 145, 152, *152*
  proximal connective, 140
  radial fiber Rf, 132, *132*
  striated distal, 142, *144*, 145
fibrillar spiral, *see* transition zone type, 2
field instruments, 406
filaments, *12*, *16*, 28
  branched, 2, 8, 10, 15, 21, 28, 32, 35
  false branching, 28, *33*
  multiseriate/pluriseriate, 28, *34*
  simple, *17*, 28, *32*
  true branching, 28, *34*
  unbranched, 2, 8, 15, 28, 53, 315
  uniseriate, 28, *34*
flagella, 122
  anisokont, 12, 123
  hairs, 126, 128, 156–157
  heterokont, 19, 156, 182
  internal features, 128
  isokont, 12, *123*, 123–124, 156, 159, *160*, 182
  mastigonemes, 12, 19
  scales, 123, *125*
  shape, 123
  spines, 128
  trailing, *126*, *157*, *176*, *177*
flagellar
  beating, 162, 165
  motor, 170
Florideophyceae, **3**, 9–10, 35, 110, 191, 307, 312–314, **324**, 327, 329, 332, **333**, 334, 348–349, 351, 354–355, **355**
fluorescence, 184, 387–388, *388*, 401–402, *see also* microscopy
foraminifera, *see* oxygen and carbon cycle
Forster type energy transfer (FRET), 185
fossil-based products, 366
fragmentation, *see* reproduction
freshwater media, 265
  Aaronson's medium, **268**
  BG11 medium, **266**
  Bold basal medium, **269**–**270**
  Cramer and Myers medium, **268**–**269**
  CY-II Cyanophora paradoxa medium, **271**–**272**
  diatom medium, **267**
  DY-III medium, **267**
  Jaworski's medium, **271**
  MES-Volvox medium, **270**–**271**
  Sueoka's medium, **269**
  Zarrouk's medium, **272**
frustules, 107, 110, 154, *see also* cell membrane type, 2
  areolae, 109
  epitheca, 107
  fultoportulae, 109, *110*
  hypotheca, 107
  portules, 109
  raphe, 109, 167
  rimoportulae, 109, *110*
  silica, 89–90
functional absorption cross-section, *see* photosynthesis-irradiance response curve (P-VS-E CURVE)
functional foods, 336–337
  dietary fibers, 311, 337, **338**, 342
  nutraceuticals, 308, 336–337, 364, 370–372
  phlorotannins, **338**, 367
  polysaccharides, 297, 329, **338**, 339, 341–342, 372, 375
  polyunsaturated fatty acids (PUFAs), 337, **338**, 340–341, 372

G

Gastropoda, 53, *see also* biotic interactions
  freshwater snails, 53
  mollusks, 43
girdle lamellae, 17, 19, 26, 192–195, 198
glacial–interglacial variations, 75
Glaucophyceae, **3**, 8–9, 133, 178, 260, **284**
Glaucophyta, **3**, **6**, 7–9, **29**, 63–65, 128, 133, *134*, 137, 177, 189, 191, 227, 229, *236*
  cyanelles, 139, 189
  dorsiventral construction, 8
  polyphosphate granules, 189
  root systems, 139, *140*
global warming, 75–76
Great Oxygenation Event, *see* oxygen and carbon cycle
green algae, 26, 35, 38, 41, 50–55, 60–61, 63–65, 87, 122, 136, 142, 199–200, 229, 231, 241, 250, 257, 323
greenhouse effect, 75
  gas, 49, 57, 90, 94, 377–378
growth
  constant, 303
  curve, 38, 287, *288*, **288**, 289, 303
  generation time, 61, 303, 356
  maximum alga growth rate, 95
  maximum population growth rate, 95
  rate, 53, 62, 84, 95–96, 264–265, 287, 289, 290, 303, 315, 340, 353
growth media, 264, 284, 373
  buffers, 277
  chelators, 274
  defined/undefined, 265–266
  k-selected species, 265
  nutrients, 274
  preparation, 264
  r-selected species, 265
  sea water base, 273
  sea water constituents, **275**
  soil extract, 277
  trace metals, 274
  vitamins, 276, *277*

H

Haber-Bosch process, 77
Haptonema, 17, 128, *129*, 145, *146*, *147*

Haptophyta, **3**, **6**, 17, **29**, 65, 74, 104, 123, 134, *134*, 136–137, 154, 169, 173–175, 177, *238*, 324
chloroplasts, 192
ejectile organelle, 203, *203*
root system, 145, *146*, *147*
scales, 104–105, 124
Harmful Algal Blooms (HABs), 47–48, 95, 346–348, 350, 354, 358
Alzheimer's dementia, 351
amyothrophic lateral sclerosis (ALS), 351
brown tides, 348
dictyoles, 354
didymo, 348, *349*
green tides, 348
Parkinson's dementia, 351
red tides, 349, 352
toxic algae, 355, **355**
heavy metals, *see* bioremediation
Helicosporidia, 56
apicomplexan malaria parasite, 56
cryptic plastid, 56
obligate parasites, 56
heterocystous cyanobacteria, 61, 79
heterocysts, *see* nitrogen fixation
high nutrient low chlorophyll (HNLC) regions, 85
horizontal gene transfer (HGT), 2, 63–65
hydrocolloids, 327–329, 331, 336, 371
agar, 329, **333**, 341, **370**, 371, 327–328
agarose, 329
alginates, 330
alginic acid, 111, 327, 330, **338**, 342
carrageenan, 313, 328, 331–332, **333**, 336, **338**, 341, 371
hypnospores, *see* resting stages
hypnozygote, *see* resting stages

I

illuminance, 414
intraflagellar
accessory structures, 130
transport, 170
iron chemical forms, 83
iron cycle, 83
atmospheric dust deposition, 84, 86
Great Oxidation Event (GOE), 227
iron fertilization experiments, 87
iron hypothesis, John Martins, 84
iron-limited regions, 86–87
iron-oxidizing/reducing microrganisms, 83
iron permease, 85, 87
iron quota, 86, 87
river inputs, 84

K

Kareniaceae, 67
kelp, 21, 297, 315, 317, **324**, 331, 334, 368
kinetosomes, *see* basal bodies
Klebsormidiophyceae, **3**, 15
kleptoplastids, 67, 195, *see also* endosymbiosis
Bacillariophyceae, **195**
Cryptophyceae, **195**
dinoflagellates, **195**

L

lab instruments, 394
lateral gene transfer (LGT), 2
Law of the Minimum von Liebig's Law, 94, 96
life cycle assessment (LCA), 377–378
global warming potential (GWP), 377–378
net energy ratio (NER), 377–378
life cycles
alternation of generation, 11, 42, 312, 317, 321–323
diplohaplontic or sporic, 42
diplontic or gametic, 42
haplontic or zygotic, 10, 41
heteromorphic, 10, 17, 42, 312, 315
isomorphic, 10, 42, 368
triphasic reproduction cycle, 10
life phases
carposporophyte, 10
conchocelis phase, 10, 312
egg, 41, *44*, *46*, *47*, *175*, 179, 181
gametophyte, 10, 42, *44*, *45*, *46*, *47*, 368
sperm, 15, 41, *44*, *46*, *47*
sporophyte, 10, 42, *44*, *45*, *46*, *47*, 315, 317–318, 321, 368
vegetative cell, 38, 41, *43*, 80, *80*
vegetative diploid, 42
zygote, 10, 41, *42*, 44, 46, 47, 58, 172, 181, 181, 260, 318
light, 385
absorption, 386, *386*
diffraction, 392, *394*
dispersion, *393*
electromagnetic radiation, 408, 215, 385
electromagnetic spectrum, *216*, 408
electromagnetic waves, 385, 389
frequency, 385, 389, 412
interference, *385*, 389
Rayleigh criterion, 399, *400*
reflection, 389, 390, *390*
refraction, 391–392, *392*
scattering, 385
velocity, 385, 392
light-limited environments, 247
black corals, 251
compensation depth/irradiance/point, 244–245, 248, 251
dark-purple crustose coralline algae, 74, 249
deep-water dwelling, 248
hypogea, 251
maintenance respiration rate, 96, 246
maximum depth, 248–251
troglobitic algae, 251
zooxanthellate corals, 250–251
limiting nutrient, 96, 276, 290, 82, 94–95
loricas, *see* cell membrane type, 2
low nutrient low chlorophyll (LNLC) regions, 85
Lugol's solution, 257–258, 298–299

M

maerl, *see* fertilizers
Mamiellophyceae, **3**, 12, 87, 122, 124–126, 140, 178, 325
marine media, 265, 273
ASN-III medium, **279**

CHU-11 medium, **279**–**280**
ESAW medium, **282**–**283**
f/2 medium, **281**
Johnson's medium, 282
K medium, **281**–**282**
PCR-S11 medium, **280**–**281**
Walne's medium, **278**, **279**
market scenarios, *see* algae-based products
meiosis, 38, 41, 42, *42*, *43*, *44*, *45*, *46*, *47*, 198
Mesostigmatophyceae, **3**, 15, 140, 178
metaboly, 26, 117, *see also* cell membrane type, 4
metagenomics, *see* environmental monitoring
microscopy, 394, 398
Abbe's formula, 399
Airy Disk, 399, *400*
bright field microscope, 394, 396
dichromatic mirror, 402
epi-illuminator, 401–402
filters, 419
fluorescence, 387, 401
lens, *395*
light sources, 402
microspectrophotometry, 80, *80*, 174, 184, **195**, 196, 359, 403
numerical aperture, 398–399, 402
Rayleigh criterion, *400*
resolution, 393, 398–399
steps in establishing Köhler Illumination, 396–397, *397*, 402
microtubular
dyneins, 128, 170
rootlets, 12, 142, 153
roots, 138, 140–142, *142*, *143*, *144*, 145–152, *147*, *148*, *149*, *150*, *151*
system, 118
triplets, 136, 138
microtubules, 12, 114, 118, 121–122, 126, 128, 130, 138–142, 145, *147*, 148–150, 153, 167, 170–171, 175, 199–201, 209
milking, 339–340
mineralization processes, 73, 77
Miozoa, *see* Dinophyceae
mitochondrion, 10–11, 59, 63–64, 67, 89, 138, 146, 198, 229, 234, 243, 252, *see also* endosymbiosis
chondrome, 198
proteobacterium, 63
mitosis, 28, 32, 39, 42, 198–202
closed, 199–201
open, 200
Monod equation or Michaelis-Menten equation, 95
half-saturation coefficient, 95
half-saturation constant, 241
nutrient-limited growth, 95
uptake rate, 95
movements other than swimming, 165
buoyancy control/regulation, 7, 94, 154, 168–169
flotation, 168
gliding, 163, 167, **168**
sinking, 91, 154–155, 169
slime extrusion, 167
mucilages, mucus coating, *see* cell membrane type, 2
mucocysts, 21, 206–208, *208*

N

Nephroselmidophyceae, **3**, 12, 124, 126, 140
neurotoxic shellfish poisoning (NSP), 349
nitrogen cycle, 76–81
anthropogenic fixed N, 77
assimilation, 76
atmospheric fixation, 77
denitrification, 76
fixation, 76
mineralization, 76
nitrate reductase, 80–81, 94, 365
nitrite reductase, 80–81, 231, 365
nitrification, 76
nitrogen fixation, 77–80
alternative nitrogenases, 78
heterocysts, 7–8, *8*, 61, 79–80, *80*
nitrogenase, 77–80, 86–87, 94
non heterocystous cyanobacteria, 78–79, 86
transamination reaction, 81
Nostocaceae, 62
nucleus, 19, 26, 41, 63–65, 67, 89, 114, 137–138, 140, *141*, 145, *146*, 147–149, *149*, 151, *152*, 153–154, 192–193, 195, 198–201, *202*
centrioles, 9, 10, 199–200
division, 198, 201
envelope, 11, 17, 19, 150, 192–193, 198–202
spindle, 199–201
nutrition, 17, 20, 26, 37–38, 251
autotrophy, 37, 56
facultative mixotrophic, 38
heterotrophy, 20
mixotrophy, 37
obligate heterotrophic, 26, 38, 55
obligate mixotrophic, 28, 38, 262
obligate photoautotrophic, 8, 10
obligate phototrophic, 38
osmotrophy, 37–38
phagotrophy, 17, 20, 37–38
photoautotrophy, 26

O

ocean heat retention, 75
ocellus, 177, *see also* photoreceptive systems type III
hyalosome, 177
pigmented cup, 177
retinoid, 177
Ochrophyta, **4**, **6**, 19, 28–29, 32, 35, 38, 42, 65, 101, 104, 107, 110–112, 123–124, 126, 130, 132, 135, 137, 156, 173–175, 177, 205, *238*, *239*, 307, 315, 324–327, 333, 348
chloroplasts, 193
root system, 147
oxygen and carbon cycles, 72
aragonite, 74
calcification, 74–75, 105, 107
calcite, 74
calcium carbonate dissolution, 75
carbonate system, 75
coccolithophores, 74–75
electron sink, 72
foraminifera, 74, 107

Great Oxygenation Event, 71
radiative budget, 75
seawater carbon system, 75
sedimentary rocks, 73–74, 82
sequestration, 74, 88, 298, 367
oxygen cycle, see oxygen and carbon cycles
oxygenic photosynthesis, 63, 71–72, 78–79, 86, 227, 367

P

Palmophyllales, 37, 250
paraflagellar/paraxial rod (PFR), 123, 129–130, 171, 176, 188
paraflagellar structures, 130
paralytic shellfish poisoning (PSP), 349–350, 353
paramylon, **6**, 26, 65, 198, *343*, 343, 346
anti-fibrotic, 344
β-1-3-glucan, 342–343, 364, 372
drought stress, 344
granules, 365
inflammatory cytokines, 342
nanofibers, 343–344, *345*, *346*
pathogen-associated molecular pattern (PAMPs), 342
pattern recognition receptors (PRR), 342
pro-inflammatory mediator, 344
unbranched triple helices, 343
parasite, 10, 23, 54, 56, 293
parasitism, 10, 43, 56
PAR detectors, 418, *418*
Parkinson's dementia, *see* Harmful Algal Blooms (HAB)
Pavlovophyceae, **3**, 17, 105, 124, 178, 324
Pedinellales, 130
Pedinophyceae, **3**, 12
Pelagophyceae, **4**, 21, 348
pellicle, 118, 121, *see also* cell membrane type, 4
Euglenophyceae, 26, 116
first level, 119
grooves/ridges, 116, *118*
overlapping strips, 116
second level, 119, *121*
strips, 121
third level, 121
Phaeophyceae, **4**, 19, 21, 35, 49, 101, 110–111, 122, 128, 132–133, 137, 150, 169, 175, 179, 193–194, 241, 307, 315, **324**, 326–327, 330, **333**, 333, 342, 348, 354–355
Phaeothanmniophyceae, **4**, 21, 103
phosphorus cycle, 71–72, 81–82
apatite, 81
dissolved phosphorus, 81
inorganic phosphorus deposits, 81
internal cycling, 82
limitation, 96
phosphate forms, 82
P luxury uptake, 83
polyphosphate granules (PolyP), 83
weathering, 81
photoacclimation, 246–247
photocycle, *see* photoreceptor
photoinhibition, 61, 245–246
photometry, 411
geometries, 417
Lambertian surfaces, 414
luminance, 414
luminous efficacy, **413**
luminous energy, 414
luminous flux, 412
luminous flux density, 414
luminous intensity, 412, *415*
photometric curves, 411
photopic/scotopic vision, 411–412, **413**
spectral sensitivity, *412*
unit conversion, 416
photoreception, 173, 177, 183, 411
behavioral and physiological features, 161, 172, 180, 182–183
photoreceptors, 20, 26, *122*, 162, 171–177, *176*, *177*, *178*, *179*, 179, *180*, 181–185, *185*, *186*, 188, 202, 217
phototaxis, 171–172, 181, 183, *187*
sampling strategies, 172, 180–181
signal transmission, 172, 180, 183
transduction, 172, 217–218
photoreceptive proteins, 172, 178, *178*
membrane spanning, 176, 183, 227–228
rhodopsin, *175*, 177, 179, 183
rhodopsin-like proteins, 174, 177, 179, *179*, 184, 251
photoreceptive systems, 173, *176*
type I, 173, *173*
type II, 175, *177*, *178*
type III, 177
photoreceptor, 179, *179*, *180*, 183–184
3D assemblage, 176
hexagonal lattice, 176–177
isomers, *184*, *186*
optical bistability, 183–184
photocycle, 179, 184, *186*
spectrum, *185*
retinal, 179, *180*
type I crystal, 177, 183
photorespiration, 240, 242–243
photosynthesis, 37, 52–53, 56–58, 61–63, 67, 71–73, 75, 78–79, 83–84, 86–89, 91, 96, 154, 168, 171, 215, 217–220, 226–227, 229, 232, 234–235, 242–244, 246–249, 251, 294, 339, 341, 362, 367, 418–419
anoxygenic, 226
ATP-synthase, 229, 234
balance sheet, 251
electron transfer chains (ETCs), 225–228, 232, 245
electron transport, 218–220, 227, 229–231, *233*, 243–244
energy-transfer molecules, 76
Great Oxidation Event (GOE), 227
light-dependent reactions, 219, 235, 243–244
Light-Harvesting complexes (LHCs), 64, *220*, 226–229, 246
light-independent reactions, 219, 234–235, 244
phosphorylation, 226, 232, 234–235, 242, 246, 250
plastoquinone (PQ), 79, 226, 228, 230–232
proton transport, 232
Z-scheme, 232, *233*
photosynthesis-irradiance response curve (P-VS-E CURVE), 243–244, *245*, 247
functional absorption cross-section, 96, 244, *245*, 247
irradiance compensation point, *245*
light saturation, 243, 245, 247

maximum photosynthetic rate, 57, *245*
saturating irradiance, 244–245, 248
photosynthetic active radiation (PAR) detectors, 418, *418*
Photosystem I (PSI), Photosystem II (PSII), 7, 61, 63, 64, 79, 96, 188–189, 220, *220*, 225–232, 234, 244–247
in vivo absorption spectra, *236*, *237*, *239*, *240*, *407*
pigment distribution, 234–235, *240*
structure, 227
phototaxis, *see* photoreception
phycobilins, **6**, 7, 8, 19, 219, 220, *224*, 357, 404
phycobiliviolin, *224*
phycocyanin, **6**, 7, 8, 9, 59, 189, 191–192, *225*, 228, 239, 310, 368, 372
phycocyanobilin, *224*
phycoerythrin, **6**, 7, 9, 189, 191–192, 195, 225, 228, 311
phycoerythrobilin, *224*
phycoerythrocyanin, **6**, 8, 189, 225
phycourobilin, *224*
phycobiliproteins, 9, 63–65, 80, *80*, 189, 192, 196, 220, 225, 227, 235–236, 249, 251, 310
phycobilisomes, 7, 8, 9, 19, 64–65, 189, *190*, *191*, 191–192, 227–228, 248, 251
Picophagophyceae, **4**, 21
pigments, *see* carotenoids; chlorophylls; phycobilins; xanthophylls
Pinguiophyceae, **4**, 21
Plantae, **3**, 63–64, 177
plastids, 26, 56, 63–65, 67, 179, 188, 191, 193, 195, 198, 241, *see also* endosymbiosis
blue-green, 9
origin, 29, 63–64, **195**
plastome, 198
platelet ice, 56–57
poisoning, 349–350
cyanotoxin, 349
fish, 349, 353
food, 349
human, 87, 95, 352, 354
shellfish, 87, 95, 349–350, 353
polar bears, 55, *see also* biotic interactions
captivity, 55
fur coloration, 55
hair, 55
polyphosphate granules (PolyP), *see* phosphorus cycle
Porphyridiophyceae, **3**, 11
Prasinodermatophyceae, **3**, 104, 124, 126, 136
Prasinodermatophyta, **3**, **6**, 11, **29**, 104, 124
chloroplasts, 191
ejectile organelle, 203
intranuclear mitosis, 199
root system, 139
primary productivity, 46, 83, 85, 95, 248
Prochlorophyta, 2
Prochlorophytes, 2, 7, 8, 26, 63, 228, 248
protothecosis, 55–56, *see also* biotic interactions
achlorophyllic unicells, 55
bovine mastitis, 55
Protozoa, 2, **4**, 23, 260, 290
Prymnesiophyceae, 348, 350–351
Pyramimonadophyceae, **3**, 12, 104, 125–126, 138, 203
pyrenoid, 19, 26, 50–51, 191–192, 194, 312
central naked, 197
double-sheeted, 198
pear-shaped, 194
semi-immersed, 194
spindle-shaped, 192

Q

Quartz, 88, 285, **393**

R

radiative budget, *see* oxygen and carbon cycle
radiolarians, 90
radiometry, 408–411
radial intensity, 410
radiance, 410
radiant energy, 71, 408–409, 414, 418
radiant flux, 409
radiant flux density, 409
solid angles, 401, 408, 410–412, 417–418
spectral radiance, 410
spectral radiant energy, 408
spectral radiant flux, 409
spectral radiant flux density, 410
spectral radiant intensity, 411
Raphidophyceae, **4**, 21, 48, 137, 149, 193–194, 201, 205, 241, 342, 348, 350, 352, **355**
root system, 149
thylakoids, 193
trichocystis, 21, 205
red algae, 9–11, 35, 59, 64–65, 191–192, 199, 250, 329, 334, 342, 354
Redfield ratio, 96
stoichiometric balance, 96
reflection, *see* light
refractive index, 392, *392*, **393**, 398
Snell's law, 392
reproduction, asexual, vegetative, 2, 8, 11, 28, 38, *42*, 55
aplanospores, 38
autocolony formation, 38
autospores, 9, 38, 55, 200
binary fission/cell division, 11, 19, 26, 38
endospores, 10
fragmentation, 38
monospores, 11
resting stages, 40
zoospores, 26
reproduction, sexual, 2, 9–11, 19, 38, 41, *42*, 188
anisogamy, 41
fusion of non-flagellate gametes, 15
heterogamy, 26, 41
isogamy, 41
karyogamy, 38
oogamy, 41
plasmogamy, 38
reserve polysaccharides, 14, 19
α-1-4-glucan, **6**, 9
β-1-3-glucan, **6**, 20, 26, 65, 194, 337, **338**, 341, 343–344, 364
β-1-4-mannan, 14
arginine, **6**, 7
asparagine, **6**
chrysolaminarin, 17, 19

cyanophycean starch, 7
floridean starch, **6**, 9
fucoidan, 337, **338**, 341
laminaran, **338**, 342
mannose, 111
paramylon, 26, 364–365
porphyran, 341
starch, 8, 9, 26, 65
ulvan, **338**
xylose, 111, 342
respiration, 46, 51–52, 72–73, 77–79, 83, 89, 96, 218, 227, 242, 244, 248–249, 252
cutaneous, 53
respiratory carbon loss, 248
respiratory electron flow, 79
respiratory electron transport chains, 83, 227
respiratory metabolism, 93
respiratory pathways, 97, 243–244
respiratory process, 79
respiratory rates, 96
resting stages, 40
akinetes, 40
hypnospores, 40
hypnozygotes, 40–41, *40*
statospores, 40–41
Reynolds number, *see* swimming
rhizoplast, 140, *141*, 145, 147–148, *149*
Rhodellophyceae, **3**, 11
Rhodophyta, **3**, **6**, 7, 9, **29**, 35, 42, 64, 74, 103, 110, 139, 165, 167, 177, 189, 225, 227, 229, 236, 241, 249, 307, 310, 327, 332, 342
chloroplasts, 191
encircling thylakoids, 10, 11, 191
incomplete cytokinesis, 9, 199
nuclear associate organelles (NAOs), 199
nucleus, 199
pit connection/plug, 9–10, 199
rhodopsin, *see* photoreceptive proteins
ribulose-1, 5-bisphosphate carboxylase/oxygenase (RuBisCO), 79, 235, 240–243
carbon fixation, 37, 51, 75, 96, 235, 243, 287
carboxysomes, 8–9
oxygenation, 240–243
reductive carboxylation, 240

S

salinity, 263, 273–274, 291, 296, 341, 355
scales, 124, *125*, *see also* cell membrane type, 2
body, 123–124
box shaped, 104, *104*
calcified, 17, 104–105
crown-shaped, 104
fused, 12, 102, 104
hair, 124
limuloid, *125*
naviculoid, 104
spider-web, *125*
Schizocladophyceae, **4**
seasonal blooming, 95
seaweed, 1, 9, 49, 168, 246, 296–298, 307, 311, 313, 322, 327, 329, 331–332, 334, 336, 367–368, 370–373, 378
secondary metabolites, 57, 339, 353–354, 367, 370–373
sessile micro-algae, 23, 296
sheaths, *see* cell membrane type, 2
Sherwood number, *see* swimming
siderophore-producing bacteria, 85–86
siderophores, 85–87
silica (SiO_2), 41, 90–91, 97, 104, 107, 109–110, 124, 154, 262
amorphous, 88–89, 91
biogenic, 89, 109
dissolved, 88
silicic acid $Si(OH)_4$ 88–91, 97
Donnan equilibrium, 89
silicon, 72
silicon cycle, 88–91, 96–97, 109
diatomites, 90
frustules, 19, 89–90, 97, 102, 107, 109–110, 154
silica-forming organisms, 90
silicoflagellates, 20, *22*, 90–91, 112
sponges, 90
sloths, 43, 53–54, *see also* biotic interactions
camouflage, 54–55
epibiotic symbionts, 54
hair, 54
harpy eagle, 54
three-fingered, 54
two-fingered, 54
Ulvophyceae, 54
snow algae, 58
solar/sun radiation, 215, *216*, *216*, 217, 385, 418
Beer-Lambert's law, 217
energy, 216
intensity, 217
photons, *216*, 216–217
Planck's constant, 216
Planck's law, 216
reflection, 92
scattering, 385
spectral regions, 215
space, 62
bioregenerative life support system, 63
Carl Sagan terraforming vision, 62
European Space Agency (ESA), 62
Micro-Ecological Life Support System (MELiSSA), 62
microgravity effect, 62
on-board sustainable life-support systems, 62
spaceflight experiments, 62
spores, 10, 38, 42, *47*, 57, 58, 137, 312, 317–318, 321–323, *see also* reproduction
aplanospores, 38
autospores, *9*, 38, 55, 200
carpospores, 10
endospores, 10
monospores, 11
motile, 15, 38
resting, 58
zoospores, 38
statosphore, *see* resting stages
stellate pattern, *see* transition zone type, 5
stephanokont zoospore, 122, 138, 141, 143
sterilization, *see* culturing

storage products, *see* reserve polysaccharides
stumpy mutant, *51*, 162, *164*
Stylonematophyceae, **3**, 11
sulfur cycle, 92
  assimilatory/dissimilatory sulfate reduction, 93
  bacteria, 92, 94
  dimethyl sulfide (DMS), 93–94
  dimethylsulfonium propionate (DMSP), 93–94
  dissolved organic sulfur (DOS), 92
  volatile sulfur compounds, 92–93
swimming, 154–156, *166*, **168**
  patterns, 156–157, *158*, *159*, *160*, *161*, *163*, *164*, 165, *166*
  pullers, 154, 164
  pushers, 154, 164
  Reynolds number, 155–156
  Sherwood number, 155
  track reconstruction, 162
symbiosis, 43, 52–53, 67
symbiotic cyanobacteria, 61, 189
Synchromophyceae, **4**, 21
Synurales, 19

T

tabulation system, 116, *see also* cell membrane type, 3
  Kofoid, Charles, 116
target markets, *see* bio-based economy
Thalassiosirales, 109
thallus, structure of, 28, **29**
  apocyte/coenocyte, 32
  blade-like, 10
  coccoid, 23, 26
  coenobium, 28, *30*, *31*, 38, *40*
  colony, 28
  discoid, 15
  filamentous, 28
  foliose, 10, 310, 312
  giant-celled, 13, 28
  multicellular, 11–13, 21, 28
  multinucleate, 13, 15, 28, 32, 35
  palmelloid, 36
  parenchymatous, 35
  pseudofilamentous, 11
  pseudoparenchymatous, 35
  siphonocladous, 28
  siphonous, 32
  unicell, 28
thermal environments, 58, 59, *see also* extreme habitats
  C-phycocyanin, **6**, 59, *225*
  Cyanidiales, 59
  geothermal environments, 10, 60
  hydrothermal vents, 58
  temperature-resistant protein, 59
  thermo-acidophile prokaryotes, 59
thylakoids
  encircling, 10, 191
  grana, 14, 188–189, 192, 226
  lamellae, 189
  not stacked, 191, 226
  single, 174
  stacked, 65
toxic algae, *see* Harmful Algal Blooms (HABs)
toxins, 346–347, 349–351, 353–354, **355**, 356
  2-methylisoborneol (MIB), 349
  acrylic acid, 94, 351
  anatoxins, 350, **355**
  B-N-methylamino-L-alanina (BMAA), 351, **355**
  brevetoxins, 352–353, **355**
  ciguatoxins (CTX), 353
  cyanotoxin, 349
  cylindrospermopsin, 350
  dinophysystoxins, 353, **355**
  domoic acid (DA), 87, 351–352, **355**
  endotoxic lipopolysaccharides, 351
  geosmin, 349
  hemolytic substances, 351, **355**
  hepatotoxic cyclic pentapeptides, 350
  hepatotoxin, 349
  maitotoxins (MTX), 353
  microcystins, 350
  neurotoxic alkaloids, 350
  neurotoxic aminoacid, 351
  nodularins, 350, **355**
  okadaic acid (OA), 353, **355**
  palytoxin, 354
  polyunsaturated aldehyde (PUA), 351–352
  prymnesin, 351, **355**
  saxitoxin, 350, **355**
  toxic galactolipids, 349, **355**
trace elements, *see* growth media
transition zone (region), 130, 132, *134*, *135*, 138, 142
  basal plate, 132, 134–136, *142*, 142, *144*
  transitional helix, 135
  transitional plate, 138
  type 1, 132, *133*
  type 2, 132, *133*
  type 3, *134*
  type 4, *135*
  type 5, *136*
Trebouxiophyceae, **3**, 12, 54–56, 61–62, 65, 103, 178, 308
trichome, 102
  apical cell, *103*, 174, 181
  movement, 181
tubulins, 128, 170

U

Ulvophyceae, **3**, 12–13, 15, 31, 36, 49, 53–54, 65, 122, 138, 142, 145, 178, 307, 321, **324**, 327, 348, 354–355
unit conversion, 416
upwelling, 84–85, 90–91
urea $(NH_2)_2CO$, 77, 89–90, 274, 347

V

viral shunt, 46
viruses, 44–48, *see also* biotic interactions
  algal-infecting viruses, 48
  cyanophages, 48
  double-stranded DNA (ds-DNA), 47–48
  single-stranded DNA (ss-DNA), 48

vitamins, 28, 37, 50, 92, 262, 265, 273, 276–277, 308, 310–311, 316–317, 320, 325–326, 337, **338**, 367
α-tocopherol, 325, **338**
biotin, 276, *277*, 326
cobalamin, vitamin B_{12}, 49, 276, *277*, 326
folates, 326
niacin, 316, 325
pantothenic acid, 325
pyridoxine, 326
retinol, 326, **338**, 319
riboflavin, 325
thiamine, vitamin B_1, 49, 276, *277*, 277
vitamin D, 326

W

wastewater, 364–365, *366*
biodegradability index, 365
biodegradable contaminants, 364
biological oxygen demand (BOD), 364–365
biological treatment, 364
chemical oxygen demand (COD), 364–365
food industry, 364
tertiary treatment, 364
treatment, 82–83, 374–376
weathering, 78, 81, 88–90, 92, 103, *see also* carbonation reaction (Urey reaction)
white water phenomenon, 74

X

Xanthophyceae, **4**, 23, 101, 110–111, *135*, 135, 137, 148, 175, 193–194, 199, **284**, 342
xanthophylls, **6**, 8, 14, 26, 57–58, 192, 194–196, 198, 219–220, 227, 235, *236*, *237*, *238*, *239*, *240*, 247, 249, 339
allophycocyanin, **6**, 7–9, 189, 191–192, *225*, 227
alloxanthin, **6**, 195, *222*
astaxanthin, *222*, 292, 295, 337, **338**, 339, 341, 367, **369**, 372
cantaxanthin, 372
diadinoxanthin, **6**, 26, 183, 194, *223*
dinoxanthin, **6**, 26
echinenone, **6**, 26, *223*, 405
fucoxanthin, 367, **6**, 17, 19, 26, 67, 192–195, *223*, 249, 295, **338**, 341
gyroxanthin diester, **6**, 26
lutein, **6**, 191–192, 194, *223*, 246–247, 367
neoxanthin, **6**, *223*
peridinin, **6**, 26, 65, 67, 195, *223*
vaucheriaxanthin, 19, 194
violaxanthin, **6**, 192, 194, *223*, 246
zeaxanthin, **6**, 8, 192, *223*, 246, **338**, 372

Z

zooxanthellae, *see* corals
Zygnematophyceae, **3**, 15, 17, 58, 103, 145, 192, 348, 354–355

Index

Note: Page numbers in *italics* indicate illustrations. Numbers in **bold** indicate tables

A

Acanthophora, 349, 355
Acaryochloris marina, 220, 253, 255
Acetabularia, 13, *15,* 32, 188
Acetabularia acetabulum, 178
Acris crepitans, 53
Acrochaete wittrockii, 122
Acrosiphonia, 137
Agaricia, 250
Agarophyton chilense, **333**
Ahnfeltia, 332, **333**
Ahnfeltiopsis concinna, **324**
Alaria, 315
Alaria esculenta, 315, *315,* **324**, 327
Alexandrium, 114, 353, **355**
Alexandrium hiranoi, 175
Alexandrium minutum, 357
Alexandrium tamarense, 357
Alteromonas, 352
Ambystoma maculatum, 51
Amphidinium, 206, 349
Amphidinium carterae, 114, 195
Amphidinium lacustre, 175
Amphidinium latum, **195**
Amphidinium poeciliochroum, **195**
Anabaena, 41, 79–80, *80,* 167, 178, 189, 350, **355**
Anabaena azotica, 61
Anabaena bergii, 350, **355**
Anabaena cylindrica, 41
Anabaena flos-aquae, 169
Anabaena siamensis, 62
Anabaena variabilis, 79, 167, 174, 337
Anacystis, **29**
Anadyomene, 31
Aphanizomenon flos-aquae, 291, 350, **355**
Artemia, 325, 343
Arthrospira, **3**, 62, 167, 189, *236,* **284**, 291–293, 295, 307–310, **324**, 336–337, 368, **369**, 372
Arthrospira indica, 62
Arthrospira platensis, 308, 364
Ascoglena, **29**
Ascophyllum nodosum, 168, *239,* 326, 331, **333**, **338**
Asparagopsis taxiformis, **324**
Asterochloris, 178
Asterococcus, 103
Aurearena, **4**, 21
Aureococcus, 348
Aureococcus anophagefferens, 348
Aureodinium pigmentosum, 114

B

Bangia, 10
Basicladia, 53
Basicladia chelonum, 53
Basicladia crassa, 53
Basicladia ramulosa, 53
Basicladia sinensis, 53
Basicladia vivipara, 53
Bellis perennis, 235
Bellotia eriophorum, 23
Biddulphia, 109, *111,* 137, 149
Bigelowiella, 159
Bigelowiella natans, 150, *151,* 157, **168**, 178, 205, *205*
Bjornbergiella, **29**
Blastodinium, 201
Botryocladia, 10
Botryococcus, 368
Bradypus, 54, 55
Bradypus pygmaeus, 54
Bradypus torquatus, 54
Bradypus tridactylus, 54
Bradypus variegatus, 54
Bryopsis, **29**, 32
Bufo americanus, 53
Bufo americanus charlesmithi, 52
Bumilleria, 199

C

Callophyllis variegata, 314, **324**
Calothrix, **29**
Calothrix elenkinii, 337
Calyptrosphaera sphaeroidea, 105
Capsosiphon, 307
Capsosiphon fulvescens, 371
Caulerpa, 307, 348, 371
Caulerpa lentillifera, 323, *323,* **324**
Caulerpa racemosa, 323
Caulerpa racemosa var. cylindracea, 35, *35*
Cephaleuros, 36
Ceramium rubrum, **338**
Ceratium, 116, 169, 201
Ceratium furca, 131, *132*
Chaetoceros, 48, 109, 169, 291, 325
Chaetoceros calcitrans, 324
Chaetoceros concavicornis, 349
Chaetoceros convolutus, 349
Chaetoceros muelleri, 342
Chaetomorpha, 142, 355
Chaetosphaeridium, 145
Chara, 15, 355
Chattonella, 149, **168**, 193, 352
Chattonella antiqua, 349
Chattonella marina, 352, **355**
Chilomonas, 146
Chlamydomonas, 36, 41, *42,* 61, 122, 137–138, 158–159, 162, 165, 174, 362, *363, 412*
Chlamydomonas nivalis, 58
Chlamydomonas polypyrenoideum, 364

Chlamydomonas reinhardtii, 49, 62, 87, 123, 174, 241, 341, 362
Chlorarachnion, *27*, **29**
Chlorarachnion reptans, 150, 157, **168**
Chlorella, **3**, *13*, **29**, 38, 47, 55, 62, *237*, 290, 292–295, 308, 325, 362, *363*, 363, 364, 368, **369**, 372
Chlorella ellipsoidea, 62
Chlorella kessleri, 362
Chlorella ohadii, 61
Chlorella pyrenoidosa, 62, 338
Chlorella sorokiniana, 62
Chlorella vulgaris, 61, 62, 178, 295, 335, 364, 368
Chlorococcum, 40
Chlorococcum humicola, 61
Chlorogonium, 52, 53
Chlorokybus, **3**, **29**
Chlorokybus atmophyticus, 15
Chloromonas rubroleosa, 58
Choloepus, 54
Choloepus didactylus, 54
Choloepus hoffmanni, 54
Chondracantus canaliculatus, **333**
Chondracantus chamissoi, 369
Chondria armata, 351
Chondria armata domoi, **355**
Chondrus crispus, 48, 313, *313*, **324**, 328, 332, **333**, **338**
Chroomonas, 103, 116, *118*, 174, **195**, 196–197
Chrysemis rubriventris, 53
Chrysochromulina, **29**, 105, *105*, *129*, 136
Chrysochromulina parva, 123
Chrysococcus, 111
Chrysophaeum, **4**
Cladophora, 28, 31, *34*, 53, 142, 348, 355
Cladosiphon, 321, 348, 355
Cladosiphon okamuranus, 321, **324**
Closterium, **3**
Clostridium, 78
Coccolithus, 74
Coccolithus pelagicus, 105
Cocconeis, 249
Codium, **3**, *14*, 307
Codium edule, **324**
Codium fragilen, 168, **338**, **369**, 371
Colacium, **29**, 119, *119*, 198
Coleochaete, **3**, **29**, 145, 200
Compsopogon, 11
Conchocelis rosea, 312
Corallina, 10
Coronocyclus, **3**
Cosmarium, **29**
Crassostrea gigas, 325
Crocosphaera, 87
Crocosphaera watsonii, 87
Crustomastix, **3**
Crypthecodinium cohnii, 291, **338**, 340, 341
Cryptomonas, *18*, **29**, 116, 147, **168**, 183, 196, 199
Cryptoperidiniopsis, **195**
Cyanidioschyzon, 10, 59
Cyanidium, 10, 59
Cyanidium caldarium, 59
Cyanoderma, **29**
Cyanophora, **3**, **29**, 133, 139, *236*
Cyanophora paradoxa, 178–179, *180*, *191*, 260, *261*, **271**, **272**, **284**
Cyanothece, *7*, 64, 79, 87
Cylindrocapsa, 199–200
Cylindrospermopsis raciborskii, 350, 355

D

Desmaretia, 35
Desmococcus olivaceus, 61
Devaleraea mollis, 327
Diacronema, 145
Diacronema lutheri, 324
Diatoma vulgare var. ovalis, 61
Dictyopteris plagiogramma, 324
Dictyota, 128, 348, 355
Dictyota dichotoma, 122
Dinobryon, 111, 113
Dinobryon divergens, 38
Dinoclonium, **29**
Dinococcus, **29**
Dinophysis, 169, 195, 206, 353, **355**
Dinophysis acuminata, 67, **195**
Dinophysis mitra, **195**
Diplonema, 208
Diplopsalis, 207
Discosphaera tubifera, 106
Distephanus, **4**
Disthepanus speculum, *22*
Distigma, 117
Dunaliella, **29**, 50, *123*, *124*, 158–159, 162, 174, 191, *237*, **284**, 290, 293, 307, 325, **338**, 341, **369**
Dunaliella atacamensis, 50–51
Dunaliella salina, 50, *51*, *160*, 162, *164*, **168**, 178, 182, 188, 291–292, 339, 368
Dunaliella salina mutant, 50
Dunaliella salina var. bardawil, 292
Durinskia baltica, 67
Durvillaea, 307
Durvillaea potatorum, **333**
Dydimosphenia geminata, 348, *349*
Dysmorphococcus, 111

E

Ecklonia, **333**
Ecklonia cava, 320, *320*, **338**
Ecklonia maxima, 333
Ectocarpus, **29**
Ectocarpus siliculosus, 49
Eisenia bicyclis, 320
Emiliana, 74, 390
Emiliana huxleyi, 105
Enteromorpha, 307
Entosiphon, 117, 136, 207–208, *209*
Entosiphon sulcatum, 132
Erythrocladia, **3**, 11
Erythropsidinium, 177
Erythropsidinium agile, 26
Eucheuma, 307, 322, 332, **370**, 371
Eucheuma cottonii, **338**
Eucheuma denticulatum, 332, **333**
Eucheuma denticulatum (spinosum), 332

Eudorina, 28, *31,* 362–363, *363*
Eudorina unicocca, 362
Euglena, **4**, 38, *39*, *127*, *163*, *177*, 179, *180*, 183, *366*, **369**, *407*
Euglena acus, 199, 202
Euglena communis, 202
Euglena gracilis, 27, *37*, 38, *118*, *121*, *122*, *131*, *134*, *158*, *177*, *178*, *179*, *180*, *197*, *202*, *343*, 364, *407*
Euglena mutabilis, 153
Euglena obtusa, 198
Euglena spirogyra, 202
Eunotia exigua, 60
Eutreptia, 65, 130, 198
Eutreptiella, 65, 130
Eutreptiella gymnastica, 127

F

Fischerella, 251
Fragilariopsis sublineata, 57
Fragilidium subglobosum, 38
Fucus, **29**, 35, 42, *44*, *150*, 150, 333, 342, 372
Fucus serratus, **338**
Fucus vesicolosus, 168

G

Galdieria, 10, 59
Galdieria daedala, 59
Galdieria maxima, 59
Galdieria partita, 59
Galdieria sulphuraria, 59, 241
Galeidinium, 67
Gambierdiscus toxicus, 353, **355**
Gelidiella, 322
Gelidium, 329, *330*, 368
Gelidium lingulatum, **333**
Geminella, 103
Gigartina, 307, **324**, 332
Gigartina canaliculata, **333**
Gigartina radula, 332
Gigartina skottsbergii, 332, **333**, **338**
Glaucocystis, **29**, 139
Glaucocystis nostochinearum, 9
Glaucosphaera, **3**, 11, 189
Glenodinium, 199
Glenodinium foliaceum, 116, 175
Gloeobacter violaceous, 178
Gloeocapsa, 61, 62
Gloeocystis, 103
Gloeodinium, **29**
Gloeodinium montanum, 103
Gloeothece, 79
Gloeotrichia, 189
Golenkinia minutissima, 128
Goniotricum, **29**
Gonium pectorale, 178
Gonyaulax, 25, **29**, 201
Gonyaulax polyedra, 200, *206*, 241
Gracilaria, 307, 313–314, 322, 329, **338**, 349, 354, 368, **370**, 371
Gracilaria chilensis, 314, **333**
Gracilaria coronopifolia, **324**
Gracilaria parvispora, **324**
Gracilaria verrucosa, **324**
Gracilariophila oryzoides, 10
Gracilariopsis andersonii, 10
Guillarda theta, 178
Gymnochlora, **4**, *237*
Gymnodinium, 67, 157, 207, *239*, 353, **355**
Gymnodinium acidotum, 195–196, *196*, 197, 260, *261*
Gymnodinium catenatum, 357
Gymnodinium chlorophorum, 67
Gymnodinium galathealum, 195
Gymnodinium gracilentum, 38, **168**, **195**
Gymnodinium mikimotoi, 175
Gymnodinium veneficum, 114
Gyraudiopsis, **4**
Gyrodinium, 207
Gyrodinium aureolum, 195
Gyrodinium lebouriae, 130

H

Haematococcus, 36, 174, 278, 292–293, 296, 308, 338, **369**, 370
Haematococcus pluvialis, 295, *295*, 339, 368
Halimeda, **3**, 74, 338
Haliotis, 296
Haliotis discus, 327
Haliotis rufescens, 327
Haliotis tubercolata, 327
Halomicronema hongdechloris, 220
Halymenia floresii, 11
Hantzschia amphioxys, 61
Haramonas dimorpha, 342
Harpia harpyja, 54
Hassallia byssoidea, 33
Helicosphaera carteri, 18
Helicosporidium, 55, 56
Heterocapsa, 48, 67
Heterosigma, **4**, 48, 352
Heterosigma akashiwo, 24, 349, 352, **355**
Hibiscus esculentus, 309
Hildenbrandia, 35
Himanthalia, 128
Hormosira, 128
Hormotila, 103
Hydra viridis, 48
Hydrodictyon, 28
Hydropuntia edulis, 327
Hydrurus, 28, *30*, 137
Hyla versicolor, 53
Hypnea, 329, *333*
Hypnea valentiae, **338**

I

Ictalurus punctatus, 349
Iridaea, 333
Isochrysis, 291, 324, 325
Isochrysis galbana, 324

K

Kappaphycus, 322, **338**, **370**
Kappaphycus alvarezii, 307, 332, **333**, 342, 371

Kappaphycus alvarezii (cottonii), 332
Karenia, 195, *239*
Karenia brevis, 353, **355**
Karenia mikimotoi, 67, 349
Karlodinium micrum, 67
Katagnymene, 78, 79
Kirchneriella, **3**
Klebsormidium, **3**, *16*, **29**
Kordia algicida, 49
Kryptoperidinium, 195
Kryptoperidinium foliaceum, 67

L

Laminaria, 35, 42, 331, 342
Laminaria hyperborea, 331
Laminaria japonica, 307
Laminaria religiosa, 341
Laurencia, 349, 355
Lepidodinium, 67, 195
Lepidodinium chlorophorum, 67
Lepidodinium viride, 67
Leptolyngbya, 103, **168**, 174, 181, *182*, *236,* 251
Lessardia elongata, 117
Lessonia, 331
Lessonia nigrescens, **333**
Lessonia trabiculata, **333**
Lithodesmium, 137
Lithothamnion, 10
Lithothamnion corallioides, 334
Lobophora variegata, 250
Lymnodynastes tasmaniensis, 51
Lyngbya cryptovaginatus, 61
Lyngbya lagerheimii, 337
Lyngbya maiuscola, 79

M

Macrocystis, 35, 307, 331, **338**, 368
Macrocystis pyrifera, 327, *328*, 331, **333**, **370**
Mallomonas, 107, 124, 137
Mallomonas crassisquama, 108
Mamiella gilva, 125
Mantoniella squamata, 122, 140
Mazzaella, 307
Mazzaella laminaroides, **333**
Melosira, **4**
Melosira arctica, 57
Mesostigma, **3**, 15, 29, 140
Mesostigma grande, 15
Mesostigma viride, 178
Mesotaenium berggrenii, 58
Microcoleus vaginatus, 61
Microcystis, 350, **355**
Microcystis flos-aquae, 102
Micromonas, 325
Micromonas pusilla, 48, 178
Monodus subterraneum, 342
Monostroma, 307, 321, 322, 323, **338**
Monostroma latissimum, 321
Monostroma nitidum, **324**, **370**, **371**
Myrmecia, 54
Mytilus edulis, 352
Mytilus trossulus, 325

N

Nannochloropsis, **4**, *22*, 28, 38, *112*, *194*, *238*, 325, **338**, 340–341, **369**, 377
Navicula, 296, 325
Navicula cryptocephala, 61
Nematodinium, 206
Nematopsides, 177
Neopyropia tenera, **338**
Neosadocus, 50
Nephroselmis, **3**, 126, 140
Nephroselmis spinosa, 124, 125
Nereocystis, **324**
Nereocystis luetkeana, 374, 378
Nitella, **3**, *16*, 355
Nitzschia, 325, 340
Nitzschia alba, 340
Nitzschia laevis, 340
Nitzschia ovalis, 60
Nitzschia stellata, 57
Nitzschia thermalis, 60
Noctiluca, 114, 130, 169, 201, 207
Noctiluca scintillans, 195
Nodularia, 350
Nodularia spumigena, 350–351, **355**
Nostoc, 61–62, 79, 102, 308, 337, 351, **355**
Nostoc commune, 102
Nostoc commune var. *sphaeroides,* 62
Nostoc ellipsosporum, 337
Nostoc flagelliforme, 61, 308, **324**
Nostoc sphaeroides, 62, 308

O

Ochromonas, **4**, 19, *20*, 28, **29**, 41, 101, *135*, 137, 147, *149*, 156, *238*, **284**, 342
Ochromonas danica, 126, *135*, *157*, *158*, **168**, 176, *176*, 179, 182, 193
Oedogonium, 12, 122, 138, 141, 191
Oophila ambystomatis, 51
Oscillatoria, 28, *32*, 79, 110, 167, **168**, 189
Oscillatoria limosa, 78, 79
Oscillatoria raciborskii, 337
Ostrea edulis, 325
Ostreobium, 250
Ostreococcus, 87, 178
Ostreococcus lucimarinus, 87
Ostreococcus tauri, 341
Ostreopsis ovata, 350, 354, **355**
Oxyrrhis marina, 114, 127, 130, 172, 178, 201

P

Padina pavonia, **338**
Padina tetrastomatica, **338**
Palmaria, **29**, 35
Palmaria (Rhodymenia) palmata, 312, **324**
Palmaria palmata, 36, **338**
Palmella, 36, 50, 103
Palmellococcus miniatus, 61
Palmoclathrus, 250
Palmophyllum, **3**, 11, **29**, 250
Pandorina, 174
Paramecium bursaria, 48

Parietochloris incisa, 338
Patinopecten yessoensis, 325
Paulinella cromatophora, 64
Pavlova, **3**, 17, 105, 124, 145, *238*, 325
Pavlova lutheri, 178, 341
Pavlova salina, **168**
Pediastrum, 28, 38, 39, *40*, 169
Pediastrum simplex, 31
Pedinomonas, 3
Pedinomonas noctilucae, 195
Peranema, **4**, *12*, 65, 117, 207, 342
Peranema trichophorum, 208
Peridinium, 67, 157, *160*, 174, 201
Peridinium balticum, 175
Peridinium gatunense, 342
Peridinium quinquecorne, 67
Peridinopsis, 206
Petalomonas, 117
Petalonia binghamiae, 341
Pfiesteria piscicida, **195**
Phacotus, 111, 112
Phacus, **4**, 29, 197
Phaeobacter inhibens, 49
Phaeocystis, 203, 351
Phaeocystis pouchetii, 351, **355**
Phaeodactylum, 87, *239*
Phaeodactylum tricornutum, 295, **338**, 340–341, 367
Phaeopolykrikos, 138
Phaeothamnion, **4**, 103
Phalachroma, 353, 355
Phitophora oedogonia, 355
Phormidium, 79, 167, 174
Phormidium cebennse, 337
Phormidium crosbyanum, 102
Phormidium retzi, 189
Phormidium tenue, 61, 337
Phormidium uncinatum, 167
Phyllophora, **3**
Phymatolithon calcareum, 334
Picophagus, **4**
Pilayella littoralis, 355
Pinguiococcus, **4**
Pinnularia acoricola, 60
Pinnularia quadratarea, 57
Planktothrix, 350, 355
Planktothrix perornata, 349
Plasmodium falciparum, 56
Plectonema boryanum, 78, 79
Pleurocapsa, **29**
Pleurochrysis, 145, 147
Pleurochrysis carterae, 105
Ploeotia, 117, 208
Polykrikos kofoidi, 206, *207*
Polysiphonia lanosa, 236
Polytomella agilis, 122
Porphyra, **3**, 10, 42, *47*, 307, 310–312, **324**, 327, **338**, 342, 368, **370**, 371–372
Porphyra purpurea, 10
Porphyra tenera, **338**
Porphyra umbilicalis, 10, 312
Porphyra yezoensis, **324**
Porphyridium, **3**, 11, **29**, 165, 167, **168**, 191, *236*, **338**, 342
Porphyridium aerugineum, 342
Porphyridium cruentum, 192
Prasinoderma, **3**, **29**
Prochlorococcus, 228, 241, 248
Prochloron, 7, 29, 110, 189, 228, 248
Prochlorothrix, 29, 228, 248
Prorocentrum, **4**, 157, 159, 199, 239, 353, 355
Prorocentrum donghaiense, 178
Prorocentrum micans, 116
Prorocentrum minimum, 347
Prorocentrum nanum, 116
Protoperidinium, 201, 207
Protoperidinium steinii, 116
Prototheca, 55
Prototheca blashkeae, 55
Prototheca moriformis, 55
Prototheca stagnorum, 55
Prototheca ulmea, 55
Prototheca wickerhamii, 55
Prototheca zopfii, 55
Prymnesium parvum, 349, 351, **355**
Prymnesium polylepis, 349, 351, **355**
Pseudanabaena, 79, 174
Pseudoisochrysis paradoxa, 324
Pseudomonas, 352
Pseudomonas protegens, 49
Pseudo-nitzschia, 87–88, 351–352, **355**
Pseudo-nitzschia delicatissima, 352, **355**
Pseudo-nitzschia granii, 87
Pseudo-nitzschia multiseries, 49, 87
Pseudosphaerocystis, **29**
Pterocladiella, 329, **333**
Pteromonas, 111–112
Pteromonas protracta, 113
Pyramimonas, **3**, 104, *125*, 125, 140, 203
Pyramimonas longicauda, 13
Pyramimonas lunata, 138
Pyramimonas octopus, 138
Pyramimonas orientalis, 126
Pyrocystis, **4**
Pyrocystis lunula, 178
Pyrodinium, 353, **355**
Pyropia, 10, 307, 310–311, 368, **370**, 371
Pyropia abbottae, 311
Pyropia tenera, 311
Pyropia torta, 311
Pyropia yezoensis, 311

R

Rana palustris, 51
Rana sylvatica, 51
Rebecca salina, 342
Rhabdomonas, 65
Rhipiliopsis profunda, 250
Rhodomonas, **3**, 195, *238*
Rhodomonas salina, **195**
Rhodosorus, **3**
Rhodymenia palmata, 312, 324
Rhoicosphenia, 109
Rhopalodia gibba, 64
Rodomella subfusca, **338**
Rosenvingiella radicans, 62
Roseobacter, 49

S

Saccharina, 46, 316–317, 320–321, **324**, 326, 331, **333**, **338**, 342
Saccharina angustata, 316
Saccharina coriacea, 316
Saccharina digitata, 326, **333**
Saccharina hyperborea, **333**
Saccharina japonica, 307, 316, *316*, 331, **333**, **338**, **370**
Saccharina latissima, **338**, 374, 378
Saccharina longissima, 316
Saccharina ochotensis, 316
Saccharina saccharina, **333**
Salmonella, 351
Sarcopeltis skottsbergii, **333**
Sarcothalia, 307
Sarcothalia crispata, 332, **333**
Sargassum, 168, 307, 320, 333, **338**, 348, 354–355, **370**
Sargassum echinocarpum, **324**
Sargassum fluitans, 355
Sargassum fusiforme, 319, **324**, **338**, 371
Sargassum natans, 355
Scenedesmus, 169, 364
Scenedesmus dimorphus, 378
Scenedesmus obliquus, 62, 377
Scherffelia, 104
Schizochytrium, 340, 368, **369**
Schizochytrium limacinum, 340
Schizocladia, **4**
Scrippsiella, 114
Scytomonas pusilla, 137
Scytonema, 28, *33*, 251
Scytonema burmanicum, 337
Scytonema javanicum, 61
Scytosiphon lomentaria, 341
Silvetia, 181
Silvetia compressa, 174, *175*, 179, 181
Skeletonema, 109, 291, 325
Skeletonema costatum, 49, 292, 324, 352, **355**
Spermatozopsis, 174
Sphaerocystis sphaerocystiformis, 62
Sphaleromantis sp, 124
Spirogyra, *17*, 28, 103, 188, 355
Spirulina, 290, 336, 368
Spyridia filamentosa, 355
Spyrogyra, 40
Stephanodiscus, *110*
Stigonema mamillosum, 28, *34*
Stigonema ocellatum, 28, *34*
Strombomonas verrucosa, 119, *120*
Stylonema, **3**, 11
Symbiodinium, **168**, 178, 250–251
Symploca, 79
Synchroma, **4**
Synechococcus, **29**, 59, 85, **168**, 241, 248
Synechococcus lividus, 59
Synechococcus planctibus, 189
Synechocystis, 85, 167
Synechocystis pevalekii, 61
Synura, **4**, 28, **29**, 107, 124, 137
Synura petersenii, *107*
Synura uvella, *21*
Syracosphaera oblonga, 106

T

Tetraflagellochloris mauritanica, 28, *30*, 138, *139*, *142*, *143*, 160, *161*, 162, 164, **168**, *172*, *210*
Tetraparma, **4**
Tetraselmis, **3**, 38, *39*, 104, 124, *125*, 125, 126, 140, *237*, 291, 325, 368
Tetraselmis subcordiformis, 178
Tetraselmis suecica, 138, **168**, 324, 377
Tetraspora, 37
Thalarctos maritimus, 55
Thalassiosira, 87, 110, 291
Thalassiosira pseudonana, 325, 341
Thalassiosira rotula, 352, **355**
Thraustochytrium, 340
Tolypothrix, 28
Trachelomonas, **4**, 119–120, 197
Trentepohlia, 54, 145, 307
Trentepohlia arborum, *14*
Triceratium, **29**, *108*
Trichodesmium, 78–79, 86, 169
Trichophilus, 54
Trichormus azollae, *8*

U

Udotea, 74
Ulothrix, 28, **29**, *32*, 40, 142
Ulva, **29**, 35, 42, *45*, 142, 168, 171, 174, 321, *322*, 323, 355
Ulva clathrata, 369
Ulva fasciata, 324
Ulva intestinalis, 322
Ulva lactuca, 327, 338, 342
Ulva mutabilis, 49
Ulva prolifera, 324, 348, 371
Umbellosphaera, **3**
Undaria, **4**, 317–318, 320–321, 341
Undaria pinnatifida, 307, 317, *318*, **324**, **338**, 341, **370**, 371

V

Vaucheria, **4**, **29**, 32, 148
Vaucheria sessilis, *24*
Verdigellas, 250
Viviparus malleatus, 53
Volvox, 28, **29**, 38, 159, 174
Volvox aureus, *30*
Volvox carteri, 178, 183

W

Warnowia polyphemus, 26
Warnowia pulchra, 26
Woloszynskia coronate, 114, 174
Wrightiella blodgettii, 355

X

Xiphophora, 128

Z

Zygnema, 188